

AFFDL-TR-71-62  
VOLUME VII

Volume VII. Wind Tunnel Test of the Aerodynamics  
and Dynamics of Rotor Spinup, Stopping and  
Folding on a Semispan Folding Tilt-Rotor Model

Dirk van Wagenveld  
Frank J. McHugh  
Leon N. Delarm  
Walter L. Lapinski  
John P. Magee  
The Boeing Company, Vertol Division  
Philadelphia, Pennsylvania

TECHNICAL REPORT AFFDL-TR-71-62, VOLUME VII

October 1971

APPROVED FOR PUBLIC RELEASE  
DISTRIBUTION UNLIMITED

Air Force Flight Dynamics Laboratory  
Aeronautical Systems Division  
Air Force Systems Command  
Wright-Patterson Air Force Base, Ohio

# Contracts

## FOREWORD

This report was prepared by the Boeing Company, Vertol Division, Philadelphia, Pennsylvania, for the Air Force Flight Dynamics Laboratory, Wright-Patterson Air Force Base, Ohio, under Phase II of Contract F33615-69-C-1577. The contract objective is to develop design criteria and aerodynamic prediction techniques for the folding tilt rotor concept through a program of model testing and analysis.

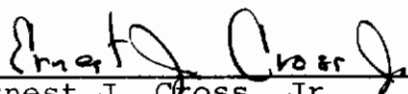
The contract was administered by the Air Force Flight Dynamics Laboratory with Mr. Daniel E. Fraga (FV) as Project Engineer.

This report covers the period from January to July 1971.

The reports published under this contract for Design Studies and Model Tests of the Stowed Tilt Rotor Concept are:

Volume I	Parametric Design Studies
Volume II	Component Design Studies
Volume III	Performance Data for Parametric Study
Volume IV	Wind Tunnel Test of the Conversion Process of a Folding Tilt Rotor Aircraft Using a Semi-Span Unpowered Model
Volume V	Wind Tunnel Test of a Powered Tilt Rotor Performance Model
Volume VI	Wind Tunnel Test of a Powered Tilt Rotor Dynamic Model on a Simulated Free Flight Suspension System
Volume VII	Wind Tunnel Test of the Dynamics and Aerodynamics of Rotor Spinup, Stopping and Folding on a Semi-Span Folding Tilt Rotor Model
Volume VIII	Summary of Structural Design Criteria and Aerodynamic Prediction Techniques
Volume IX	Value Engineering Report

This report has been reviewed and is approved.

  
Ernest J. Cross, Jr.  
Lt. Colonel, USAF  
Chief, Prototype Division

## ABSTRACT

Wind tunnel test data obtained with a 1/9 scale, semispan, unpowered, dynamically-scaled Model 213 stowed/tilt rotor are reported.

The objectives of the tests were to obtain aerodynamic, structural, and dynamics data during the spinup, feather and blade fold cycles of this vehicle.

## SUMMARY

A wind tunnel test (BVWT 071) of a 1/9 scale, semi-span, unpowered, dynamically-scaled Model 213 was conducted in the Boeing V/STOL tunnel for the Air Force Flight Dynamics Laboratory under USAF Contract No. F33615-69-C-1577. The test results comprise performance, stability, rotor loads and dynamics data during the conversion cycles of this vehicle (windmilling, feather, fold, deploy and spinup) to provide verification of prediction techniques and establish design criteria. The report is divided into performance, stability, rotor loads and dynamics sections and a brief summary of each section follows:

Performance - Total aircraft performance data are presented in Section 5.0 and show that a spinup and feather schedule of 3 to 4 seconds duration using a linear collective schedule will produce a transient axial force of less than 0.1 g's. This can be achieved either by starting the conversion cycle from 70% rpm or by providing simple thrust modulation to balance the change in steady drag from windmilling to feathered. The interaction effects of the rotor on the airframe are small. Flatwise blade folding is shown to produce less drag than edgewise folding.

Stability - Stability test data shown in Section 6.0 indicate that the Model 213 with rotors operating is a statically stable vehicle ( $\partial C_M / \partial C_L = -0.116$ ). Blade folding and deployment can be accomplished with a smooth change in stability margin. No large transient changes in stability were observed during spinup and feather. Rotor blade dynamics and couplings have a large stabilizing effect on rotor stability derivatives for a soft in-plane hingeless rotor. The effects of wing circulation on the rotor derivatives have been measured. The rotor-airframe aerodynamic interactions are small and do not influence the contribution of the tail to static stability.

Rotor Loads - Rotor loads data are presented in Section 7.0. Spinup and feather can be accomplished without excessive alternating blade loads. The increase in blade loads due to angle of attack and wing flap setting have been measured and show that the use of flap to maintain airplane lift at low speed produces lower blade loads than changing the aircraft attitude. Near zero loads were observed during blade folding and steady loads are less than the feathered blade case for both edgewise and flatwise folding.

## SUMMARY

Dynamics - Whirl flutter and divergence did not occur for the scaled Model 213 wing spar stiffness. Air resonance was found and the inception of this instability is correctly predicted. Static divergence and whirl flutter data were measured using a reduced stiffness spar.

TABLE OF CONTENTS

	<u>PAGE</u>
1.0 INTRODUCTION . . . . .	1
2.0 OBJECTIVES . . . . .	2
3.0 TEST INSTALLATION . . . . .	4
3.1 MODEL DESCRIPTION . . . . .	4
3.2 MODEL INSTRUMENTATION AND DATA PROCESSING . . . . .	15
3.3 MODEL INSTALLATION IN THE WIND TUNNEL . . . . .	17
4.0 TEST PROGRAM . . . . .	21
4.1 SCALING OF WIND TUNNEL TEST SPEEDS . . . . .	21
4.2 DESCRIPTION OF TEST RUNS . . . . .	21
4.3 OBSERVATIONS MADE DURING THE TEST . . . . .	22
5.0 PERFORMANCE. . . . .	27
5.1 STEADY STATE WINDMILLING PERFORMANCE. . . . .	27
5.2 SPINUP AND FEATHER PERFORMANCE. . . . .	30
5.3 FOLDING AND DEPLOYMENT PERFORMANCE. . . . .	33
5.4 CONCLUSIONS . . . . .	65
6.0 STABILITY. . . . .	66
6.1 STEADY STATE WINDMILLING STABILITY. . . . .	66
6.2 SPINUP AND FEATHER STABILITY. . . . .	138
6.3 FOLDING AND DEPLOYMENT STABILITY . . . . .	143
6.4 CONCLUSIONS . . . . .	146
7.0 ROTOR LOADS. . . . .	147
7.1 ROTOR BLADE FREQUENCIES . . . . .	147
7.2 STEADY WINDMILLING . . . . .	147
7.3 SPINUP AND FEATHER LOADS . . . . .	176
7.4 FOLD AND DEPLOYMENT LOADS . . . . .	202
7.5 CONCLUSIONS . . . . .	213

TABLE OF CONTENTS

	<u>PAGE</u>
8.0 DYNAMICS . . . . .	214
8.1 WING FREQUENCY AND DAMPING NOMINAL SPAR. . . . .	214
8.1.1 Blade Folding Test	215
8.2 REDUCED STIFFNESS SPAR . . . . .	215
8.3 CONCLUSIONS . . . . .	216
9.0 CONCLUSIONS . . . . .	229
10.0 RECOMMENDATIONS . . . . .	232
11.0 REFERENCES . . . . .	233
APPENDICES . . . . .	234

LIST OF ILLUSTRATIONS

FIGURE NO.		PAGE
3-1	MODEL INSTALLATION IN WIND TUNNEL . . . . .	5
3-2	CALCULATED BLADE FREQUENCY SPECTRUM OF 1/9 SCALE MODEL 213 BLADES. . . . .	8
3-3	BLADE TWIST AND ORIENTATION OF GAGES AT .125R . . . . .	9
3-4	ROTOR BLADE ORIENTATION AND MOUNTING DETAILS . . . . .	11
3-4A	FLAT FOLDING HUB DETAILS . . . . .	12
3-4B	WING CONSTRUCTION DETAILS . . . . .	14
3-5	1/9 SCALE MODEL 213 SEMISPAN. . . . .	18
3-6	1/9 SCALE MODEL 213 (SEMISPAN). . . . .	19
3-7	INSTALLATION OF 1/9 SCALE VR076D IN B.V.W.T..	20
4-1	BASELINE RUNS (WITHOUT ROTOR) . . . . .	25
4-2	STEADY STATE WINDMILLING RUNS . . . . .	26
5-1	AIRFRAME LIFT/ANGLE OF ATTACK VARIATION FOR FLAP DEFLECTIONS OF 0°, 15°, 30°, AND 45° . . . . .	35
5-2	AIRFRAME DRAG/LIFT VARIATION FOR FLAP DEFLECTIONS OF 0°, 15°, 30°, AND 45°. . . . .	36
5-3	DEFINITION OF INDUCED DRAG AND AIRFRAME EFFICIENCY . . . . .	37
5-4	BLADE COLLECTIVE/ROTOR RPM VARIATION FOR STEADY WINDMILLING. . . . .	38
5-5	BLADE COLLECTIVE/ADVANCE RATIO VARIATION FOR STEADY WINDMILLING. . . . .	39
5-6	ROTOR DRAG/ROTOR RPM VARIATION AS INFLUENCED BY FORWARD SPEED AND FLAP DEFLECTION (STEADY WINDMILLING). . . . .	40
5-7	ROTOR PERFORMANCE DURING WINDMILLING OPERATION . . . . .	41



## LIST OF ILLUSTRATIONS

<u>FIGURE NO.</u>	<u>TITLE</u>	<u>PAGE</u>
5-8	AIRFRAME LIFT/ANGLE OF ATTACK VARIATION FOR FLAP DEFLECTIONS OF $0^\circ$ , $15^\circ$ , $30^\circ$ , AND $45^\circ$ . . . . .	42
5-9	AIRFRAME LIFT/ANGLE OF ATTACK VARIATION FOR FLAP DEFLECTIONS OF $0^\circ$ AND $30^\circ$ . . . . .	43
5-10	AIRFRAME PITCHING MOMENT/ANGLE OF ATTACK VARIATION FOR FLAP DEFLECTIONS OF $0^\circ$ , $15^\circ$ , $30^\circ$ AND $45^\circ$ . . . . .	44
5-11	AIRFRAME PITCHING MOMENT/ANGLE OF ATTACK VARIATION FOR FLAP DEFLECTIONS OF $0^\circ$ AND $30^\circ$ . . . . .	45
5-12	EFFECT OF ROTOR RPM AND FORWARD SPEED ON AIRCRAFT LIFT $\alpha=0^\circ$ $\delta_F=30^\circ$ (STEADY WINDMILLING) . . . . .	46
5-13	EFFECT OF ROTOR RPM AND FORWARD SPEED ON AIRCRAFT DRAG, $\alpha=0^\circ$ $\delta=30^\circ$ (STEADY WINDMILLING) . . . . .	47
5-14	EFFECT OF COLLECTIVE RATE ON ROTOR DRAG DURING SPINUP AT $V=85$ FPS $\alpha=0^\circ$ $\delta_F=30^\circ$ (LINEAR COLLECTIVE RATE) . . . . .	48
5-15	EFFECT OF COLLECTIVE RATE ON ROTOR DRAG DURING FEATHER AT $V=85$ FPS $\alpha=0^\circ$ $\delta_F=30^\circ$ (LINEAR COLLECTIVE RATE) . . . . .	49
5-16	EFFECT OF COLLECTIVE RATE ON ROTOR DRAG DURING SPINUP AT $113$ FPS $\alpha=0^\circ$ $\delta_F=15^\circ$ . . . . .	50
5-17	EFFECT OF COLLECTIVE RATE ON ROTOR DRAG DURING FEATHER AT $V=113$ FPS $\alpha=0^\circ$ $\delta_F=15^\circ$ . . . . .	51
5-18	EFFECT OF FLAP DEFLECTION ON ROTOR DRAG DURING SPINUP AT $V=113$ FPS $\alpha=0^\circ$ (LINEAR COLLECTIVE RATE) . . . . .	52

# Contracts

## LIST OF ILLUSTRATIONS

<u>FIGURE NO.</u>	<u>TITLE</u>	<u>PAGE</u>
5-19	EFFECT OF FLAP DEFLECTION ON ROTOR DRAG DURING FEATHER AT $V=113$ FPS $\alpha=0^\circ$ (LINEAR COLLECTIVE RATE) . . . . .	53
5-20	EFFECT OF FORWARD SPEED ON ROTOR DRAG DURING SPINUP FOR 4.5 SECOND LINEAR COLLECTIVE RATE, FINAL RPM = 950 . . . . .	54
5-21	EFFECT OF FORWARD SPEED ON ROTOR DRAG DURING FEATHER FOR 4.5 SECOND LINEAR COLLECTIVE RATE $\alpha = 0$ INITIAL RPM = 950 . . . . .	55
5-22	EFFECT OF FORWARD SPEED ON ROTOR DRAG DURING SPINUP FOR 4.5 SECOND LINEAR COLLECTIVE RATE, FINAL RPM = 715 . . . . .	56
5-23	EFFECT OF FORWARD SPEED ON ROTOR DRAG DURING FEATHER FOR 4.5 SEC LINEAR COLLECTIVE RATE, INITIAL RPM = 715 . . . . .	57
5-24	COMPARISON OF LINEAR AND PARABOLIC COLLECTIVE RATES FOR SPINUP $V=85$ FPS FINAL RPM = 950 .	58
5-25	COMPARISON OF LINEAR AND PARABOLIC COLLECTIVE RATES FOR FEATHER $V=85$ FPS INITIAL RPM=950	59
5-26	COMPARISON OF VARIOUS PARABOLIC COLLECTIVE RATES FOR SPINUP $V=113$ FPS FINAL RPM=715 . .	60
5-27	COMPARISON OF VARIOUS PARABOLIC COLLECTIVE RATES FOR FEATHER $V=113$ FPS INITIAL RPM 715	61
5-28	AIRCRAFT DRAG VARIATION WITH BLADE FOLDING AT $\alpha=0^\circ$ $\xi_F = 0^\circ$ (FLATWISE FOLD) . . . . .	62
5-29	TOTAL AIRCRAFT DRAG VARIATION DURING 3 SECOND TRANSIENT FOLD AND DEPLOY . . . . .	63
5-30	COMPARISON OF EDGEWISE AND FLATWISE BLADE FOLDING DRAG LEVELS $\alpha=0^\circ$ $\xi_F=0^\circ$ . . . . .	64

# Contracts

## LIST OF ILLUSTRATIONS

<u>FIGURE NO.</u>	<u>TITLE</u>	<u>PAGE</u>
6-1	AIRFRAME LIFT/ANGLE OF ATTACK VARIATION FOR FLAP DEFLECTIONS OF $0^{\circ}, 15^{\circ}, 30^{\circ}, 45^{\circ}$ . . .	73
6-2	AIRFRAME PITCHING MOMENT/LIFT VARIATION FOR FLAP DEFLECTIONS OF $0^{\circ}, 15^{\circ}, 30^{\circ}$ AND $45^{\circ}$ . . . . .	74
6-3	ROTOR PITCHING MOMENT/RPM VARIATION FUSELAGE ATTITUDE = $4^{\circ}$ $\delta_F=0^{\circ}$ (STEADY WINDMILLING) . . . . .	75
6-3A	RATIO OF NET OUT-OF-PLANE FLAPPING/UNIT SHAFT ANGLE OF ATTACK . . . . .	76
6-4	ROTOR NORMAL FORCE/RPM VARIATION FUSELAGE ATTITUDE = $+4^{\circ}$ $\delta_F=0^{\circ}$ (STEADY WINDMILLING) . . . . .	77
6-5	ROTOR YAWING MOMENT/RPM VARIATION FUSELAGE ATTITUDE = $+4^{\circ}$ $\delta_F=0^{\circ}$ (STEADY WINDMILLING) . . . . .	78
6-6	ROTOR SIDE FORCE/RPM VARIATION FUSELAGE ATTITUDE = $+4^{\circ}$ $\delta_F=0^{\circ}$ (STEADY WINDMILLING) . . . . .	79
6-7	ROTOR PITCHING MOMENT/NACELLE ANGLE OF ATTACK FOR ROTOR RPM = 600 $\delta_F=0^{\circ}$ . . . . .	80
6-8	ROTOR PITCHING MOMENT/NACELLE ANGLE OF ATTACK FOR ROTOR RPM = 700 $\delta_F=0^{\circ}$ . . . . .	81
6-9	ROTOR PITCHING MOMENT/NACELLE ANGLE OF ATTACK FOR ROTOR RPM = 800 $\delta_F=0^{\circ}$ . . . . .	82
6-10	ROTOR PITCHING MOMENT/NACELLE ANGLE OF ATTACK FOR ROTOR RPM = 900 $\delta_F=0^{\circ}$ . . . . .	83
6-11	ROTOR PITCHING MOMENT/NACELLE ANGLE OF ATTACK FOR ROTOR RPM = 950 $\delta_F=0^{\circ}$ . . . . .	84
6-12	ROTOR PITCHING MOMENT/NACELLE ANGLE OF ATTACK FOR ROTOR RPM = 600 $\delta_F=30^{\circ}$ . . . . .	85

LIST OF ILLUSTRATIONS

<u>FIGURE NO.</u>	<u>TITLE</u>	<u>PAGE</u>
6-13	ROTOR PITCHING MOMENT/NACELLE ANGLE OF ATTACK FOR ROTOR RPM = 800 $\delta_F=30^\circ$ . . . . .	86
6-14	ROTOR PITCHING MOMENT/NACELLE ANGLE OF ATTACK FOR ROTOR RPM = 950 $\delta_F=30^\circ$ . . . . .	87
6-15	ROTOR PITCHING MOMENT DERIVATIVE VARIATION WITH ROTOR RPM, $\delta_F = 0^\circ$ . . . . .	88
6-16	ROTOR NORMAL FORCE/NACELLE ANGLE OF ATTACK FOR ROTOR RPM = 600 $\delta_F=0^\circ$ . . . . .	89
6-17	ROTOR NORMAL FORCE/NACELLE ANGLE OF ATTACK FOR ROTOR RPM = 700 $\delta_F=0^\circ$ . . . . .	90
6-18	ROTOR NORMAL FORCE/NACELLE ANGLE OF ATTACK FOR ROTOR RPM = 800 $\delta_F=0^\circ$ . . . . .	91
6-19	ROTOR NORMAL FORCE/NACELLE ANGLE OF ATTACK FOR ROTOR RPM = 900 $\delta_F=0^\circ$ . . . . .	92
6-20	ROTOR NORMAL FORCE/NACELLE ANGLE OF ATTACK FOR ROTOR RPM = 950 $\delta_F=0^\circ$ . . . . .	93
6-21	ROTOR NORMAL FORCE/NACELLE ANGLE OF ATTACK FOR ROTOR RPM = 600 $\delta_F=30^\circ$ . . . . .	94
6-22	ROTOR NORMAL FORCE/NACELLE ANGLE OF ATTACK FOR ROTOR RPM = 800 $\delta_F=30^\circ$ . . . . .	95
6-23	ROTOR NORMAL FORCE/NACELLE ANGLE OF ATTACK FOR ROTOR RPM = 950 $\delta_F=30^\circ$ . . . . .	96
6-24	ROTOR NORMAL FORCE DERIVATIVE VARIATION WITH ROTOR RPM $\delta_F = 0^\circ$ . . . . .	97
6-25	ROTOR YAWING MOMENT/NACELLE ANGLE OF ATTACK FOR ROTOR RPM = 600 $\delta_F=0^\circ$ . . . . .	98
6-26	ROTOR YAWING MOMENT/NACELLE ANGLE OF ATTACK FOR ROTOR RPM = 700 $\delta_F=0^\circ$ . . . . .	99

LIST OF ILLUSTRATIONS

<u>FIGURE NO.</u>	<u>TITLE</u>	<u>PAGE</u>
6-27	ROTOR YAWING MOMENT/NACELLE ANGLE OF ATTACK FOR ROTOR RPM = 800 $\delta_F=0^\circ$ . . . . .	100
6-28	ROTOR YAWING MOMENT/NACELLE ANGLE OF ATTACK FOR ROTOR RPM = 900 $\delta_F=0^\circ$ . . . . .	101
6-29	ROTOR YAWING MOMENT/NACELLE ANGLE OF ATTACK FOR ROTOR RPM = 950 $\delta_F=0^\circ$ . . . . .	102
6-30	ROTOR YAWING MOMENT/NACELLE ANGLE OF ATTACK FOR ROTOR RPM = 600 $\delta_F=30^\circ$ . . . . .	103
6-31	ROTOR YAWING MOMENT/NACELLE ANGLE OF ATTACK FOR ROTOR RPM = 800 $\delta_F=30^\circ$ . . . . .	104
6-32	ROTOR YAWING MOMENT/NACELLE ANGLE OF ATTACK FOR ROTOR RPM = 950 $\delta_F=30^\circ$ . . . . .	105
6-33	ROTOR YAWING MOMENT DERIVATIVE VARIATION WITH ROTOR RPM, $\delta_F = 0^\circ$ . . . . .	106
6-34	ROTOR SIDE FORCE/NACELLE ANGLE OF ATTACK FOR ROTOR RPM = 600 $\delta_F=0^\circ$ . . . . .	107
6-35	ROTOR SIDE FORCE/NACELLE ANGLE OF ATTACK FOR ROTOR RPM = 700 $\delta_F=0^\circ$ . . . . .	108
6-36	ROTOR SIDE FORCE/NACELLE ANGLE OF ATTACK FOR ROTOR RPM = 800 $\delta_F=0^\circ$ . . . . .	109
6-37	ROTOR SIDE FORCE/NACELLE ANGLE OF ATTACK FOR ROTOR RPM = 900 $\delta_F=0^\circ$ . . . . .	110
6-38	ROTOR SIDE FORCE/NACELLE ANGLE OF ATTACK FOR ROTOR RPM = 950 $\delta_F=0^\circ$ . . . . .	111
6-39	ROTOR SIDE FORCE/NACELLE ANGLE OF ATTACK FOR ROTOR RPM = 600 $\delta_F=30^\circ$ . . . . .	112
6-40	ROTOR SIDE FORCE/NACELLE ANGLE OF ATTACK FOR ROTOR RPM = 800 $\delta_F=30^\circ$ . . . . .	113

LIST OF ILLUSTRATIONS

<u>FIGURE NO.</u>	<u>TITLE</u>	<u>PAGE</u>
6-41	ROTOR SIDE FORCE/NACELLE ANGLE OF ATTACK FOR ROTOR RPM = 950 $\delta_F=30^\circ$ . . . . .	114
6-42	ROTOR SIDE FORCE DERIVATIVE VARIATION WITH ROTOR RPM, $\delta_F = 0^\circ$ . . . . .	115
6-43	EFFECT OF WING LIFT ON ROTOR PITCHING MOMENT (V = 113 FPS, RPM = 600) . . . . .	116
6-44	EFFECT OF WING LIFT ON ROTOR PITCHING MOMENT (V = 113 FPS, RPM = 700) . . . . .	117
6-45	EFFECT OF WING LIFT ON ROTOR PITCHING MOMENT (V = 113 FPS, RPM = 800) . . . . .	118
6-46	EFFECT OF WING LIFT ON ROTOR PITCHING MOMENT (V = 113 FPS, RPM = 900) . . . . .	119
6-47	EFFECT OF WING LIFT ON ROTOR PITCHING MOMENT (V = 113 FPS, RPM = 950) . . . . .	120
6-48	ROTOR PITCHING MOMENT/NACELLE ANGLE OF ATTACK FOR ROTOR RPM = 600 $\delta_F=0^\circ$ (CIRCULATION EFFECTS REMOVED) . . . . .	121
6-49	ROTOR PITCHING MOMENT/NACELLE ANGLE OF ATTACK FOR ROTOR RPM = 950 $\delta_F=0^\circ$ (CIRCULATION EFFECTS REMOVED) . . . . .	122
6-50	ROTOR NORMAL FORCE/NACELLE ANGLE OF ATTACK VARIATION FOR ROTOR RPM = 600 $\delta_F=0^\circ$ (CIRCULATION EFFECTS REMOVED) . . . . .	123
6-51	ROTOR NORMAL FORCE/NACELLE ANGLE OF ATTACK VARIATION FOR ROTOR RPM = 950 $\delta_F=0^\circ$ (CIRCULATION EFFECTS REMOVED) . . . . .	124
6-52	COMPARISON OF ROTOR PITCHING MOMENT DERIVATIVE WITH AND WITHOUT WING CIRCULATION EFFECTS $\delta_F=0^\circ$ . . . . .	125

LIST OF ILLUSTRATIONS

<u>FIGURE NO.</u>	<u>TITLE</u>	<u>PAGE</u>
6-53	COMPARISON OF ROTOR NORMAL FORCE DERIVATIVE WITH AND WITHOUT WING CIRCULATION EFFECTS	126
6-54	COMPARISON OF ROTOR YAWING MOMENT DERIVATIVE WITH AND WITHOUT WING CIRCULATION EFFECTS	127
6-55	COMPARISON OF ROTOR SIDE FORCE DERIVATIVES WITH AND WITHOUT WING CIRCULATION EFFECTS	128
6-56	ROTOR PITCHING MOMENT DERIVATIVE VARIATION WITH ROTOR RPM (WING CIRCULATION EFFECTS REMOVED) . . . . .	129
6-57	ROTOR NORMAL FORCE DERIVATIVE VARIATION WITH ROTOR RPM (WING CIRCULATION EFFECTS REMOVED)	130
6-58	ROTOR YAWING MOMENT DERIVATIVE VARIATION WITH ROTOR RPM (WING CIRCULATION EFFECTS REMOVED) . . . . .	131
6-59	ROTOR SIDE FORCE DERIVATIVE VARIATION WITH ROTOR SIDE FORCE (WING CIRCULATION EFFECTS REMOVED) . . . . .	132
6-60	EFFECT OF ROTOR RPM AND FORWARD SPEED ON AIRCRAFT LIFT $\alpha=0^\circ \delta_F=30^\circ$ (STEADY WINDMILLING) . . . . .	133
6-61	EFFECT OF ROTOR RPM AND FORWARD SPEED ON AIRCRAFT PITCHING MOMENT $\delta_F=30^\circ \alpha=0^\circ$ (STEADY WINDMILLING) . . . . .	134
6-62	VARIATION OF TAIL LIFT WITH AIRFRAME LIST DURING AN ANGLE OF ATTACK SWEEP $\delta_F=30^\circ$ ROTOR OFF . . . . .	135
6-63	VARIATION OF TAIL LIFT WITH AIRFRAME LIFT DURING ANGLE OF ATTACK SWEEP FOR $\delta_F=30^\circ$ , ROTOR STEADY WINDMILLING . . . . .	136

LIST OF ILLUSTRATIONS

<u>FIGURE NO.</u>	<u>TITLE</u>	<u>PAGE</u>
6-64	CONTRIBUTION OF PROP/ROTOR AND HORIZONTAL TAIL TO AIRCRAFT STABILITY FOR STEADY WINDMILLING $\delta_F = 30^\circ$ . . . . .	137
6-65	COMPARISON OF STEADY STATE AND TRANSIENT ROTOR NORMAL FORCE FOR PARABOLIC COLLECTIVE RATES AT V = 113 FPS, FINAL RPM = 715 . . . . .	139
6-66	COMPARISON OF STEADY STATE AND TRANSIENT ROTOR PITCHING MOMENT FOR PARABOLIC COLLECTIVE RATES AT V = 113 FPS, FINAL RPM = 715 . . . . .	140
6-67	AIRCRAFT PITCHING MOMENT VARIATION DURING PARABOLIC COLLECTIVE SCHEDULES $\alpha = 0^\circ$ $\delta_F = 30^\circ$ V=113 FPS . . . . .	141
6-68	AIRCRAFT PITCHING MOMENT VARIATION WITH RPM DURING PARABOLIC COLLECTIVE SCHEDULES $\alpha = 0^\circ$ $\delta_F = 30^\circ$ V=113 FPS . . . . .	142
6-69	TOTAL AIRCRAFT PITCHING MOMENT VARIATION DURIN DURING THE FLATWISE BLADE FOLD TRANSIENT $\alpha = 2^\circ$ $\delta_F = 30^\circ$ V=113 FPS . . . . .	144
6-70	CONTRIBUTION OF HORIZONTAL TAIL AND FEATHERED ROTOR TO AIRCRAFT STABILITY $\delta_F = 30^\circ$ . . . . .	145
7-1	COMPARISON OF EXPERIMENTAL AND DESIGN ROTOR BLADE FREQUENCIES . . . . .	150
7-2	1ST HARMONIC CONTENT OF WINDMILLING BLADE LOADS . . . . .	151
7-3	SECOND HARMONIC CONTENT OF WINDMILLING BLADE LOADS . . . . .	152
7-4	THIRD HARMONIC CONTENT OF WINDMILLING BLADE LOADS . . . . .	153
7-5	FOURTH HARMONIC CONTENT OF WINDMILLING BLADE LOADS . . . . .	154



## LIST OF ILLUSTRATIONS

<u>FIGURE NO.</u>	<u>TITLE</u>	<u>PAGE</u>
7-6	ALTERNATING CHORD BENDING LOADS FOR STEADY WINDMILLING $\alpha = 0^\circ \delta_F = 0^\circ$ . . . . .	155
7-7	ALTERNATING FLAP BENDING LOADS FOR STEADY WINDMILLING $\alpha = 0 \delta_F = 0$ . . . . .	156
7-8	ALTERNATING BLADE CHORD BENDING FOR STEADY WINDMILLING $\alpha = -2^\circ \delta_F = 0^\circ$ . . . . .	157
7-9	ALTERNATING BLADE FLAP BENDING STEADY WINDMILLING $\alpha = -2^\circ \delta_F = 0^\circ$ . . . . .	158
7-10	ALTERNATING BLADE CHORD BENDING 0.125R STEADY WINDMILLING $\alpha = 2^\circ \delta_F = 0^\circ$ . . . . .	159
7-11	ALTERNATING BLADE FLAP BENDING 0.125R STEADY WINDMILLING $\alpha = 2^\circ \delta_F = 0^\circ$ . . . . .	160
7-12	ALTERNATING BLADE CHORD BENDING 0.125R STEADY WINDMILLING $\alpha = 4^\circ \delta_F = 0^\circ$ . . . . .	161
7-13	ALTERNATING BLADE FLAP BENDING 0.125R STEADY WINDMILLING $\alpha = 4^\circ \delta_F = 0^\circ$ . . . . .	162
7-14	ALTERNATING BLADE TORSION AS A FUNCTION OF RPM AND TUNNEL SPEED . . . . .	163
7-15	ALTERNATING BLADE CHORD BENDING FOR THREE TUNNEL SPEEDS AND VARIOUS NACELLE ANGLES AT 950 RPM . . . . .	164
7-16	ALTERNATING BLADE FLAP BENDING AT .125R FOR THREE TUNNEL SPEEDS AND VARIOUS NACELLE ANGLES AT 950 RPM . . . . .	165
7-17	ALTERNATING BLADE CHORD BENDING AS A FUNCTION OF FLAP DEFLECTION AND THREE TUNNEL SPEEDS AT 950 RPM . . . . .	166
7-18	ALTERNATING BLADE FLAP BENDING AS A FUNCTION OF FLAP DEFLECTION AND THREE TUNNEL SPEEDS AT 950 RPM . . . . .	167

LIST OF ILLUSTRATIONS

<u>FIGURE NO.</u>	<u>TITLE</u>	<u>PAGE</u>
7-19	ALTERNATING BLADE CHORD BENDING AT .125R AS A FUNCTION OF MODEL LIFT, AIR SPEED AND FLAP DEFLECTION TO 30° AT 950 RPM . . .	168
7-20	ALTERNATING BLADE FLAP BENDING AT .125R AS A FUNCTION OF MODEL LIFT, AIR SPEED AND FLAP DEFLECTION TO 30° AT 950 RPM . . . . .	169
7-21	ALTERNATING BLADE FLAP BENDING AT .125R AS A FUNCTION OF MODEL LIFT, AIR SPEED AND FLAP DEFLECTION TO 30° AT 700 RPM . . .	170
7-22	ALTERNATING BLADE CHORD BENDING AT .125R AS A FUNCTION OF MODEL LIFT, AIR SPEED AND FLAP DEFLECTION TO 30° AT 700 RPM . . . . .	171
7-23	STEADY BLADE FLAP BENDING AT .125r/R WITH $\alpha_F = 0^\circ$ $\delta_F = 0^\circ$ . . . . .	172
7-24	STEADY BLADE CHORD BENDING AT .125r/R WITH $\alpha = 0^\circ$ $\delta_F = 0^\circ$ . . . . .	173
7-25	STEADY BLADE CHORD BENDING $\alpha_F = +4^\circ$ $\delta_F = 0^\circ$ . .	174
7-26	STEADY BLADE FLAP BENDING AT .125r/R WITH $\alpha = +4^\circ$ $\delta_F = 0^\circ$ . . . . .	175
7-27	ALTERNATING BLADE CHORD BENDING DURING SPINUP $V = \text{FT/SEC}$ $\alpha = 0^\circ$ $\delta_F = 30^\circ$ (LINEAR COLLECTIVE RATES) . . . . .	178
7-28	ALTERNATING BLADE CHORD BENDING DURING FEATHERED $V = 85 \text{ FT/SEC}$ $\alpha = 0^\circ$ $\delta_F = 30^\circ$ (LINEAR COLLECTIVE RATES) . . . . .	179
7-29	ALTERNATING BLADE FLAP BENDING DURING SPINUP $V = 85$ $\alpha = 0^\circ$ $\delta_F = 30^\circ$ . . . . .	180
7-30	ALTERNATING BLADE FLAP BENDING DURING FEATHER $V = 85$ $\alpha = 0^\circ$ $\delta_F = 30^\circ$ . . . . .	181

LIST OF ILLUSTRATIONS

<u>FIGURE NO.</u>	<u>TITLE</u>	<u>PAGE</u>
7-31	ALTERNATING BLADE CHORD BENDING DURING SPINUP - EFFECT OF WING FLAP DEFLECTION $V = 113 \alpha = 0^\circ$ . . . . .	182
7-32	ALTERNATING BLADE FLAP BENDING DURING SPINUP EFFECT OF FLAP DEFLECTION $V = 113 \alpha = 0^\circ$ . .	183
7-33	ALTERNATING BLADE CHORD BENDING DURING FEATHER EFFECT OF FLAP DEFLECTION $V = 113 \alpha = 0^\circ$ . .	184
7-34	ALTERNATING BLADE FLAP BENDING DURING FEATHER EFFECT OF FLAP DEFLECTION $V = 113 \alpha = 0$ . .	185
7-35	ALTERNATING BLADE CHORD BENDING DURING SPIN- UP . . . . .	186
7-36	ALTERNATING BLADE CHORD BENDING DURING FEATHER . . . . .	187
7-37	ALTERNATING BLADE FLAP BENDING DURING SPIN-UP . . . . .	188
7-38	ALTERNATING BLADE FLAP BENDING DURING FEATHER . . . . .	189
7-39	ALTERNATING BLADE CHORD BENDING DURING SPINUP - EFFECT OF COLLECTIVE SCHEDULE . . .	190
7-40	ALTERNATING BLADE FLAP BENDING DURING SPINUP - EFFECT OF COLLECTIVE SCHEDULE . . .	191
7-41	ALTERNATING BLADE CHORD BENDING DURING FEATHER - EFFECT OF COLLECTIVE SCHEDULE . .	192
7-42	ALTERNATING BLADE FLAP BENDING DURING FEATHER - EFFECT OF COLLECTIVE SCHEDULE . .	193
7-43	ALTERNATING BLADE CHORD BENDING DURING SPINUP - VARIOUS PARABOLIC COLLECTIVE SCHEDULES . . . . .	194

LIST OF ILLUSTRATIONS

<u>FIGURE NO.</u>	<u>TITLE</u>	<u>PAGE</u>
7-44	ALTERNATING BLADE FLAP BENDING DURING SPIN-UP - VARIOUS PARABOLIC COLLECTIVE SCHEDULES . . . . .	195
7-45	ALTERNATING BLADE FLAP BENDING DURING FEATHER - VARIOUS PARABOLIC COLLECTIVE SCHEDULES . . . . .	196
7-46	ALTERNATING BLADE CHORD BENDING DURING FEATHER - VARIOUS PARABOLIC COLLECTIVE SCHEDULES . . . . .	197
7-47	ALTERNATING BLADE CHORD BENDING DURING SPIN-UP - VARIOUS PARABOLIC COLLECTIVE SCHEDULES . . . . .	198
7-48	ALTERNATING BLADE FLAP BENDING DURING SPIN-UP - VARIOUS PARABOLIC COLLECTIVE SCHEDULES . . . . .	199
7-49	ALTERNATING BLADE CHORD BENDING DURING FEATHER - VARIOUS PARABOLIC COLLECTIVE SCHEDULES . . . . .	200
7-50	ALTERNATING FLAP BENDING DURING FEATHER - VARIOUS PARABOLIC COLLECTIVE SCHEDULES . . .	201
7-51	STEADY BLADE LOADS DURING DYNAMIC FOLD AND DEPLOY, $r/R = 0.125$ . . . . .	203
7-52	STEADY BLADE LOADS DURING DYNAMIC FOLD AND DEPLOY, $r/R = 0.125$ . . . . .	204
7-53	STEADY BLADE LOADS DURING DYNAMIC FOLD AND DEPLOY, $r/R = 0.125$ . . . . .	205
7-54	STEADY BLADE LOADS DURING DYNAMIC FOLD AND DEPLOY, $r/R = 0.125$ . . . . .	206
7-55	STEADY BLADE LOADS DURING DYNAMIC FOLD AND DEPLOY . . . . .	207

# Contracts

## LIST OF ILLUSTRATIONS

<u>FIGURE NO.</u>	<u>TITLE</u>	<u>PAGE</u>
7-56	STEADY BLADE LOADS DURING DYNAMIC FOLD AND DEPLOY, $r/R = 0.125$ . . . . .	208
7-57	STEADY BLADE LOADS DURING DYNAMIC FOLD AND DEPLOY, $r/R = 0.125$ . . . . .	209
7-58	STEADY BLADE LOADS DURING DYNAMIC FOLDING AND DEPLOYMENT $r/R = 0.125$ . . . . .	210
7-59	STEADY BLADE LOADS DURING FOLDING $r/R = 0.125$ . . . . .	211
7-60	STEADY BLADE LOADS DURING FOLDING $r/R = 0.125$ . . . . .	212
8-1	WING 1ST HARMONIC ALTERNATING RESPONSE AT DISCRETE ROTOR SPEEDS - NOMINAL WING $V = 85$ FPS, RUN 69 (4-44) . . . . .	218
8-2	FREQUENCY SPECTRUM FOR NOMINAL STIFFNESS WING SPAR-WINDMILLING CONDITION, $V = 140$ FPS . . . . .	219
8-3	DAMPING SPECTRUM FOR NOMINAL STIFFNESS WING SPAR - WINDMILLING CONDITION, $V = 140$ FPS . . . . .	220
8-4	CORRELATION OF TEST AIR RESONANCE INSTABILITY WITH ANALYSIS - NOMINAL WING, $V = 104$ FPS WING FLAP BENDING MODE, RUN 49 . . . . .	221
8-5	MEASURED DAMPING IN WHIRL MODE ( $\Omega - \omega_2$ ) - REDUCED TORSION STIFFNESS SPAR, RUN 126 . . . . .	222
8-6	WHIRL FLUTTER INSTABILITY BOUNDARY - RE- DUCED TORSIONAL STIFFNESS SPAR . . . . .	223
8-7	MEASURED WING TORQUE WITH NACELLE ANGLE OF ATTACK = $2^\circ$ , REDUCED TORSION STIFFNESS SPAR . . . . .	224

LIST OF ILLUSTRATIONS

<u>FIGURE NO.</u>	<u>TITLE</u>	<u>PAGE</u>
8-8	ELASTIC TWIST RESULTING FROM WING TORQUE AND DIVERGENCE VELOCITY PROXIMITY - REDUCED WING TORSION STIFFNESS SPAR, RUN 126 . . . . .	225
8-9	STATIC DIVERGENCE BOUNDARY EXTRACTED FROM TEST DATA - RUN 126 - REDUCED TORSION STIFFNESS SPAR . . . . .	226
8-10	BLADE MODE DAMPING RESULTING FROM DISTURBANCE - $V = 85$ FPS, RUN 123 . . . . .	227
8-11	WAVE TRACES ILLUSTRATING BLADE RESPONSE TO DISTURBANCE . . . . .	228

# Contracts

## LIST OF TABLES

<u>Table No.</u>		<u>Page</u>
3-1	SIGNIFICANT MODEL DIMENSIONS . . . . .	6
3-2	PHYSICAL CHARACTERISTICS OF MODEL COMPONENTS . . . . .	7
3-3	INSTRUMENTATION ON 1/9 SCALE MODEL 213 . . . . .	16
6-1	WING CIRCULATION EFFECTS ON ROTOR DERIVATIVES. . . . .	70
8-1	WING FREQUENCY SUMMARY (NORMAL SPAR). . . . .	214
8-2	NATURAL FREQUENCIES MEASURED BY BANG TESTS (CPS) . . . . .	217

LIST OF SYMBOLS

<u>SYMBOL</u>		<u>UNITS</u>
A	Rotor Disc Area	FT <sup>2</sup>
C <sub>D</sub>	Airframe Drag Coefficient $\frac{D}{qS}$	-
C <sub>L</sub>	Aircraft Lift Coefficient $\frac{L}{qS}$	-
C <sub>N</sub>	Rotor Normal Force Coefficient $\frac{NF}{\rho AV_T^2}$	-
C <sub>SF</sub>	Rotor Side Force Coefficient $\frac{SF}{\rho AV_T^2}$	-
C <sub>PM</sub>	Rotor Pitching Moment Coefficient $\frac{PM}{\rho AV_T^2 R}$	-
C <sub>YM</sub>	Rotor Yawing Moment Coefficient $\frac{YM}{\rho AV_T^2 R}$	-
C <sub>T</sub>	Rotor Thrust Coefficient $\frac{T}{\rho AV_T^2}$	-
D	Airframe Drag	LB
L	Airplane Lift	LB
MAC	Mean Aerodynamic Chord	-
NF	Normal Force	LB
PM	Pitching Moment	FT-LB
q	Dynamic Pressure $\frac{1}{2} \rho V^2$	LB/FT <sup>2</sup>
R	Rotor Radius	FT
r/R	Radial Location on Blades	-
SF	Side Force	LB



# Contracts

## LIST OF SYMBOLS (CONT.)

<u>SYMBOL</u>		<u>UNITS</u>
S	Wing Area	FT
T	Rotor Thrust	LB
V	Freestream Velocity	FT/SEC
V <sub>D</sub>	Divergence Speed	FT/SEC
V <sub>S</sub>	Stall Speed	FT/SEC
V <sub>T</sub>	Rotor Tip Speed	FT/SEC
YM	Yawing Moment	FT-LB
$\alpha_F$	Fuselage Angle of Attack	DEG
$\delta_F$	Trailing Edge Flap Deflection	DEG
$\theta_{.75}$	Rotor Blade Collective Pitch at Three Quarter Radius	DEG
$\mu$	Advance Ratio $\frac{V}{V_T}$	-
$\rho$	Air Density	LB-SEC/FT
$\Omega$	Rotor Angular Velocity	RAD/SEC
W	Rotor Blade Natural Frequency	RAD/SEC
$\omega_{LAG}$	Rotor Blade Natural Frequency for Lag Motion	RAD/SEC
$\left(\frac{\omega}{\Omega}\right)$	Blade Frequency Ratio	-
$\omega_{FLAP}$	Rotor Blade Natural Frequency for Flap Motion	RAD/SEC
$\omega_1$	Rotor Blade First Coupled Natural Frequency (Usually Predominantly Lag at Operating RPM)	RAD/SEC
$\omega_2$	Rotor Blade Second Coupled Natural Frequency (Usually Predominantly Flap At Operating RPM)	RAD/SEC

*Continued*  
LIST OF DATA PLOTTING SYMBOLS

RUN	SYMBOL	RUN	SYMBOL	RUN	SYMBOL	RUN	SYMBOL
1	△	29	■	57	▴	85	◐
2	□	30	▴	58	◑	86	▴
3	▴	31	◑	59	▴	87	◑
4	◑	32	▴	60	◑	88	◑
5	▴	33	●	61	◑	89	◑
6	○	34	◆	62	◑	90	◑
7	◇	35	◑	63	◑	91	◑
8	◑	36	■	64	◑	92	◑
9	□	37	◑	65	◑	93	◑
10	◑	38	◑	66	◑	94	◑
11	◑	39	◑	67	◑	95	◑
12	◑	40	◑	68	◑	96	◑
13	◑	41	◑	69	◑	97	◑
14	◑	42	◑	70	◑	98	◑
15	◑	43	◑	71	◑	99	+
16	◑	44	◑	72	+	123	☆
17	◑	45	+	73	☆	124	◑
18	+	46	☆	74	◑	125	◑
19	☆	47	◑	75	◑	126	◑
20	◑	48	◑	76	◑	127	◑
21	◑	49	◑	77	◑	128	◑
22	△	50	◑	78	◑	129	◑
23	◑	51	◑	79	◑	130	◑
24	◑	52	◑	80	◑	131	◑
25	◑	53	◑	81	◑	132	◑
26	◑	54	◑	82	◑	133	◑
27	◑	55	◑	83	◑	134	◑
28	▲	56	◑	84	◑	135	◑

## 1.0 INTRODUCTION

The stowed/tilt rotor aircraft hovers, executes transition and cruises at low speed in the same manner as a pure tilt rotor aircraft. When the aircraft reaches conversion speed, the rotors are feathered and folded, propulsion being maintained by convertible fan engines. The Boeing Company is conducting a program of parametric design, analysis and wind tunnel testing to establish design criteria and aerodynamic prediction techniques for this concept under Contract No. F33615-69-C-1577 from USAF Flight Dynamics Laboratory. This program consists of two phases. Phase I studies (Reference 1) included the preliminary design of stowed tilt-rotor vehicles for (1) high-speed, long-range rescue, (2) capsule recovery, and (3) VTOL transport and laid the ground work necessary to plan Phase II. Phase II consists of a series of four wind tunnel tests designed to provide experimental data on which to base design criteria and prediction methods and to verify preliminary design information.

This volume describes the investigations and results of a test conducted on the 1/9 scale semi-span Model 213 stowed/tilt rotor aircraft with a 5.5 ft. diameter, soft in-plane hingeless rotor in the 20'X 20' Boeing V/STOL wind tunnel. The investigations were directed towards obtaining more information on the conversion cycles of this vehicle.

This report therefore covers the results of investigations on steady state windmilling, spinup and feathering, folding and deployment of the rotors.

## 2.0 OBJECTIVES

Listed below are the objectives for this test program with reference to the appropriate sections of this report, which contain the detailed results of the investigation:

1. Determine the blade loads and folding hinge moments during blade folding  
Section 7.4
2. Determine blade loads and folding hinge moments as a function of aircraft attitude.  
Section 7.4
3. Determine the effects of blade folding on drag and stability derivatives.  
Section 6.3
4. Establish the collective pitch schedule for spinup and feathering operations which has the minimum effect on aircraft drag and blade loads.  
Sections 5.2 and 7.3
5. Determine the effect of aircraft pitch attitude on drag and blade loads of the rotors.  
Sections 5.2 and 7.3
6. Establish the effect of the rotor conversion on wing performance, aircraft stability derivatives and rotor stability derivatives.  
Sections 5.2, 5.3, 6.2 and 6.3
7. Establish the effect of the wing on the blade loads and conversion performance.  
Sections 5.2, 5.3, 7.3 and 7.4
8. Determine the rotor drag and aircraft stability derivatives when the rotors are stopped and establish the effect of aeroelastic deflections of wing and rotors on the stability derivatives.  
Sections 6.2 and Appendix A
9. Determine the rotor drag and rotor and aircraft stability derivatives when the rotors are windmilling, and establish the effect of aeroelastic deflections on these parameters. Sections 5.1, 6.1 and Appendix A

# *Contrails*

10. Determine the effect of rotor conversion on the tail lift.  
Section 5.1

For a subsequent Boeing-funded test, the following objective was set:

11. Establish the effect of a torsionally soft wing on the divergence, whirl flutter and air resonance boundaries of the aircraft.  
Section 8.2

## 3.0 TEST INSTALLATION

### 3.1 Model Description

The 1/9 scale semi-span conversion model used during this test as installed in the 20 X 20 foot test section of the Boeing-Vertol V/STOL Wind Tunnel is shown in Figure 3-1.

The model consists of a four-bladed rotor, a rotor nacelle, a half-span wing, a wing mounted dummy fan thrust engine nacelle, a half fuselage and a half span horizontal stabilizer.

The model wing nacelles and blades are geometrically and dynamically scaled from the full-scale Model 213 design. (See Volume II of this report).

Significant model dimensions are listed in Table 3-1 and Table 3-2.

#### Rotor Blades

The blades are a Froude and reduced frequency scaled representation of those designed for the Model 213 stowed rotor aircraft. The blades consist of a steel spar around which foam was molded to create the blade contour. In order to obtain the correct blade weight distribution tantalum balance weights were bonded to the steel spar.

The predicted wind tunnel model blade physical properties in comparison to true, scaled down, properties of the Model 213 blades are shown in Appendix E.

Figure 3-2 shows the calculated frequency spectrum of the blades. The frequencies are a function of the blade collective setting and to illustrate this two lines are presented. The solid lines show the frequency variation for collective settings as required at a tunnel speed of 100 fps and the dotted lines indicate the frequency variation for a constant collective setting of 10°.

The strain gages to measure blade chord and flap bending were bonded to the steel spar. Due to the twist in the blade and the spar, the orientation of the gages is a function of their location along the spar and the blade collective setting. To illustrate this, Figure 3-3 is presented which shows the orientation of the gages at .125R for the feathered position and the 900 rpm at the 85 fps tunnel speed condition.

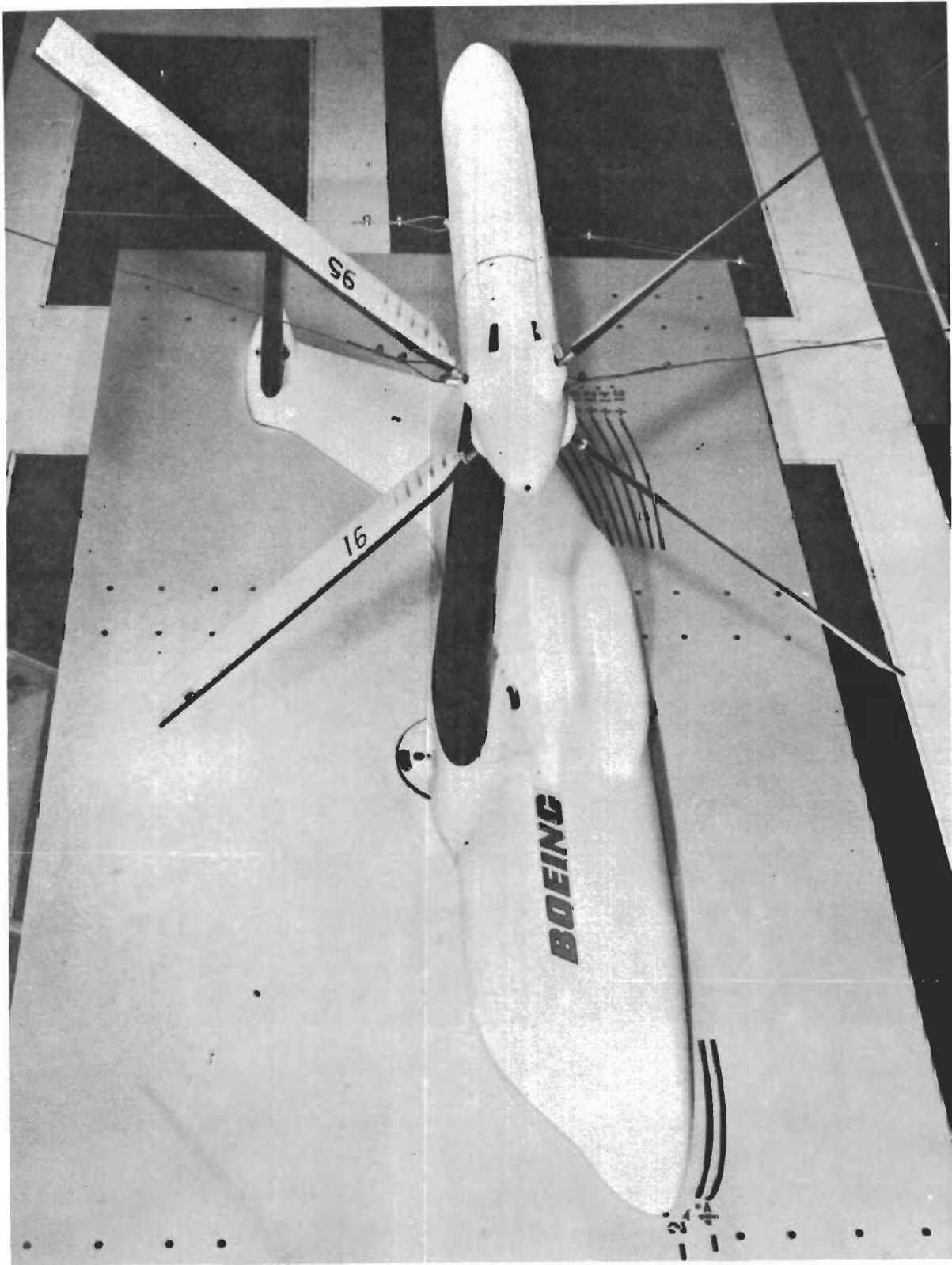


FIGURE 3-1. MODEL INSTALLATION IN WIND TUNNEL

TABLE 3-1SIGNIFICANT MODEL DIMENSIONS

Overall fuselage length including tail	91.92 in.
Wing semi-span to inboard side of tip nacelle	37.88 in.
Wing semi-span to centerline of rotor shaft	40.78 in.
Wing mean aerodynamic chord	16.55 in.
Wing area from fuselage centerline to inboard side of tip nacelle	624.50 sq.in.
Wing chord at centerline	24.59 in.
Wing chord at tip	12.705 in.
Wing incidence with respect to fuselage W.L.	3.0°
Horizontal tail semi-span	18.75 in.
Horizontal tail area	175.00 sq.in.
Blade radius	32.80 in.
Blade chord	2.50 in.
Rotor solidity	0.0994
Blade twist from 0.20R to 1.00R linear	23.5°



TABLE 3-2

PHYSICAL CHARACTERISTICS OF MODEL COMPONENTS

Weight of rotating system including blades	4.50 lb
Inertia of rotating system including blades	849 lb in <sup>2</sup>
Shaft bearing friction without hub loads	0.42 in.-lbs
Pitch inertia of tip nacelle	1230 lb in <sup>2</sup>
Weight of tip nacelle	8.07 lb
Nacelle stiffness (rotor hub to wing attachment) (pitch and yaw)	70,600 $\frac{\text{in.}\cdot\text{lb}}{\text{rad}}$
Wing spar flapwise stiffness at tip	64 lb-in.
Wing spar chordwise stiffness at tip	214 lb-in.
Wing spar torsional stiffness at tip	9200 in-lb/rad
Blade collective control torsional stiffness	316 in-lb/rad
Wing spar torsional stiffness at tip for torsionally soft wing	2300 in-lb/rad

# Contrails

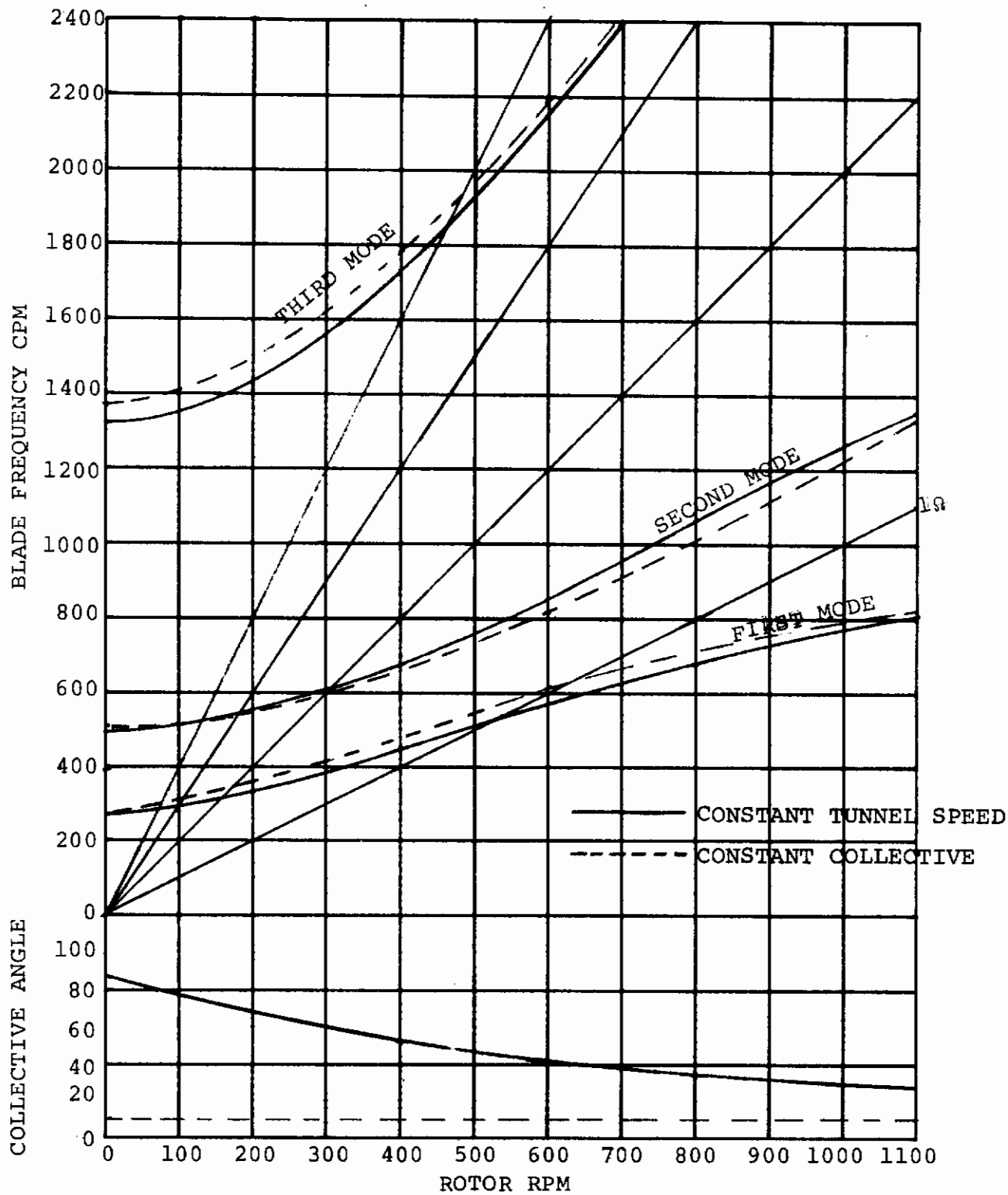


FIGURE 3-2. CALCULATED BLADE FREQUENCY SPECTRUM OF 1/9 SCALE MODEL 213 BLADES

# Contrails

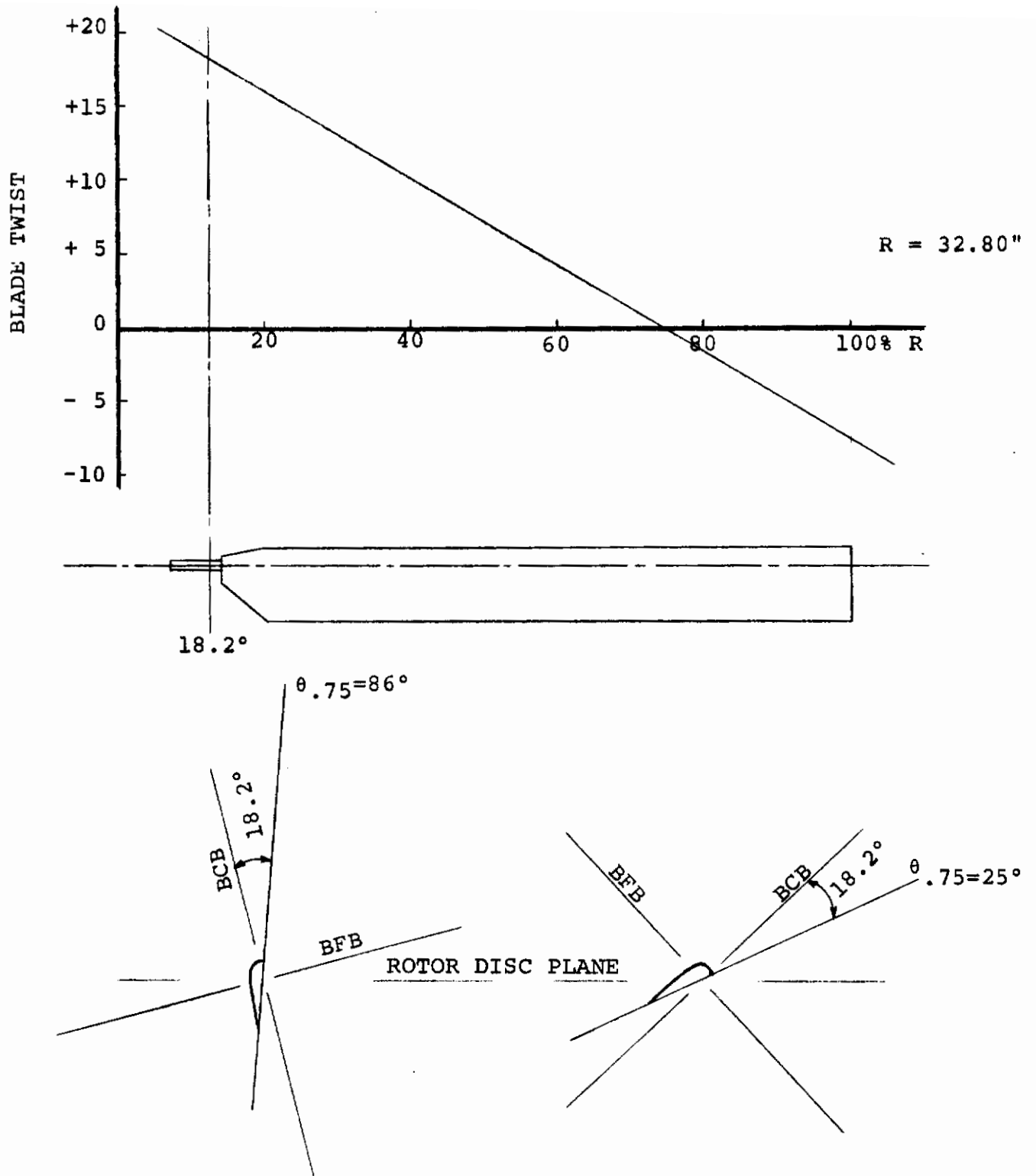


FIGURE 3-3. BLADE TWIST AND ORIENTATION OF GAGES AT .125R

# Contrails

## Rotor Hubs

Two rotor hubs are available for the model. A rotating hub used for the steady state windmilling, spinup and feathering tests and a non-rotating hub used for the folding tests. Blade serial numbers are indicated in Figure 3-4 by S/N.

The rotating hub contains an electric collective drive motor which via a worm and gear drive sets and controls the collective setting of the blades. The motor is a variable speed motor and can change the collective angle up to a maximum rate of 45 degrees per second. The motor is driven by a power supply which was developed for the unpowered model of Test Program I.

The folding hub does not rotate and the blade azimuthal positions are fixed as indicated on Figure 3-4. This position was selected as the optimum for blade folding since it resulted in the smallest diameter tip nacelle. Both flat and edgewise folding systems were fixed in that position. A variable speed electric motor is connected to a lead screw. Arms attached to a Saginaw ball nut drive connecting rods leading to the blade root retentions. The fold hinge radial location of the flat folding system was at the correctly scaled radius but the edgewise fold hinge was half an inch further out. The flat folding hub incorporated a camplate and cam follower to change the collective angle of the blades prior to their nesting around the nacelle. The camplates for the blades have a schedule which permits the blades to fold back over a 70° arc without a pitch change from the feathered position. In the last 20° fold arc the blade collective angle is changed to suit the individual blade to its proper nesting position. The flat folding hub is shown in Figure 3.4a.

The edgewise folding system does not need this feature as the blades are folded back over their full folding arc without a collective angle change.

The fold motor was driven by a variable voltage power supply to move the blades at rates up to 45 degrees per second.

## Rotor Nacelles

Two rotor nacelles are available for the model, one for flat folding and one for edgewise folding.

The flat folding nacelle has cavities in its outer surface matching either the upper or lower contour of the blades dependent on the mode each blade is folded back on the nacelle. Except for the most forward section of the nacelle where enough clearance must be provided for the inboard trailing edge of the blades to allow them to rotate to the flat position, those cavities are only half a blade thickness deep.

# Contrails

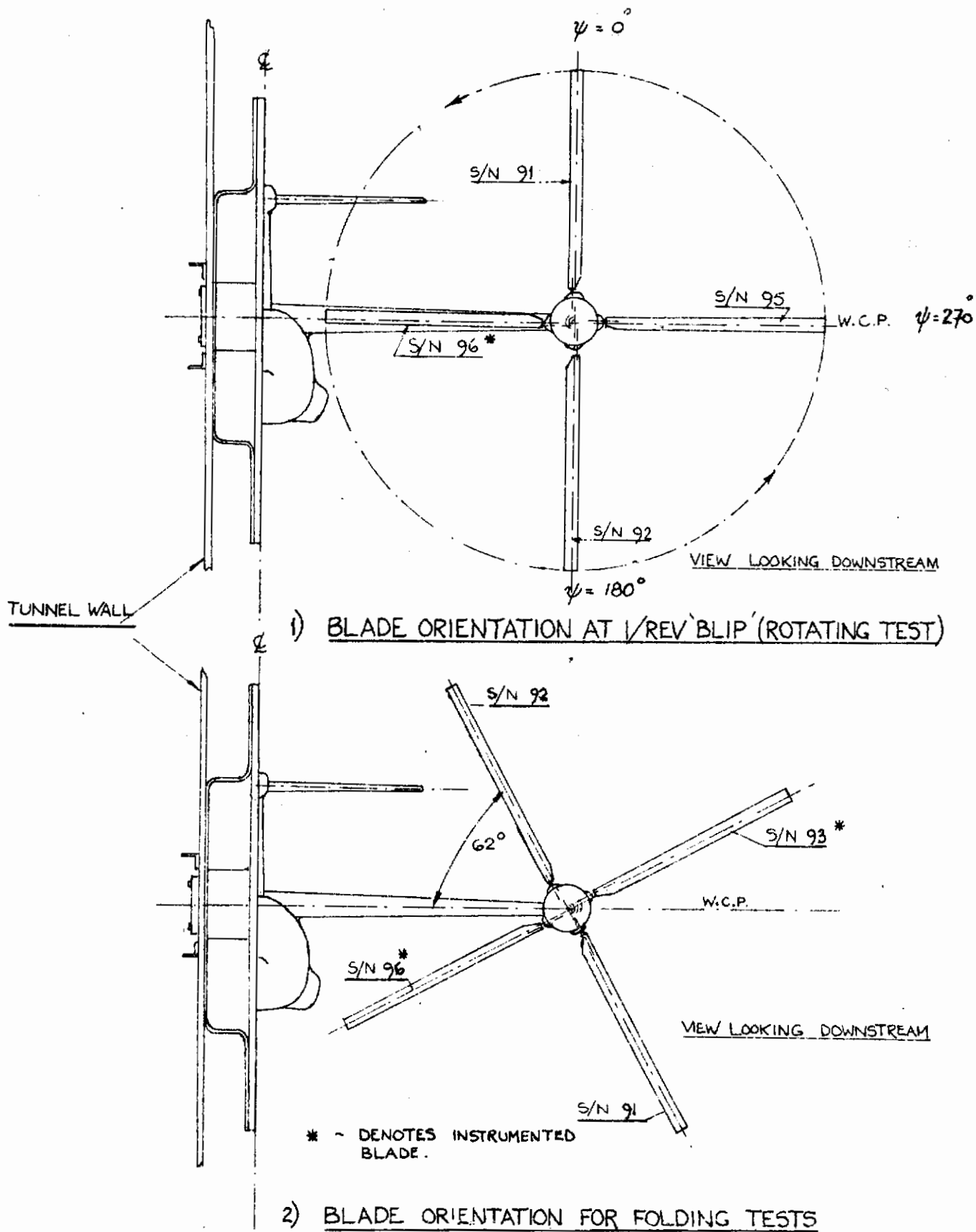


FIGURE 3-4. ROTOR BLADE ORIENTATION AND MOUNTING DETAILS.

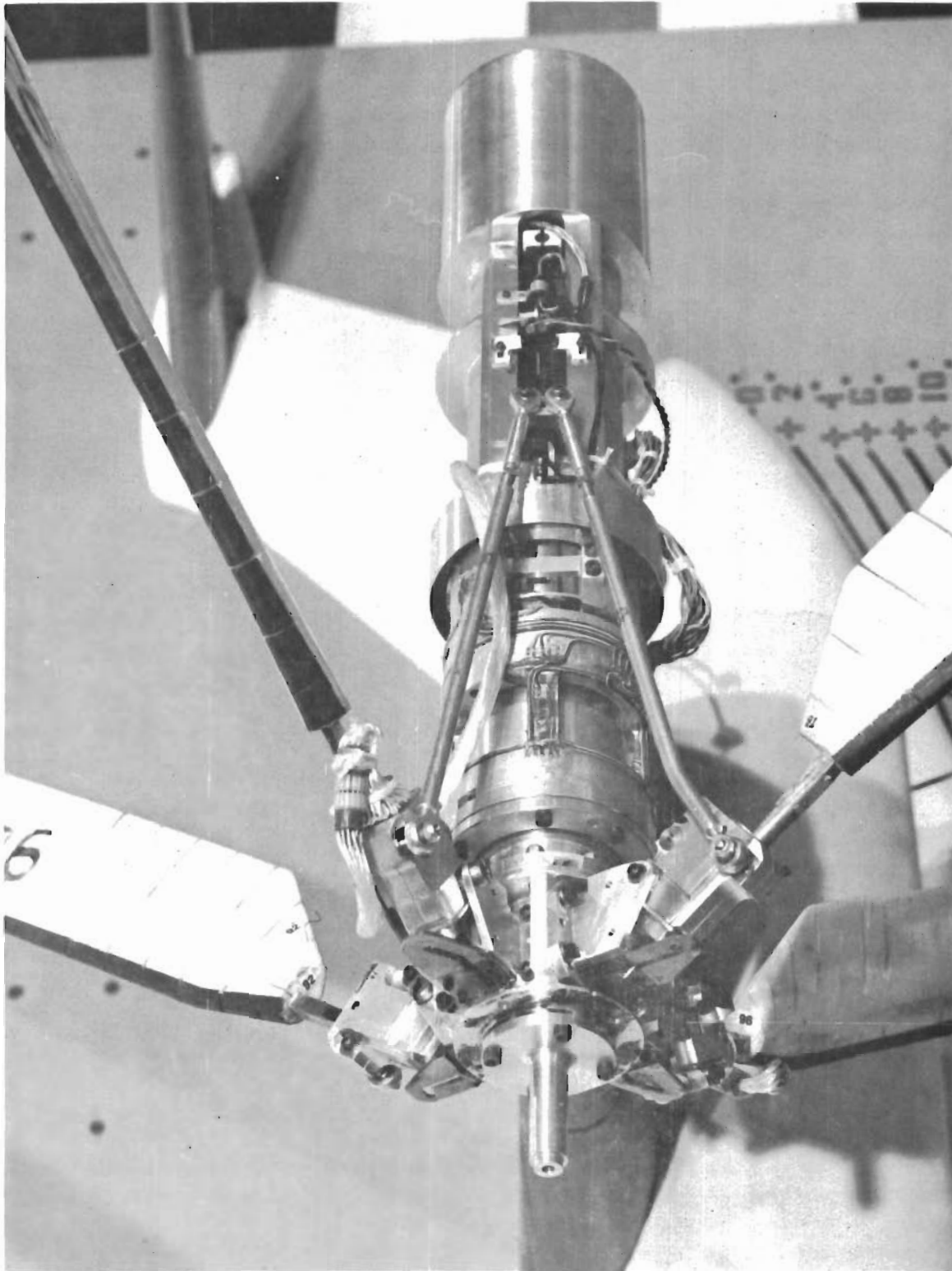


FIGURE 3-4a. FLAT FOLDING HUB DETAILS

# Contrails

The edgewise folding nacelle has foam inserts, which were cut out to allow for space for the trailing edge of the blades. Although it was never intended for the entire blade to fold into the nacelle (60% of the blade chord was supposed to stay outside the nacelle) due to the wing fold hinge location approximately 70% chord protrudes outside the nacelle. The cavities in the foam are 7/8" wide at the outer surface of the nacelle tapering down to approximately 1/4 inch. The slots are 0.9" deep and curved to allow for the gravity deflection of the blades. Inside the nacelles a five component balance can measure hub forces and moments except rotor torques. This balance was used during all phases of the test.

The balance is mounted between the hub and a balance support structure which in turn is connected to the wing spar. The nacelle incidence can be changed over  $\pm 3^\circ$  with respect to a fuselage waterline although this feature was not used during the test. The tests were conducted with the nacelle parallel to the fuselage.

## Wing

The dynamically-scaled wing has stiffness and weight properties as shown in Appendix E. The wing inboard section has a 30% chord trailing edge flap and the outboard section is equipped with a flaperon with a chord varying from 30% to 25%. The flap and flaperon were manually adjustable to  $45^\circ$  down. The flaperon is a quick-acting flap which also acts as an aileron.

An unpowered aerodynamic and mass representation of a turbo-fan engine nacelle is located underneath the inboard section of the wing. This nacelle can be removed from the wing maintaining the aerodynamic contours of the wing.

The wing airfoil contour is a Boeing-developed transonic airfoil. The wing is constructed with a main spar which provides the stiffness characteristics and five non-interconnected wing boxes, which have a two-point connection with the spar. Details are shown on Figure 3.4b.

The wing spar is instrumented to measure lift, drag, rolling, yawing and pitching moment.

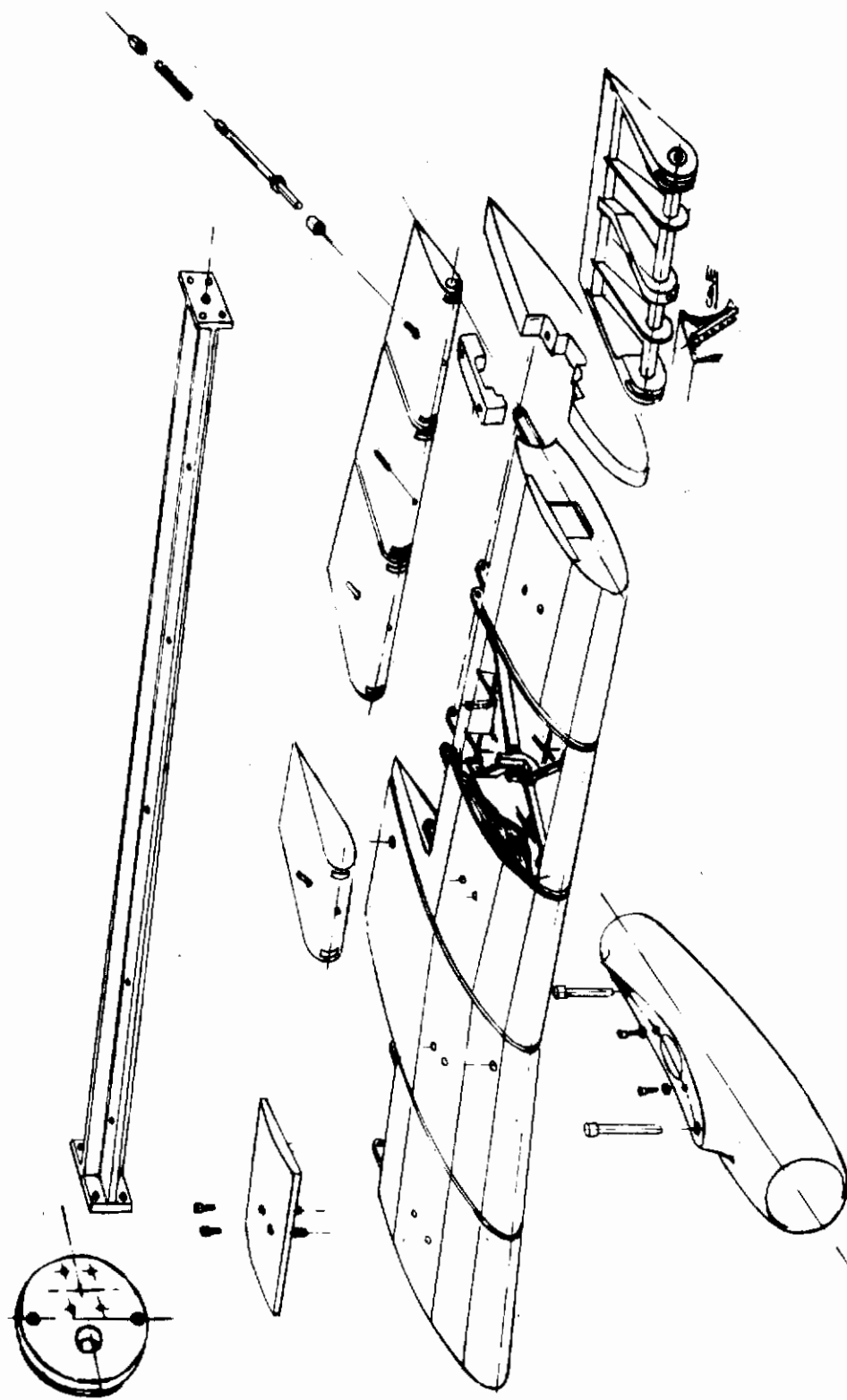


FIGURE 3-4b. WING CONSTRUCTION DETAILS



Another wing spar with equal chord and flap stiffness but a torsional stiffness of one quarter of the nominal stiffness was installed during a subsequent Boeing-funded test program (BVWT-072).

## Horizontal Tail

The semi-span horizontal tail is a geometric representation of the tail designed for the Model 213. It has a NACA 0015 airfoil. The tail incidence can be manually changed over a range of  $+4^{\circ}$  to  $-14^{\circ}$  but this feature was not used during this test. The spar of the tail is instrumented to measure tail lift only.

## Fuselage

The half fuselage is a geometric representation of the Model 213 fuselage. It contains the manually adjustable model pitch mechanism ( $-4^{\circ}$  to  $+16^{\circ}$ ), the axis of which goes through the one quarter chord of the MAC. The fuselage rotates against the 5 x 9' splitter plate, which was located 6 inches from the vertical tunnel wall.

## 3.2 Model Instrumentation and Data Processing

During the rotating tests, due to slipring limitations, only one instrumented blade was connected to the recording instrumentation. This blade has six strain gauge bridges to record blade moments and torsion at four inboard locations on the blade.

During the folding tests the signals did not have to go through a slipring and two identically instrumented blades were connected to the recording instrumentation. The outputs of both the five component nacelle balance and the five component wing balance were recorded during all tests.

Rotor speed, rotor azimuth, collective pitch and blade fold angle were recorded during the test runs. Lift on the horizontal tail was also recorded. Table 3-3 lists all available instrumentation. All parameters were calibrated prior to the test and calibration checks were performed whenever mechanical changes on the model could have affected the original calibration.

INSTRUMENTATION ON 1/9 SCALE MODEL 213

Parameter	Recorded During		Recorded On	
	Steady State Spinup and Feather	Folding	Osc.	Digital Magnetic Tape
<u>Blade 96</u>				
Flap Bending Moment .065R	X	X	X	X
.125R	X	X		X
.200R	X	X		X
Chord Bending Moment .125R	X	X	X	X
.200R	X	X		X
Blade Torsion .150R	X	X	X	X
<u>Blade 93</u>				
Flap Bending Moment .065R		X		X
.125R		X	X	X
.200R		X		X
Chord Bending Moment .125R		X	X	X
.200R		X		X
Blade Torsion .150R		X	X	X
<u>Rotor Nacelle Thrust</u>				
Normal Force	X	X	X	X
Side Force	X	X	X	X
Pitching Moment	X	X	X	X
Yawing Moment	X	X	X	X
<u>Wing Lift</u>				
Drag	X	X	X	X
Rolling Moment	X	X		X
Yawing Moment	X	X		X
Pitching Moment	X	X	X	X
<u>Horizontal Tail Lift</u>				
Rotor Speed	X			X
Blade Collect. Angle	X		X	X
Blade Fold Angle		X	X	X
<u>Torsionally-Soft</u>				
<u>Wing Dynamics Test</u>				
Nacelle Vertical Acceleration	X		X	X
Nacelle Longitudinal Acceleration in addition to above mentioned instrumentation	X		X	X

# Contrails

Selected parameters were recorded on oscillograph as indicated on Table 3-3. All parameters were recorded on magnetic tape via an IBM 1800 computer and processed on and off line with computer programs appropriate for the data presentations or analysis requirements.

During all test runs the information obtained from the nacelle, wing and tail balances was recorded and processed for steady state values. In addition to a printout of tunnel conditions, model configuration and model forces aerodynamic parameters were calculated and printed.

It should be noted that the fuselage is not mounted on the balance and that references to "airframe" lift/drag ratio are based on the total forces measured on the wing root balance.

During most rotating tests on line stress data of blade and model loads and moments was printed following the steady state aerodynamic data.

An off line harmonic analysis program was able to harmonically analyze all parameters recorded on magnetic tape.

Nacelle and wing balance outputs were processed via interaction matrices to obtain pure loads and moments at or about designated points on the model.

Loads and moment reference centers and sign convention are indicated on Figure 3-5 and 3-6.

### 3.3 Model Installation in the Wind Tunnel

The model installation design required it to be installed at the lengthwise center of the test section at a height where the tunnel flow is uniform. The mounting hardware utilized a slot in the tunnel wall and therefore the slot at the eight foot level above the tunnel floor was selected. To avoid the necessity to work with ladders or workstands for the model maintenance at that level, a four foot high fixed ground plane was installed. The model installation arrangement is shown on Figure 3-7.

The wind tunnel has been calibrated for flow uniformity and a uniform flow exists over the model at the chosen location. The model is Froude number scaled, in the cruise configuration (low down wash) and is windmilling at low negative thrust. The model to tunnel ratios indicate that the tunnel wall corrections are less than data scatter.

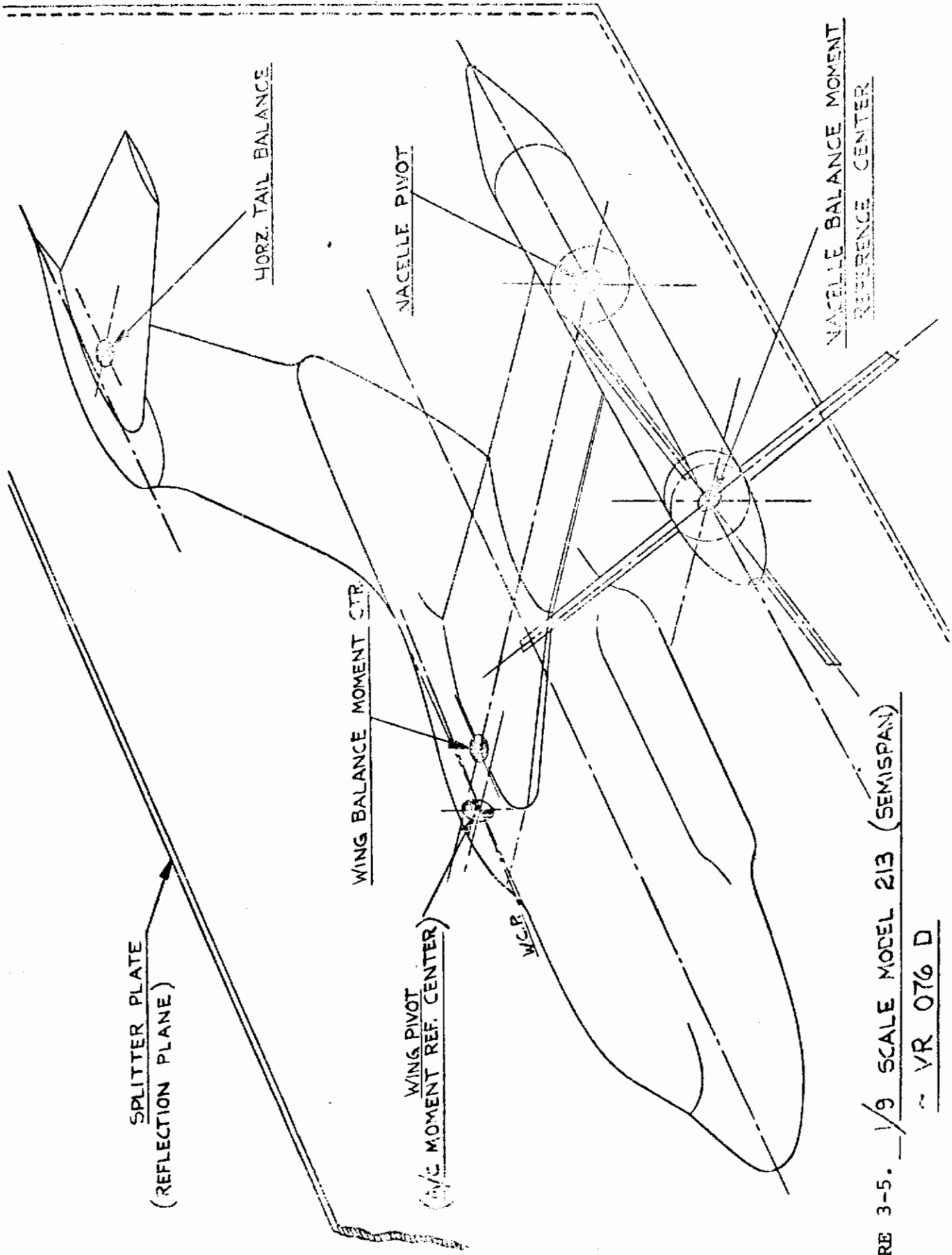


FIGURE 3-5. 1/9 SCALE MODEL 213 (SEMISPAN)

~ VR 076 D

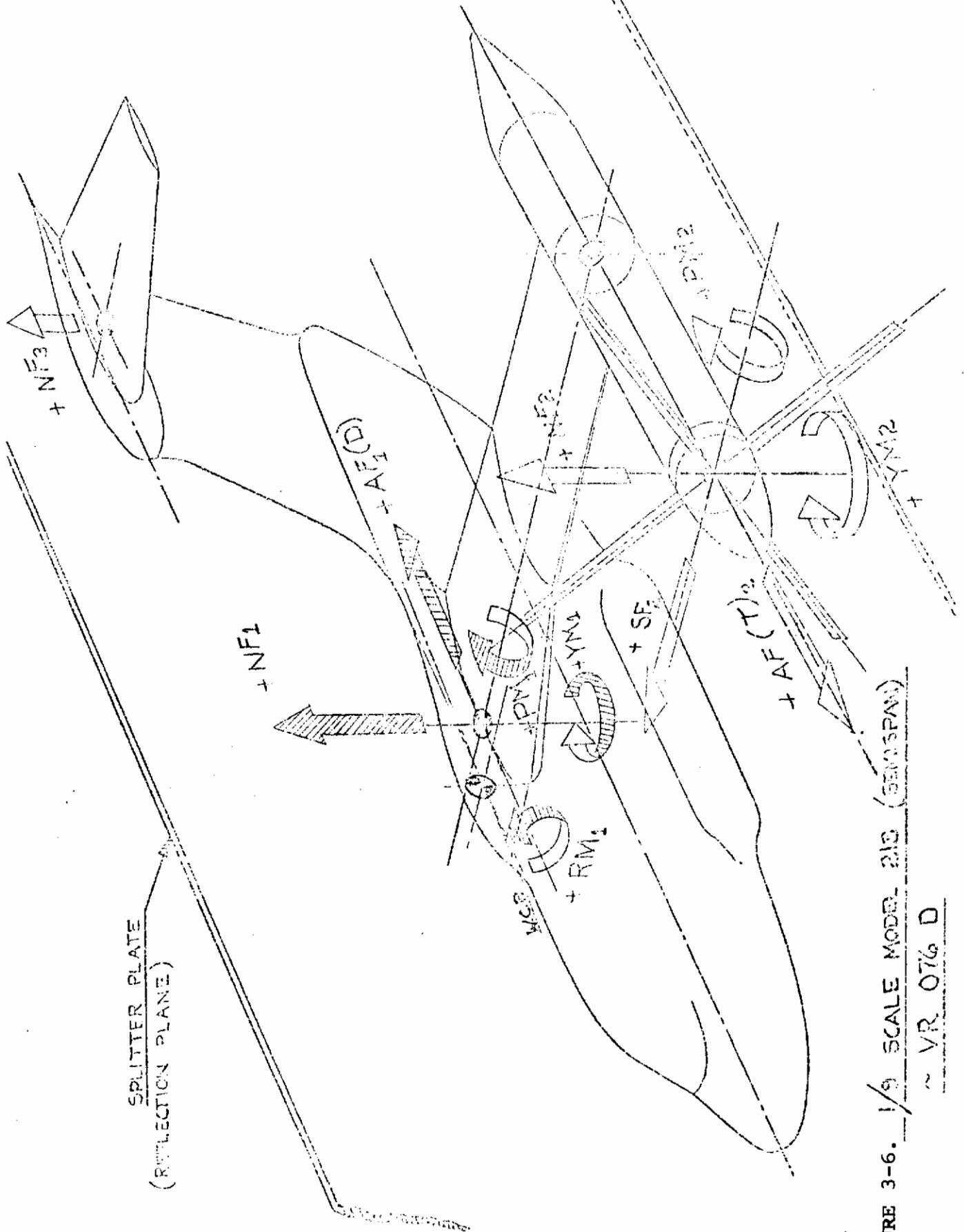


FIGURE 3-6. 1/9 SCALE MODEL 210 (BEMSPAN)

~ VR 076 D

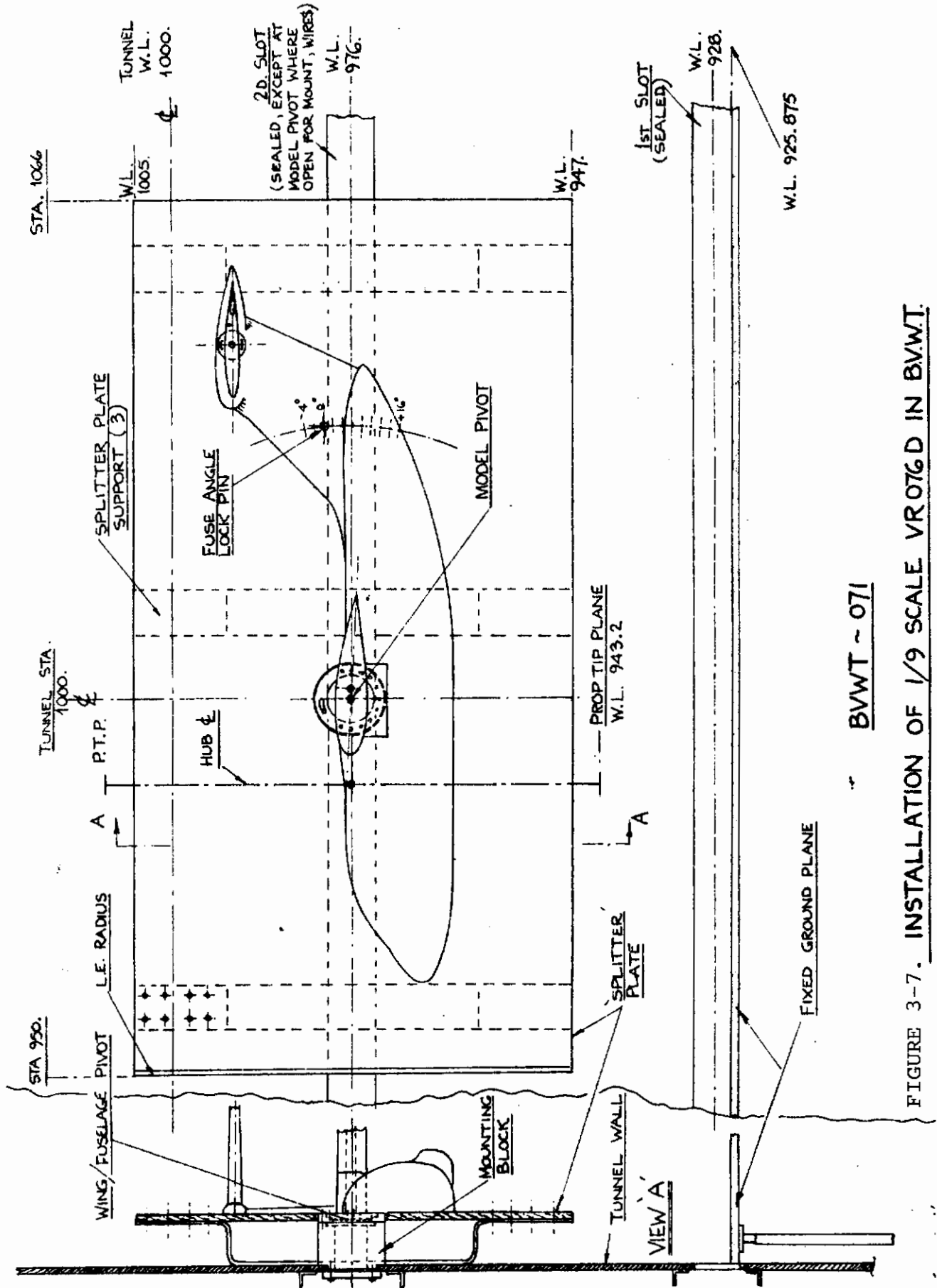


FIGURE 3-7. INSTALLATION OF 1/9 SCALE VRO76D IN BVWT.

BVWT ~ 071

## 4.0 TEST PROGRAM

### 4.1 Scaling of Wind Tunnel Test Speeds

The Model 213 aircraft is designed for a maximum speed of 400 knots in the rotor folded cruise mode. The maximum speed in the rotors deployed cruise mode is 250 knots. Conversion from the rotors deployed cruise mode to the rotors folded cruise mode must be performed in the speed range of  $1.2 V_S$  flaps down to 250 knots. The  $1.2 V_S$  flaps down speed, assuming a wing loading of 90 pounds per square foot and a  $C_{LMAX}$  of 2.15 is 134 knots. The model is geometrically 1/9 full scale. Froude number and reduced frequency similarity was used to obtain dynamic characteristics similar to the full-scale aircraft. These criteria provided a velocity scale factor of 1/3.

The tunnel speed range of interest is therefore 75 fps up to 141 fps. Testing below a Reynolds number of 750,000 for the model wing was considered undesirable and the tunnel speed range was therefore selected to be 85 fps to 141 fps with an intermediate velocity of 113 fps as the third point in this speed range. The maximum structural rotor speed for the model is 1100 RPM. At 1050 RPM the model displayed onset of an air resonance instability and in order to stay clear of that range most test runs were terminated between 950 and 1000 RPM.

The time scale factor is also 1/3 of the full-scale time and therefore collective and folding rates tested were three times faster than the contemplated full-scale aircraft rates.

To get a better impression of the type of motions of the full-scale aircraft, motion pictures were taken at 72 frames per second, three times faster than the regular playback speed of 24 frames per second.

### 4.2 Description of Test Runs

A summary of all data runs is presented in Appendix F. Runs with a wing tip snubber by which the wing vertical and torsional motions could be restricted or suppressed were conducted to establish the stability boundaries of the model prior to the data runs.

As indicated on the run log, the test program was started with baseline and steady state windmilling runs, followed by spinup and feather and folding tests.

The baseline runs were conducted with the blades removed from the hub and the openings in the spinner covered with tape. The spinner was free to rotate and the operation of the wing tip nacelle balance was not impaired.

The baseline tests were conducted over the range of fuselage angles, flap deflections and tunnel speeds shown in Figure 4-1. Only steady state data were collected during these runs. These data were used to determine the effects of the rotor on the model characteristics.

Steady state windmilling runs were conducted at various fuselage and flap angles shown in Figure 4-2 and for some configurations three tunnel speeds. Oscillograph, steady state and dynamic data was collected during these runs. Rotor speed sweeps were performed with increments of 100 RPM maximum unless resulting blade and/or balance loads prohibited continuous operations at certain rotor speed ranges.

Spinup and feathering runs were conducted at one fuselage ( $\alpha_F=0$ ) angle, two flaps angles ( $\delta_F=15^\circ$  and  $30^\circ$ ) and two tunnel speeds ( $V=85$  and  $113$  fps). A variety of collective schedules were tested to evaluate the effect of collective rate and schedule shapes on aircraft drag changes and rotor loads.

Rotor fold step runs were conducted at four fuselage angles and two flap angles. Automatic continuous folding and deployment runs at various rates were conducted at a fuselage angle of  $+2^\circ$  and a  $30^\circ$  flap deflection.

### 4.3 Observations Made During the Test

#### Steady State Windmilling

Each test run was started with the blades in the feathered position. Feathering of the blades did not present any problems at the three test speeds of this program. The blades bend due to the twist in the blades and although the curvature in the blades is quite pronounced at the 141 fps tunnel speed, this did not affect their ability to be feathered.

The bending in the blades occurs primarily outboard of 50% radius where no instrumentation was installed. Steady blade bending moment could therefore not be recorded.



# Contrails

When feathered, the blade azimuthal location was observed to be almost the same for all conditions. The blade above the wing would always stop within an arc between an estimated 30 and 60 degrees with respect to the wing. This was an equilibrium position probably caused by the wing induced flow field, and the blades would always assume this position and could not be stopped in any other position. The model was not equipped with instrumentation to record and measure the exact feathering position.

By making a small collective change the blades would rotate slowly. This rotation is not at a constant RPM but whenever a blade approaches the leading edge of the wing it accelerates until it has passed the wing at which point it slows down, thereby accelerating and decelerating the entire rotor system. This acceleration was caused by the fact that the wing induced flow provided an equilibrium position for the stopped rotor blades as discussed above. Between 200 and 400 RPM at tunnel speeds above 85 fps, loads and moments exceeding the endurance allowables of nacelle balance and blades were observed and limited data was taken for that rotor speed range.

Above 400 RPM complete sweeps could be conducted up to approximately 950 RPM. During one of the first model checkout runs a predicted air resonance instability was noticed at 1050 RPM. To stay clear of the instability, the rotor speed was limited to a maximum of 1000 RPM during the subsequent test.

## Spinup and Feathering

During the spinup and feathering runs it was observed that blade and model motions were higher at the low rotor speeds when the collective sweep rate was low. Fast collective rates at the low rotor speeds decreased the monitored blade loads noticeably. Optimum spinup and feathering schedules within the constraints of the capabilities of the collective control circuit were developed.

## Blade Folding and Deployment

The blade position during the folding test was fixed as indicated on Figure 3-4. This position was based on design considerations which led to the smoothest nesting of the blades around the nacelle. The blades do not always normally assume that position when they are feathered as has been discussed in the paragraph on Steady State Windmilling. This resulted in a torque on the rotor shaft despite the fact that the blade collective setting

# *Contrails*

was adjusted to the feathering angle. The nacelle balance did not have a torque measuring strain gage bridge and a check revealed that the thrust measurement was affected by torque. The data obtained during these tests has therefore a lower accuracy than the data obtained from the rotating rotor tests.

At tunnel speeds above 85 fps, blade bending was quite pronounced but this bending reduced rapidly when the blades folded towards the nacelle. The blades were dynamically stable during all folding tests. When the blades were close to and on the nacelle for the flatwise system or close to and on the nacelle for the edgewise fold system, the blade position in the airstream for both flat and edgewise folding was steady and they never missed their pockets on the nacelle.

# *Contrails*

## With engine nacelle

Run	$\alpha_f$	$\delta_f$
19	0	0
20	0	15
21	0	30
22	0	45
23	-4	45
24	-4	30
25	-4	15
26	-4	0
27	+4	0
28	+4	15
29	+4	30
30	+4	45
31	+8	0
32	+8	15
33	+8	30
34	+8	45
38	0	0

## Without engine nacelle

Run	$\alpha_f$	$\delta_f$
37	0	0
39	0	30
40	+4	30
41	+4	0
44	+8	0
43	+8	30
44	12	30
45	12	0
46	16	0
47	14	0

All runs at tunnel speeds ranging from 85 to 140 fps

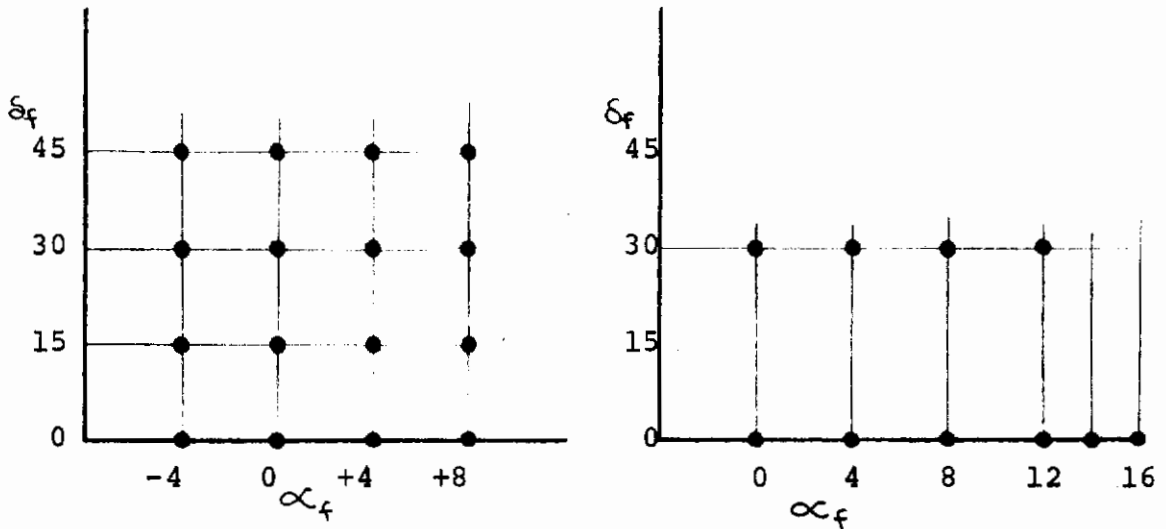


FIGURE 4-1. BASELINE RUNS (WITHOUT ROTOR)

# Contrails

Run	$\alpha_f$	$\delta_f$	V
55	0	0	85-113
56	0	0	142
57	0	30	85-113-142
59	-2	0	85-113-142
60	+2	0	85-113-142
61	+4	0	85-113-142
62	+4	30	85-113-142
67	0	15	85
68	0	45	85
69	0	0	85

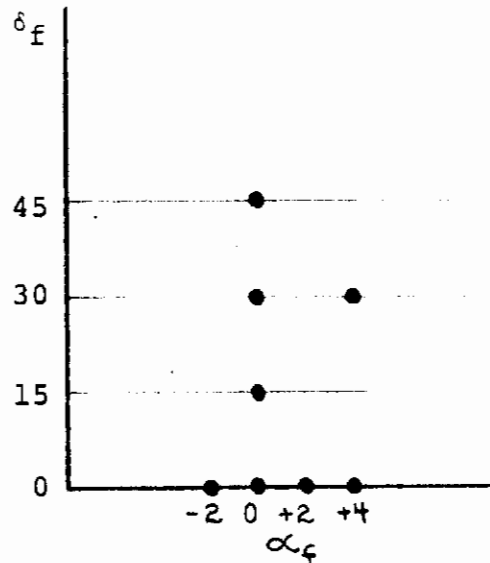


FIGURE 4-2. STEADY STATE WINDMILLING RUNS

## 5.0 PERFORMANCE

Performance data were obtained from the 1/9 scale conversion model in three regimes of operation:

- ° Steady windmilling
- ° Spinup and feather
- ° Blade fold and deployment

These three areas will be addressed in the following sections and the analysis presents the relationship of the transient data obtained in spinup/feather and blade fold/deployment to the steady windmilling condition. Also presented is a comparison between edgewise and flatwise blade folding.

### 5.1 Steady State Windmilling Performance

Steady windmilling is the mode of rotor operation at the end of transition before the blades are stowed to the cruise configuration. It forms the basis for comparison with the transient operation. The data analysis presented here addresses the airframe (wing and nacelle) and the rotor individually and then together as the aircraft. Figures 5-1 and 5-2 present the lift and drag characteristics of the airframe obtained without the rotor blades. Airframe lift variation with wing angle of attack is shown in Figure 5-1 for flap deflections ( $\delta_F$ ) of 0°, 15°, 30° and 45°.

The forces and moments measured are those outboard of the balance located at 11 percent of the semi-span. Using Anderson's (Reference 5) method to define the spanwise lift distribution, an approximation of the lift on the inboard 11 percent can be made and an estimate of the lift curve slope can be made for the full wing. Integrating the spanwise lift distribution indicated that 15 percent of the lift is generated by the inboard portion of the wing. This results in the measured loads being 85 percent of the actual values.

The "airframe" (wing and nacelle) data presented in this report are not corrected for the lift, drag or pitching moment inboard of the 11% wing span. The "airframe" data are included so that increments in lift and drag due to model changes can be evaluated.

# Contrails

A lift curve slope ( $C_{L\alpha}$ ) of 0.052 per degree was obtained for zero degrees flap deflection and 0.062 for 15°, 30° and 45° flap deflection. The increase in  $C_{L\alpha}$  achieved with flap deflection is a result of improved flow circulation about the wing. This improvement is higher than normal but the 0.062 is more representative of the full scale wing. The model was designed and constructed to achieve the dynamic characteristics of the full scale wing and results in a wing with chordwise slots with foam rubber filler. This contributes to the reduction in lift efficiency; as the flap is deflected the circulation is improved and is more representative of the full scale aircraft.

The lift curve slope, when corrected for the inboard wing lift not measured by the balance, is 0.073 for the wing with the flap deflected. This is the same as the prediction for this wing.

Figure 5-2 presents the airframe lift/drag variation for flap deflections of 0°, 15°, 30° and 45° obtained without the rotor blades. To define the airplane efficiency factor ( $e$ ), the data of Figure 5-2 was replotted as the airframe drag variation with the square of the lift coefficient in Figure 5-3. The resulting slope is 0.10 and is equal to  $1/\pi A R e$ . Adjusting this slope to account for lift and drag on the wing inboard of the balance reduces it to 0.085 and defines an airplane efficiency factor of 0.75. This is within the expected range of 0.7 to 0.85 for conventional airplanes even though the model has a large wing tip nacelle and the simulated engine nacelle.

The rotor operation in steady windmilling is defined as the specific combination of forward speed and blade collective that produces a steady rotor speed for zero rotor torque. Figure 5-4 presents the variation of blade collective and rotor speed (RPM) for forward speeds of 85 and 113 feet per second. Since the aerodynamic characteristics of the blade define the relationship between the rotational speed and the forward speed that produces zero torque, this relationship should produce a unique trend of blade collective with advance ratio ( $\mu$ ), the ratio of forward speed to rotor tip speed. Figure 5-5, based on run 133, shows that the variation of blade collective with advance ratio does form a single trend.

Included on Figure 5-5 is a prediction of the blade collective variation with advance ratio that was developed as part of the pretest predictions. The predictions are indicated by the X symbols and show excellent agreement with the test data.

# Contrails

The rotor performance associated with the steady windmilling operation is presented in Figure 5-6 as the variation of rotor drag with rotor speed for various forward speeds. These data are presented for flap deflections of  $0^\circ$ ,  $15^\circ$  and  $30^\circ$  and indicate that there is an insignificant influence of flap deflection on rotor drag. As indicated previously, there is a specific trend of blade collective with advance ratio and therefore there must be an associated trend in rotor thrust for steady windmilling operation. Converting the data of Figure 5-6 to rotor thrust coefficient and presenting this variation against advance ratio as in Figure 5-7 does show a unique trend. This indicates that the change in circulation from  $\delta_F = 30^\circ$  to  $\delta_F = 0^\circ$  flap deflection does not have a significant effect on the rotor axial force. There is a distinct change in the slope at an advance ratio of approximately 1.20 which is in the low rotor RPM range (0 to 300 RPM). This could be a Reynold's Number effect on the rotor drag since  $R_N$  is between 100,000 and 200,000 for this condition.

The variation in wing circulation does not appear to have a significant effect on the rotor thrust but the rotor influence on the airframe characteristics can be seen in Figure 5-8 through 5-11. Rotor interference on wing lift can be seen from Figures 5-8 and 5-9. The rotor produces an increment in aircraft lift coefficient of 0.03 for both  $0^\circ$  and  $30^\circ$  flap deflection. Pitching moment is also influenced by the rotor. As indicated by Figures 5-10 and 5-11, there is a  $-0.006$  change in aircraft pitching moment for  $0^\circ$  flap deflection and a  $-0.014$  change for  $30^\circ$  flap deflection. This decrease in pitching moment indicates that there must be a shift aft in the center of lift resulting from the rotor influence on the flow about the wing.

The total aircraft performance in steady windmilling is presented in Figures 5-12 and 5-13 for a level fuselage attitude ( $\alpha = 0^\circ$ ) and a flap deflection of  $30^\circ$ . This configuration is representative of one "g" cruise at 200 knots where conversion would be initiated. Figure 5-12 presents the variation of aircraft lift with rotor RPM. The rotor contribution to total aircraft lift is small at all rotor speeds. However, the rotor drag in steady windmilling is large and increases the airframe drag coefficient by approximately 0.07 as indicated in Figure 5-13. The rotor drag includes a spinner drag increment of 0.01. This results in an incremental aircraft drag coefficient of 0.06 which is equivalent to a 0.1 "g" deceleration.

## 5.2 Spinup and Feather Performance

The second regime of operation in conversion is the spinup and the feathering of the rotor. This is the process of bringing the rotor up to speed from the feathered condition or feathering the rotor from the windmilling condition and is achieved by an exchange of energy between the airstream and the rotor. The rotor takes energy from the airstream to accelerate in the spinup and therefore there is a transient drag force produced. Energy is given up to the airstream during the feather operation resulting in a transient propulsive force. The schedule of the blade collective pitch variation with time defines the magnitude of the transient drag and propulsive force. During the transient two effects are observed. The change in operating conditions of the rotor during spinup produces a trim change in axial force and also puts a brief deceleration on the passengers and crew. Examination of existing data, Reference 1, shows that a transient force of 0.1 to 0.2g is commonplace in everyday transportation. The level of 0.1g was adopted as a design goal to provide good ride qualities for the vehicle and, as shown in this section, this level can be met without undue sophistication.

For the Model 213, at a minimum operating gross weight of 50,000 lbs., this amounts to a transient force of 2500 lbs per rotor. For the wind tunnel model this reduces to 3.4 lbs drag above the feathered rotor drag or 3.4 lbs thrust above the windmilling rotor drag.

Testing was performed at 85 fps and 113 fps to define a collective schedule that would meet the 0.1 "g" transient force objective. These speeds are representative of full scale conversion speeds of 150 knots and 200 knots respectively. Figure 5-14 presents the effect of collective rate on the rotor drag during the spinup to the maximum RPM at a forward speed of 85 fps with the flap deflected 30 degrees. Three linear collective schedules of 3.0, 4.5 and 6.0 seconds from feather to windmilling are presented. Indicated on the top of the figure is the actual rotor collective and RPM variation with time that was achieved and on the bottom is the resulting rotor drag. The transient drag above the feathered rotor drag (zero time) is 9.4 pounds for the 3-second schedule and 6.4 pounds for the 6-second schedule which are well above the 0.1 "g" indicated goal. The steady windmilling drag is the asymptote to the envelope of the transient drag peaks and permits an extrapolation of the drag envelope. This results in a schedule of approximately 10 seconds for the model to meet 0.1g. The associated full scale schedule is then 30 seconds since time is factored by the square root of the model scale factor for Froude scale testing and this would be too long from operational considerations. Figure 5-15 presents the effect of collective rate on rotor drag



# Contrails

for the feathering operation of the rotor at 85 fps utilizing the same schedules as in the spinups. Regardless of the schedule (3.0, 4.5 or 6.0 seconds) there is a transient peak at approximately 0.5 seconds.

Since the feather rotor drag is 2.8 pounds less than the windmilling drag, this indicates that the collective schedule must be long to meet the 0.1g objective of 3.4 pounds. It is estimated that it would require a schedule of approximately 10 seconds again to attain the objective.

Figures 5-16 and 5-17 present the spinup to maximum RPM (950) and feather with a flap deflection of 15 degrees and a forward speed of 113 fps which is equivalent to a full-scale conversion speed of 200 knots. The steady windmilling drag is 3.4 pounds above the feathered drag which is the equivalent of 0.1 "g", therefore, the collective schedule would have to be very long to avoid a transient drag peak.

Flap deflection had no significant effect on rotor axial force in steady windmilling and it was tested during the transient to verify this trend. As indicated by Figures 5-18 and 5-19 changing the flap deflection from 30 to 15 degrees had very little effect on the rotor drag during the spinup and feather at a forward speed of 113 fps and a 6-second linear collective schedule.

A comparison of the speed effects presented in Figures 5-14 to 5-17 for a 4.5 second collective schedule is shown in Figures 5-20 and 5-21. The net rotor drag developed during the spinup transient, shown in Figure 5-20, is approximately the same for both speeds and the only difference in the drag variation is a result of the feathered rotor drag. During the feathering there is a difference in incremental drag below the steady windmilling level with the 113 fps forward speed transient having a 5.2 pound thrust and the 85 fps transient having 6.2 pounds thrust. A similar comparison was made for spinning-up to a lower RPM (715 in Figure 5-22). This exhibits a similar trend in the net drag, the peak being the same, for the two forward speeds tested at approximately 6 pounds. This is considerably less than the 9 pounds obtained when spinning up to 950 RPM. It is of particular significance that with the 4.5 second linear collective schedule 0.1 "g" transient drag can be met when the spinup is to 715 RPM. The corresponding feather or spin-down in Figure 5-23 indicates that both forward speeds

# Contrails

have a transient thrust increment from the steady windmilling level within 0.1 "g". Thus, the 0.1 "g" goal can be met by starting and finishing the conversion cycle at 715 RPM instead of 950.

Since the drag increases at a low rate at the beginning of the spinup and increases at a rate that is directly related to the collective in the mid portion of the transient, a collective schedule can be defined that will reduce the peak drag to a minimum. A parabolic schedule rate that has a high collective rate at the beginning and a low rate at the end would take advantage of the low drag rise at the beginning and mid portion of the spinup. A number of parabolic variations were tested. Figures 5-24 and 5-25 show the comparison of two parabolic and a linear collective schedule for spinup to 950 RPM and feather at a forward speed of 85 fps. For the 4.5 second schedule in Figure 5-24 the drag increment above the feathered level is reduced from 9 pounds to 7.6 pounds by using a slight parabolic variation for the spinup. Decreasing the collective at a very high rate initially, presented for a 3.0 second schedule, results in a small drag peak at 0.3 seconds which is the end of the steep collective rate and the main drag peak is at 2.7 seconds. The maximum transient drag increment above the feathered drag level is 5.8 pounds which is the same as the 4.5 second parabolic discussed above. Comparison of the parabolic and linear schedules in the feathering operation is made in Figure 5-25. There is an incremental thrust peak at approximately 0.5 seconds of 6.3 pounds for the linear and 5.5 for both parabolic schedules. The parabolic schedules from 950 RPM shown in Figure 5-24 and 5-25 do not meet the 0.1 "g" transient drag goal.

The parabolic schedules do reduce the drag during spinup but not enough to allow spinup to hover RPM. Since the linear schedule spinning up to 715 RPM at 113 fps forward speed just met the criteria, a non-linear schedule would be within it. Figures 5-26 and 5-27 present three parabolic variations for schedules of 1.0, 2.0 and 6.0 second durations. The 1.0 second schedule had a drag increment of 15.5 pounds occurring at 0.25 seconds and the 2.0 second schedule has a drag increment of 4.8 occurring at 1.0 second. Neither of these meet 0.1 "g" (3.4 pounds) but the 6.0 second schedule has a transient drag increment of 2.5 pounds, well within 3.4 pounds. Developing an envelope of the drag peaks indicates that a schedule of approximately 3.0 seconds or greater would satisfy the criteria for the spinup.

There are two non-linear spin down schedules shown at 2.0 and 4.5 seconds and a 6.0 second linear schedule presented in Figure 5-27. The non-linear schedules are composed of two linear rates; the first portion has a low rate and the last portion has a high rate. The point at which transition from the low rate to the high rate is defined by the desired schedule length. Neither of these meet 0.1 "g" objective but the 6 second linear schedule has a drag increment of 2.6 pounds and is better than the criteria. Referring back to Figure 5-23, the 4.5 second linear schedule has a drag increment of 3.0 pounds. This would indicate that a spin down with a linear schedule with a duration of 3.0 to 4.0 seconds would meet the 0.1 "g" transient thrust goal or as indicated by the trend in Figure 5-25 a parabolic feather schedule would have a transient thrust even less than 0.1 "g". Therefore, a three to four second spinup and feather can be performed with the model while meeting the 0.1 "g" transient thrust drag objective. This time scales up to a schedule that is 9 to 12 seconds for the full scale aircraft.

Each of the figures indicates the feathered and windmilling drag levels. This provides an indication of the increment in transient drag that is acting on the airframe and would be added to the rotor contribution to the total aircraft performance presented in Figure 5-13.

### 5.3 Folding and Deployment Performance

The third regime of the conversion is the blade fold and deployment which is the process of folding the blades from the feathered position into the wing tip nacelle. As the blades are folded, the total aircraft drag is reduced. When folding the blades from the feathered position, the easiest method would be to fold them directly into the nacelle edgewise. In that case the blades cannot be completely retracted into the nacelle contour and they are partially exposed or require blade covers which would increase the frontal area of the nacelle. A better aerodynamic configuration for the nacelle can be achieved by folding the blades flat against the nacelle. This is accomplished by rotating the blade 90 degrees in the last portion of the folding process to achieve the flatwise fold. Figure 5-28 shows the variation of the total aircraft drag with blade fold angles for a flatwise fold. Indicated for reference is the aircraft drag with the blades feathered, shown at 90 degrees and the blades removed shown at 0 degrees.

# Contrails

The drag with the blades removed is used as a base level to indicate the drag increment of the rotor shown as the shaded area. A slight increase in drag from the feathered rotor drag level is attributed to the blade folding mechanism and a slight discrepancy in the blade collective angle setting. As the blades are folded, the drag decreases steadily until 30 degrees. At this angle the drag level is the same as with the rotor blades removed.

It remains constant as the blade folding continues to 15 degrees where the total aircraft drag coefficient becomes less than the rotors off drag coefficient as the blade folding is completed. Since the model nacelles had flat areas for the blades to fit on and a small step aft of where the folded blade would be, to achieve a relatively smooth contour in the folded configuration, the folded blade improved the contour of the nacelle and thereby reduces the drag coefficient by 0.01.

Figure 5-29 presents the variation of aircraft drag for the transient flatwise fold and deploy. This drag data is uncorrected and is included only to indicate the trend during the transient. There is no difference in the drag level during fold or deploy; there is no transient drag peak, and the trend of drag with blade fold angle is the same as indicated for the steady state fold data of Figure 5-28. This indicates that the steady state blade folding data can be used to define the performance during the transient fold process.

The increment in aircraft drag for the rotor when folded flatwise, represented by the shaded area in Figure 5-28, is presented in Figure 30 to show the comparison of edgewise to flatwise blade folding. There appears to be a large difference in rotor drag for the edgewise and flatwise with the rotors deployed. This difference results from the incorrect setting in blade collective and they both should be at the level indicated for the feathered drag. As the blade is folded, the drag decreases in a smooth trend but when completely folded the edgewise folded blade has a higher incremental aircraft drag coefficient than the flatwise folded blade. The flatwise folding provides a drag reduction of approximately 5.6 sq. ft equivalent flat plate drag area from the edgewise folding configuration to result in a total aircraft  $C_D$  of 20.79 sq. ft.

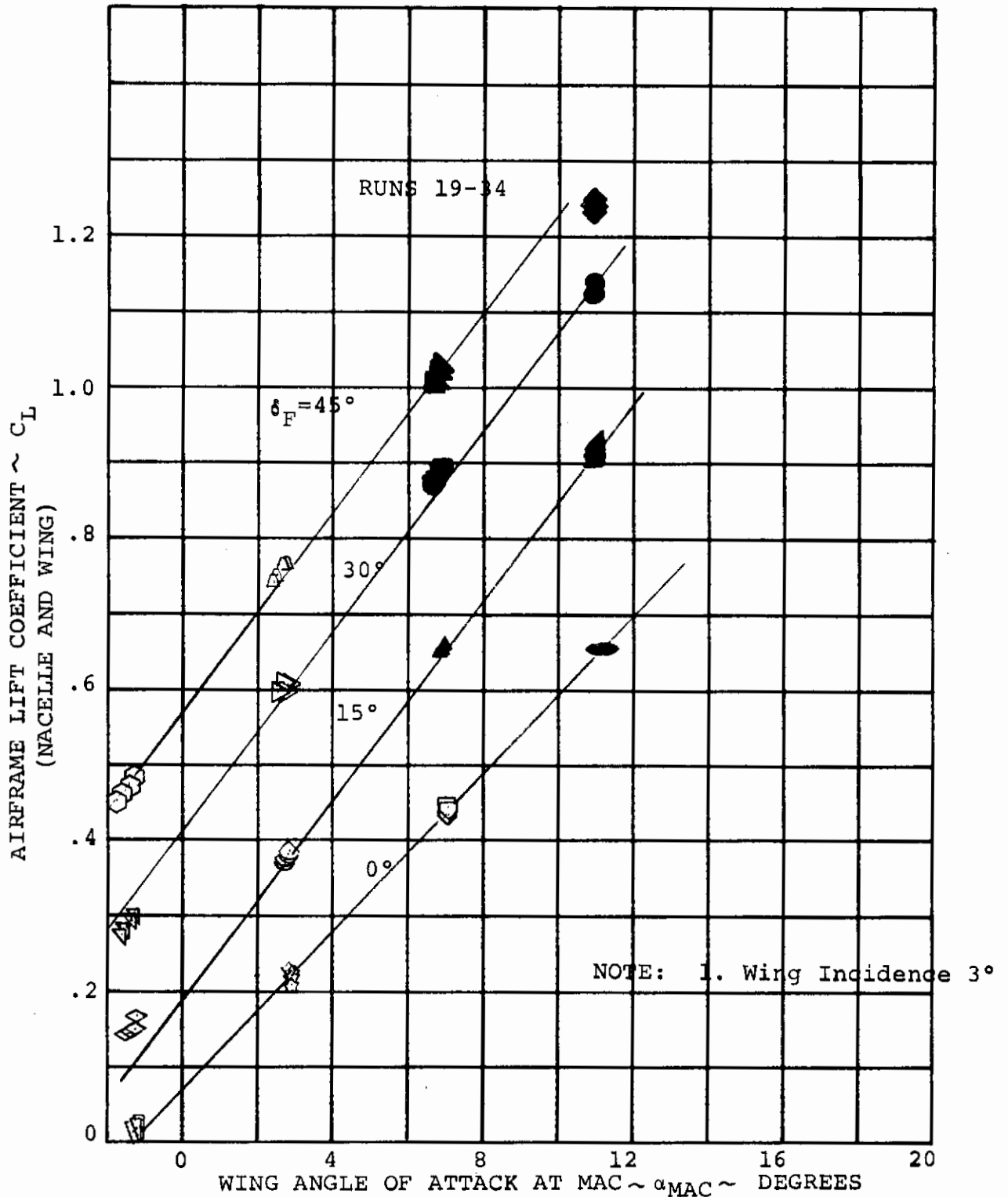


FIGURE 5-1 AIRFRAME LIFT/ANGLE OF ATTACK VARIATION FOR FLAP DEFLECTIONS OF 0°, 15°, 30°, 45°

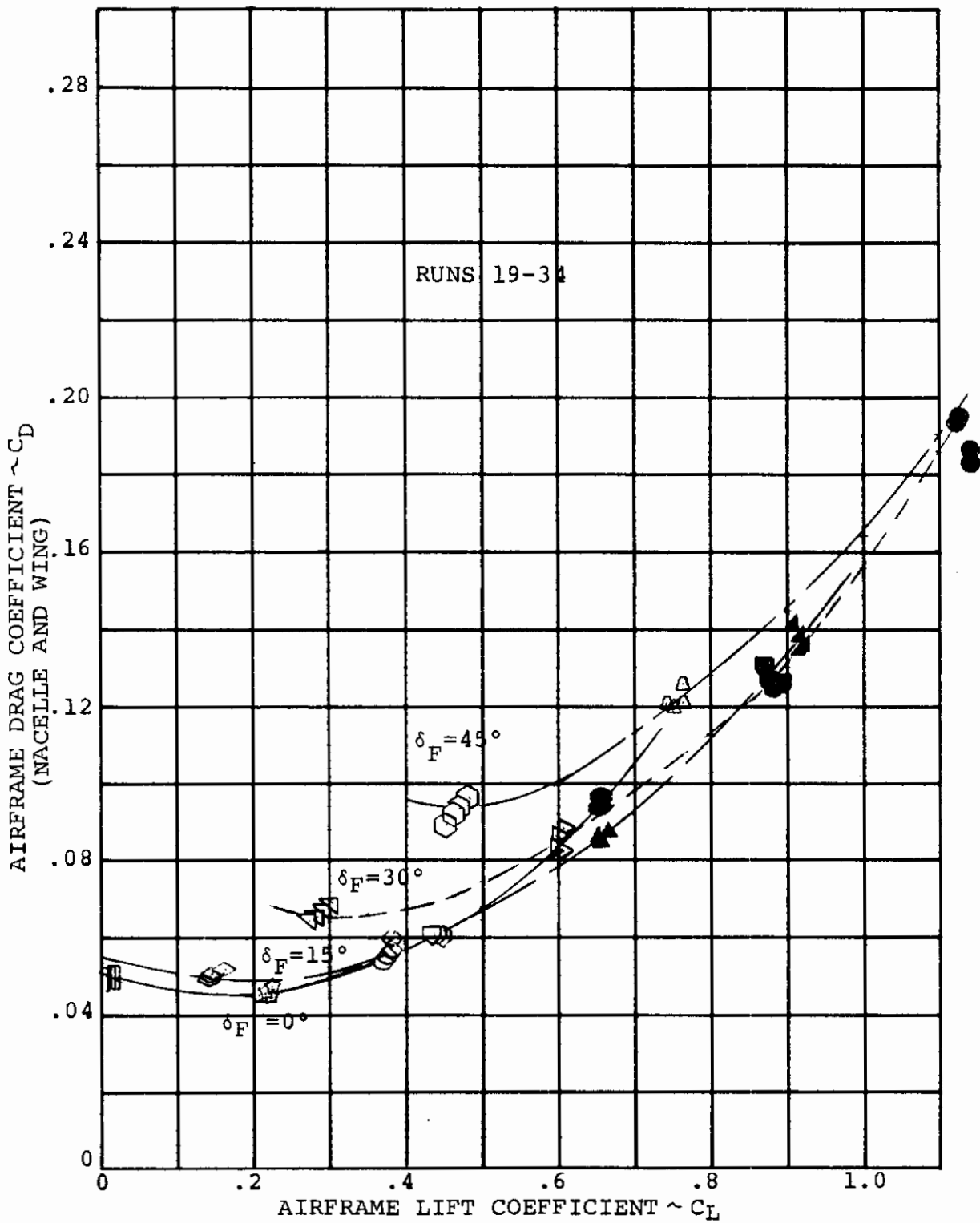


FIGURE 5-2 AIRFRAME DRAG/LIFT VARIATION FOR FLAP DEFLECTIONS OF 0°, 15°, 30° and 45°

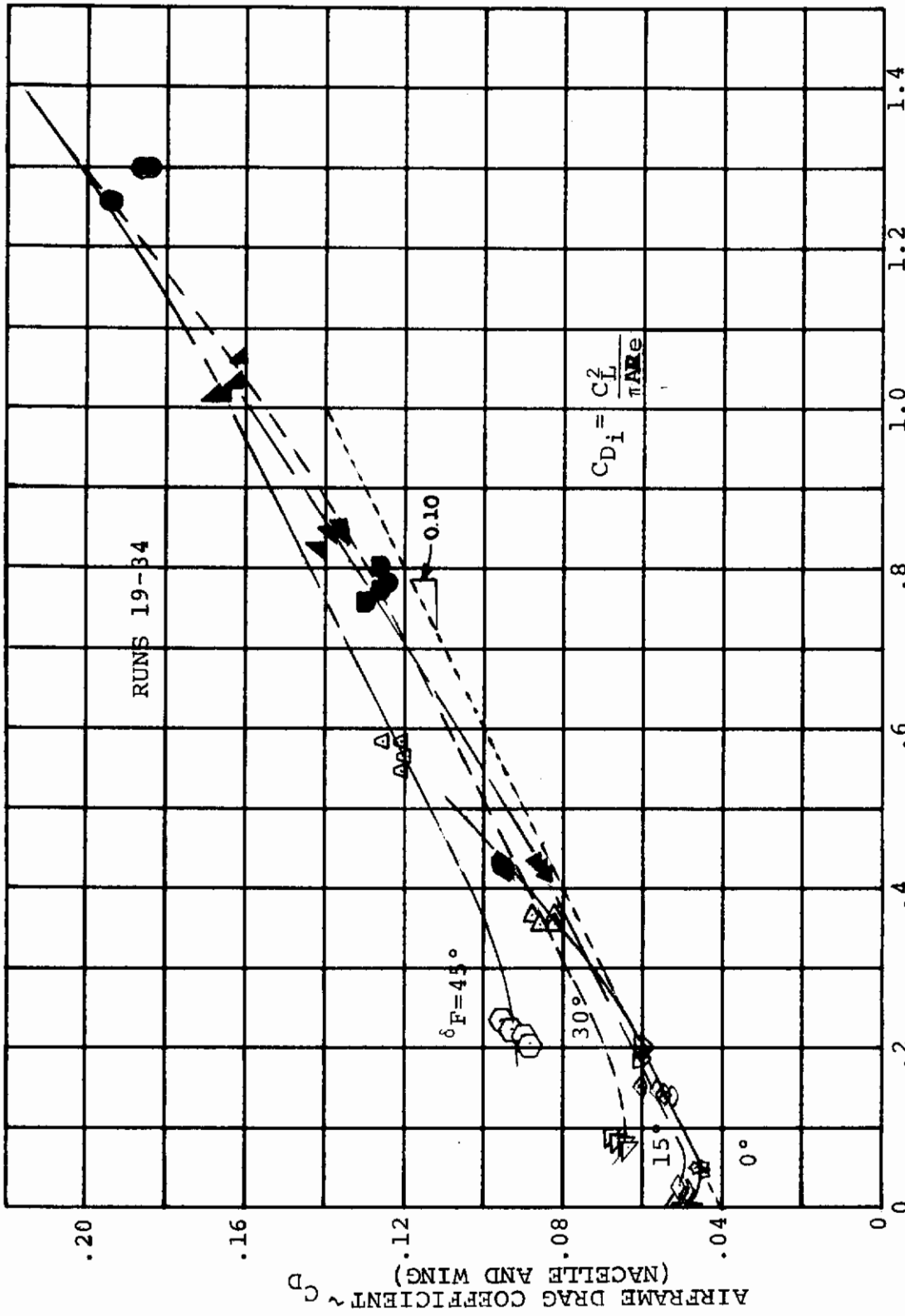


FIGURE 5-3 DEFINITION OF INDUCED DRAG AND AIRFRAME EFFICIENCY (NACELLE AND WING) AIRFRAME LIFT COEFFICIENT SQUARED  $\sim C_L^2$

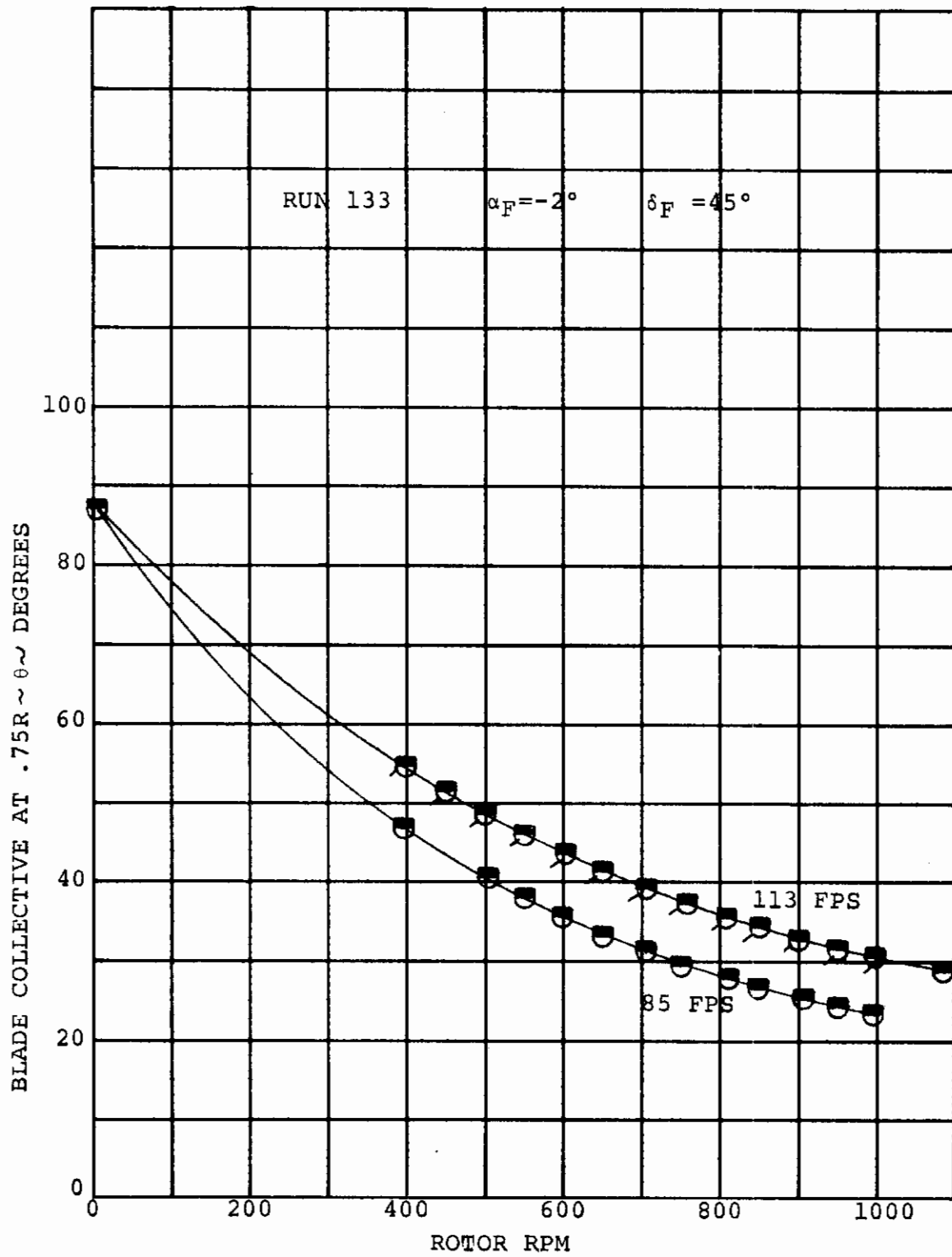


FIGURE 5-4 BLADE COLLECTIVE/ROTOR RPM VARIATION FOR STEADY WINDMILLING



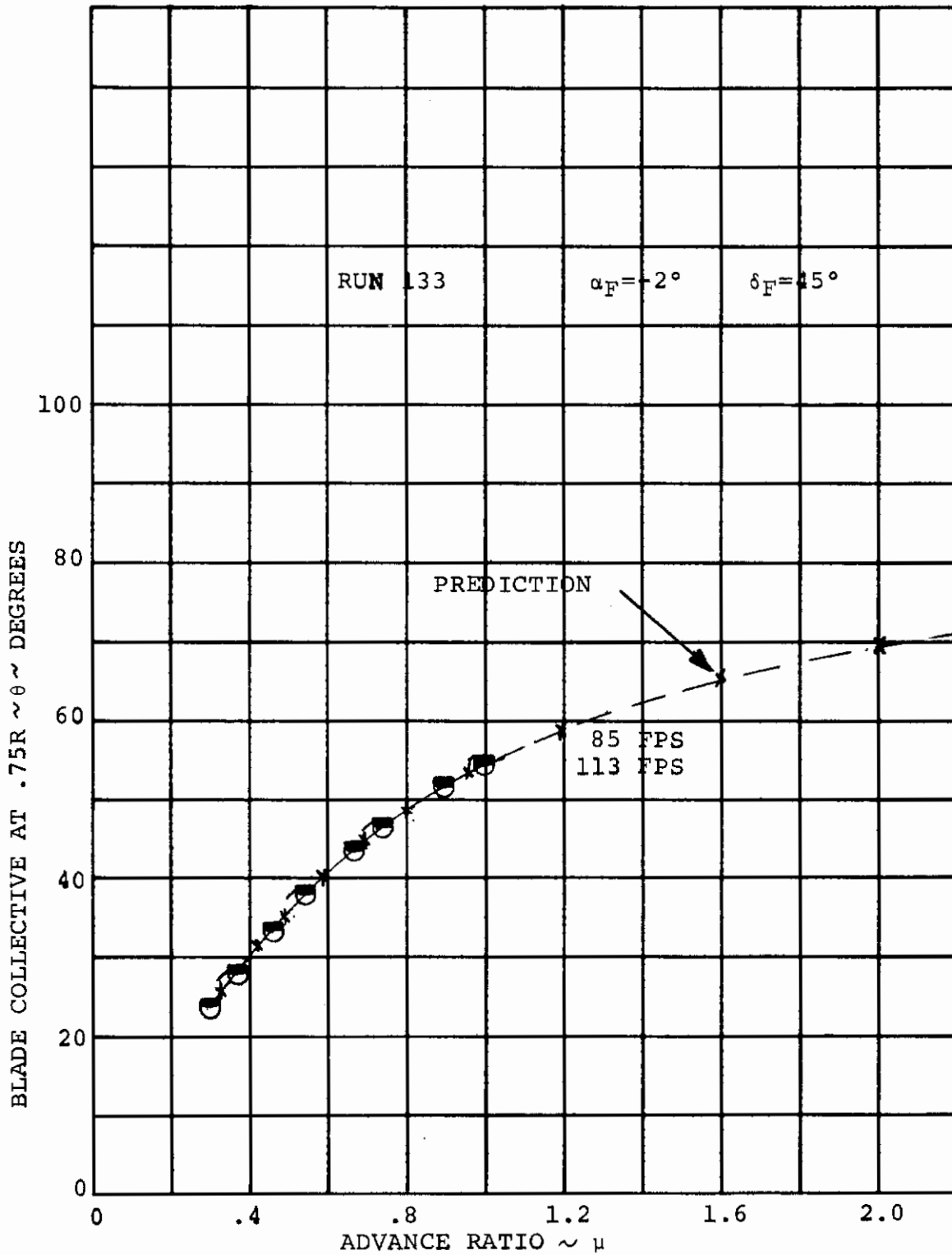


FIGURE 5-5 BLADE COLLECTIVE/ADVANCE RATIO VARIATION FOR STEADY WINDMILLING

# Contrails

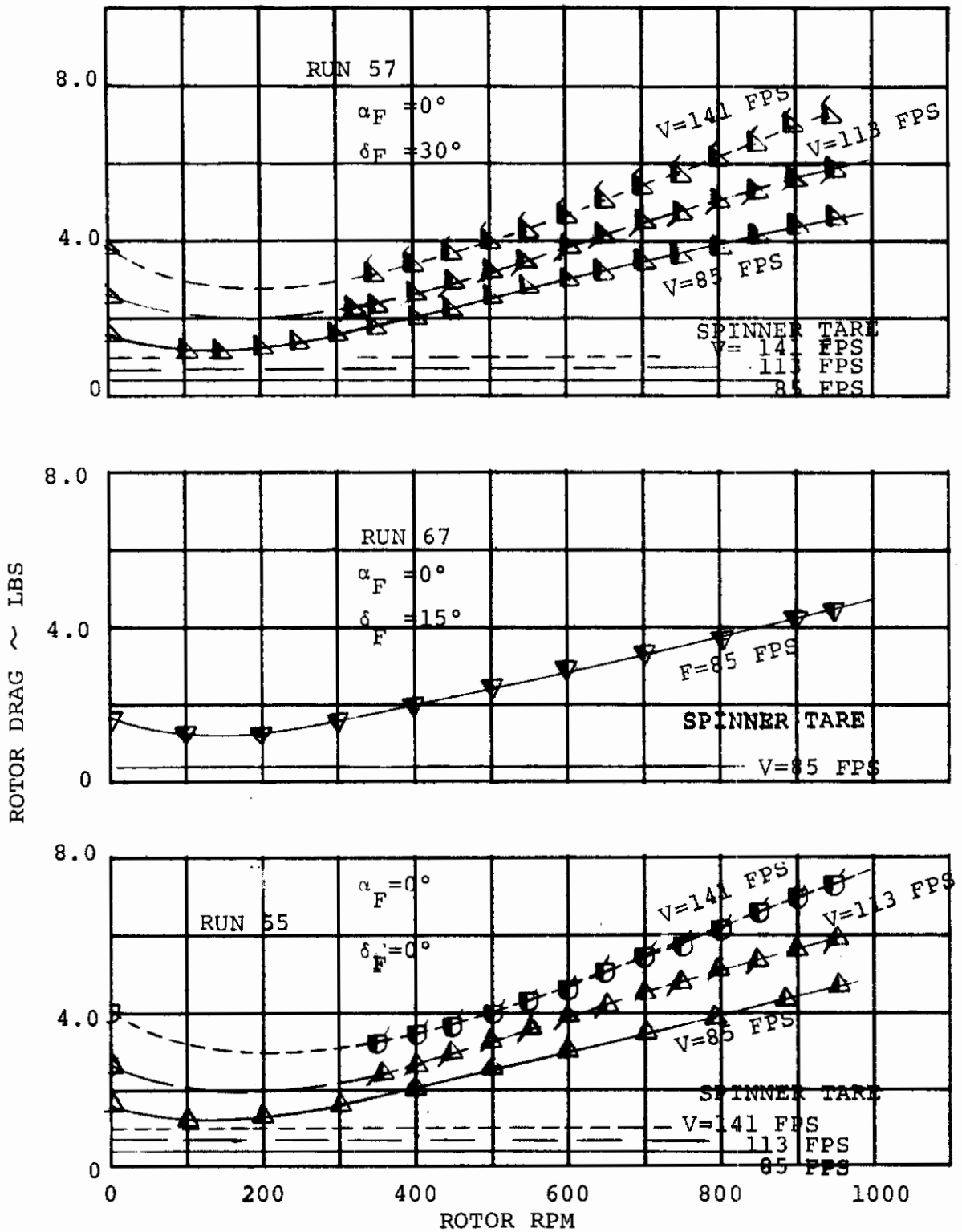


FIGURE 5-6 ROTOR DRAG/ROTOR RPM VARIATION AS INFLUENCED BY FORWARD SPEED AND FLAP DEFLECTION (STEADY WINDMILLING)

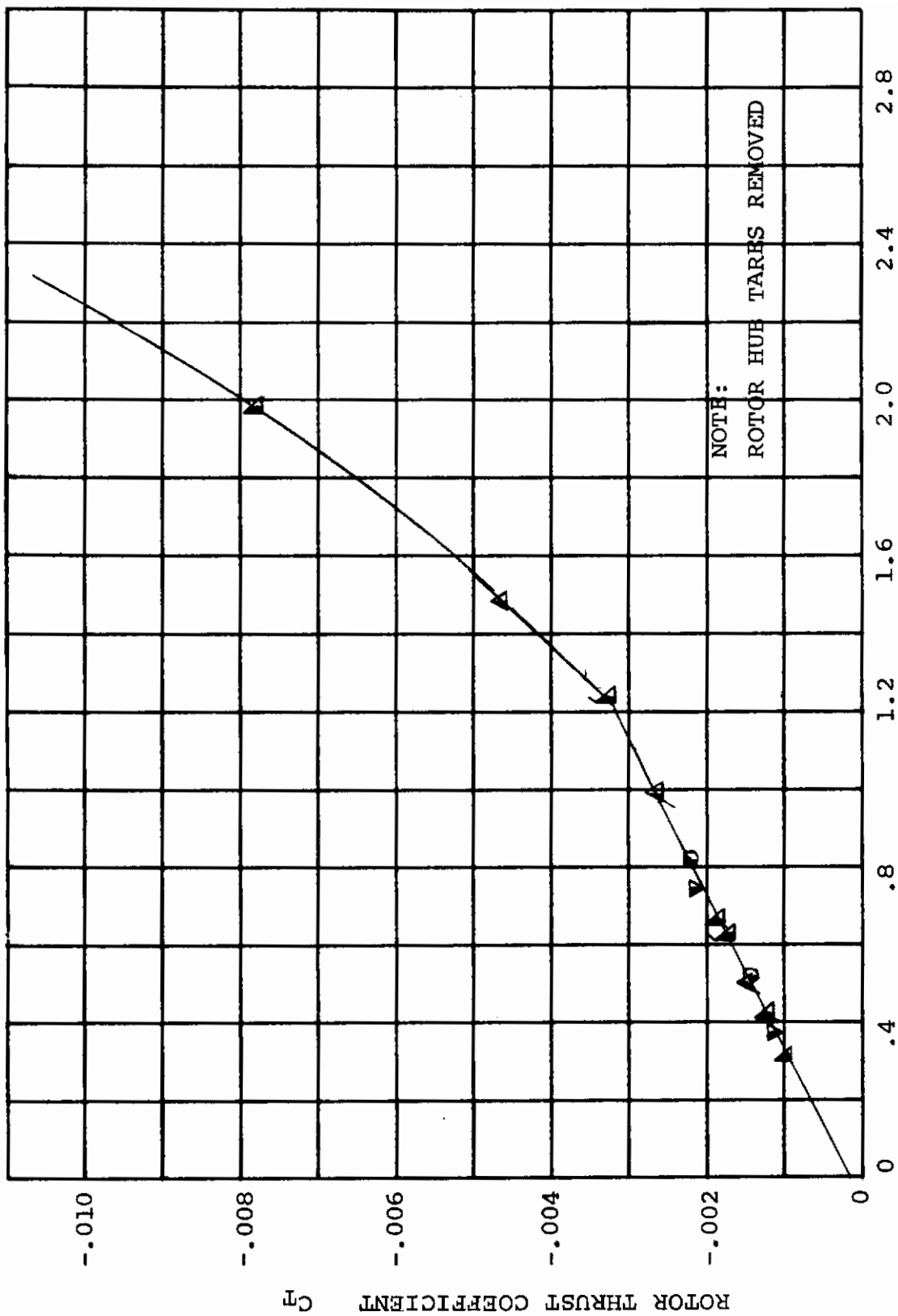


FIGURE 5-7. ROTOR PERFORMANCE DURING WINDMILLING OPERATION

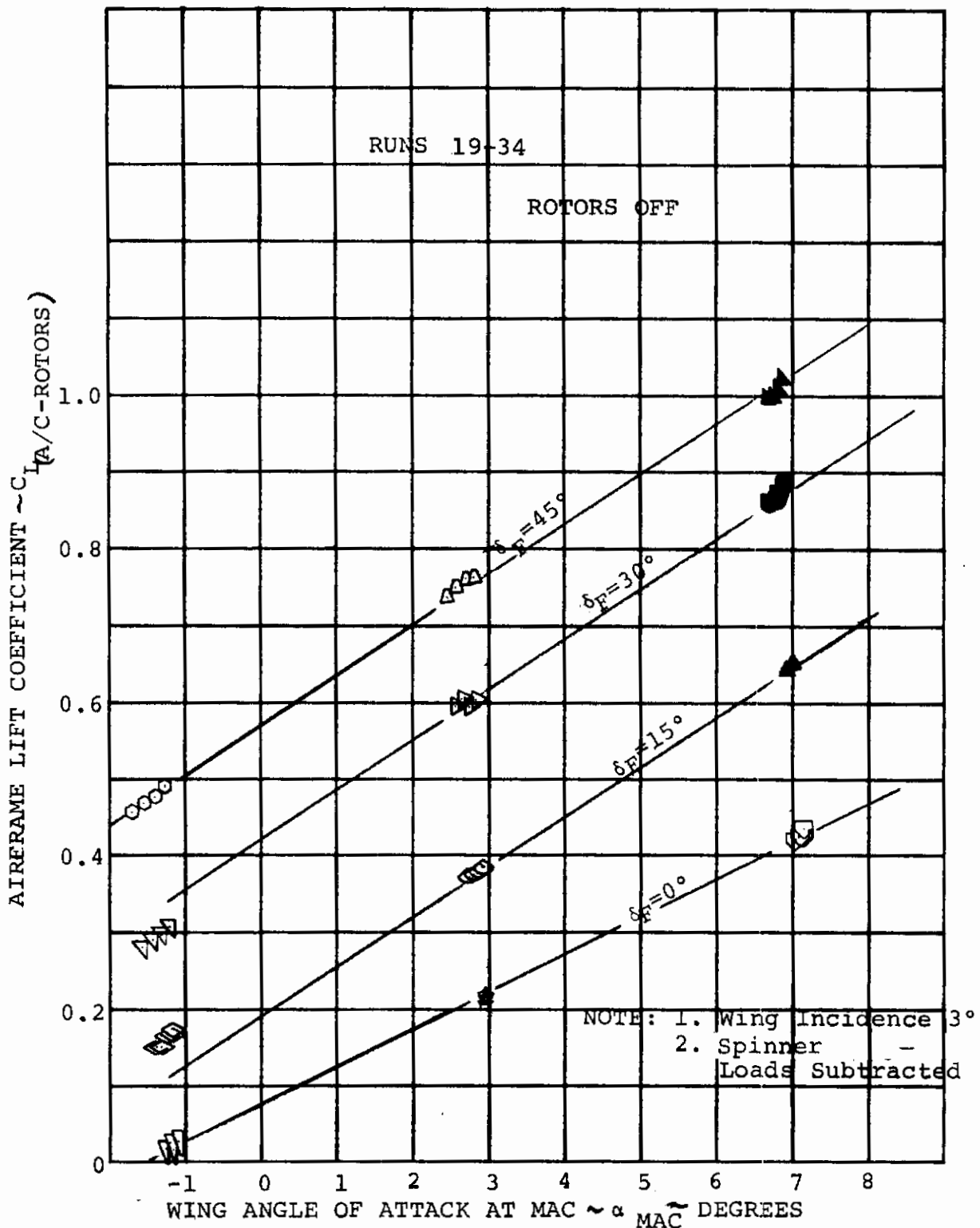


FIGURE 5-8 AIRFRAME LIFT/ANGLE OF ATTACK VARIATION FOR FLAP DEFLECTIONS OF 0°, 15°, 30°, 45°

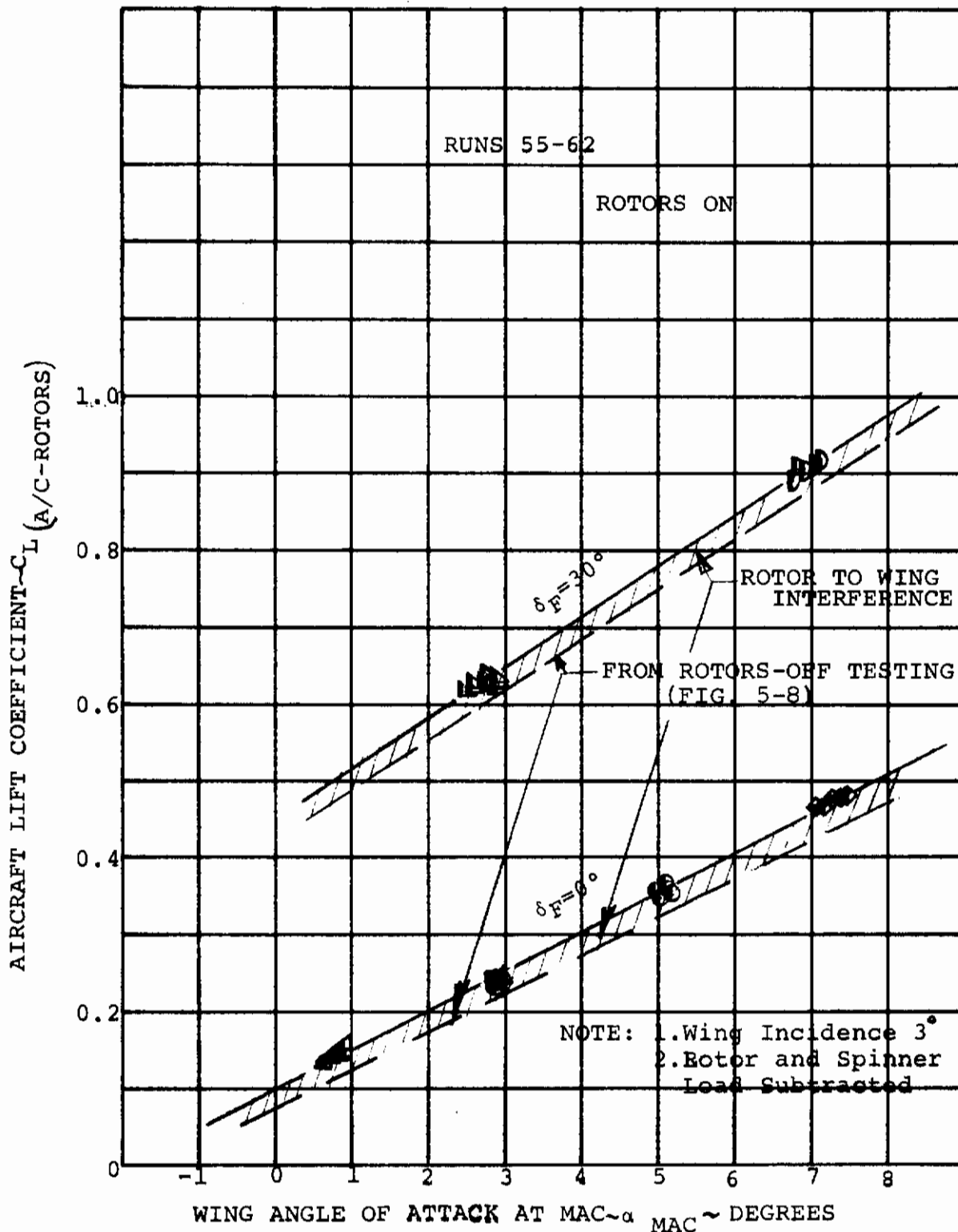


FIGURE 5-9 AIRFRAME LIFT/ANGLE OF ATTACK VARIATION FOR FLAP DEFLECTIONS OF  $0^\circ$  AND  $30^\circ$

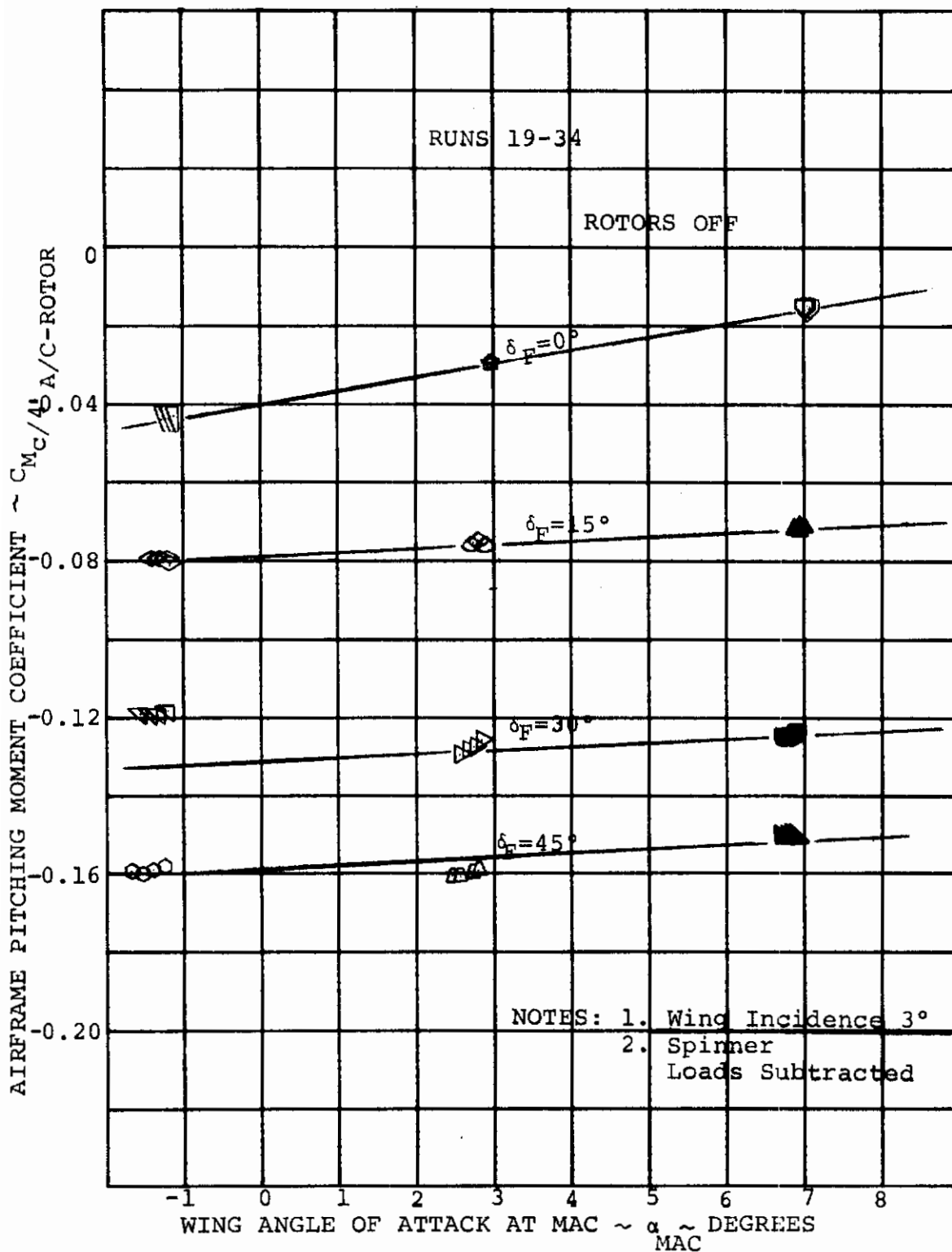


FIGURE 5-10 AIRFRAME PITCHING MOMENT/ANGLE OF ATTACK VARIATION FOR FLAP DEFLECTIONS OF  $0^\circ$ ,  $15^\circ$ ,  $30^\circ$  AND  $45^\circ$

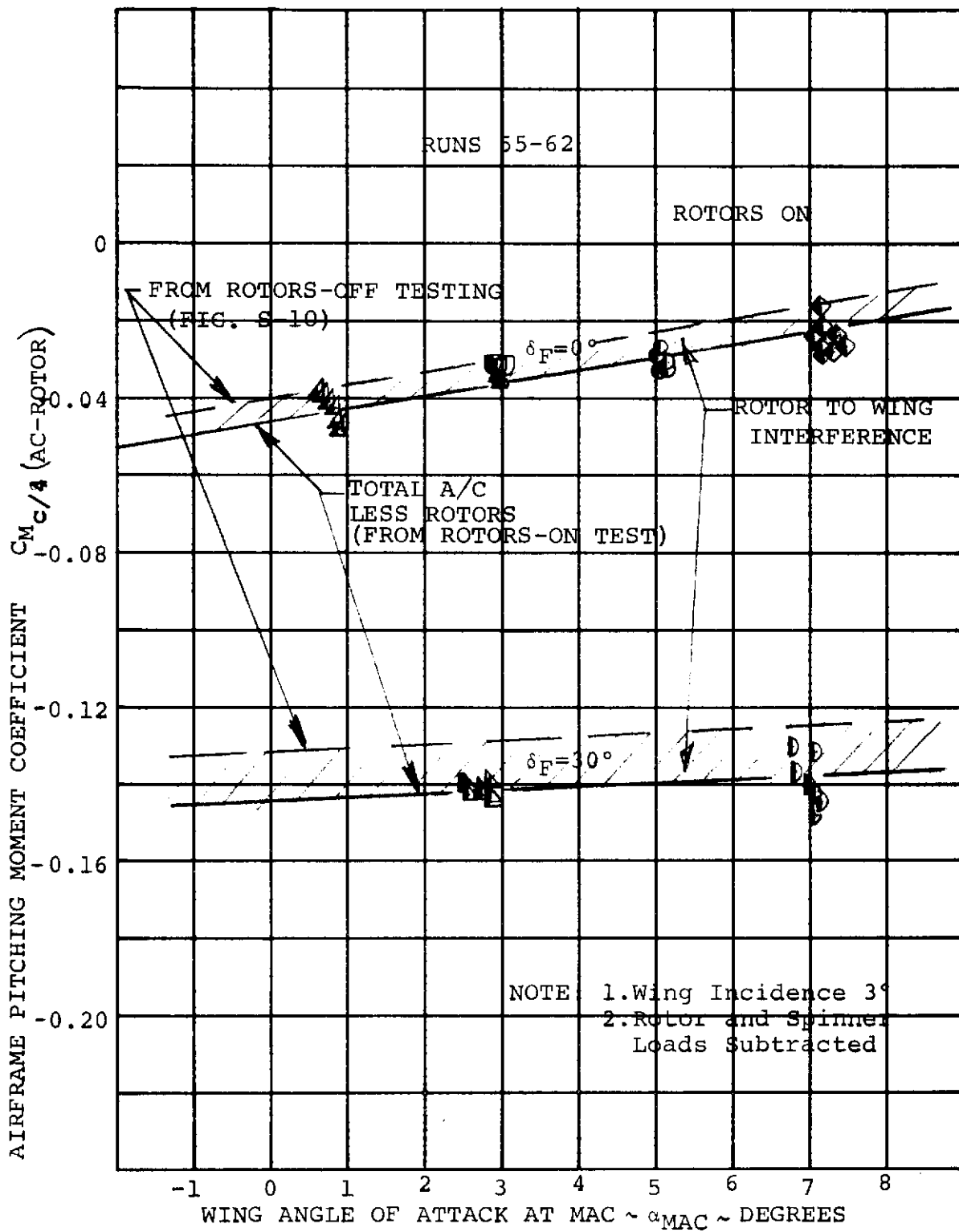


FIGURE 5-11 AIRFRAME PITCHING MOMENT/ANGLE OF ATTACK VARIATION FOR FLAP DEFLECTIONS OF  $0^\circ$  AND  $30^\circ$

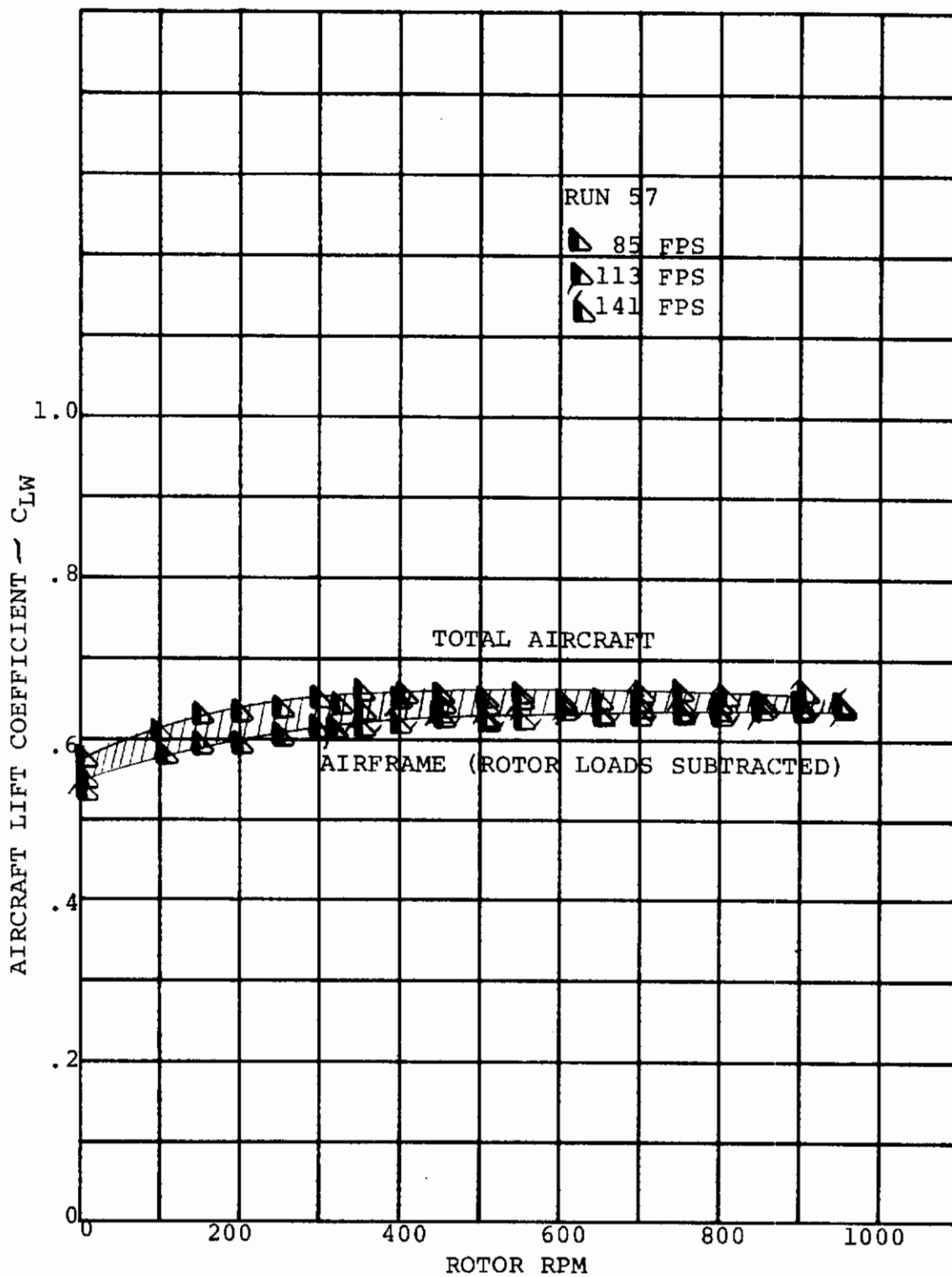


FIGURE 5-12 EFFECT OF ROTOR RPM AND FORWARD SPEED ON AIRCRAFT LIFT  $\alpha=0^\circ$   $\delta_F=30^\circ$  (STEADY WINDMILLING)



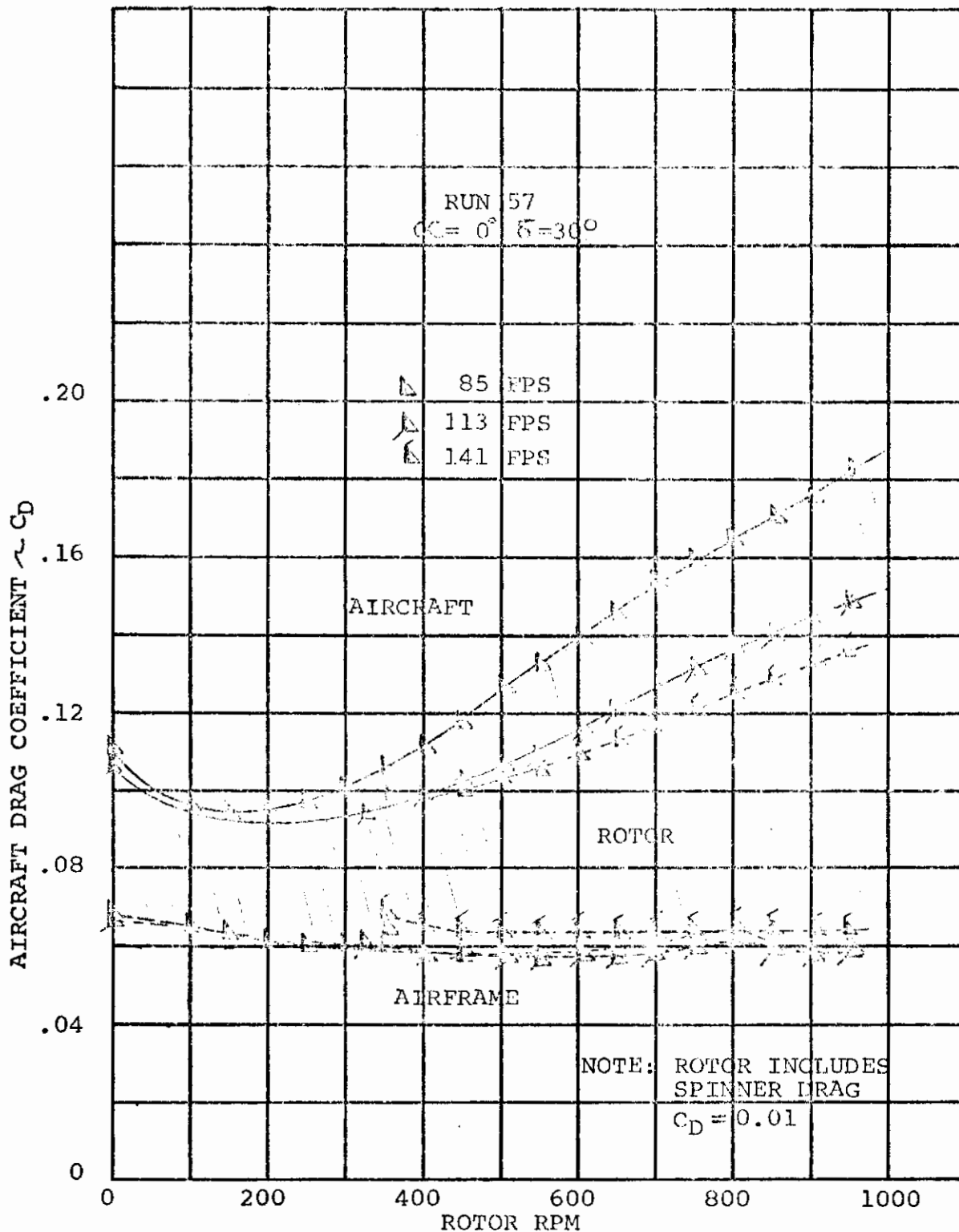


Figure 5-13. EFFECT OF ROTOR RPM AND FORWARD SPEED ON AIRCRAFT DRAG,  $\alpha = 0^\circ$   $\beta = 30^\circ$  (STEADY WINDMILLING)

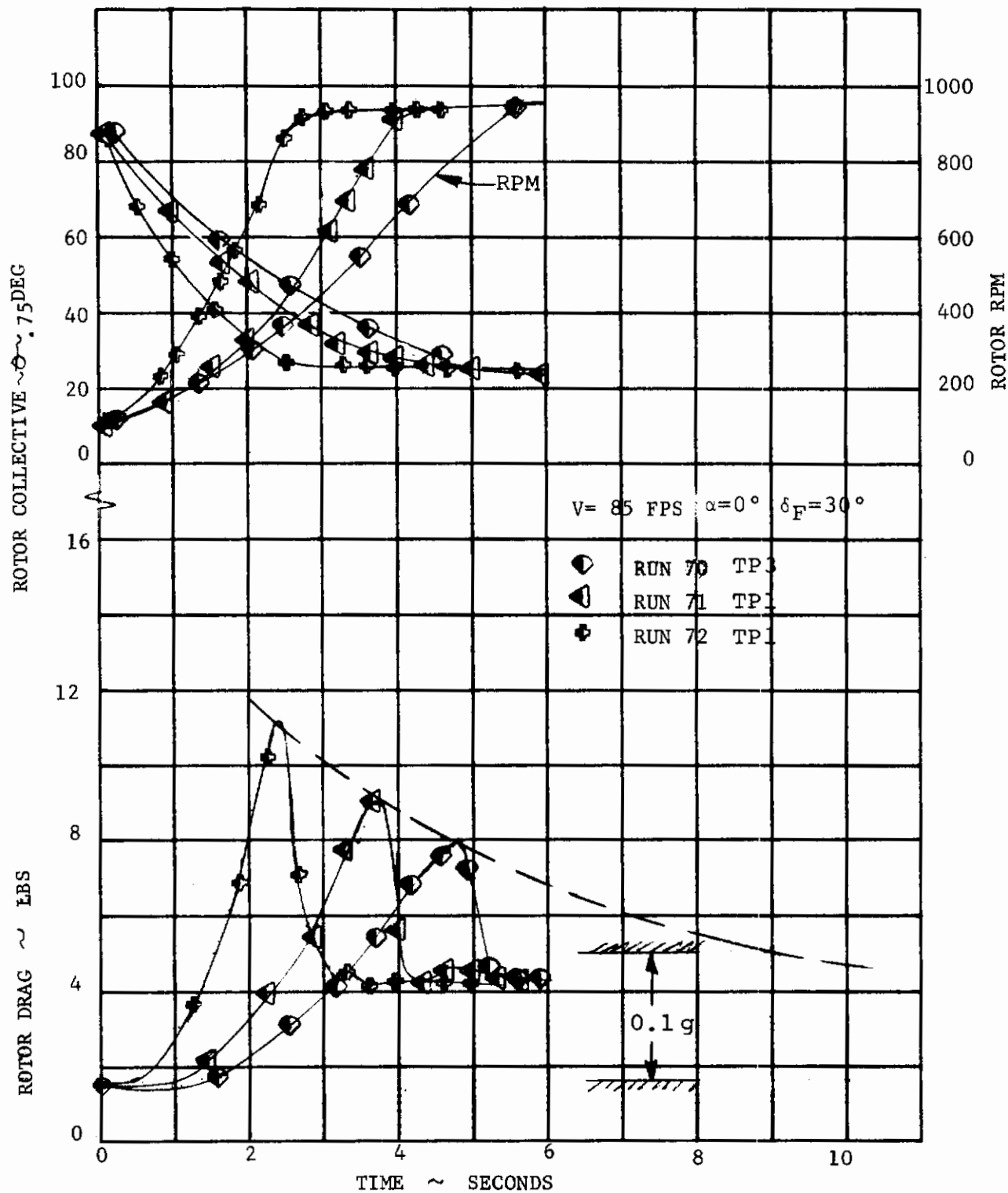


FIGURE 5-14 EFFECT OF COLLECTIVE RATE ON ROTOR DRAG  
 DURING SPINUP AT  $V=85 \text{ FPS}$   $\alpha=0^\circ$   $\delta_F=30^\circ$   
 (LINEAR COLLECTIVE RATE)

# Contrails

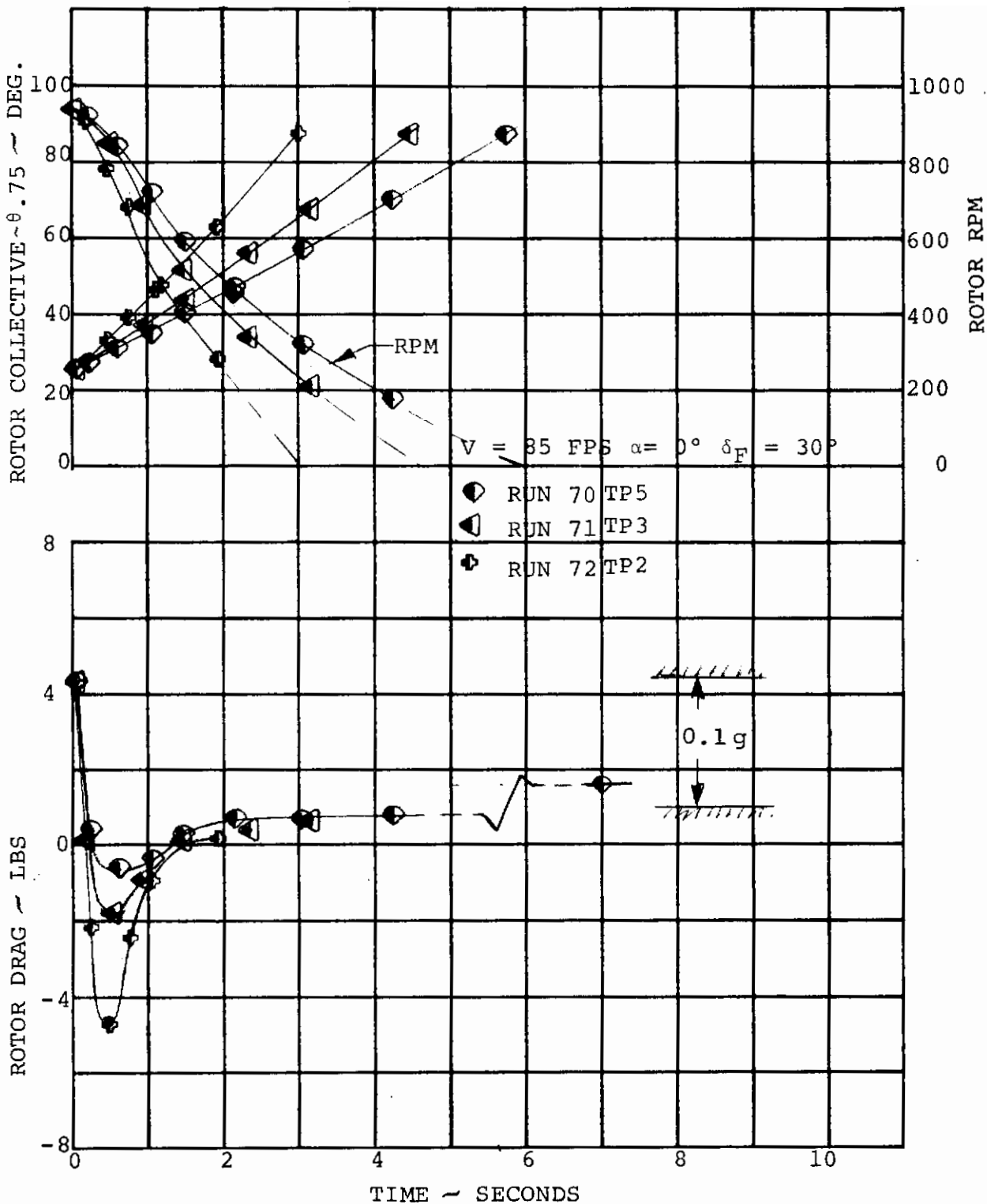


FIGURE 5-15 EFFECT OF COLLECTIVE RATE ON ROTOR DRAG  
 DURING FEATHER AT  $V=85 \text{ FPS}$   $\alpha=0^\circ$   $\delta_F=30^\circ$   
 (LINEAR COLLECTIVE RATE)

# Contrails

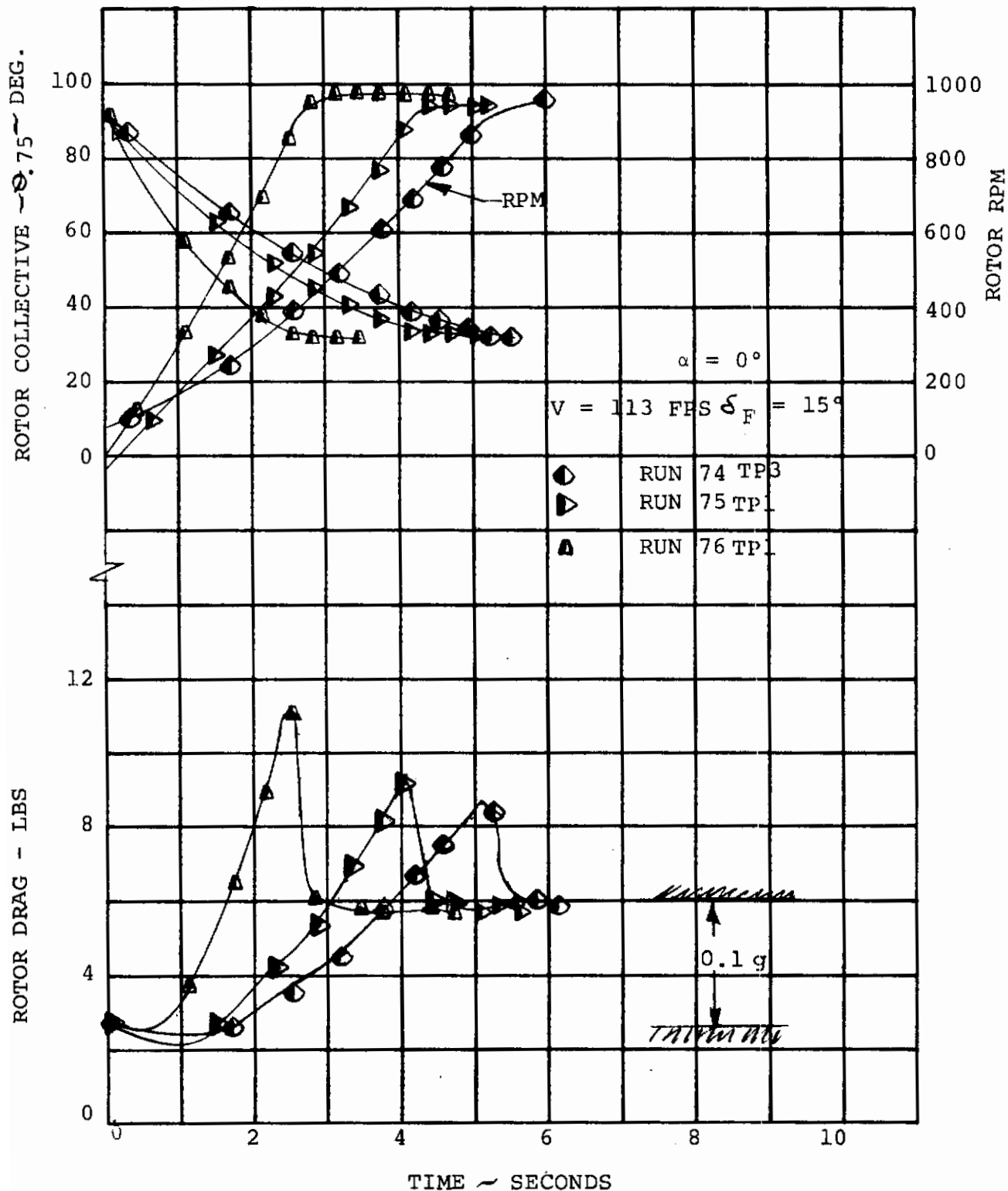


FIGURE 5-16 EFFECT OF COLLECTIVE RATE ON ROTOR DRAG  
 DURING SPINUP AT 113 FPS  $\alpha=0^\circ \delta_F=15^\circ$   
 (LINEAR COLLECTIVE RATE)

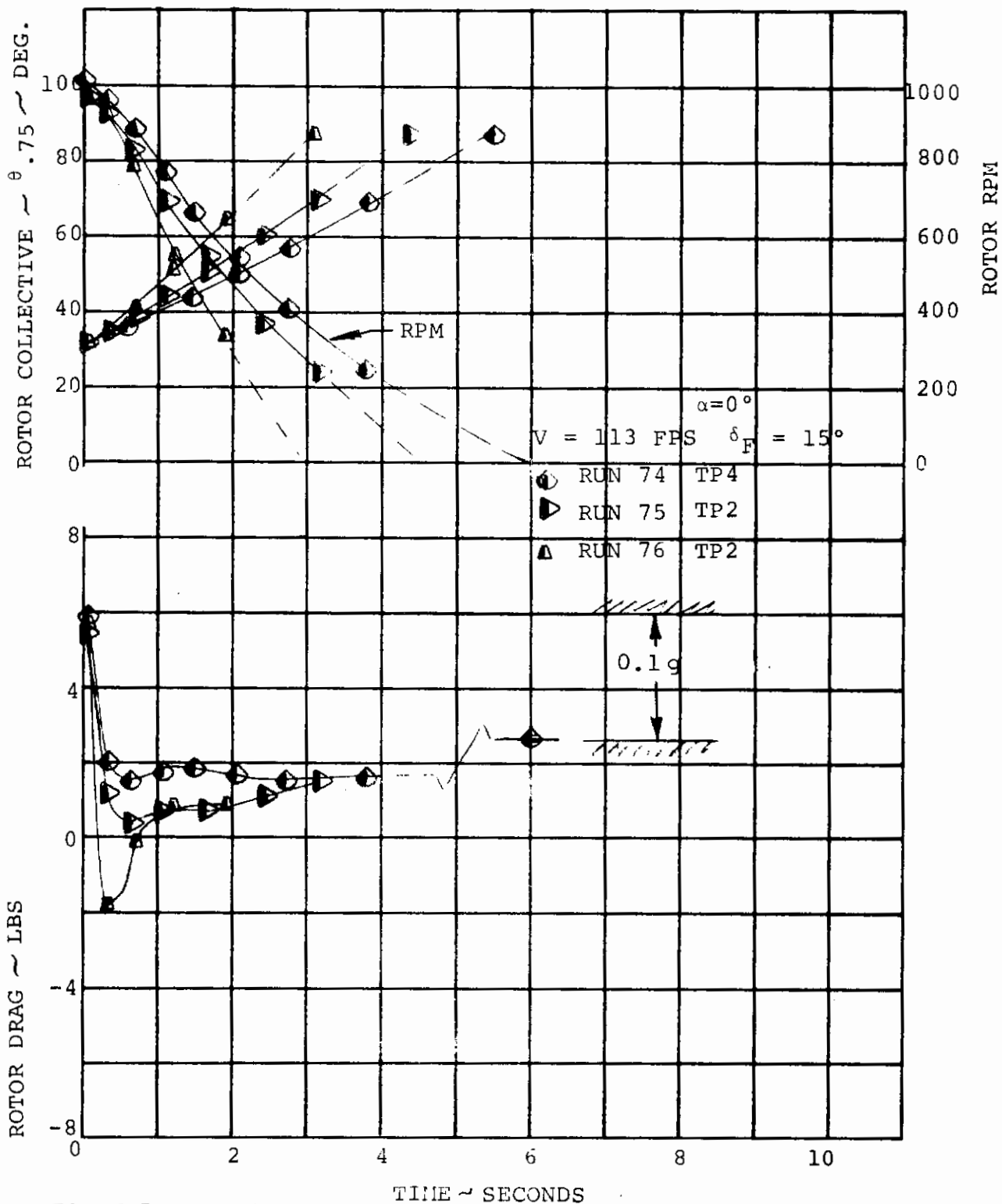


FIGURE 5-17 EFFECT OF COLLECTIVE RATE ON ROTOR DRAG DURING FEATHER AT  $V = 113 \text{ FPS}$   $\alpha = 0^\circ$   $\delta_F = 15^\circ$

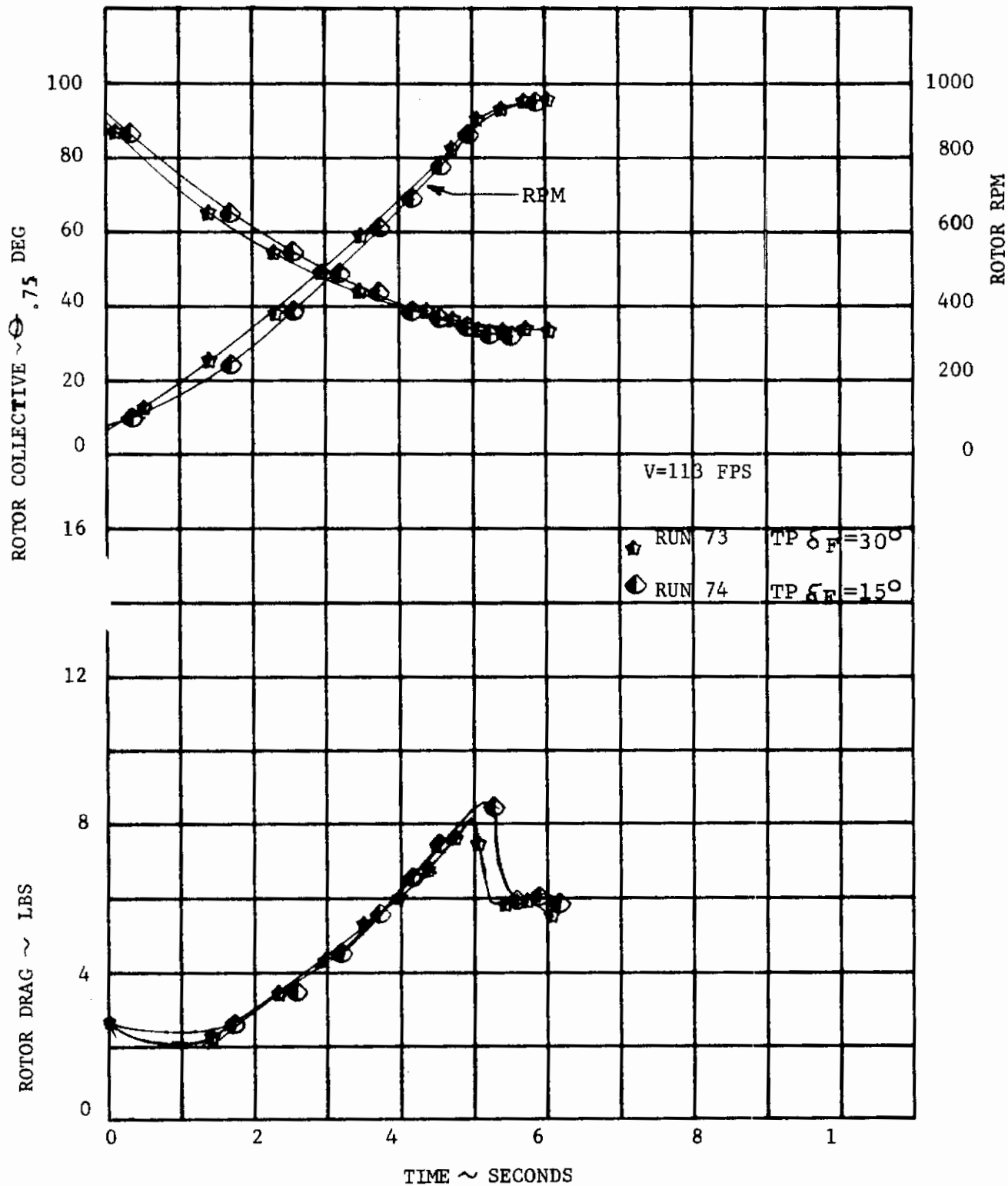


FIGURE 5-18 EFFECT OF FLAP DEFLECTION ON ROTOR DRAG  
 DURING SPINUP AT  $V = 113 \text{ FPS}$   $\alpha = 0^\circ$   
 (LINEAR COLLECTIVE RATE)

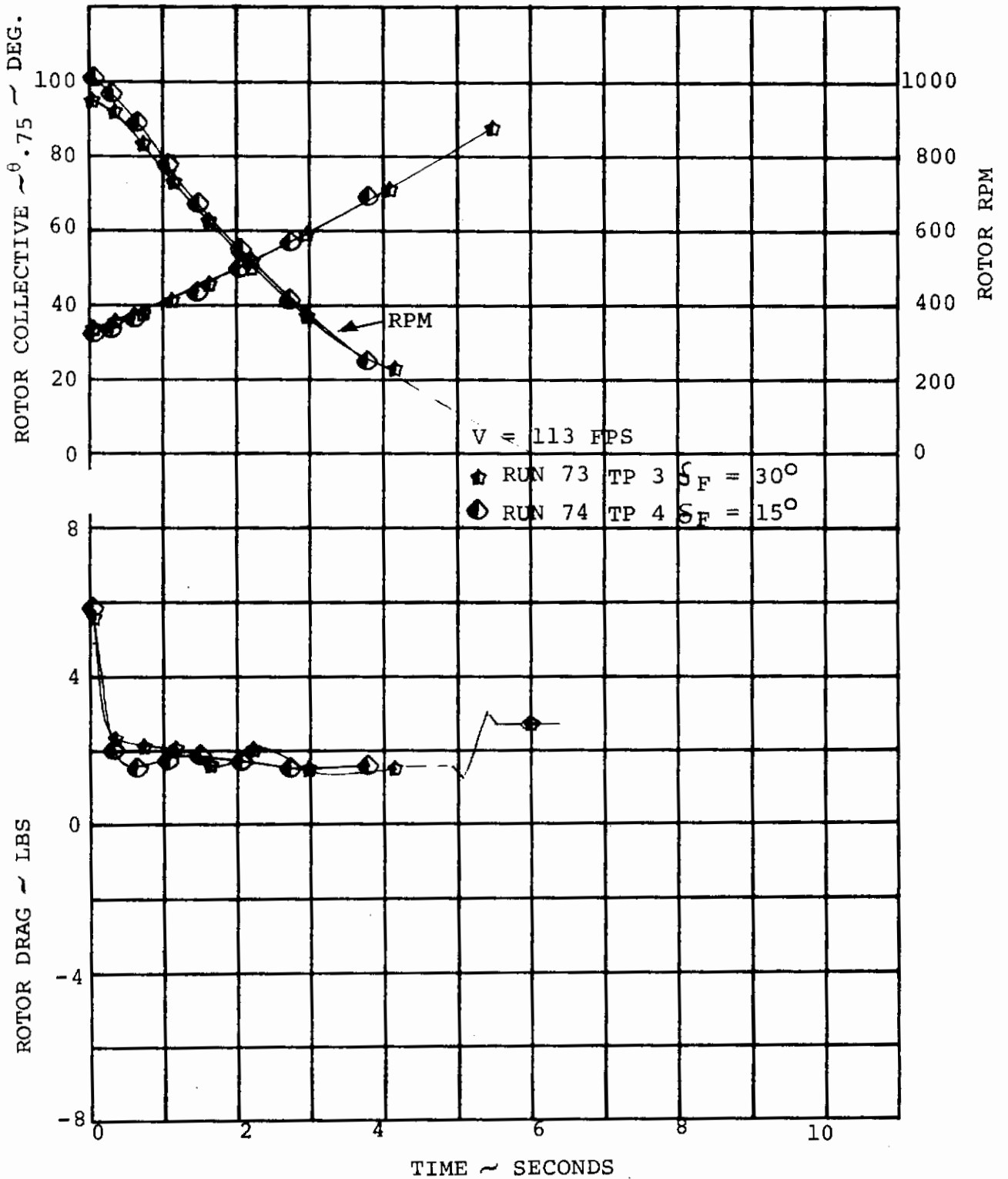


FIGURE 5-19 EFFECT OF FLAP DEFLECTION ON ROTOR DRAG DURING FEATHER AT  $V = 113$  FPS  $\alpha = 0^\circ$  (LINEAR COLLECTIVE RATE)

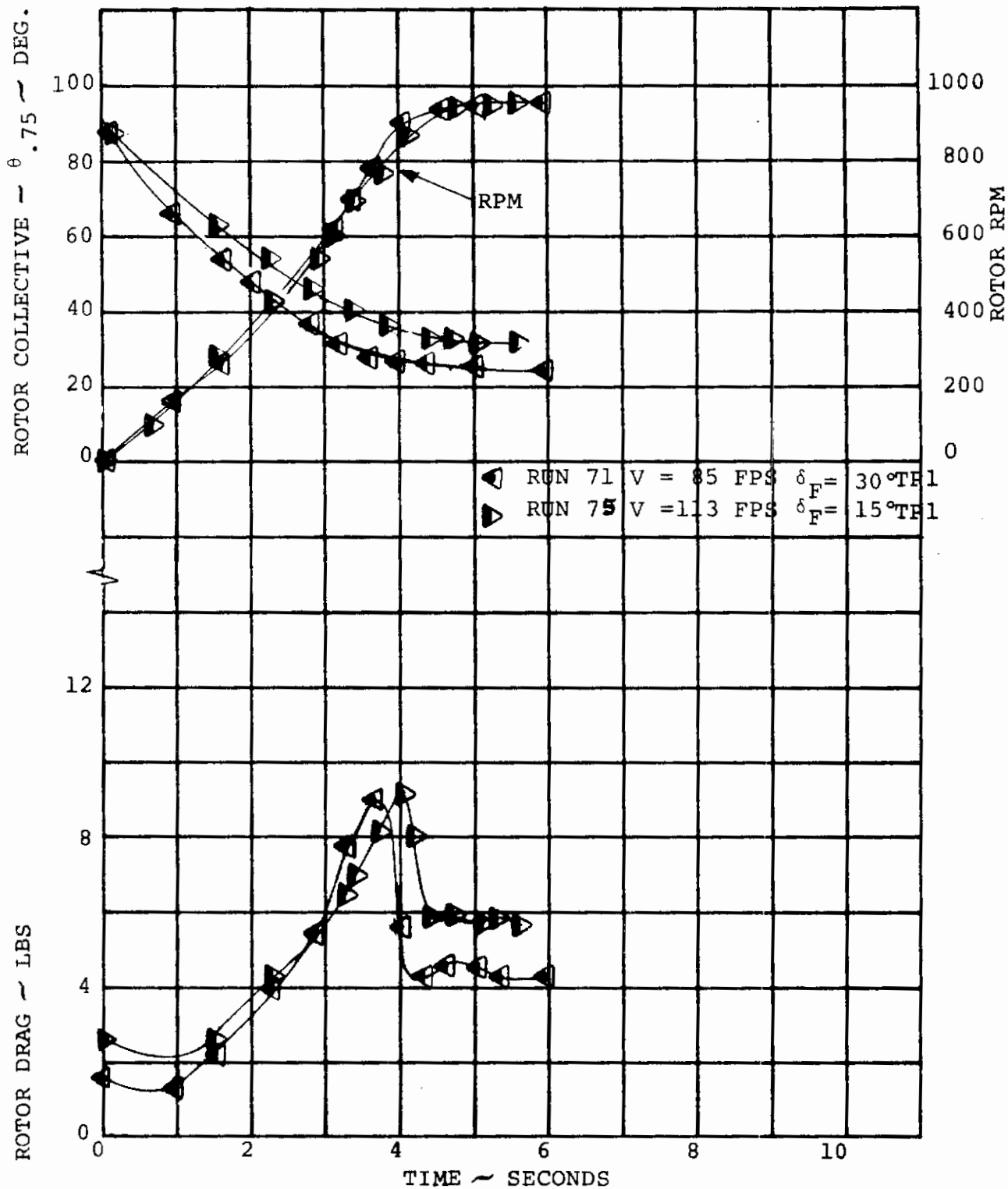


FIGURE 5-20 EFFECT OF FORWARD SPEED ON ROTOR DRAG DURING SPINUP FOR 4.5 SECOND LINEAR COLLECTIVE RATE, FINAL RPM = 950



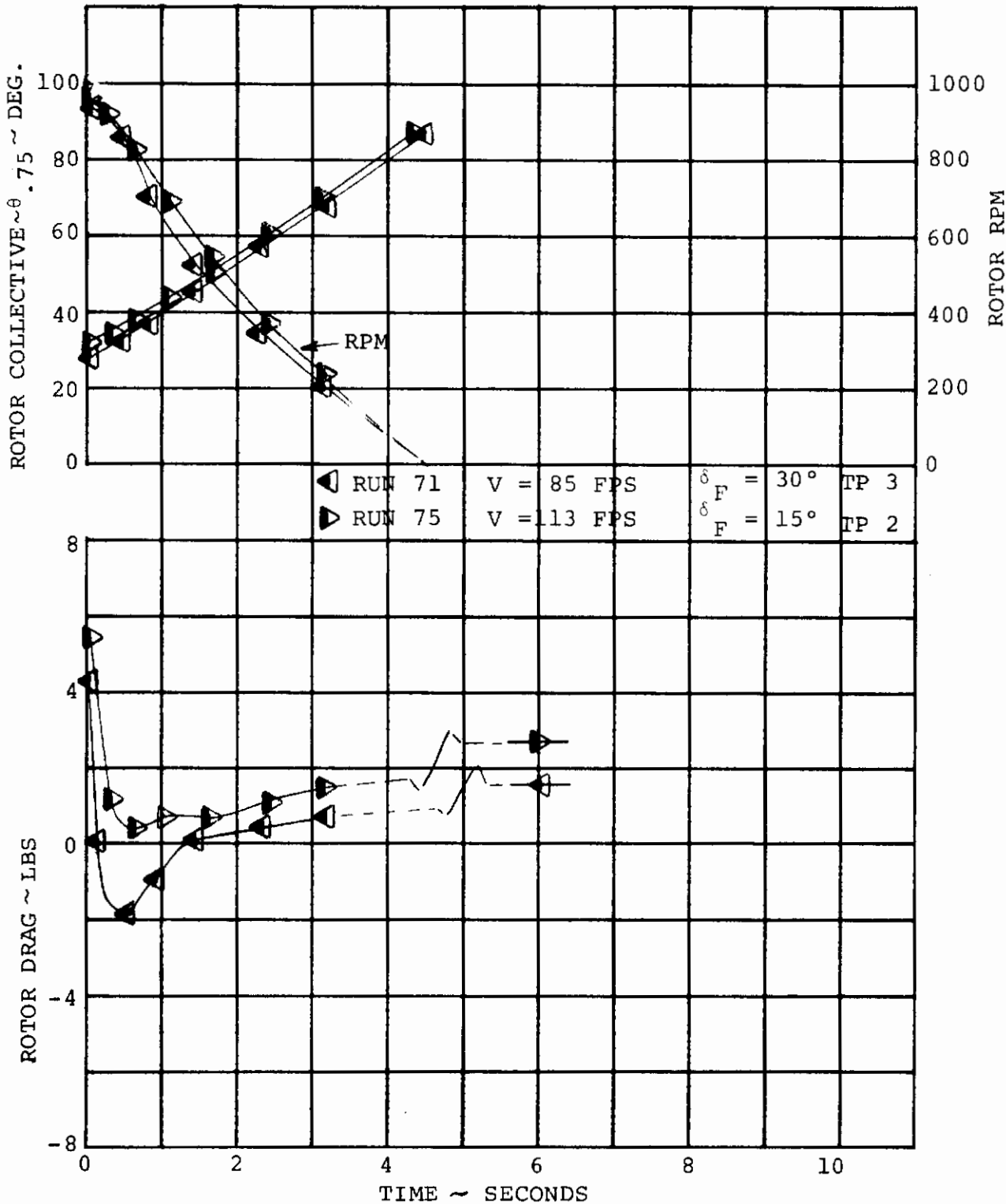


FIGURE 5-21 EFFECT OF FORWARD SPEED ON ROTOR DRAG DURING FEATHER FOR 4.5 SECOND LINEAR COLLECTIVE RATE  
 $\alpha = 0$  INITIAL RPM = 950

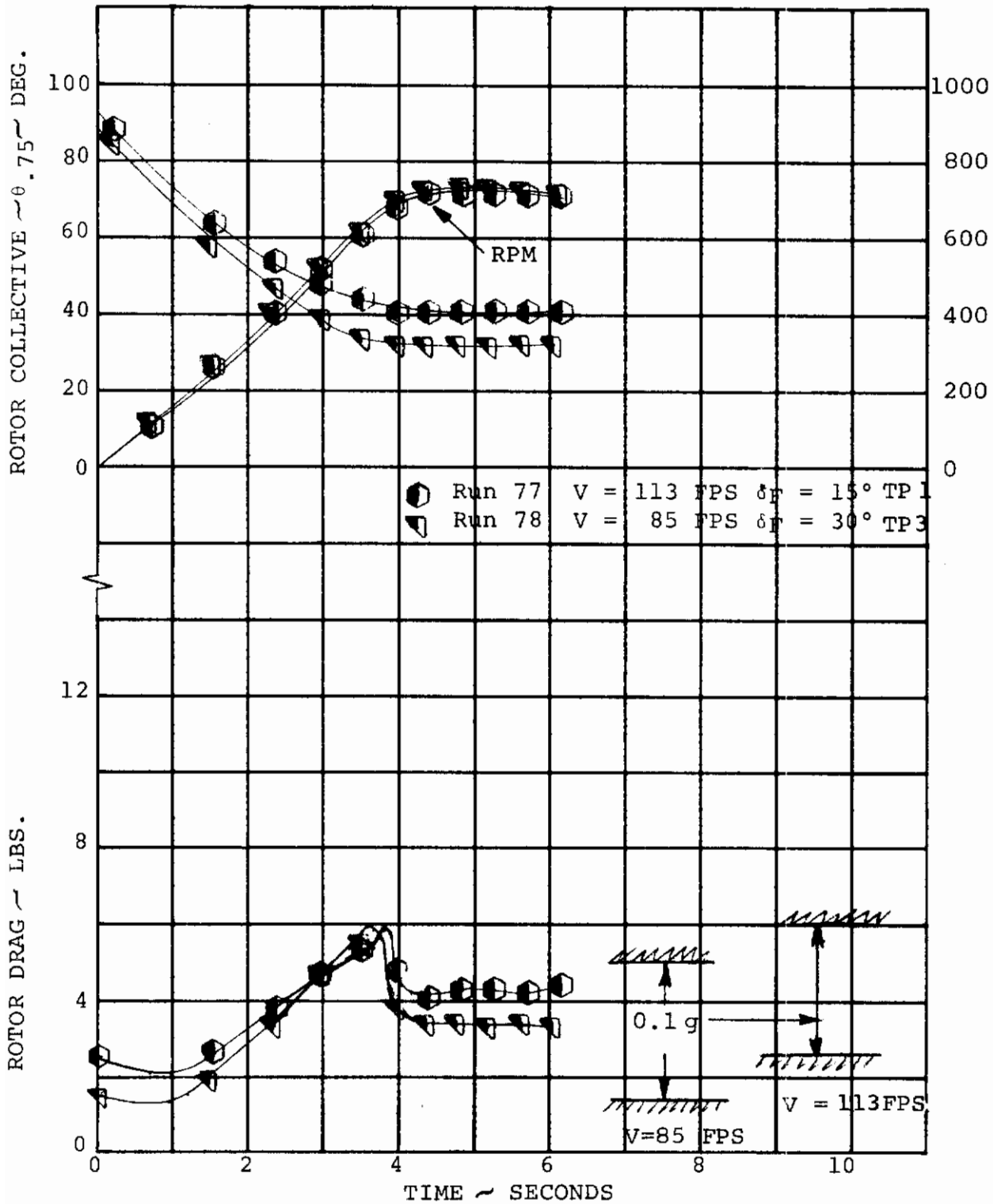


FIGURE 5-22 EFFECT OF FORWARD SPEED ON ROTOR DRAG DURING SPINUP FOR 4.5 SECOND LINEAR COLLECTIVE RATE, FINAL RPM = 715

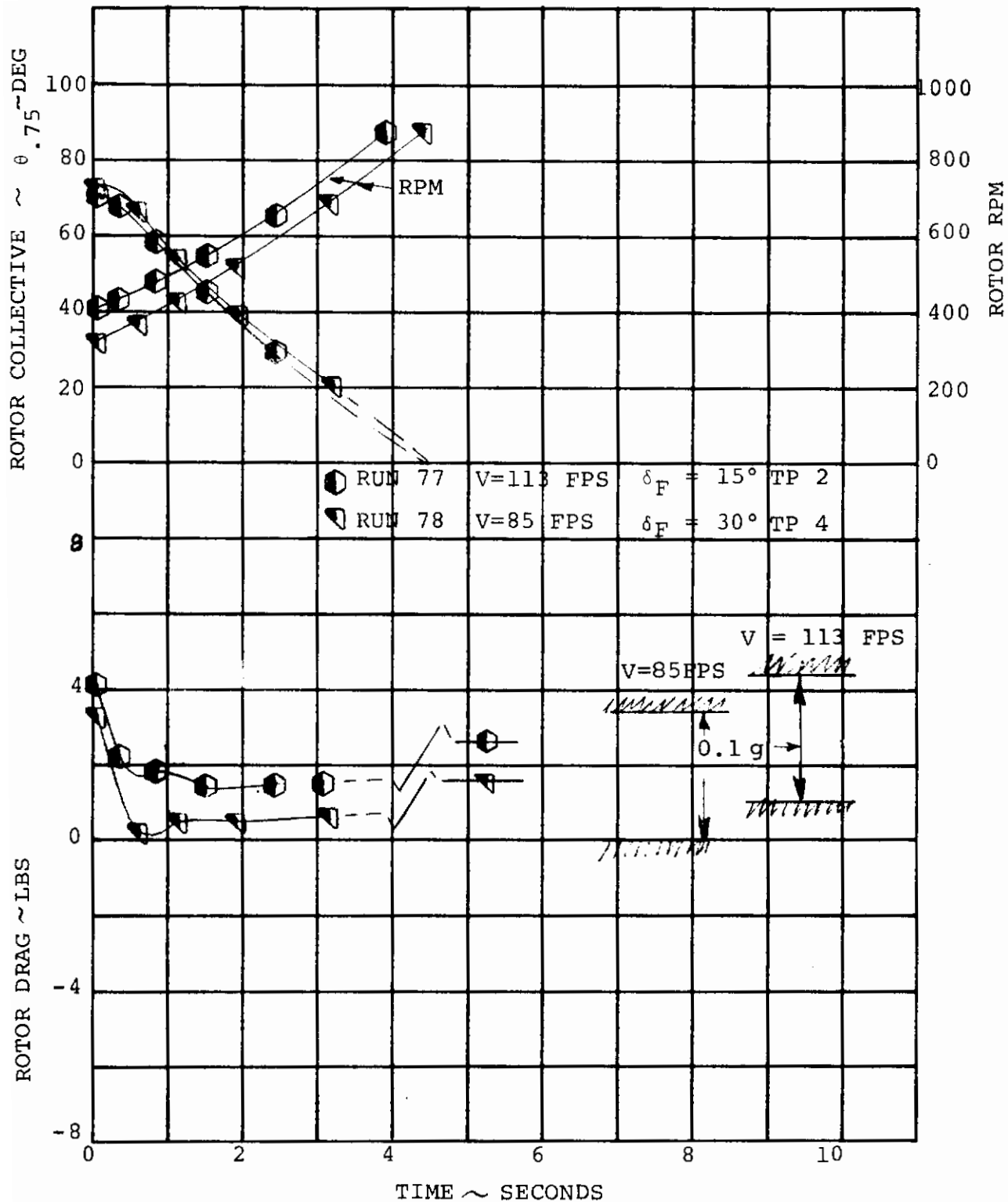
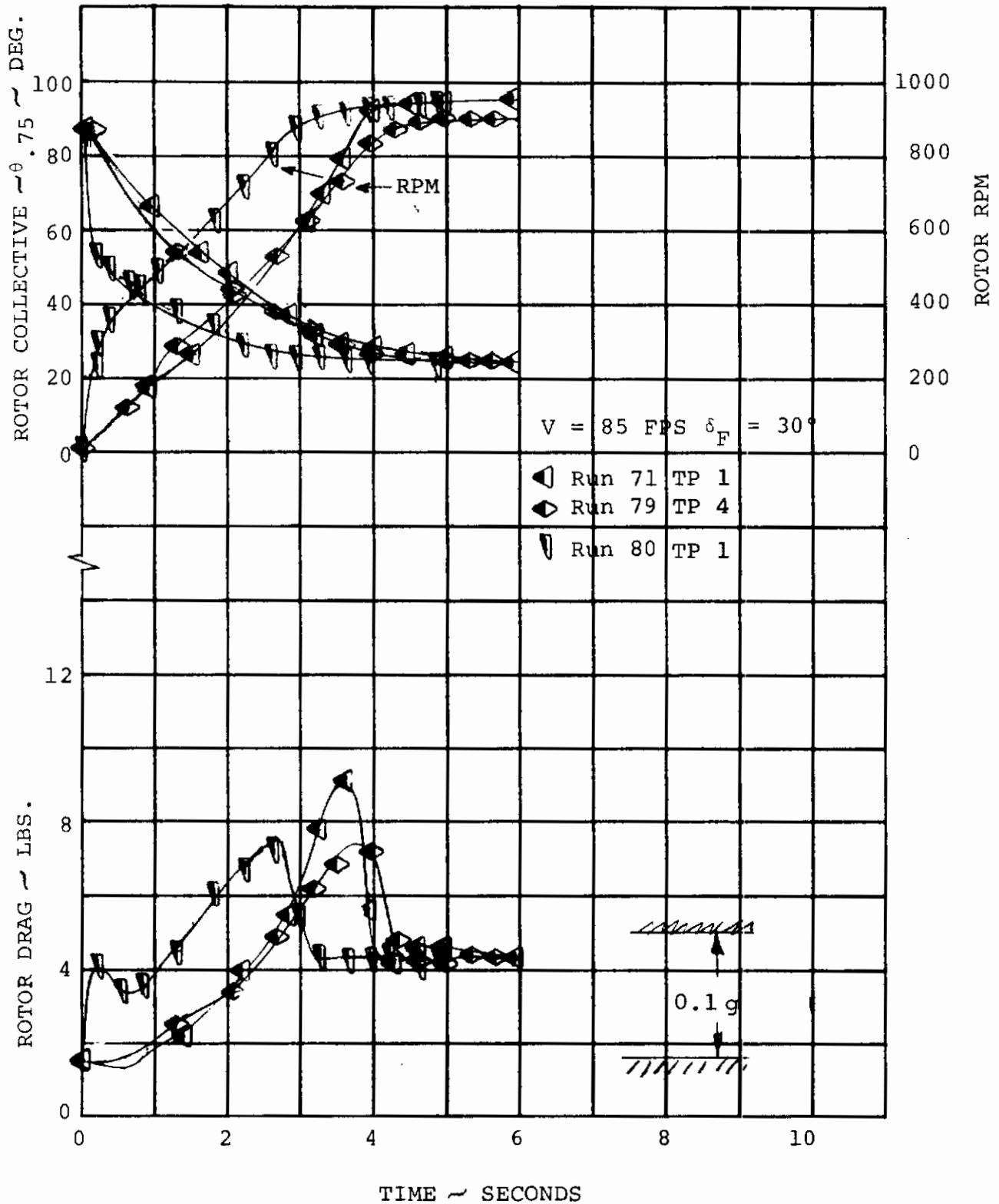


FIGURE 5-23 EFFECT OF FORWARD SPEED ON ROTOR DRAG DURING FEATHER FOR 4.5 SEC LINEAR COLLECTIVE RATE, INITIAL RPM = 715

# Contrails



TIME ~ SECONDS

FIGURE 5-24 COMPARISON OF LINEAR AND PARABOLIC COLLECTIVE RATES FOR SPINUP  $V = 85 \text{ FPS}$   
FINAL RPM = 950

# Contrails

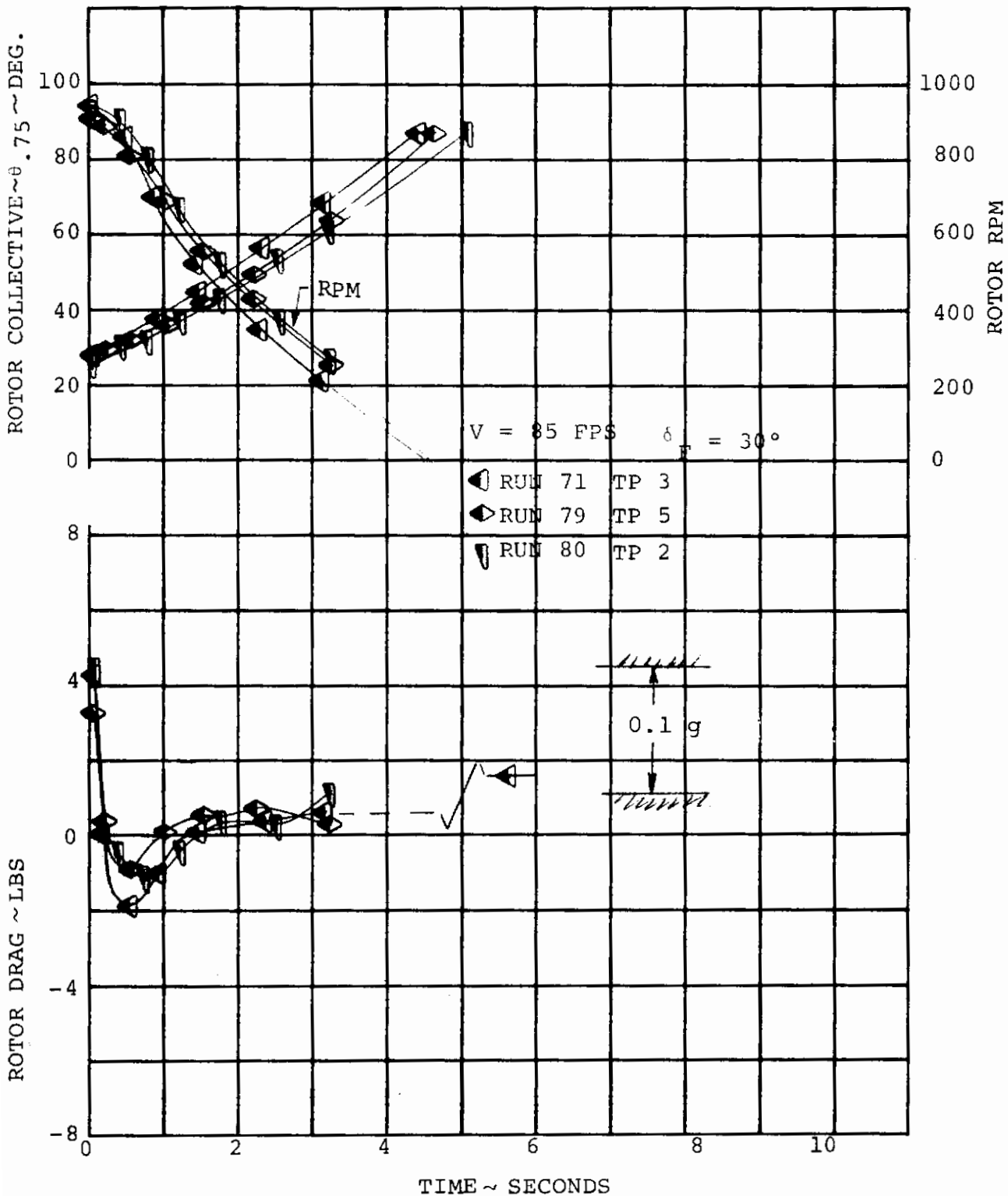


FIGURE 5-25    COMPARISON OF LINEAR AND PARABOLIC COLLEC-  
 TIVE RATES FOR FEATHER  
 $V = 85 \text{ FPS}$     INITIAL RPM=950

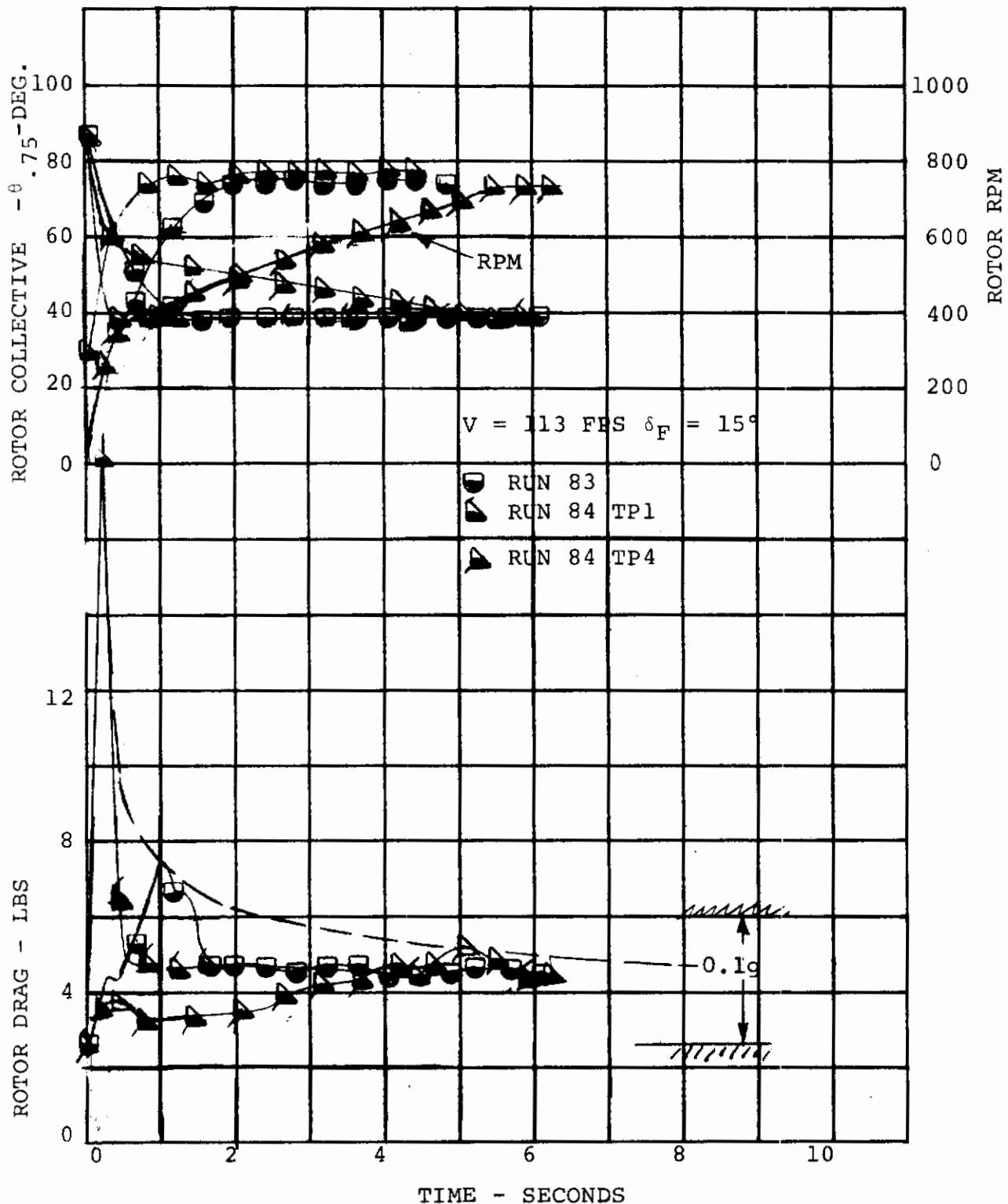


FIGURE 5-26 COMPARISON OF VARIOUS PARABOLIC COLLECTIVE RATES FOR SPINUP  
 V = 113 FPS FINAL RPM = 715

# Contrails

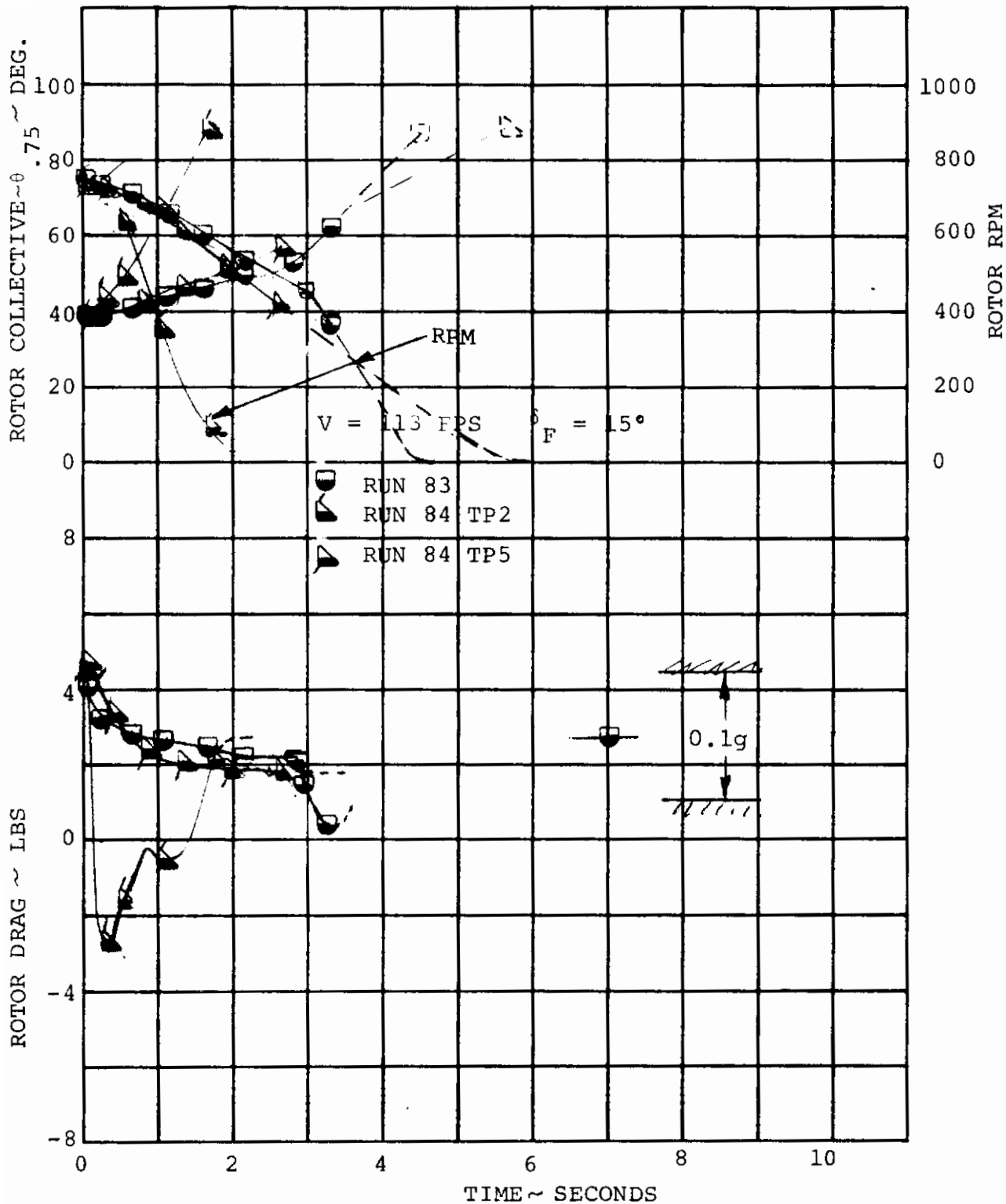


FIGURE 5-27 COMPARISON OF VARIOUS PARABOLIC COLLECTIVE RATES FOR FEATHER  $V = 113 \text{ FPS}$  INITIAL RPM 715

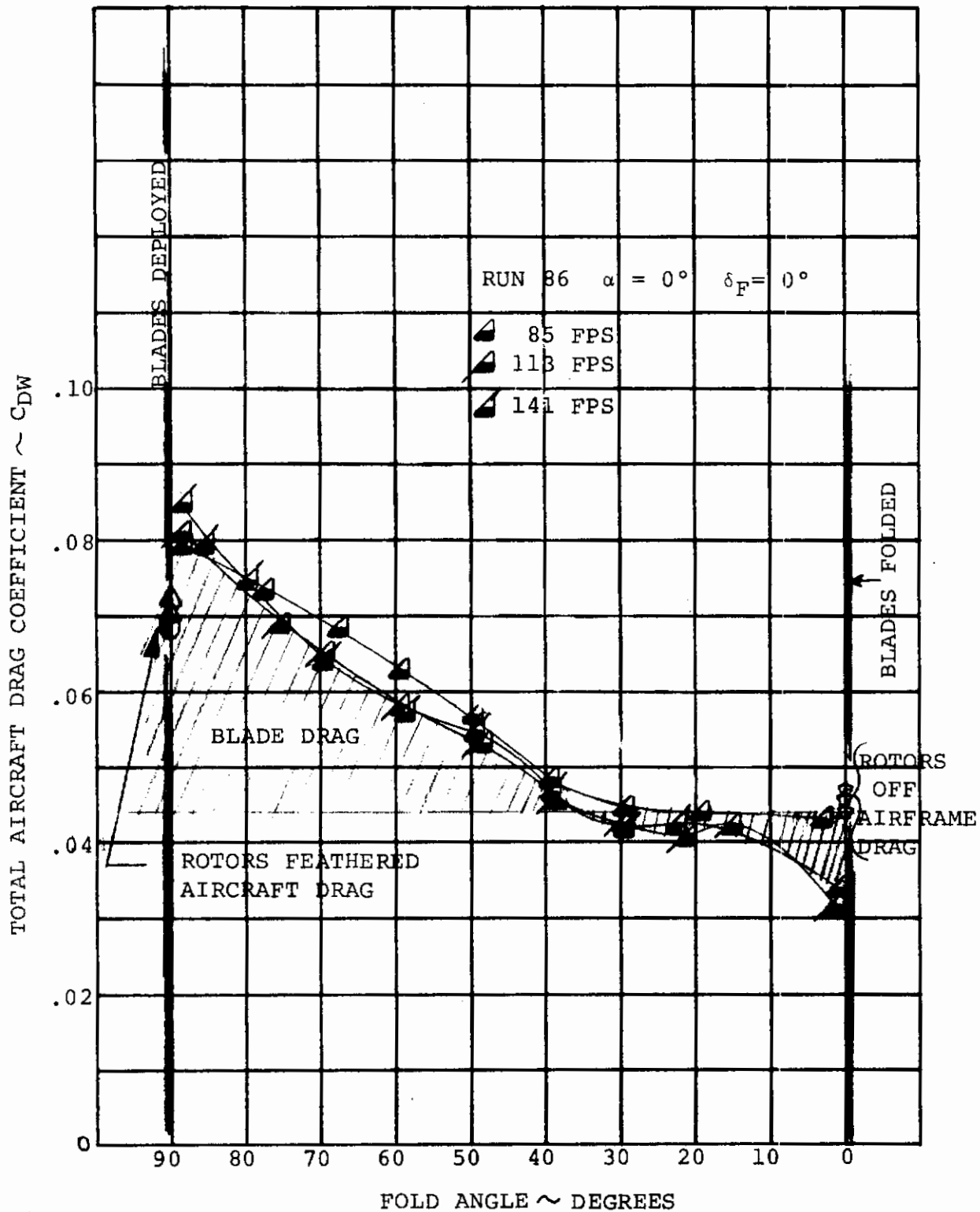


FIGURE 5-28 AIRCRAFT DRAG VARIATION WITH BLADE FOLDING AT  $\alpha = 0^\circ$   $\delta_F = 0^\circ$  (FLATWISE FOLD)



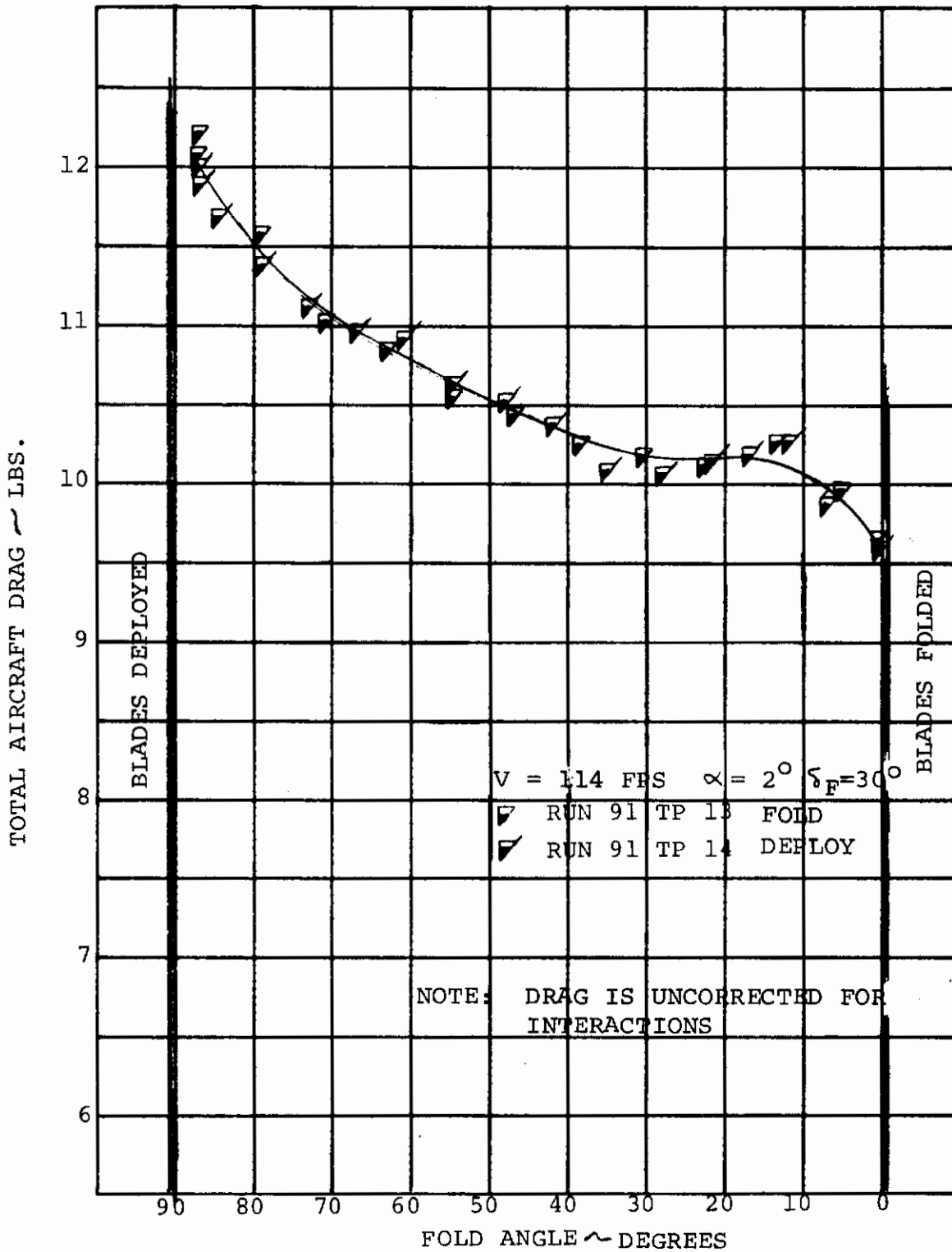


FIGURE 5-29. TOTAL AIRCRAFT DRAG VARIATION DURING 3 SECOND TRANSIENT FOLD AND DEPLOY

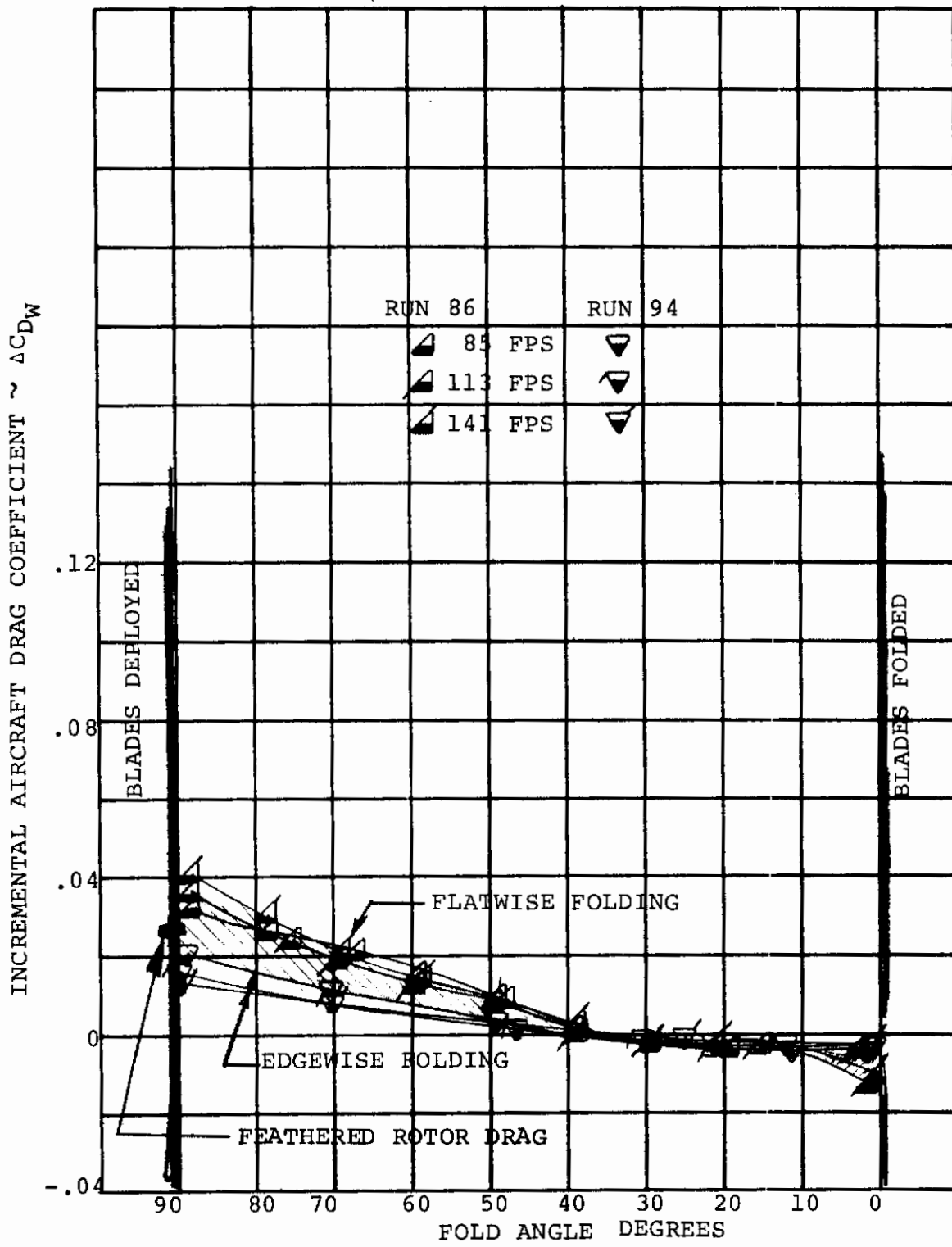


FIGURE 5-30 COMPARISON OF EDGEWISE AND FLATWISE BLADE FOLDING DRAG LEVELS  $\alpha = 0^\circ$   $\delta_F = 0^\circ$

## 5.4 Conclusions - Performance

Analysis of the performance test data presented here allows the following conclusions to be made:

### Windmilling

1. Flap setting effects on rotor axial force are small.
2. The rotor has a small effect on the aircraft lift and pitching moment but a large effect on drag.
3. Prediction of the rotor speed variation with airspeed and collective pitch in steady windmilling agrees with test.

### Spinup/Feather

1. A 3 to 4 second spinup/feather with a linear collective schedule will meet the 0.1g transient force criteria if the cycle is started at 70% hover RPM.
2. A small further reduction in drag transient can be obtained from a non-linear schedule.
3. Low accelerations can also be achieved from 100% hover RPM by using simple thrust modulation to balance the changes in steady drag between the windmilling and feathered configurations.

### Folding/Deploy

1. Flatwise blade folding provides a minimum drag configuration.

## 6.0 STABILITY

The following three areas of the conversion process were tested in Test Program III to obtain stability data for the 1/9 scale conversion model:

- ° Steady windmilling
- ° Spinup and feather
- ° Blade fold and deployment

These three areas will be discussed in the following sections. The analysis of the transient operation of spinup/feather and blade fold/deploy will address those schedules recommended Section 5.

### 6.1 Steady State Windmilling Stability

When the transition is completed, nacelle incidence is zero and the conversion can be made to the cruise configuration for the Model 213. The conversion is initiated by reducing collective and power to the rotor, thus operating in the steady windmilling state before the transient feather is initiated. Conversely, the conversion from the cruise configuration has steady windmilling as the last step before power and collective are increased to initiate transition. Steady windmilling stability characteristics are representative of cruise for the tilt rotor mode of operation and serve as a base for comparison for the transient spinup and feather. The data analysis presented here addresses the airframe (wing and nacelle) and the rotor separately and then together as the aircraft.

Airframe characteristics, shown in Figures 6-1 and 6-2, present the lift variation with angle of attack and the aircraft pitching moment variation with lift. This indicates that the aerodynamic center of the wing nacelle combination is approximately 9 percent ahead of the quarter chord when the flaps are retracted. As the flaps are deflected to 15, 30 and 45 degrees, the aerodynamic center moves aft and is only 4 percent ahead of the quarter chord, thereby decreasing the unstable characteristics of the plain wing/nacelle. The influence of the nacelle produces the major portion of the unstable characteristics and results in the forward location of the aerodynamic center at 16 percent of the MAC.

# Contrails

The rotor was then installed and the model was tested in steady windmilling to define the rotor stability characteristics in conversion as well as provide an insight into the rotor derivatives representative of the cruise mode for this soft inplane rotor. The rotor contribution to airplane stability is large and for flexible rotors the major rotor terms are dependent upon the out-of-plane flapping of the blades as shown theoretically and experimentally in References 2 and 3. The test model of Reference 3 was stiff inplane with an inplane or lag frequency of 1.7 or 2.0 compared to the test model of this report where  $\frac{\omega}{n} < 1.0$  at near design RPM. The soft inplane rotor, as tested in this case, has a further major contribution to the rotor derivatives. The lag-flap coupling of the rotor radically changes the out-of-plane ( $\omega$  flap) response of the rotor blades to one per rev disturbances (e.g., angle of attack) especially in the region of the RPM spectrum close to the lag natural frequency ( $\omega$  lag). A theoretical plot of the blade out-of-plane response for different lag frequencies is shown in Figure 6-3A and is included to serve as an introduction to the rotor derivative data obtained. The test rotor traverses the range of lag frequencies from stiff inplane at low RPM to soft inplane in excess of 600 RPM.

Figures 6-3 through 6-6 present the variation of rotor force and moment characteristics with rotor RPM at a fuselage attitude of 4 degrees and zero flap deflection. Similar data obtained at other angles of attack and flap deflection are included in Appendix B. Figure 6-3 presents the rotor pitching moment coefficient variation with RPM. There is a peak in the coefficient at 200 RPM; it rapidly decreases to a minimum at approximately 600 RPM then increases sharply to approximately 850 RPM and then it levels off. Nondimensionalizing by rotor tip speed causes the apparent peak in the coefficient at 200 RPM when there is a peak between 300 and 400 RPM in the absolute pitching moment. This peak occurs in the same RPM region as the wing vertical bending natural frequency. The minimum shown at approximately 600 RPM appears to be the result of passing through the 1/rev first rotor mode crossover which is the lag mode for this rotor. A description of blade natural frequencies is given in Section 7.1 and in Figure 7.1. The "lag mode" here refers to the in-plane mode. This produces a change in rotor flapping resulting from this lag/flap coupling. Normal force coefficient variation with RPM, presented in Figure 6-4, shows a rapid decrease with increasing RPM up to approximately 600. The slope becomes almost zero and then drops off rapidly as the RPM is increased by 950. The plateau illustrates the effect of passing through the 1/rev lag frequency crossover. Figure 6-5 presents the yawing moment coefficient

# Contrails

variation with rotor RPM. Here is a complete reversal in the trend of yawing moment with RPM between 500 and 700 RPM. This appears to be caused by the 1/rev lag frequency crossover producing a change in the flapping phase angle from the second/fourth to the first/third quadrant of the rotor disc. The pitching moment, presented in Figure 6-3, goes from positive to negative at approximately 500 RPM and remains negative until approximately 700 RPM indicating this phase shift in the flapping. Figure 6-6 shows the rotor sideforce variation with RPM. There is a distinct bucket at 600 RPM again indicating the impact of the 1/rev lag frequency crossover. These trends are typical for the data obtained at other positive angles of attack and flap deflections. The trends for negative angle of attack are inverted.

Since the model was quite flexible, a deflection test was conducted to define the incremental pitch and yaw angle changes induced by the aerodynamic loads developed by the wing and the rotor. The deflection test data is included in Appendix A. This provided the information to correctly define the nacelle angle of attack. Utilizing this angle of attack and the rotor characteristics of Appendix B, rotor derivatives could be obtained. Figures 6-7 to 6-14 present the rotor pitching moment coefficient variation with angle of attack at 85, 113 and 141 fps forward speed for 600, 700, 800, 900 and 950 RPM for zero flap deflection and 600, 800, and 950 RPM for 30 degrees flap deflection. At 600 RPM the pitching moment derivatives are highly stable (-.000103 to -.000197) and as the RPM increases these derivatives become unstable (+.000047 to +.000089) as in Figures 6-7 to 6-11. Deflecting the flap to 30 degrees increases the derivative in the unstable direction as indicated by the derivatives at 600 RPM (-.000094 to -.000160) in Figure 6-12. A summary of the pitching moment derivative ( $\partial C_{PM}/\partial \alpha$ ) variation with RPM and forward speed is presented in Figure 6-15 for the zero flap deflection.

The rotor normal force coefficient trend with nacelle angle of attack at constant rotor RPM is presented in Figures 6-16 to 6-20 for forward speeds of 85, 113 and 141 fps and zero flap deflection. There is almost no change in the slope of normal force coefficient with angle of attack between 600 and 700 RPM. As the RPM is further increased, the slope decreases rapidly. This indicates that the 1/rev lag frequency crossover causes a leveling or reduction in the normal force derivative with RPM.

# Contrails

Figures 6-21 to 6-23 present the normal force/angle of attack variation for a 30 degree flap deflection. This data indicates that flap deflection increases the normal force derivatives. A summary of the normal force derivatives for zero flap deflection is presented in Figure 6-24. Additional data has been added which indicates that the derivative decreases with RPM from 400 to 500 RPM then changes slope from negative to positive up to 700 RPM then a negative slope is shown between 700 and 950 RPM. The plateau is a result of the 1/rev lag frequency crossover.

Rotor yawing moment coefficient variation with angle of attack for specific rotor speeds are shown in Figures 6-25 to 6-29 for zero flap deflection. The data indicates that there is a sharp increase in the rotor yawing moment derivative between 600 and 700 RPM. As the rotor speed is increased further to 950 RPM, the derivative becomes smaller. The trend of the yawing moment derivative resembles the trend of the coefficient with RPM for a fixed angle as discussed earlier. The change in the trend is a result of the change in flapping phase angle which results in a change in the yawing moment derivative slope with RPM between 500 and 700 RPM. Yawing moment/nacelle angle of attack variations for 30 degrees flap deflection are presented in Figures 6-30 to 6-32. This indicates flap deflection increases the magnitude of the derivatives. A summary of the derivatives of zero degrees flap deflection is presented in Figure 6-33.

Rotor side force coefficient variation with nacelle angle of attack is presented in Figures 6-34 to 6-38 for zero flap deflection. At 600 RPM there is a large negative derivative that diminishes and becomes positive as the RPM is increased. There is just a slight effect of the flap deflection on the side force derivative as indicated by Figures 6-39 to 6-41. A summary of the rotor side force derivatives is presented in Figure 6-42 to define the variation with rotor RPM with zero flap deflection.

As indicated in the data presented in Figures 6-7 through 6-42, there is a definite increase in the magnitude of the rotor derivatives with flap deflection. This is a trend similar to that shown on the 1/10 scale performance model tested in Test Program II, indicating that the wing circulation produces a change in the local flow through the rotor disc resulting in increased rotor derivatives. To define the circulation effects and establish the rotor derivatives without circulation effects, the rotor data was plotted against airframe lift for constant nacelle angles of attack at various flap deflections. Figures 6-43 through 6-47 present the pitching moment coefficient variation with airframe lift coefficient ( $C_{LA}/C_{L-Rotors}$ ) for a forward speed of 113 fps

at rotor speeds of 600, 700, 800, 900 and 950 RPM. This indicates the influence of lift producing a negative increment in pitching moment at 600 RPM but produces a positive increment at the higher RPM (700 to 950). Extrapolating these constant nacelle angle of attack lines back to zero lift provides the pitching moment variation without any circulation, thereby defining the derivatives equivalent to an isolated rotor. This was repeated for the rotor normal force, yawing moment and side force at forward speeds of 85, 113 and 141 fps and is included in Appendix C. The rotor derivatives without circulation effects were then defined and are presented in Appendix D. Figures 6-48 through 6-51 present a few of the curves from Appendix D to provide a basis for comparison with data that include the circulation effects that were presented earlier in this section. Pitching moment variation with angle of attack at the rotor speeds associated with the 1/rev lag frequency crossover (600 RPM) and the maximum tested (950 RPM) are presented in Figures 6-48 and 6-49 respectively. The corresponding normal force variations with angle of attack are shown in Figures 6-50 and 6-51. A comparison of the derivatives obtained from these figures with the derivatives that include the circulation effects are tabulated below.

TABLE 6-1

WING CIRCULATION EFFECTS ON ROTOR DERIVATIVES

Coefficient	RPM	Circulation Effects	Derivatives		
			V=85 FPS	V=113 FPS	V=141 FPS
Pitching Moment	600	in	-0.00103	-0.000150	-0.000197
Pitching Moment	600	out	-0.000102	-0.000148	-0.000191
Pitching Moment	950	in	+0.000047	+0.000074	+0.000089
Pitching Moment	950	out	+0.000039	+0.000061	+0.000070
Normal Force	600	in	0.000194	0.000390	0.000656
Normal Force	600	out	0.000176	0.000358	0.000588
Normal Force	950	in	0.000075	0.000153	0.000280
Normal Force	950	out	0.000072	0.000144	0.000260

This comparison indicates that the wing circulation increases the pitching moment derivative by 1 to 27 percent and the normal force derivative by 4 to 12 percent. The circulation effect on the rotor forces and moments are a function of speed and lift coefficient; therefore, the impact on rotor derivatives would be a function of speed and lift curve slope.



# Contrails

For zero flap deflection the rotor derivative is a function of speed only since the lift curve slope is a constant. To verify this, the pitching moment derivatives without circulation were plotted against the derivatives with the circulation effects in Figure 6-52. This indicates one unique trend for rotor speeds of 85, 113 and 141 FPS. This trend has a slope of 0.93 and test derivative intercept of 0.000008. The shaded area between the line of exact agreement and the trend through the data is the wing circulation effect. A similar comparison is made for the normal force derivatives with and without circulation in Figure 6-53. Again there is a single trend for all rotor and forward speeds which also has a slope of 0.93 but has an intercept at zero test derivative. The comparison of the yawing moment derivative without and with circulation is presented in Figure 6-54. As with the normal force there is a single trend for all the rotor and forward speeds with a slope of 0.93 and an intercept at zero test derivative. Figure 6-55 presents the comparison of the side force derivatives without and with circulation effects. The slope is 0.93 but there is a test derivative intercept of 0.000015.

When the rotor characteristics are nondimensionalized by rotor tip speed there is a single trend that varies with advance ratio, as indicated in Section 5.1 for rotor axial force. If the circulation effects are nondimensionalized by tip speed they result in a quantity that is a function of advance ratio and lift coefficient; therefore, when comparing the derivatives it results in a function of advance ratio and lift curve slope. Since the rotor characteristics and the circulation effects vary as a function of advance ratio, the comparisons of Figures 6-52 to 6-55 show that the effect on the rotor coefficient derivative is a result of only the lift curve slope.

It is significant to note that both the pitching moment and the side force derivatives do not have zero intercepts in this comparison and they both result from the forces normal to the axis through the 0-180 azimuth. This would indicate that there is an influence of the yaw deflection in the pitch sweeps but removing this effect will result in a lateral shift in Figures 6-52 and 6-55 and the curves will have a zero test intercept.

A summary of the rotor derivatives without circulation effects is presented in Figures 6-56 through 6-59 for pitching moment, normal force, yawing moment and side force as influenced by rotor RPM. Imposed on these summary curves is a prediction of the derivatives by an analysis that accounts for the various mode shapes. The agreement is quite good and adequately accounts for the effects of the 1/rev first mode (lag) frequency crossover.

# Contrails

Combining the rotor and the airframe results in aircraft characteristics presented in Figures 6-60 and 6-61 for zero angle of attack and 30 degrees flap deflection. This configuration, typical for conversion at 200 knots, indicates that the rotor produces a small percentage of the lift and moment through the RPM range. The data presented so far has not included the effects of the tail on the total stability. To define the tail contribution as influenced by the wing, the tail lift is presented in Figure 6-62, as a function of wing lift for an angle of attack sweep without the rotor on. The slope of this curve when multiplied by the tail volume  $\bar{V} = \frac{(\text{tail area} \times \text{tail length})}{(\text{wing area} \times \text{wing chord})}$  defines the

moment contribution of the tail to stabilize the aircraft. Similar data is presented in Figure 6-63 for testing with the rotors on. There is no noticeable difference in the level or the slope indicating that the rotor does not significantly influence the tail for these data. This contribution of the tail is converted to an incremental moment contribution and shown on the buildup of the total aircraft moment/lift variation in Figure 6-64. This indicates that the airframe (less tail and rotors) is slightly unstable and the windmilling rotor increases the instability but the tail provides an adequate margin of stability. This buildup also indicates that the most aft cg for neutral stability is at 37 percent mac.

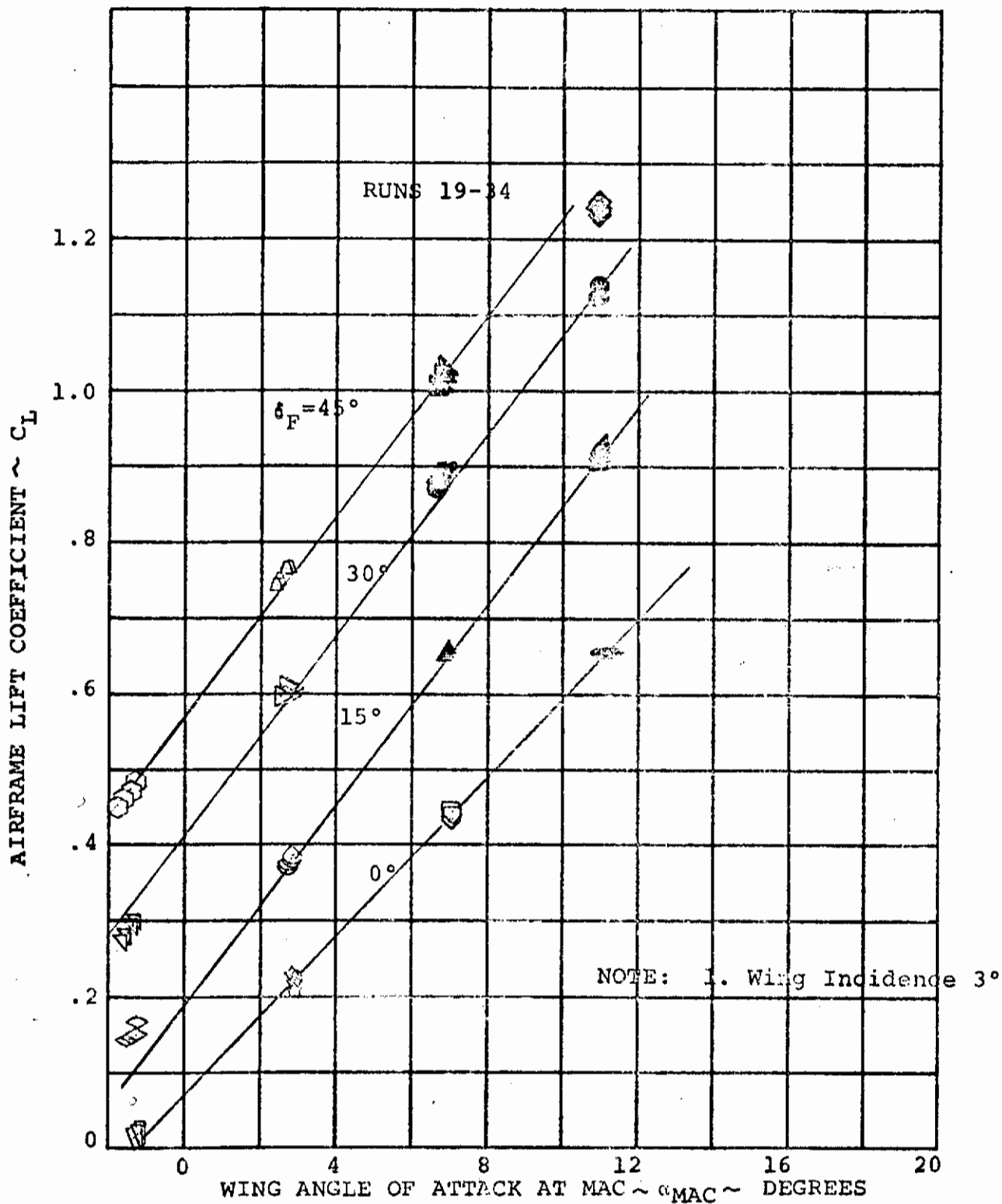


FIGURE 6-1 AIRFRAME LIFT/ANGLE OF ATTACK VARIATION FOR FLAP DEFLECTIONS OF 0°, 15°, 30°, 45°

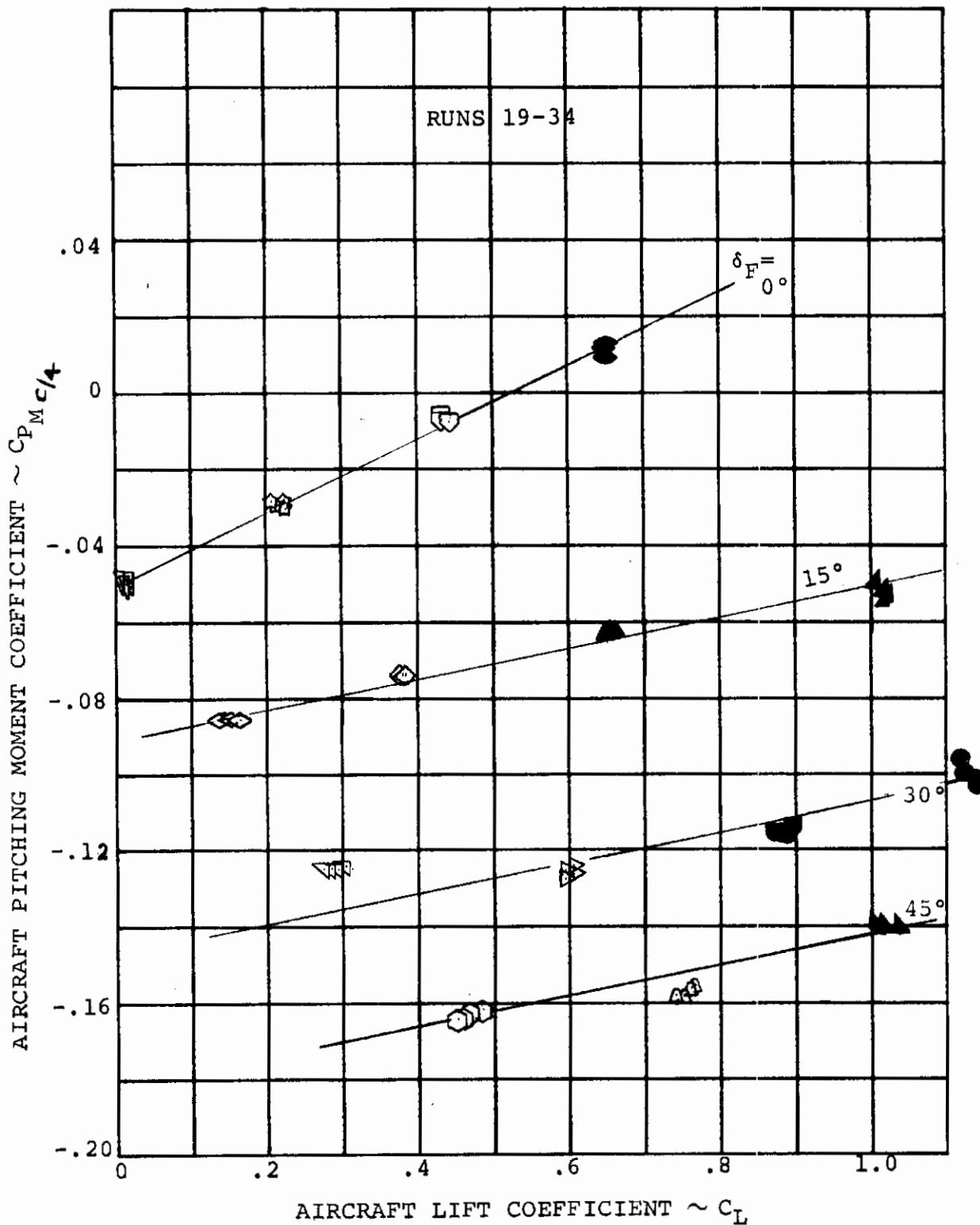


FIGURE 6-2 AIRFRAME PITCHING MOMENT/LIFT VARIATION FOR FLAP DEFLECTIONS OF  $0^\circ, 15^\circ, 30^\circ$  AND  $45^\circ$

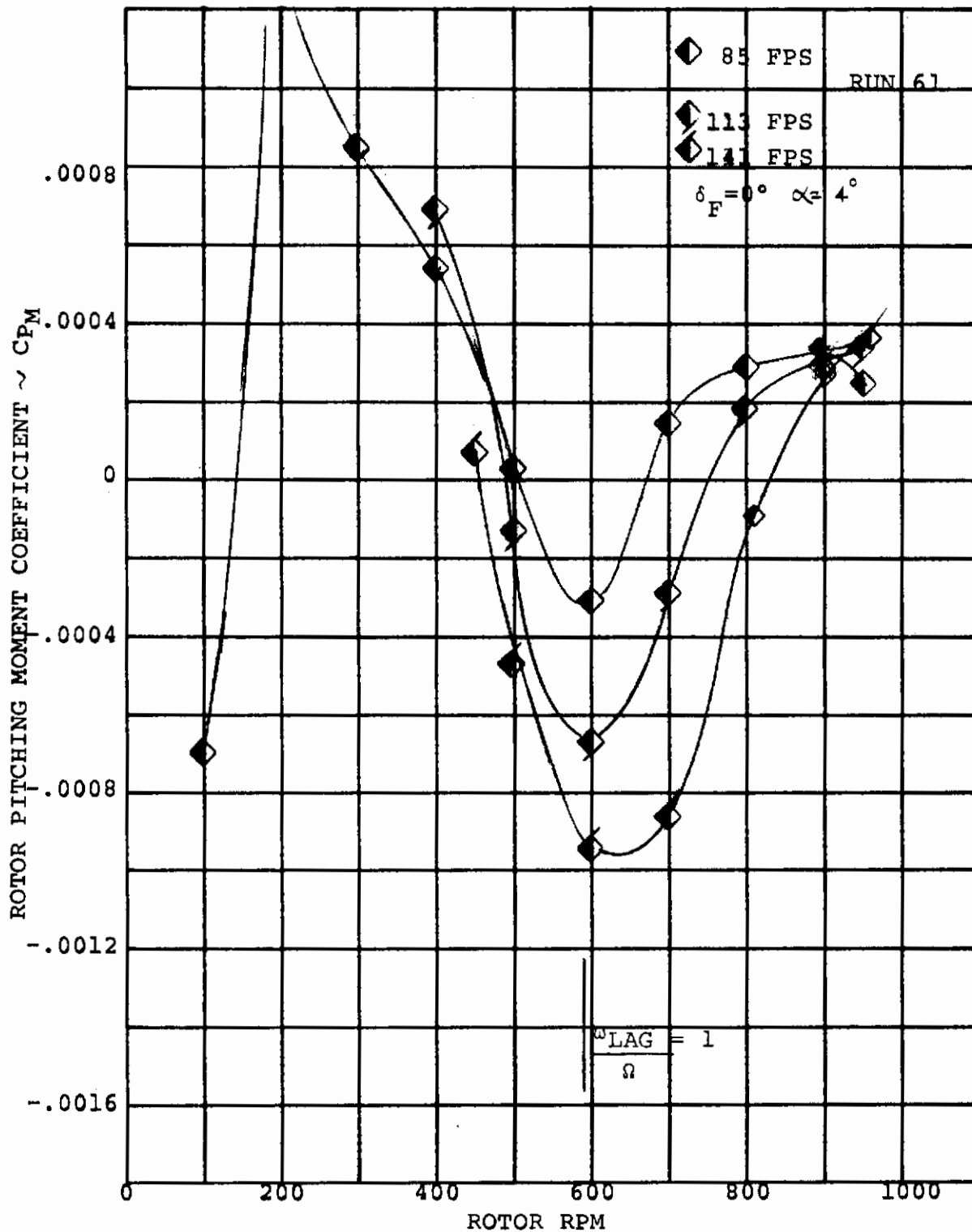


FIGURE 6-3 ROTOR PITCHING MOMENT/RPM VARIATION  
 FUSELAGE ATTITUDE =  $4^\circ$   $\delta_F = 0^\circ$   
 (STEADY WINDMILLING)

OUT OF PLANE FLAPPING  
PER DEGREE  $\alpha$

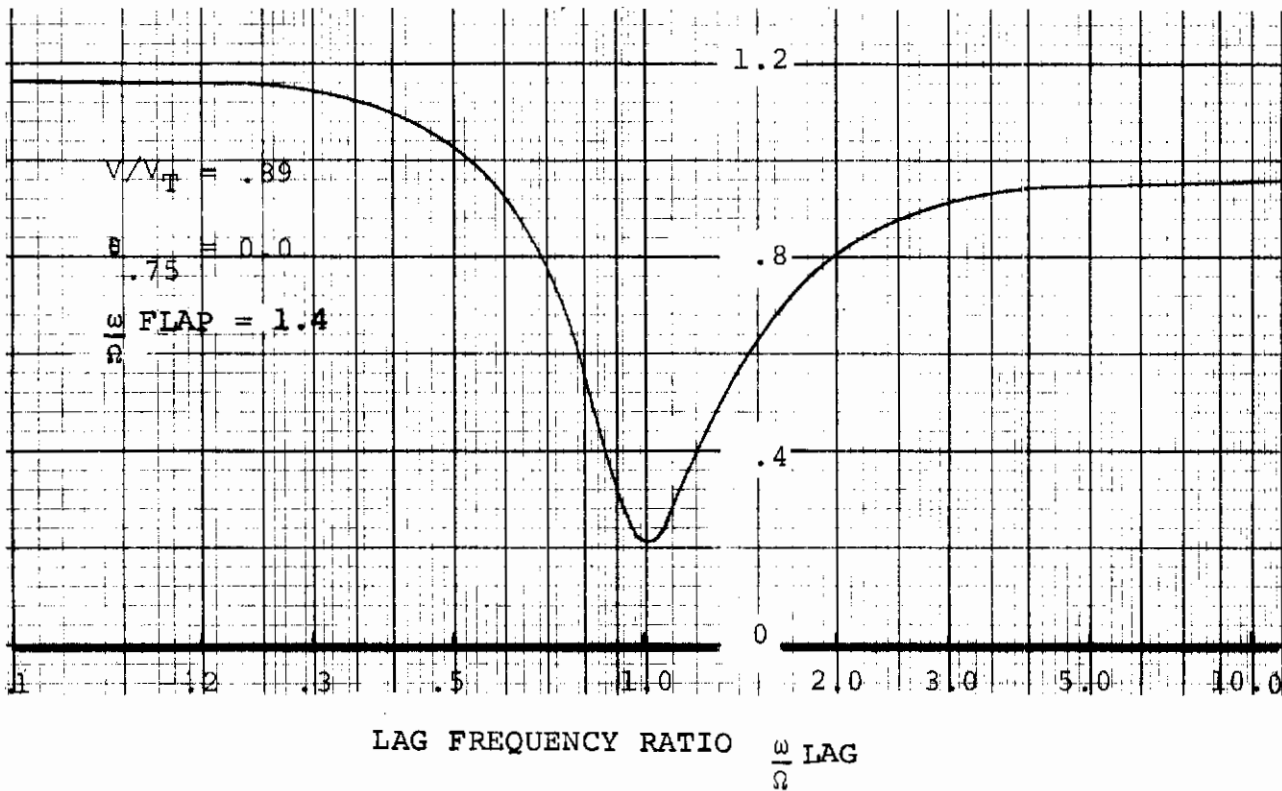


FIGURE 6-3A RATIO OF NET OUT OF PLANE FLAPPING/  
UNIT SHAFT ANGLE OF ATTACK

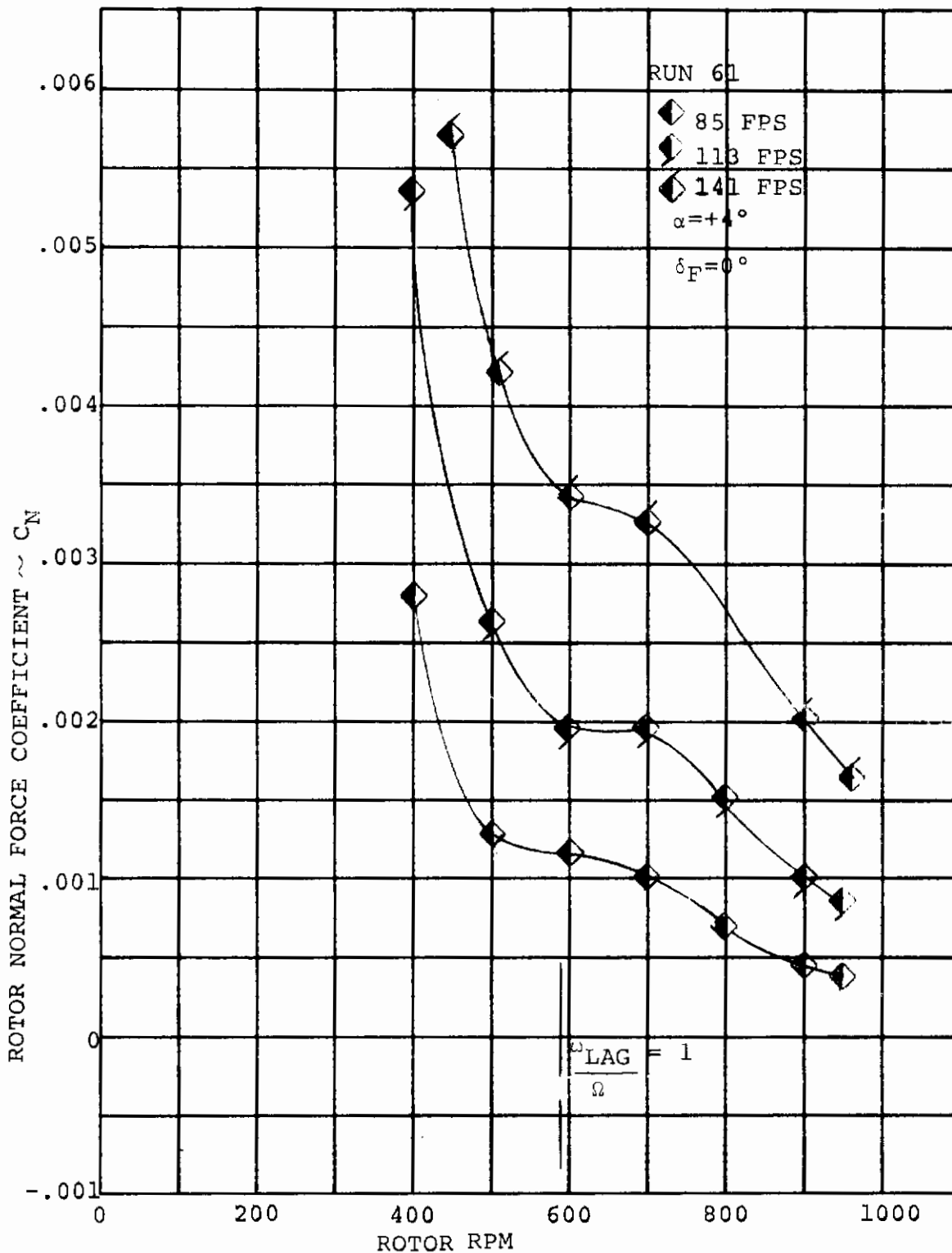


FIGURE 6-4 ROTOR NORMAL FORCE/RPM VARIATION  
 FUSELAGE ATTITUDE =  $+4^\circ$   $\delta_F = 0^\circ$   
 (STEADY WINDMILLING)

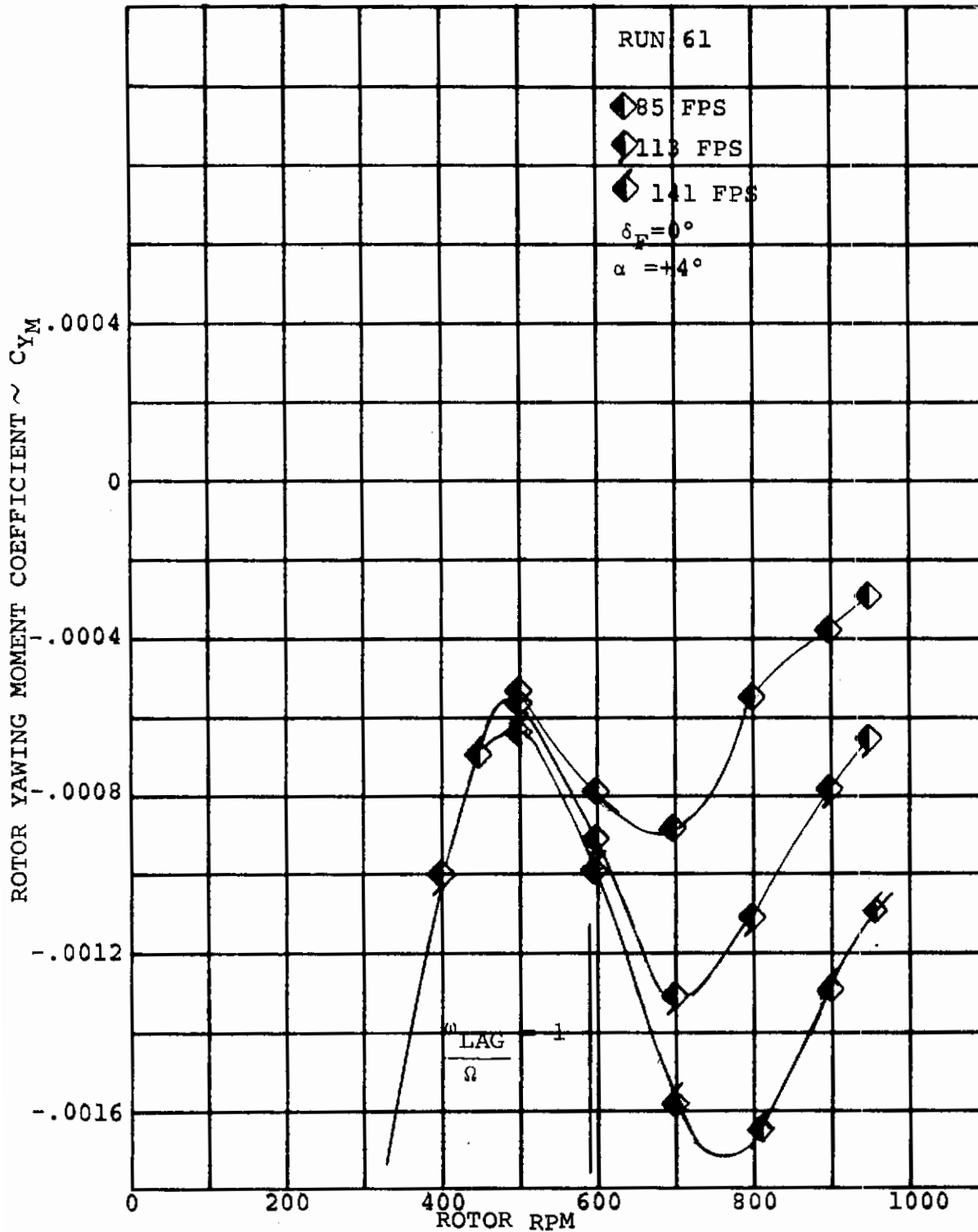


FIGURE 6-5 ROTOR YAWING MOMENT/RPM VARIATION  
 FUSELAGE ATTITUDE =  $+4^\circ$   $\delta_F = 0^\circ$   
 (STEADY WINDMILLING)



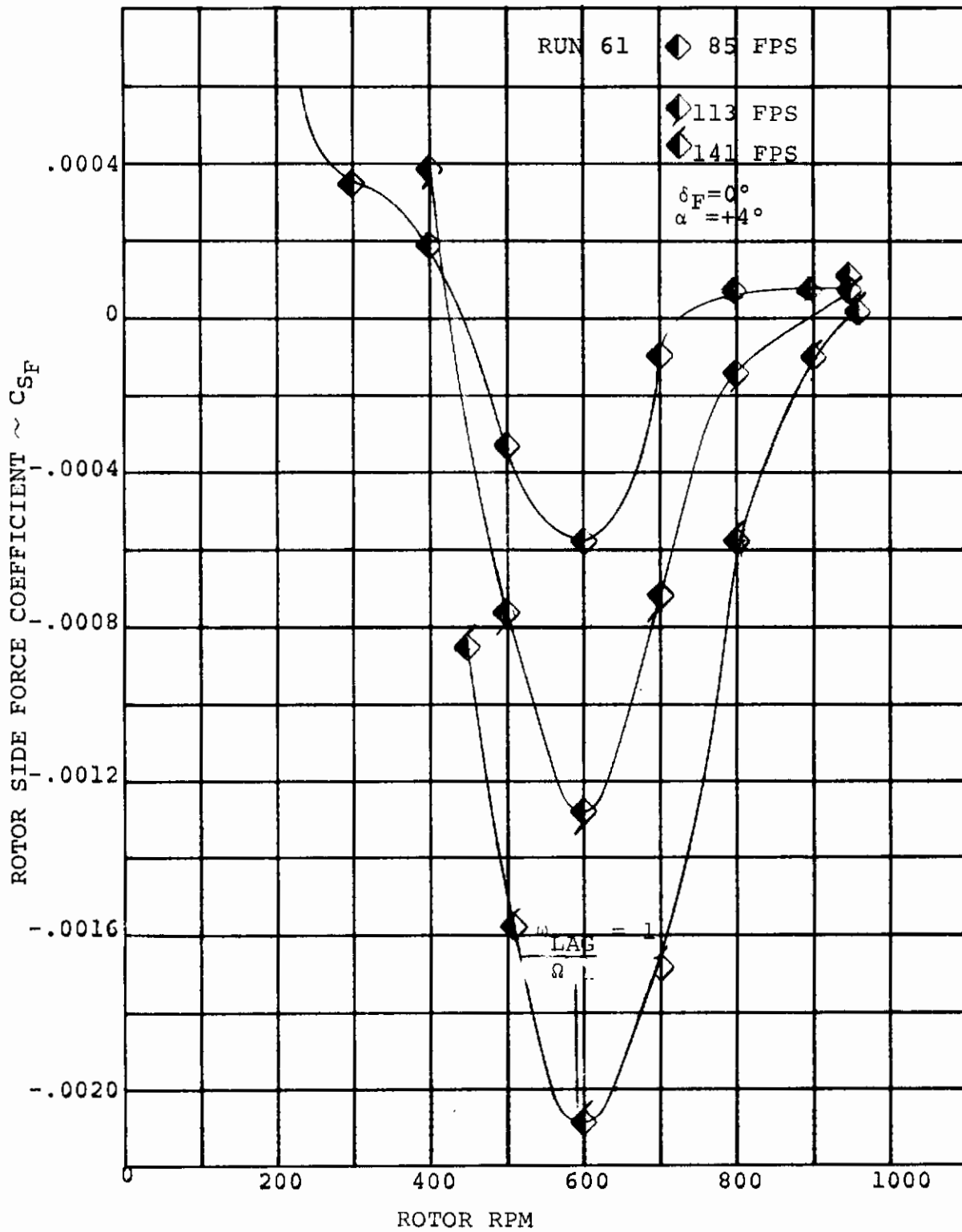


FIGURE 6-6 ROTOR SIDE FORCE/RPM VARIATION  
 FUSELAGE ATTITUDE  $=+4^\circ$   $\delta_F = 0^\circ$   
 (STEADY WINDMILLING)

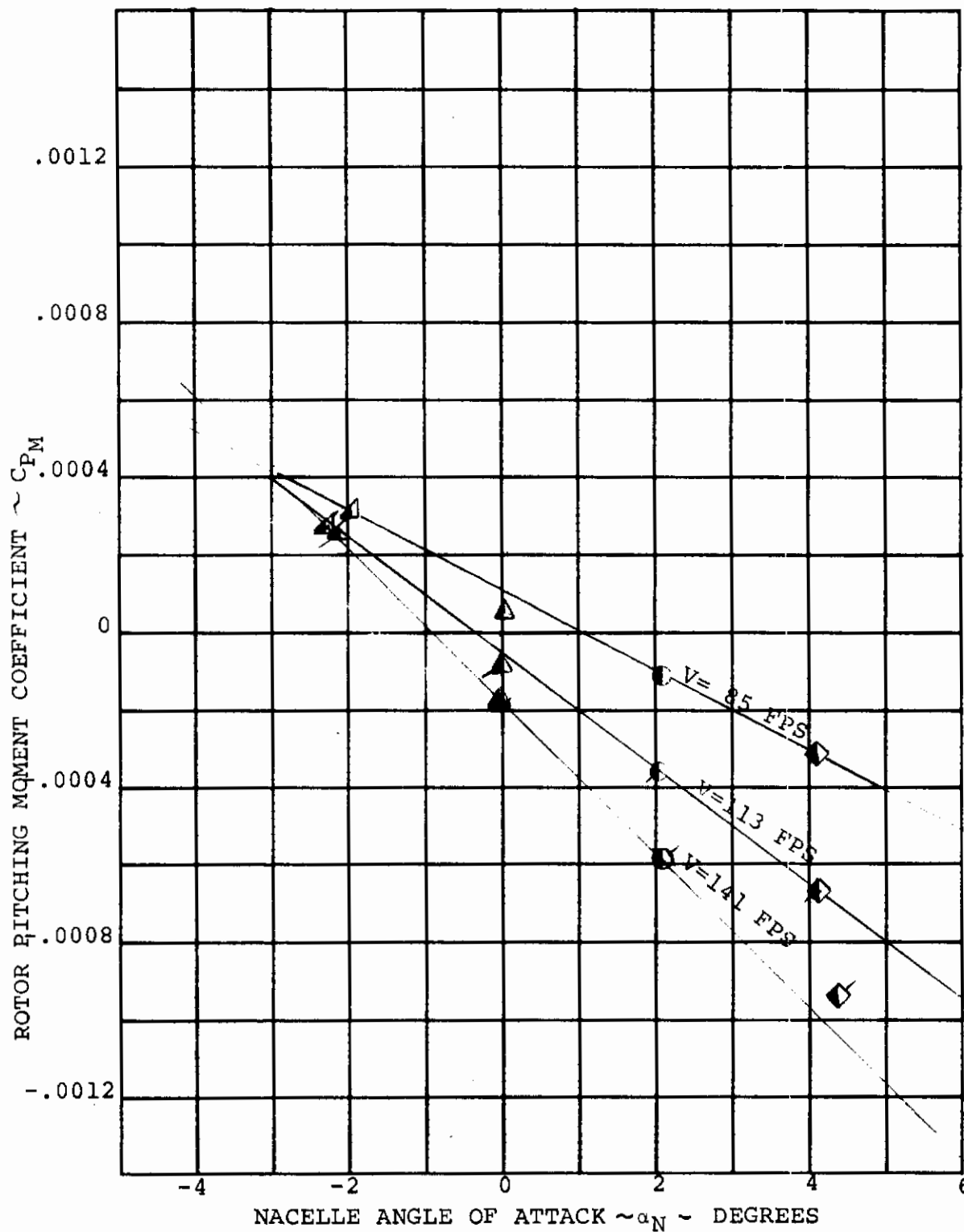


FIGURE 6-7 ROTOR PITCHING MOMENT/NACELLE ANGLE OF ATTACK FOR ROTOR RPM = 600  $\delta_F = 0^\circ$

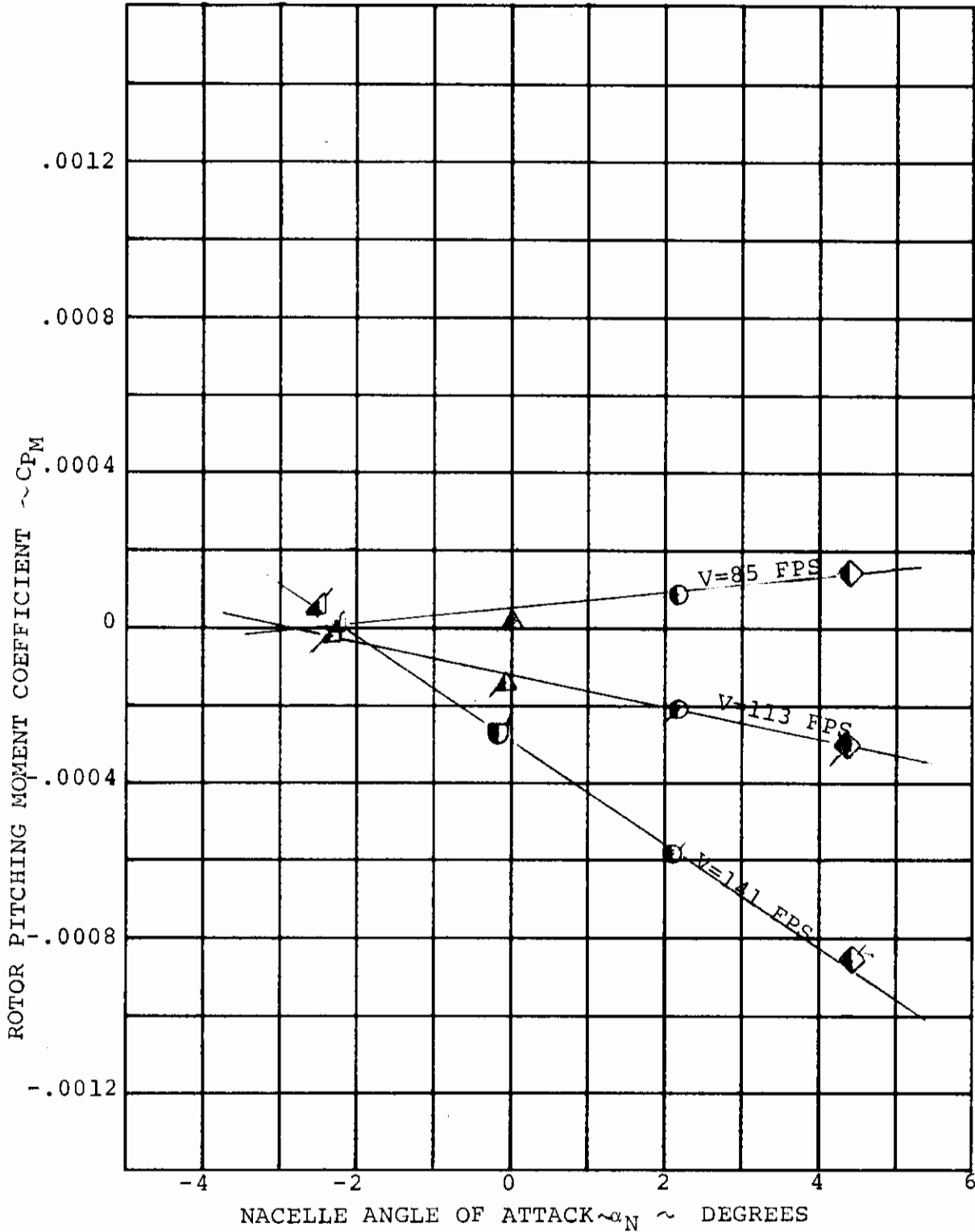


FIGURE 6-8 ROTOR PITCHING MOMENT/NACELLE ANGLE OF ATTACK FOR ROTOR RPM = 700 δ<sub>r</sub> = 0°

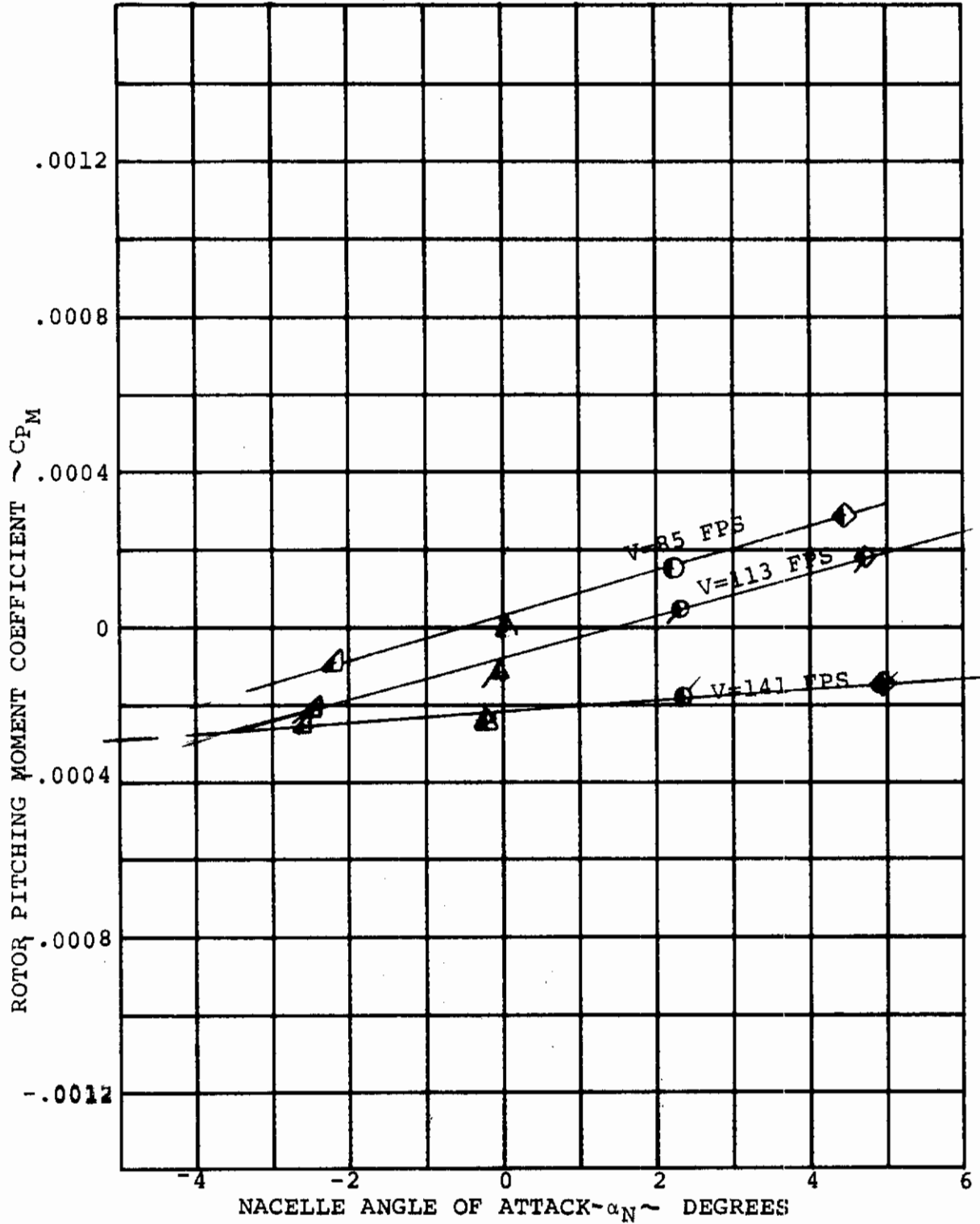


FIGURE 6-9 ROTOR PITCHING MOMENT/NACELLE ANGLE OF ATTACK FOR ROTOR RPM = 800 δ<sub>ψ</sub> = 0°

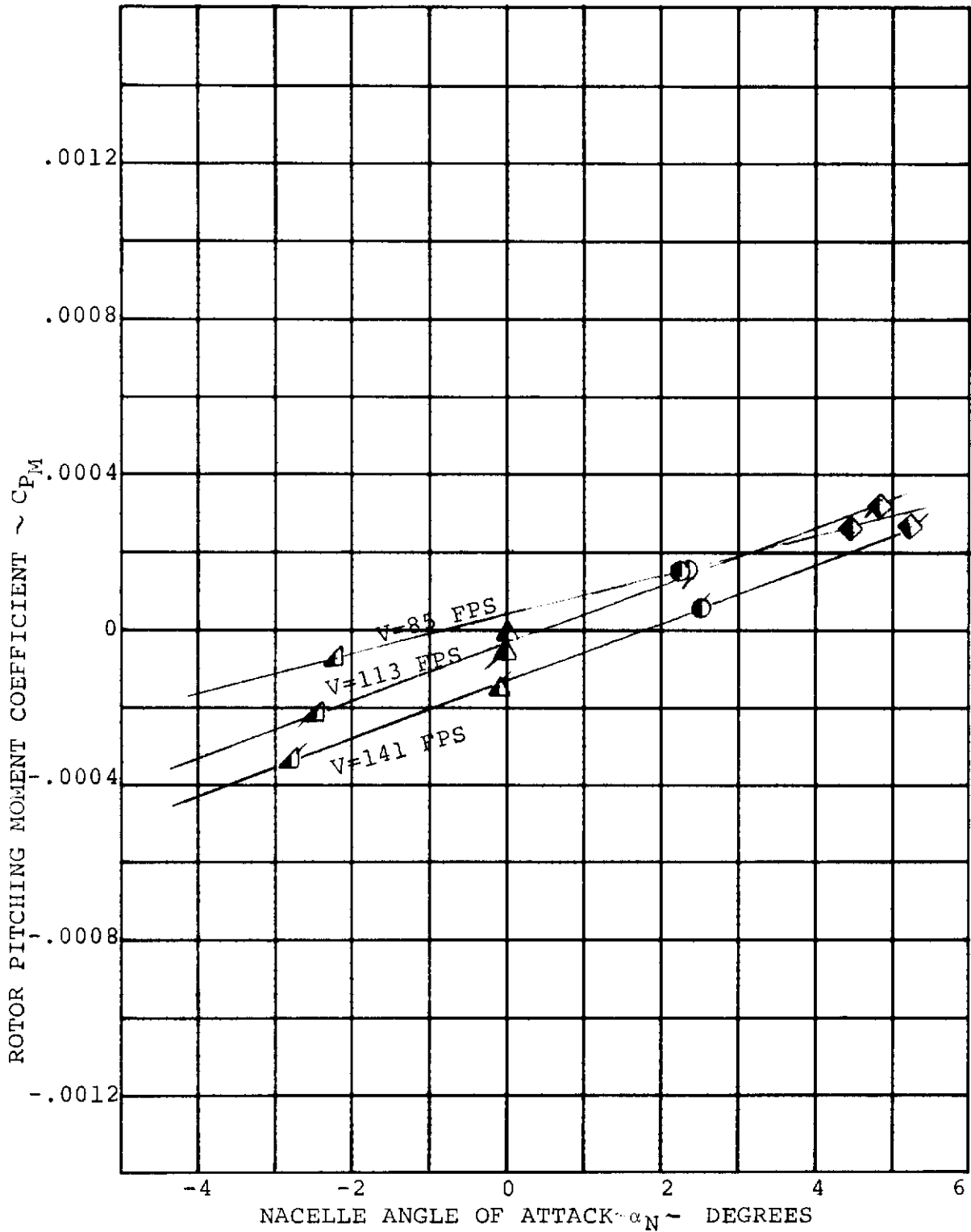


FIGURE 6-10 ROTOR PITCHING MOMENT/NACELLE ANGLE OF ATTACK FOR ROTOR RPM = 900  $\delta_F = 0^\circ$

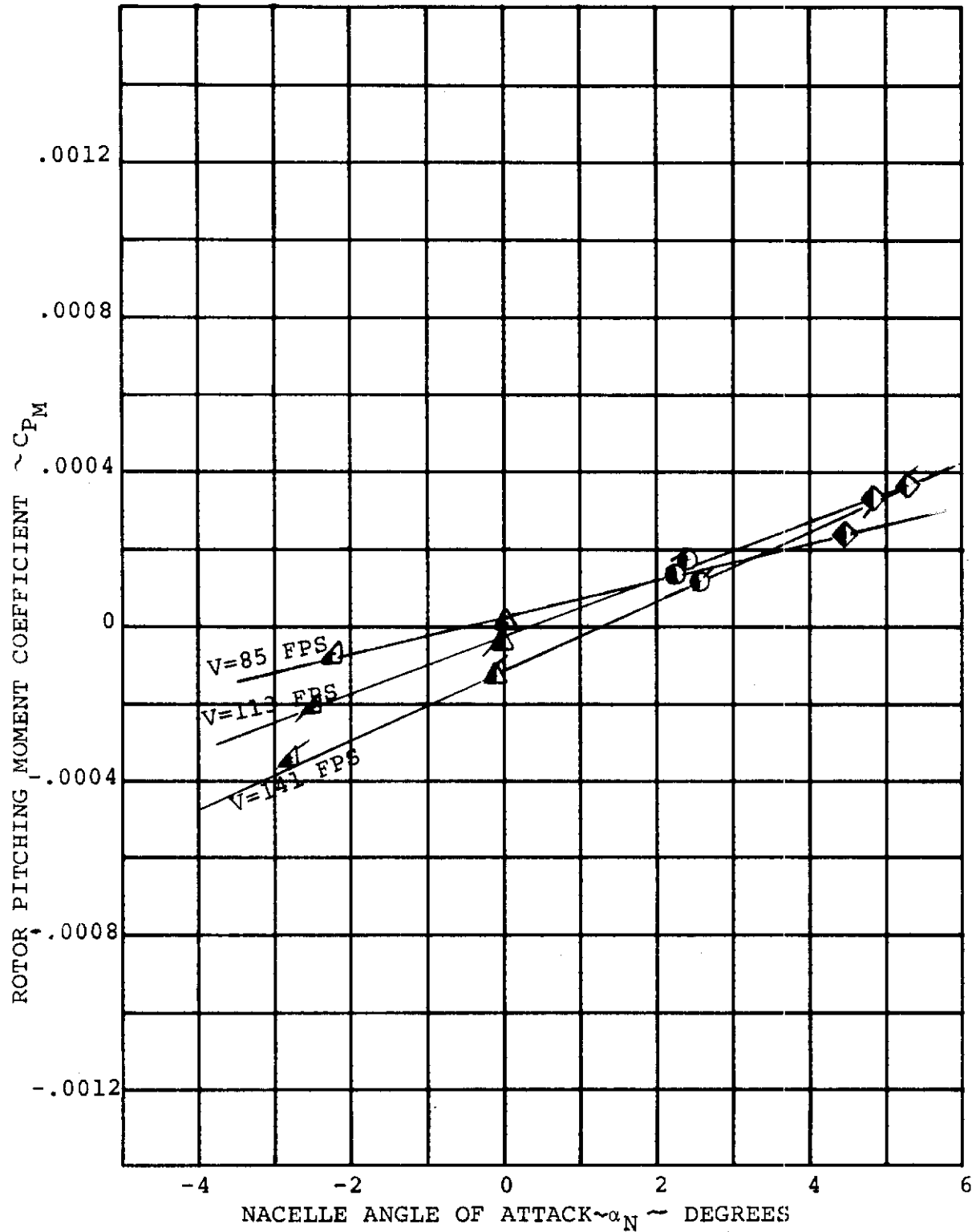


FIGURE 6-11 ROTOR PITCHING MOMENT/NACELLE ANGLE OF ATTACK FOR ROTOR RPM = 950  $\delta_f = 0^\circ$

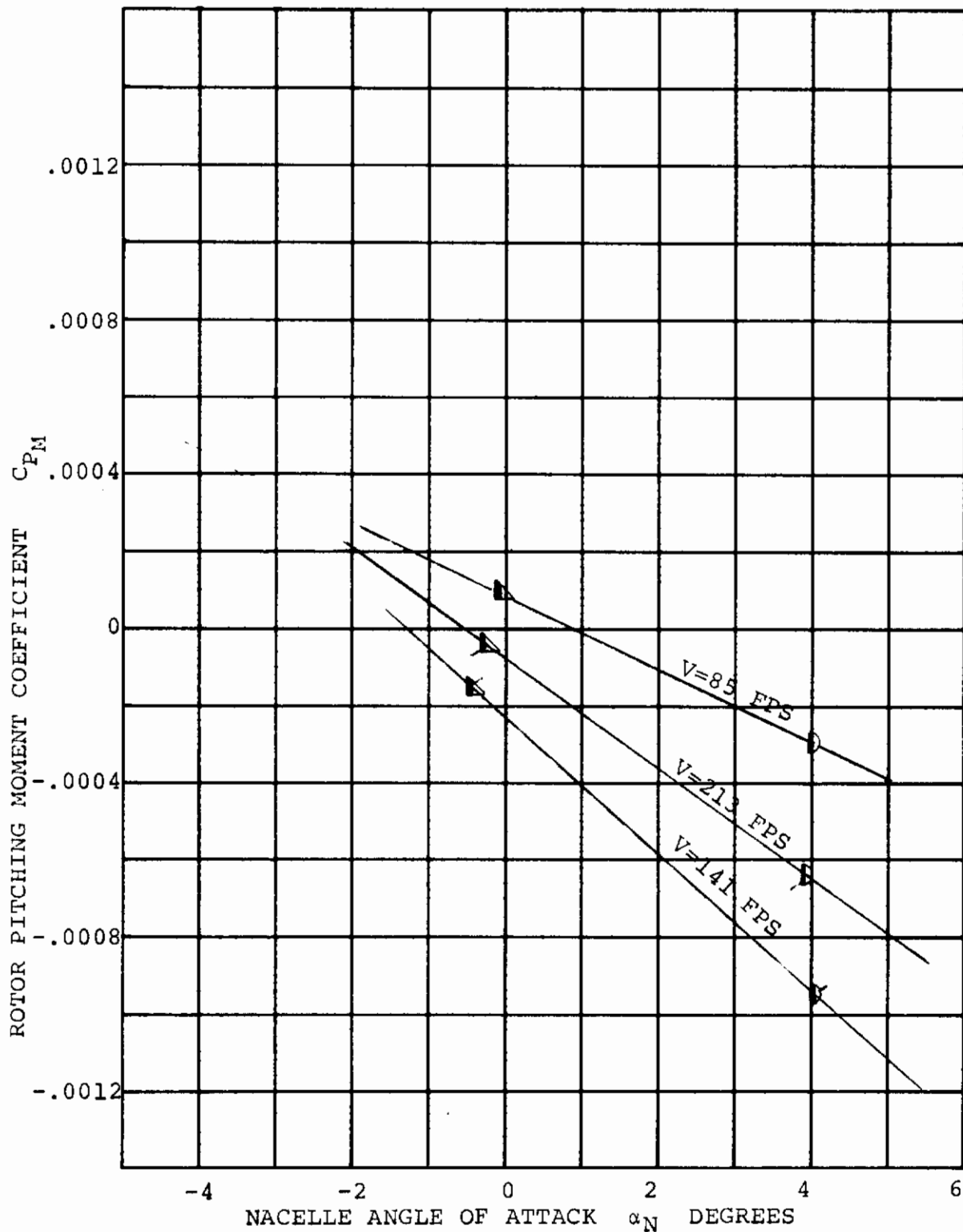


FIGURE 6-12 ROTOR PITCHING MOMENT/NACELLE ANGLE OF ATTACK FOR ROTOR RPM = 600  $\delta_F=30^\circ$

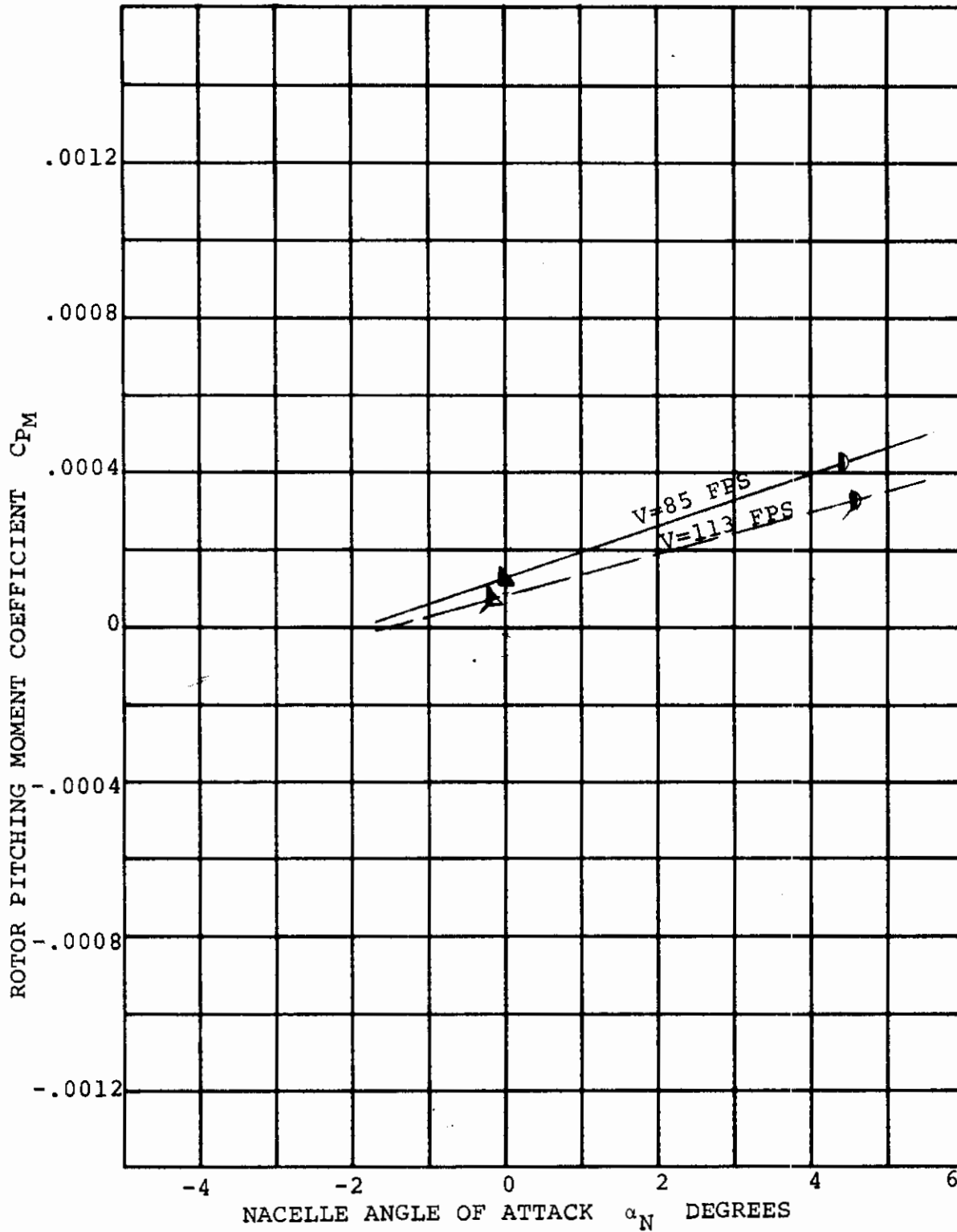


FIGURE 6-13 ROTOR PITCHING MOMENT/NACELLE ANGLE OF ATTACK FOR ROTOR RPM = 800  $\delta_F=30^\circ$



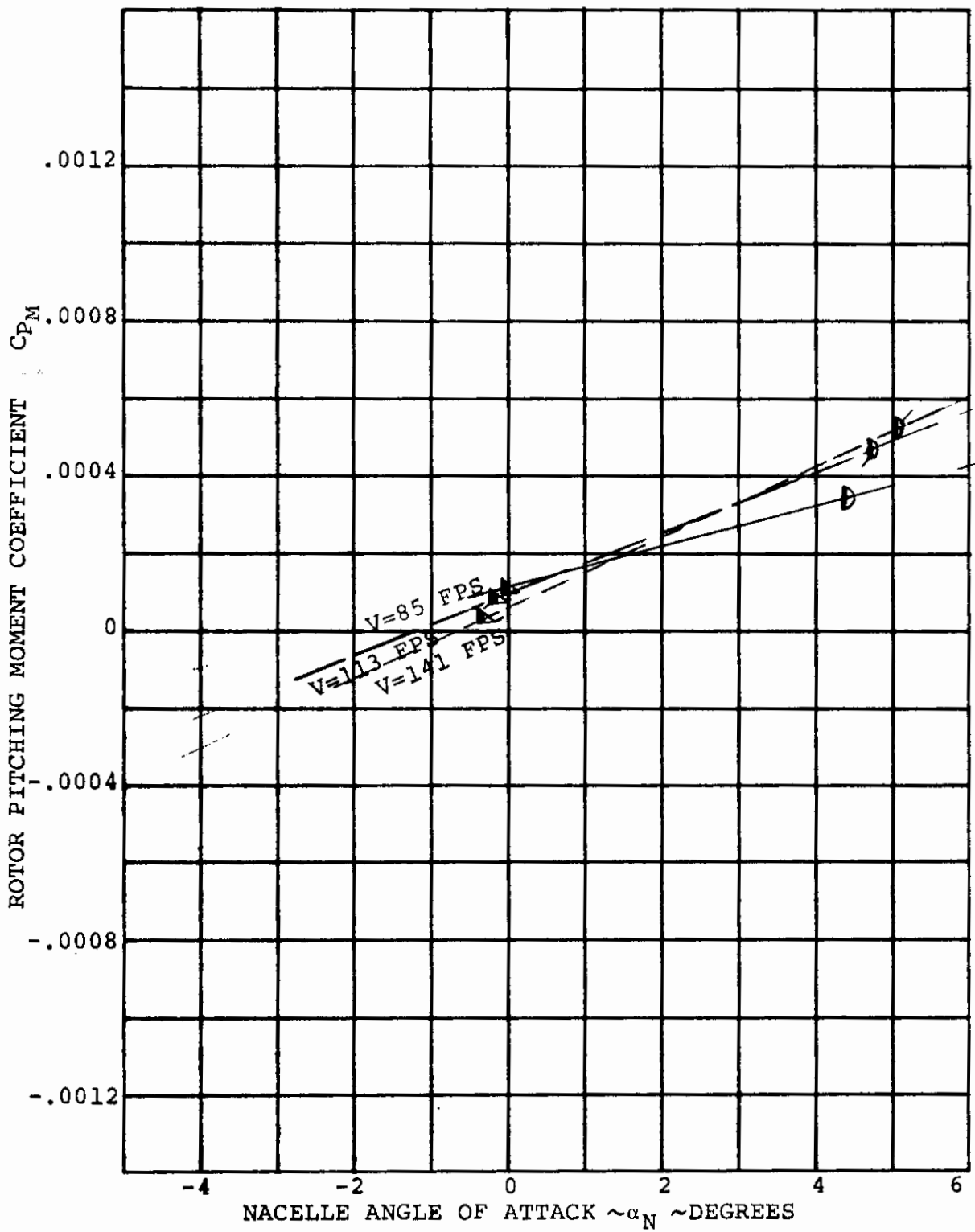


FIGURE 6-14 ROTOR PITCHING MOMENT/NACELLE ANGLE OF ATTACK FOR ROTOR RPM = 950  $\delta_F=30^\circ$

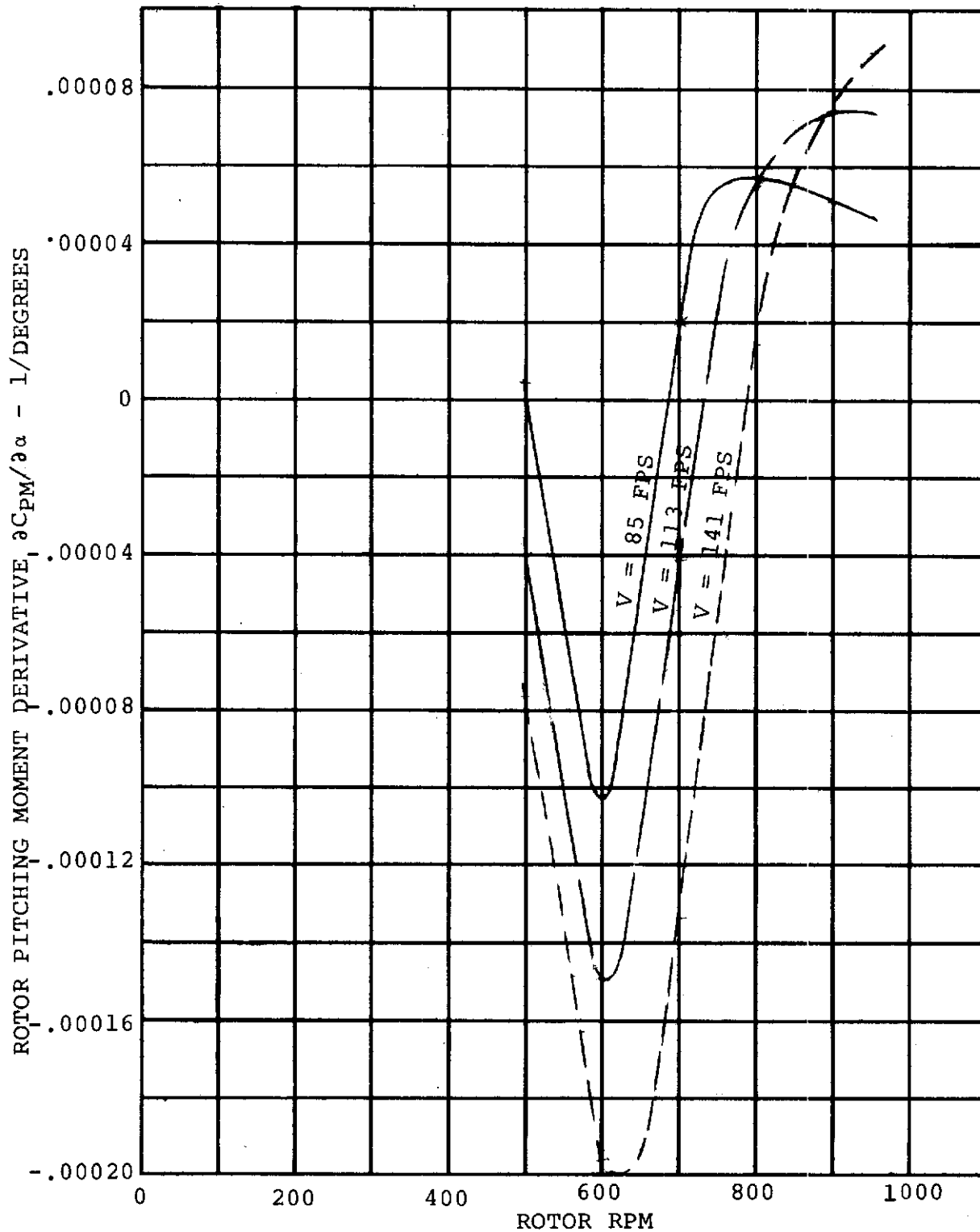


FIGURE 6-15 ROTOR PITCHING MOMENT DERIVATIVE VARIATION WITH ROTOR RPM,  $\delta F = 0^\circ$

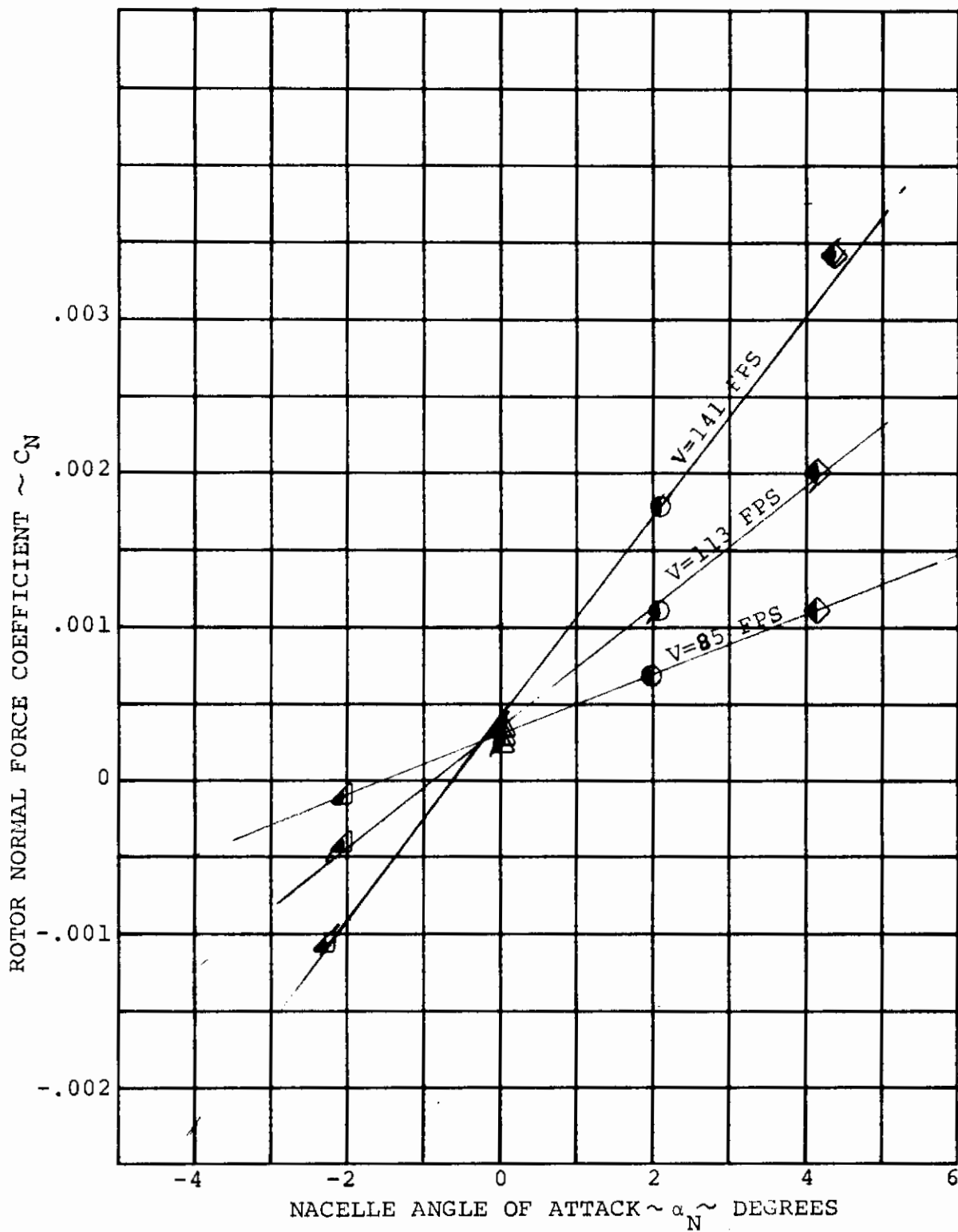


FIGURE 6-16 ROTOR NORMAL FORCE/NACELLE ANGLE OF ATTACK FOR ROTOR RPM = 600  $\delta_F=0^\circ$

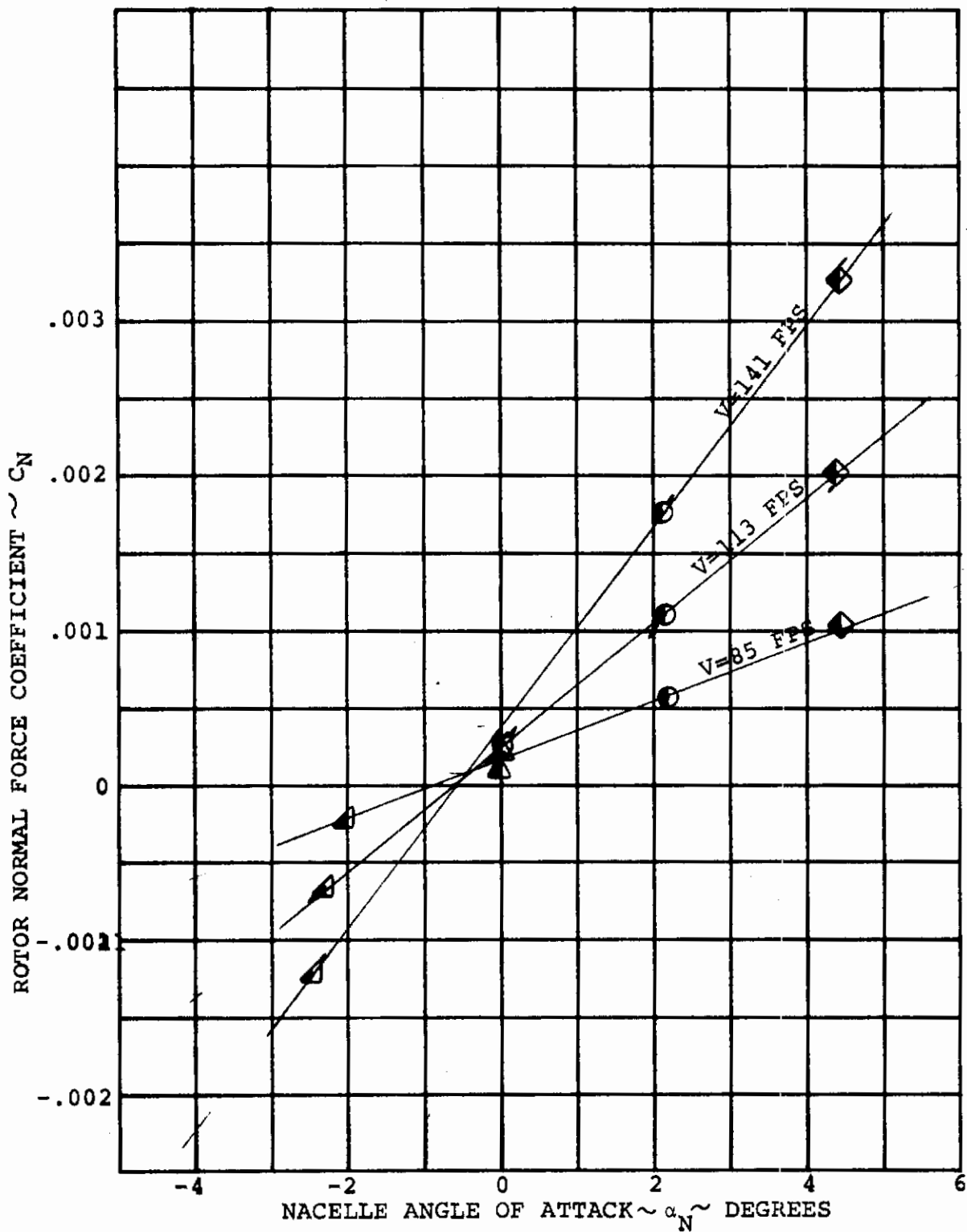


FIGURE 6-17 ROTOR NORMAL FORCE/NACELLE ANGLE OF ATTACK FOR ROTOR RPM = 700 δ<sub>F</sub> = 0°

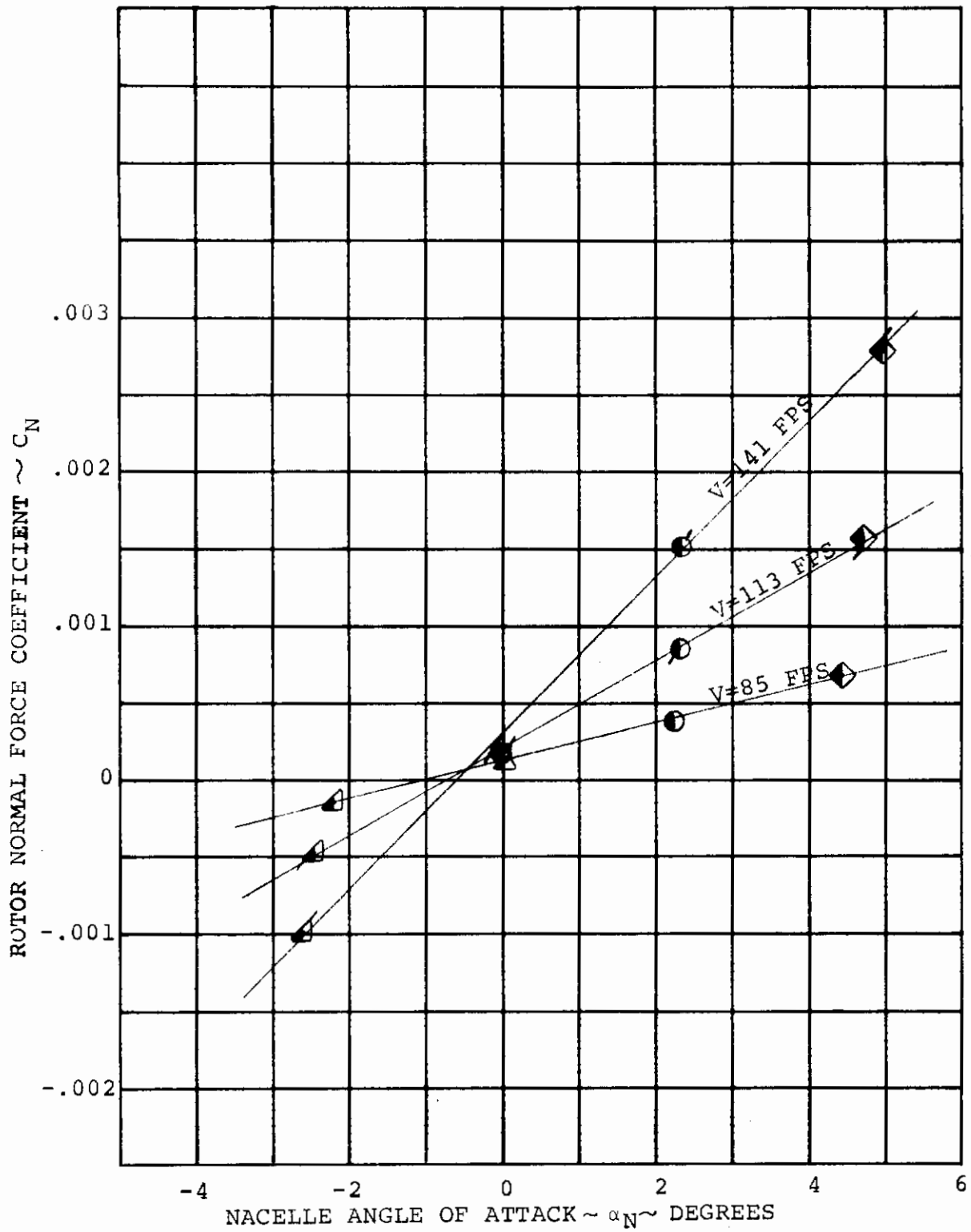


FIGURE 6-18 ROTOR NORMAL FORCE/NACELLE ANGLE OF ATTACK FOR ROTOR RPM = 800  $\delta_F=0^\circ$

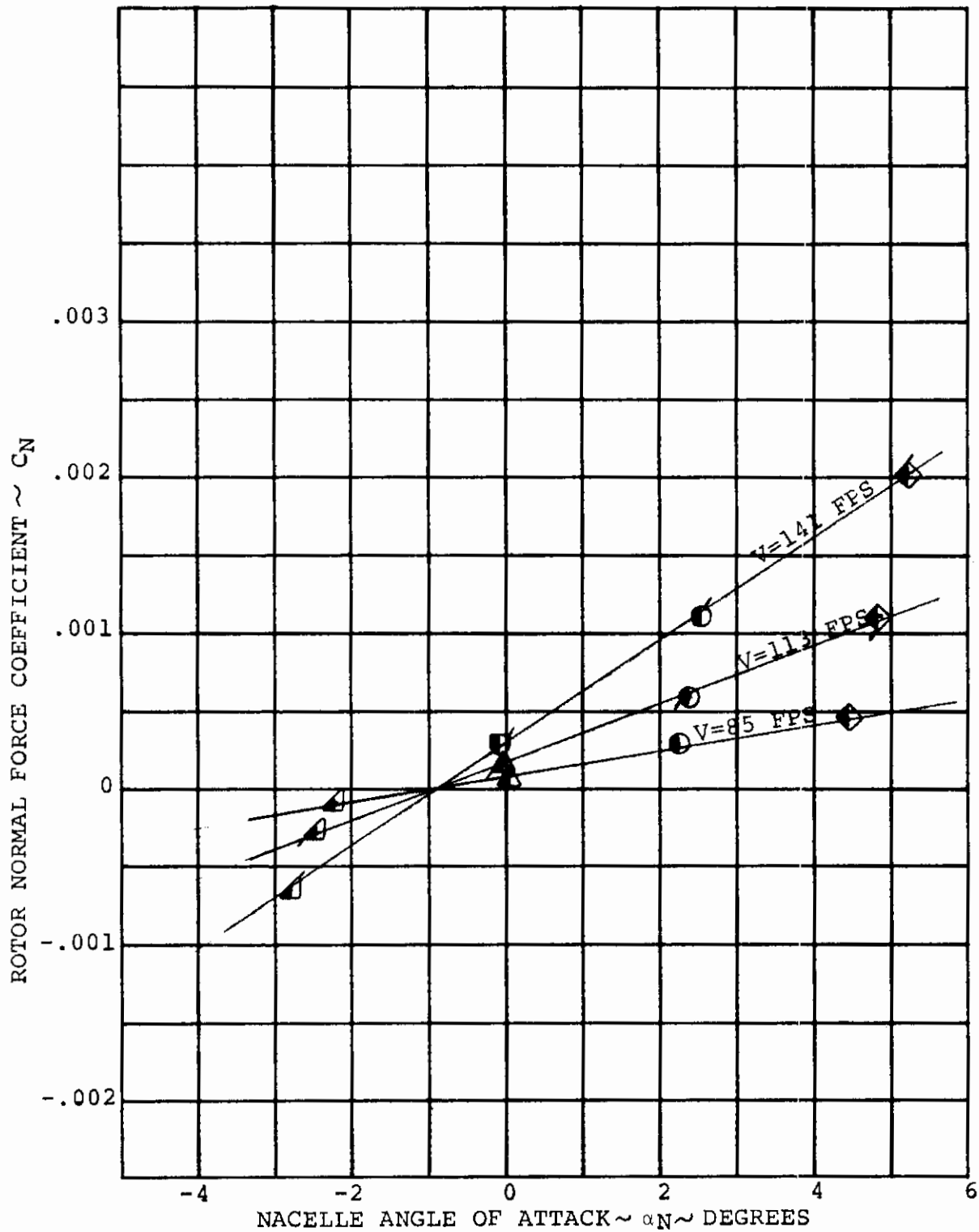


FIGURE 6-19 ROTOR NORMAL FORCE/NACELLE ANGLE OF ATTACK FOR ROTOR RPM = 900  $\delta_F = 0^\circ$

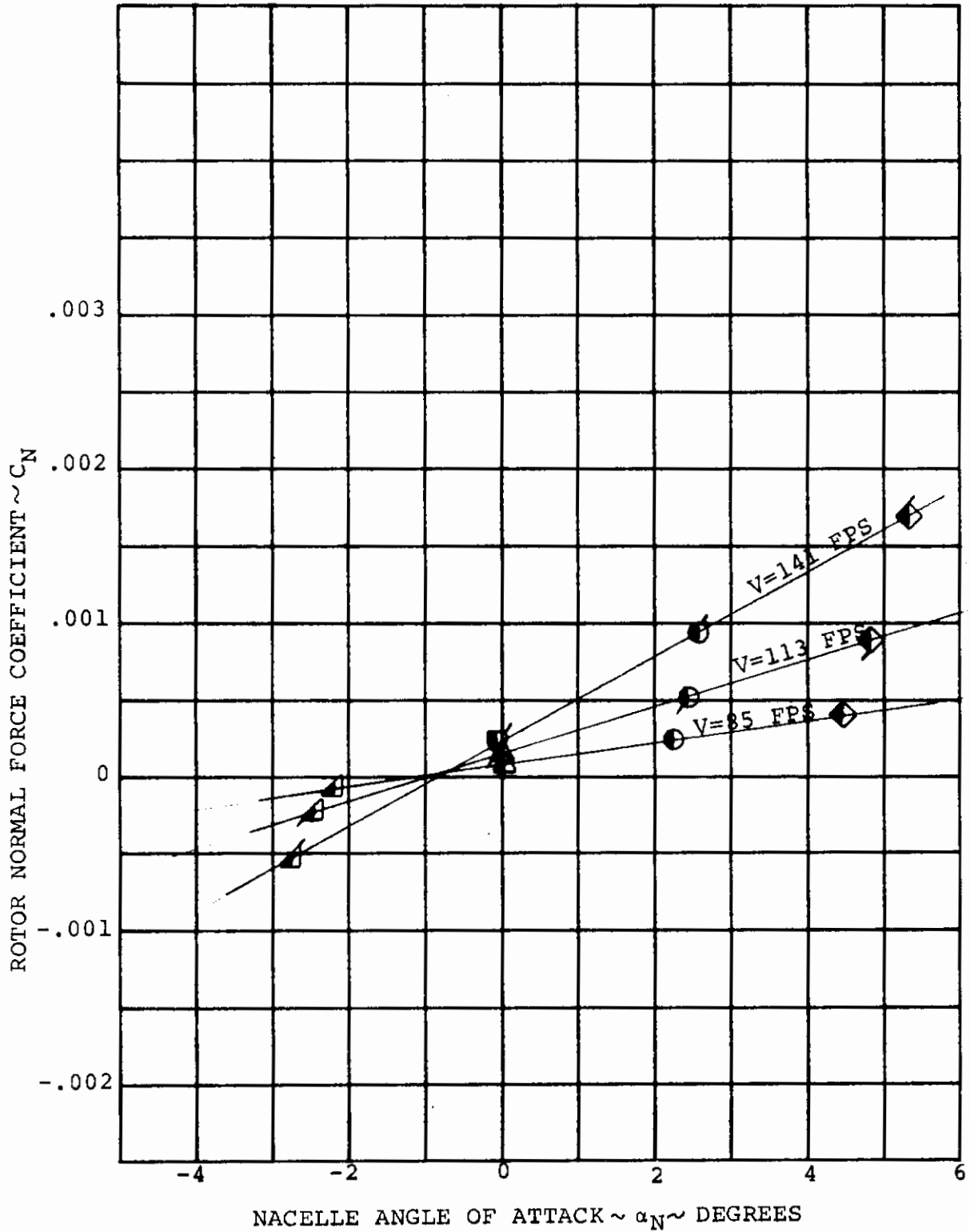


FIGURE 6-20 ROTOR NORMAL FORCE/NACELLE ANGLE OF ATTACK FOR ROTOR RPM = 950  $\delta_F=0^\circ$

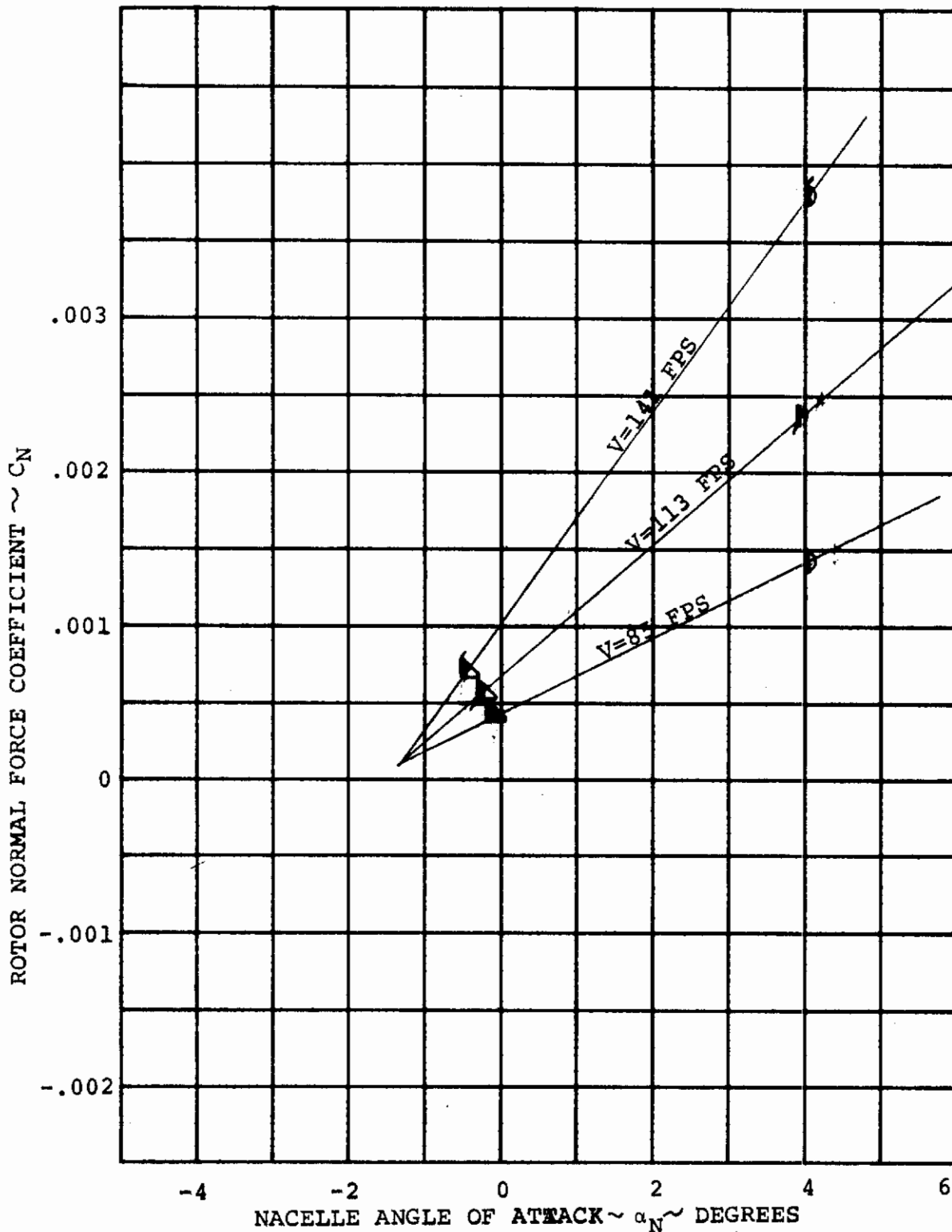


FIGURE 6-21 ROTOR NORMAL FORCE/NACELLE ANGLE OF ATTACK FOR ROTOR RPM = 600  $\delta_F=30^\circ$



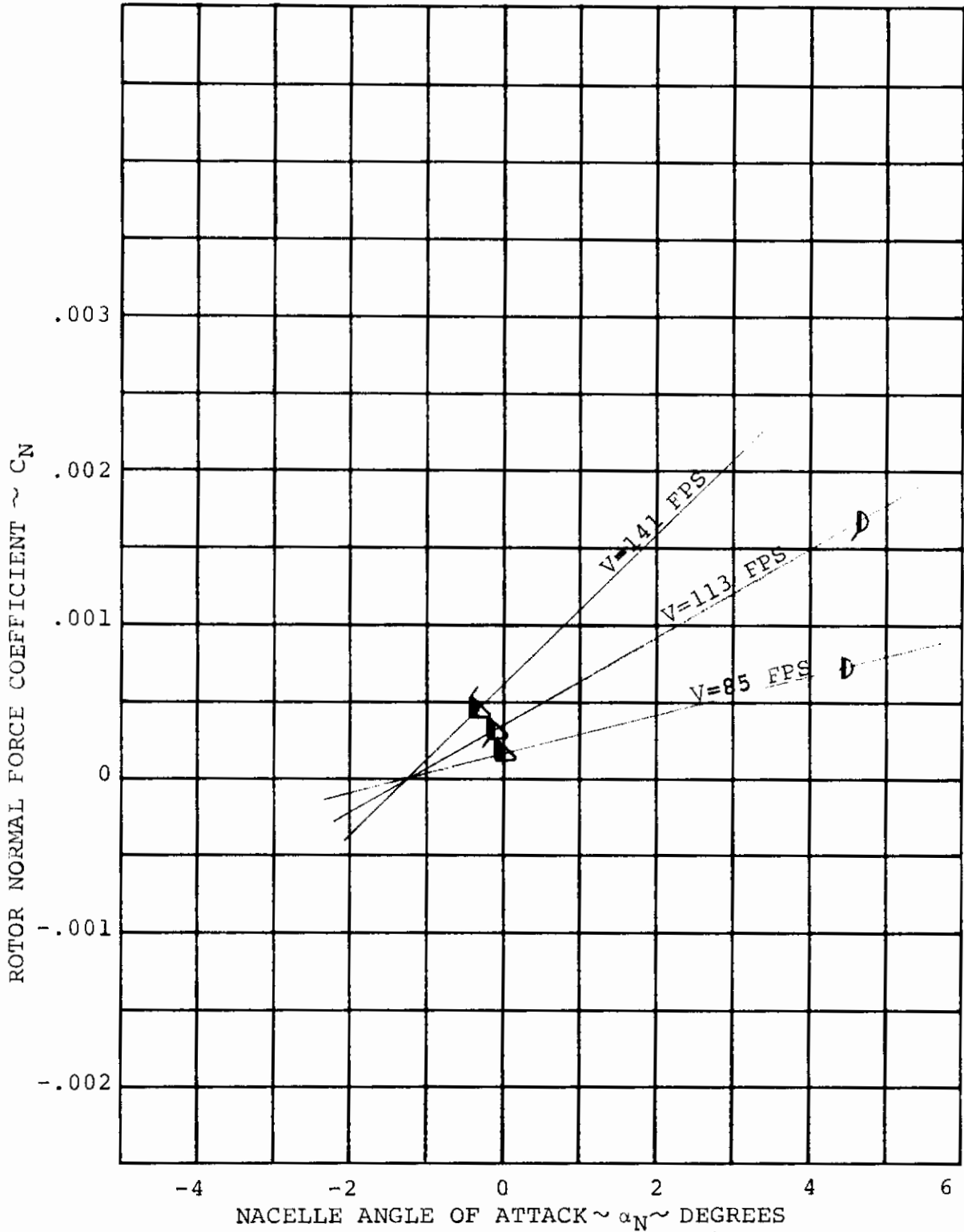


FIGURE 6-22 ROTOR NORMAL FORCE/NACELLE ANGLE OF ATTACK FOR ROTOR RPM = 800  $\delta_F=30^\circ$

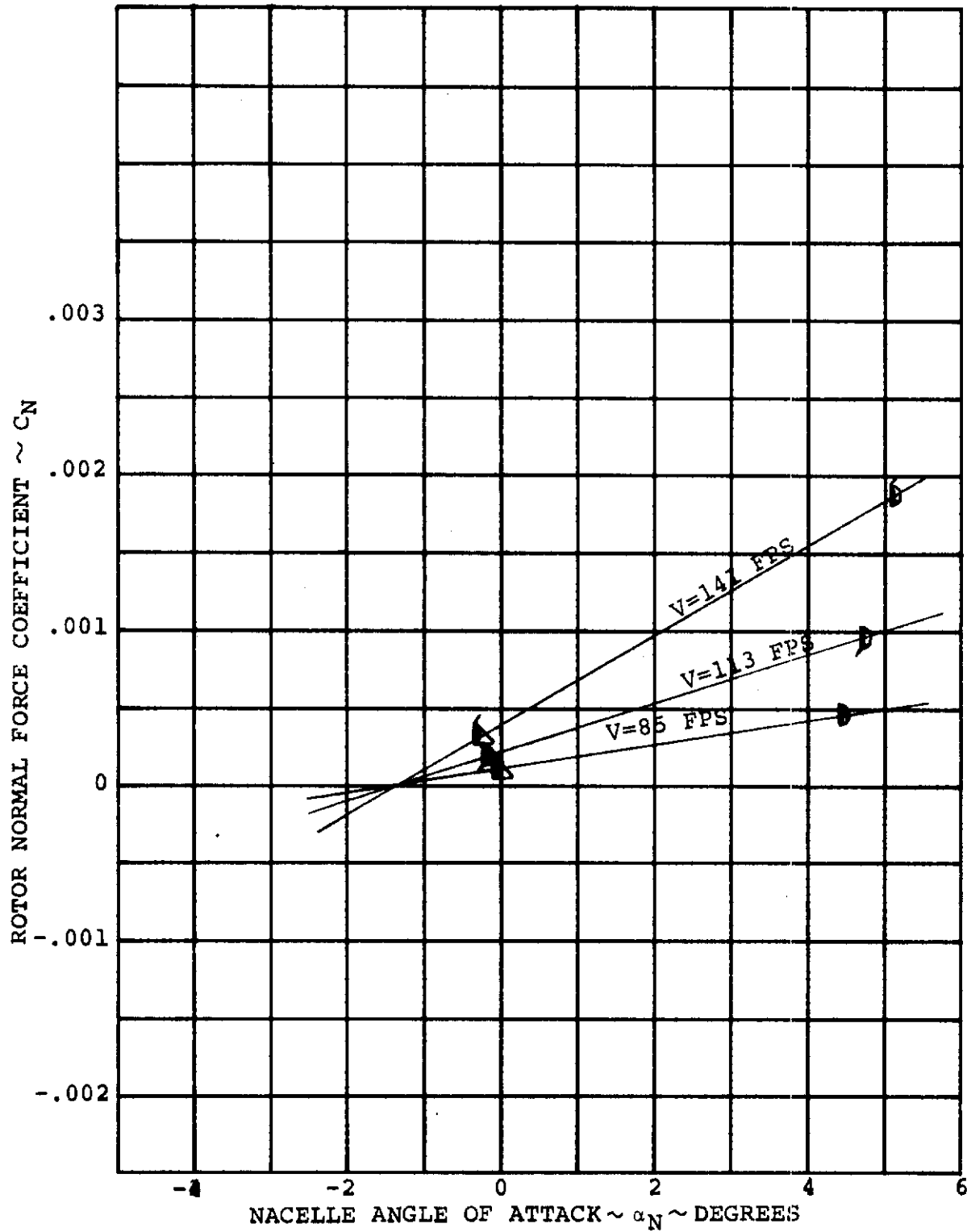


FIGURE 6-23 ROTOR NORMAL FORCE/NACELLE ANGLE OF ATTACK FOR ROTOR RPM = 950  $\delta_F = 30^\circ$

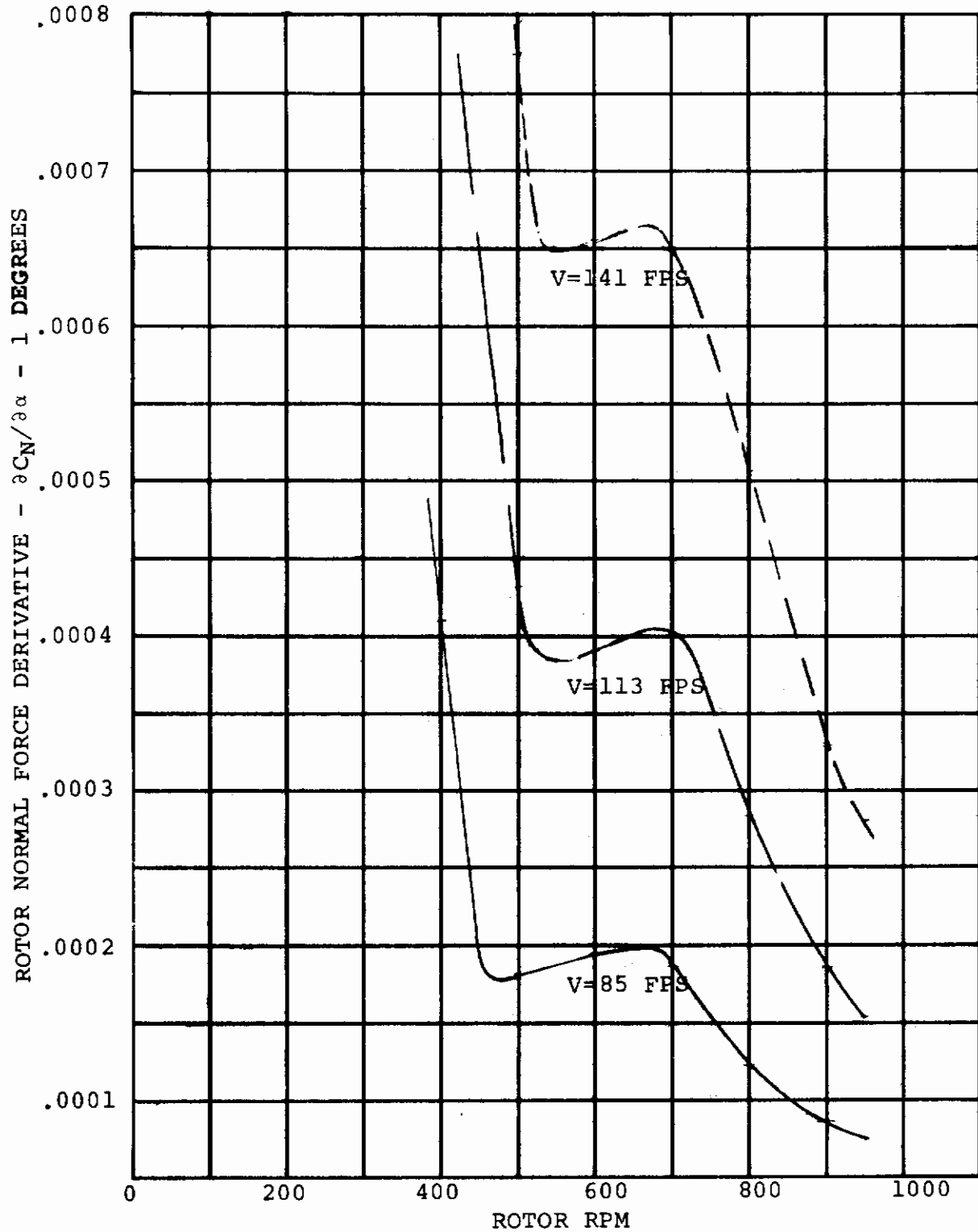


FIGURE 6-24 ROTOR NORMAL FORCE DERIVATIVE VARIATION WITH ROTOR RPM  $\delta \bar{\alpha} = 0^\circ$

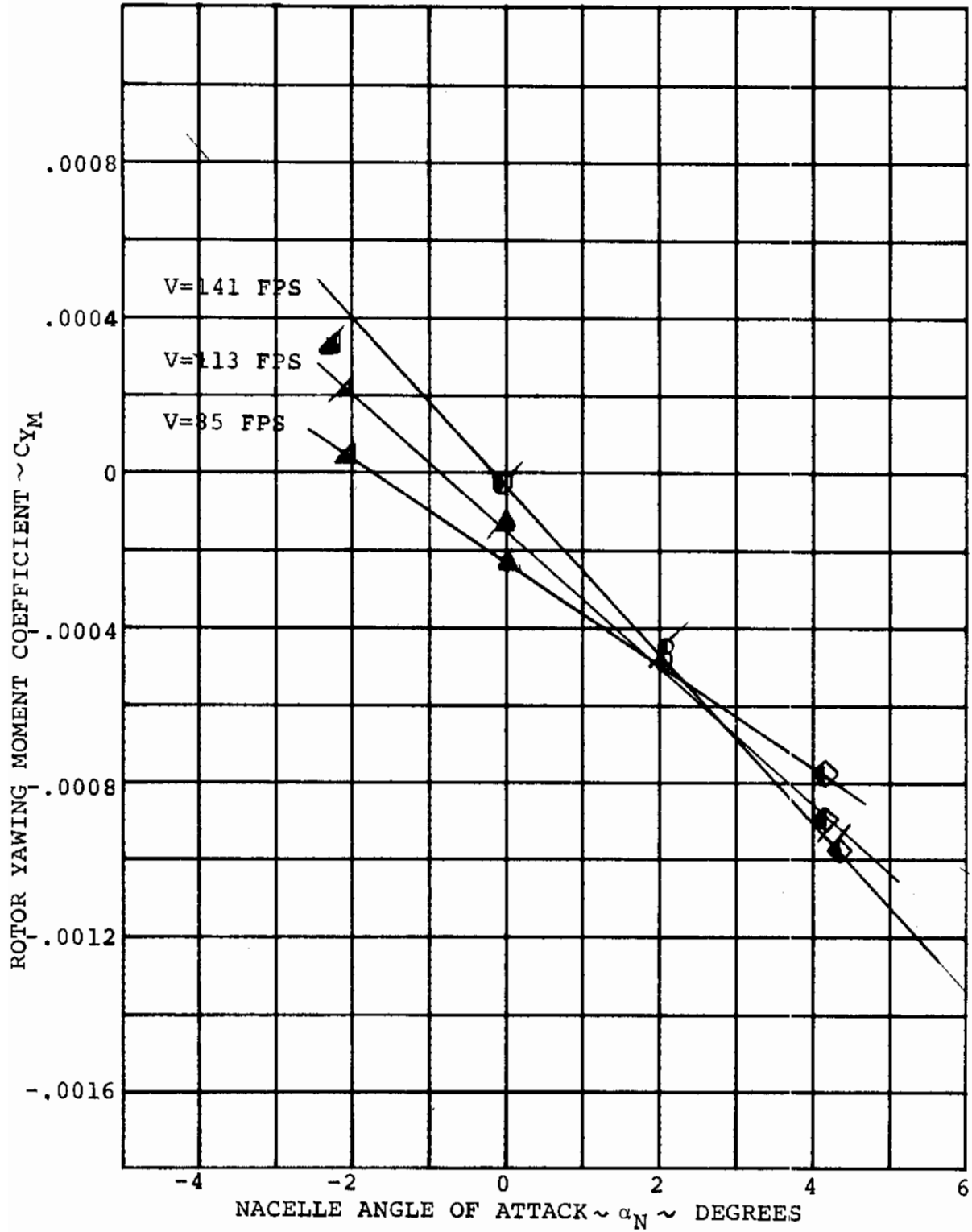


FIGURE 6-25 ROTOR YAWING MOMENT/NACELLE ANGLE OF ATTACK FOR ROTOR RPM = 600  $\delta_F = 0^\circ$

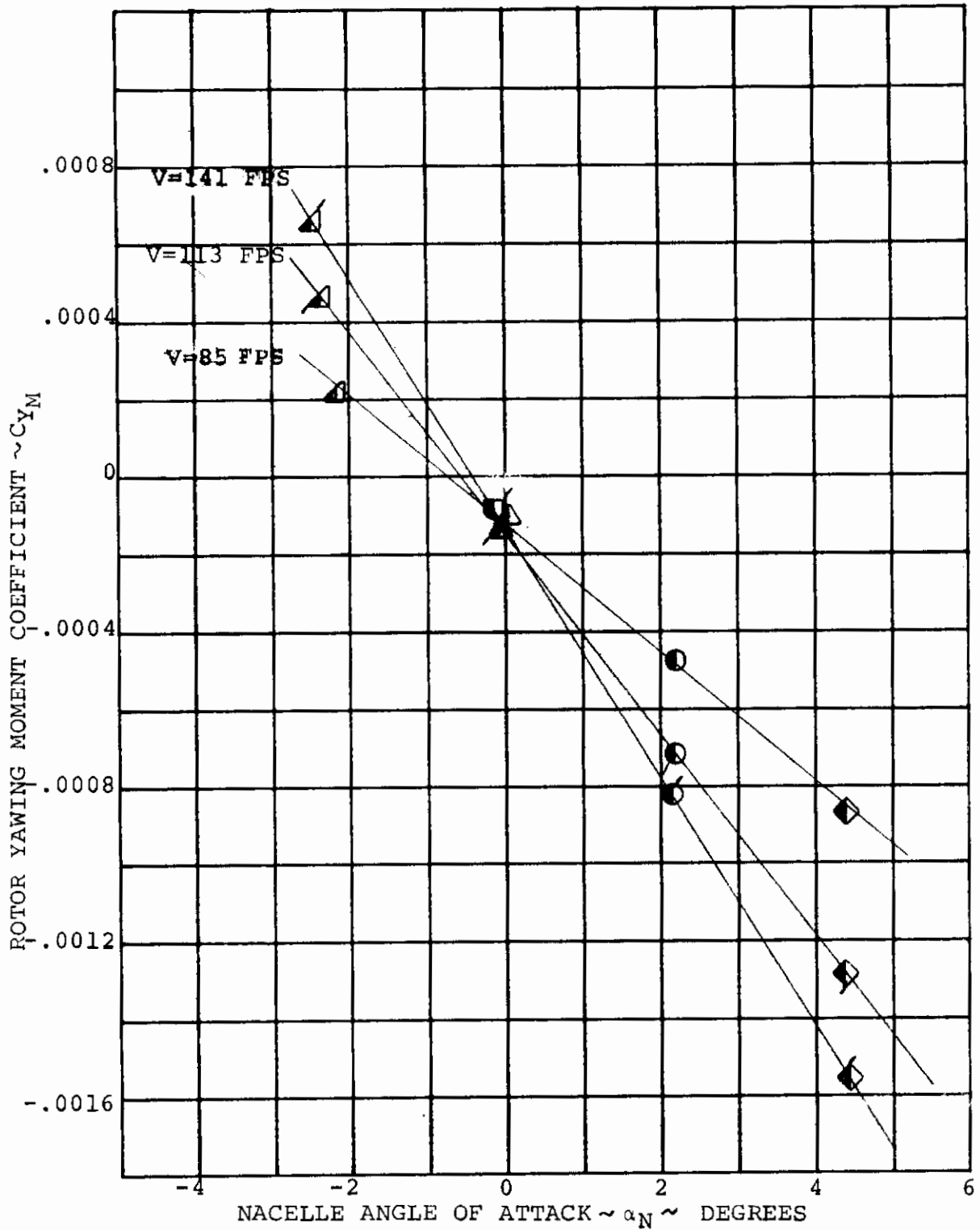


FIGURE 6-26 ROTOR YAWING MOMENT/NACELLE ANGLE OF ATTACK FOR ROTOR RPM = 700  $\delta_F = 0^\circ$

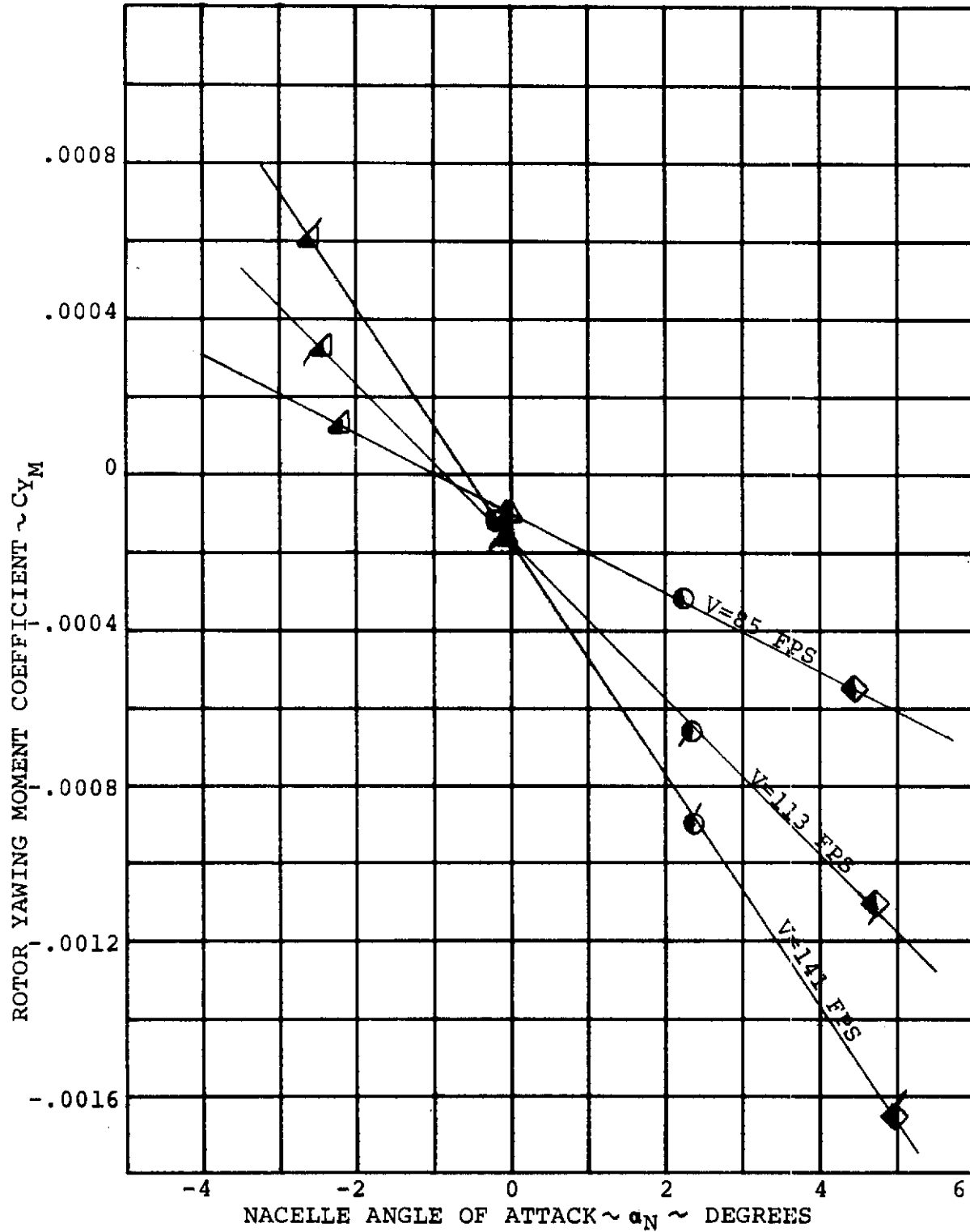


FIGURE 6-27 ROTOR YAWING MOMENT/NACELLE ANGLE OF ATTACK FOR ROTOR RPM = 800  $\delta_F = 0^\circ$

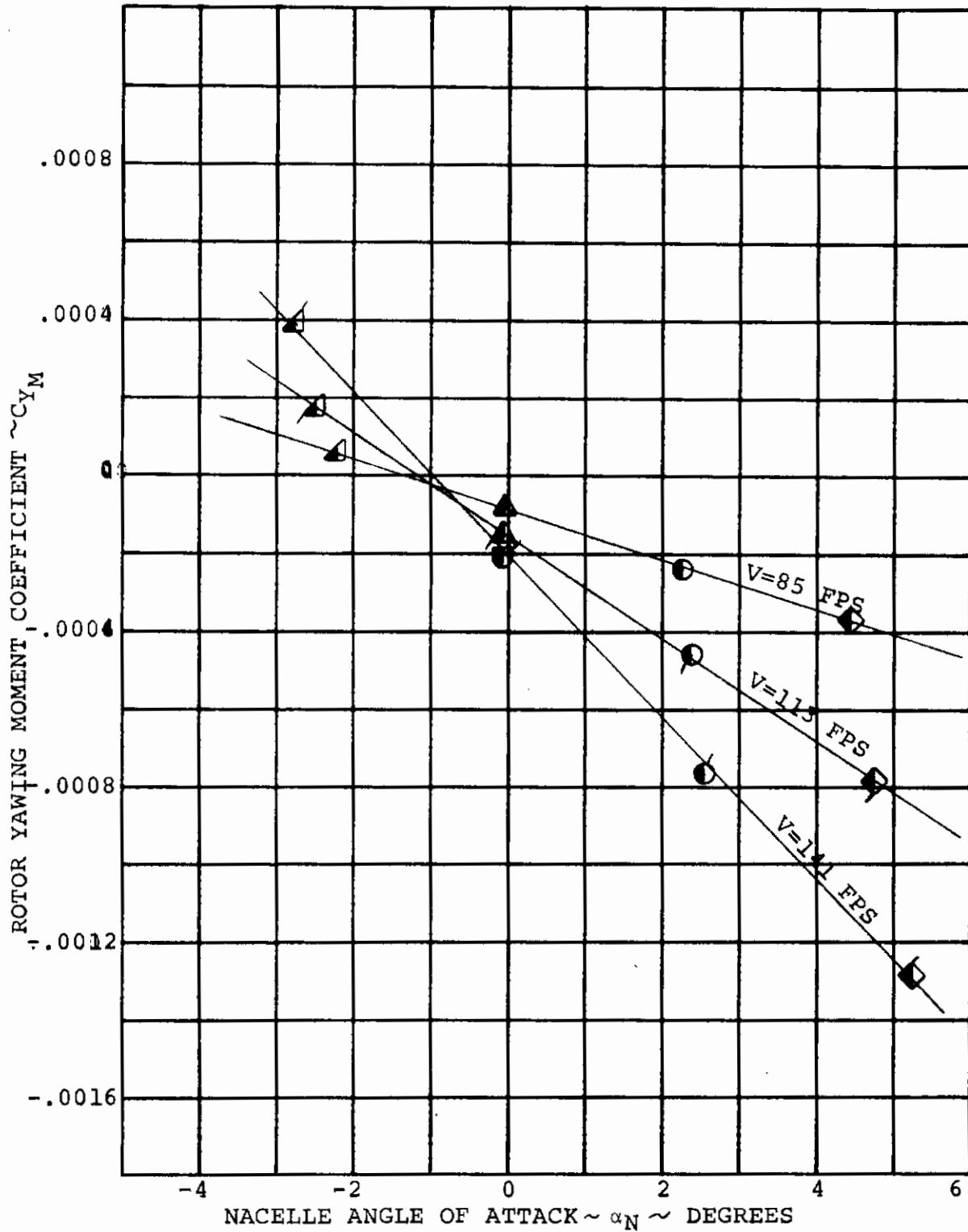


FIGURE 6-28 ROTOR YAWING MOMENT/NACELLE ANGLE OF ATTACK FOR ROTOR RPM = 900  $\delta_F = 0^\circ$

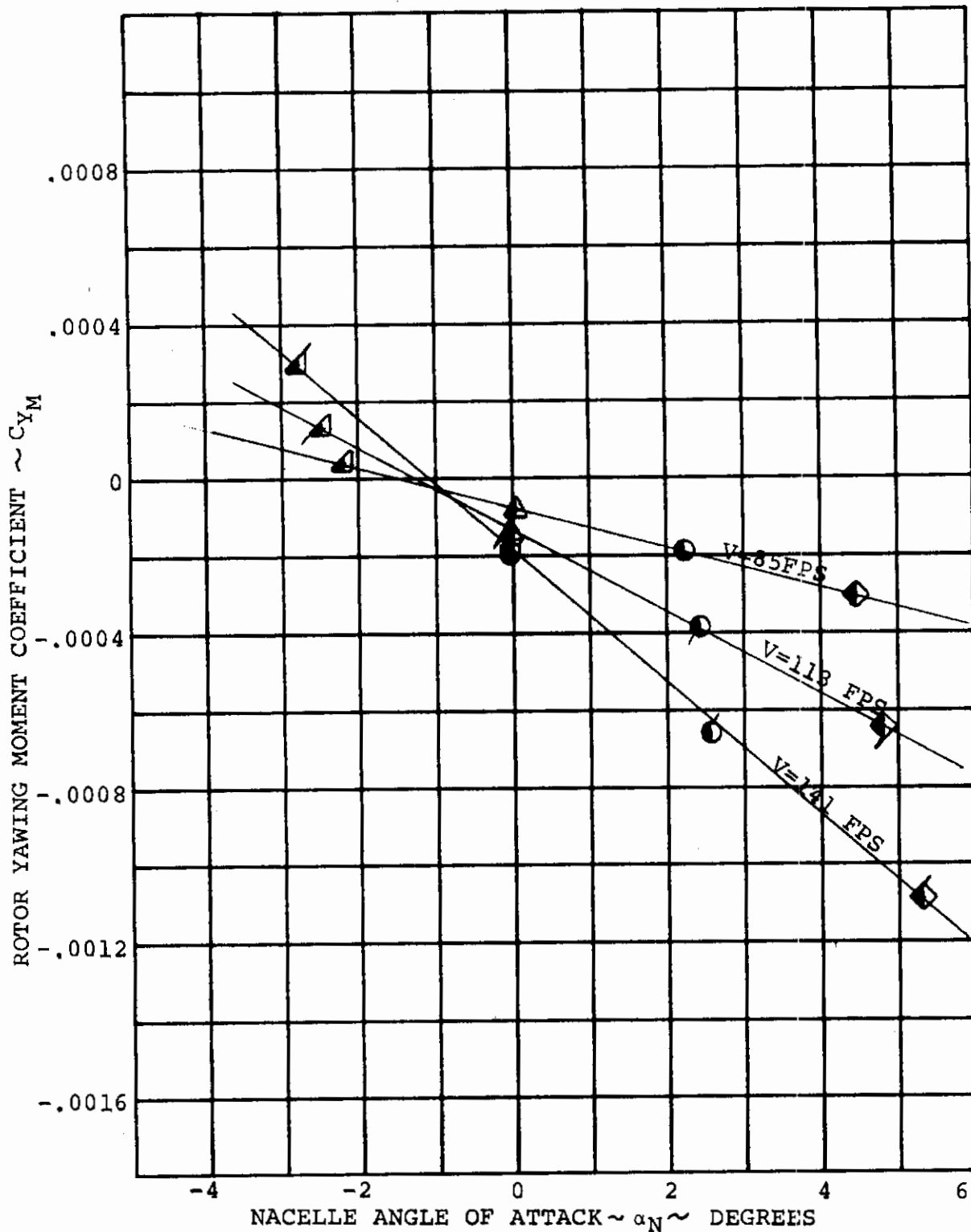


FIGURE 6-29 ROTOR YAWING MOMENT/NACELLE ANGLE OF ATTACK FOR ROTOR RPM = 950  $\delta_F = 0^\circ$



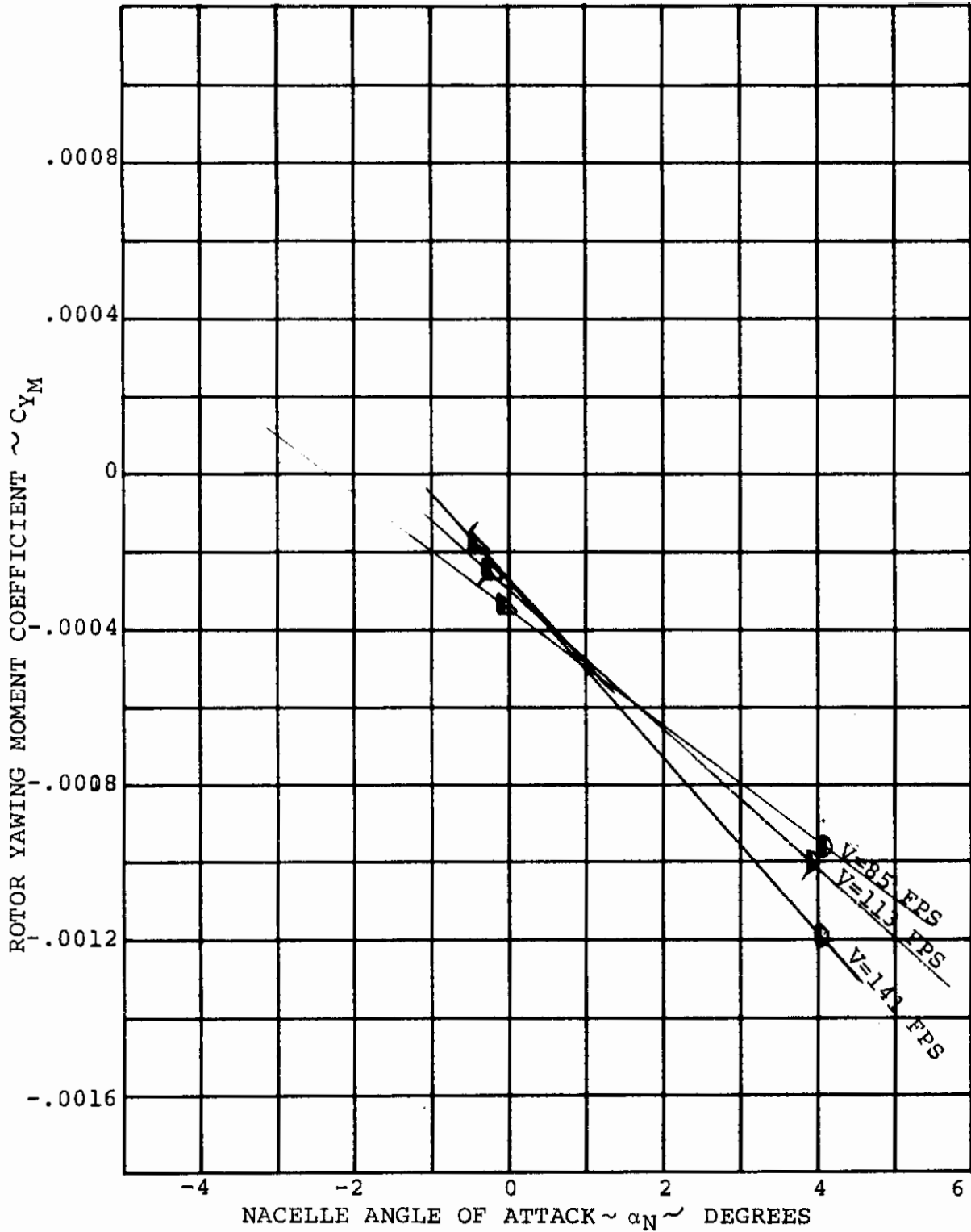


FIGURE 6-30 ROTOR YAWING MOMENT/NACELLE ANGLE OF ATTACK FOR ROTOR RPM = 600  $\delta_F=30^\circ$

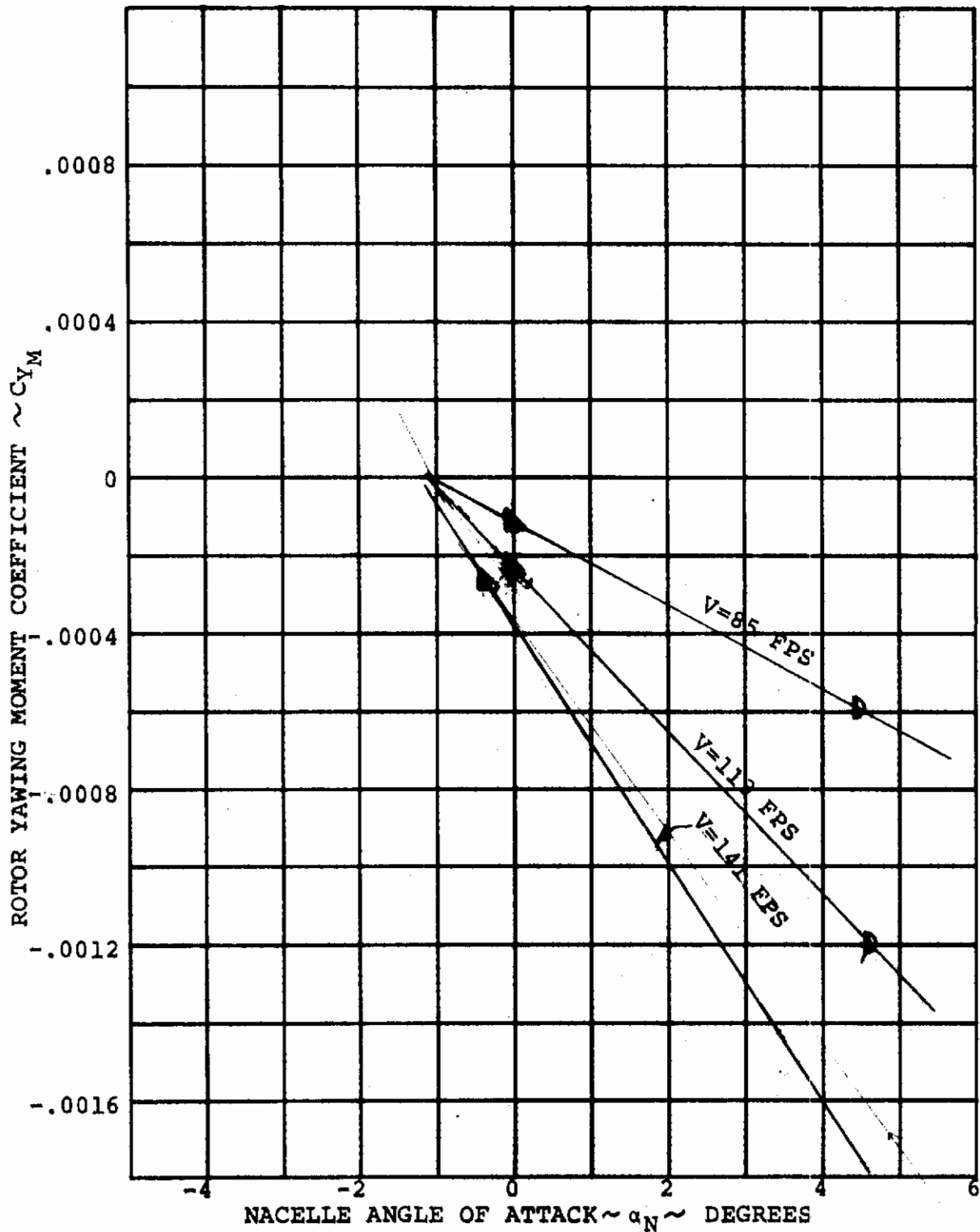


FIGURE 6-31 ROTOR YAWING MOMENT/NACELLE ANGLE OF ATTACK FOR ROTOR RPM = 800  $\delta_F=30^\circ$

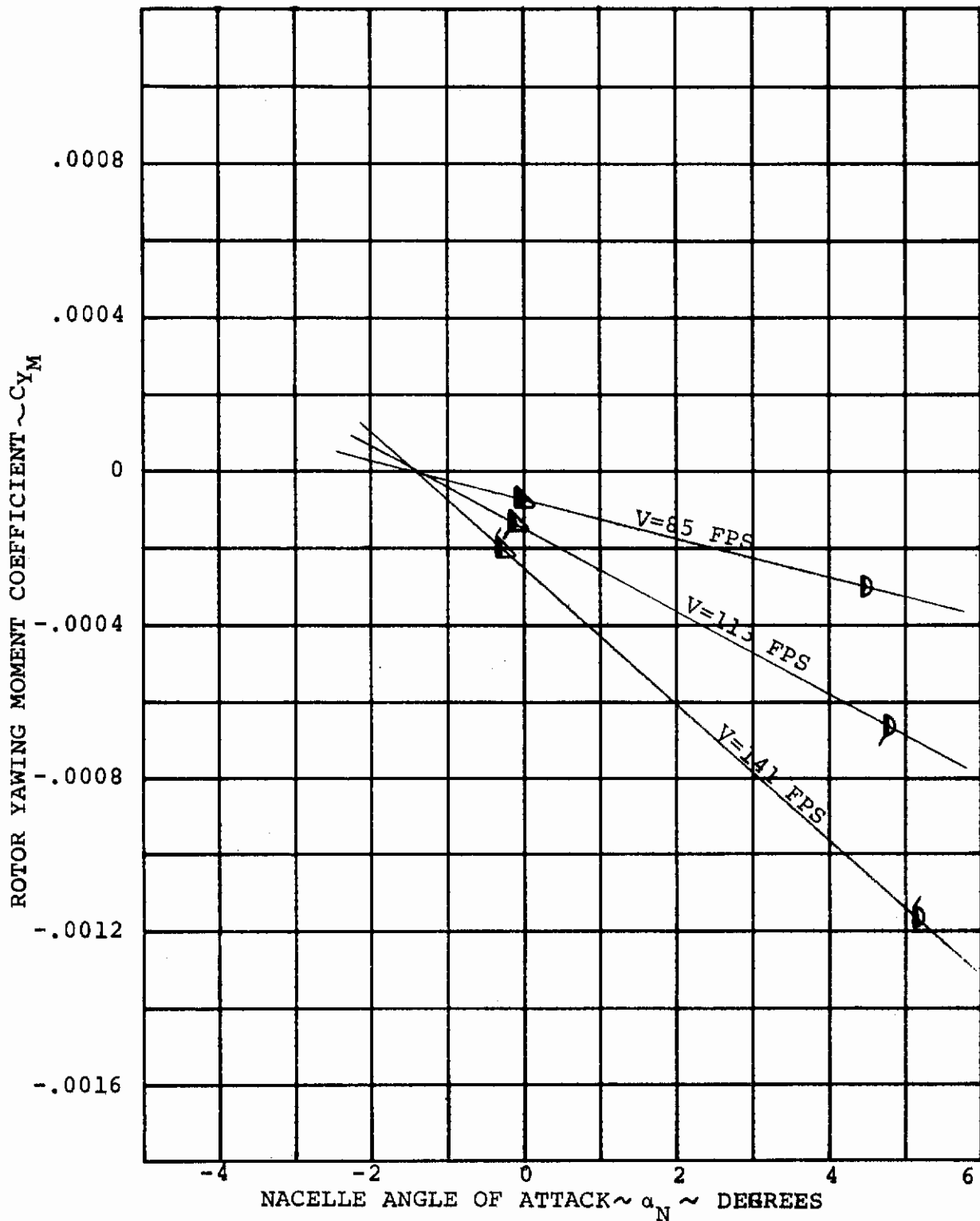


FIGURE 6-32 ROTOR YAWING MOMENT/NACELLE ANGLE OF ATTACK FOR ROTOR RPM = 950  $\delta_F = 30^\circ$

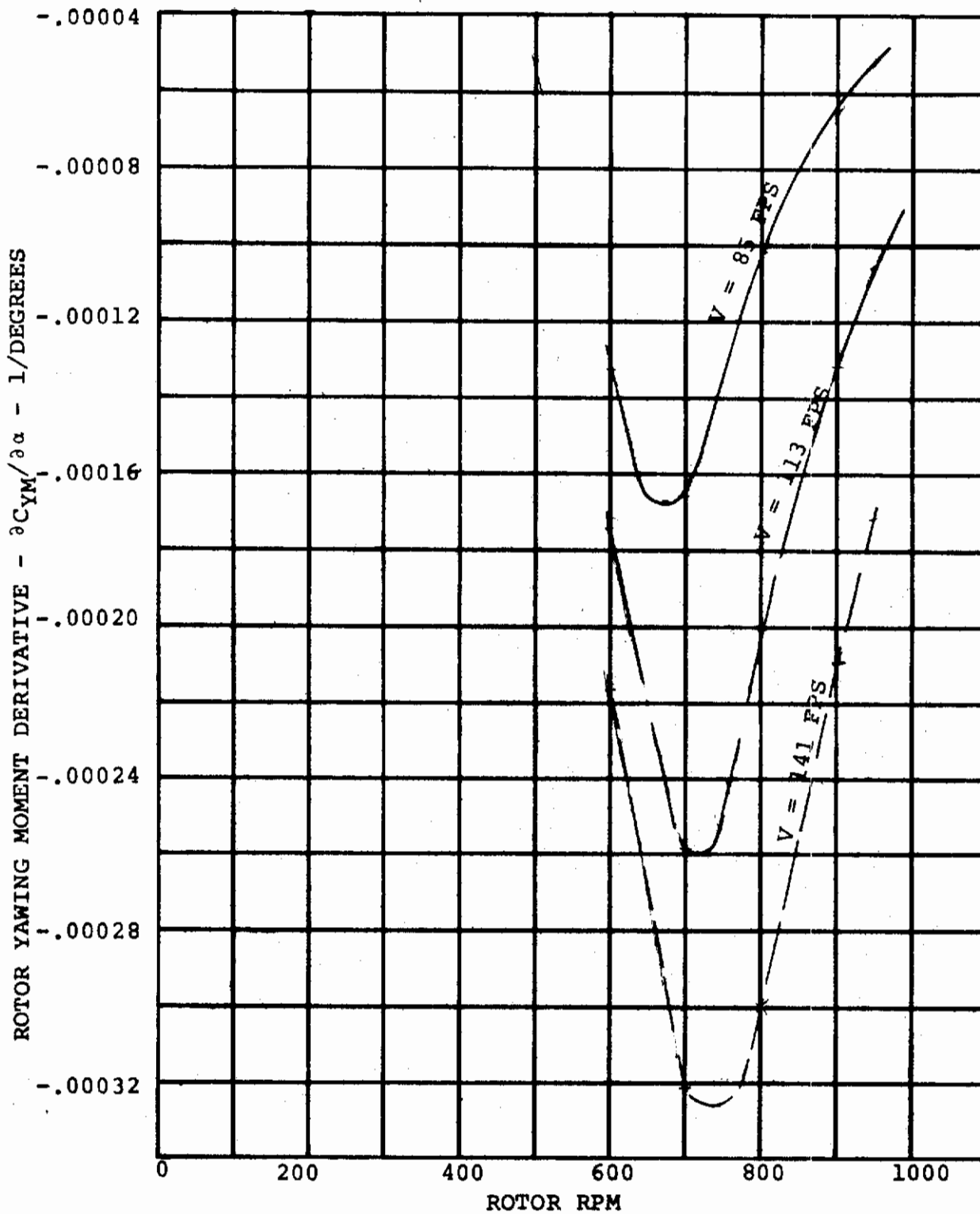


FIGURE 6-33 ROTOR YAWING MOMENT DERIVATIVE VARIATION WITH ROTOR RPM,  $\delta_F = 0.^\circ$

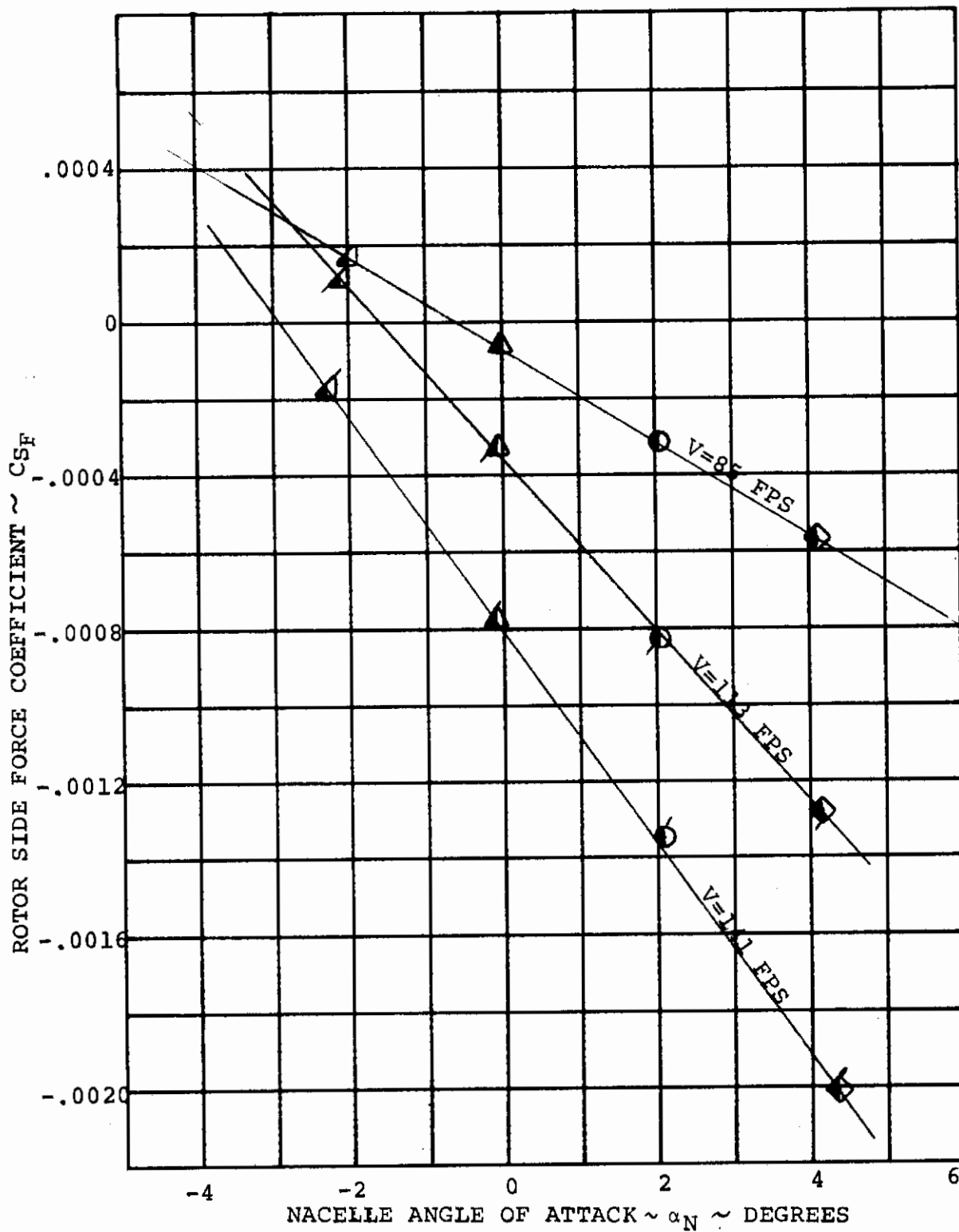


FIGURE 6-34 ROTOR SIDE FORCE/NACELLE ANGLE OF ATTACK FOR ROTOR RPM = 600 δ<sub>F</sub>=0°

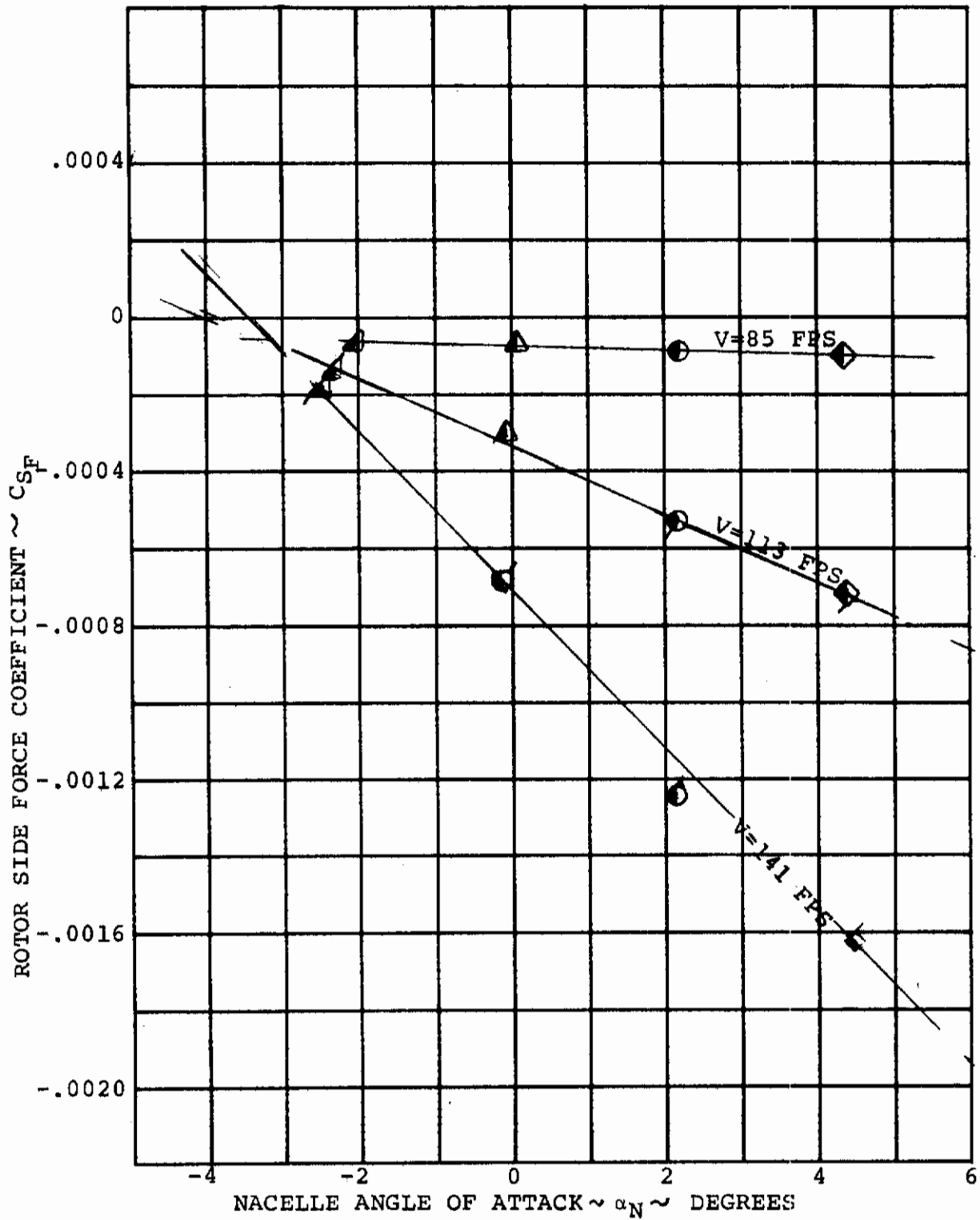


FIGURE 6-35 ROTOR SIDE FORCE/NACELLE ANGLE OF ATTACK FOR ROTOR RPM = 700  $\delta_F = 0^\circ$

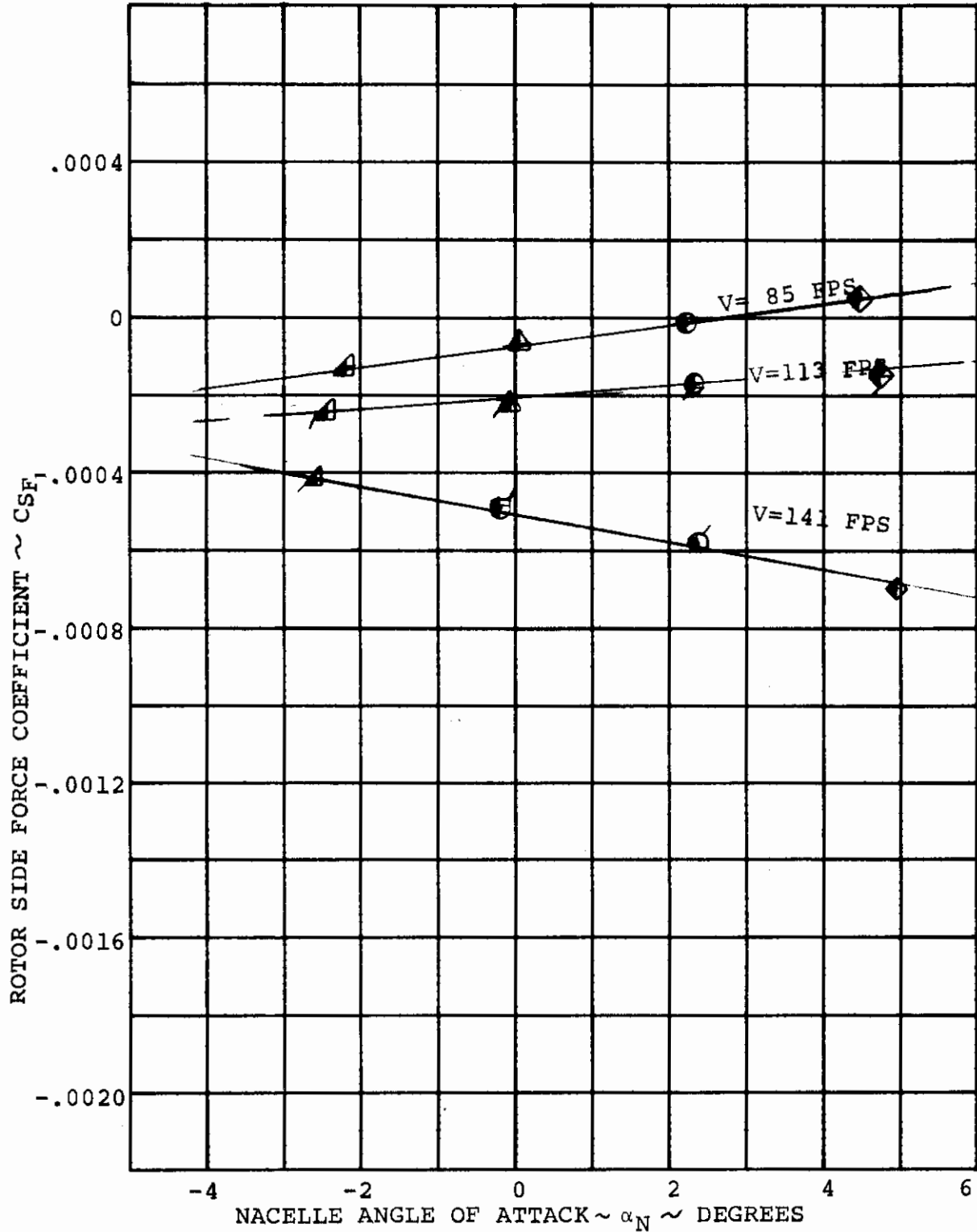


FIGURE 6-36 ROTOR SIDE FORCE/NACELLE ANGLE OF ATTACK FOR ROTOR RPM = 800 δ<sub>F</sub> = 0°

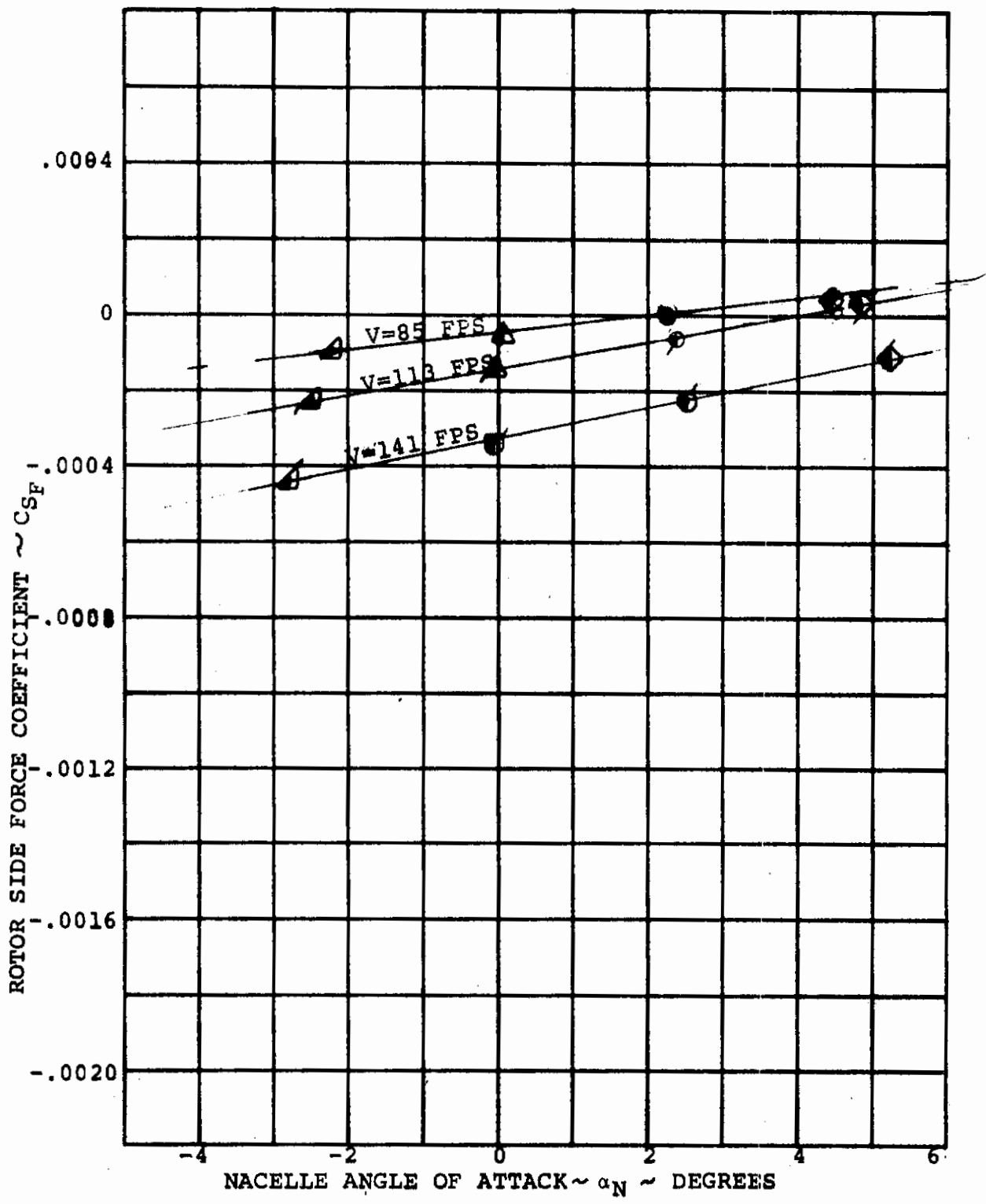


FIGURE 6-37 ROTOR SIDE FORCE/NACELLE ANGLE OF ATTACK FOR ROTOR RPM = 900  $\delta_F = 0^\circ$



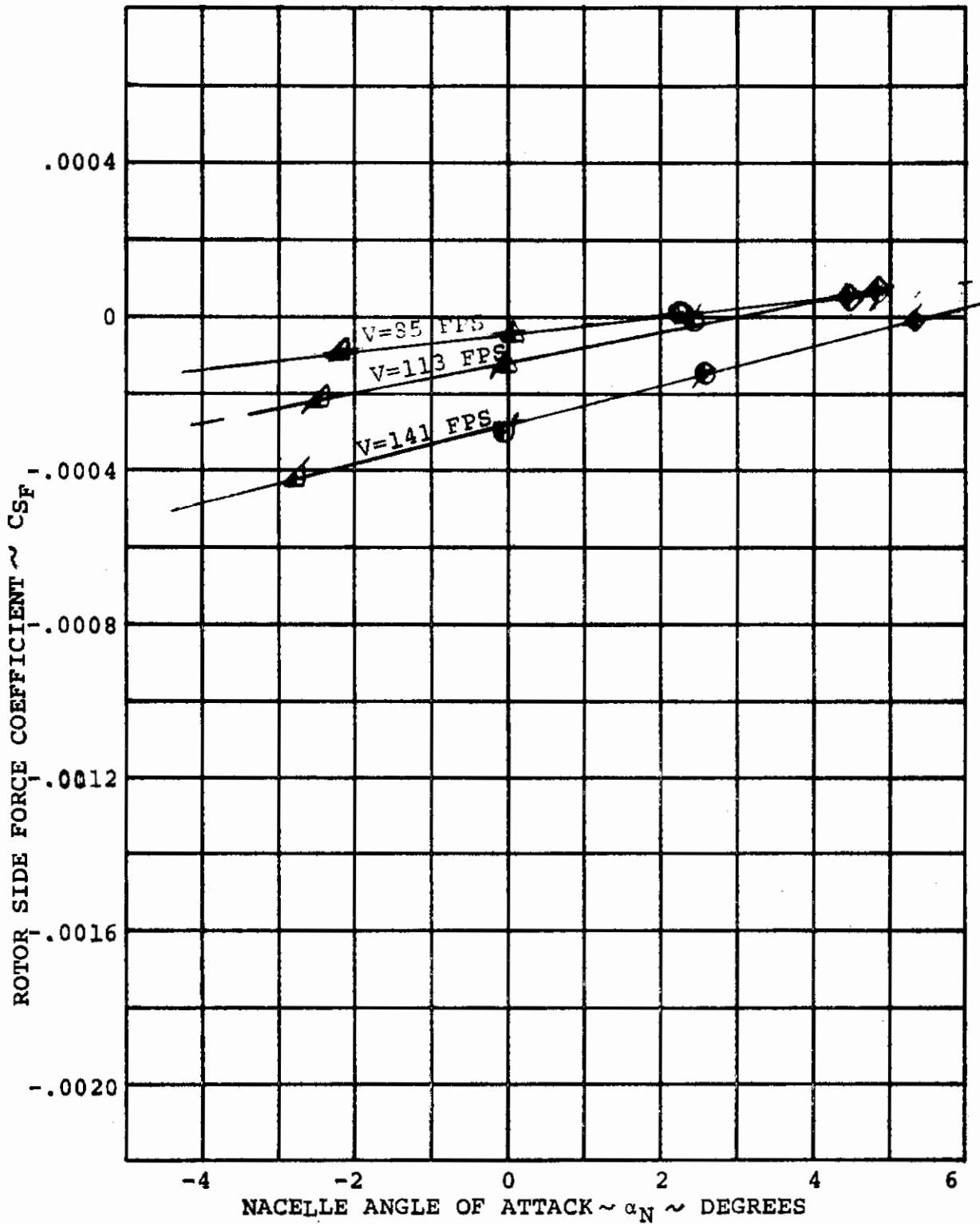


FIGURE 6-38 ROTOR SIDE FORCE/NACELLE ANGLE OF ATTACK FOR ROTOR RPM = 950 δ<sub>F</sub> = 0°

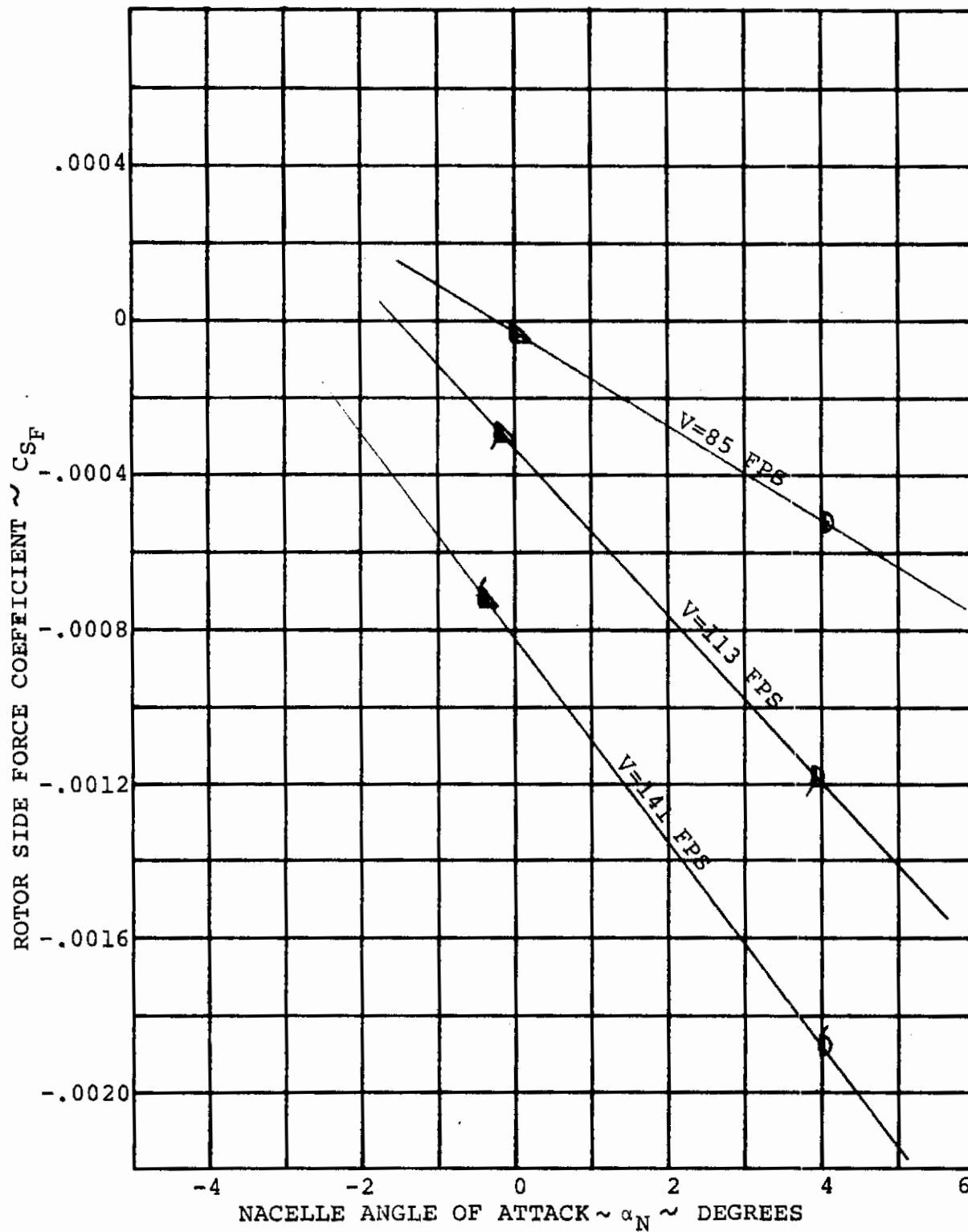


FIGURE 6-39 ROTOR SIDE FORCE/NACELLE ANGLE OF ATTACK FOR ROTOR RPM = 600  $\delta_F = 30^\circ$

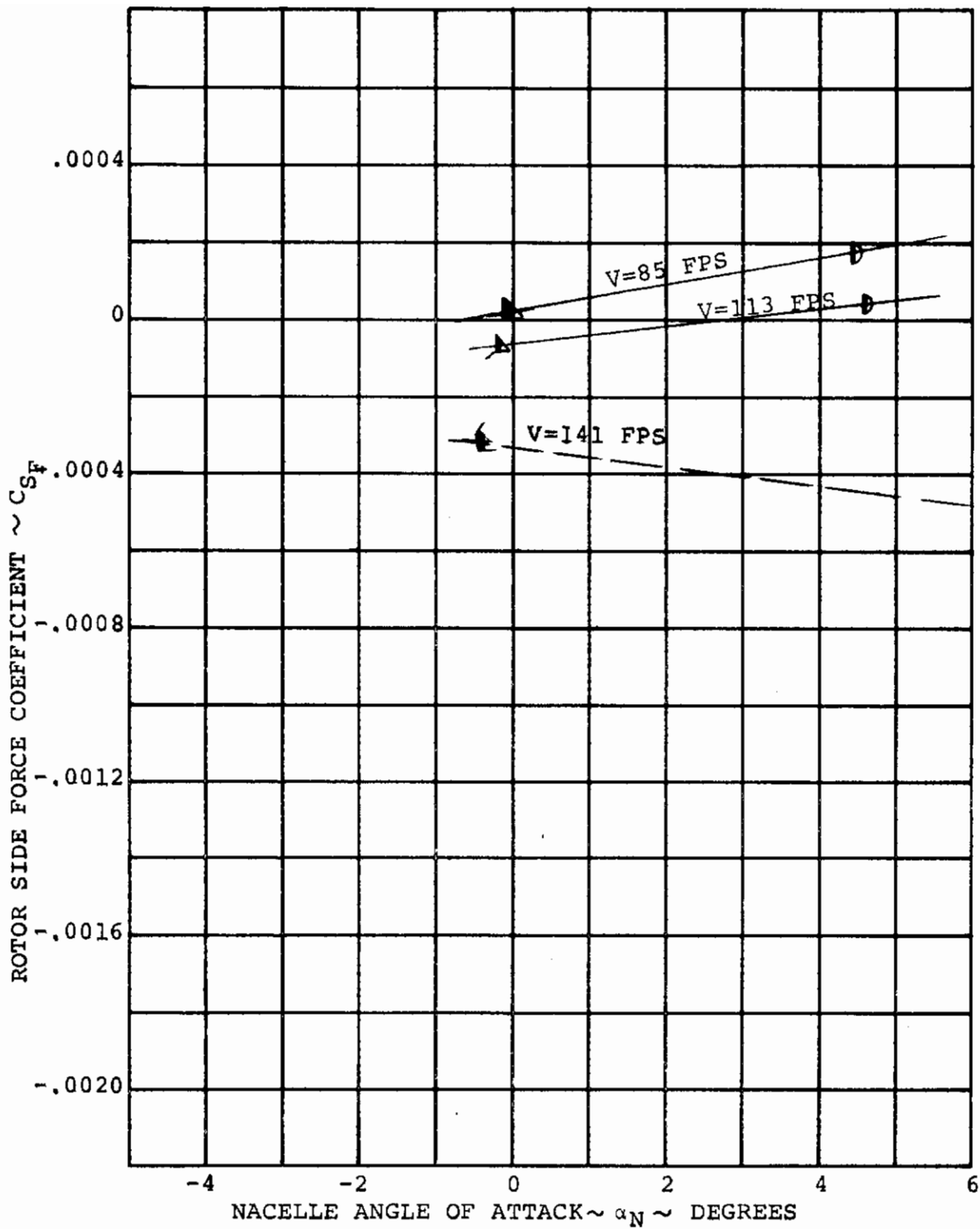


FIGURE 6-40 ROTOR SIDE FORCE/NACELLE ANGLE OF ATTACK FOR ROTOR RPM = 800  $\delta_F = 30^\circ$

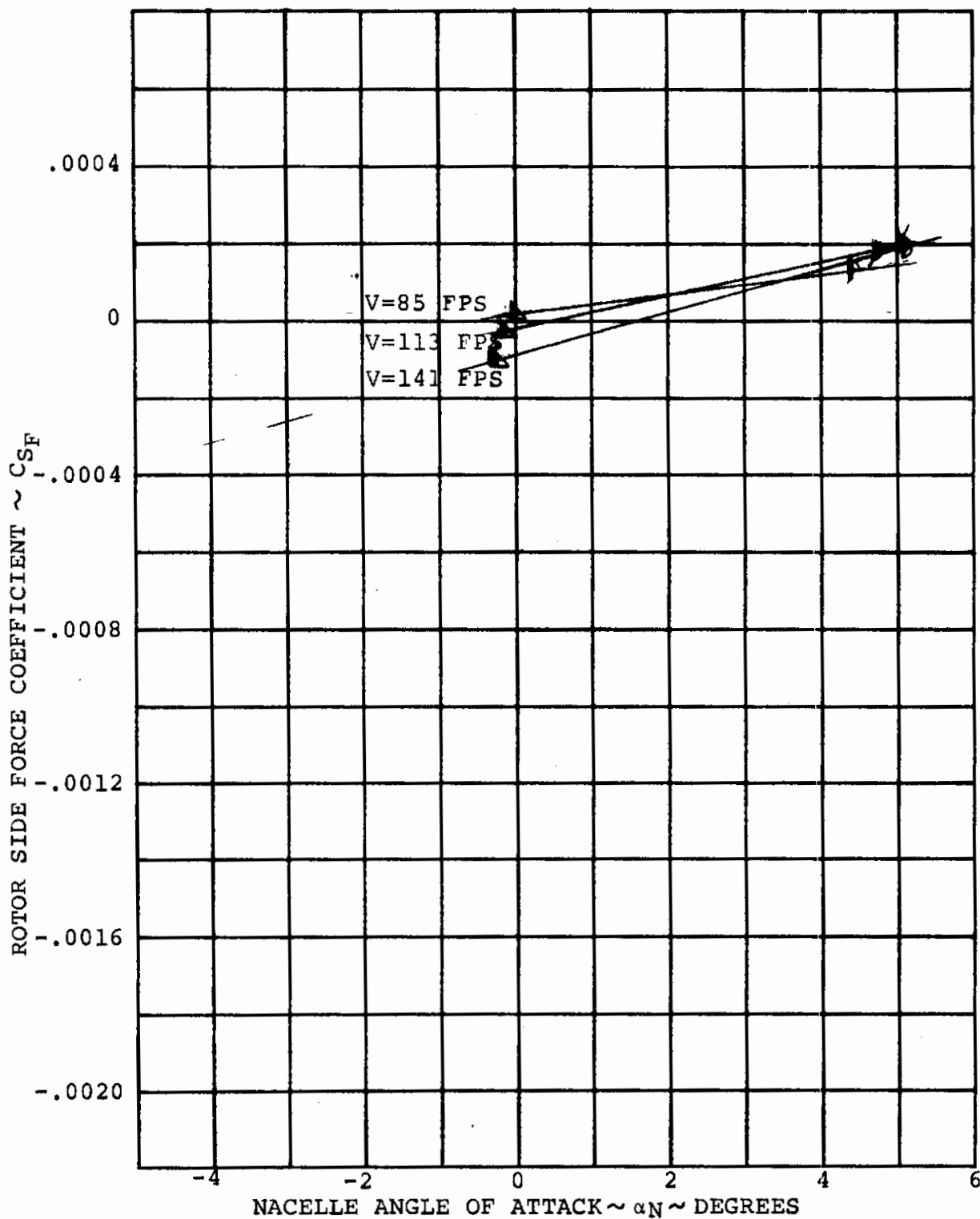


FIGURE 6-41 ROTOR SIDE FORCE/NACELLE ANGLE OF ATTACK FOR ROTOR RPM = 950  $\delta_F=30^\circ$

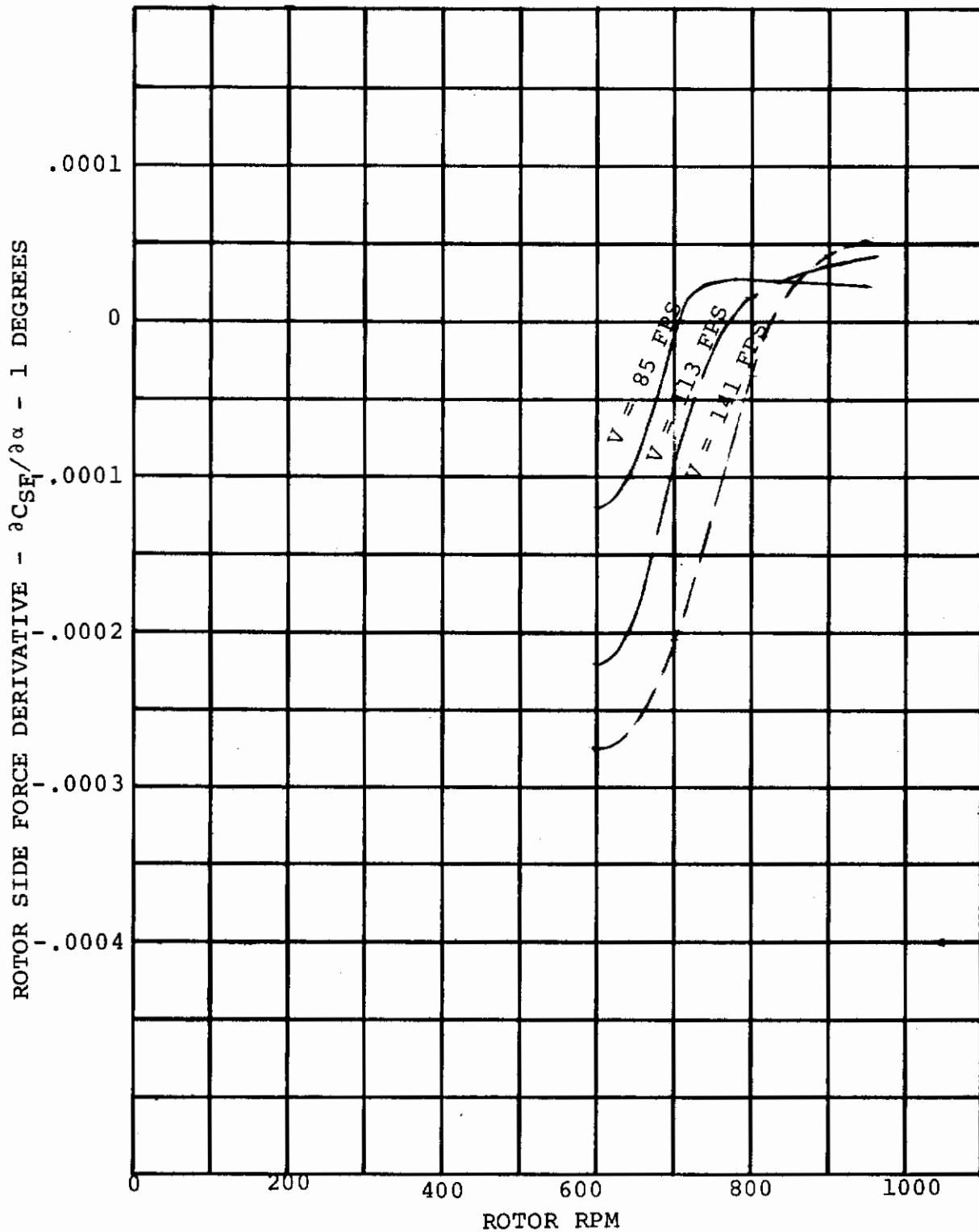


FIGURE 6-42 ROTOR SIDE FORCE DERIVATIVE VARIATION WITH ROTOR RPM,  $\delta_F = 0^\circ$

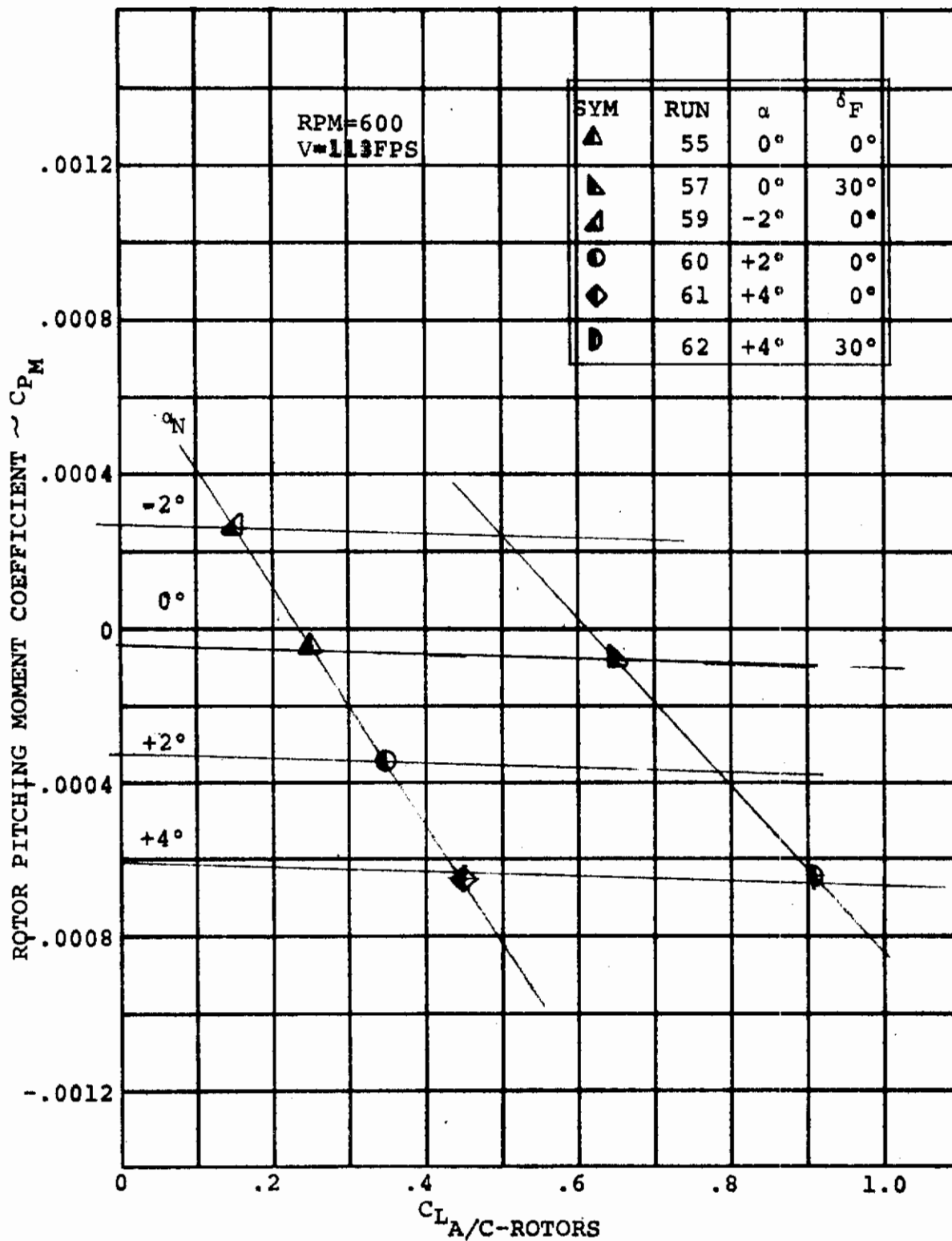


FIGURE 6-43 EFFECT OF WING LIFT ON ROTOR PITCHING MOMENT  
(V = 113 FPS, RPM = 600)

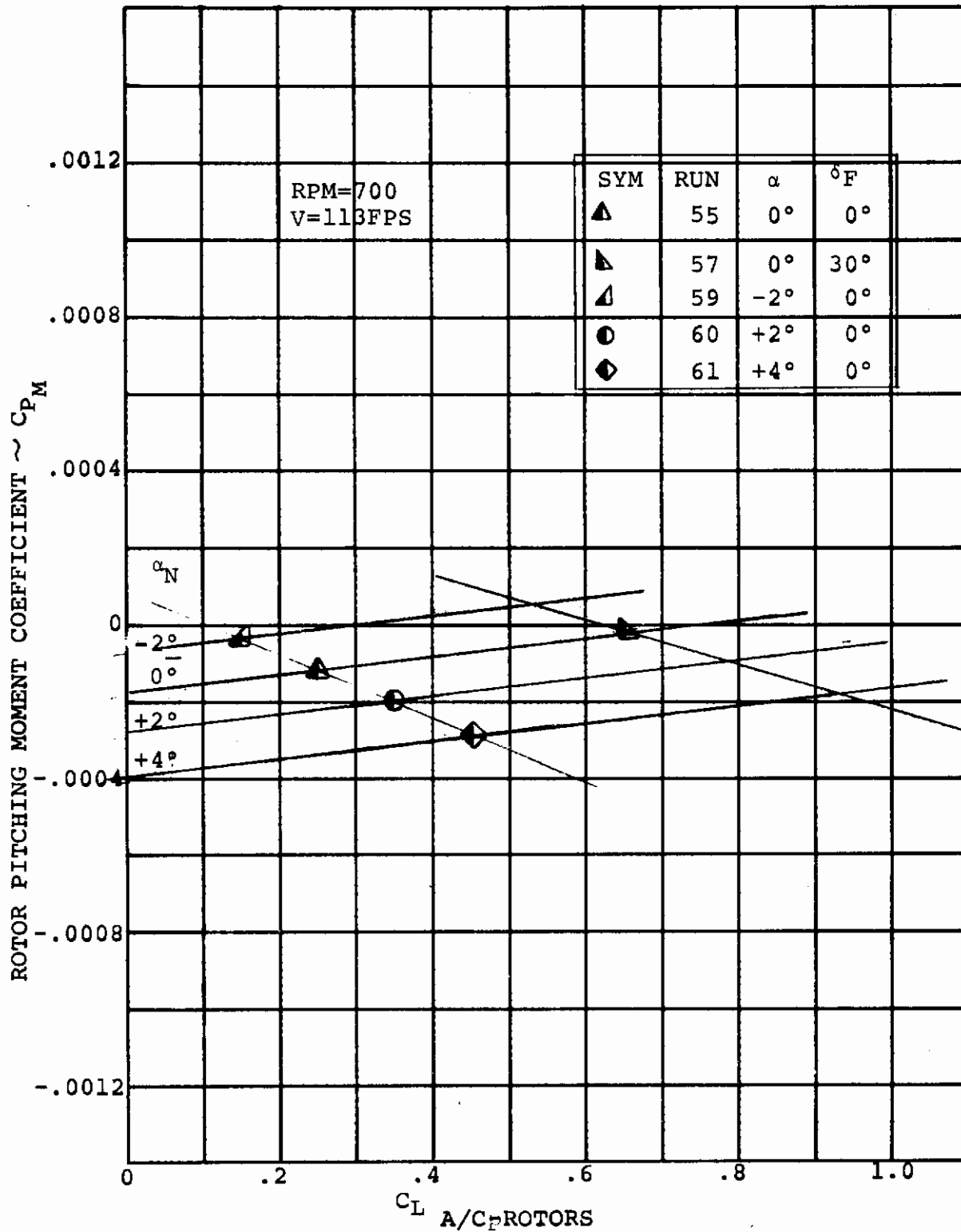


FIGURE 6-44 EFFECT OF WING LIFT ON ROTOR PITCHING MOMENT  
(V = 113 FPS, RPM = 700)

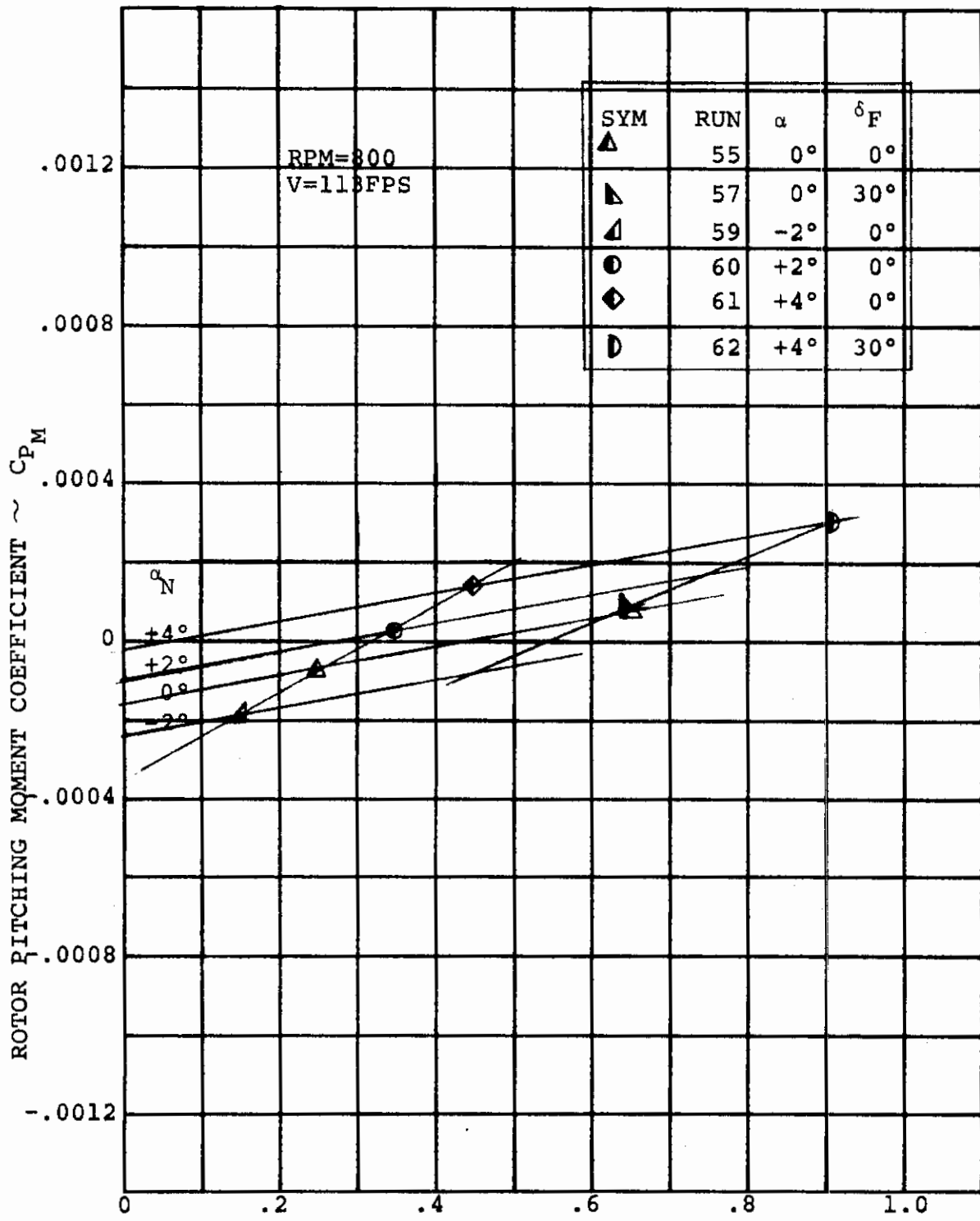


FIGURE 6-45 EFFECT OF WING LIFT ON ROTOR PITCHING MOMENT  
(V = 113 FPS, RPM = 800)



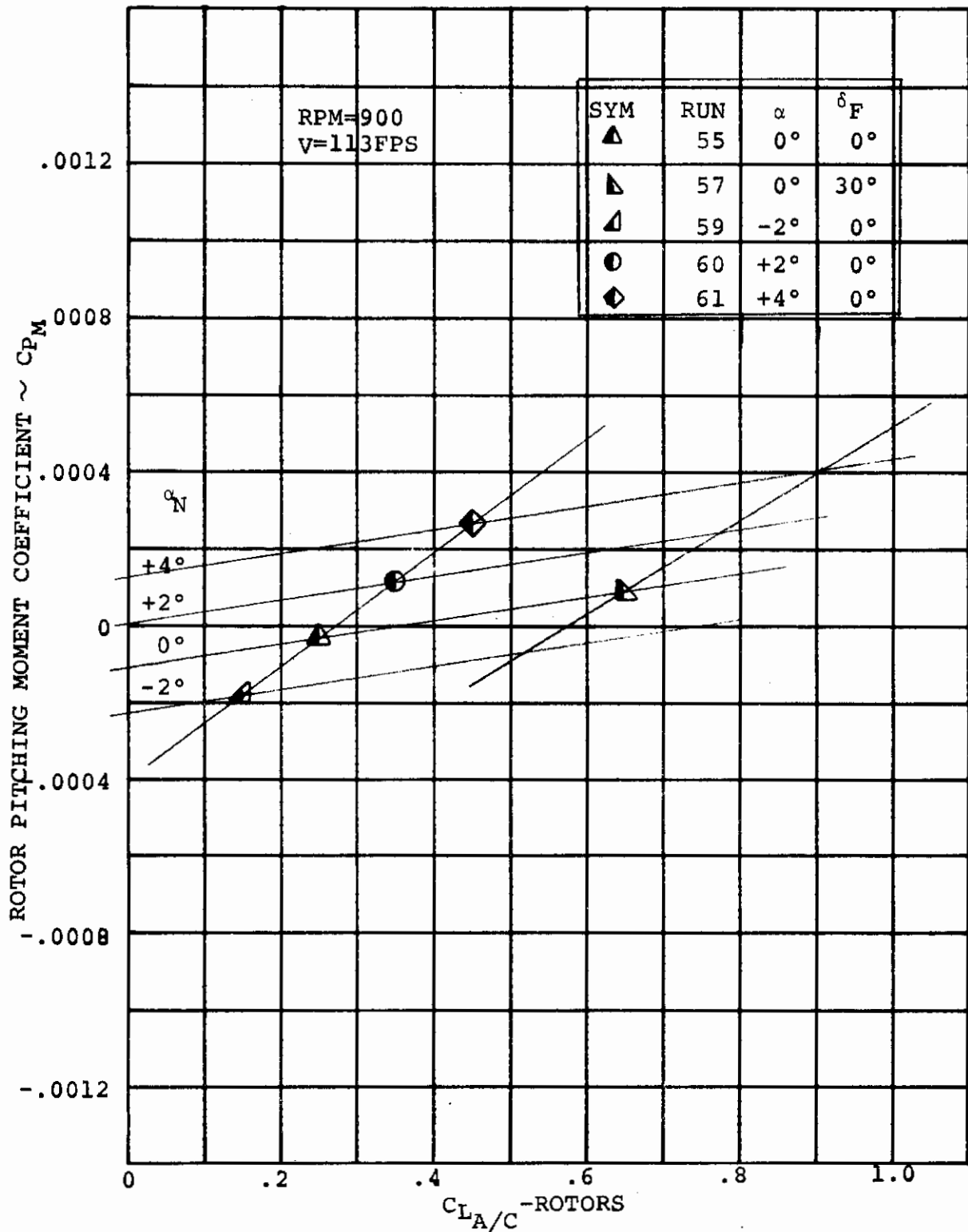


FIGURE 6-46 EFFECT OF WING LIFT ON ROTOR PITCHING MOMENT  
(V = 113 FPS, RPM = 900)

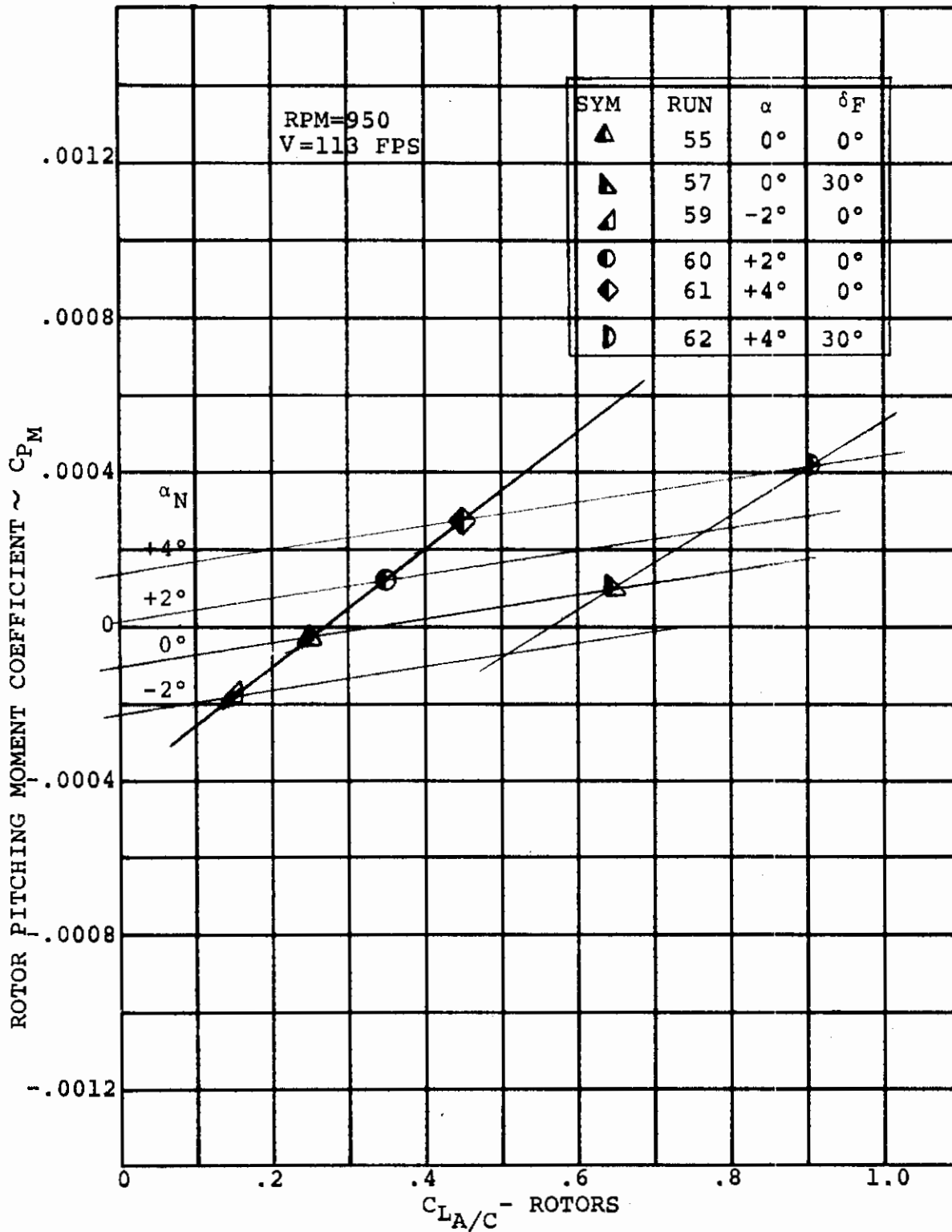


FIGURE 6-47 EFFECT OF WING LIFT ON ROTOR PITCHING MOMENT  
(V = 113 FPS, RPM = 950)

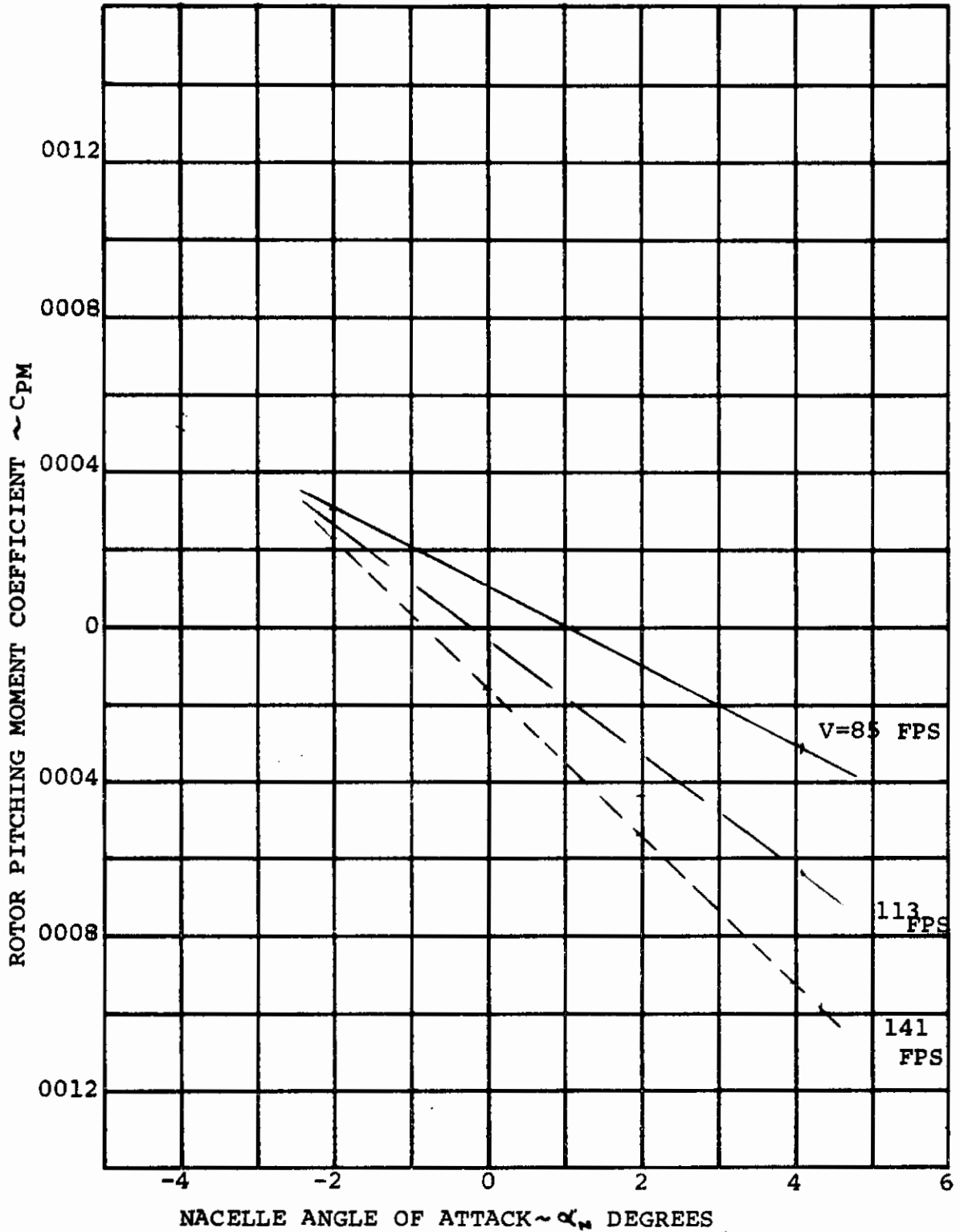


FIGURE 6-48 ROTOR PITCHING MOMENT/NACELLE ANGLE OF ATTACK FOR ROTOR RPM = 600 δ<sub>n</sub> = 0°. (CIRCULATION EFFECTS REMOVED)

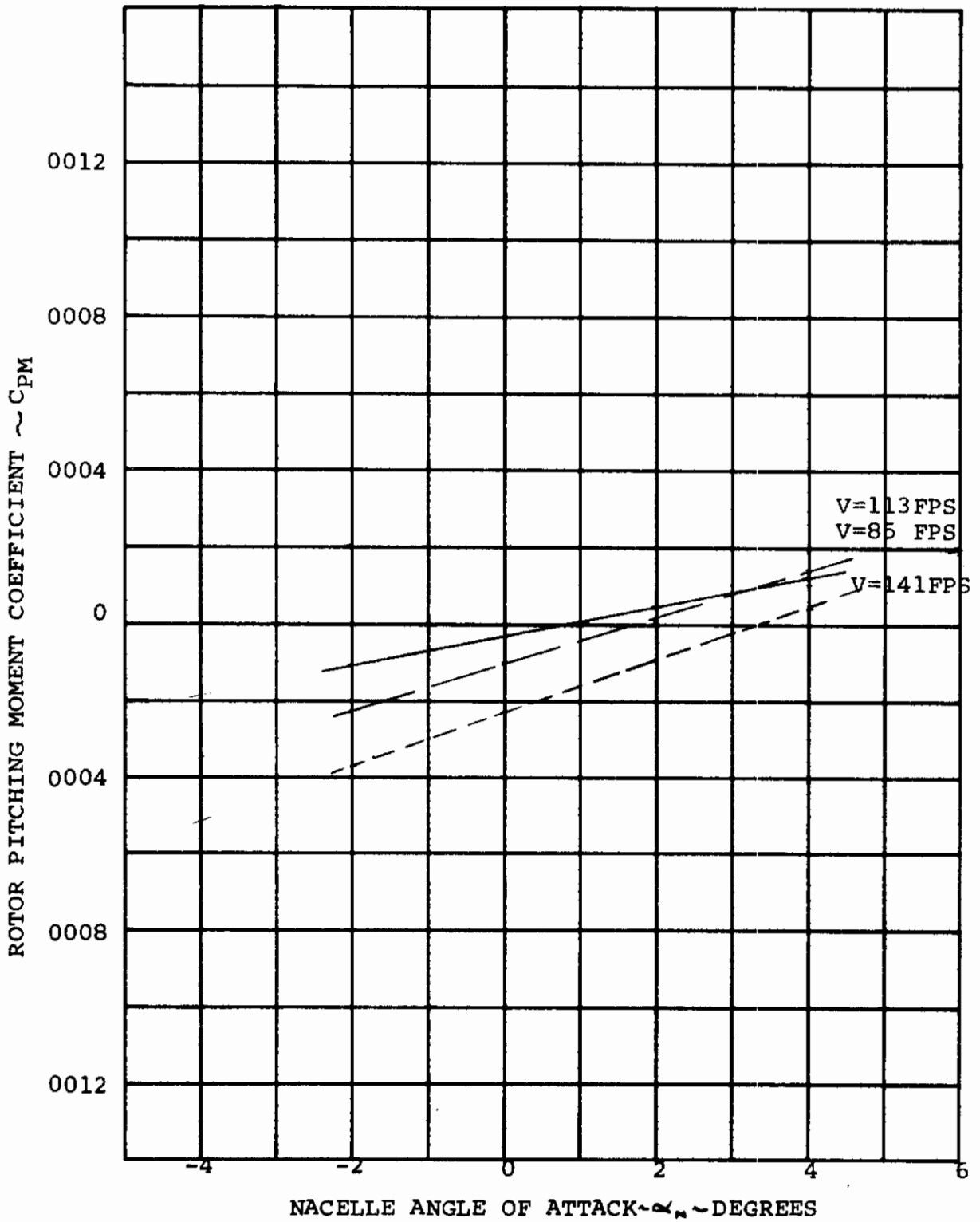


FIGURE 6-49 ROTOR PITCHING MOMENT/NACELLE ANGLE OF ATTACK FOR ROTOR RPM = 950  $\delta_r = 0^\circ$  (CIRCULATION EFFECTS REMOVED)

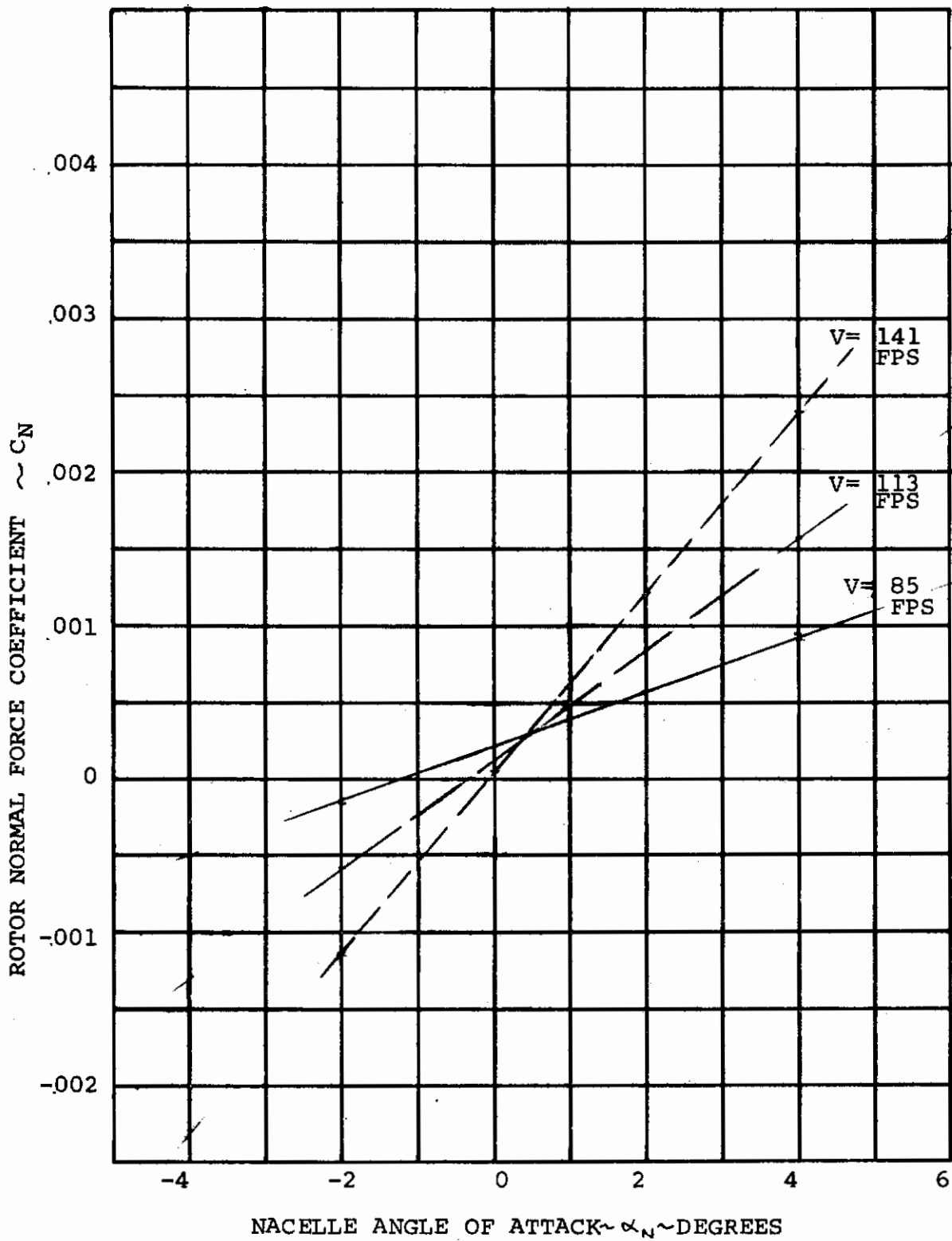


FIGURE 6-50 ROTOR NORMAL FORCE/NACELLE ANGLE OF ATTACK VARIATION FOR ROTOR RPM = 600  $\delta_F = 0^\circ$  (CIRCULATION EFFECTS REMOVED)

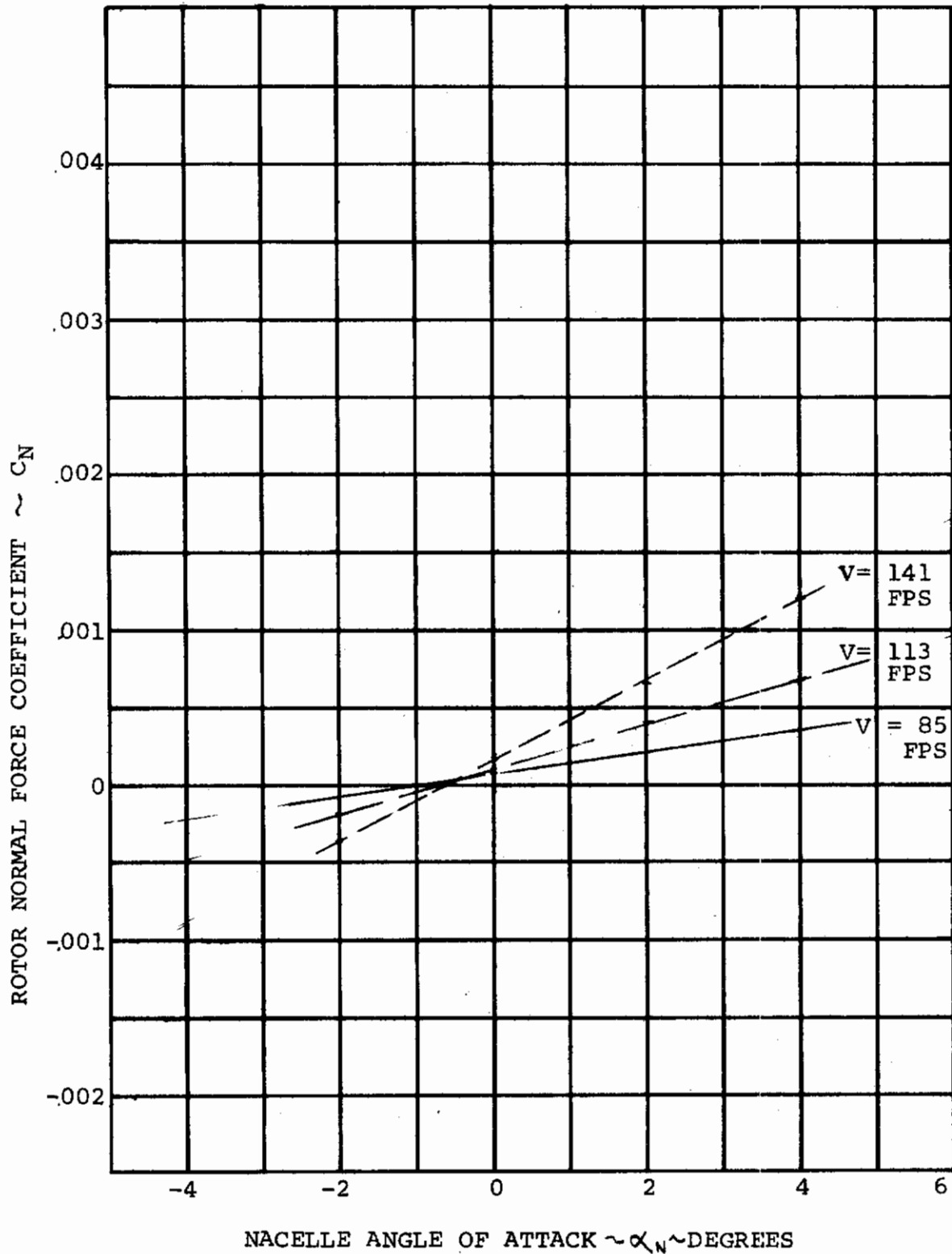


FIGURE 6-51 ROTOR NORMAL FORCE/NACELLE ANGLE OF ATTACK VARIATION FOR ROTOR RPM = 950  $\delta_F = 0^\circ$   
(CIRCULATION EFFECTS REMOVED)

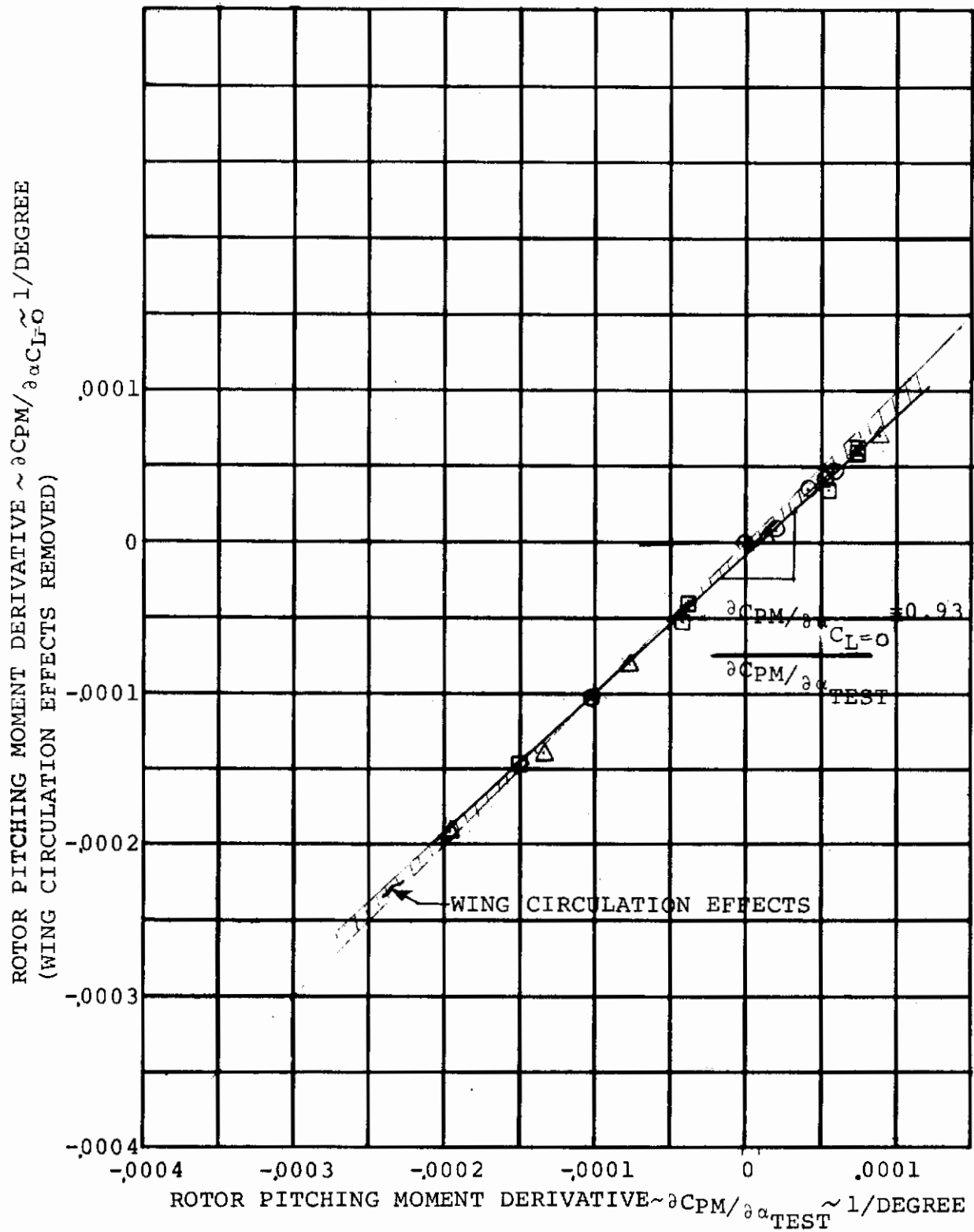


FIGURE 6-52 COMPARISON OF ROTOR PITCHING MOMENT DERIVATIVE WITH AND WITHOUT WING CIRCULATION EFFECTS

$\delta_F = 0^\circ$

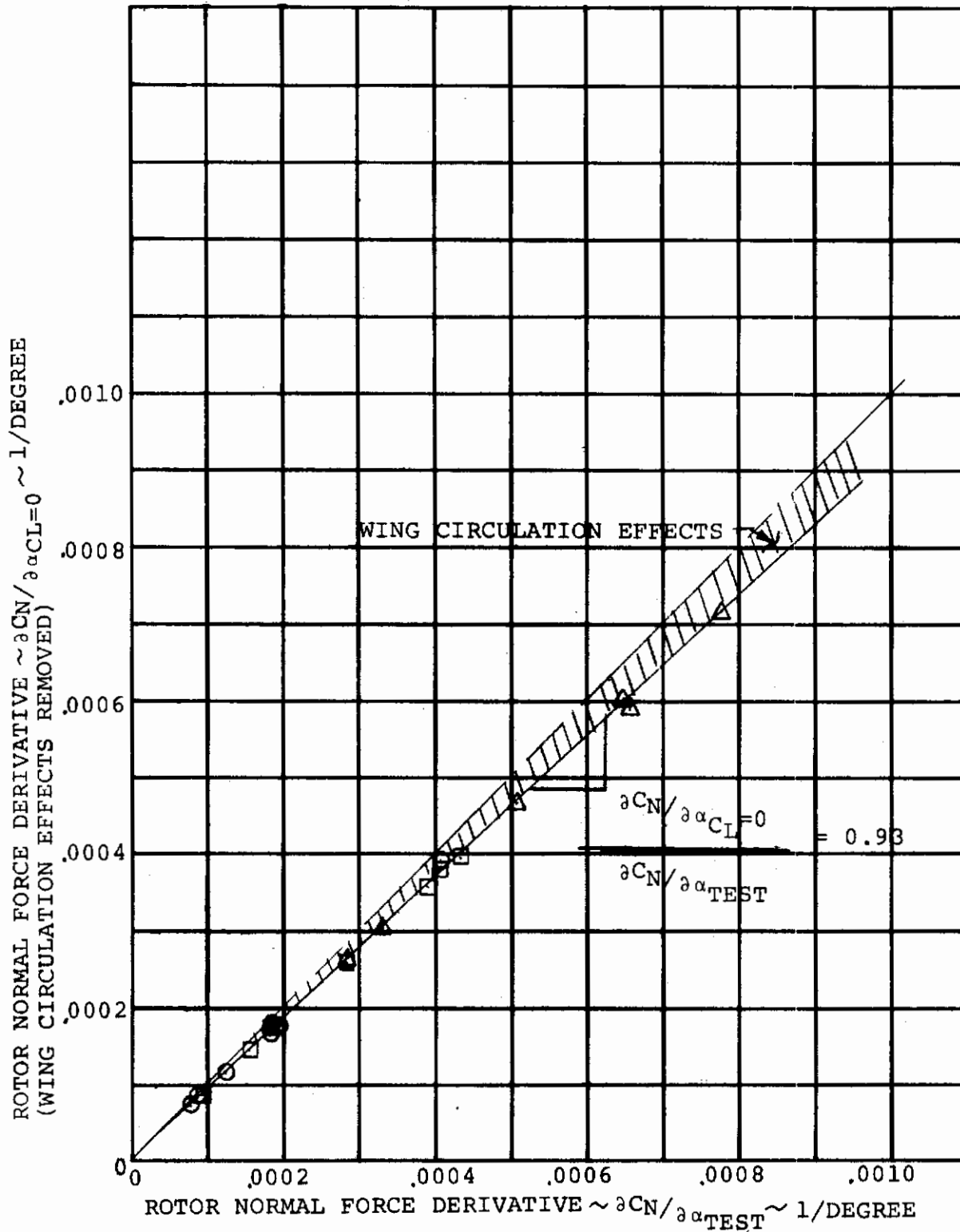


FIGURE 6-53 COMPARISON OF ROTOR NORMAL FORCE DERIVATIVE WITH AND WITHOUT WING CIRCULATION EFFECTS



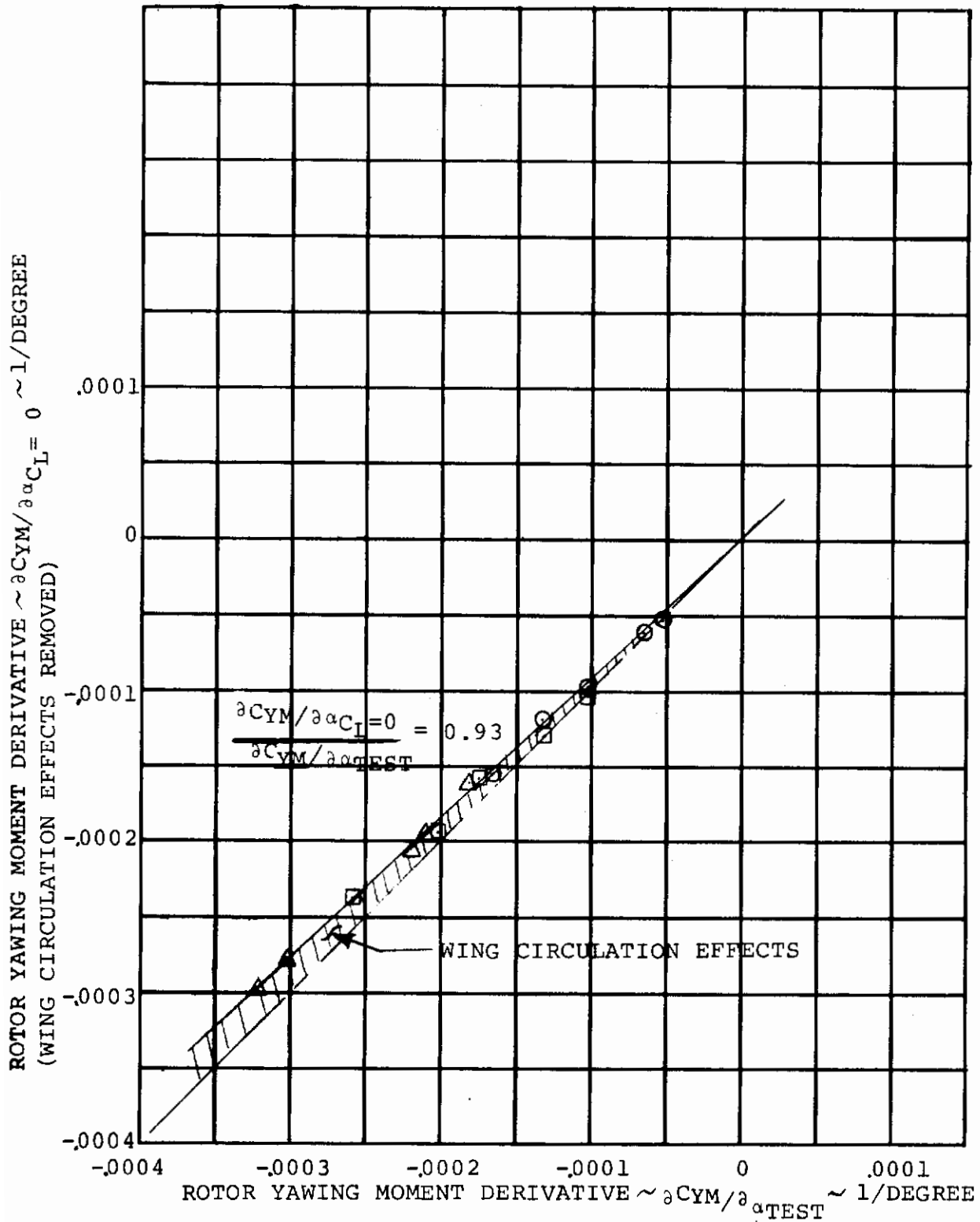


FIGURE 6-54 COMPARISON OF ROTOR YAWING MOMENT DERIVATIVE WITH AND WITHOUT WING CIRCULATION EFFECTS

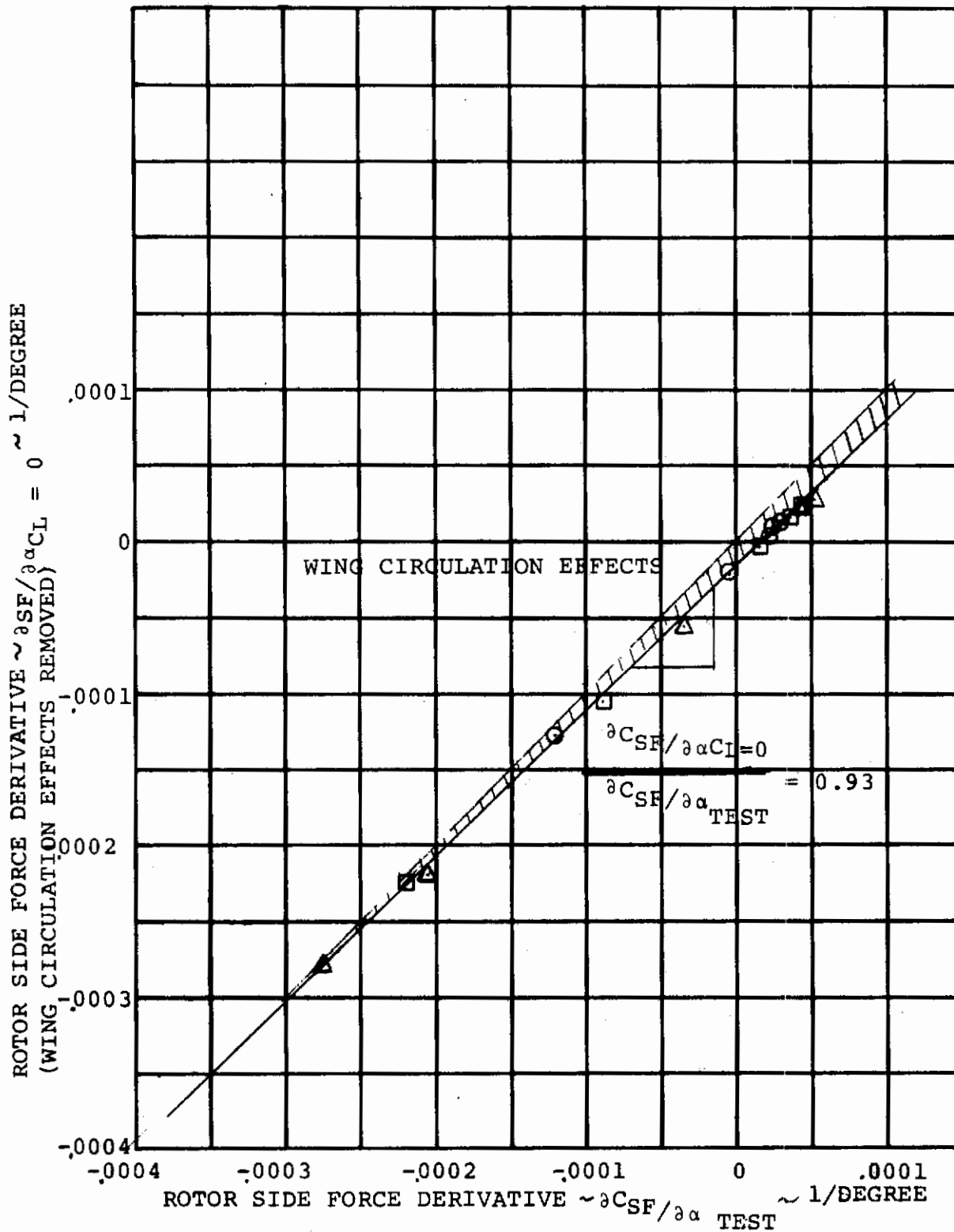


FIGURE 6-55 COMPARISON OF ROTOR SIDE FORCE DERIVATIVES WITH AND WITHOUT WING CIRCULATION EFFECTS

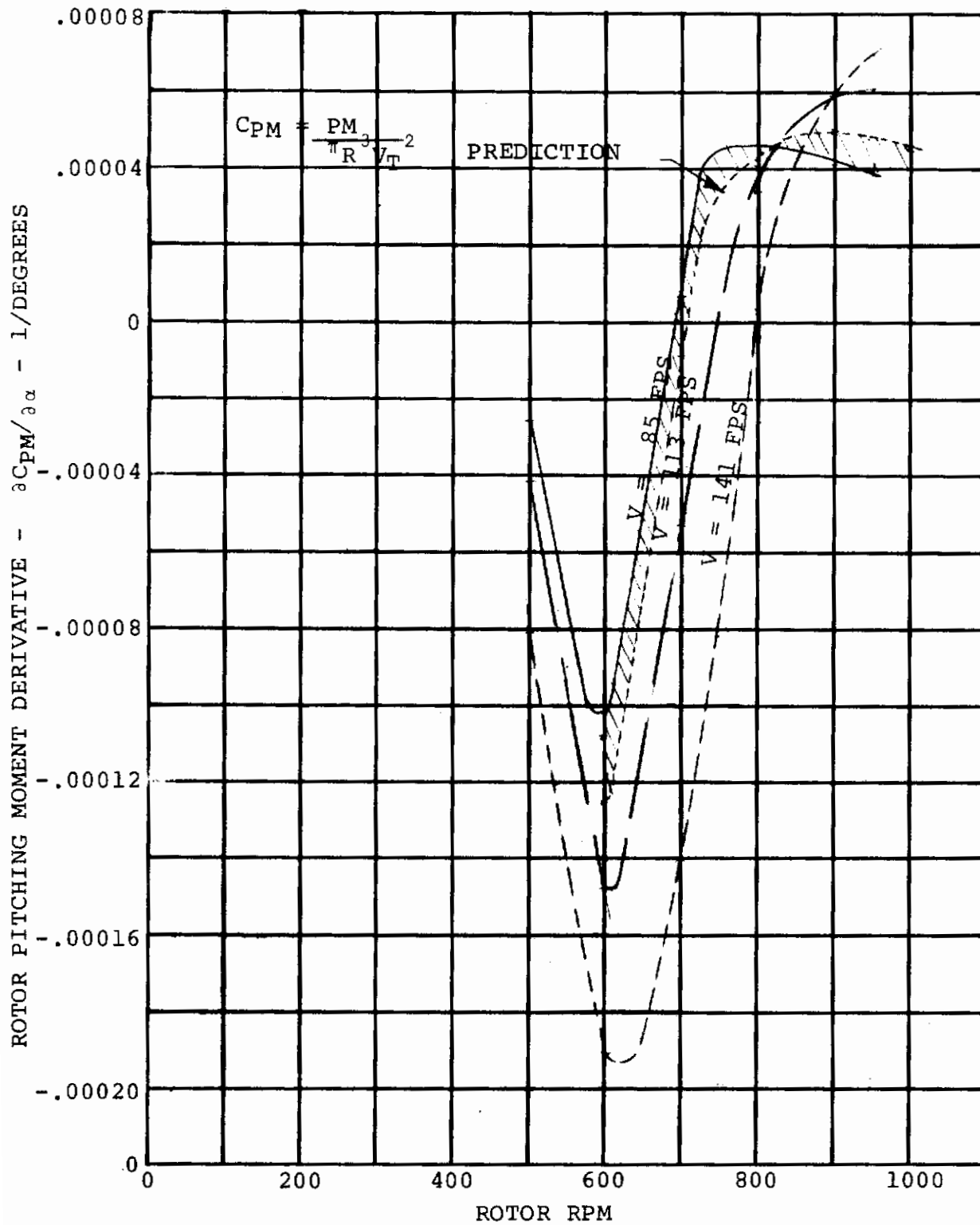


FIGURE 6-56 ROTOR PITCHING MOMENT DERIVATIVE VARIATION WITH ROTOR RPM (WING CIRCULATION EFFECTS REMOVED)

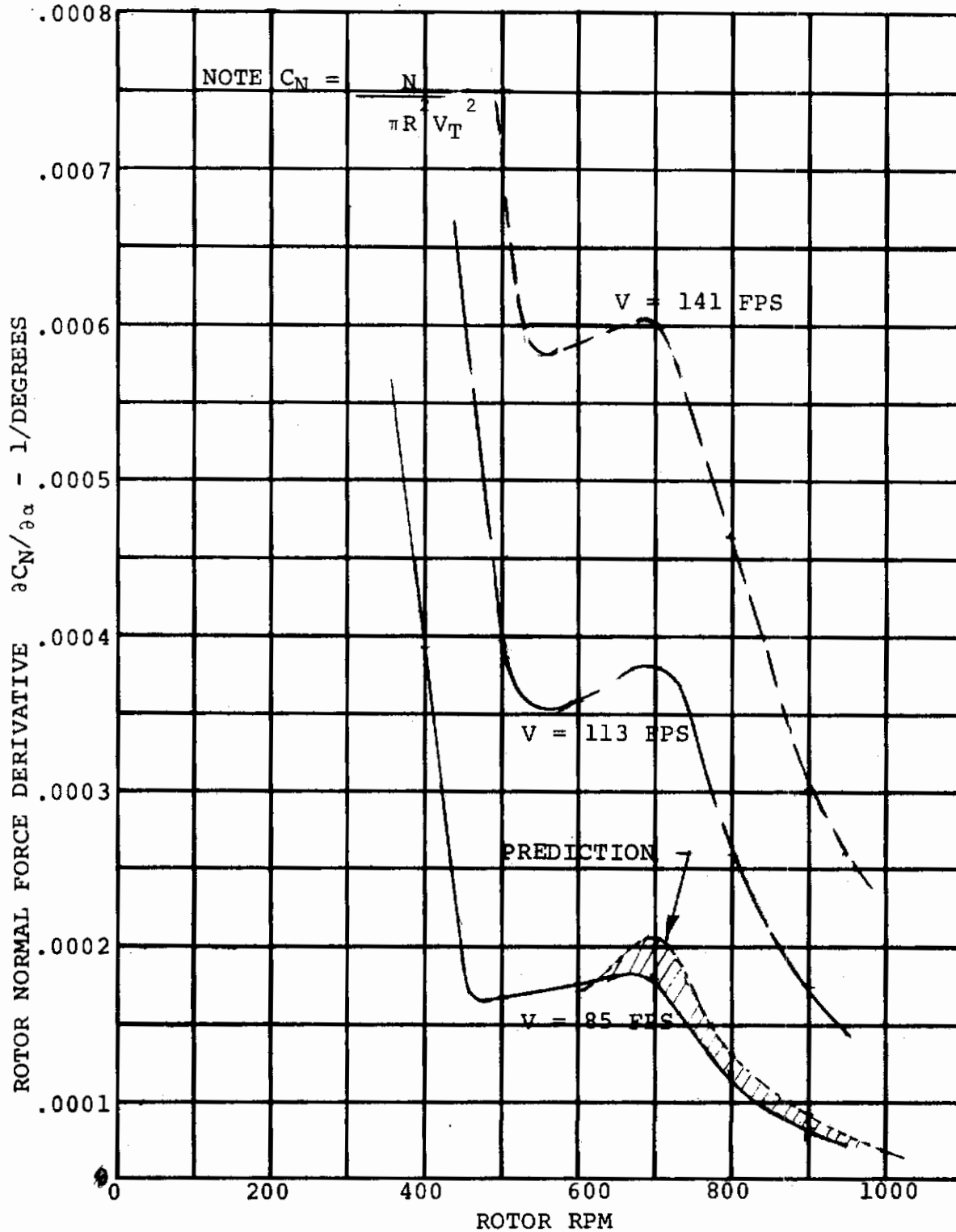


FIGURE 6-57 ROTOR NORMAL FORCE DERIVATIVE VARIATION WITH ROTOR RPM (WING CIRCULATION EFFECTS REMOVED)

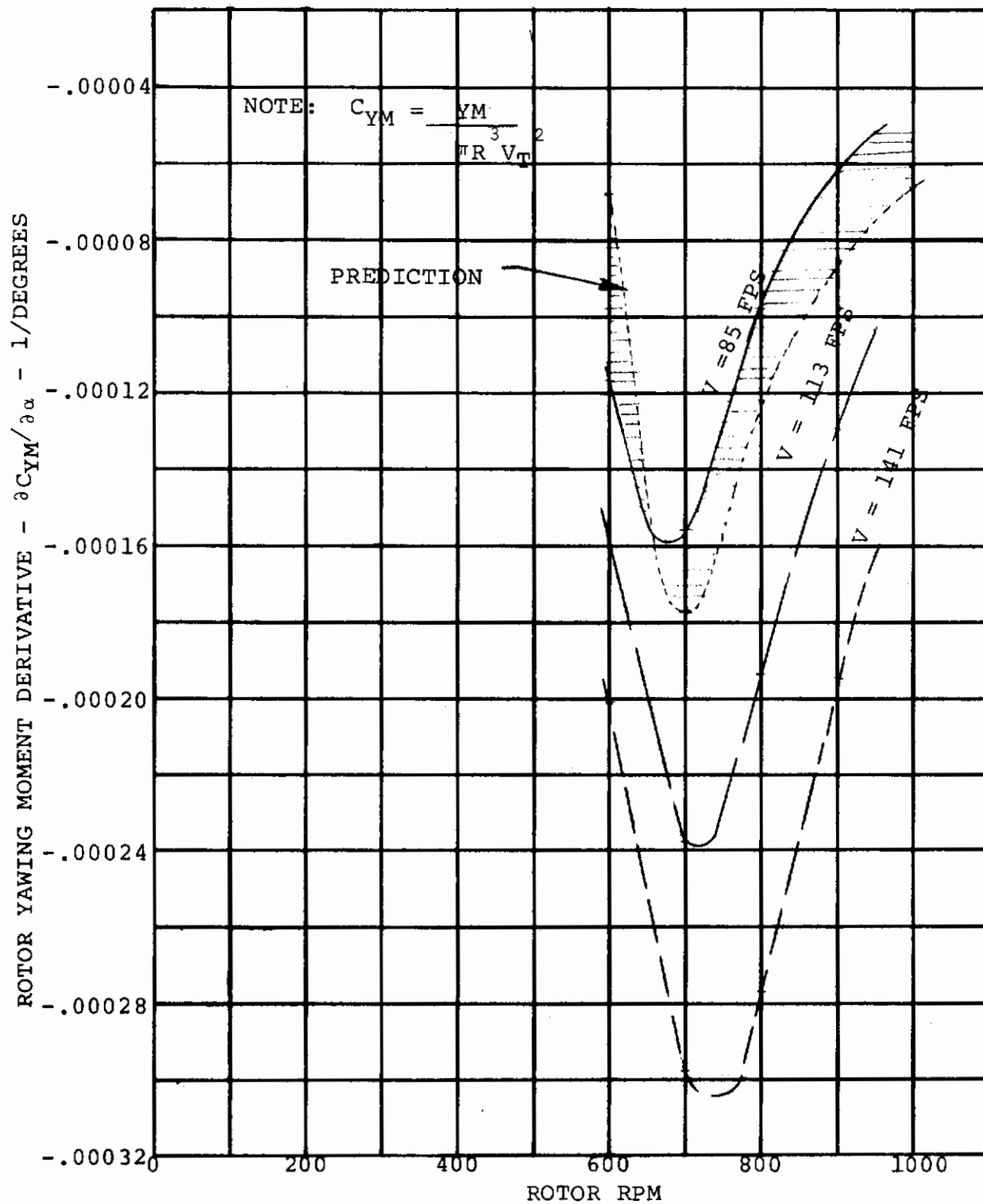


FIGURE 6-58 ROTOR YAWING MOMENT DERIVATIVE VARIATION WITH ROTOR RPM (WING CIRCULATION EFFECTS REMOVED)

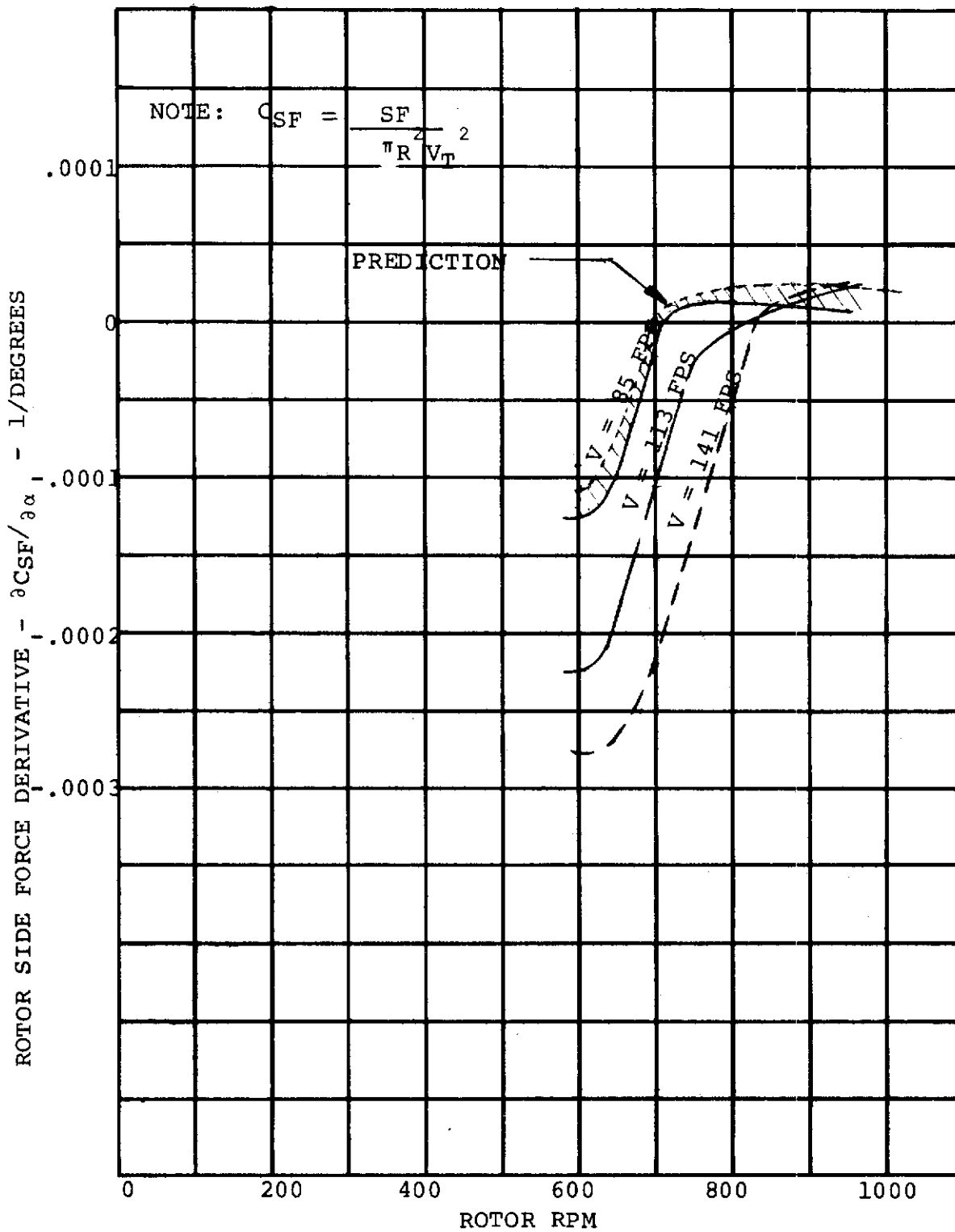


FIGURE 6-59 ROTOR SIDE FORCE DERIVATIVE VARIATION WITH ROTOR SIDE FORCE (WING CIRCULATION EFFECTS REMOVED)

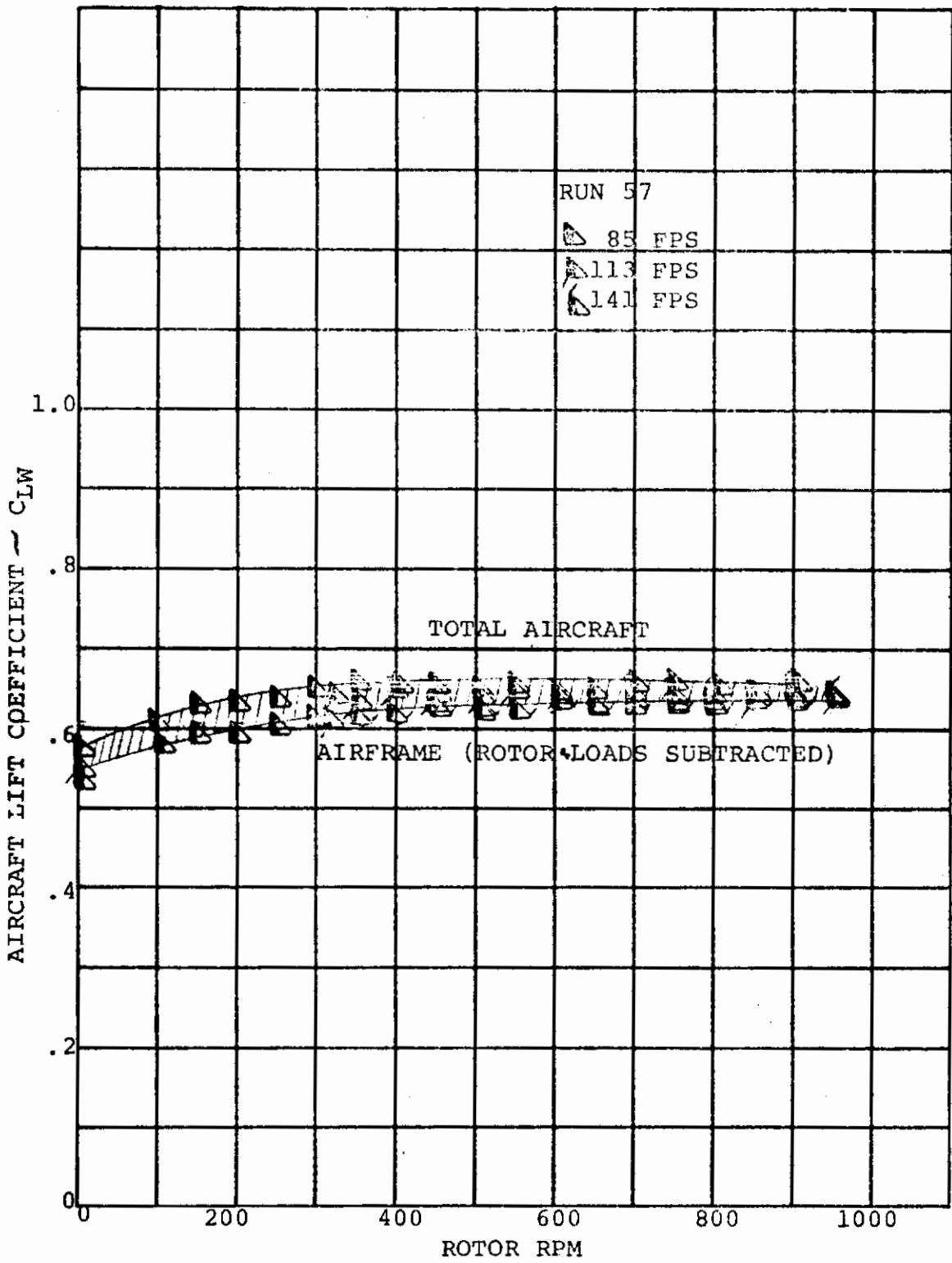


FIGURE 6-60 EFFECT OF ROTOR RPM AND FORWARD SPEED ON AIRCRAFT LIFT  $\alpha=0^\circ$   $\delta_F=30^\circ$  (STEADY WINDMILLING)

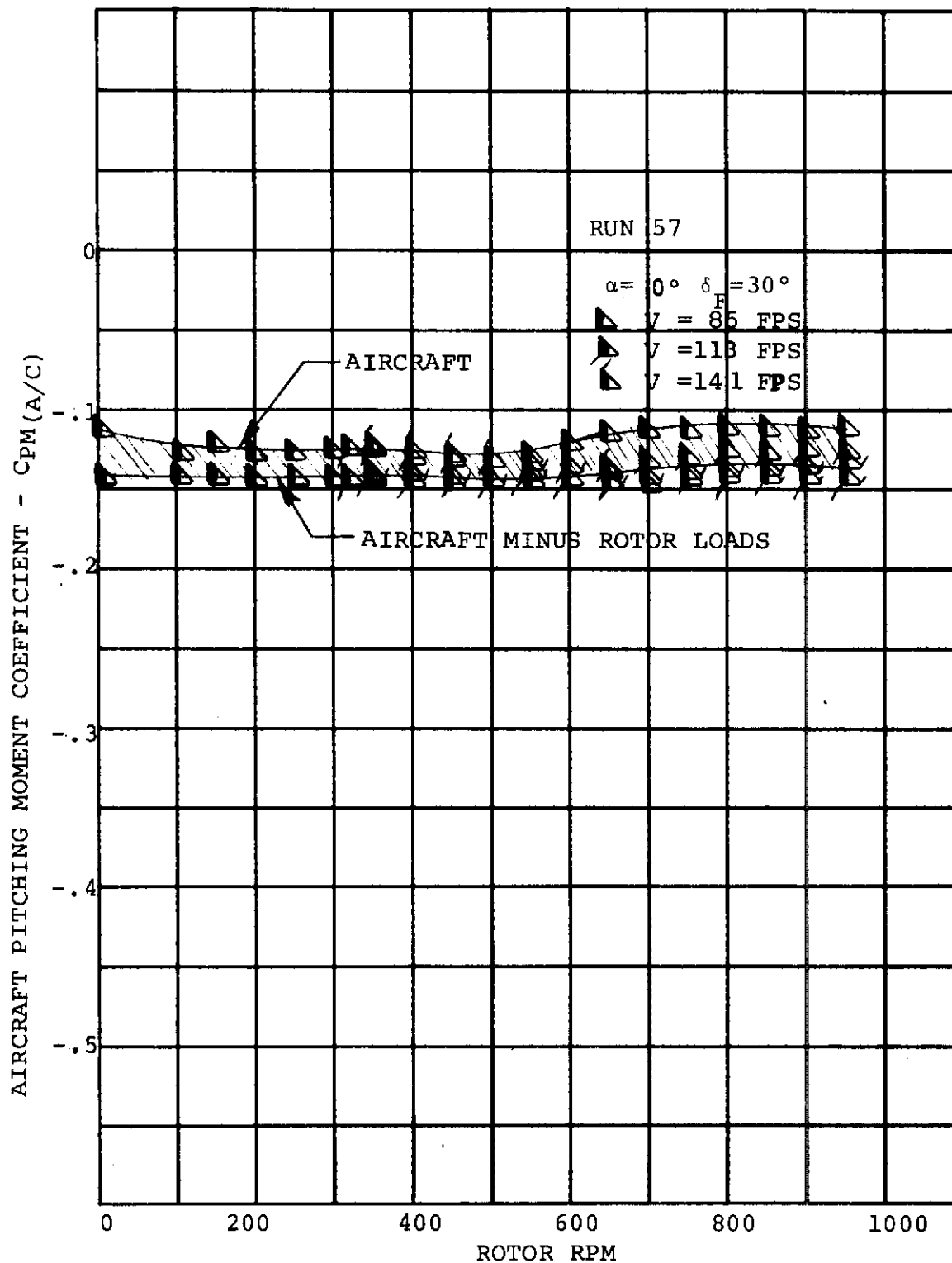


FIGURE 6-61 EFFECT OF ROTOR RPM AND FORWARD SPEED ON AIRCRAFT PITCHING MOMENT  $\alpha=0^\circ$   $\delta_F=30^\circ$  (STEADY WINDMILLING)



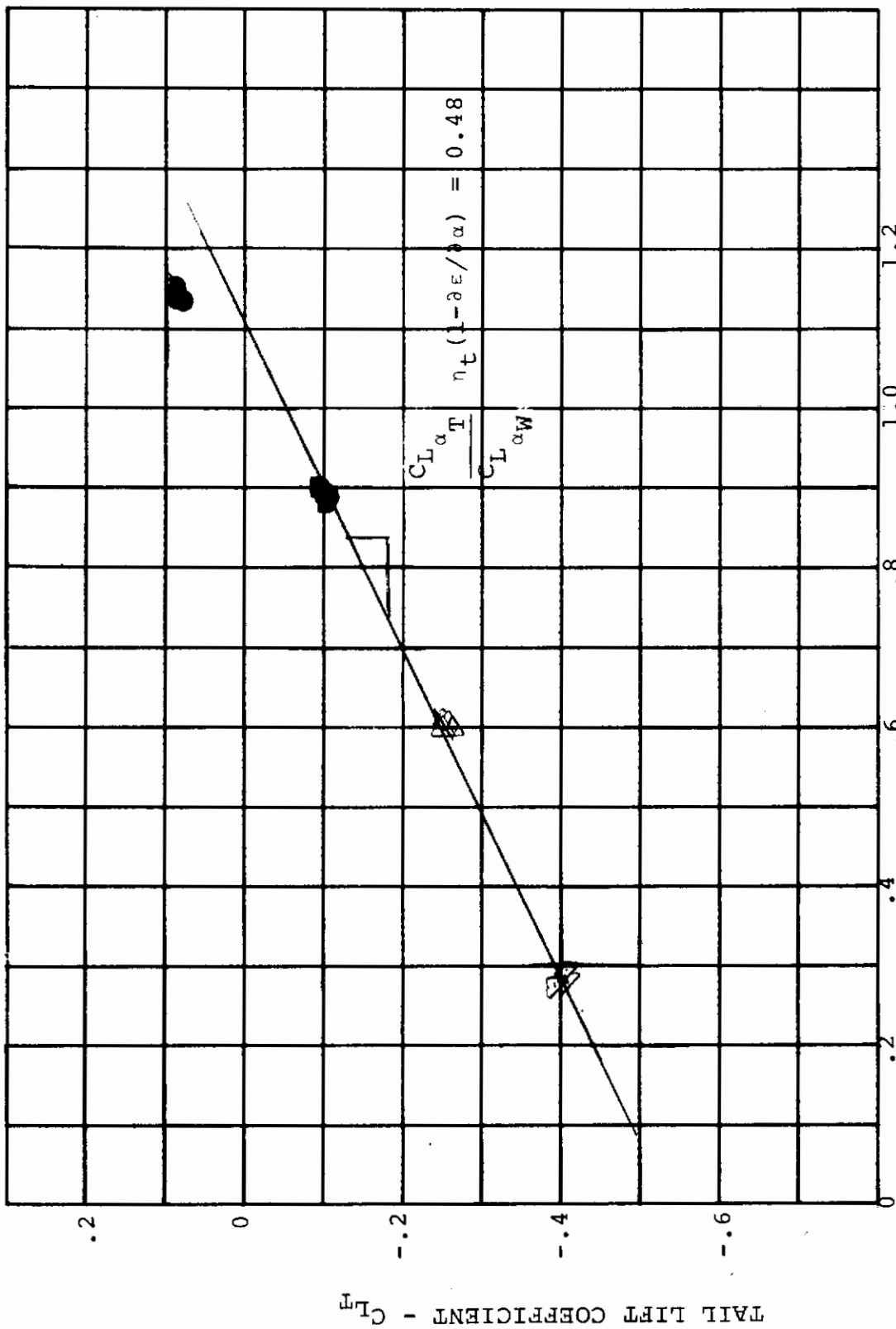


FIGURE 6-62 VARIATION OF TAIL LIFT WITH AIRFRAME LIFT DURING AN ANGLE OF ATTACK SWEEP  $\delta_F=30^\circ$  ROTOR OFF

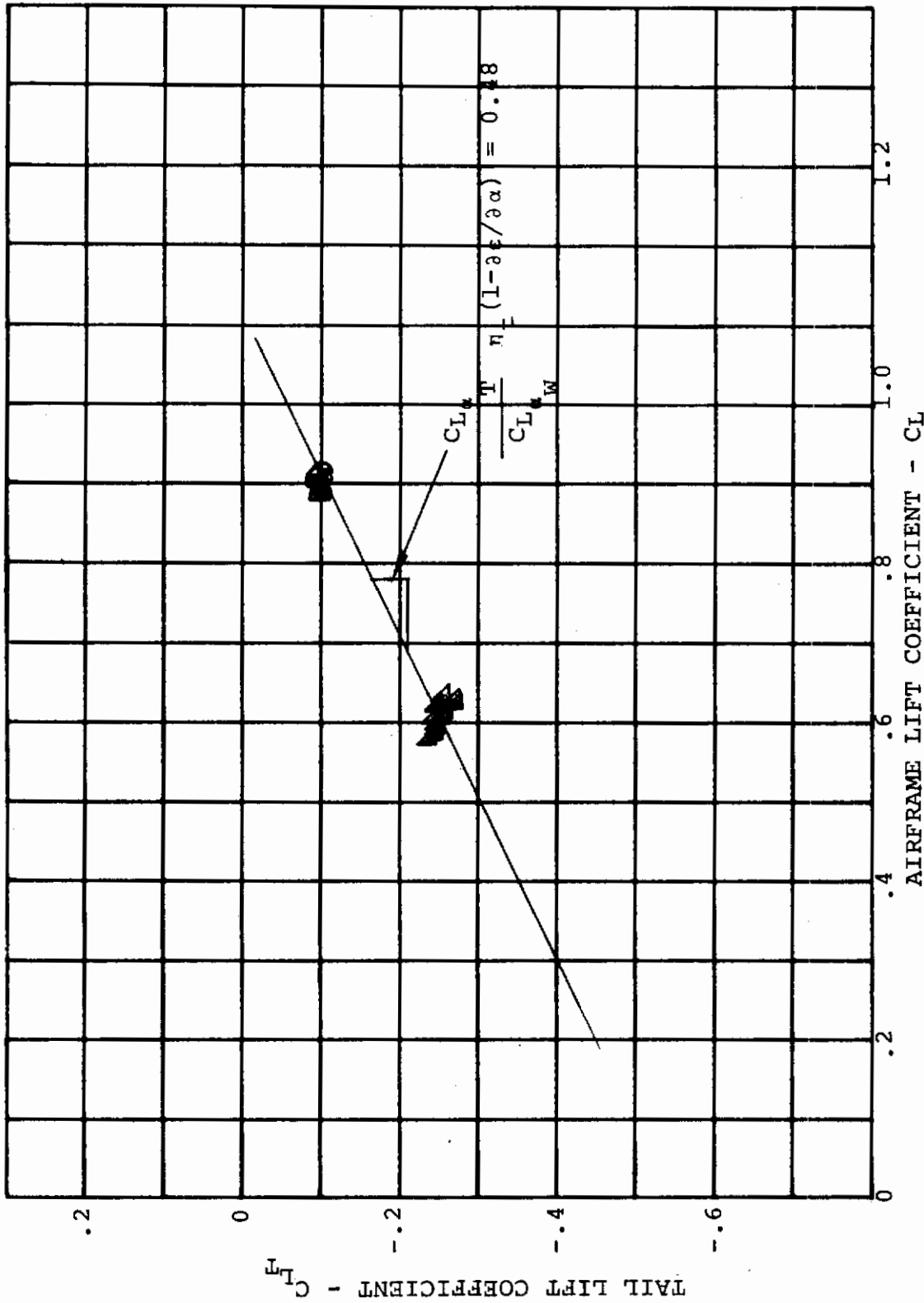


FIGURE 6-63 VARIATION OF TAIL LIFT WITH AIRFRAME LIFT DURING ANGLE OF ATTACK SWEEP FOR  $\delta_F = 30^\circ$ , ROTOR STEADY WINDMILLING

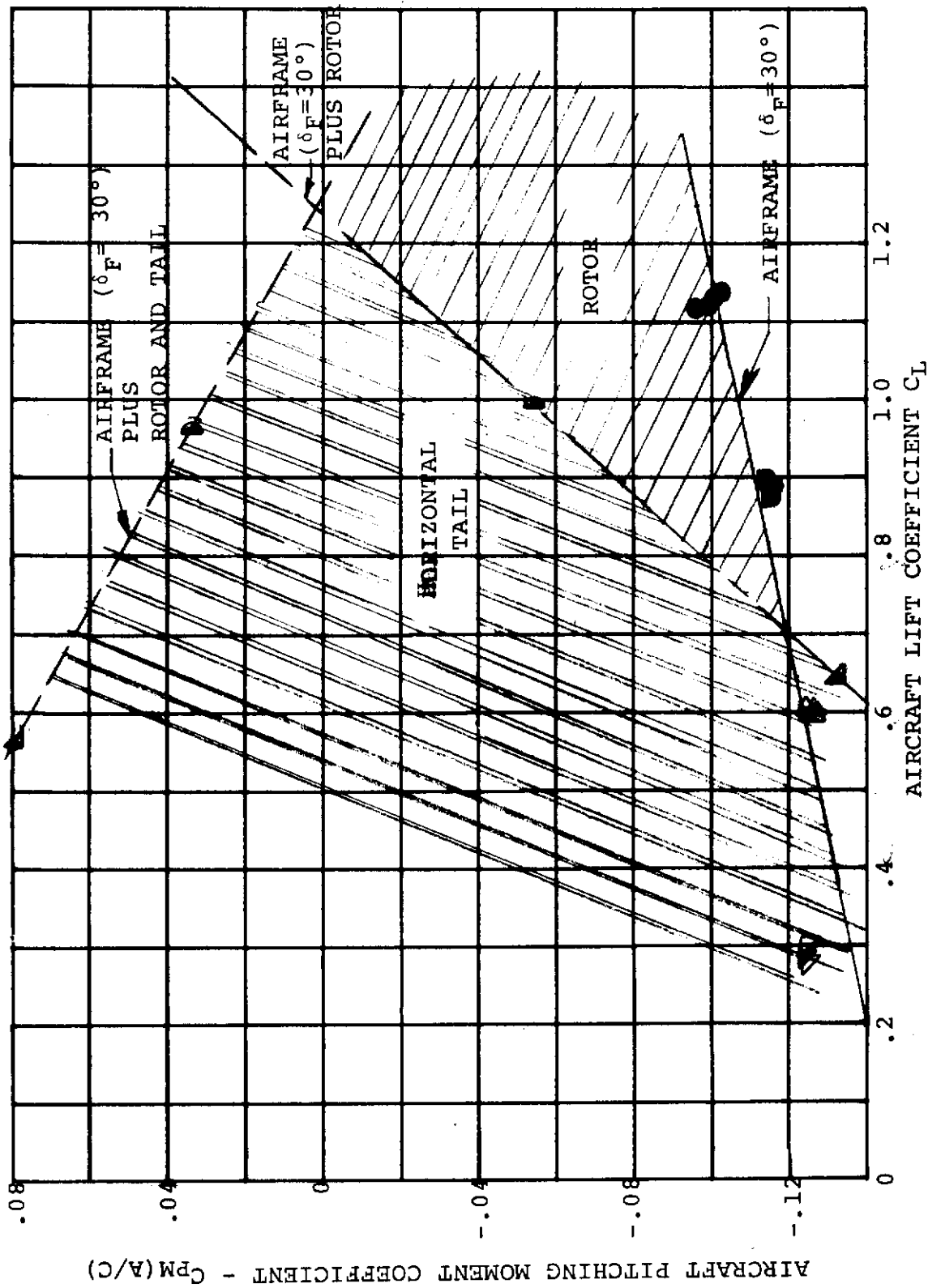


FIGURE 6-64 CONTRIBUTION OF PROP/ROTOR AND HORIZONTAL TAIL TO AIRCRAFT STABILITY FOR STEADY WINDMILLING  $\delta_F = 30^\circ$

## 6.2 Spinup and Feather Stability

The recommended spinup and feather schedule was a 3.0 to 4.0 second parabolic as indicated in Section 5.2. This was based on meeting the 0.1g transient drag/thrust force goal. The rotor stability characteristics for the same conditions as presented in Section 5.2 on Figures 5-26 and 5-27 will be presented here. Figures 6-65 and 6-66 present the rotor normal force and pitching moment variation during the transient. Imposed on this data is a trend defined by the steady state windmilling data and is represented by the dashed line. Although there are many oscillations in the transient load variation with time it shows a gradual change in the average from zero time to the end of the spinup. The average transient normal force has the same trend and magnitude as the steady state. The average pitching moment presented in Figure 6-66 changes very gradually from zero time to the end of the spinup, whereas the trend indicated by the steady state shows a peak and bucket during the RPM sweep. The large oscillations indicated in the beginning of the transient appear to be a result of the rapid acceleration of the rotor and it damps out.

This gradual change in the rotor forces and moments from the beginning to the end of the spinup would indicate that the total aircraft moments show a gradual change also. Verification of this is presented in Figure 6-67. The mean aircraft pitching moment forms a smooth trend from zero time to the end of the spinup. This data was replotted against RPM in Figure 6-68 to determine whether the oscillations mask the 1/rev lag frequency crossover. It is apparent for the 1.0 and 2.0 and 6.0 second schedule and the crossover is apparent by the peak in the pitching moment at 650 RPM shown at the top of Figure 6-68.

The highest oscillating forces shown in Figure 6-65 are about  $\pm 1$  lb, or less than  $\pm .03g$  in terms of vibration excitation.

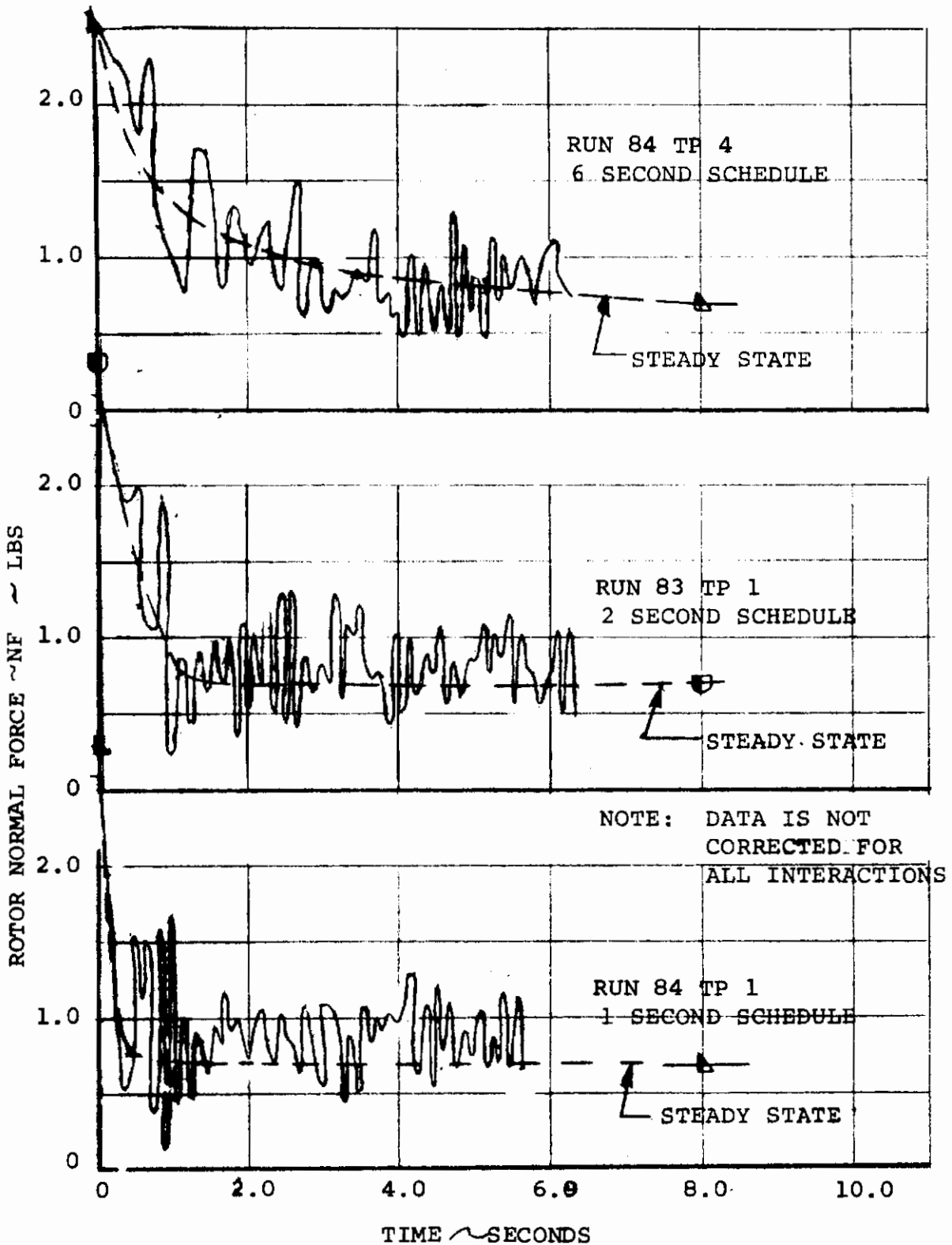


FIGURE 6-65. COMPARISON OF STEADY STATE AND TRANSIENT ROTOR NORMAL FORCE FOR PARABOLIC COLLECTIVE RATES AT V = 113 FPS, FINAL RPM = 715

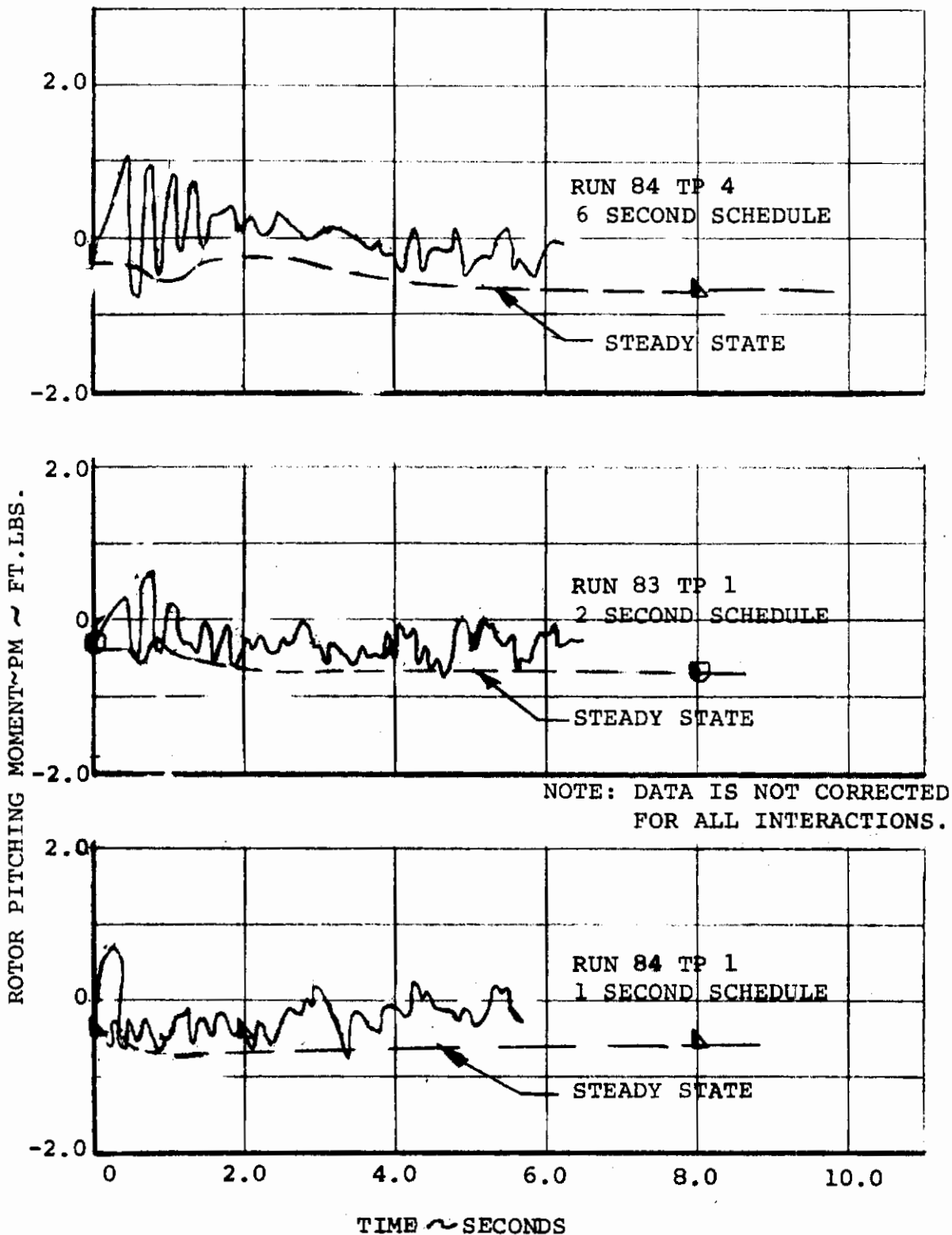


FIGURE 6-66. COMPARISON OF STEADY STATE AND TRANSIENT ROTOR PITCHING MOMENT FOR PARABOLIC COLLECTIVE RATES AT V = 113 FPS, FINAL RPM = 715

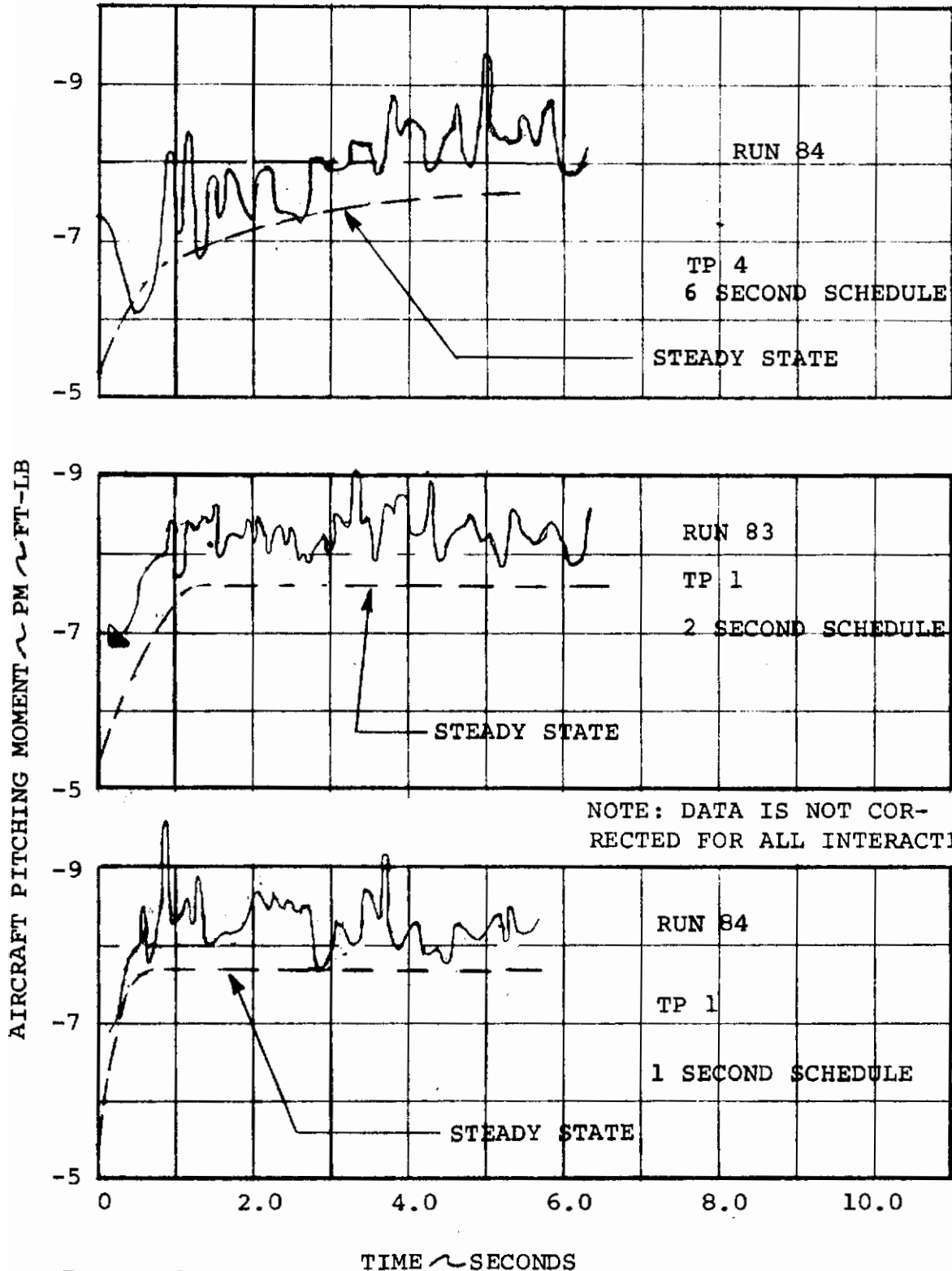


FIGURE 6-67 AIRCRAFT PITCHING MOMENT VARIATION  
 DURING PARABOLIC COLLECTIVE SCHEDULES  
 $\alpha=0^\circ$   $\delta_F=30^\circ$   $V=113$  FPS

# Contrails

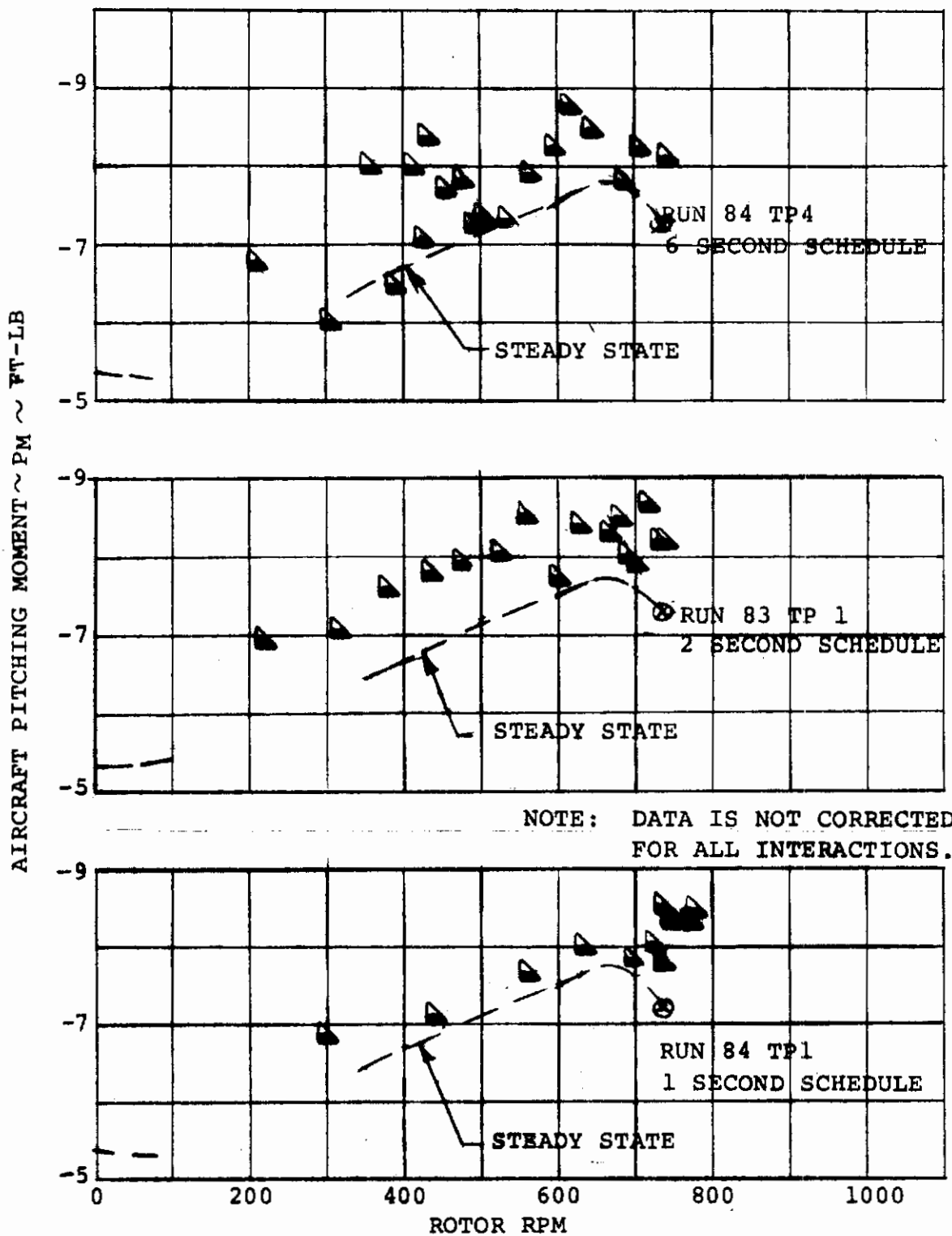


FIGURE 6-68 AIRCRAFT PITCHING MOMENT VARIATION WITH RPM DURING PARABOLIC COLLECTIVE SCHEDULES  
 $\alpha=0^\circ$   $\delta_F=30^\circ$   $V=113$  FPS



## 6.3 Folding and Deployment Stability

The blade folding impact on stability is to increase the total aircraft stability by removing the unstable rotor contribution. This results in a decrease in pitching moment slope with angle of attack but an increase in negative pitching moment. The change in pitching moment with blade fold angle is presented in Figure 6-69 and indicates a change of approximately 2.5 ft-lbs. This data, not being corrected for all the interactions, indicates the correct change in moment with blade fold angle but the level shift of -6.4 ft-lbs due to the interactions is not included. Blade folding and deployment is presented in Figure 6-69 and there is very little difference between them. Flagged symbols represent the rotor deployment. The trend in pitching moment is quite smooth with a small peak at 30 degrees blade fold angle which is very small in comparison to the total decrease in pitching; therefore, there would be a smooth blade fold operation from the stability standpoint.

The impact on the aircraft stability is presented in Figure 6-70 and indicates the change in stability from the configuration with the blades feathered to that with the blades folded. Aircraft stability with the blades feathered ( $C_M/C_L = -0.126$ ) is approximately the same as with the rotor in steady windmilling shown in Figure 6-64. As the blades are folded the stability is increased resulting in a  $C_{PM}/C_L = -0.296$  for the cruise mode.

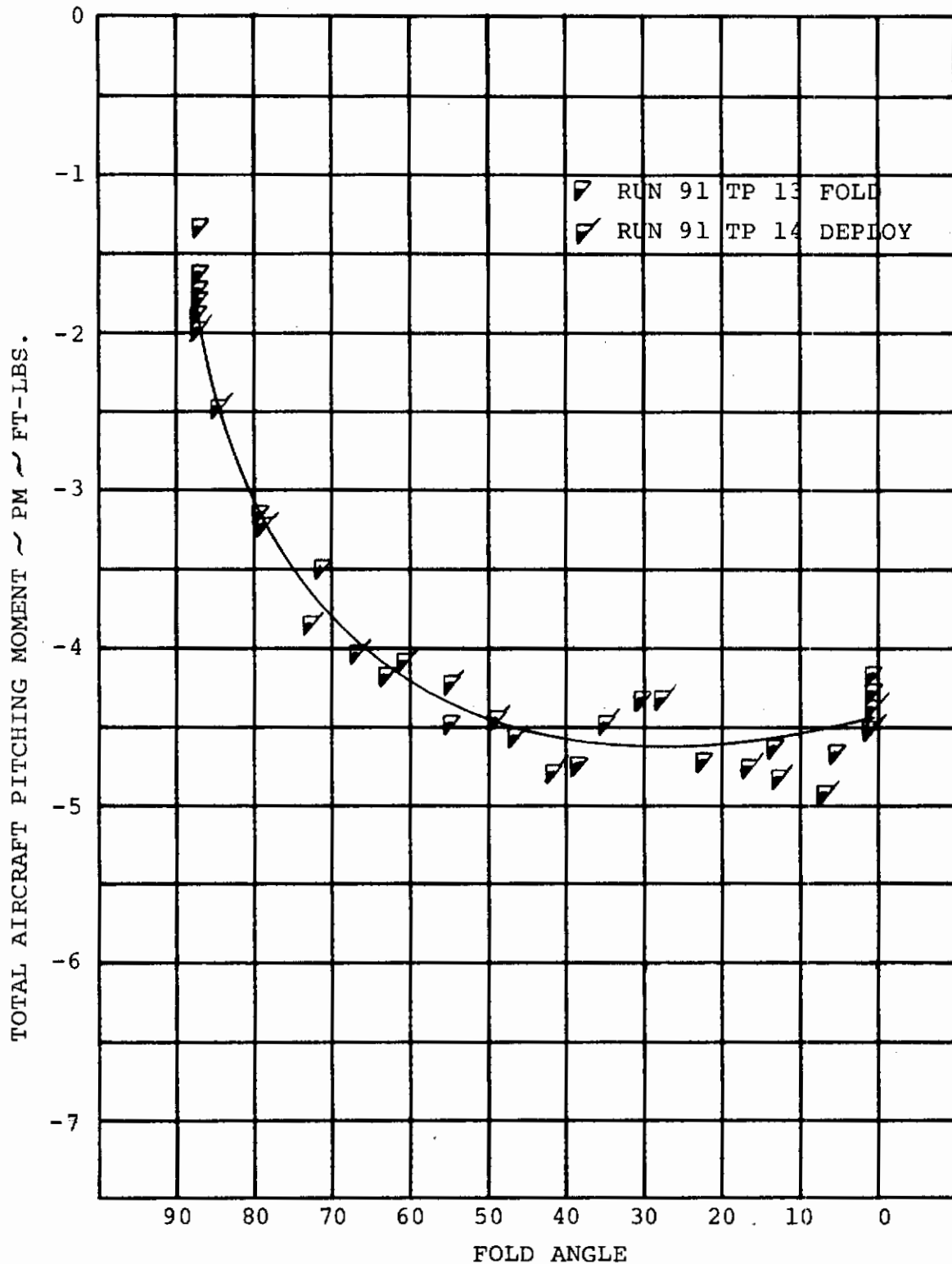


FIGURE 6-69. TOTAL AIRCRAFT PITCHING MOMENT VARIATION DURING THE FLATWISE BLADE FOLD TRANSIENT  $\alpha = 2^\circ$ ,  $\delta_F = 30^\circ$ ,  $V = 113$  FPS

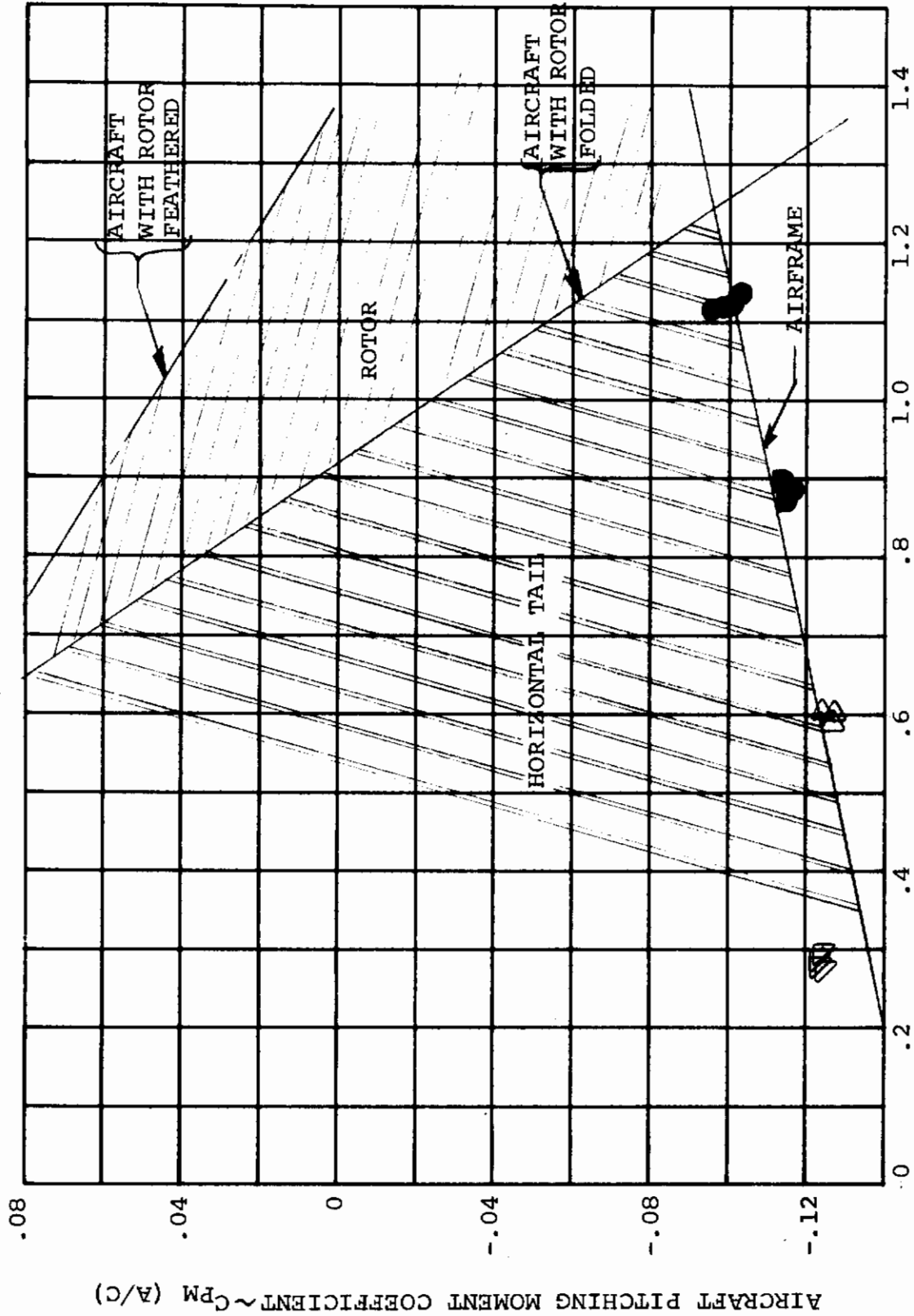


FIGURE 6-70 CONTRIBUTION OF HORIZONTAL TAIL AND FEATHERED ROTOR TO AIRCRAFT STABILITY  $\alpha_F = 30^\circ$

## 6.4 Conclusions - Stability

### Windmilling

1. The rotor stability derivatives with angle of attack are strongly affected by blade lag frequency. The pitching moment derivative varies from the typical large unstable value for a stiff in-plane rotor to a large stable value at a lag frequency of 1 per rev and back to a smaller unstable value at the lowest frequencies tested (about .79 per rev.). The normal force derivative decreases steadily as lag frequency decreases, with a flat region near 1 per rev.
2. The rotor derivatives, including their variation with blade lag frequency, are quite well predicted by current techniques.
3. The Model 213 is statically stable with rotors windmilling.
4. Flap deflection, resulting in an increase in wing circulation, increases the magnitude of the rotor derivatives.
5. Circulation effects on rotor derivatives appear to be a function of lift curve slope only.
6. The rotors do not affect the tail contribution to stability for the range of test condition covered.

### Spinup and Spin Down

During the transient spinup, rotor and aircraft stability form a smooth trend from the feathered condition to the windmilling condition.

### Folding

Blade fold and deployment can be accomplished with smooth increase in stability from a  $\partial C_{PM} / \partial C_L$  of -0.126 with blades feathered to -0.296 with blades folded.

## 7.0 ROTOR LOADS

During the conversion process power is transferred from the rotors to the convertible fan jet engines and the rotors windmill at their operational RPM. The blades are then feathered involving an RPM transient and finally folded. This section contains blade load data obtained during windmilling feathering, spinup and folding.

### 7.1 Rotor Blade Frequencies

To obtain low blade loads with a soft in-plane hingeless rotor it is important to tune the blade to specific frequencies. For this reason the first blade loads objective was to verify the blade design rotating frequencies. This procedure involves measuring the blade loads for steady windmilling RPM at points from zero to the maximum operating RPM. Harmonic analysis of these data yields peaks in the blade response at frequencies corresponding to integer times the RPM points. The frequencies deduced in this manner are compared with the design values in Figure 7-1. The experimental data agree well with the blade design frequencies, particularly at the 1st mode 1 per rev frequency crossing, which at this airspeed-collective combination is slightly less than 600 RPM.

Figures 7-2 through 7-5 show the harmonic content (1st four harmonics) of the blade flap and chord bending for various RPM's at a tunnel speed of 85 ft/sec.

The data show blade response peaks (mostly 2/rev) at 350 RPM and 800 RPM which are not attributable to the blade natural frequencies. Reference to the alternating wing loads in Section 8 identifies these points as being the coincidence of the wing flapwise frequency with the 1/rev line (350 RPM) and the wing torsion frequency (800 RPM). The vibration of the wing causes hub motions which impart 2/rev loads to the blades and accounts for the high 2/rev content shown in Figure 7-3 at these RPM.

### 7.2 Steady Windmilling Loads

#### 7.2.1 Effect of RPM

Prior to conversion the rotor windmills at constant RPM. The steady windmilling conditions experienced in flight will normally be at the normal operating RPM. In this test the whole range of RPM's has been investigated to provide comparison data with transient spinup and feather cases reported in Section 7.4. Figures 7-6 and 7-7 show the alternating blade chord and flap bending loads at three airspeeds. The loads are shown to increase with airspeed and show peaks corresponding to the frequency crossings identified in Section 7.1.

The alternating loads at the maximum RPM (950) are low and the flap bending loads show little change with airspeed. The chord bending loads are still influenced by the wing torsion frequency 1/rev crossing at 800 RPM. These data provide a measure of the frequency separation required between the wing frequencies and the operating RPM to achieve minimum loads. Blade torsional moments were found to be very low in all test conditions. Figure 7-8 shows the alternating torsional loads for the test condition ( $\alpha_F = 4^\circ$ ), which produced the highest alternating moments. At a fuselage angle of  $0^\circ$  the alternating moment exceeds 1 in.lb. only in the rotor speed range of 300 to 400 RPM but never exceeds 1.4 in.lb. Flutter did not occur at any of the tested conditions.

### 7.2.2 Effect of Angle of Attack

The alternating blade flap and chord bending loads measured throughout the RPM range are given for angles of attack from  $\alpha_F = -2^\circ$  to  $\alpha_F = 4^\circ$  in Figures 7-9 through 7-14. These data show that the loads are increased by angle of attack; however, at the maximum RPM the flap bending loads show little effect. The peaks in the chordwise load data between 600 and 800 RPM increase rapidly with angle of attack due to the increased 1/rev airload forcing applied to the blades. Figures 7-15 and 7-16 are cross plots at 950 RPM against true nacelle angle of attack (corrected for deflections using the deflection test data of Appendix A), showing these effects.

The increase in chordwise loads due to angle of attack increases with airspeed. This rate of increase is found to be in excess of the square of the tunnel speed and is due to the increase in 1/rev airloads due to increased local blade section velocities (square law) and also the added asymmetry in the velocity field due to wing circulation induced effects (proportional to  $V$ ). The response characteristics of the blade change a little also, since different collective pitch settings are required at each airspeed, resulting in slightly different blade bending mode shapes. The blade flap bending loads are low and do not show an effect due to airspeed.

### 7.2.3 Effect of Flaps and Wing Circulation

The application of wing flaps increases the wing circulation and as a result increases the asymmetry of the inflow distribution to the rotor. This effect increases the blade chord bending slightly as shown in Figure 7-17. The blade flap bending loads show no consistent increase with wing flap deflection, Figure 7-18. Figure 7-19 is a composite plot showing the effects of model lift on blade loads at three airspeeds. The plot contains points where

the lift is obtained both with angle of attack and wing flap deflection. The conclusion that can be drawn from this comparison is that the minimum conversion blade loads are achieved by using the wing flaps to maintain airplane lift rather than changing the attitude of the aircraft. The flap bending loads, Figure 7-20, are low and the application of wing flap enables high lift to be obtained with no increase in flap bending loads.

Figures 7-21 and 7-22 show similar plots at 700 RPM and again the application of wing flap proves to be the best way of obtaining lift from a blade loads viewpoint. In this instance the flap bending data shows a large effect due to angle of attack. This is the result of the high degree of coupling between the blade bending modes in the proximity of the 1/rev lag frequency crossing.

#### 7.2.4 Steady Blade Loads

The steady blade bending moments measured for zero and four degrees angle of attack are given in Figures 7-23 through 7-26 versus RPM. The steady blade loads are shown to increase almost linearly with RPM and are due to two major effects. The windmilling drag of the rotor provides a steady bending load and also the hub torque offset designed for powered flight causes a centrifugal force dependent blade moment in the zero applied torque windmilling case. The steady blade chord bending decreases with airspeed at 950 RPM but the flap bending load increases. This effect is due to the change in collective pitch required for constant RPM and changing the resolution of the bending loads in the blade section axis system.

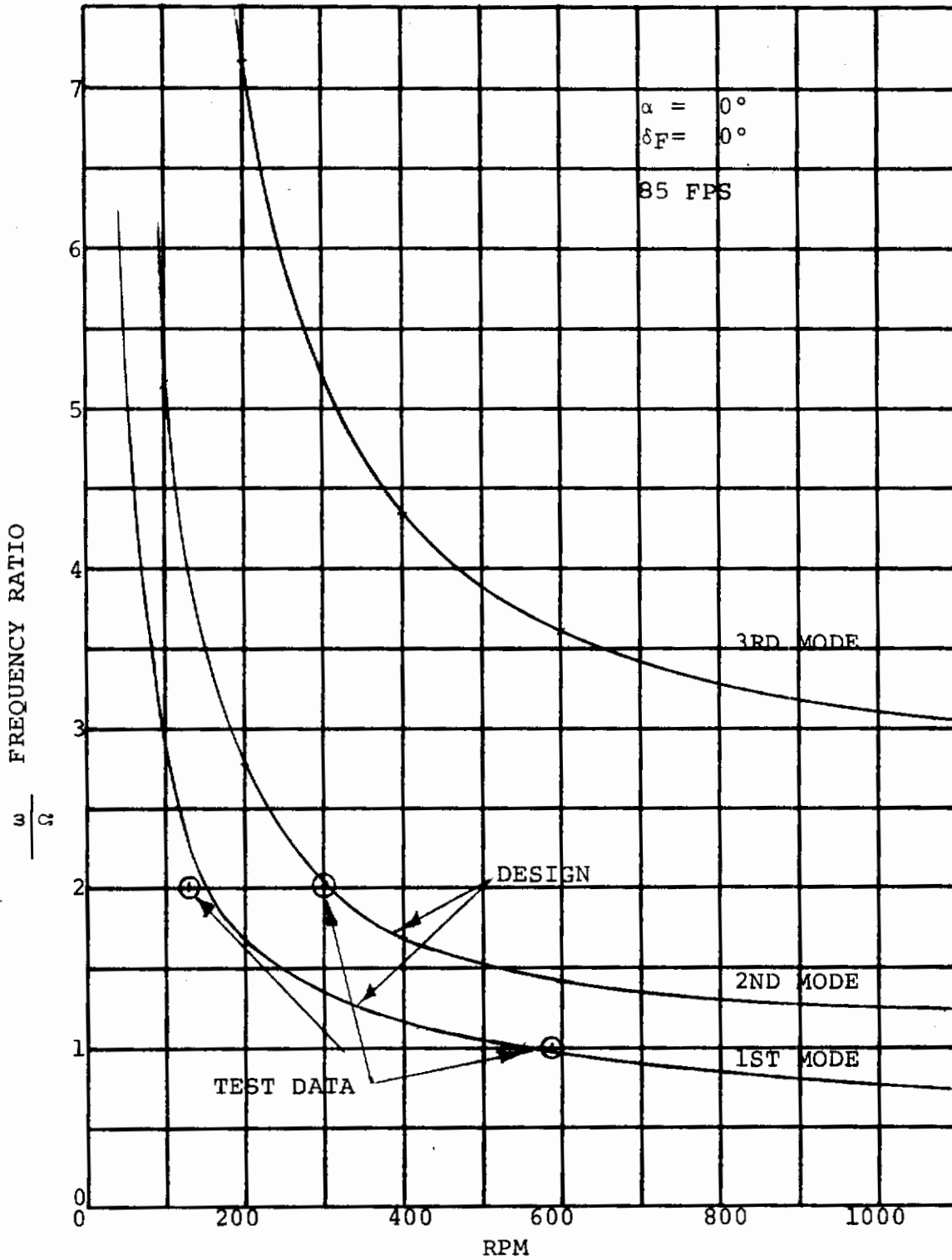


FIGURE 7-1 COMPARISON OF EXPERIMENTAL AND DESIGN ROTOR BLADE FREQUENCIES



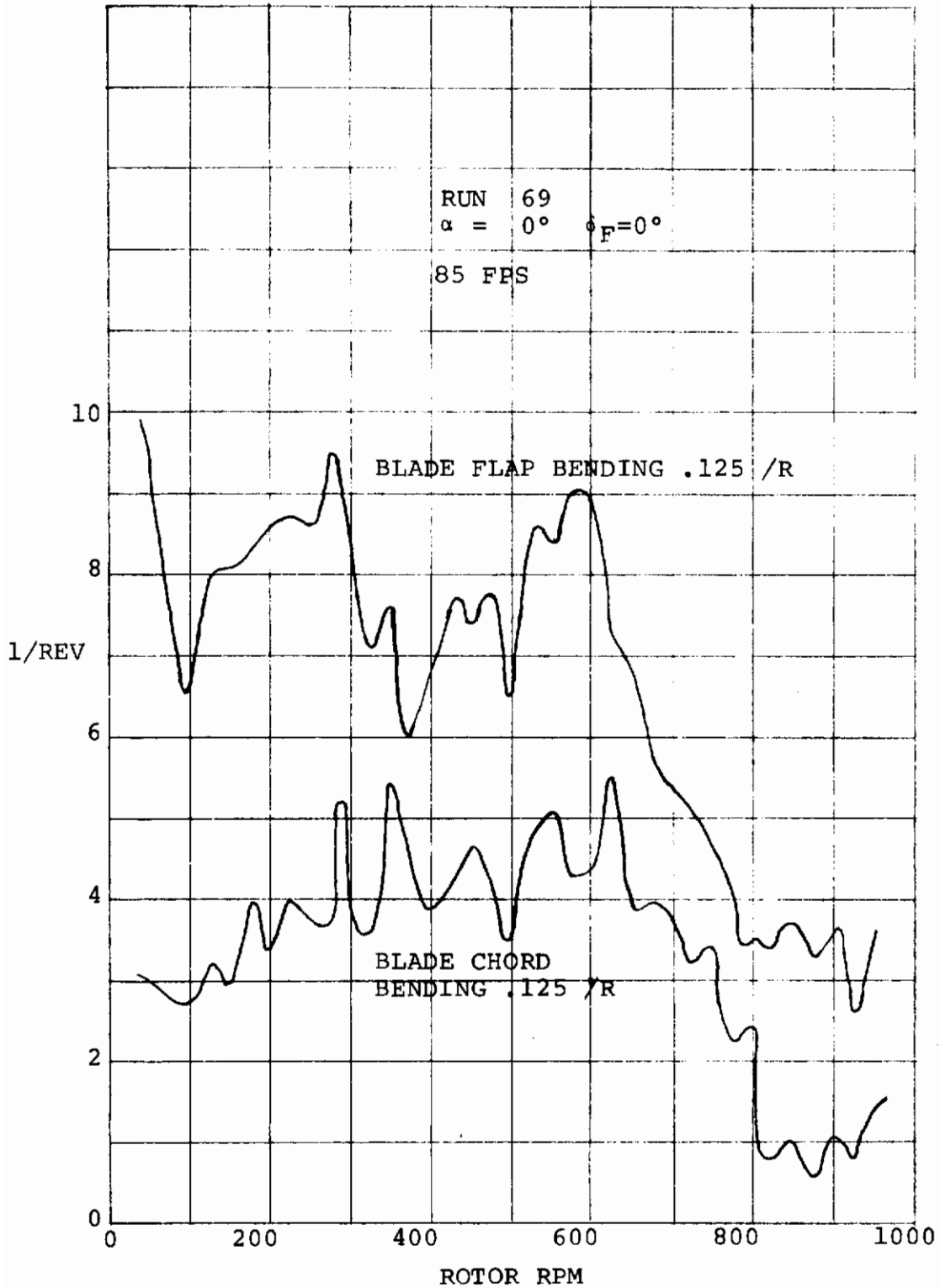


FIGURE 7-2 1ST HARMONIC CONTENT OF WINDMILLING BLADE LOADS

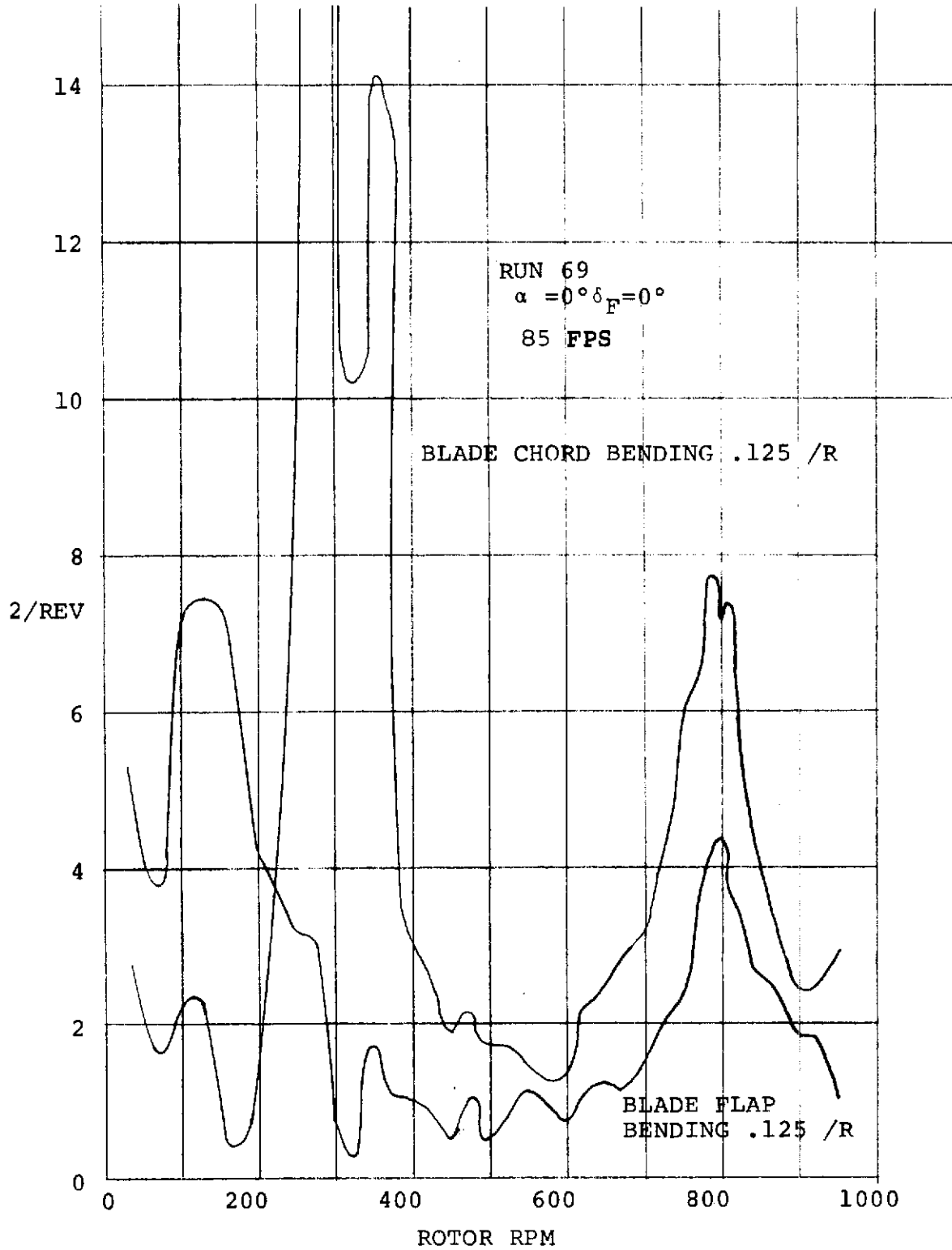


FIGURE 7-3. SECOND HARMONIC CONTENT OF WINDMILLING BLADE LOADS

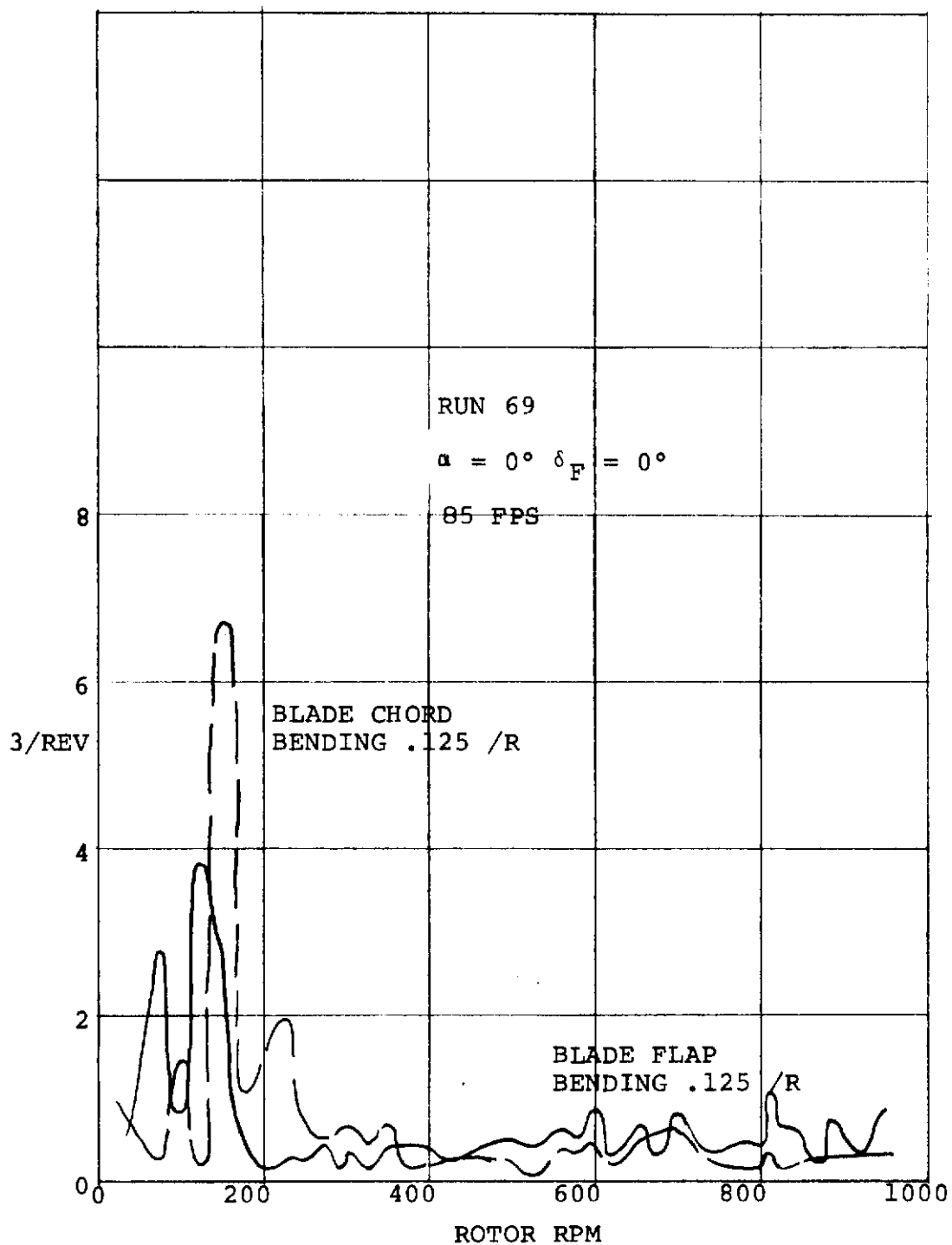


FIGURE 7-4. THIRD HARMONIC CONTENT OF WINDMILLING  
BLADE LOADS

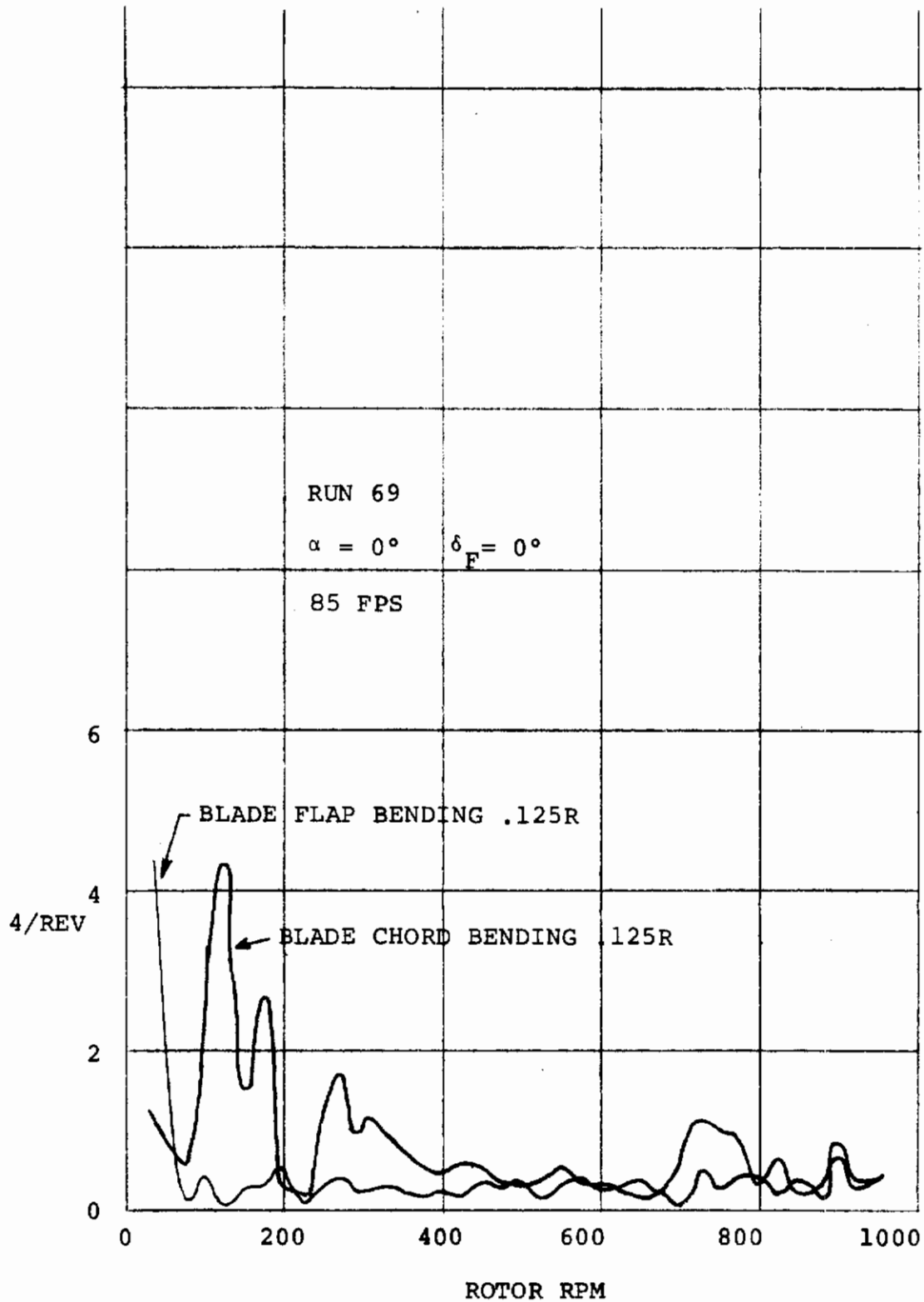


FIGURE 7-5. FOURTH HARMONIC CONTENT OF WINDMILLING BLADE LOADS

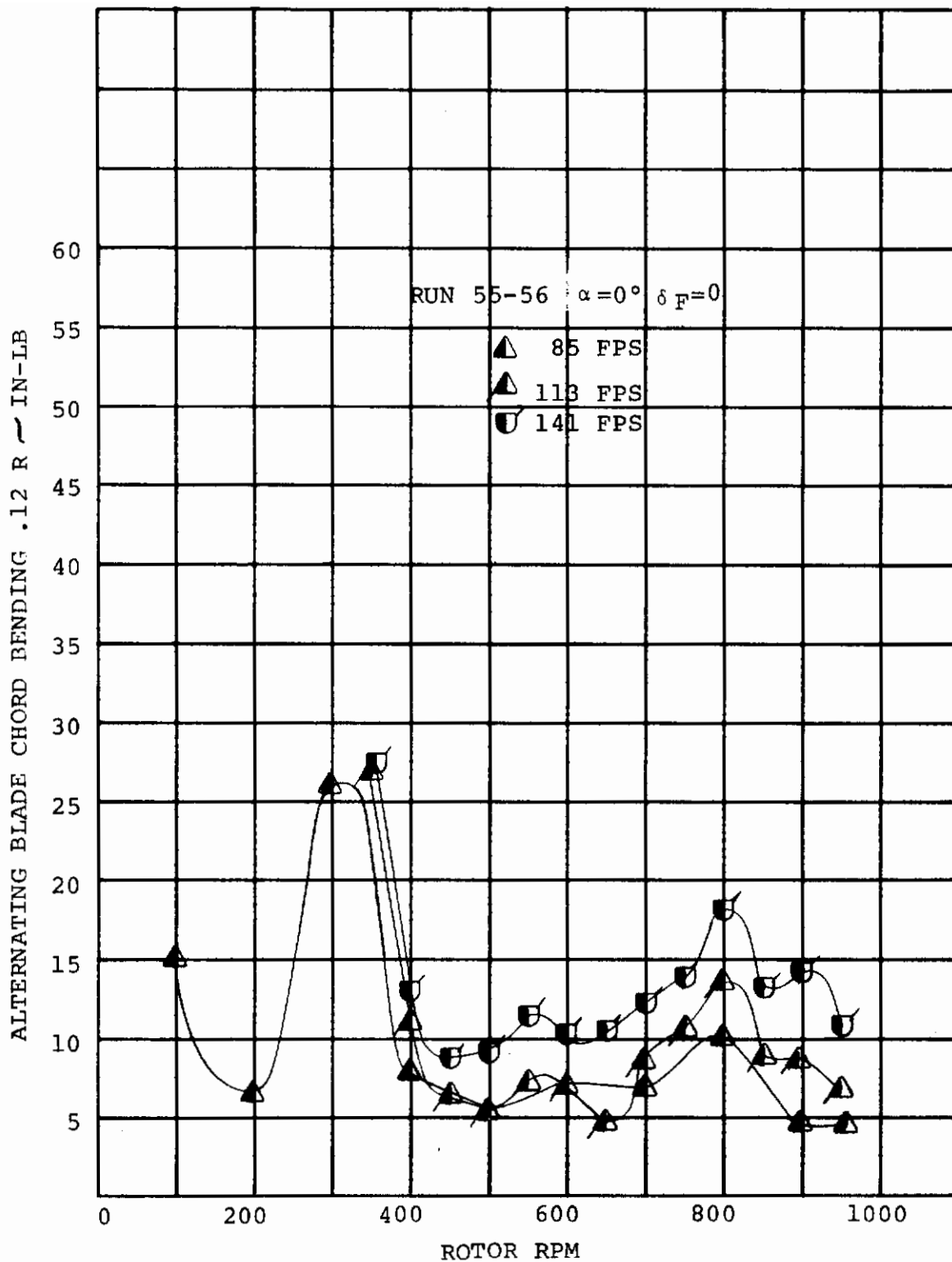


FIGURE 7-6. ALTERNATING CHORD BENDING LOADS FOR STEADY WINDMILLING  $\alpha = 0$   $\delta_F = 0^\circ$

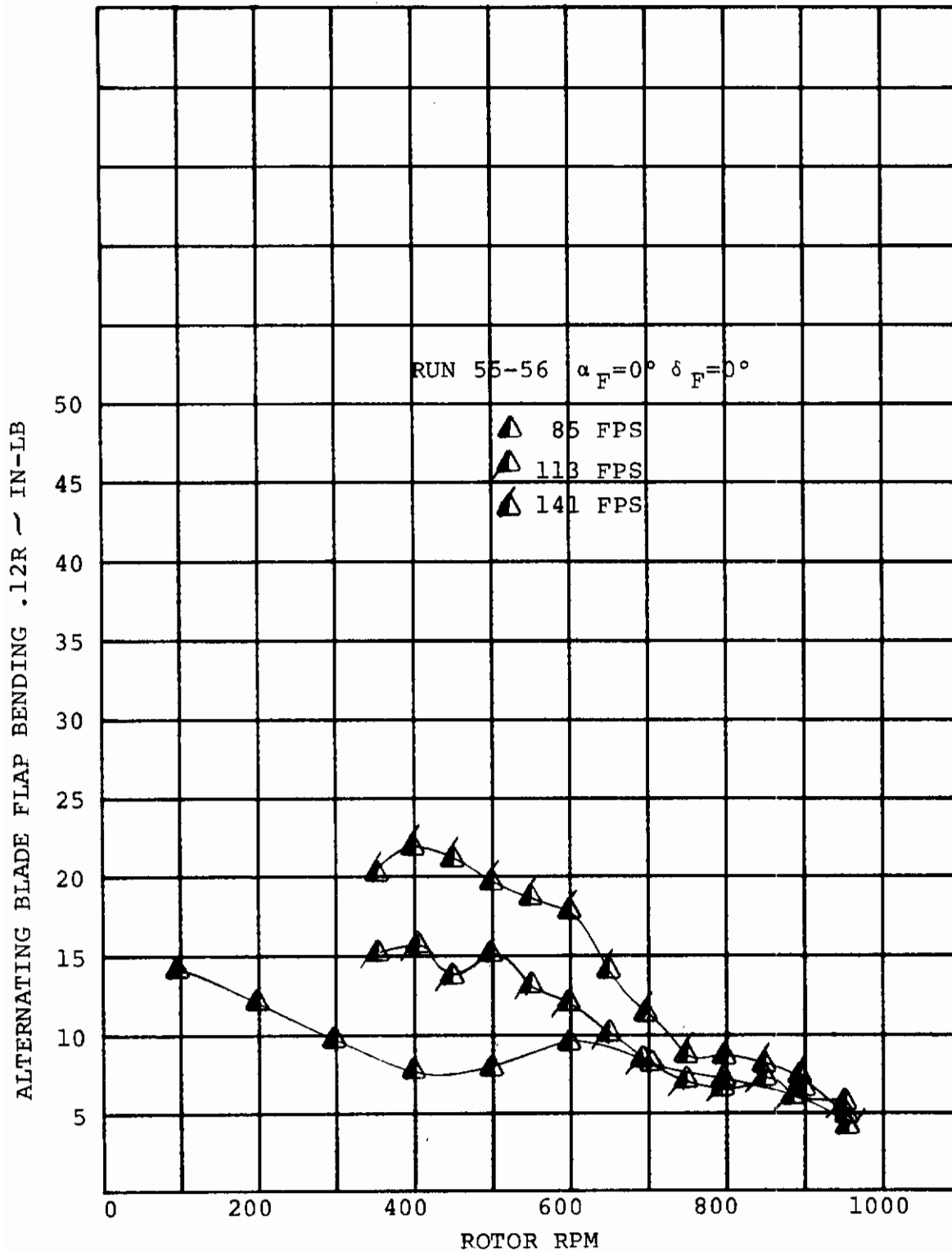


FIGURE 7-7. ALTERNATING FLAP BENDING LOADS FOR STEADY WINDMILLING  $\alpha = 0$   $\delta_F = 0$

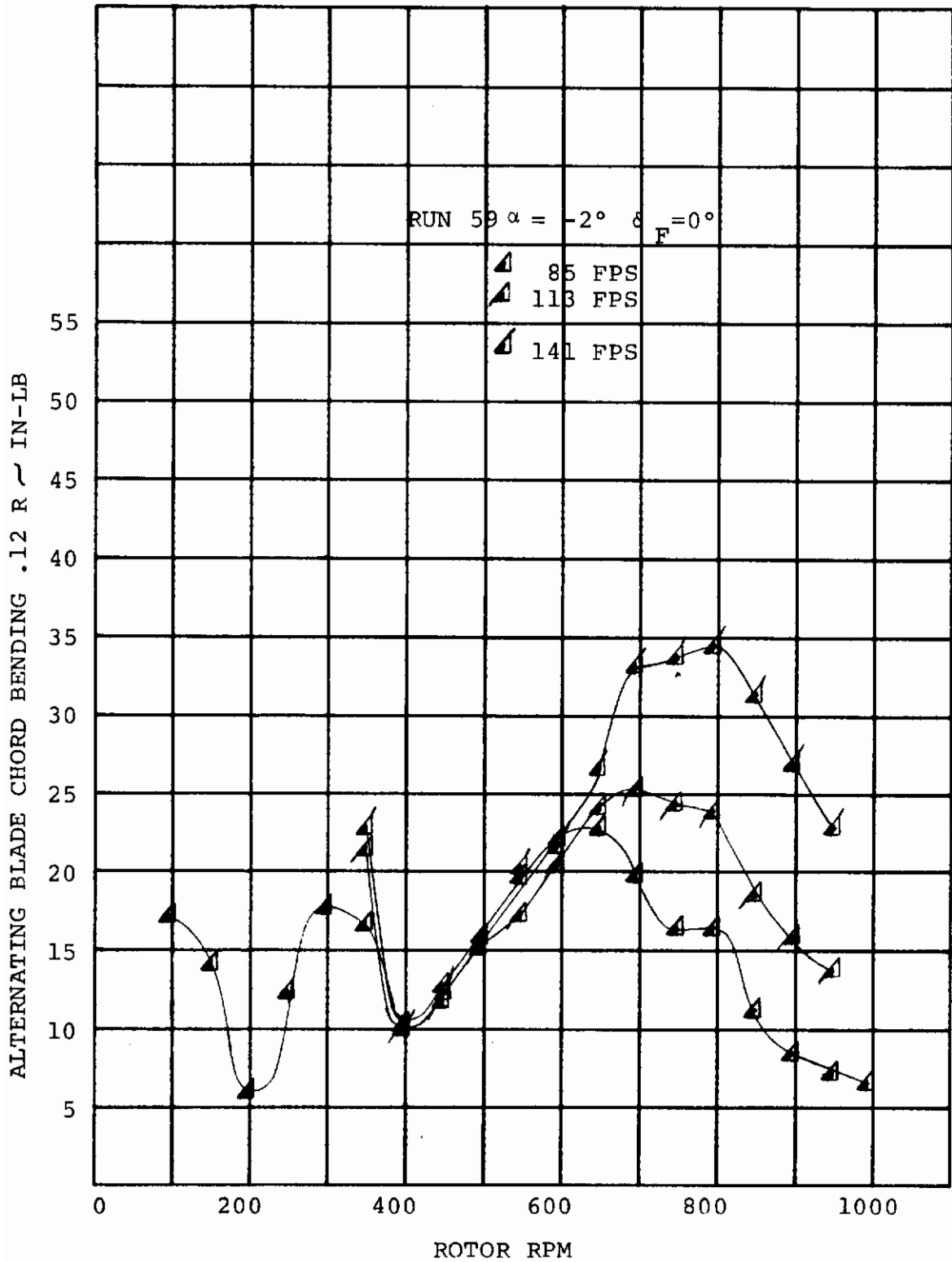


FIGURE 7-8. ALTERNATING BLADE CHORD BENDING FOR STEADY WINDMILLING  $\alpha = -2^\circ$   $\delta F = 0^\circ$

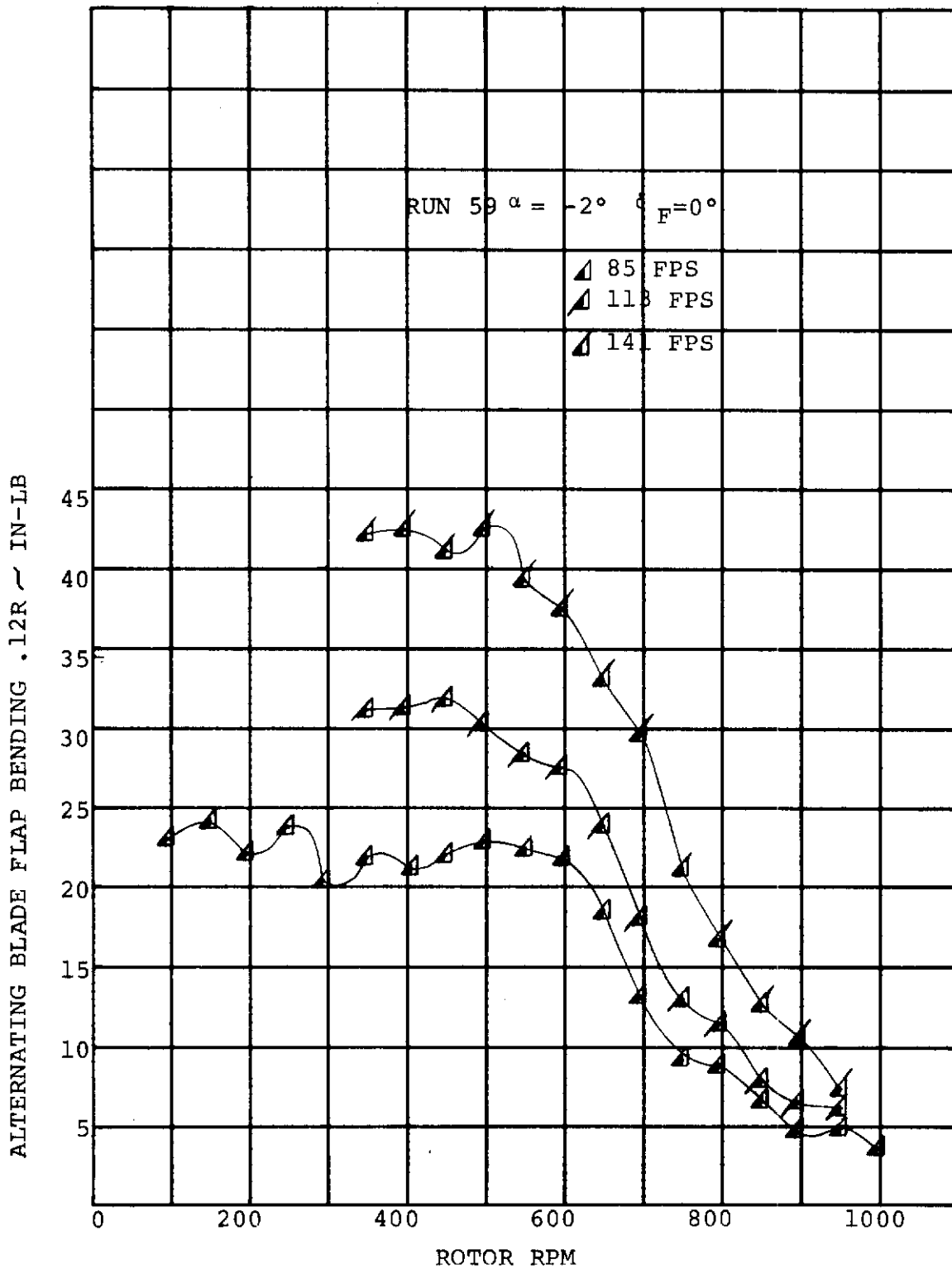


FIGURE 7-9. ALTERNATING BLADE FLAP BENDING STEADY WINDMILLING  $\alpha = -2^\circ$   $\delta F = 0^\circ$



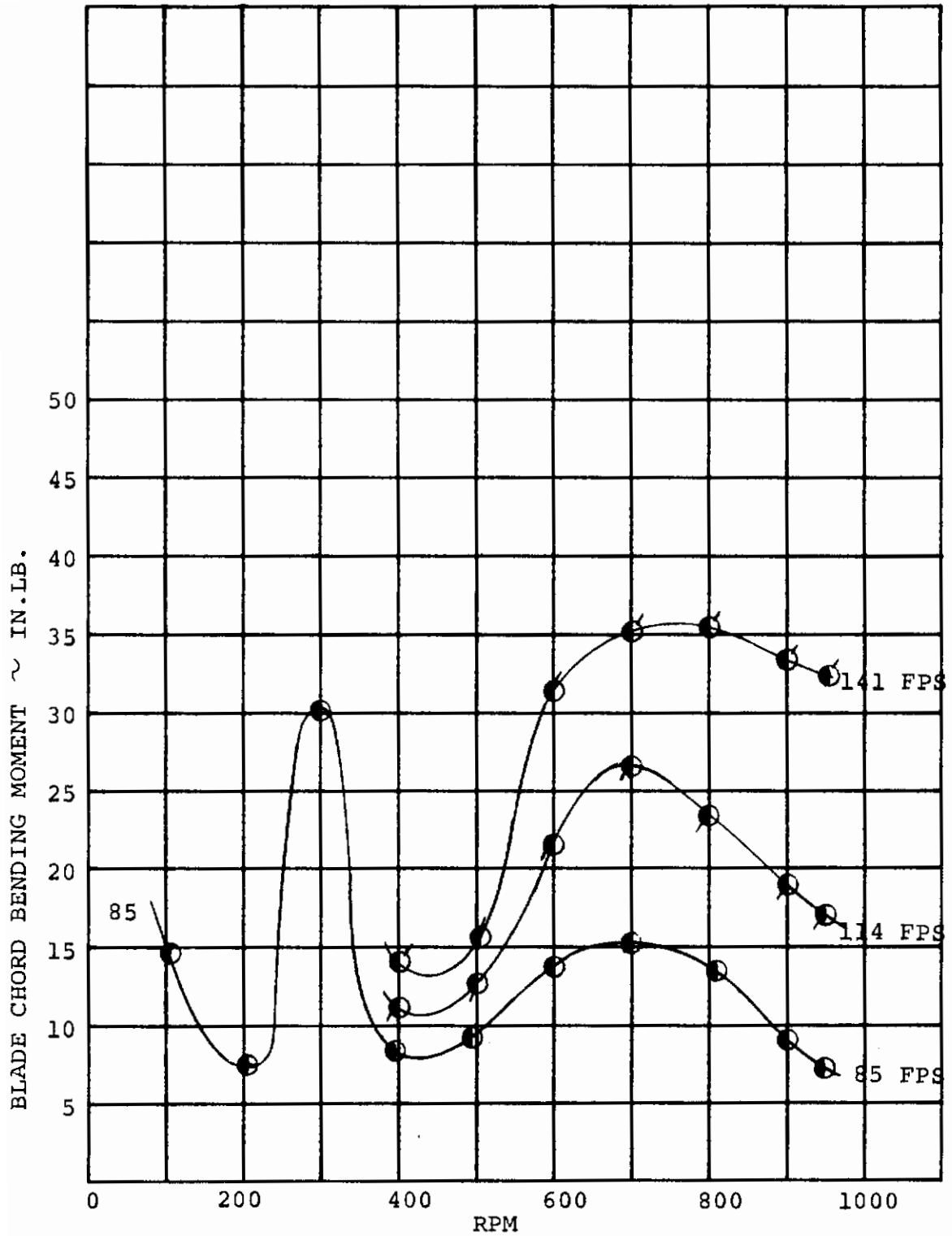


FIGURE 7-10. ALTERNATING BLADE CHORD BENDING 0.125R  
 STEADY WINDMILLING  $\alpha = 2^\circ$   $\delta_F = 0^\circ$

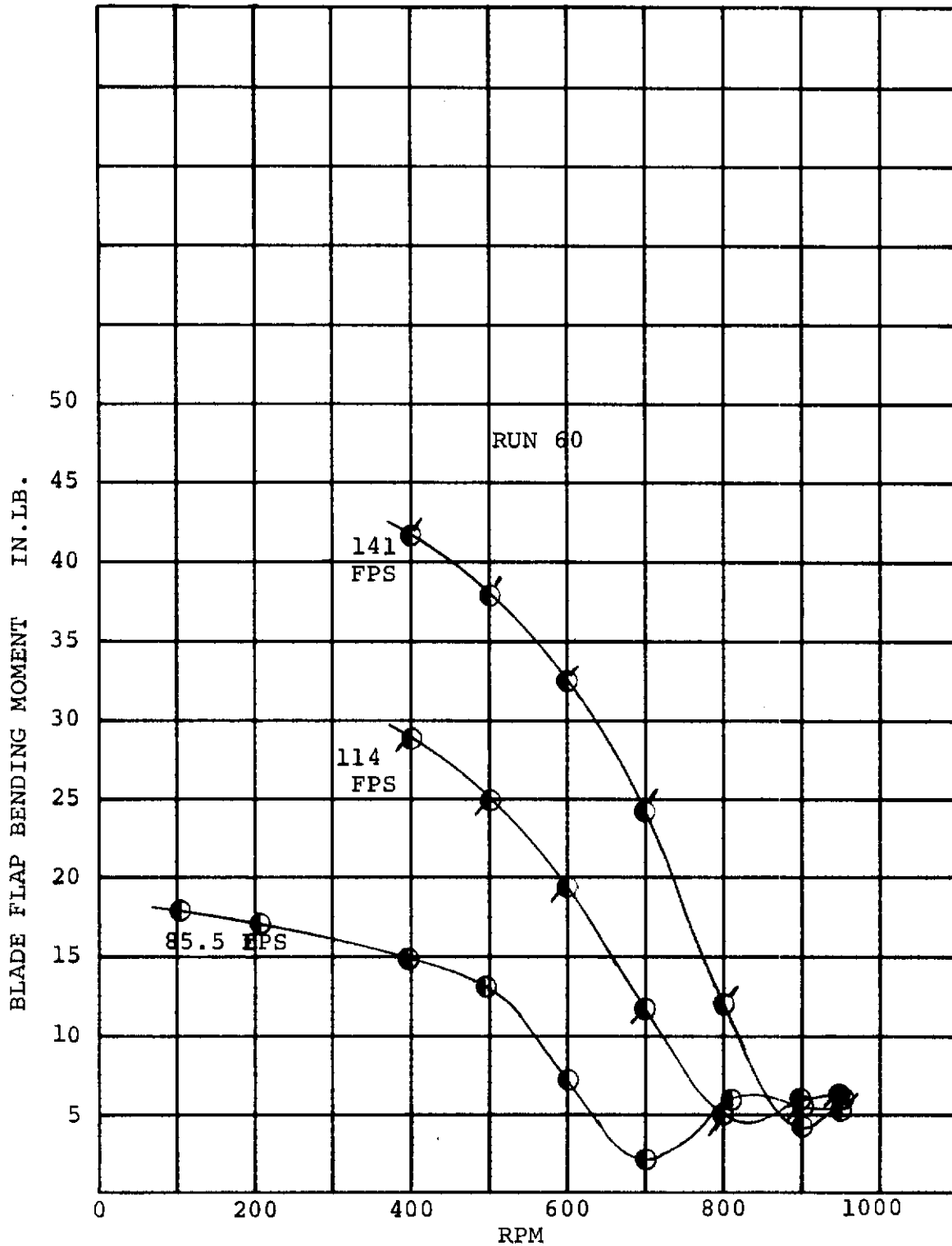


FIGURE 7-11. ALTERNATING BLADE FLAP BENDING 0.125R  
STEADY WINDMILLING  $\alpha = 2^\circ$   $\delta_F = 0^\circ$

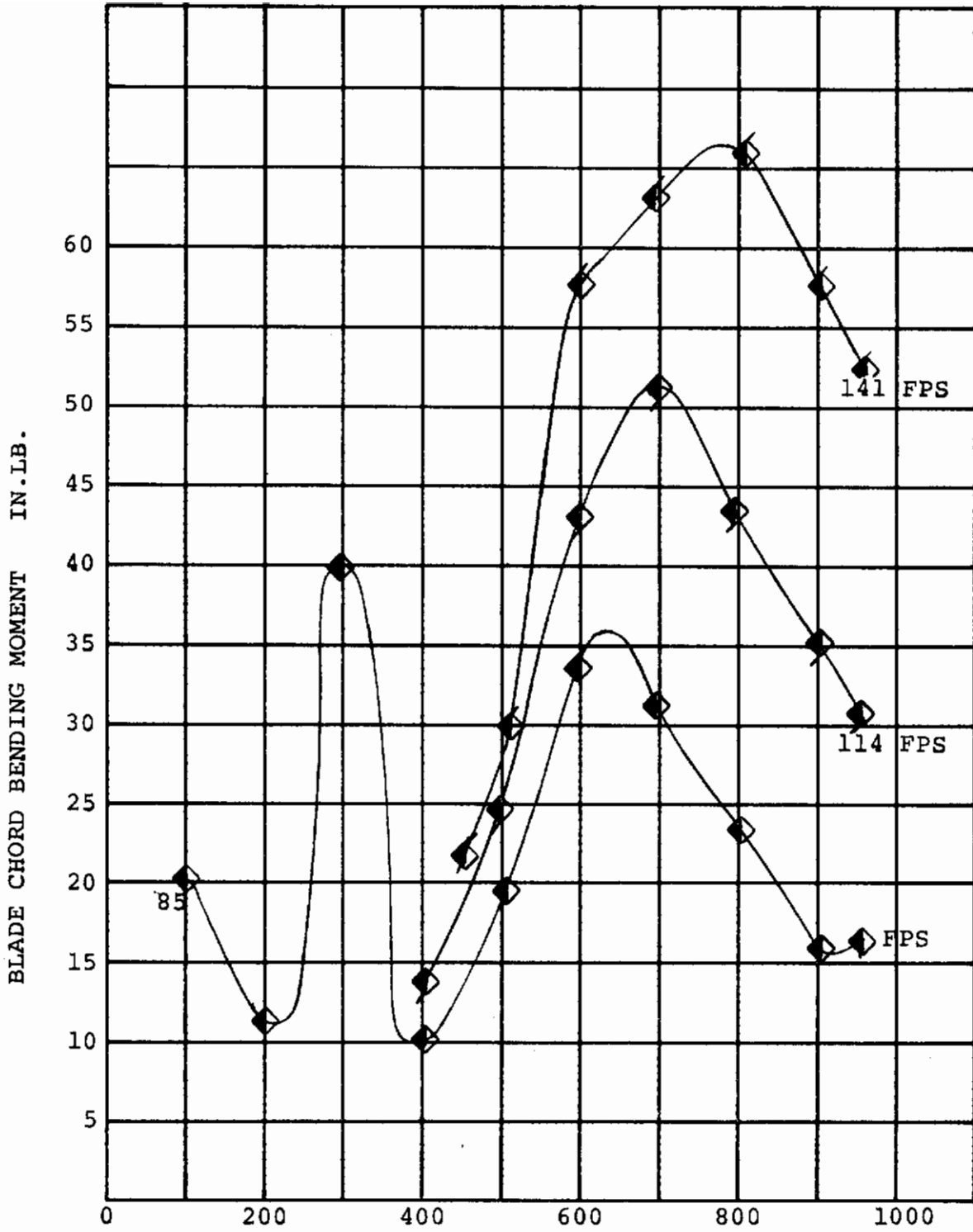


FIGURE 7-12. ALTERNATING BLADE CHORD BENDING 0.125R  
 STEADY WINDMILLING  $\alpha = 4^\circ$   $\xi_F = 0^\circ$

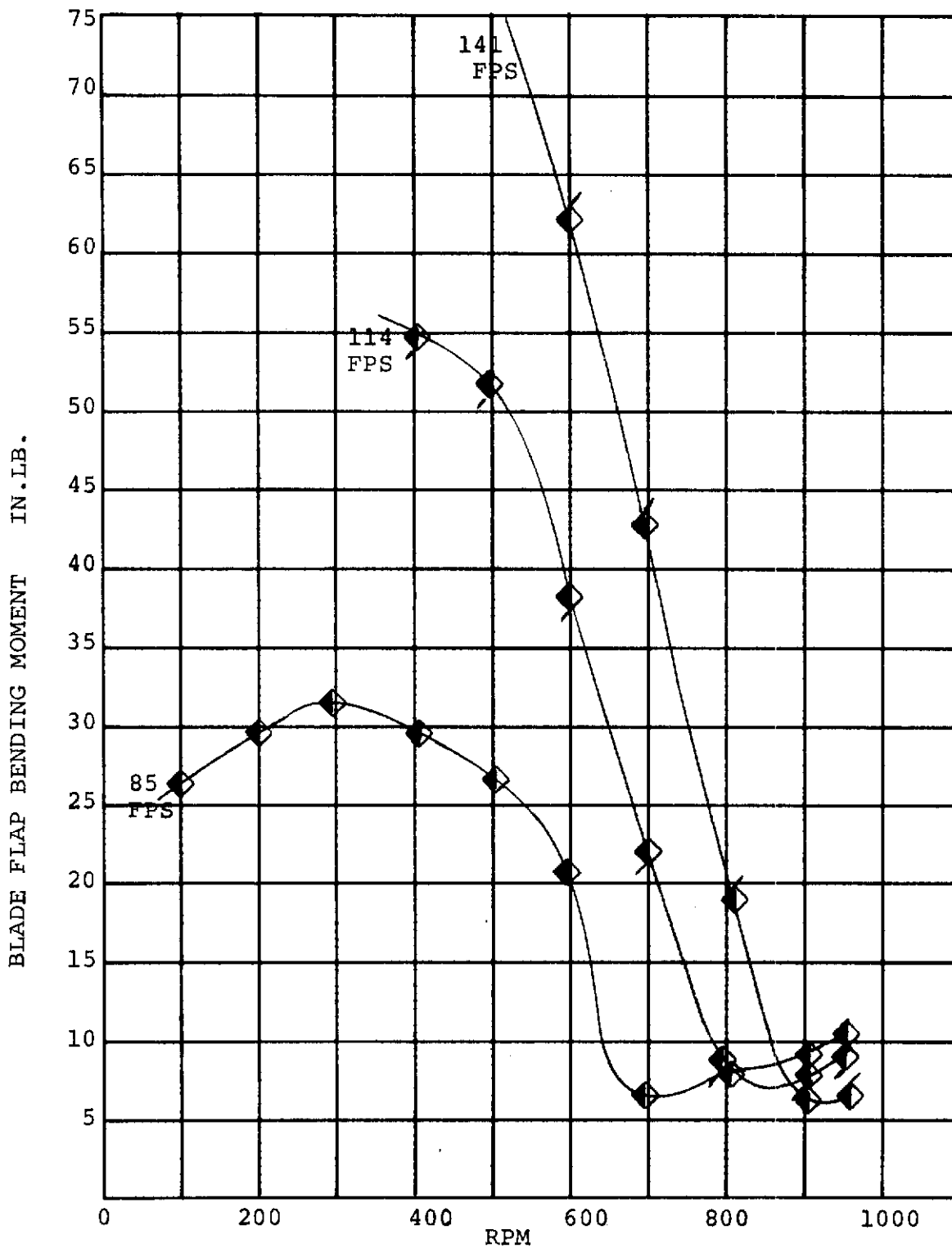


FIGURE 7-13: ALTERNATING BLADE FLAP BENDING 0.125R  
STEADY WINDMILLING  $\alpha = 4^\circ \delta_F = 0^\circ$

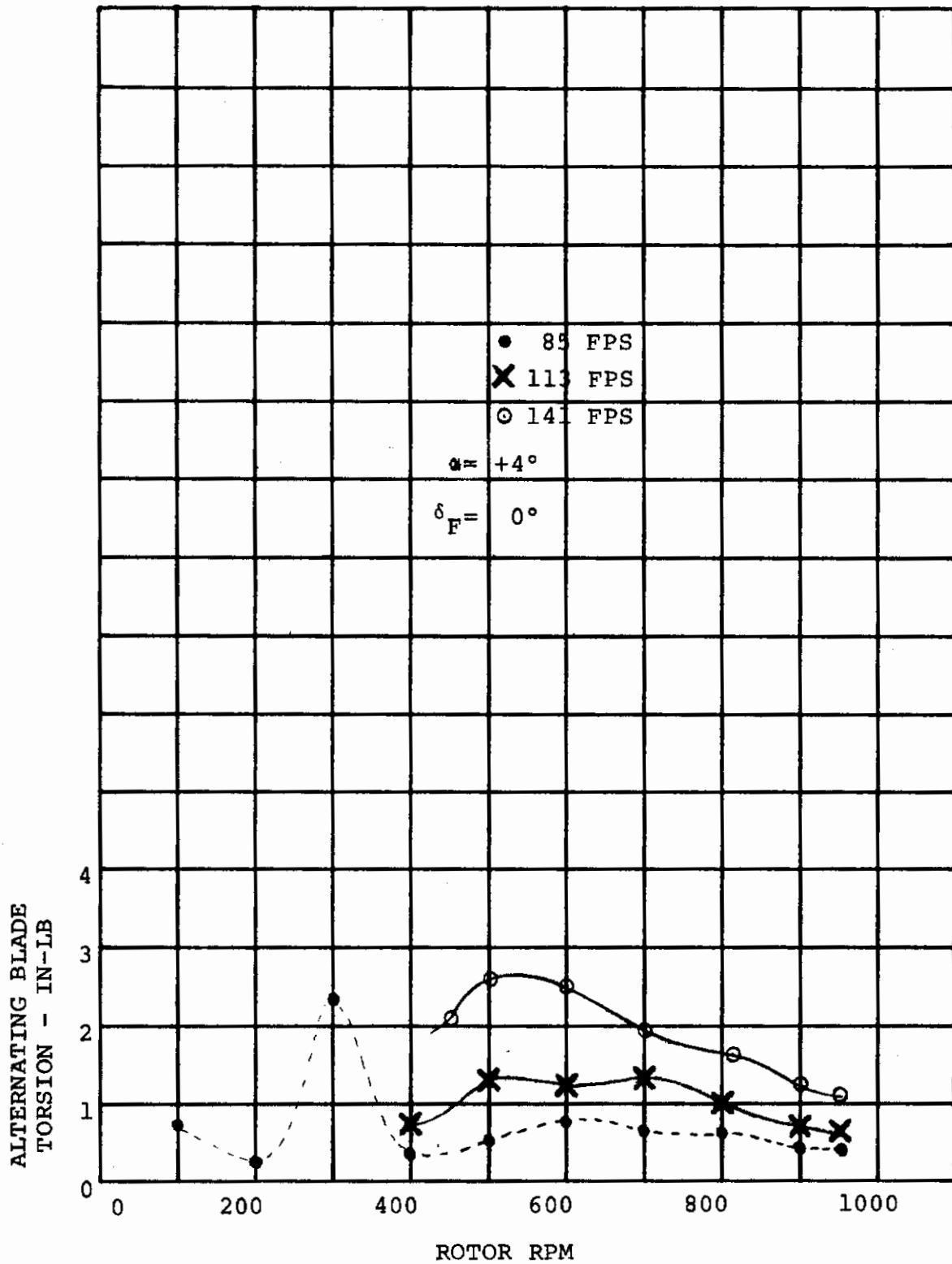


FIGURE 7-14. ALTERNATING BLADE TORSION AS A FUNCTION OF RPM AND TUNNEL SPEED

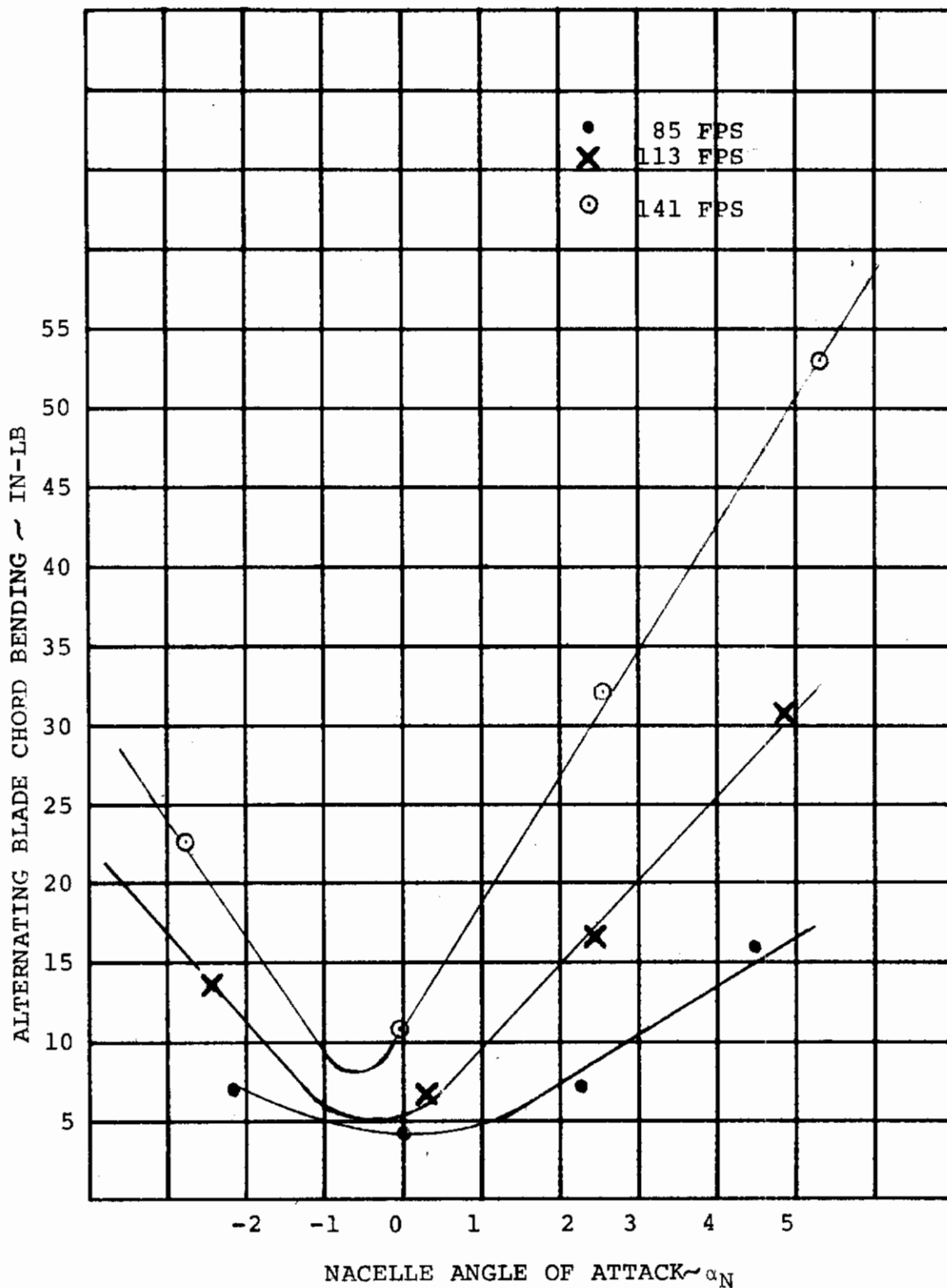


FIGURE 7-15. ALTERNATING BLADE CHORD BENDING FOR THREE TUNNEL SPEEDS AND VARIOUS NACELLE ANGLES AT 950 RPM

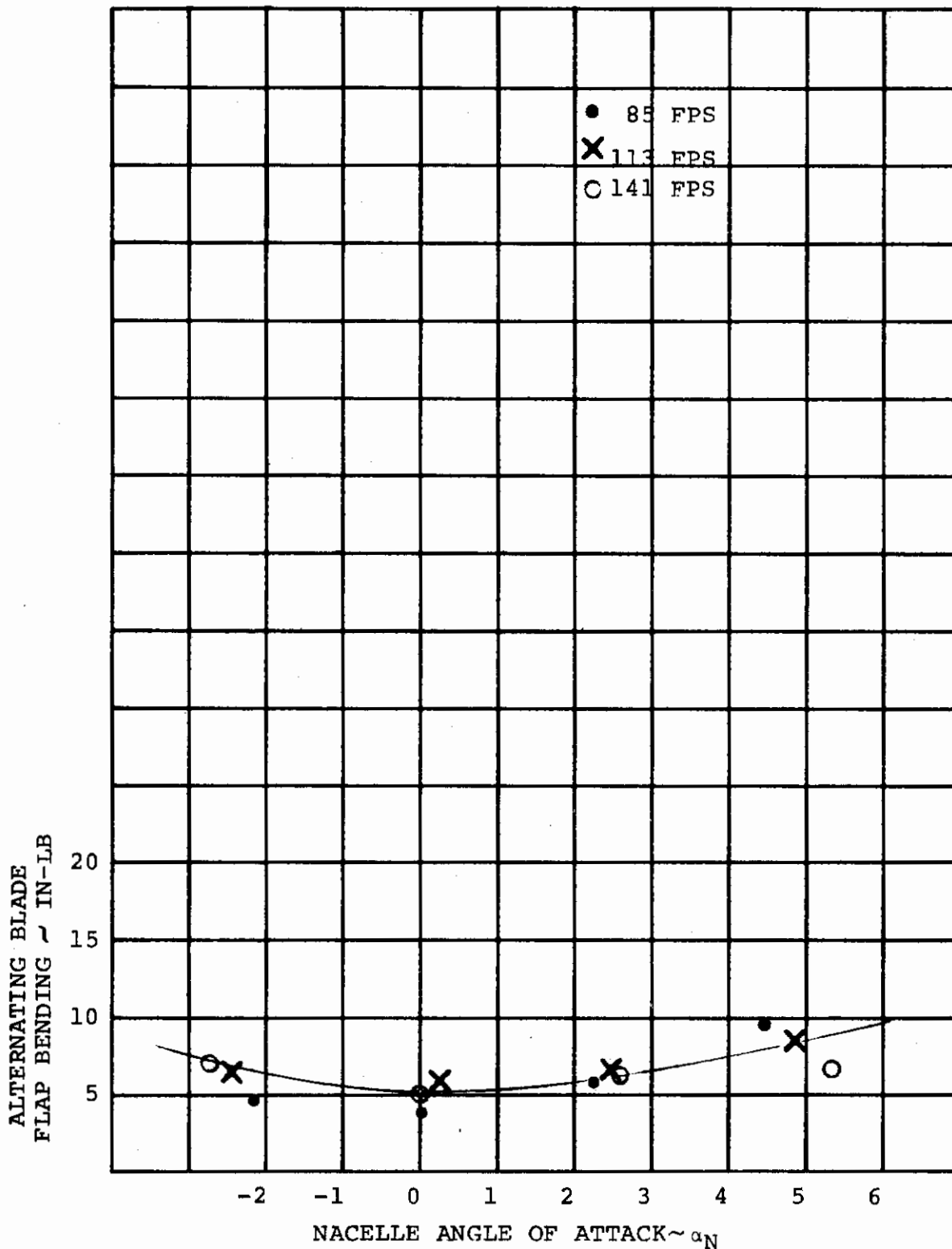


FIGURE 7-16. ALTERNATING BLADE FLAP BENDING AT .125 R FOR THREE TUNNEL SPEEDS AND VARIOUS NACELLE ANGLES AT 950 RPM

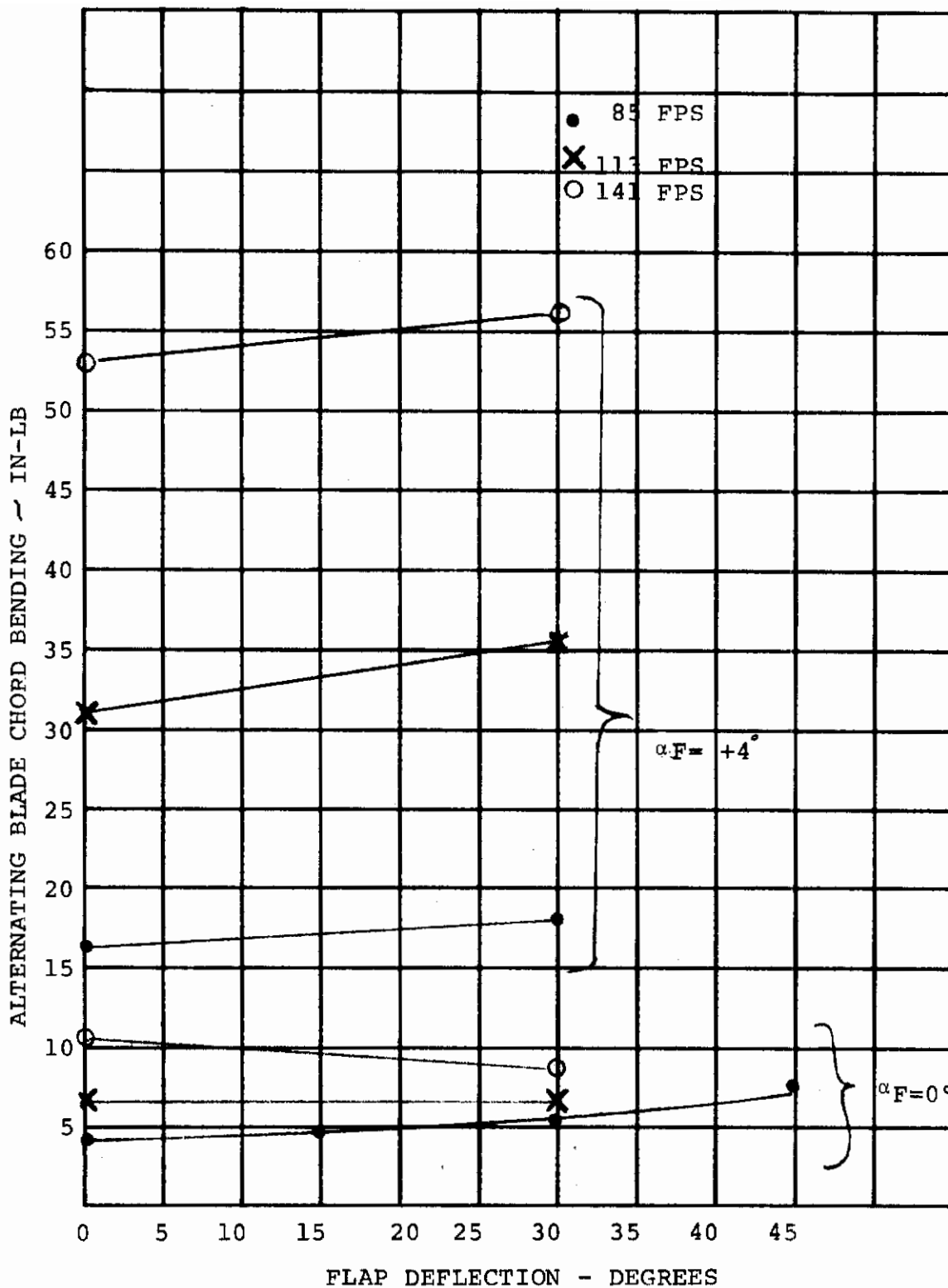


FIGURE 7-17. ALTERNATING BLADE CHORD BENDING AS A FUNCTION OF FLAP DEFLECTION AND THREE TUNNEL SPEEDS AT 950 RPM



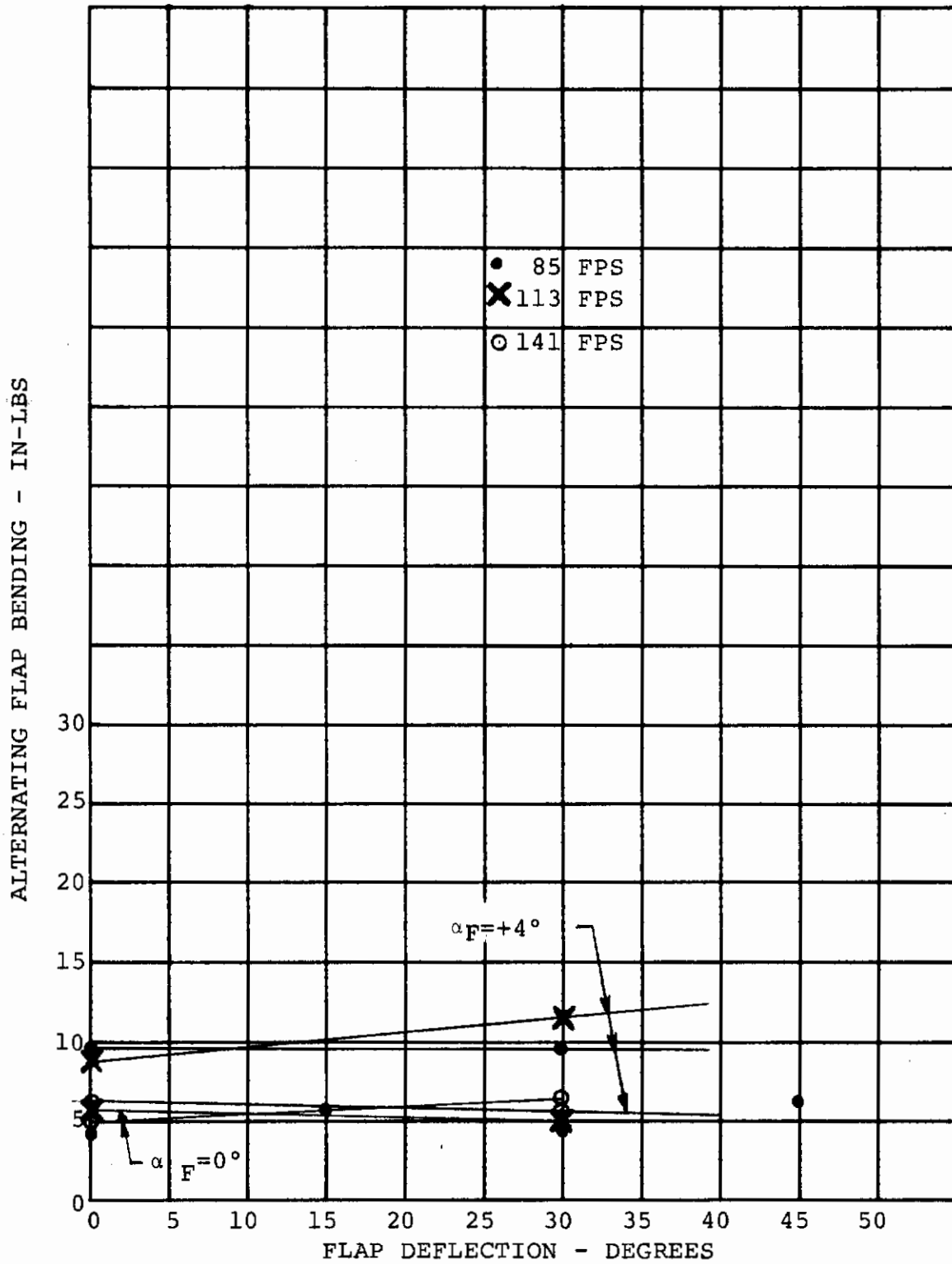


FIGURE 7-18. ALTERNATING BLADE FLAP BENDING AS A FUNCTION OF FLAP DEFLECTION AND THREE TUNNEL SPEEDS AT 950 RPM

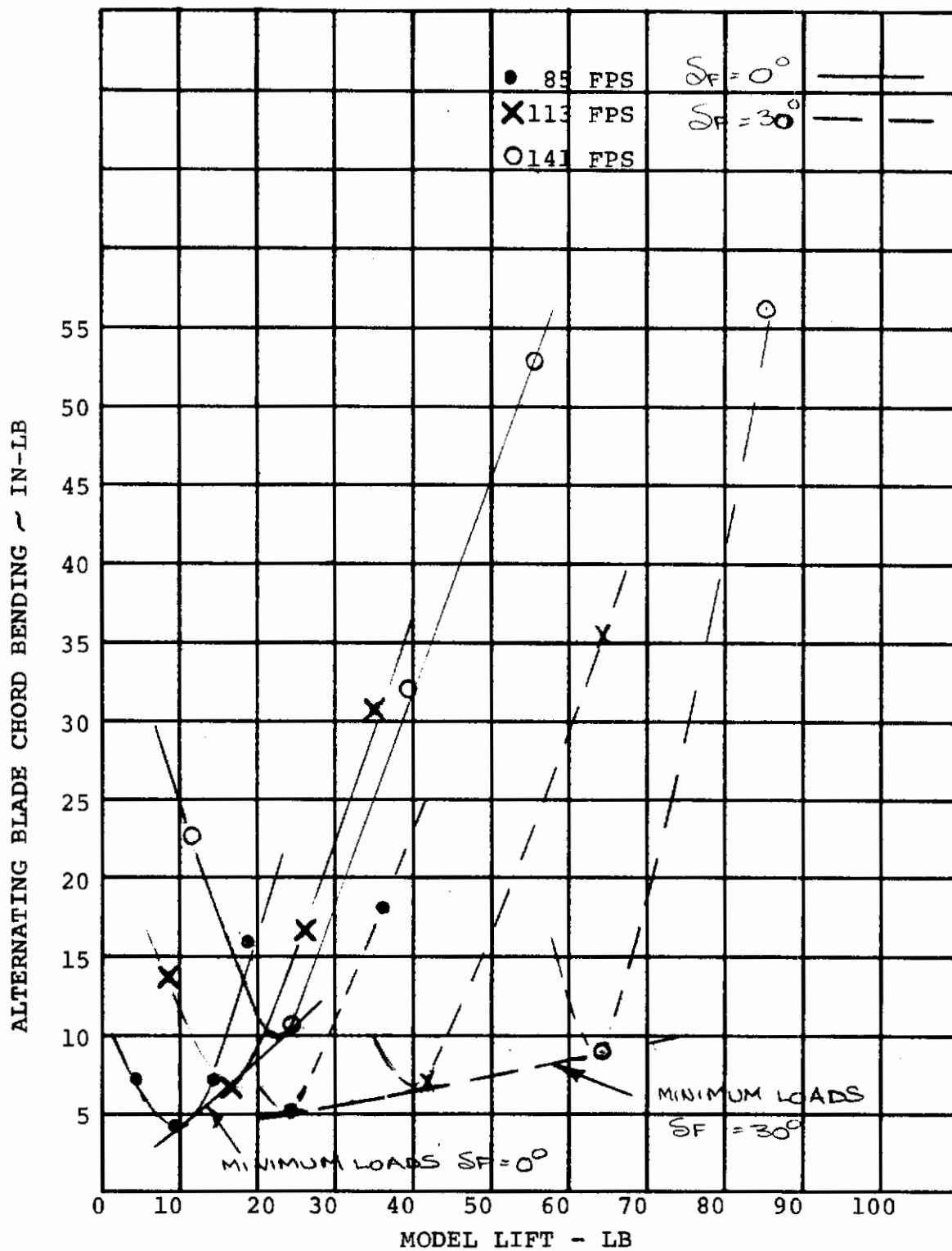


FIGURE 7-19. ALTERNATING BLADE CHORD BENDING AT .125 R AS A FUNCTION OF MODEL LIFT, AIR SPEED AND FLAP DEFLECTION TO  $30^\circ$  AT 950 RPM

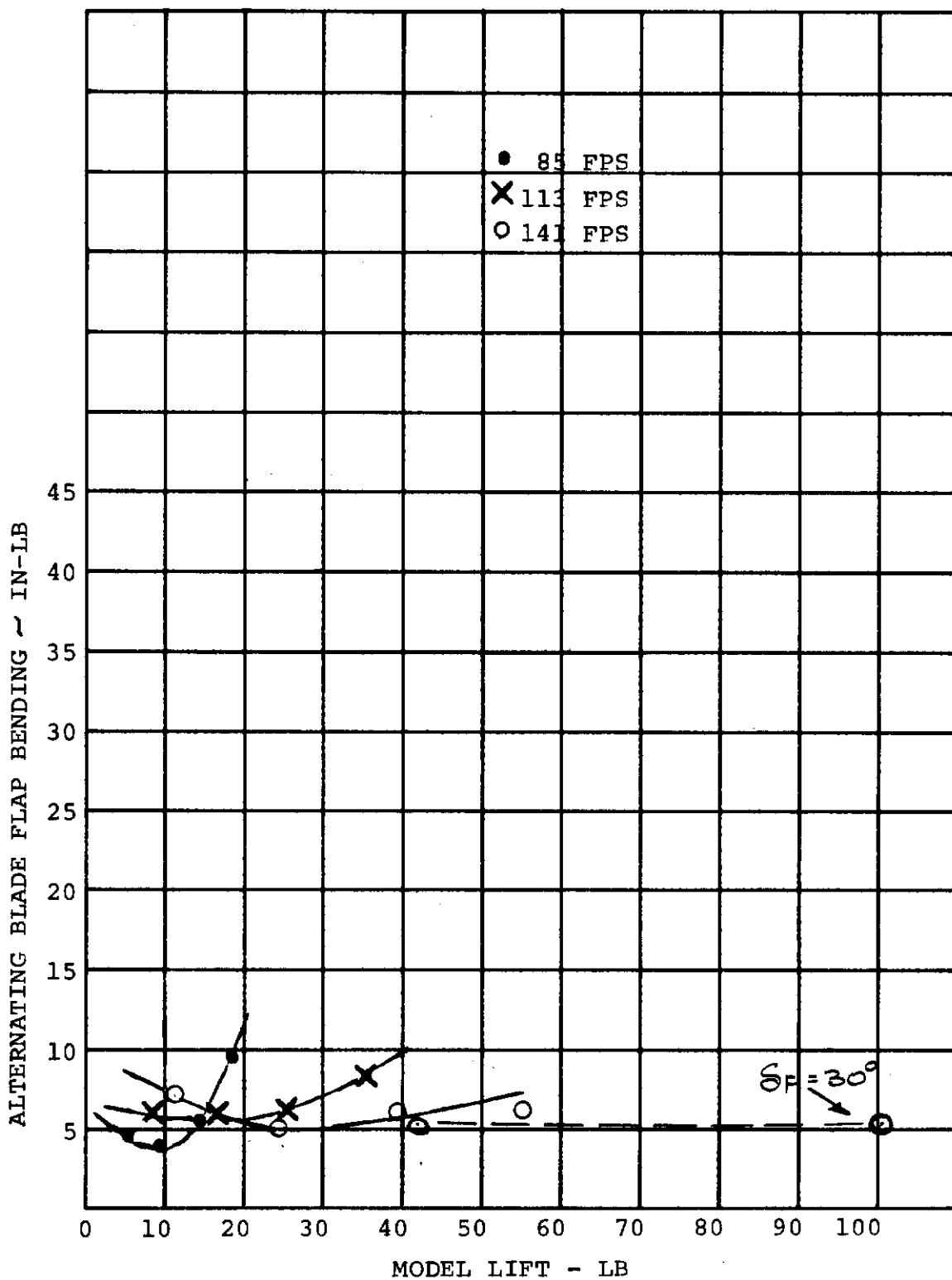


FIGURE 7-20. ALTERNATING BLADE FLAP BENDING AT .125 R AS A FUNCTION OF MODEL LIFT, AIR SPEED AND FLAP DEFLECTION TO 30° AT 950 RPM

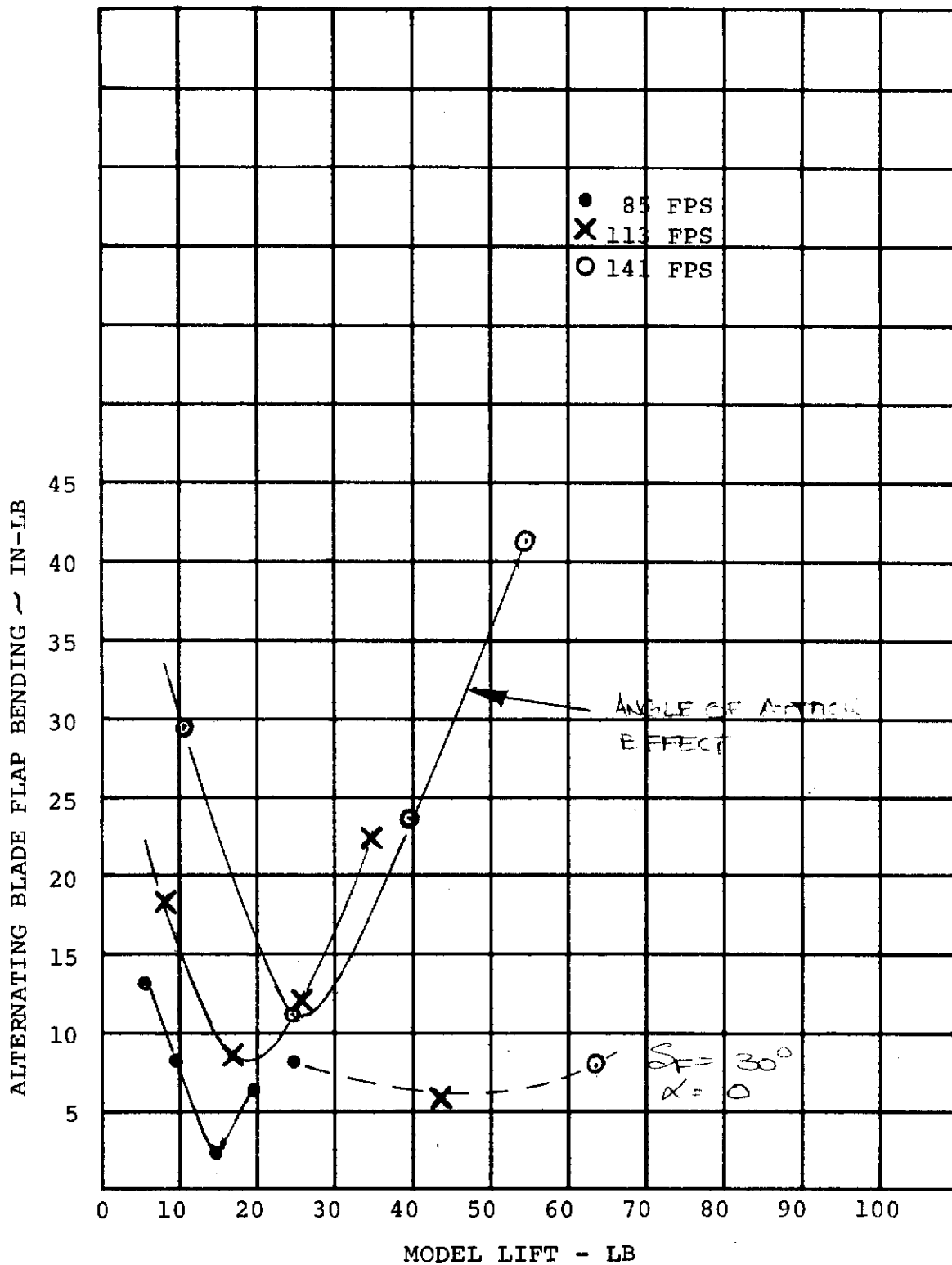


FIGURE 7-21. ALTERNATING BLADE FLAP BENDING AT .125 R AS A FUNCTION OF MODEL LIFT, AIR SPEED AND FLAP DEFLECTION TO 30° AT 700 RPM

# Contrails

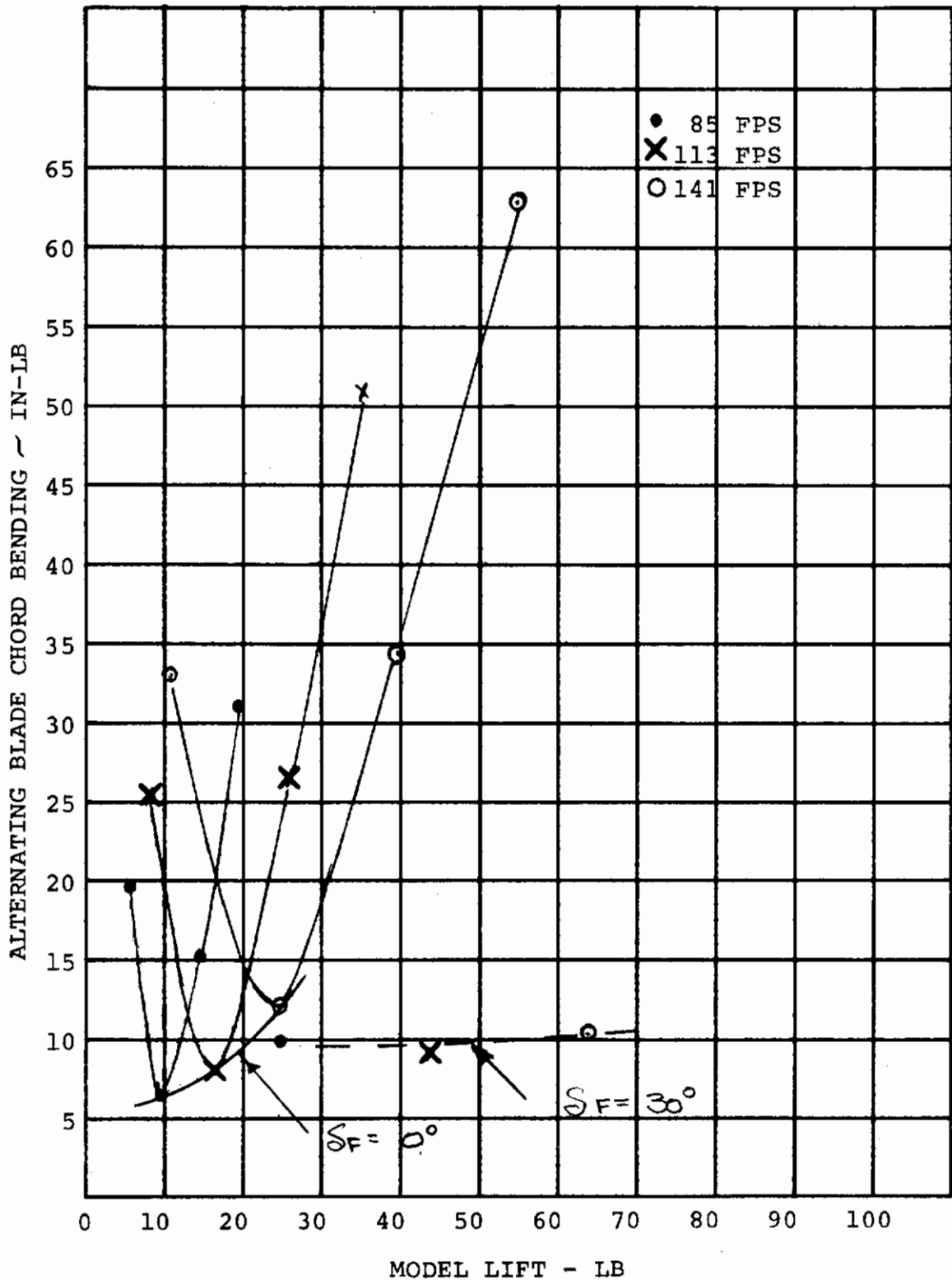


FIGURE 7-22. ALTERNATING BLADE CHORD BENDING AT .125 R AS A FUNCTION OF MODEL LIFT, AIR SPEED AND FLAP DEFLECTION TO 30° AT 700 RPM

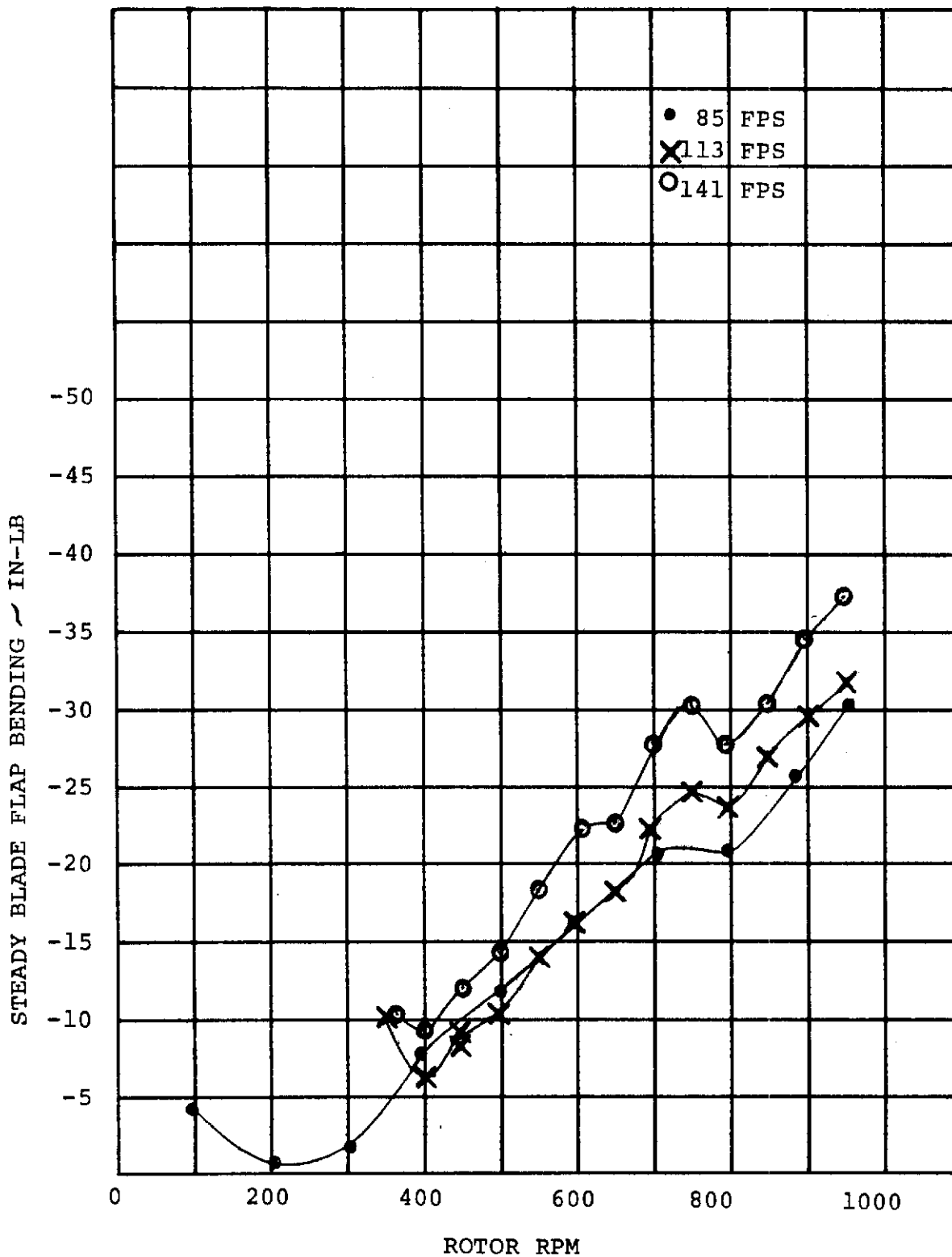


FIGURE 7-23. STEADY BLADE FLAP BENDING AT .125r/R WITH  $\alpha_F = 0^\circ$   $\delta_F = 0^\circ$

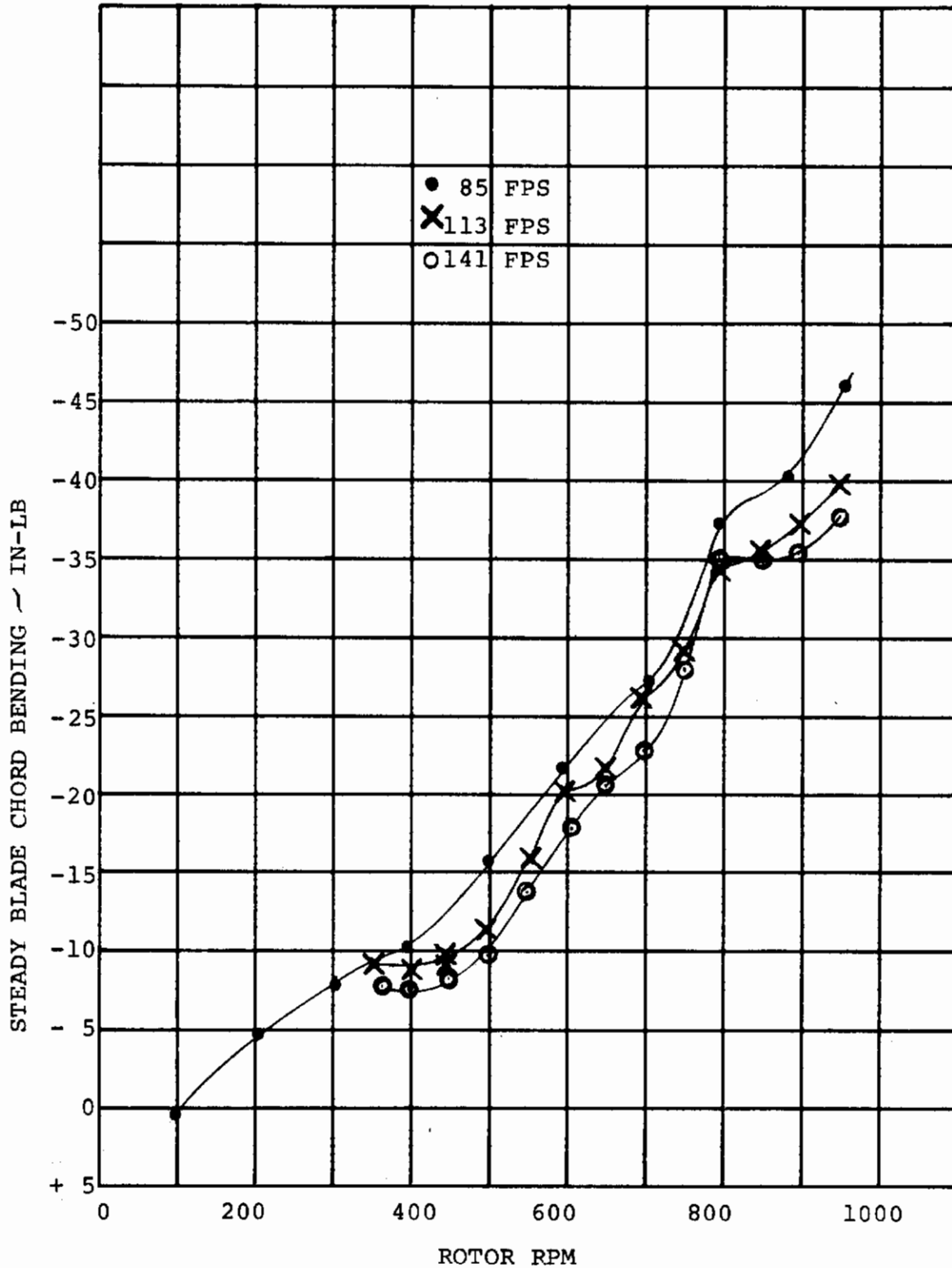


FIGURE 7-24. STEADY BLADE CHORD BENDING AT .125r/R  
WITH  $\alpha = 0^\circ$   $\delta = 0^\circ$

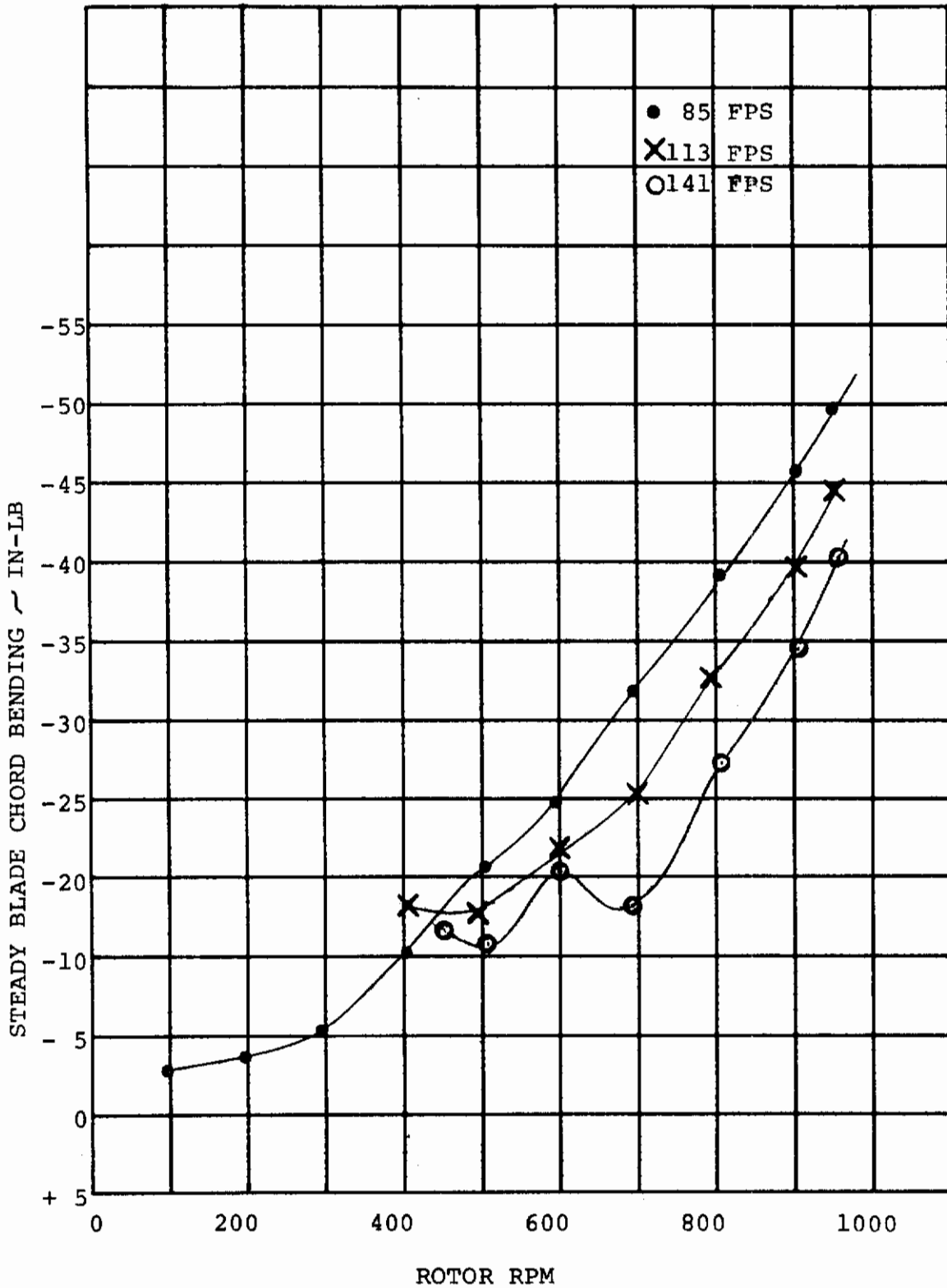


FIGURE 7-25. STEADY BLADE CHORD BENDING  $\alpha_F=+4^\circ$   $\delta_F=0^\circ$



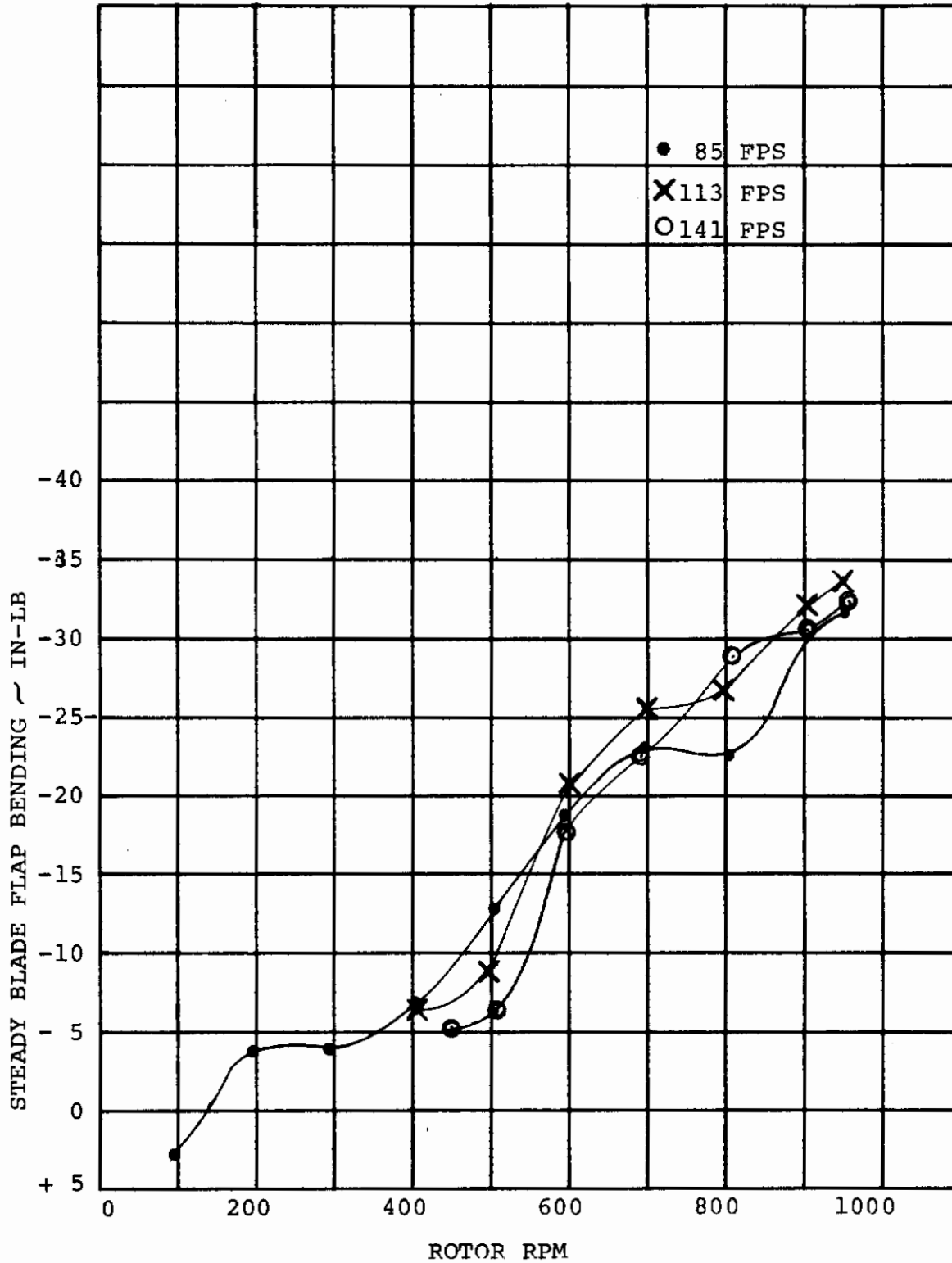


FIGURE 7-26. STEADY BLADE FLAP BENDING AT .125r/R WITH  $\alpha = +4^\circ$   $\delta_F = 0^\circ$

## 7.3 Rotor Loads During Spin-Up and Feather

Alternating blade loads measured under the transient conditions of spin-up and feather for various spin times and collective schedules are given in Figures 7-27 to 7-50.

Figures 7-27 to 7-30 compare the loads for three linear collective schedules having spin times of nominally 3.0, 4.5 and 6.0 seconds. The measured times and collective settings are given in Figures 5-14 and 5-15 in Section 5.0. The blade chord bending loads show two transient peaks at 300 to 350 RPM and at 600 to 700 RPM. The flap bending loads have no large blade response peaks. The first and predominant peaks are due to the 2/rev mode blade natural frequency at 290 RPM and the wing vertical bending natural frequency at 350 RPM as seen in the steady windmilling data. The blade loads measured at these resonance crossings decrease as the spin time is reduced and suggest that a fast initial rate of change of RPM is beneficial to blade loads since the resonance crossings are crossed too fast for the blade to respond fully.

The second peak in the chord bending loads occurs at 600 to 750 RPM. The blade lag 1/rev frequency is at 625 RPM and the wing torsion frequency is at 800 RPM. The blade response in this RPM range was not observed in steady windmilling at zero angle of attack but seems to occur whenever there is asymmetry in the inflow distribution either due to angle of attack or wing flap deflection. The differences in the alternating load levels experienced in spin-up and feather are small.

Figures 7-31 to 7-34 show the transient blade loads at 113 feet per second with different wing flap settings. The influence on the highest loads is small; however, a small change in blade response to the wing torsional frequency is observed.

Figures 7-35 to 7-38 compare alternating blade loads for two different airspeeds. The two runs shown are at different wing flap settings; however, as was previously shown the effect of flap is small. The effect of increased airspeed is to increase the alternating chord loads near the resonance peaks and to increase the flap bending loads throughout the transient except at the final RPM where the loads are small in both cases.

The influence of collective pitch schedule on the transient blade loads is shown in Figures 7-39 to 7-42. The measured collective pitch and RPM schedules corresponding to these data are shown in Figures 5-24 and 5-25. In general the loads are not greatly affected by the collective schedule. The parabolic schedule with the highest initial rate of change of RPM (Run 80) shows a reduction

# Contrails

in chord bending loads during spin-up; however, during the feather transient no differences are observed. The blade flap bending loads are low and are unaffected by collective schedule.

Figures 7-43 to 7-50 show the alternating loads for various parabolic schedules with different spin times corresponding to the performance data shown in Figures 5-26 and 5-27. The recommended collective schedule and rate from a drag standpoint is a 3-4 sec parabolic transient which is between the 2 sec transient (Run 83/1) and the 6 sec transient (Run 84/4). The measured alternating loads for these schedules are almost the same and intermediate spin times will not produce loads in excess of those shown. The peak loads are approximately the same as for steady windmilling.

# Contrails

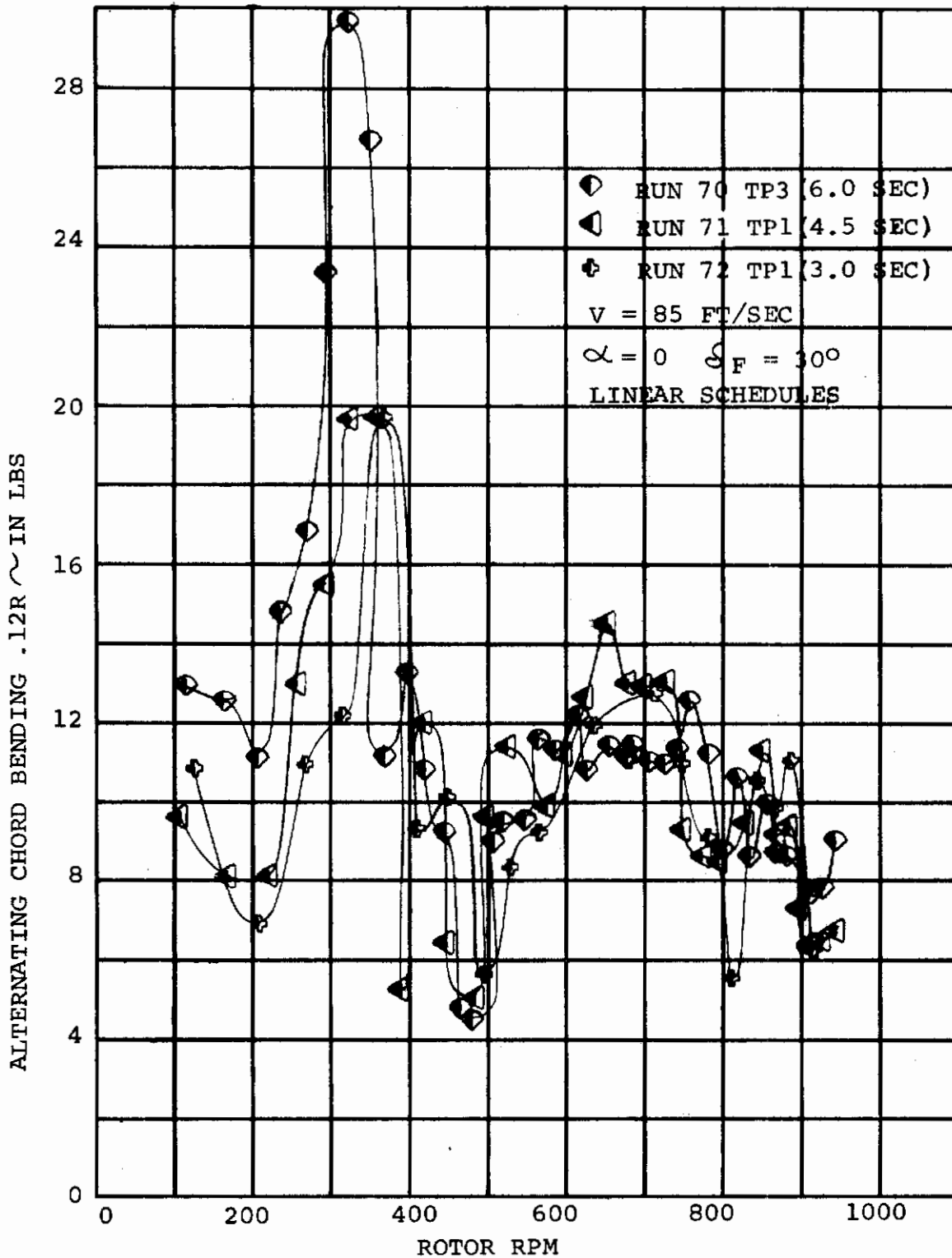


FIGURE 7-27. ALTERNATING BLADE CHORD BENDING DURING SPIN-UP  $V = 85$  FT/SEC  $\alpha_F = 0$   $\delta_F = 30$   
(LINEAR COLLECTIVE RATES)

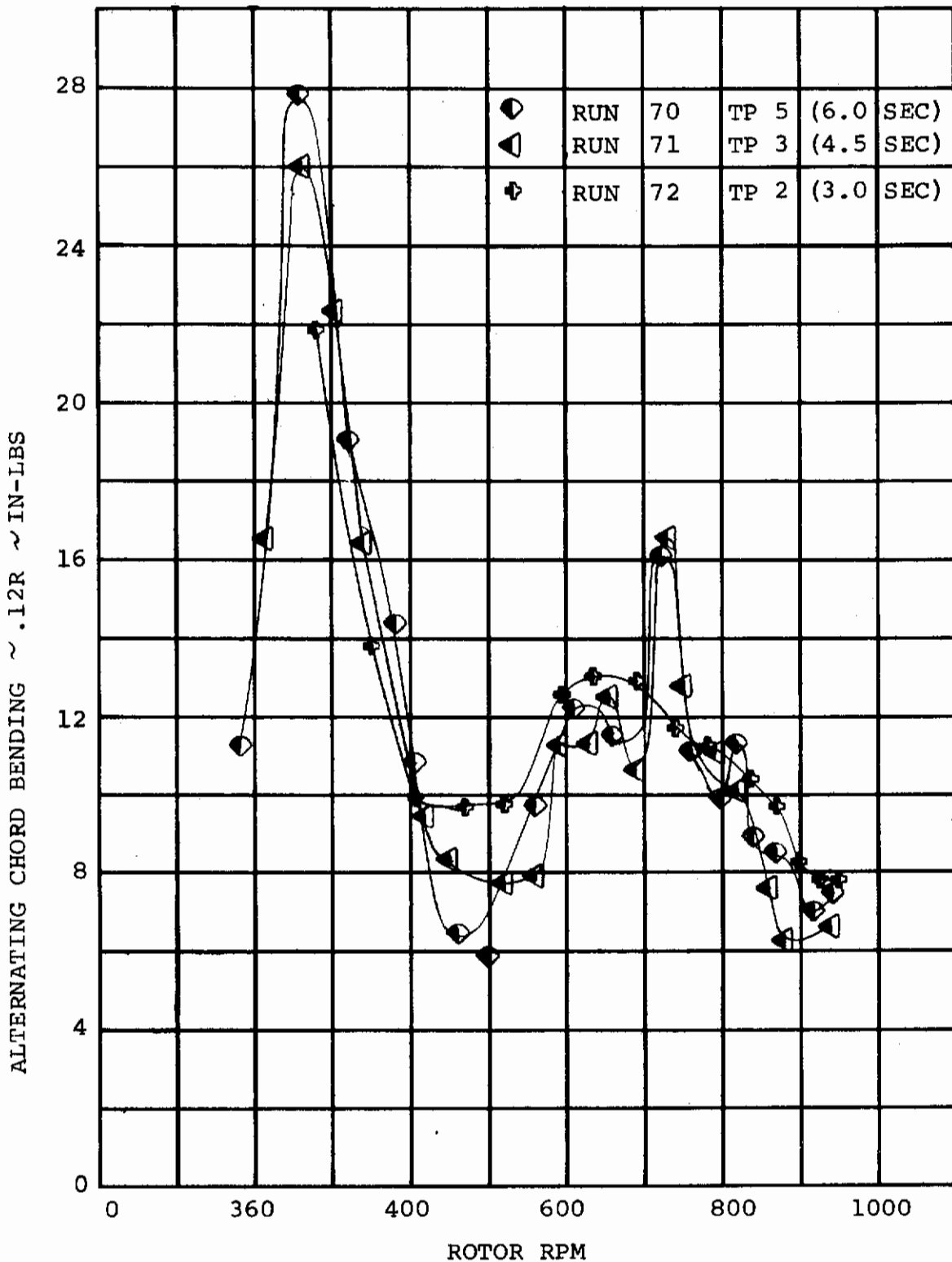


FIGURE 7-28. ALTERNATING BLADE CHORD BENDING DURING FEATHERED  $V = 85$  FT/SEC  $\alpha = 0$   $\delta_F = 30$  (LINEAR COLLECTIVE RATES)

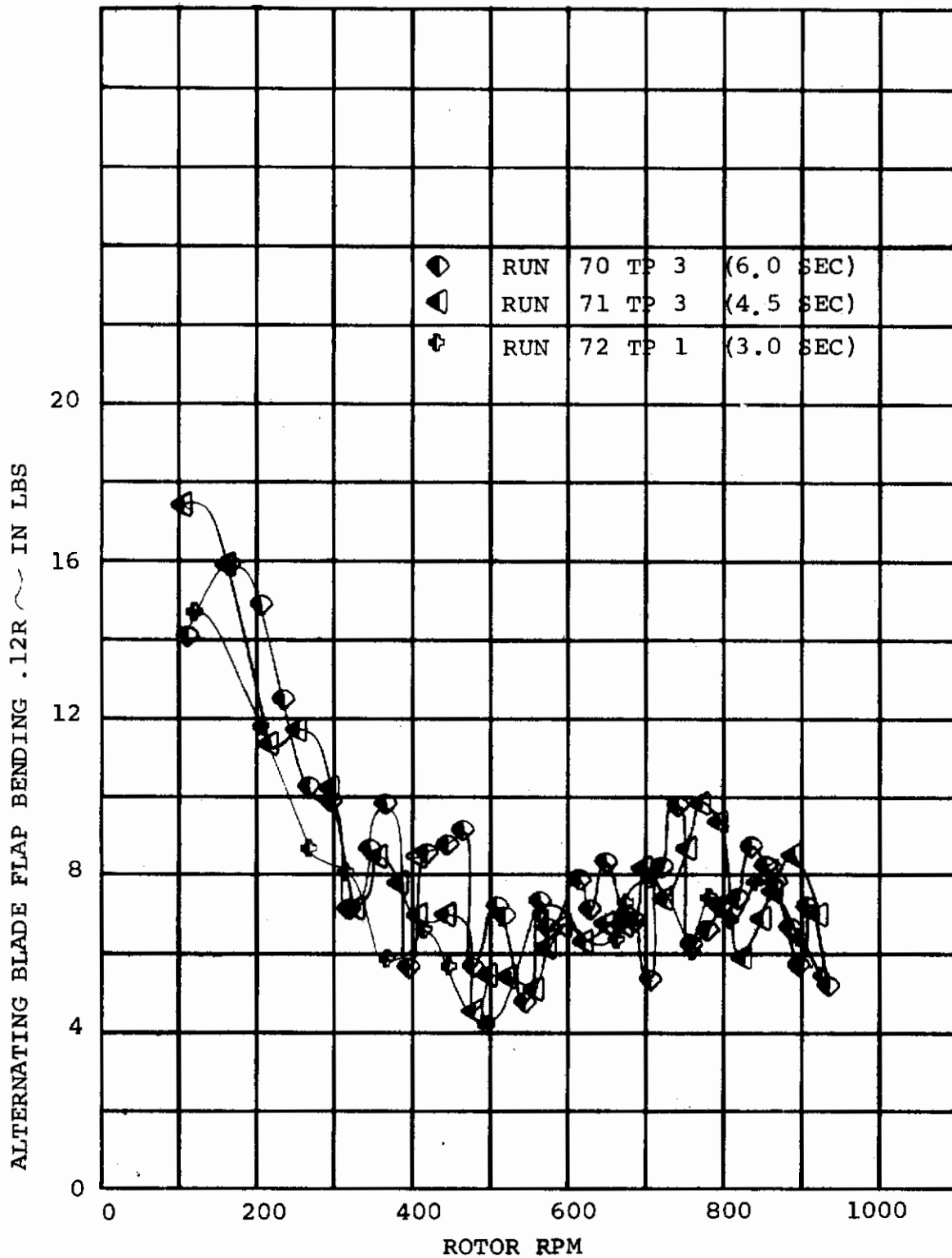


FIGURE 7-29. ALTERNATING BLADE FLAP BENDING DURING SPIN-UP  $V = 85$   $\alpha = -0$   $\delta_F = 30$   
(LINEAR COLLECTIVE RATES)

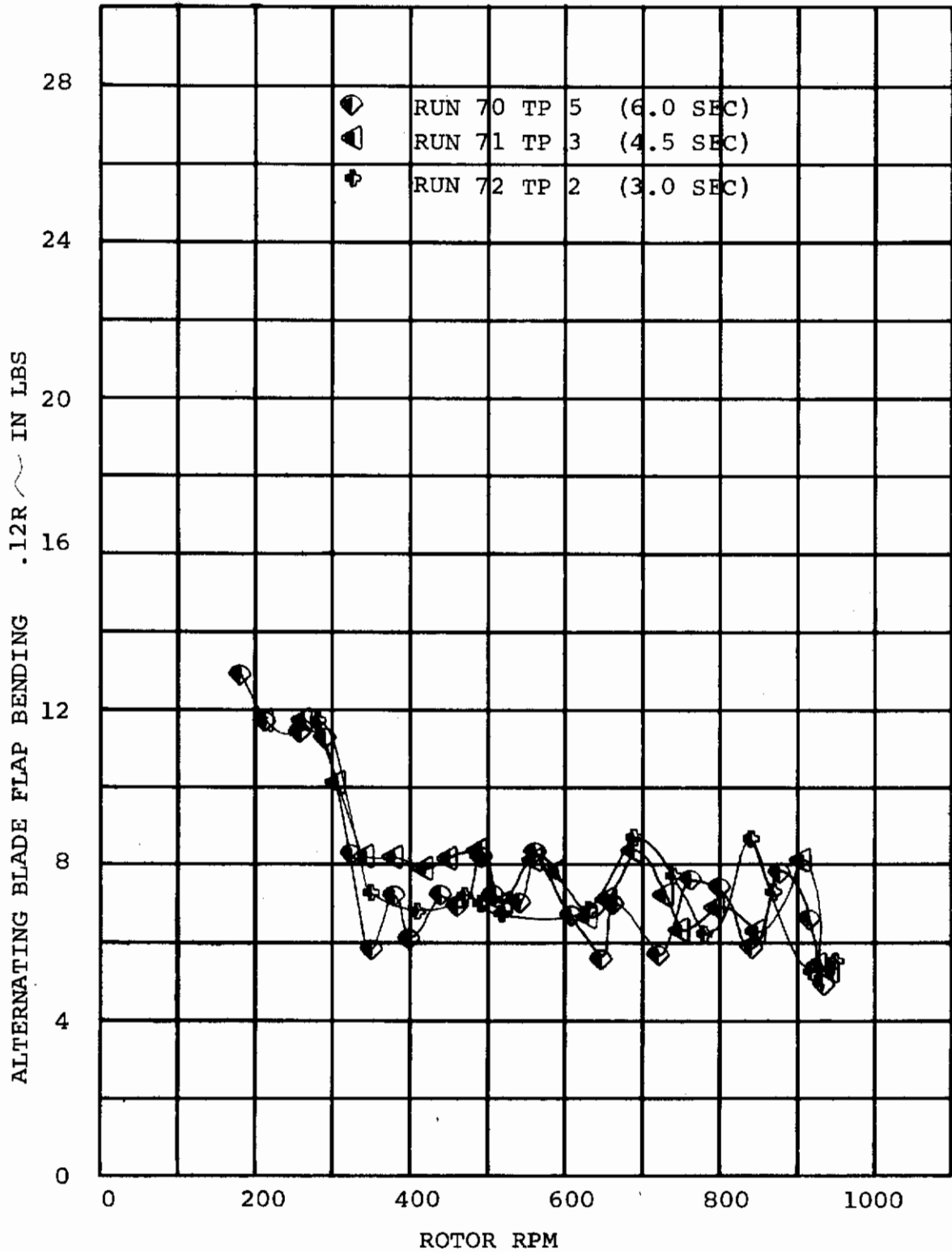


FIGURE 7-30. ALTERNATING BLADE FLAP BENDING  
 DURING FEATHER  $V = 85$   $\alpha = 0$   $\zeta_F = 30$

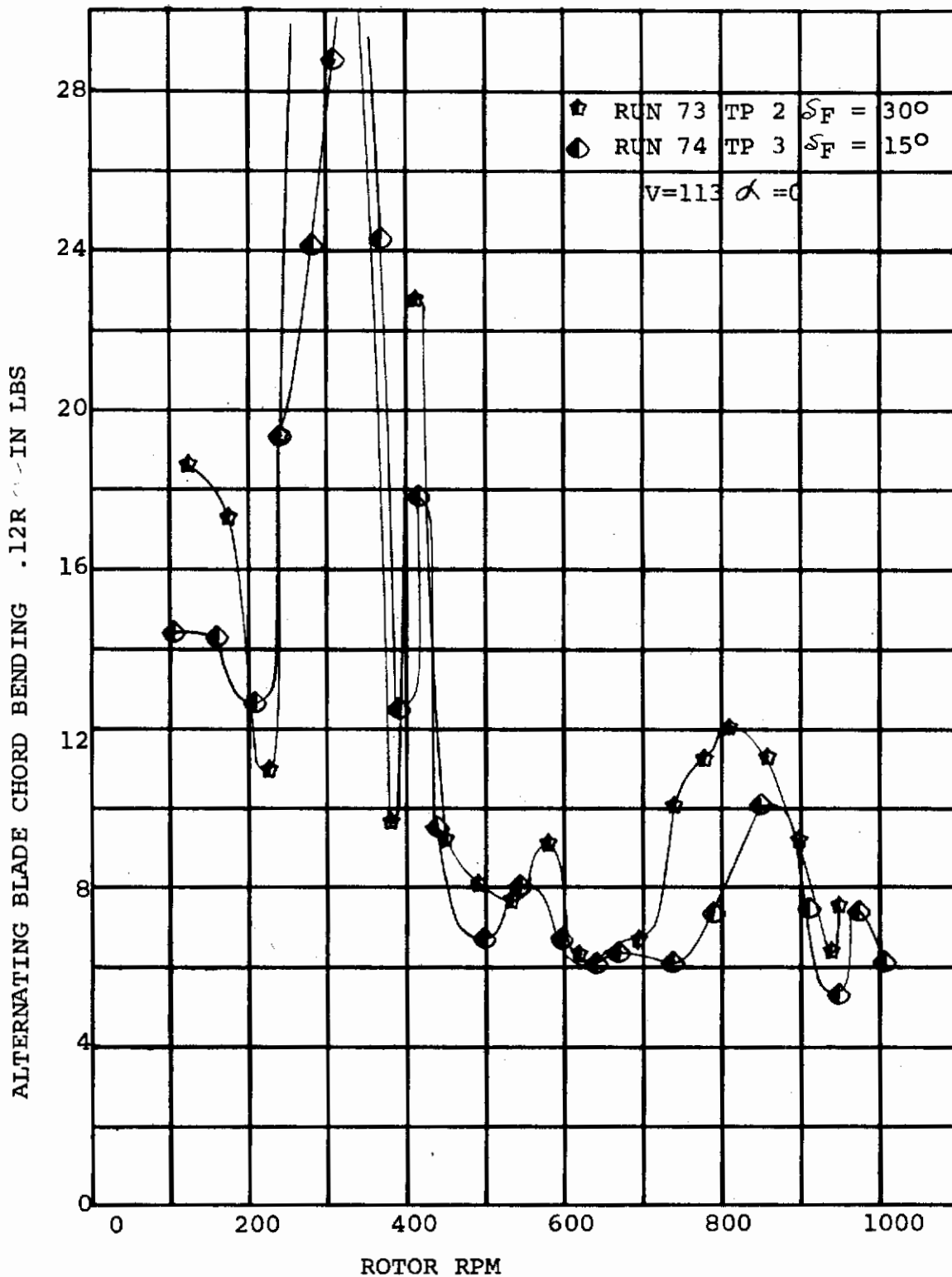


FIGURE 7-31. ALTERNATING BLADE CHORD BENDING DURING SPINUP - EFFECT OF WING FLAP DEFLECTION  $V = 113 \quad \alpha = 0$



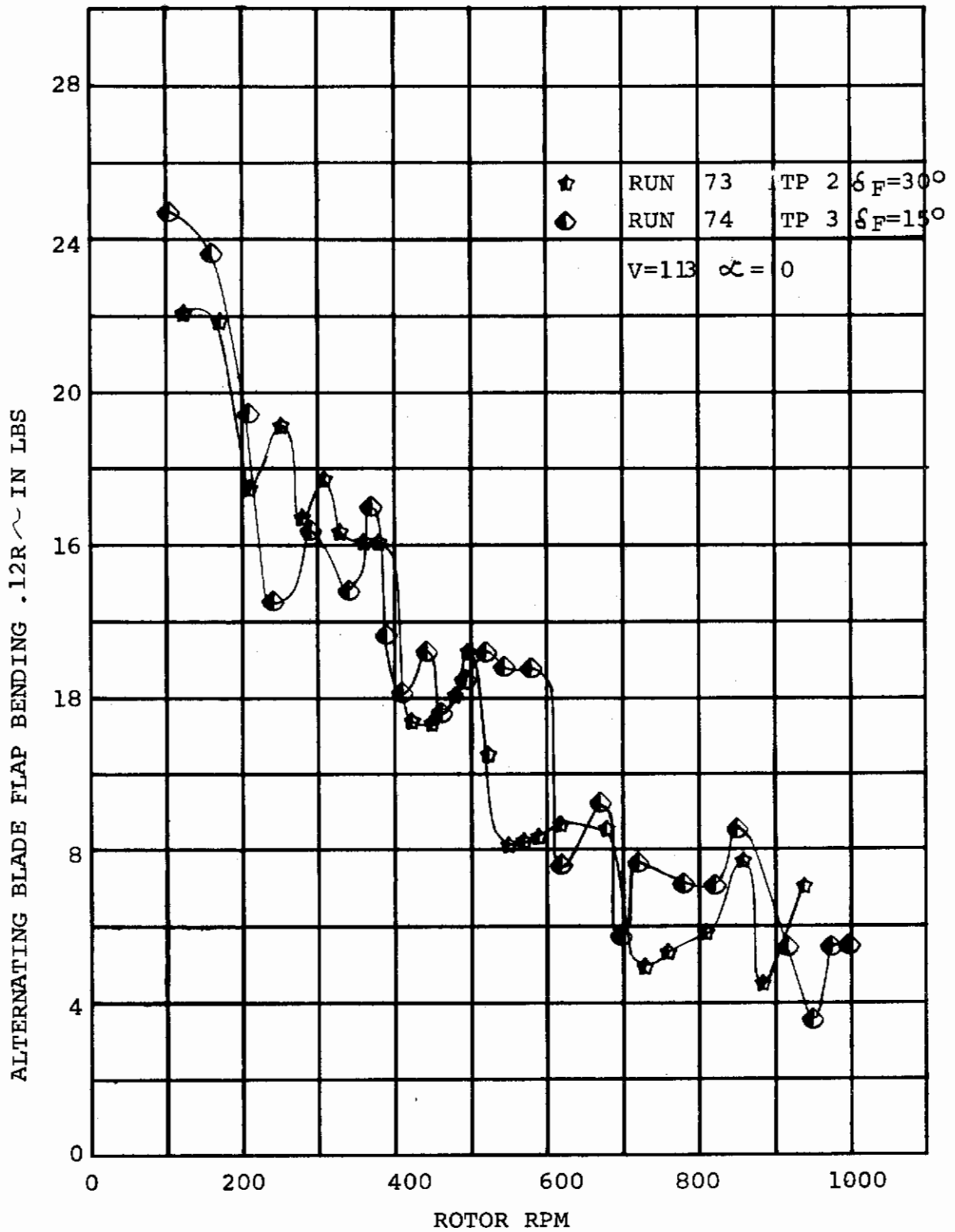


FIGURE 7-32. ALTERNATING BLADE FLAP BENDING DURING SPIN-UP EFFECT OF FLAP DEFLECTION  
 $V = 113 \quad \alpha = 0$

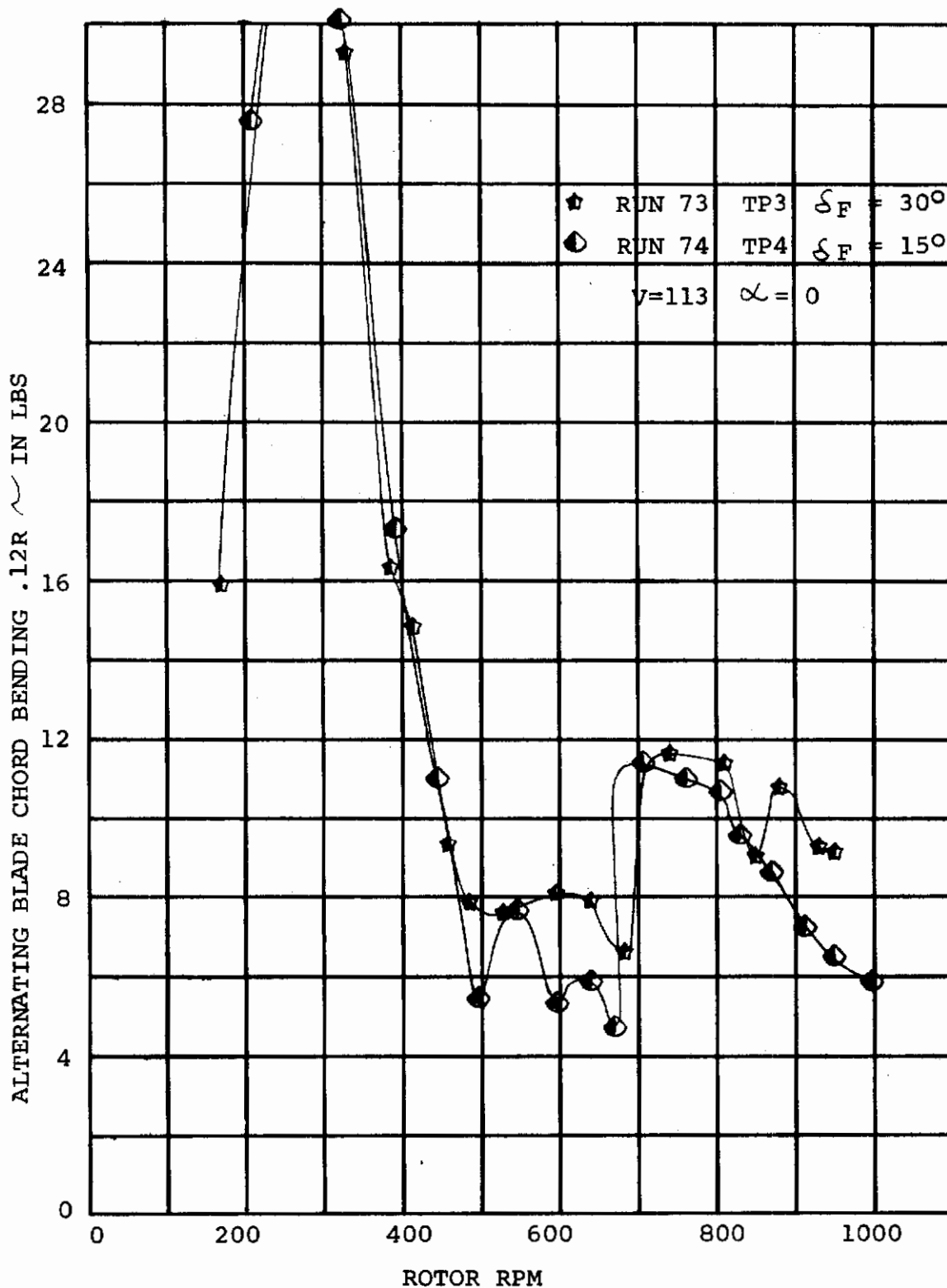


FIGURE 7-33. ALTERNATING BLADE CHORD BENDING DURING FEATHER - EFFECT OF FLAP DEFLECTION  
 $v = 113$   $\alpha = 0$

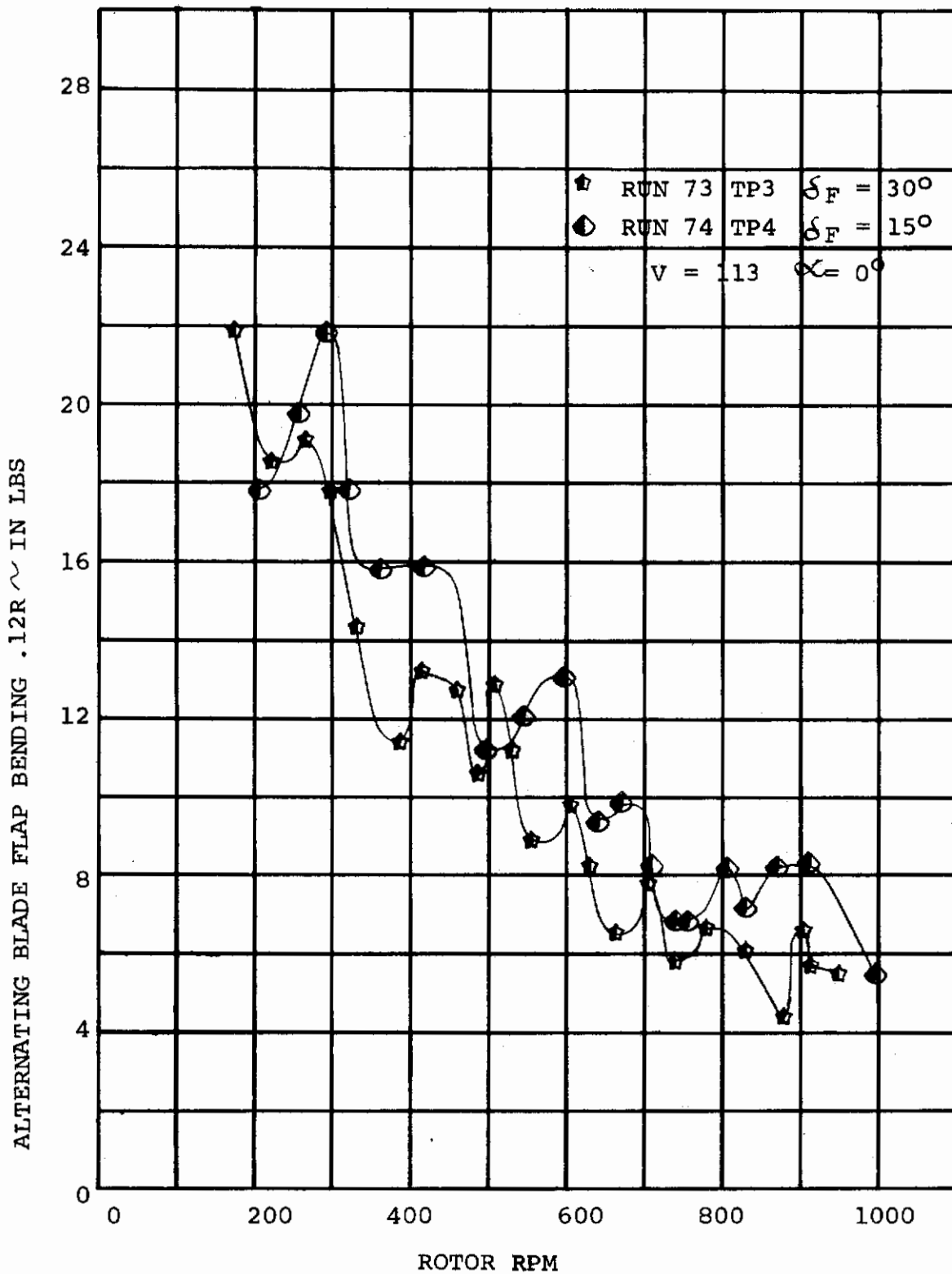


FIGURE 7-34. ALTERNATING BLADE FLAP BENDING DURING FEATHER - EFFECT OF FLAP DEFLECTION  
 V = 113  $\alpha = 0$

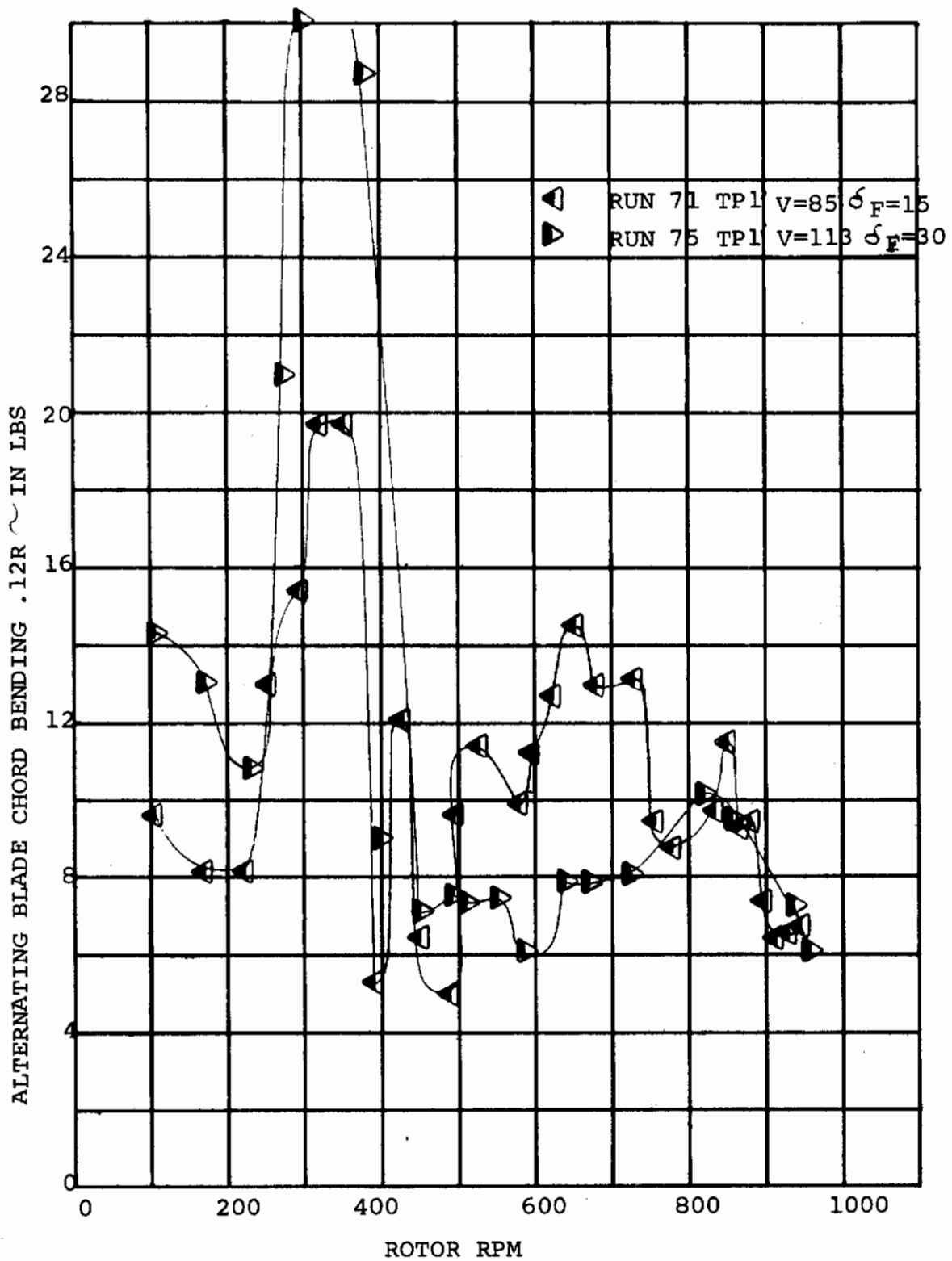


FIGURE 7-35. ALTERNATING BLADE CHORD BENDING DURING SPIN-UP

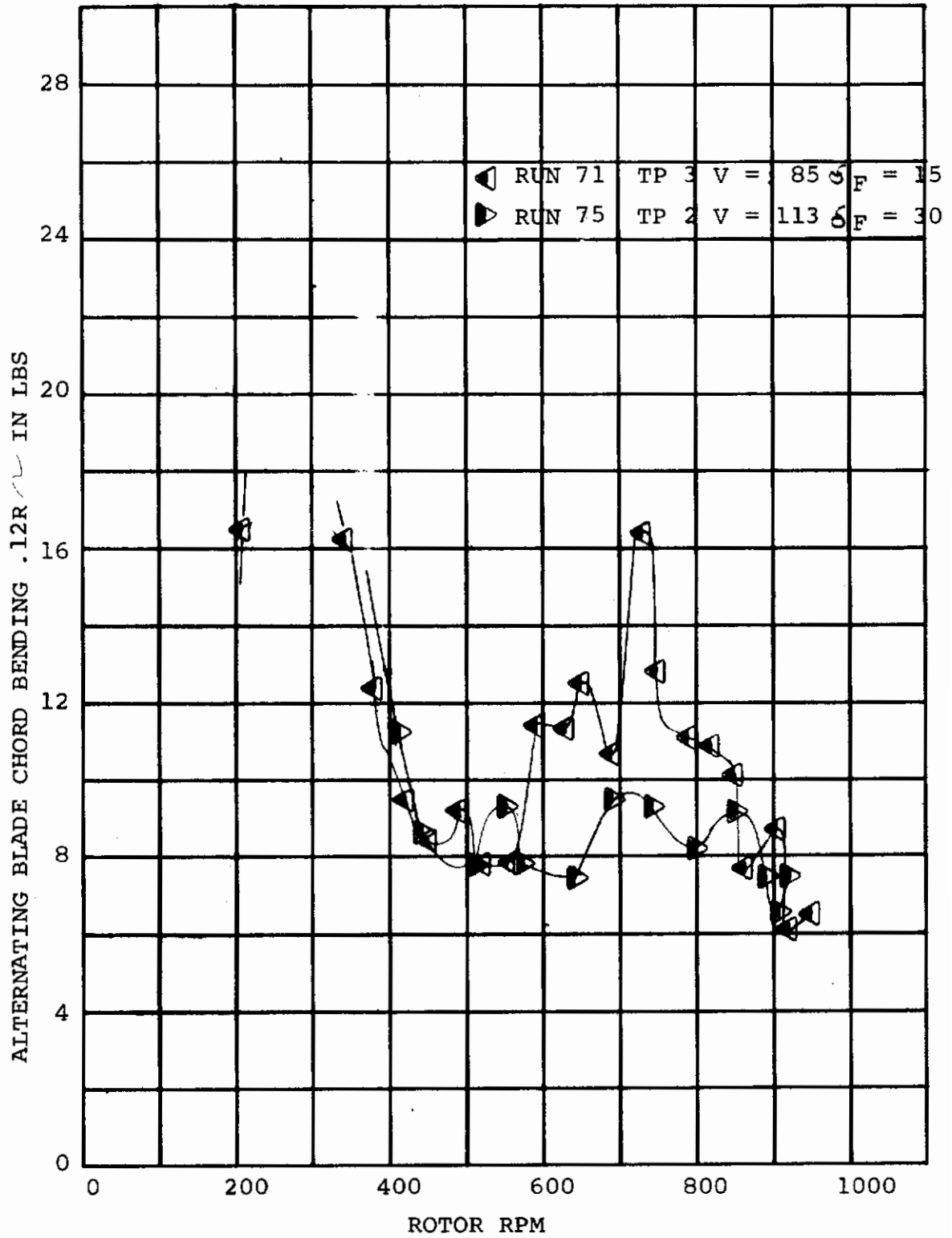


FIGURE 7-36. ALTERNATING BLADE CHORD BENDING DURING FEATHER.

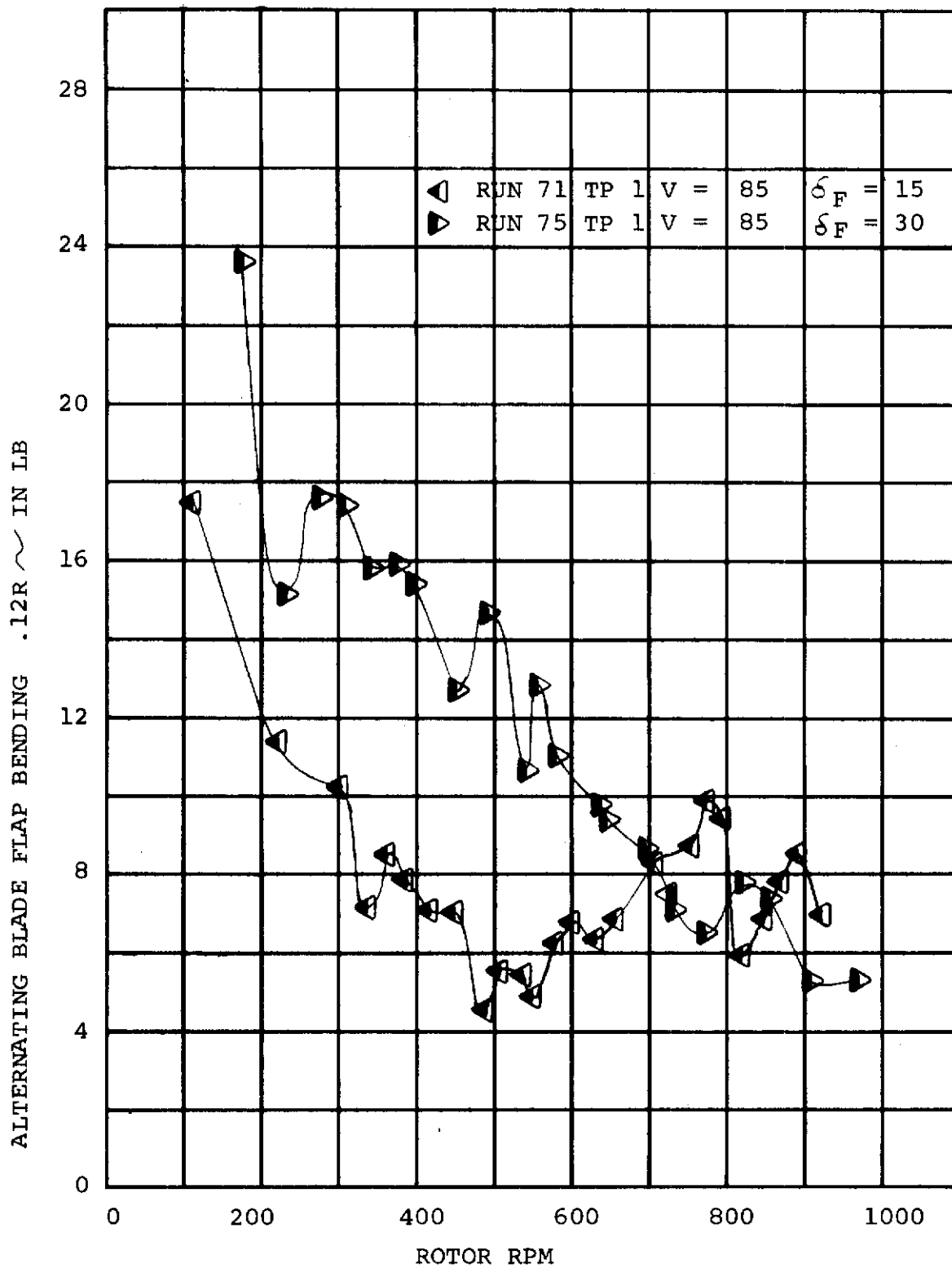


FIGURE 7-37. ALTERNATING BLADE FLAP BENDING DURING SPIN-UP.

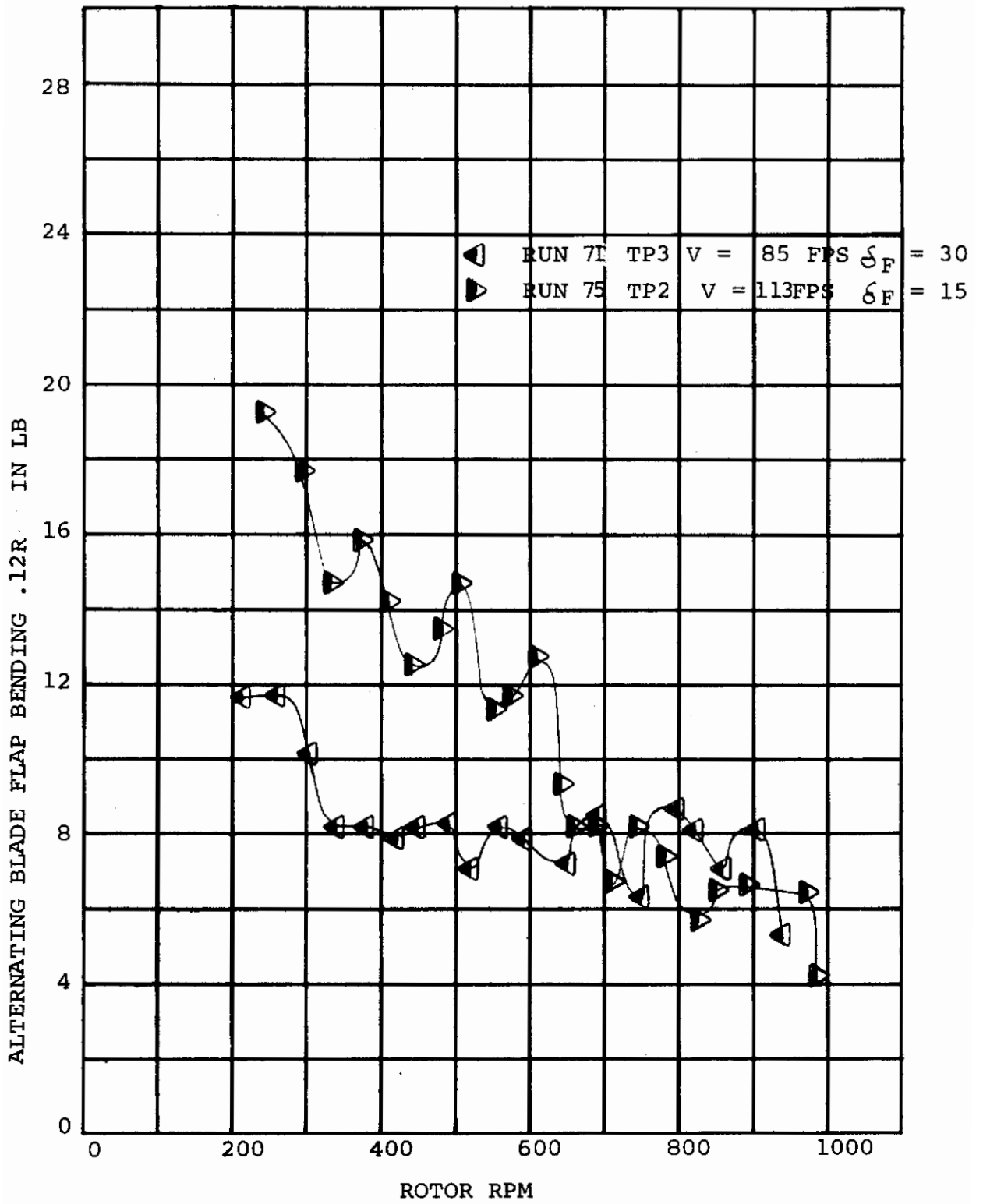


FIGURE 7-38. ALTERNATING BLADE FLAP BENDING DURING FEATHER

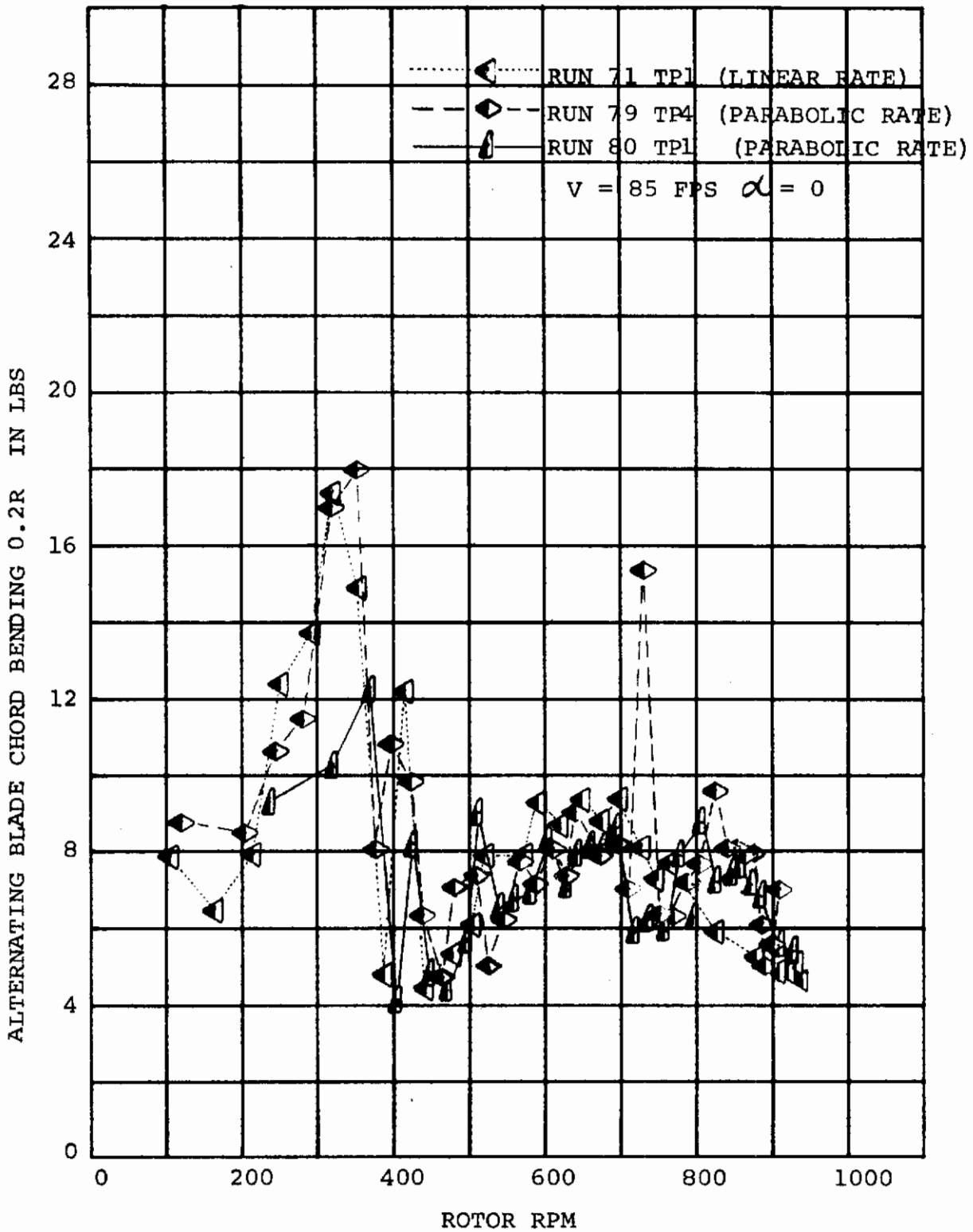


FIGURE 7-39. ALTERNATING BLADE CHORD BENDING DURING SPIN-UP - EFFECT OF COLLECTIVE SCHEDULE



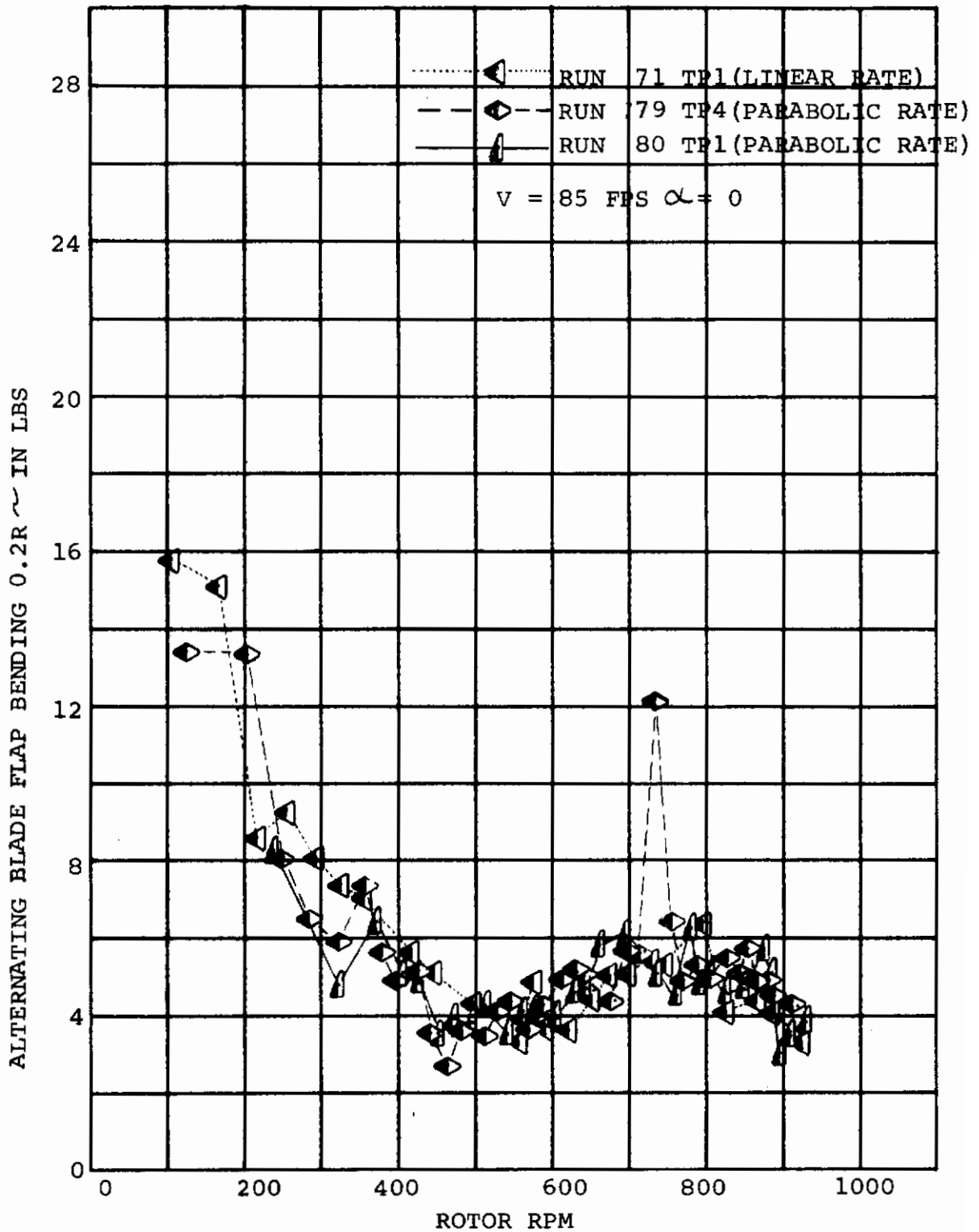


FIGURE 7-40. ALTERNATING BLADE FLAP BENDING DURING SPIN-UP - EFFECT OF COLLECTIVE SCHEDULE

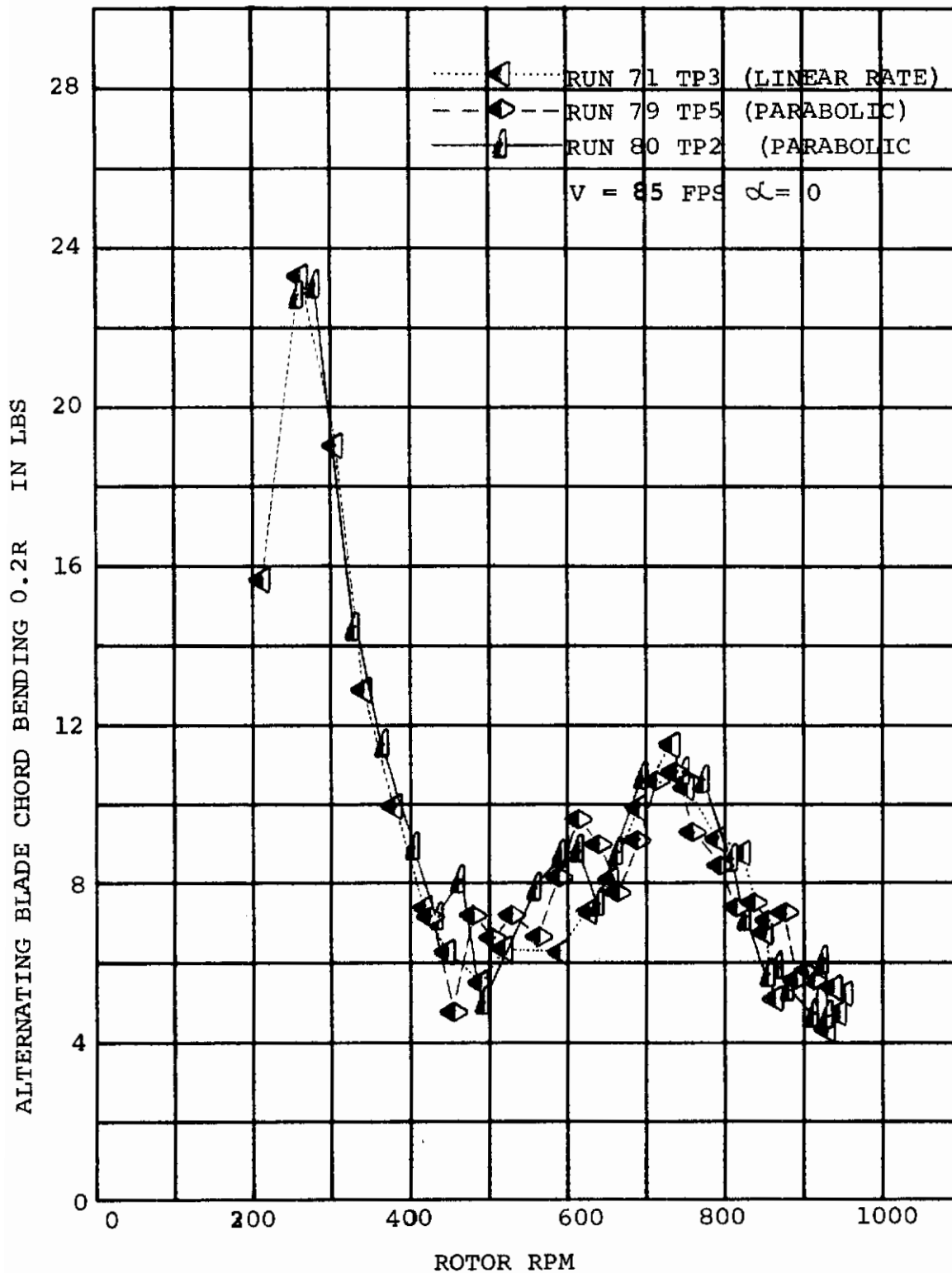


FIGURE 7-41. ALTERNATING BLADE CHORD BENDING DURING FEATHER - EFFECT OF COLLECTIVE SCHEDULE

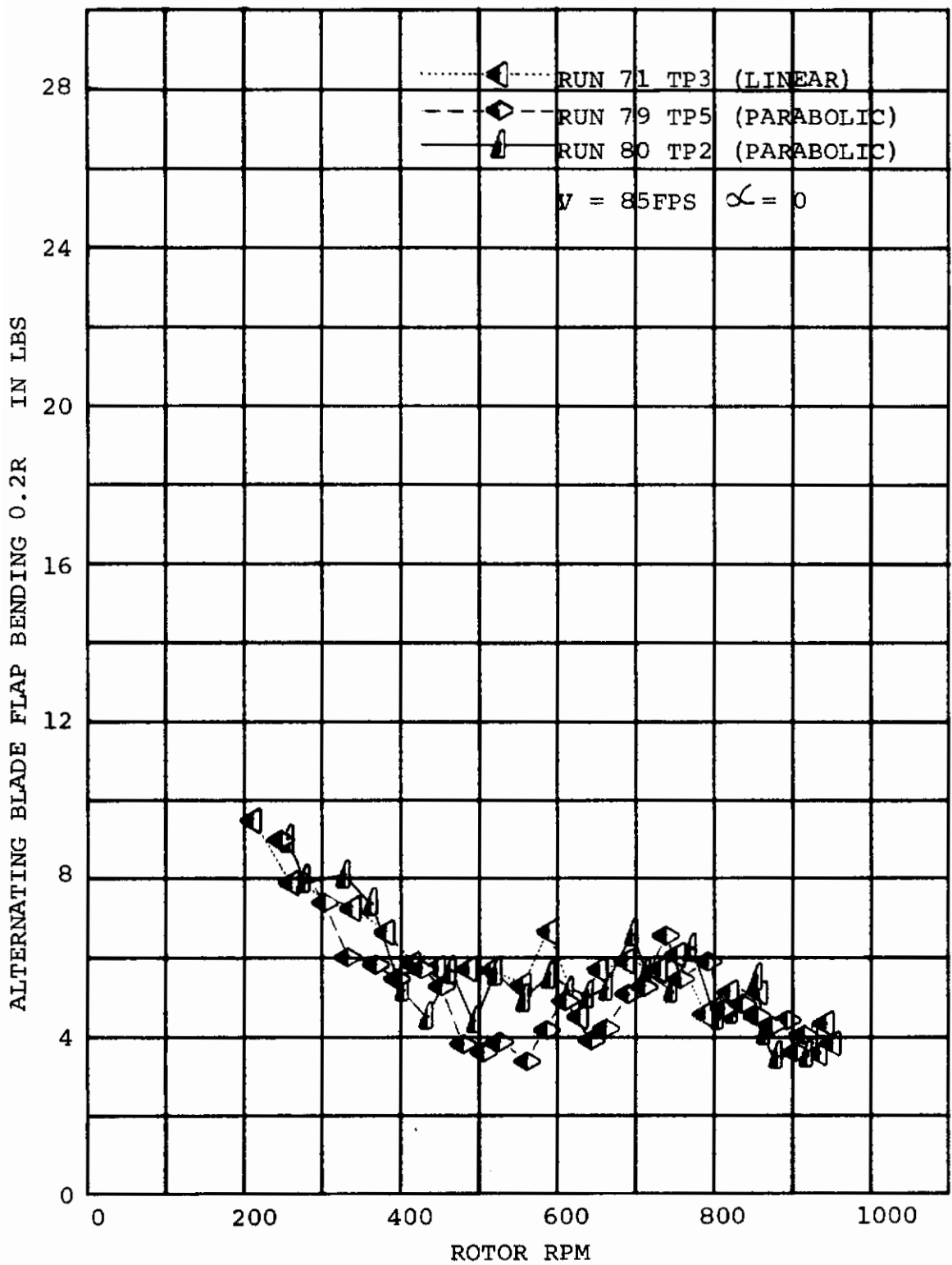


FIGURE 7-42. ALTERNATING BLADE FLAP BENDING DURING FEATHER - EFFECT OF COLLECTIVE SCHEDULE

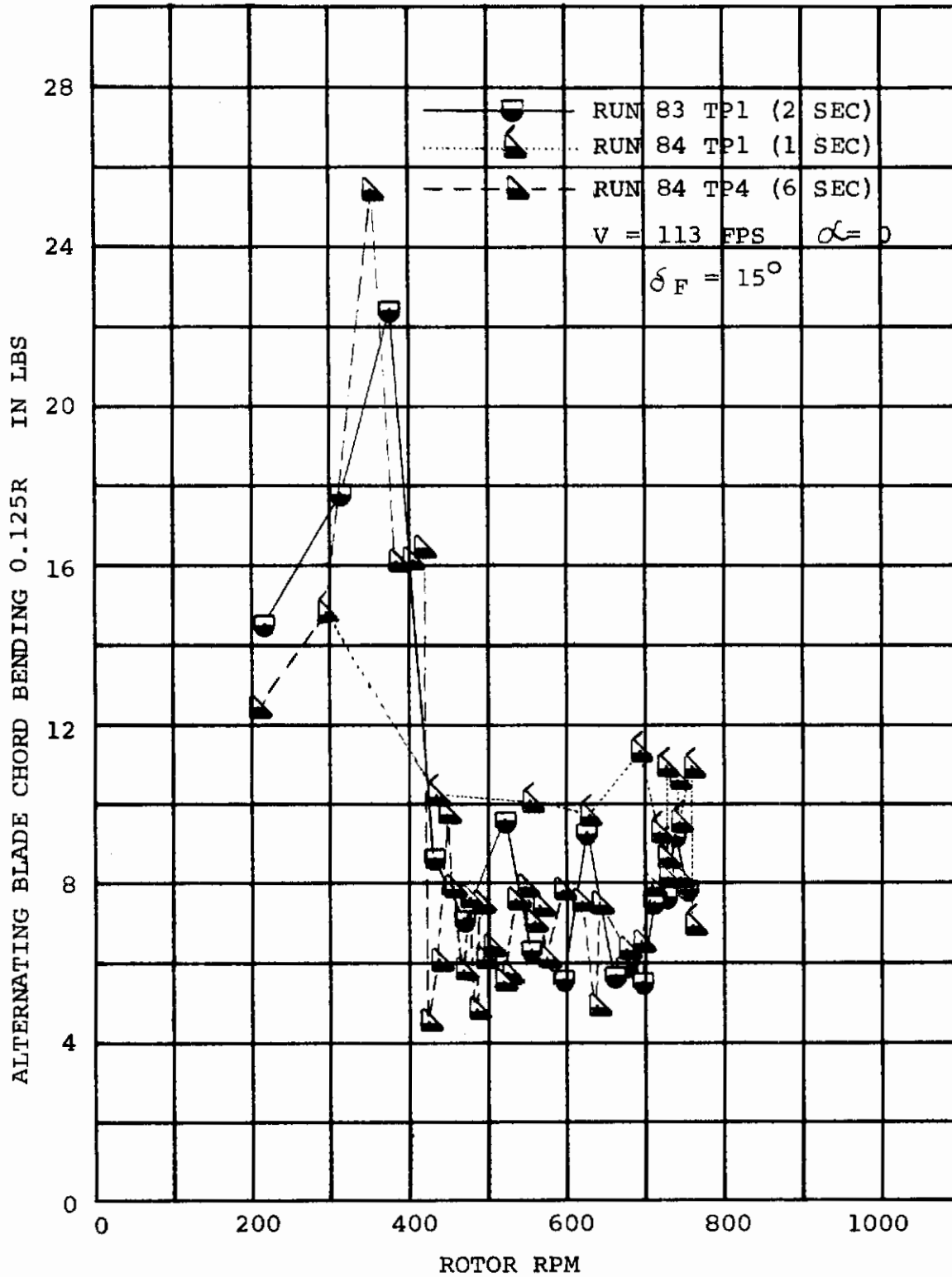


FIGURE 7-43. ALTERNATING BLADE CHORD BENDING DURING SPIN-UP - VARIOUS PARABOLIC COLLECTIVE SCHEDULES

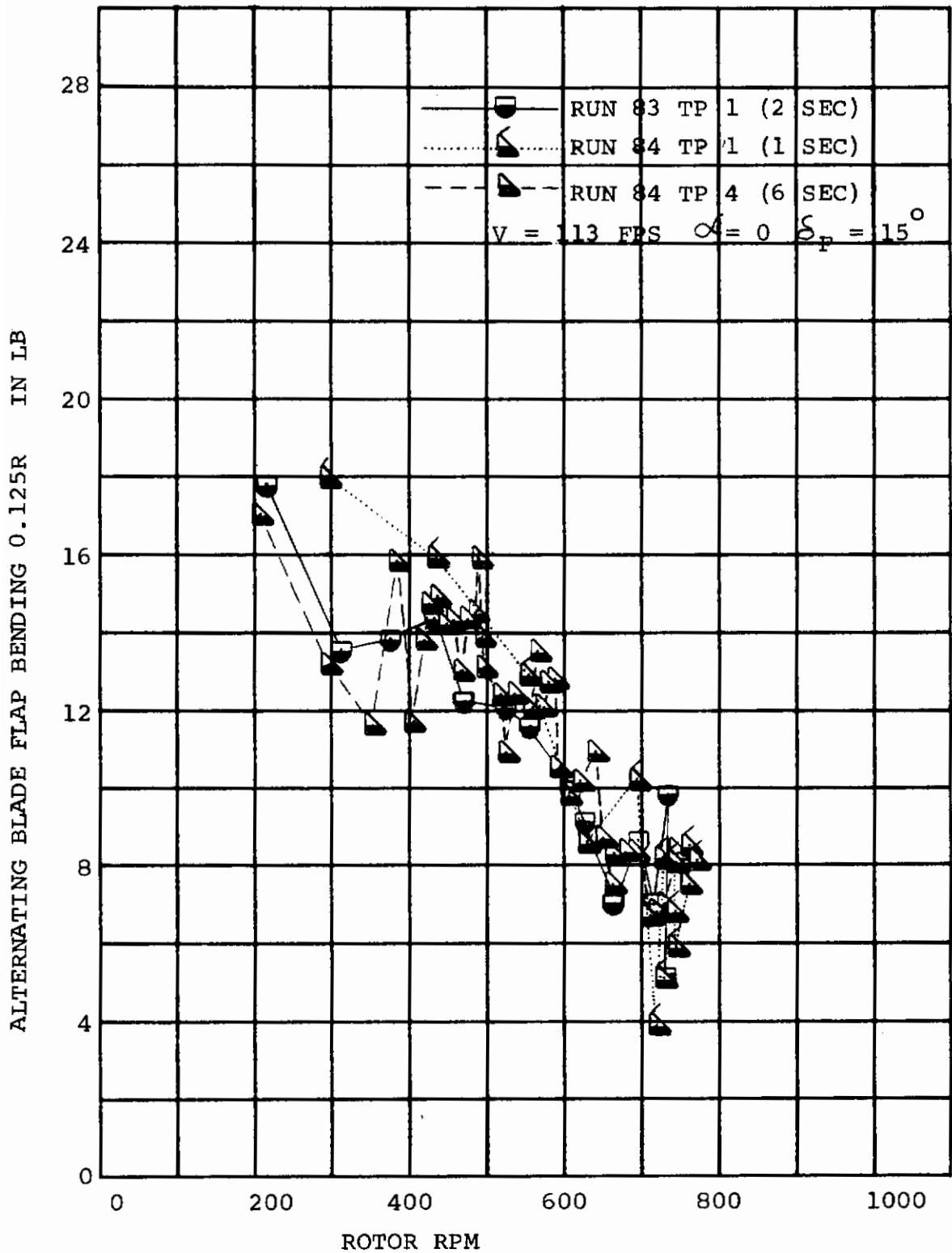


FIGURE 7-44. ALTERNATING BLADE FLAP BENDING DURING SPIN-UP - VARIOUS PARABOLIC COLLECTIVE SCHEDULES

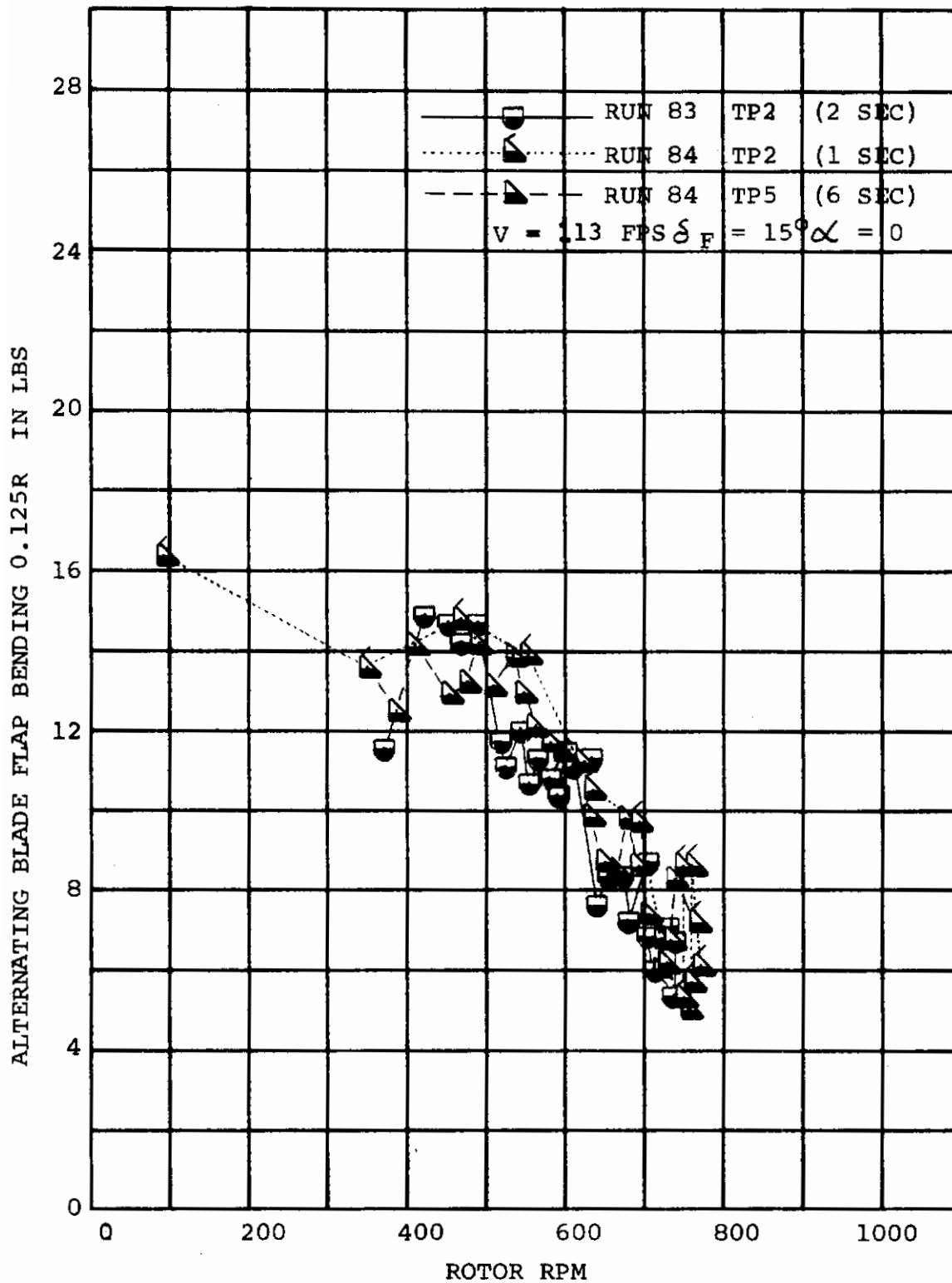


FIGURE 7-45. ALTERNATING BLADE FLAP BENDING DURING FEATHER - VARIOUS PARABOLIC COLLECTIVE SCHEDULES

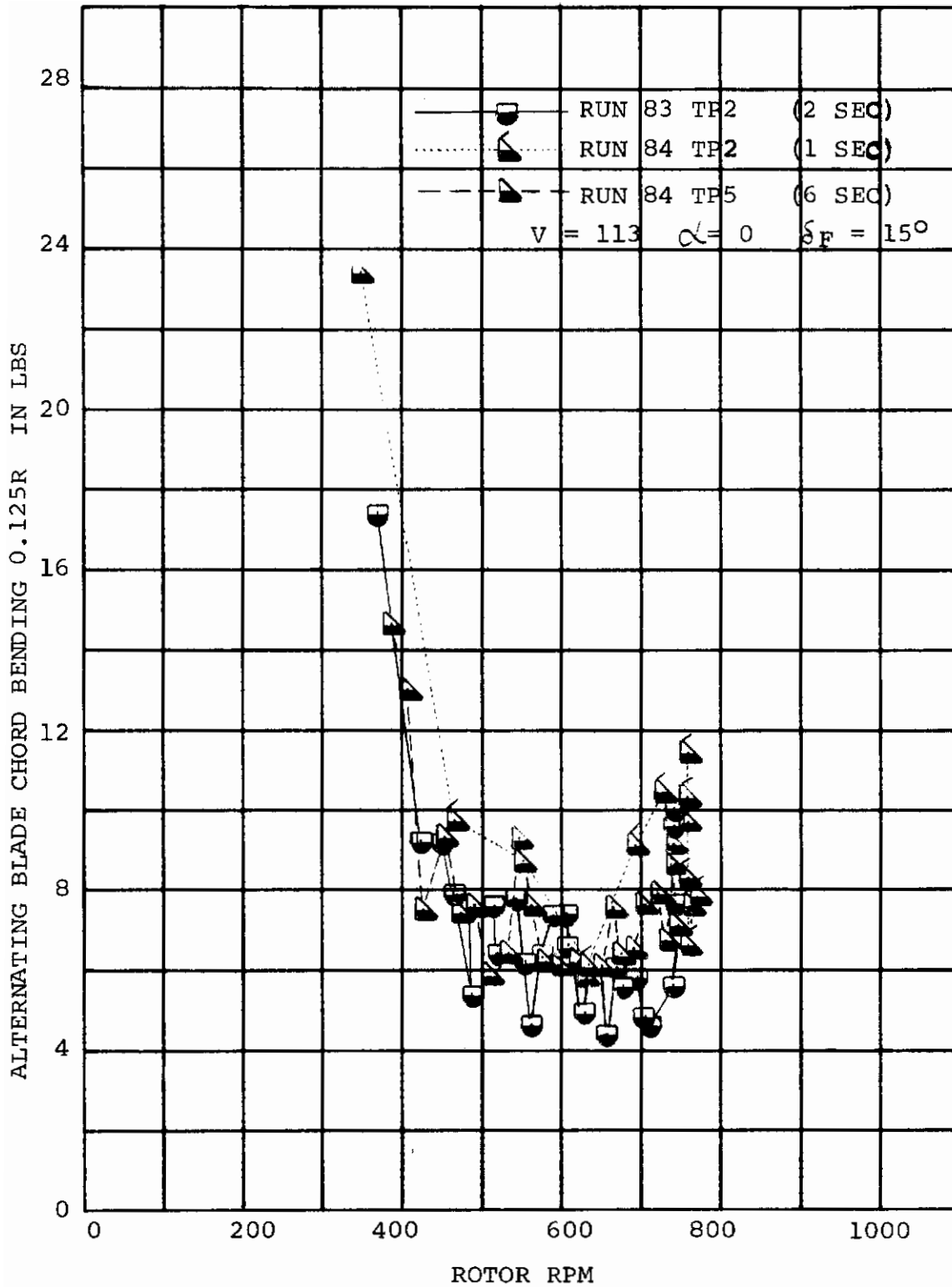


FIGURE 7-46. ALTERNATING BLADE CHORD BENDING DURING FEATHER - VARIOUS PARABOLIC COLLECTIVE SCHEDULES

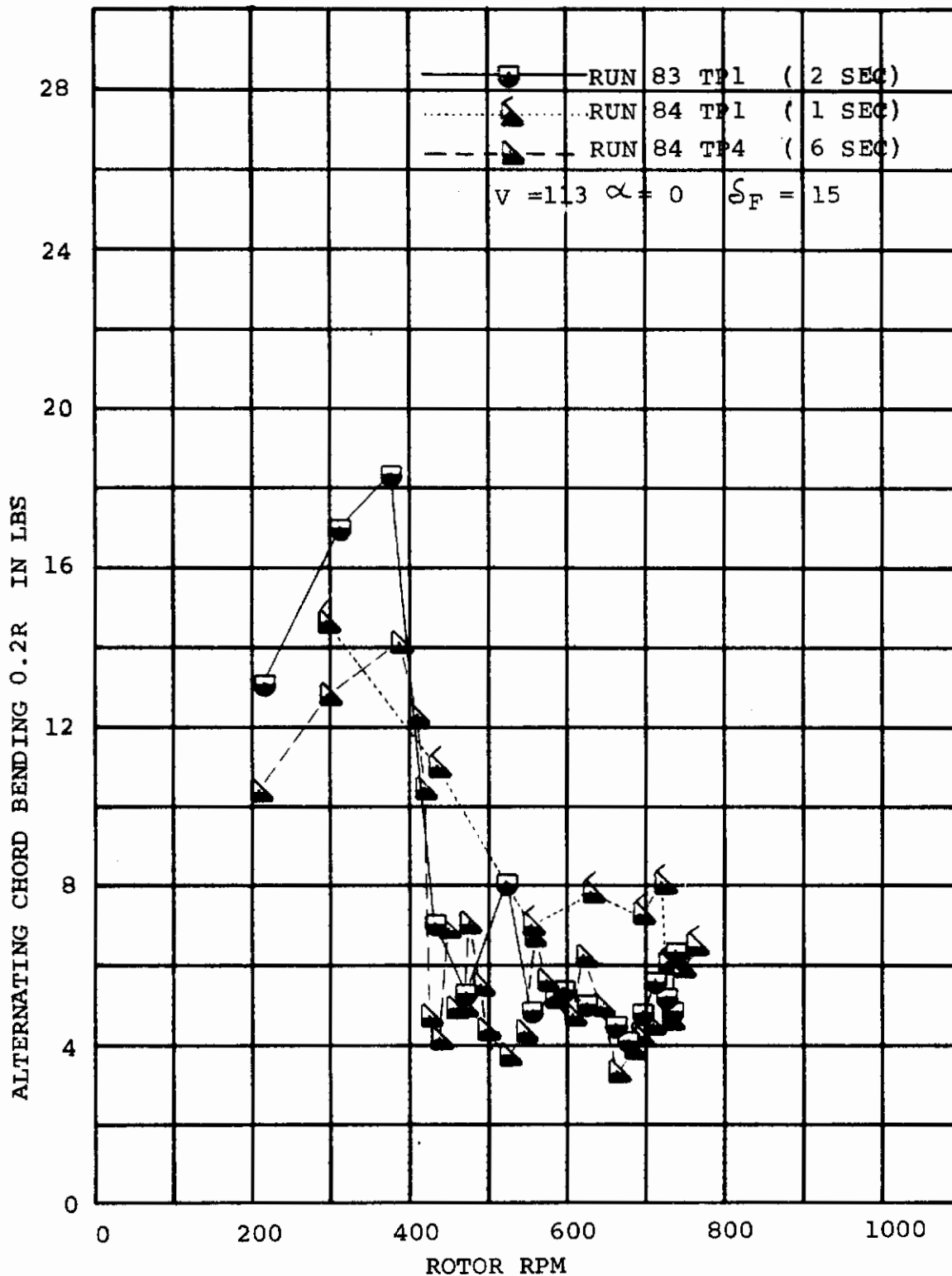
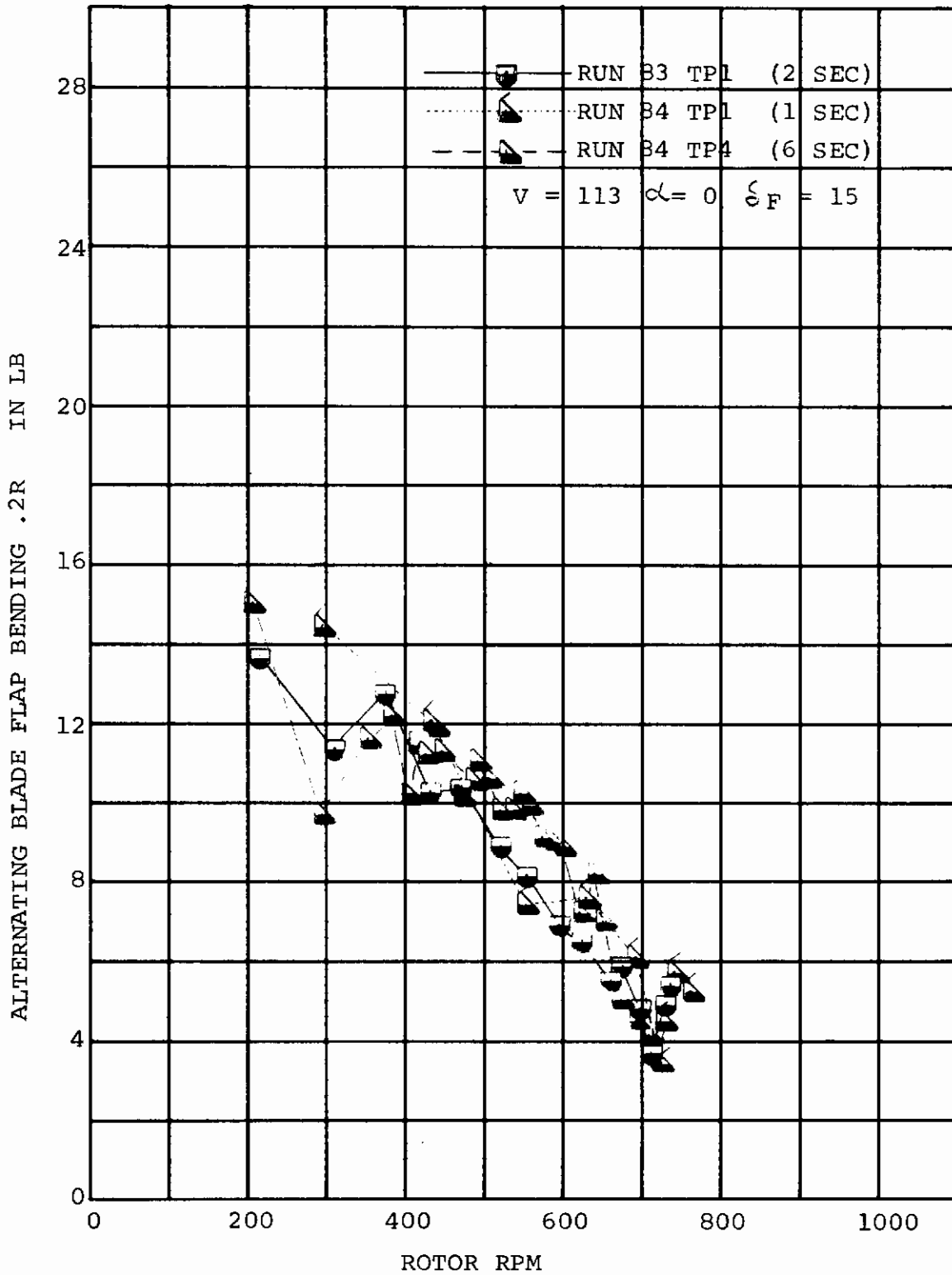


FIGURE 7-47. ALTERNATING BLADE CHORD BENDING DURING SPIN-UP - VARIOUS PARABOLIC COLLECTIVE SCHEDULES





**FIGURE 7-48** ALTERNATING BLADE FLAP BENDING DURING SPIN-UP - VARIOUS PARABOLIC COLLECTIVE SCHEDULES

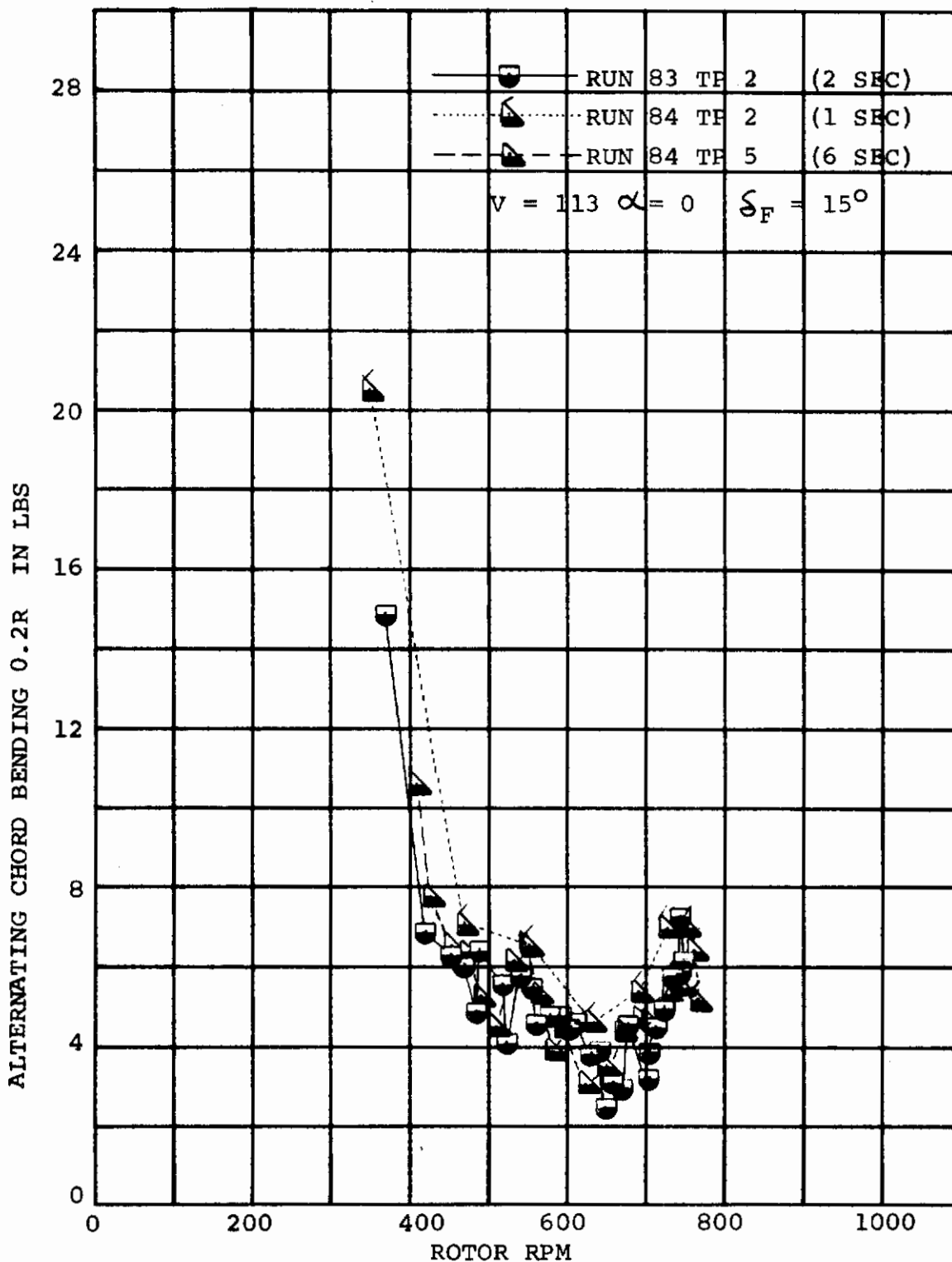


FIGURE 7-49. ALTERNATING BLADE CHORD BENDING DURING FEATHER - VARIOUS PARABOLIC COLLECTIVE SCHEDULES

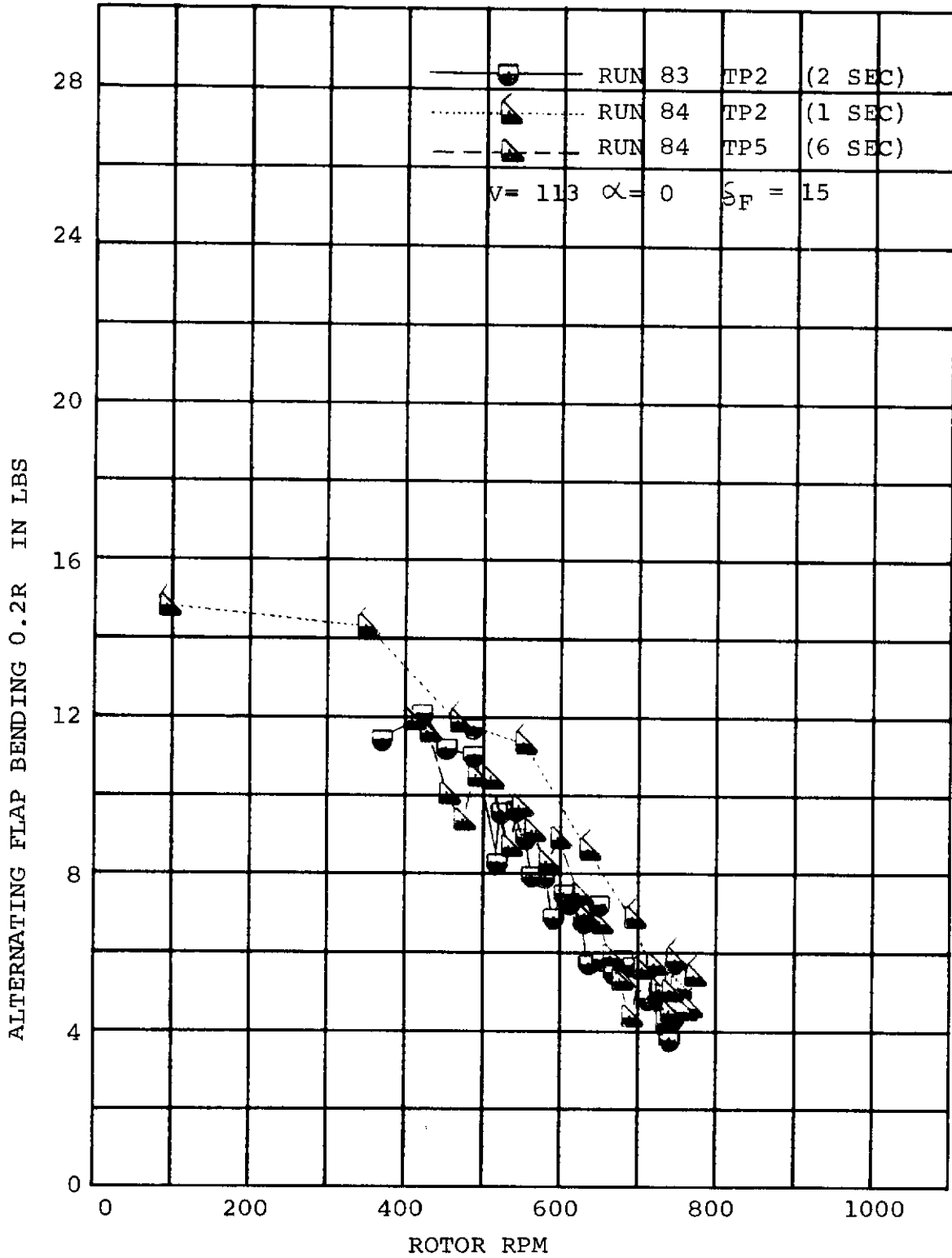


FIGURE 7-50. ALTERNATING FLAP BENDING DURING FEATHER - VARIOUS PARABOLIC COLLECTIVE SCHEDULES

## 7.4 Fold and Deploy Blade Loads

Blade folding and deployment tests were performed using two methods of folding (edgewise and flatwise). Figures 7-51 to 7-54 show the steady blade loads during flatwise folding for rates up to 45.5°/sec and for airspeeds of 85 to 113 ft/sec. Corresponding test data for the edgewise folding is shown in Figures 7-55 to 7-58.

For flatwise folding the loads are not affected by the rate at which the folding/deploy takes place. The effect of increased airspeed is to increase the steady loads at the fully deployed end but the folded loads are unchanged. This increase is proportional to airspeed squared as would be expected. In the flatwise fold case the blade collective is moved from the feathered value to the folded value in the twenty degrees before the fully folded condition. This causes a slight rise in the flapwise loads shown in Figures 7-51 to 7-54. These data show a change in loads between fold and deploy conditions at about 50° to 60° fold angle. The increase in blade loads at this fold azimuth position during deployment was due to binding of the mechanism causing a momentary non-linear motion of the blades during deployment. A slightly different fold system was employed for the edgewise folding which eliminated this binding. For edgewise folding the loads are not affected by fold rate and are increased by increased airspeed in the same manner as for flatwise folding.

No alternating loads were observed in either case. The torsion loads for all cases tested were small and less than 1 in. lb.

The deflections observed on test gave an indication of higher blade bending moments at about mid-span. The magnitude of the loads at 40% to 50% span are expected to be about twice the loads measured at .125 R in the fully deployed condition. This will be true for either method of folding. The loads in the folding/deploy flight condition are essentially governed by the feathered loads and not by the folding procedure itself. The choice of folding procedures will be governed by other considerations (i.e., drag section 5). All of the dynamic fold deploy tests were performed at 2° angle of attack and 30° of flap setting.

Loads were also measured at steady fold angles at zero angle of attack and no-flap at 141 ft/sec airspeed. These data for both folding methods are shown in Figures 7-59 and 7-60.

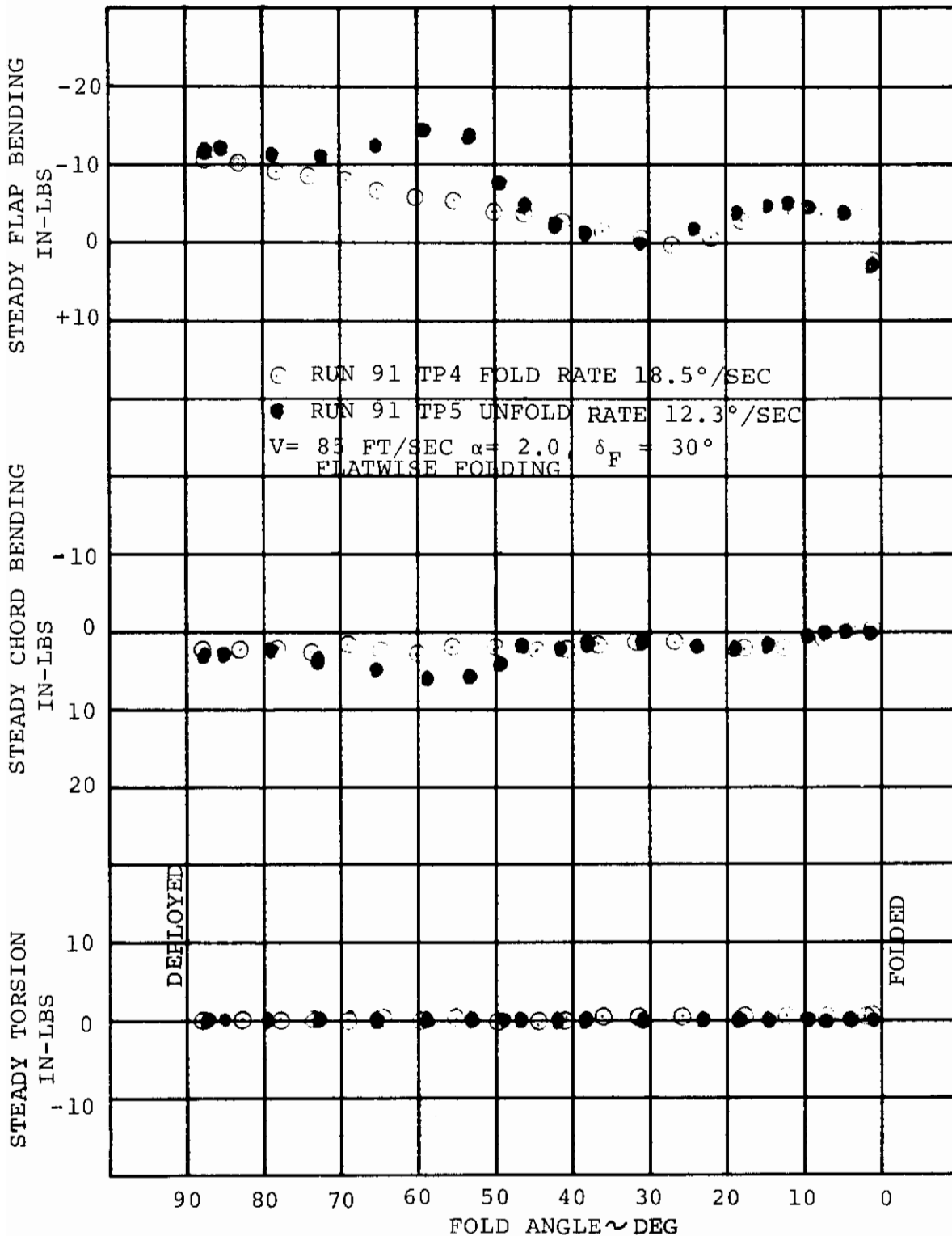


FIGURE 7-51 STEADY BLADE LOADS DURING DYNAMIC FOLD AND DEPLOY,  $r/R = 0.125$

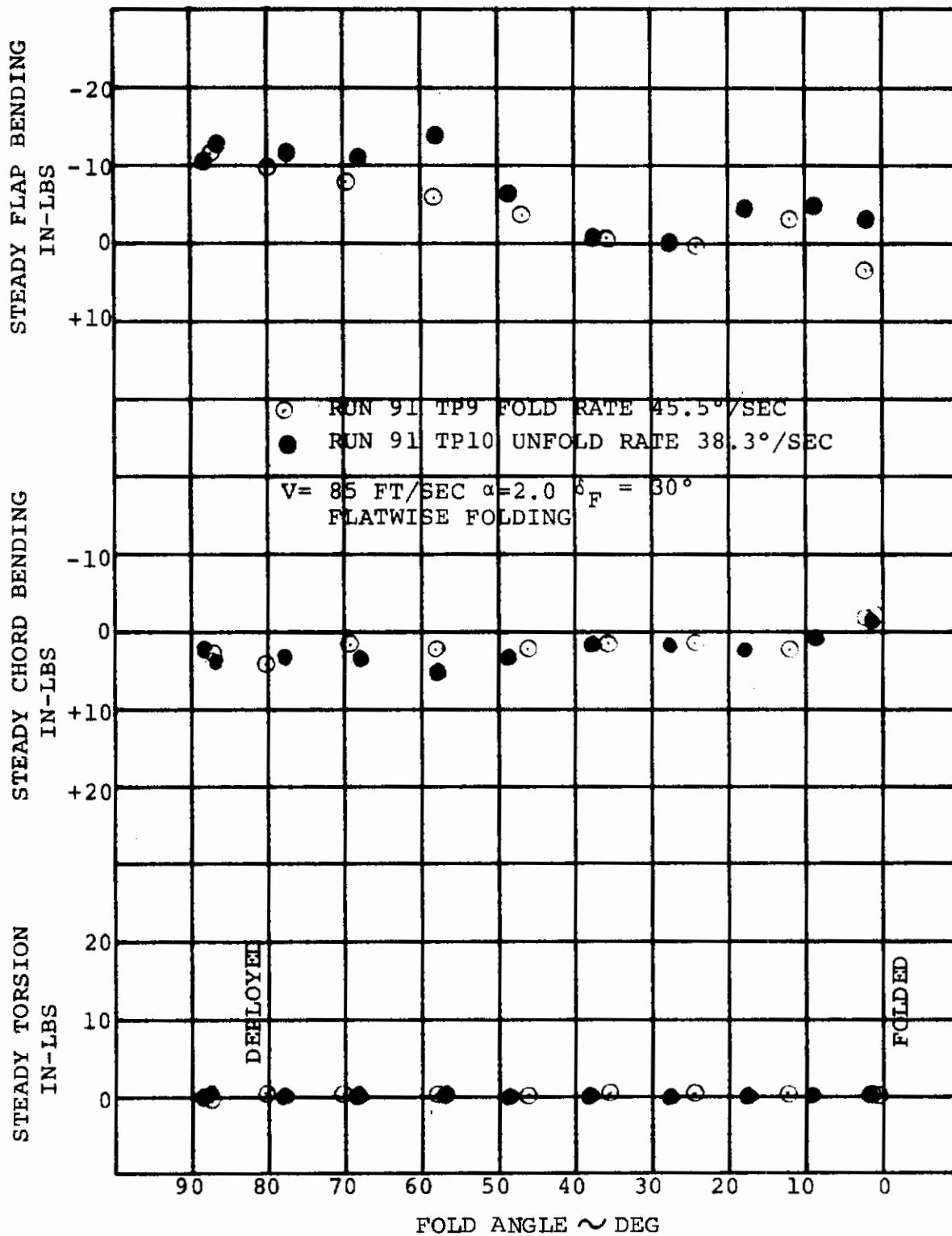


FIGURE 7-52 STEADY BLADE LOADS DURING DYNAMIC FOLD AND DEPLOY,  $r/R = 0.125$

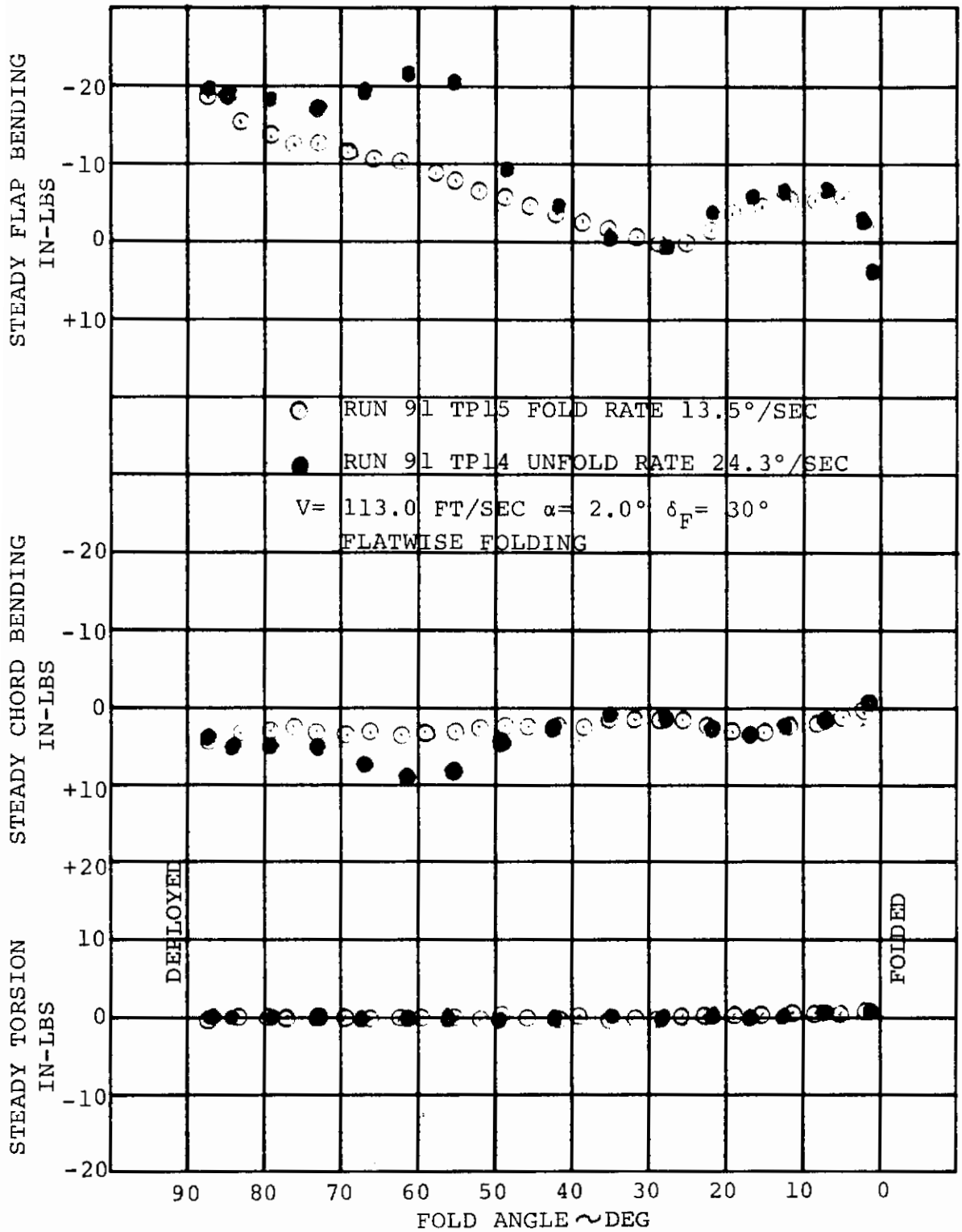


FIGURE 7-53. STEADY BLADE LOADS DURING DYNAMIC FOLD AND DEPLOY,  $r/R = 0.125$

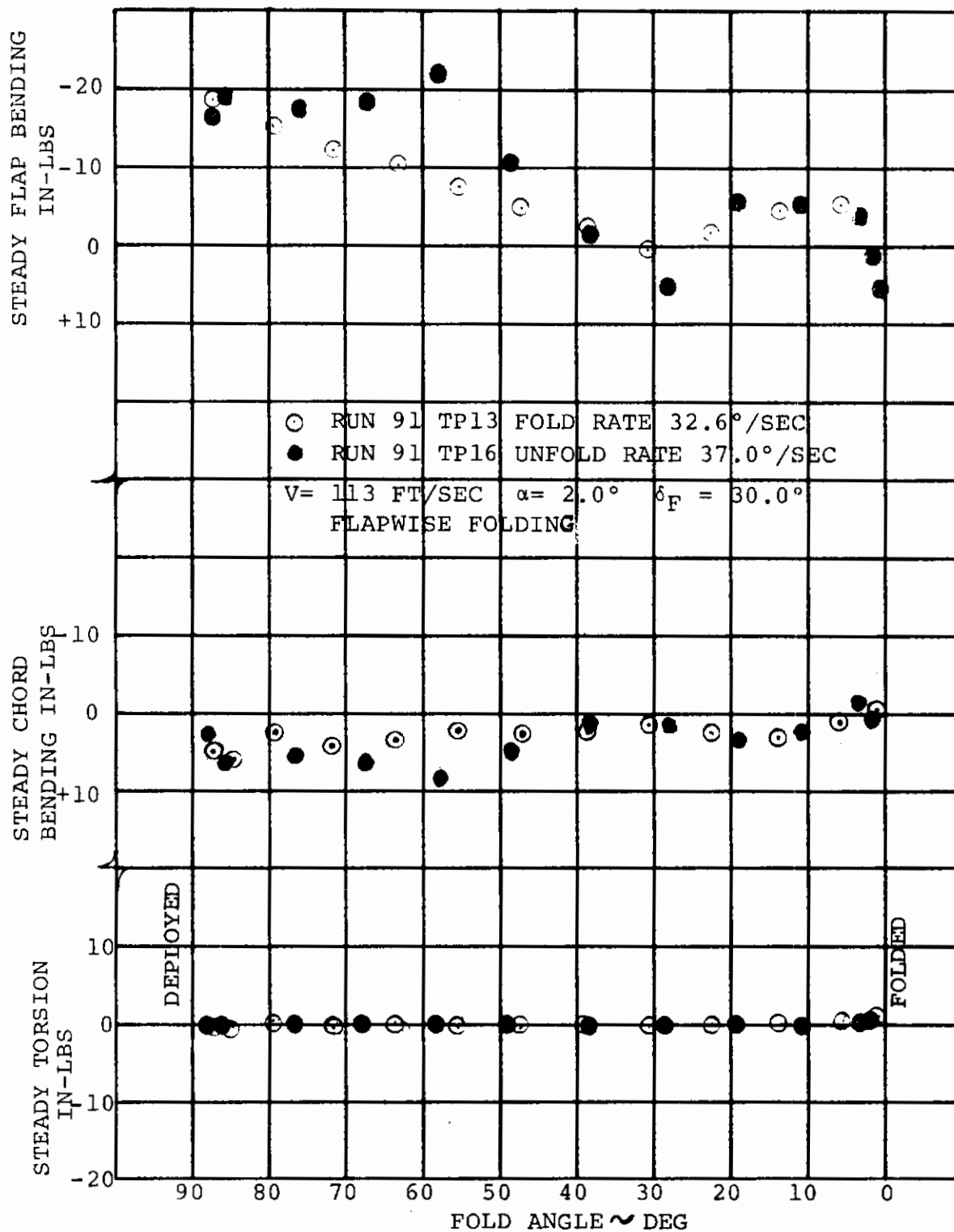


FIGURE 7-54 STEADY BLADE LOADS DURING DYNAMIC FOLD AND DEPLOY,  $r/R = 0.125$



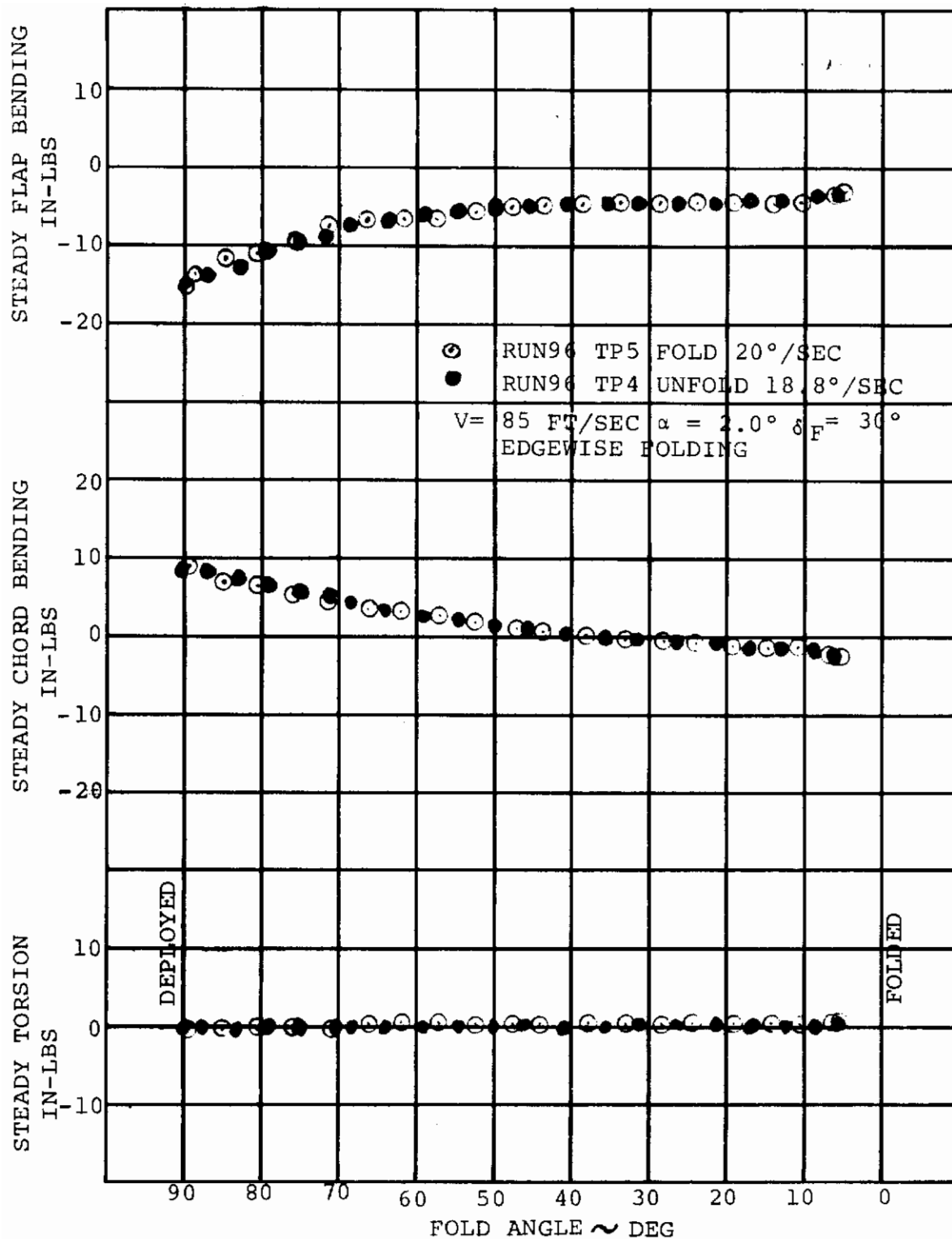


FIGURE 7-55 STEADY BLADE LOADS DURING DYNAMIC FOLD AND DEPLOY

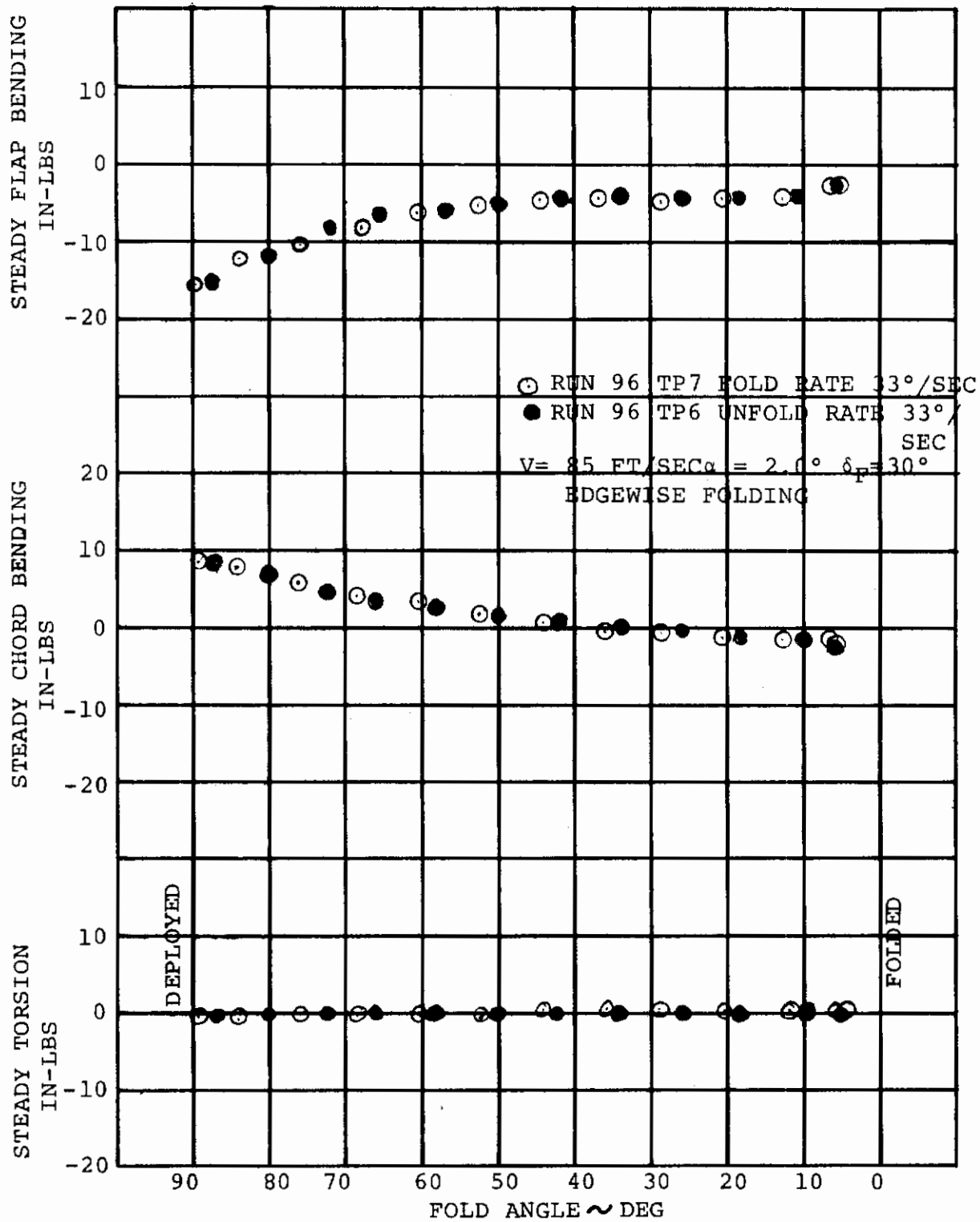


FIGURE 7-56. STEADY BLADE LOADS DURING DYNAMIC FOLD AND DEPLOY,  $r/R = 0.125$

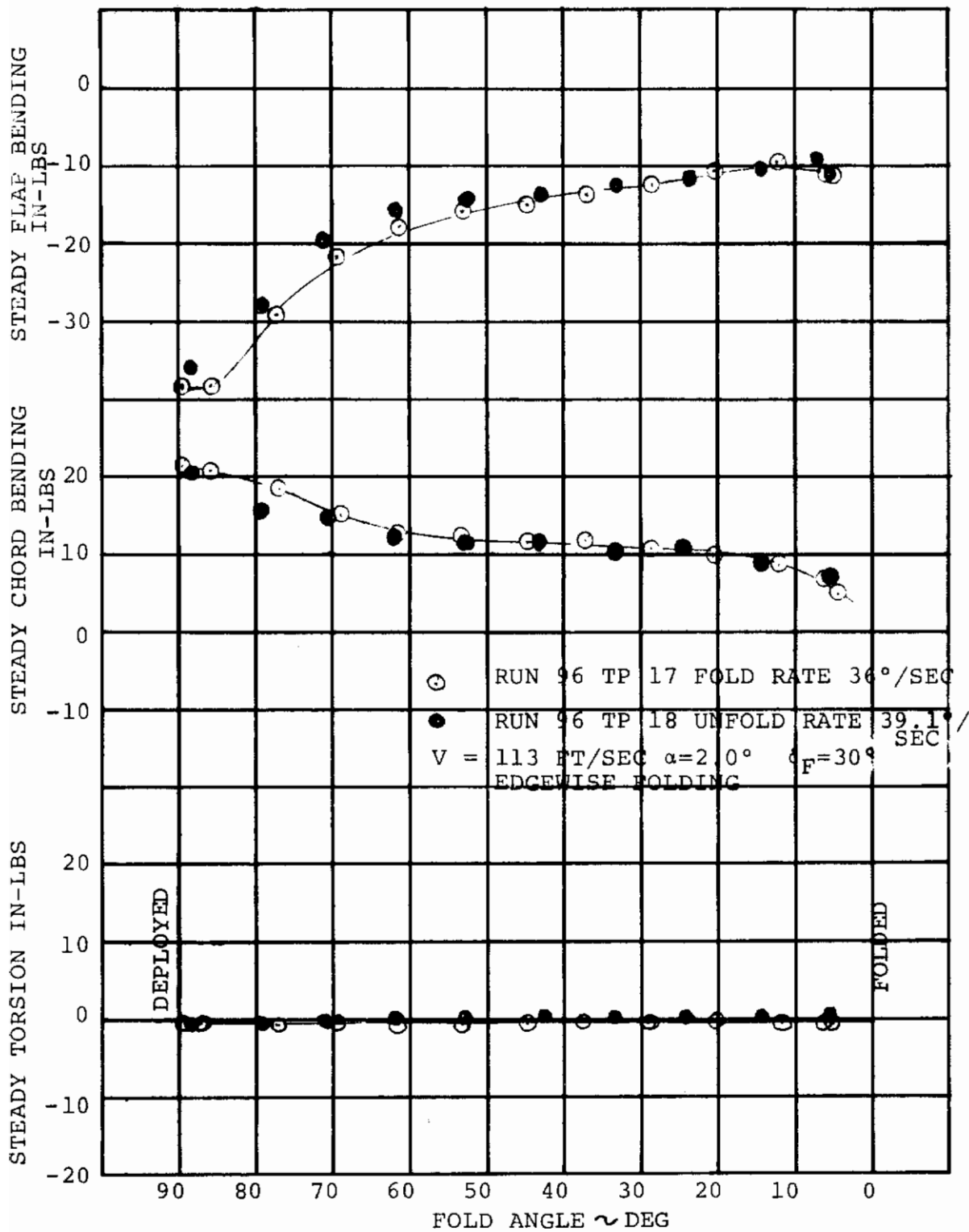


FIGURE 7-57 STEADY BLADE LOADS DURING DYNAMIC FOLD/DEPLOYMENT  $r/R = 0.125$

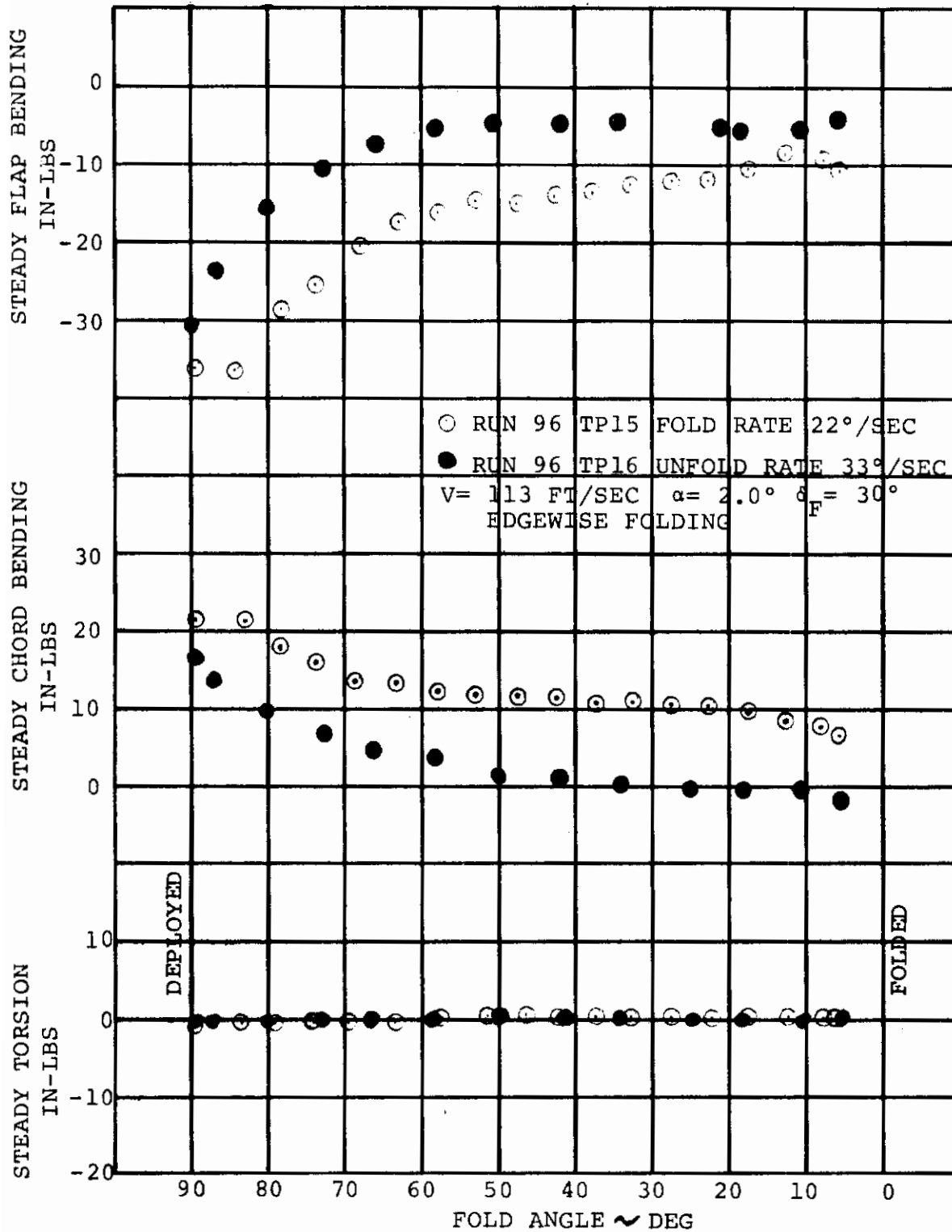


FIGURE 7-58 STEADY BLADE LOADS DURING DYNAMIC FOLDING AND DEPLOYMENT  $r/R = 0.125$

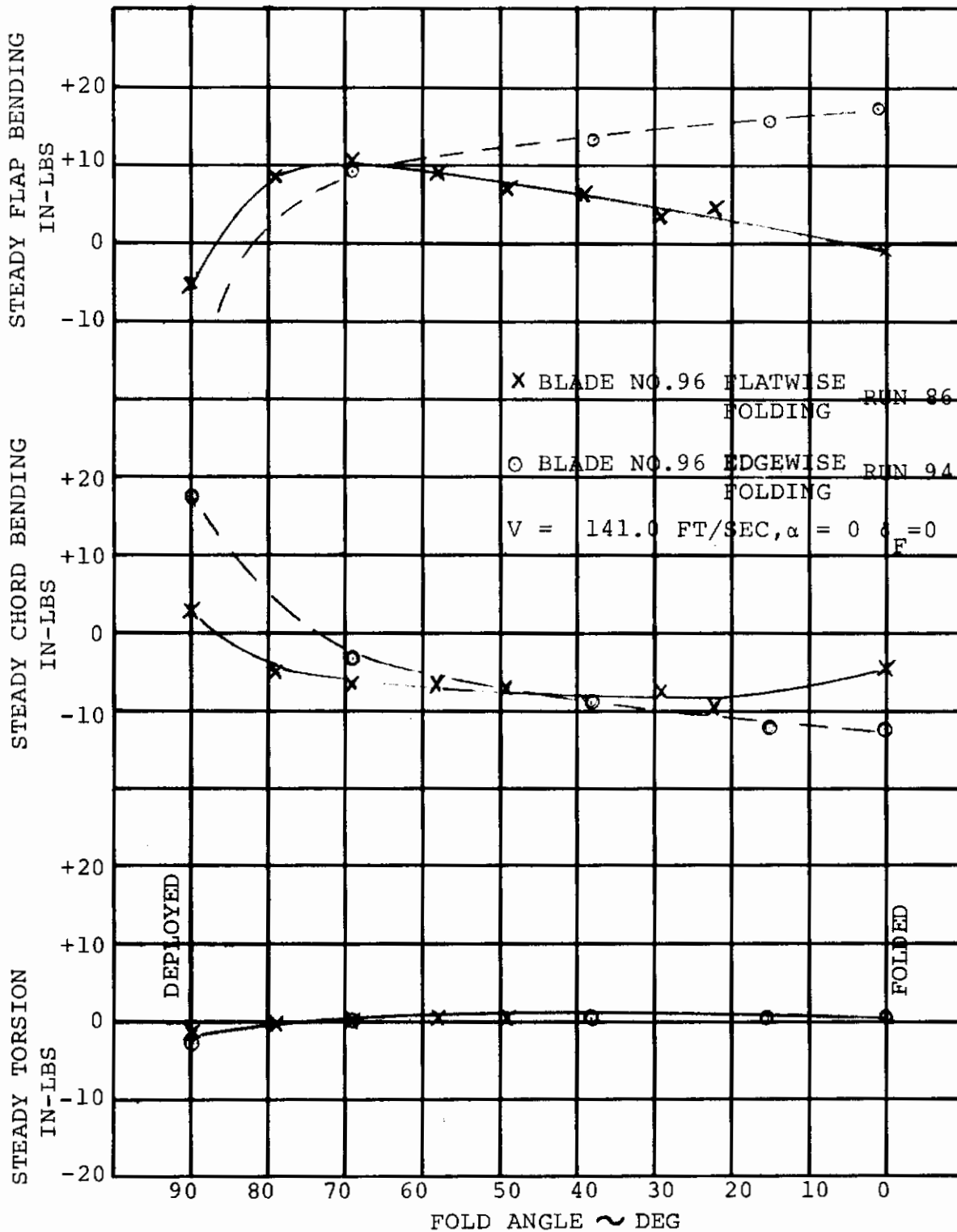


FIGURE 7-59 STEADY BLADE LOADS DURING FOLDING,  $r/R=0.125$

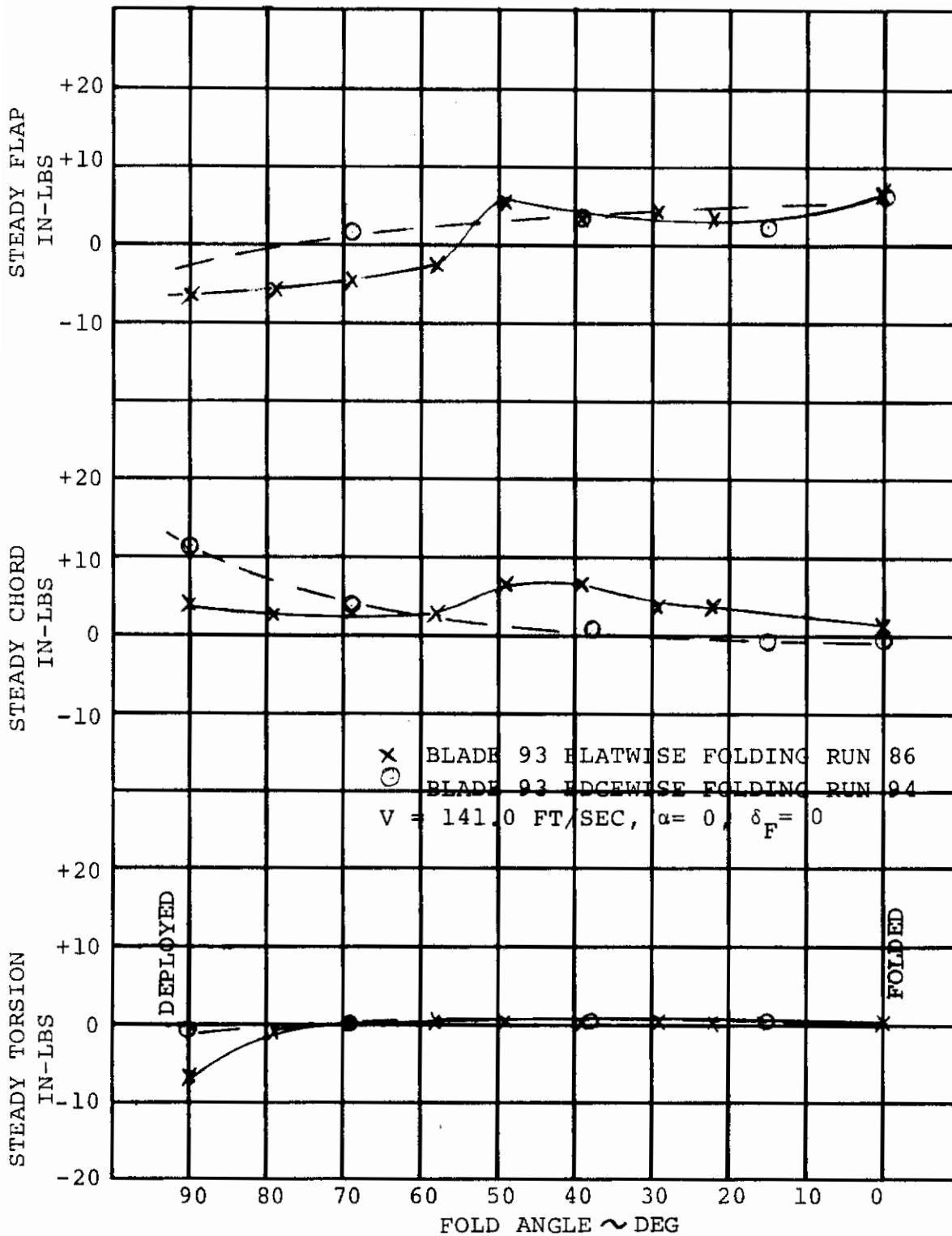


FIGURE 7-60 STEADY BLADE LOADS DURING FOLDING  $r/R=0.125$

## 7.5 Conclusions - Rotor Loads

### Steady Windmilling

1. At the operating RPM the alternating blade loads are low at zero angle of attack.
2. The alternating loads are increased by the coincidence of blade and wing natural frequencies with an integer times the RPM.
3. At operating RPM the alternating blade chord bending increases rapidly with angle of attack; blade flap bending is only slightly affected.
4. At RPM close to the 1/rev lag frequency - RPM crossing both flap and chord bending alternating loads show a strong angle of attack dependence.
5. Increased airspeed increases the alternating chord bending loads due to angle of attack - flap bending is insensitive.
6. The use of wing flaps at low speed to trim airplane lift results in much lower blade loads than would result from attitude change.
7. The steady blade loads during steady windmilling increase almost linearly with RPM and are due to the rotor drag force and the centrifugal force moment resulting from the rotor torque offset which is designed for powered flight.

### Spin-up/Feather

1. The transient alternating blade loads are approximately the same as the steady windmilling loads.
2. The effects of collective schedule and spin time on alternating blade loads are second order.
3. Blade loads will not be a constraint on the spinup and feather schedule.

### Folding

1. The steady loads measured during the blade folding and deploy procedure are the same for both edgewise and flatwise folding and are less than the feathered blade loads.
2. No alternating loads were observed in folding tests.

8.0 MODEL DYNAMICS

8.1 Wing Frequency and Damping - Nominal Spar

Wing model frequencies and viscous damping coefficients ( $\zeta = c/c_c$ ) were obtained for the non-rotating system by "tweak" tests. Wing frequencies under rotating conditions (wind on) were obtained from harmonic analysis of data recorded at discrete rotor speeds. Figure 8-1 presents the first harmonic of the wing flap bending, chord bending and torsion responses. The resonant crossovers are 350 RPM for wing flap bending and 800 RPM for wing torsion. A heavily damped wing chordwise response peaked at approximately 625 RPM. Measured dampings and frequencies (rotating and non-rotating) correlated with frequency predictions are shown by Table 8-1.

TABLE 8-1

WING FREQUENCY SUMMARY (NOMINAL SPAR)				
MODE	$\Omega = 0$		ROTATING (1P CROSSOVER)	
	TEST	CALC	TEST	CALC
FLAP BENDING	6.4 ( $\zeta = .008$ )	7.6	5.63	6.16
CHORD BENDING	11.5 ( $\zeta = .012$ )	14.16	10.4	12.91
TORSION	13.8 ( $\zeta = .010$ )	12.33	13.3	11.66

The calculated coupled wing-nacelle-rotor system modal frequencies as a function of rotor speed are presented in Figure 8-2 for the nominal stiffness spar. The blade mode frequencies change with rotor speed as expected and follow the general pattern of the isolated blade frequencies of Figure 3-2. The coupled wing frequencies are not significantly altered by rotor speed. It should be noted that the mode shape associated with a given frequency root can change from one mode to another as the rotor speed changes.



The "tweak" test frequencies (obtained at  $\Omega = 0$ ) Table 8-2 and those observed during test with wind-on are included in Figure 8-2.

The calculated modal damping values (aerodynamic plus viscous) for the windmilling rotor (varying collective) at a free stream velocity of 140 fps are shown in Figure 8-3. An air resonance instability due to the approaching coalescence of the wing flap bending and lower in-plane blade ( $\Omega - \omega_1$ ) modes was predicted at 1050 RPM. A similar instability is predicted at 104 ft/sec at 1070 RPM. During the tests a mild air resonance instability occurred at 1050 RPM at 104 fps.

Figure 8-4 shows the excellent correlation with theory. As a result of this instability, subsequent testing was limited to less than 1000 RPM.

### 8.1.1 Blade Folding Tests

Oscillograph records, visual and photographic observations indicated that the blades were absolutely stable throughout all of the folding and deployment tests.

### 8.2 Reduced Stiffness Spar

Dynamic stability testing was also performed with a spar of reduced torsional stiffness. A primary objective of the reduced torsional stiffness spar was to obtain whirl flutter and divergence data. Pre-test analysis had shown the nominal model to be free of these instabilities within the feasible test operational ranges and that a wing with torsional reduced stiffness would be required to obtain these instabilities. The reduced stiffness spar was 0.31 (2860 in-lbs/rad) of the nominal spar torsion stiffness. Coupled wing frequencies for this spar from tweak tests are given in Table 8-2.

#### 8.2.1 Whirl Flutter

Measured damping of the whirl flutter mode was obtained during the test for a series of wind velocities and rotor speeds by tweaking the model. Frequency and damping values obtained from decay decrements of the whirl flutter mode are shown in Figure 8-5. Although actual zero damping was never achieved, extrapolation to zero damping established the experimental whirl flutter boundary presented in Figure 8-6.

## 8.2.2 Static Divergence

The model was set at a 2 degree angle of attack for the divergency tests. The rate of increase of torsional deflection of the wing as divergence is approached (i.e., effective torsional spring approaching zero) is more gradual for an angle of attack. During test a maximum dynamic pressure of 29 psi was reached ( $V = 156$  fps) with a rotor speed of 800 rpm at which the induced disturbance produced a large response. The tests were terminated at this point (prior to actual static divergence) to avoid model destruction.

The measured static torque for three velocities over a rotor speed range is given in Figure 8-7. The nacelle twist and velocity ratios resulting from these torque measurements is shown in Figure 8-8. A model divergency boundary extracted from these test results (using methods of reference 4.) is presented in Figure 8-9. The data all collapse (within experimental accuracy) to define a single boundary based on the data from tests at three different velocities.

## 8.2.3 Blade Mode Damping

The model was disturbed at  $q = 8.6$  psf ( $V = 85$  fps) as it was at the higher dynamic pressures. At this velocity the whirl flutter mode was well damped and there were no tendencies to diverge. A low damped blade bending response was induced at a frequency which correlates with the calculated blade 1st mode frequency (Figure 8-10).

This indicates that the model was approaching the same air resonance mode found with the full stiffness spar.

## 8.3 Conclusions: - Dynamics

1. With the Model 213 scaled wing spar stiffness, whirl flutter and static divergence did not occur within the range of airspeed and RPM tested.
2. The inception of air resonance was found for the nominal stiffness spar and this instability is correctly predicted.
3. Using reduced torsional stiffness wing spar, test data was obtained for the whirl flutter and static divergence boundaries.
4. The rotor blades were stable during all fold tests.

*Continails*

NATURAL FREQUENCIES MEASURED BY BANG TESTS (CPS)

Bang Test No.	1	2	3	4	5	6	7	8	9	10	11
Prior to Run	1	2	19	36	59	92	101	110	123	127	132
Blade No. 96 Flap Bend.	4.60	4.50	4.45	4.51	4.45	4.58	4.29	-	-	-	4.52
Blade No. 96 Chord Bend.	7.85	7.70	7.70	7.50	8.2	7.24	8.18	7.4	-	-	7.50
Blade No. 93 Flap Bend.	-	-	-	-	-	4.38	-	-	-	-	-
Blade No. 93 Chord Bend.	-	-	-	-	-	5.55	-	-	-	-	-
Wing Flap Bend.	6.05	6.22	-	6.00	6.05	6.50	6.60	-	7.20	5.00	6.50
Wing Chord Bend.	11.7	12.4	-	11.55	11.9	10.90	-	-	11.50	10.70	11.55
Wing Torsion	14.0	-	-	13.8	14.0	12.90	15.0	-	4.65	4.45	3.70

Remarks reference to bang test no.:

1. Complete model no snubbers.
2. Model without engine nacelle, tip nacelle covers and spinner snubber on.
3. Blade frequency check only.
4. Complete model.
5. Complete model.
6. Model configured for flush folding tests.
7. Model configured for autorotation tests.
8. Check on blade chord freq.
9. Model with reduced torsional stiffness wing spar.
10. Same as for 9. plus additional 2 lb. weight in tip nacelle.
11. Complete model with soft spar and cracked wing spar web.

TABLE 8-2

# Contrails

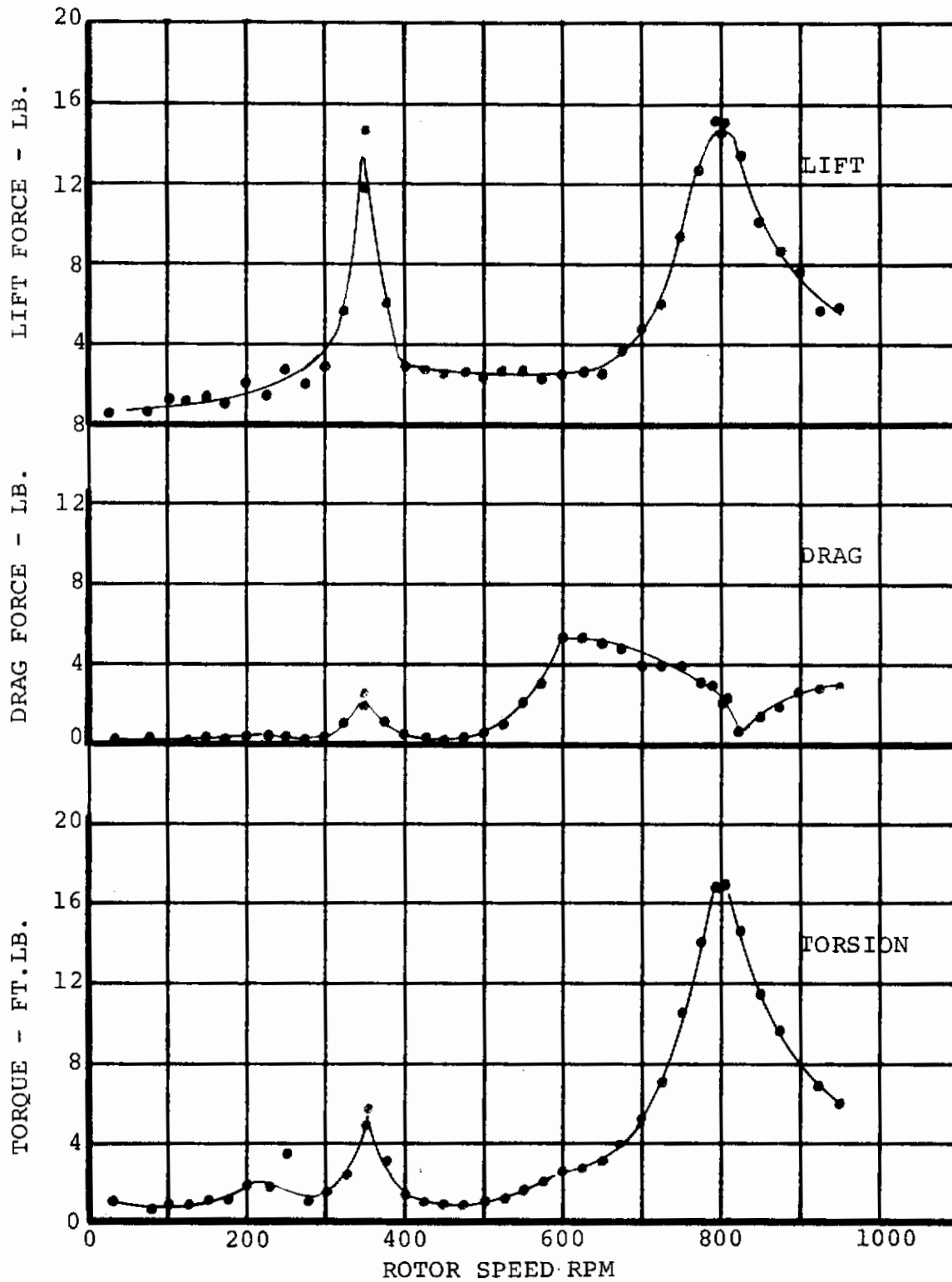


FIGURE 8-1: WING 1st HARMONIC ALTERNATING RESPONSE AT DISCRETE ROTOR SPEEDS - NOMINAL WING V = 85 FPS, RUN 69 (4-44)

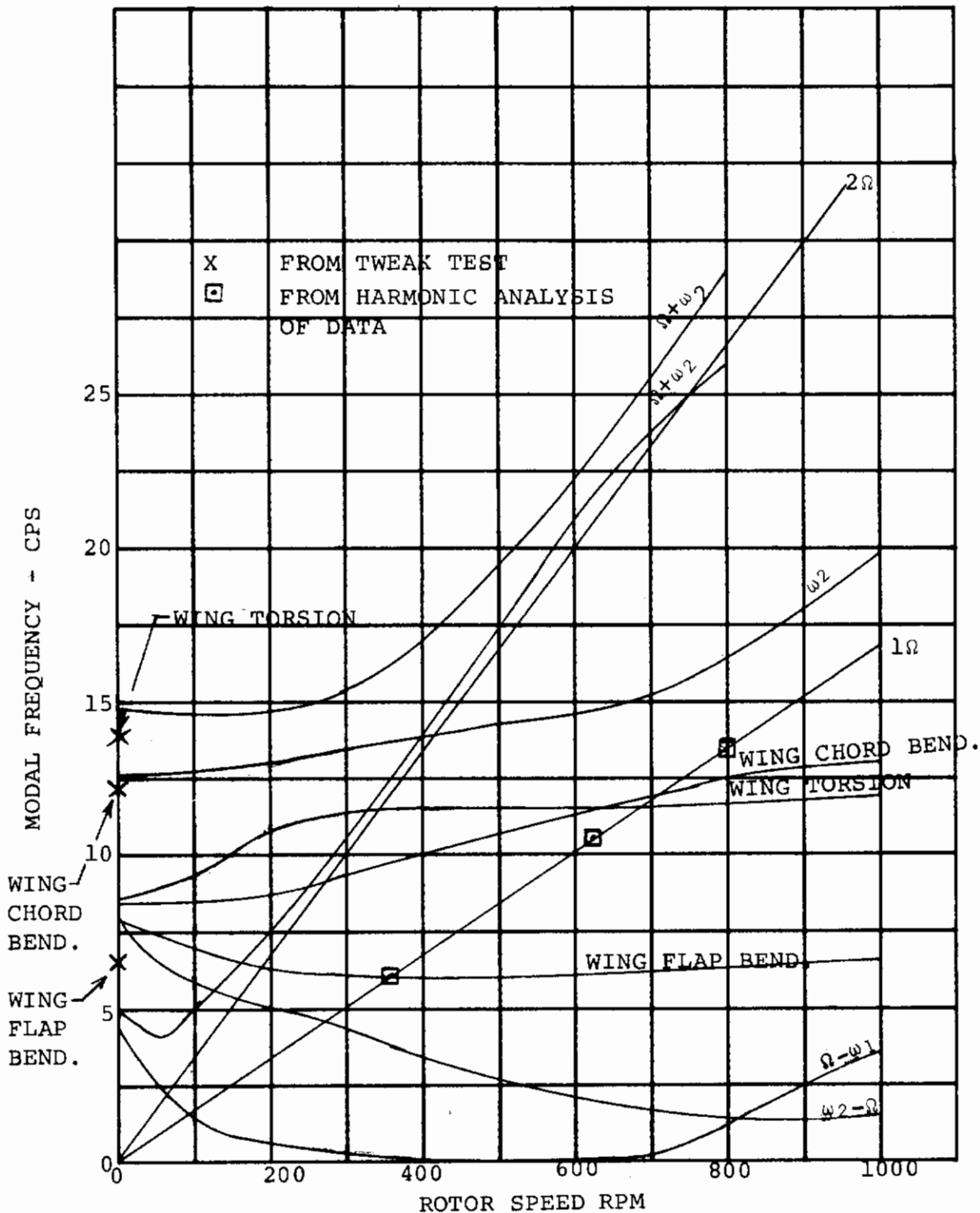


FIGURE 8-2: FREQUENCY SPECTRUM FOR NOMINAL STIFFNESS WING SPAR-WINDMILLING CONDITION, V = 140 FPS

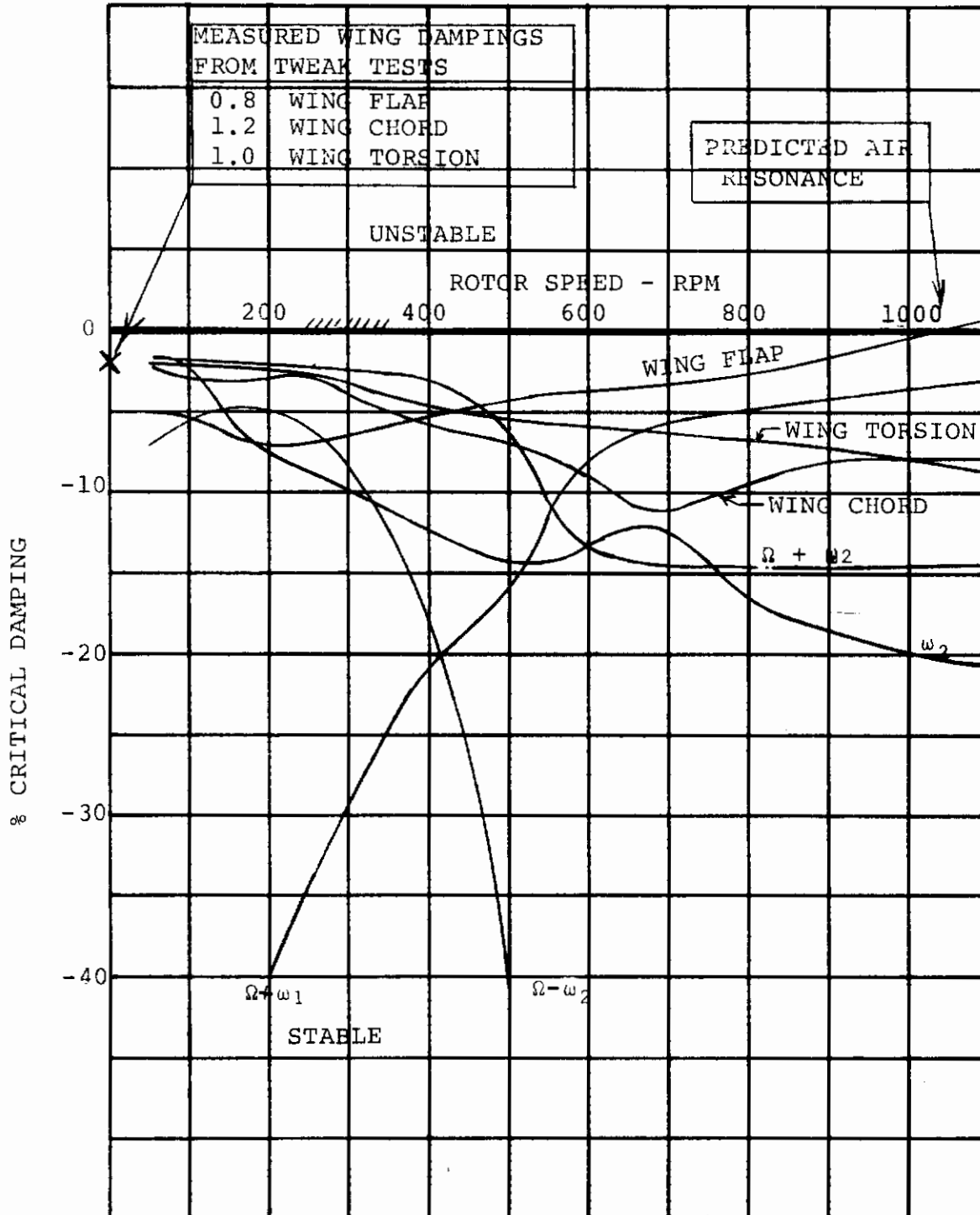


FIGURE 8-3: DAMPING SPECTRUM FOR NOMINAL STIFFNESS  
 WING SPAR - WINDMILLING CONDITION, V=140 FPS

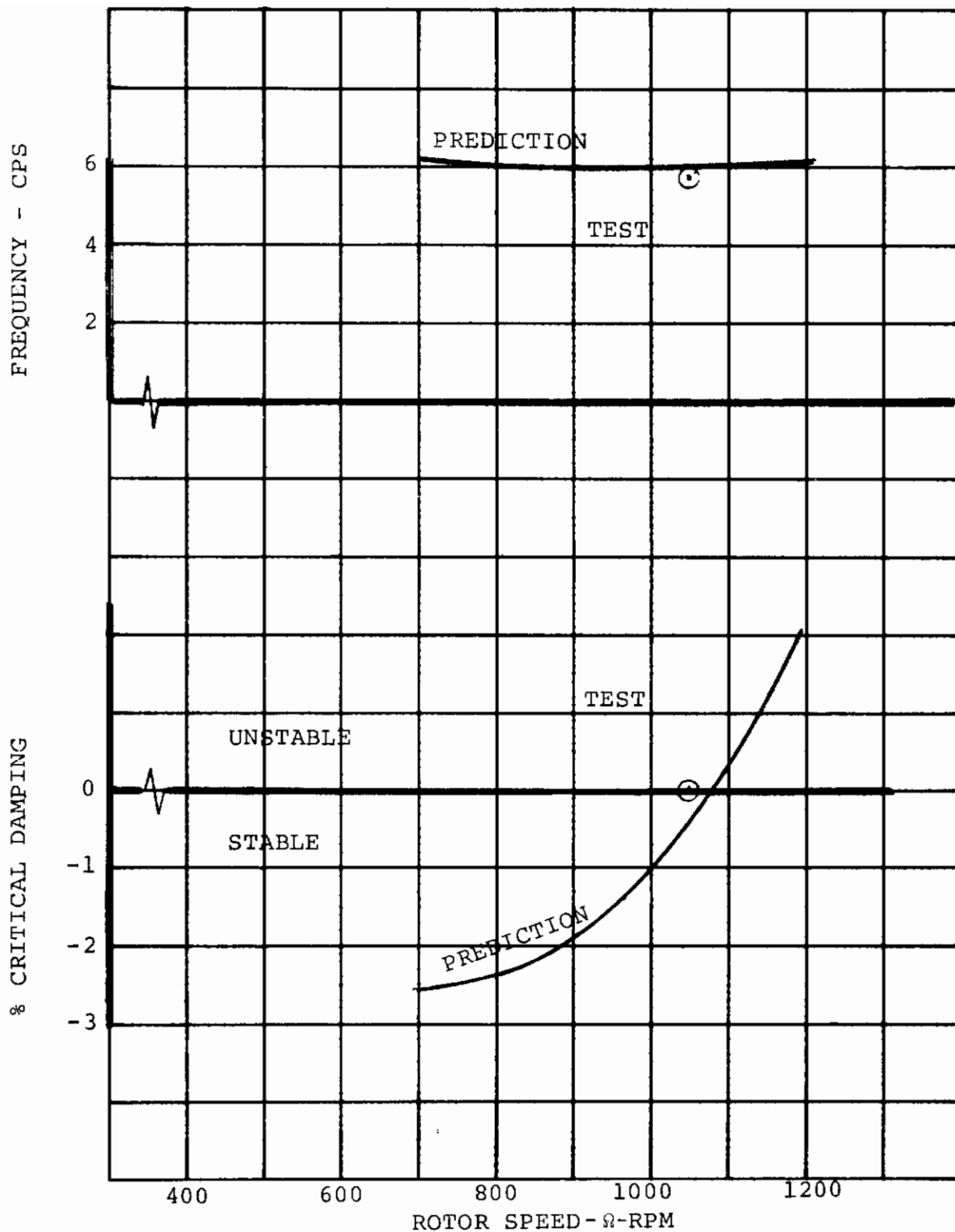


FIGURE 8-4: CORRELATION OF TEST AIR RESONANCE INSTABILITY WITH ANALYSIS - ,NOMINAL WING, V = 104 FPS - WING FLAP BENDING MODE, RUN 49

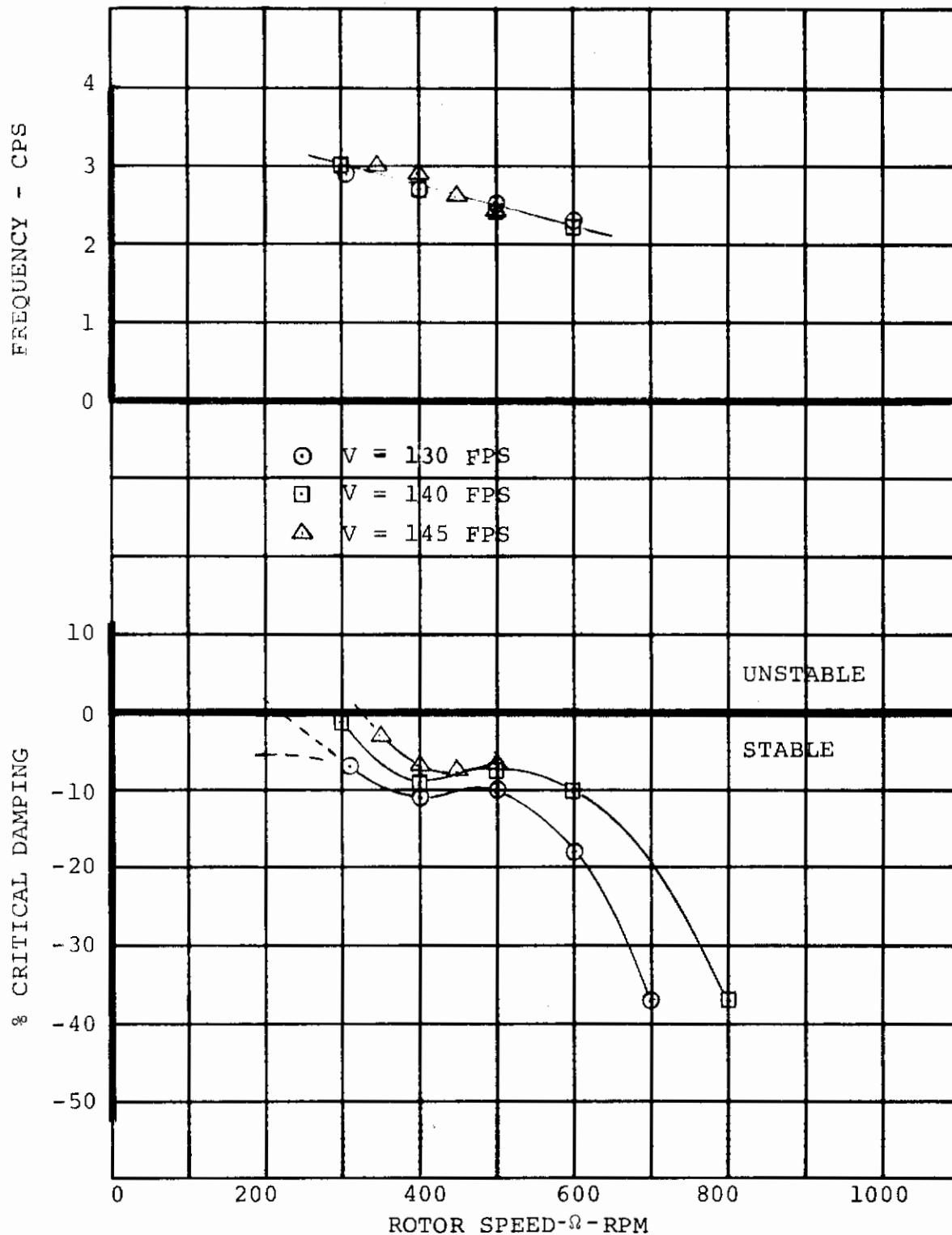


FIGURE 8-5: MEASURED DAMPING IN WHIRL MODE ( $\Omega - \omega_2$ )  
 - REDUCED TORSION STIFFNESS SPAR, RUN 126



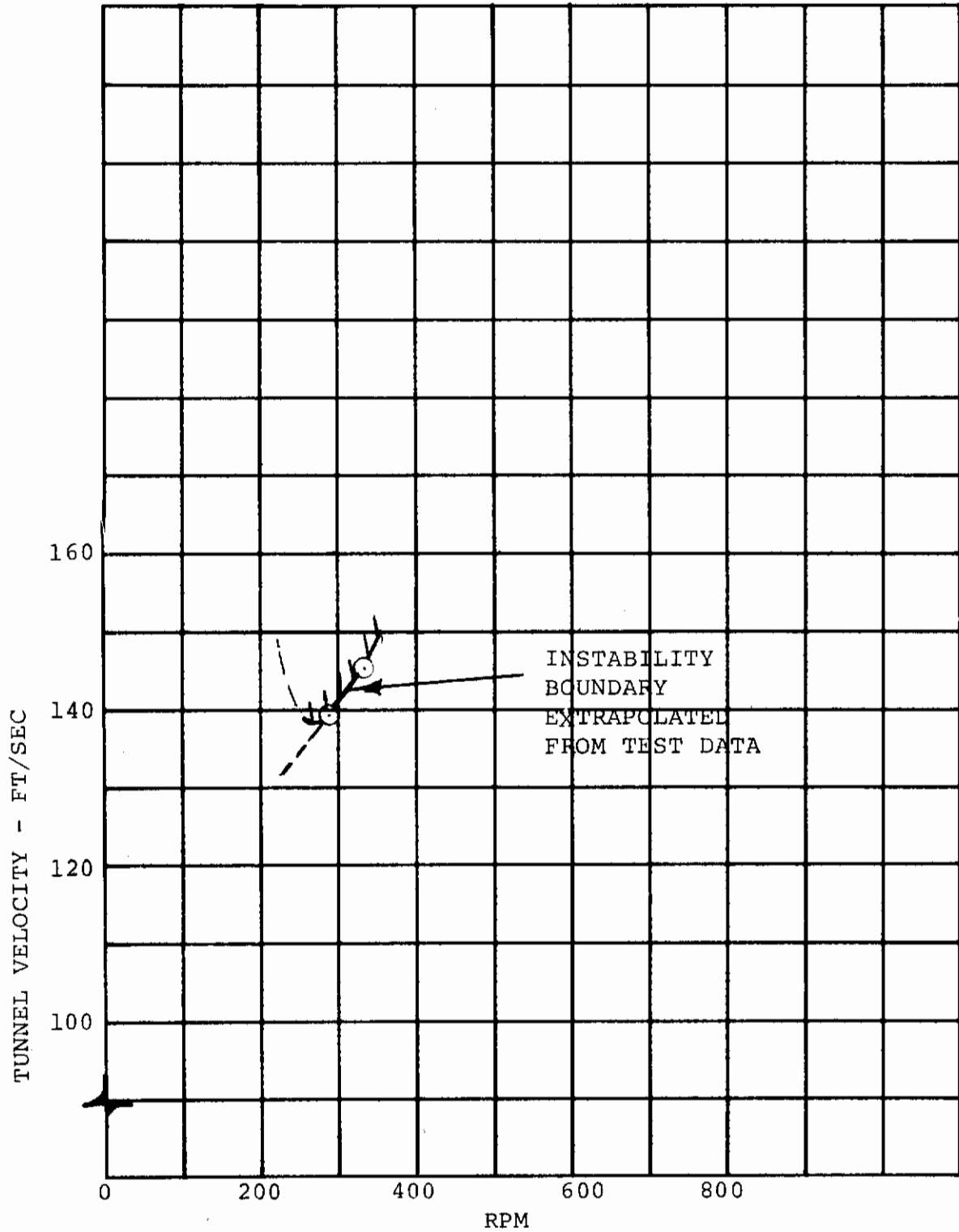


FIGURE 8-6: WHIRL FLUTTER INSTABILITY BOUNDARY - REDUCED TORSIONAL STIFFNESS SPAR

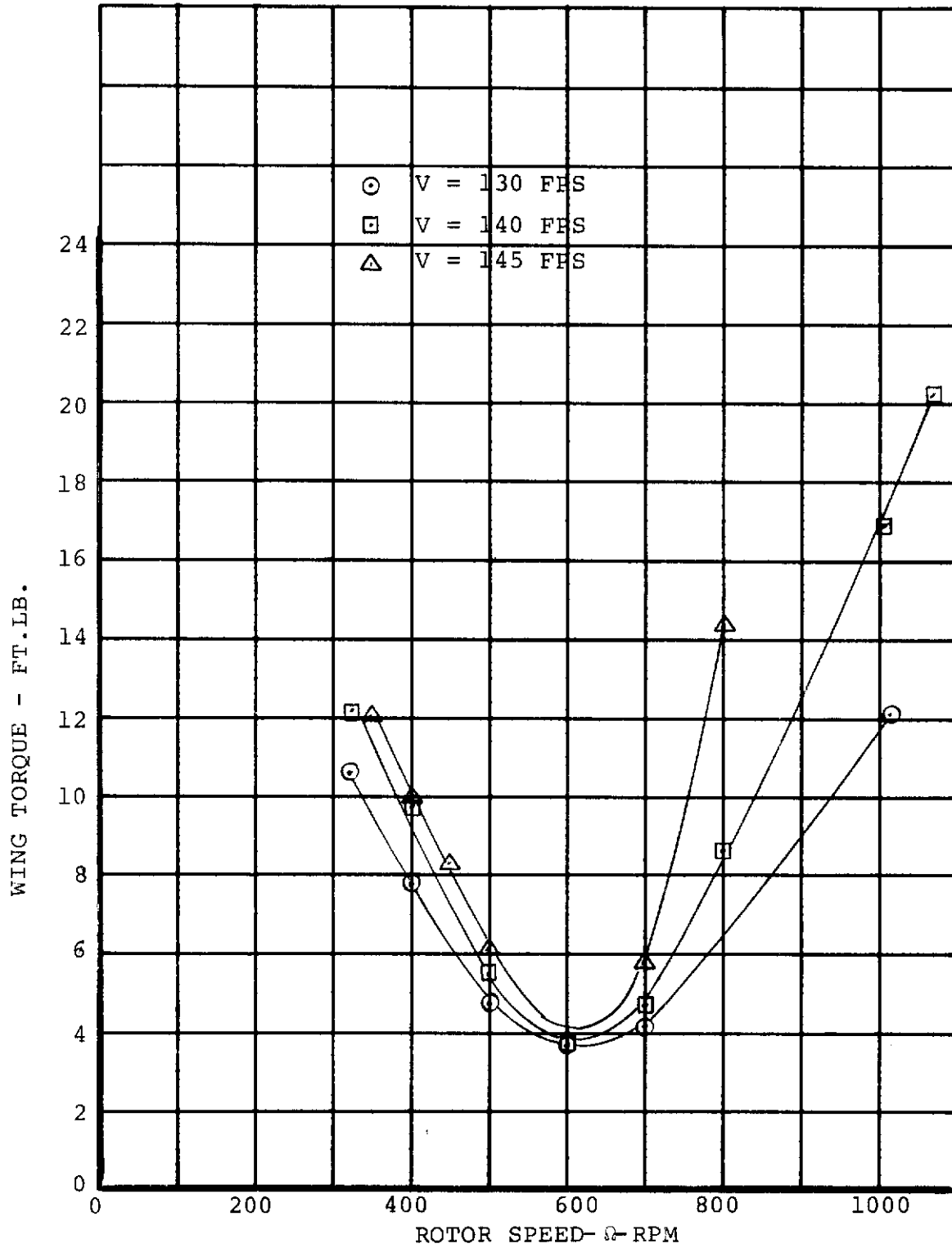


FIGURE 8-7: MEASURED WING TORQUE WITH NACELLE ANGLE OF ATTACK = 2°, REDUCED TORSION STIFFNESS SPAR

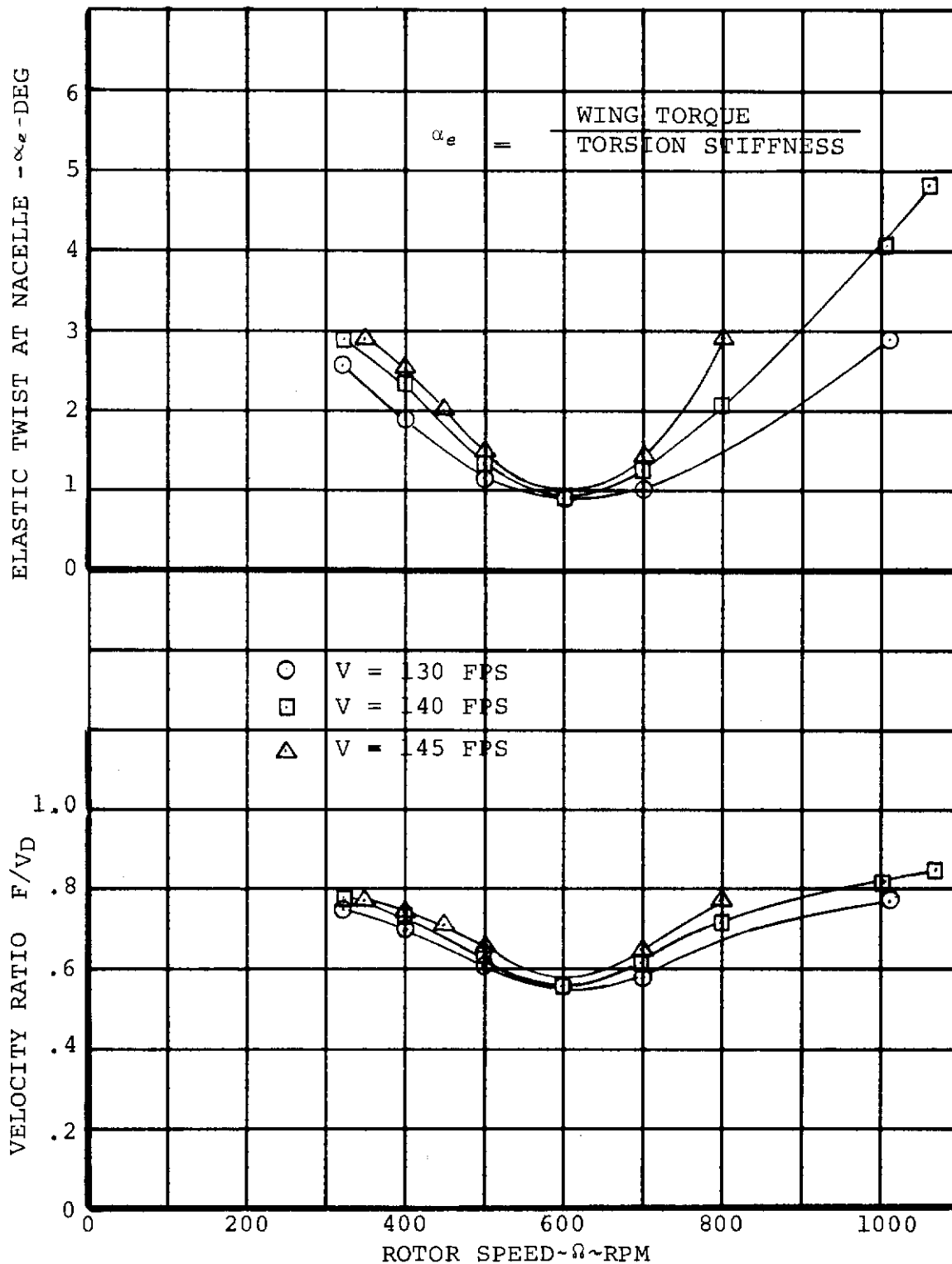


FIGURE 8-8: ELASTIC TWIST RESULTING FROM WING TORQUE AND DIVERGENCE VELOCITY PROXIMITY - REDUCED WING TORSION STIFFNESS SPAR, RUN 126

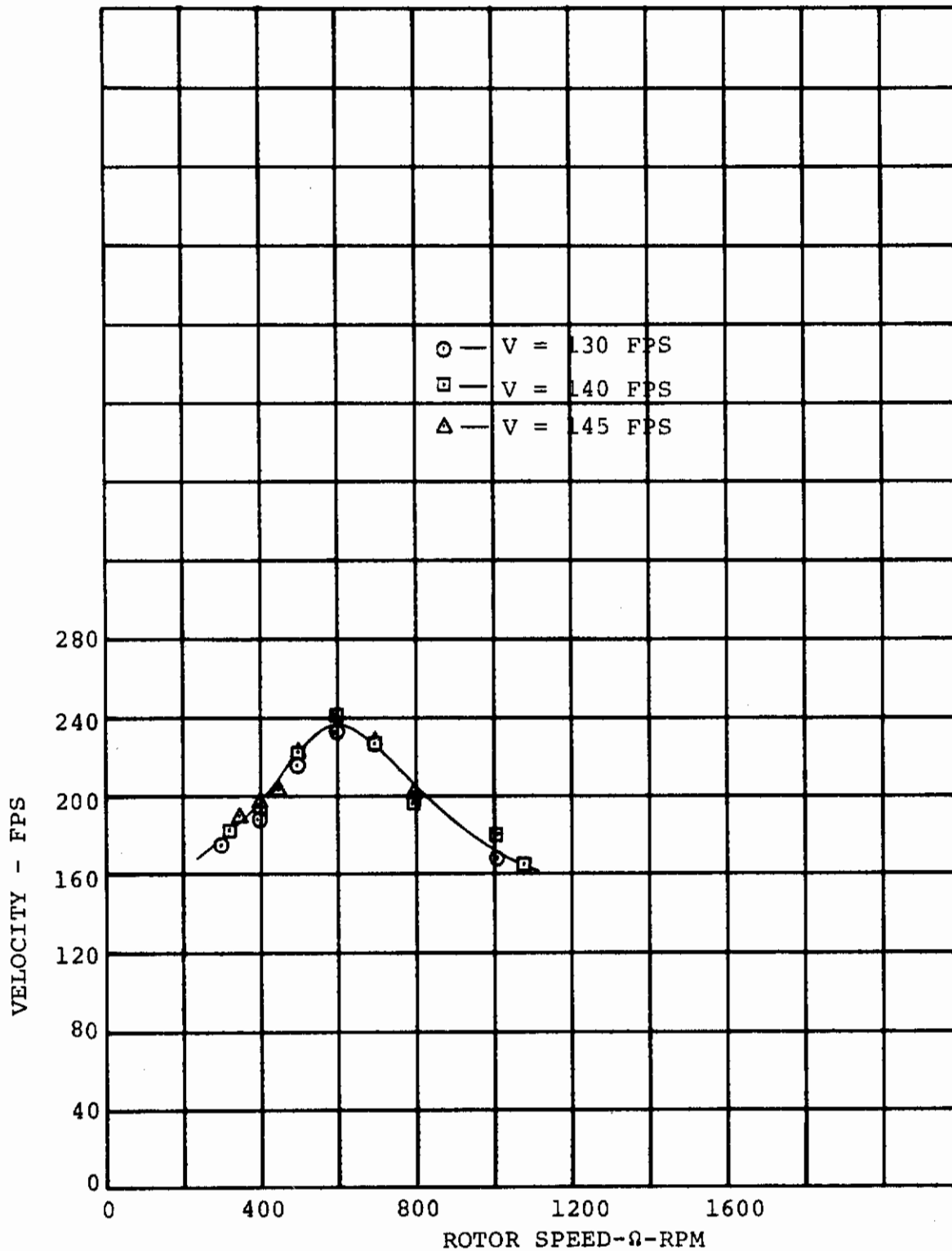


FIGURE 8-9: STATIC DIVERGENCE BOUNDARY EXTRACTED FROM TEST DATA - RUN 126 - REDUCED TORSION STIFFNESS SPAR

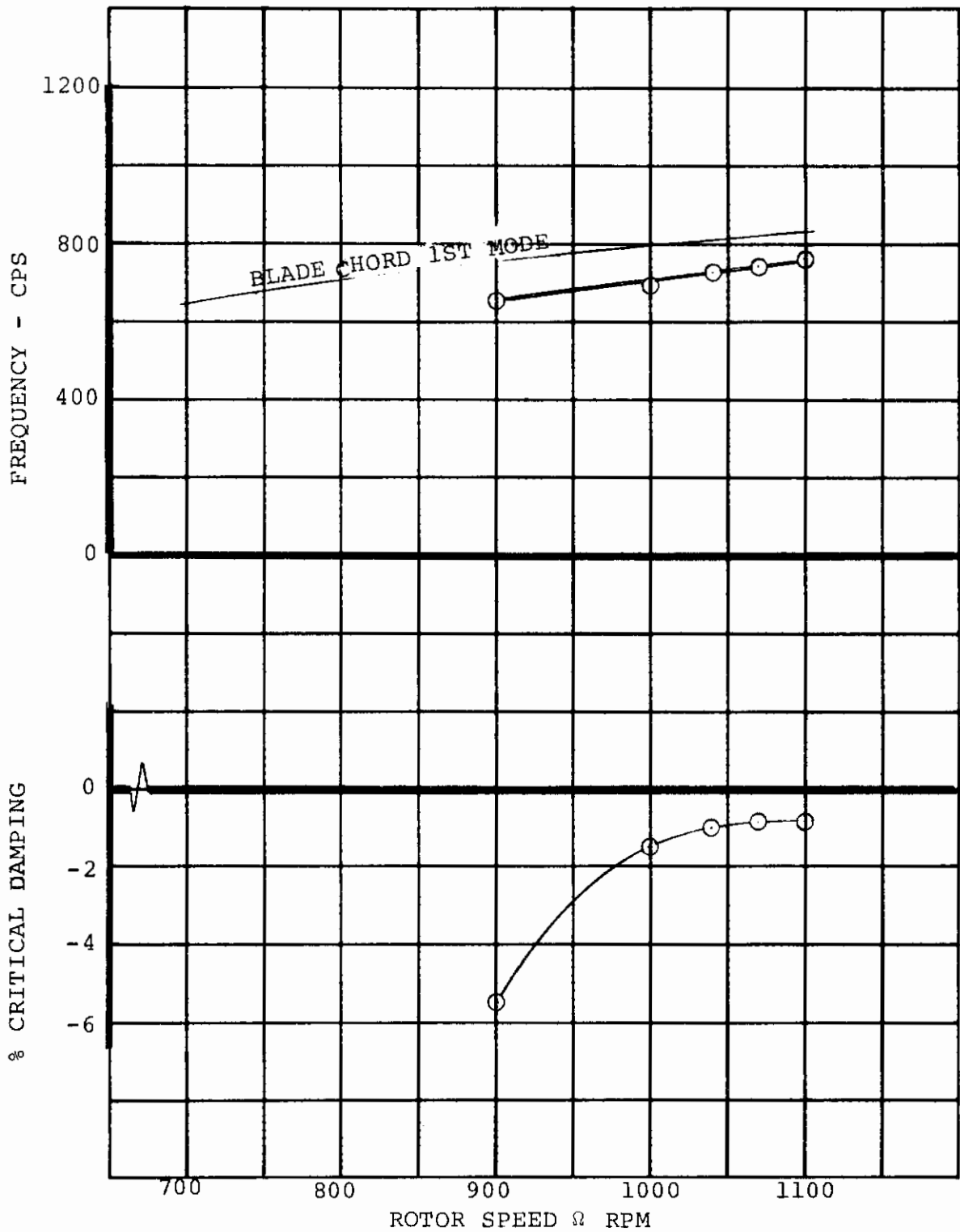
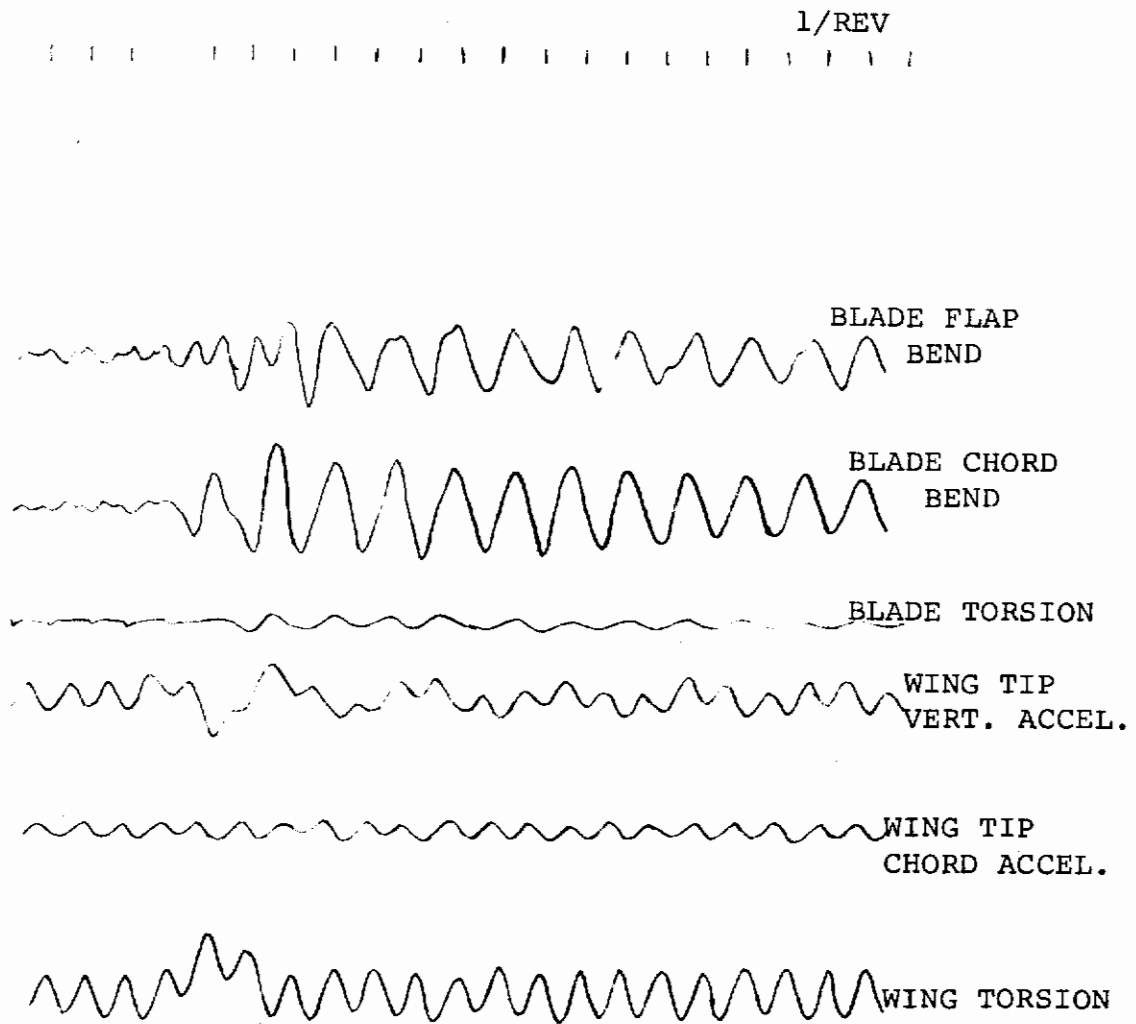


FIGURE 8-10 BLADE MODE DAMPING RESULTING FROM DISTURBANCE - V = 85 FPS, RUN 123

# Contrails



RUN 123  
 $\Omega = 1100$   
 $q = 8.6$  PSF

FIGURE 8-11: WAVE TRACES ILLUSTRATING BLADE RESPONSE TO DISTURBANCE

## 9.0 CONCLUSIONS

### 9.1 Steady Windmilling

#### Performance:-

1. The effects of rotor/airframe and airframe/rotor interactions on performance are small.
2. The windmilling rotor makes a substantial contribution to total airplane drag.

#### Stability

3. The Model 213 configuration is statically stable with rotors windmilling.
4. The low blade lag frequency of the soft in-plane hingeless rotor has a large favorable effect on the rotor contribution to airplane static stability.
5. Rotor derivatives, including lag frequency effects are well predicted by current methodology.

#### Rotor loads:-

6. At operating RPM the alternating blade loads are low.
7. The use of wing flap to trim aircraft lift results in much lower blade loads than would result from attitude change.
8. Blade loads show clearly defined peaks at RPM where blade or wing natural frequencies cross an integer harmonic.

#### Dynamics:-

9. Whirl flutter and static divergency instabilities did not occur with the scaled Model 213 wing.
10. Air Resonance was found and the onset of this instability is correctly predicted.
11. Whirl flutter and static divergence data have been obtained for correlation purposes using a reduced stiffness wing spar.

## 9.2 Spin Up and Feather

### Performance:-

1. The spin up and feather transient can be performed in 3 to 4 seconds model scale (9 to 12 sec full scale) with low transient accelerations (less than 0.1g) using a linear collective schedule and starting from 70% hover RPM.
2. The low accelerations can also be achieved from 100% hover RPM, by using simple thrust modulation to balance the changes in steady drag between the windmilling and feathered configurations.

During spin up and feather, the changes in rotor and aircraft stability derivatives are smooth with no large transient effects.

### Rotor Loads:-

3. Alternating rotor loads in transient conditions are approximately the same as for steady windmilling.
4. The effects of collective schedule and spin time on alternating blade loads are small so that blade loads will not be a constraint on the schedule.

### Dynamics:-

5. No instabilities were observed on any of the transient tests.

## 9.3 Fold/Deploy

### Performance

1. Flatwise blade folding provides less drag than edgewise blade folding.

### Stability

2. Blade folding can be accomplished with a smooth increase in static stability margin.



## Rotor Loads:-

3. The steady blade bending loads during folding/deploy are the same for both edgewise and flatwise folding. Blade root loads are less than the feathered blade loads.
4. Substantial blade bending was observed near the mid span. Instrumentation was not available to measure loads in this area.
5. No alternating loads were observed during folding.

## Dynamics:-

6. The blades were very stable during blade folding tests.

## 10.0 RECOMMENDATIONS

1. Further testing should be performed using a powered soft in-plane hingeless rotor model to extend the experimental determination of lag frequency effects to the control derivatives and also the dynamic rotor derivatives.
2. Autorotation experiments on this type of rotor system are needed including entry into autorotation from the cruise mode for various cases of failure (e.g. partial power, etc.).
3. Additional data on folding loads should be obtained with blades instrumented at several spanwise stations.

## 11.0 REFERENCES

1. "Human Engineering Guide to Equipment Design" by C. T. Morgan, J. S. Cook, A. Chapanis and M. W. Lund, Page 447. McGraw-Hill Book Company, Inc.
2. "Prediction of the Stability Derivatives of Large Flexible Prop/Rotors by a Simplified Analysis" by John P. Magee and Richard R. Pruyn. AHS National Forum presentation June 1970
3. "Wind Tunnel Test of a Powered Tilt-Rotor Performance Model" Test Program II/Volume V of this series of reports
4. "Aeroelasticity" by R. L. Bisplinghoff, H. Ashley and R. L. Halfman Addison-Wesley Publishing Co., Inc. Reading Mass.
5. "Determination of the Characteristics of Tapered Wings", R.F. Anderson. NACA Report 572, 1936.

APPENDIX A

DEFLECTION TEST

A deflection test was performed on the 1/9 Scale Conversion model to define the angular deflection of the rotor disc and the wing resulting from loads developed by the rotor and also the wing. This was done to insure correct evaluation of the angle of attack derivatives. The wing was loaded to define the deflection of the wing and also the rotor disc due to lift, drag and pitching moment. Loadings were applied at the rotor representing normal force, side force, pitching moment, yawing moment and drag. Table A-1 summarizes the deflection test data included in Figures A-1 to A-6.

TABLE A-1. SUMMARY OF DEFLECTION TEST RESULTS	
LOADINGS	BASIC MODEL SPAR
<u>Rotor Pitch Deflection</u>	
Rotor Normal Force $\frac{\partial \phi}{\partial NF}$	0.089°/Lb.
Rotor Pitching Moment $\frac{\partial \phi}{\partial PM}$	0.099°/Ft. Lb.
Wing Pitching Moment $\frac{\partial \phi}{\partial M}$	0.074°/Ft. Lb.
Wing Lift $\frac{\partial \phi}{\partial L}$	0.0 °/Lb.
<u>Wing Pitch Deflection</u>	
Rotor Normal Force $\frac{\partial \alpha}{\partial NF}$	0.078°/Lb
Rotor Pitching Moment $\frac{\partial \alpha}{\partial PM}$	0.071°/Ft. Lb.
Wing Pitching Moment $\frac{\partial \alpha}{\partial M}$	0.074°/Ft. Lb.
Wing Lift $\frac{\partial \alpha}{\partial L}$	0.0 °/Lb.
<u>Rotor Yaw Deflection</u>	
Rotor Side Force $\frac{\partial \psi}{\partial SF}$	0.018°/Lb.
Rotor Yawing Moment $\frac{\partial \psi}{\partial YM}$	0.032°/Ft. Lb.
Wing Drag $\frac{\partial \psi}{\partial D}$	0.0125°/Lb.
Wing Yawing Moment $\frac{\partial \psi}{\partial YM_{AC}}$	0.010°/Ft. Lb.

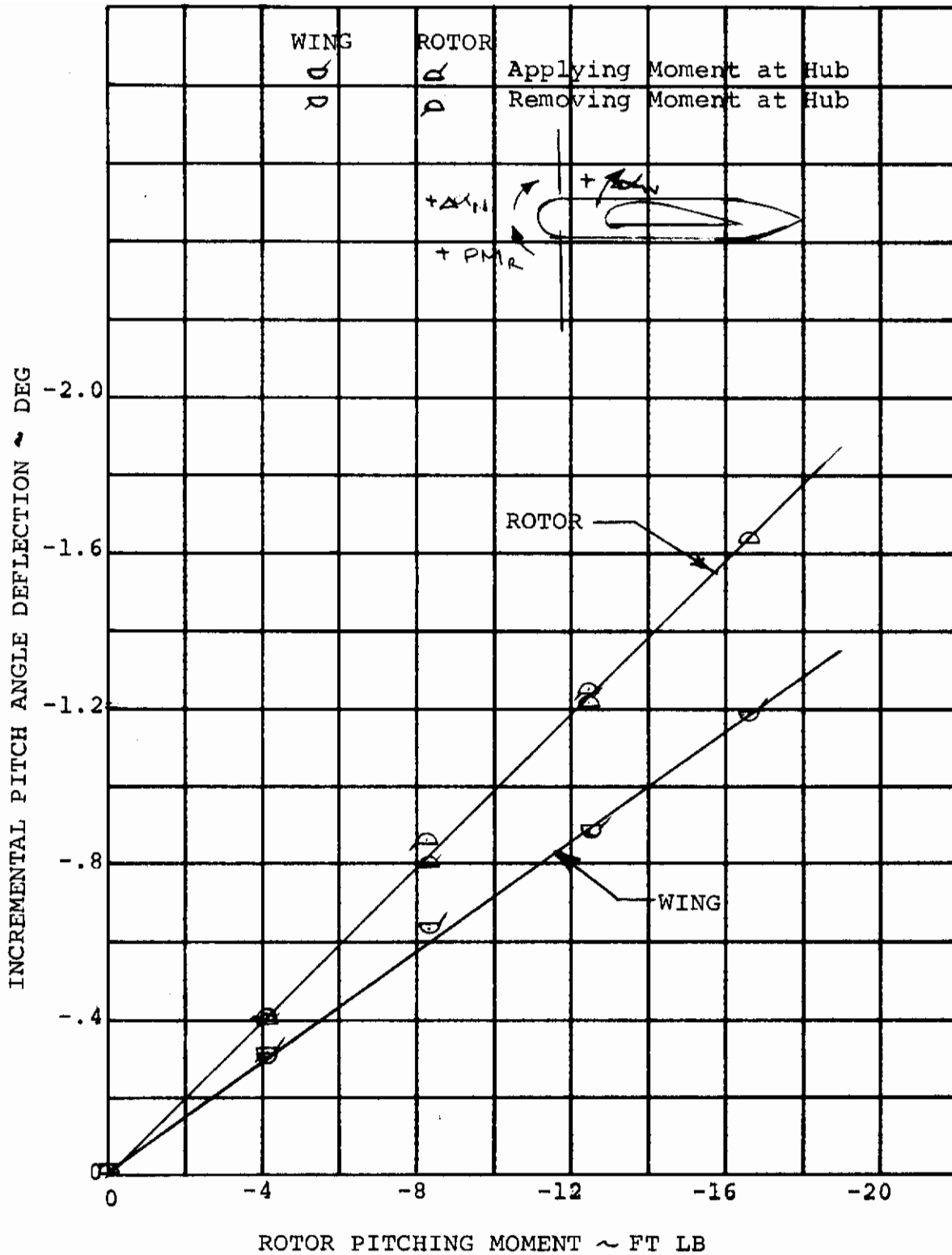


FIGURE A-1. PITCH ANGLE DEFLECTIONS OF THE ROTOR AND WING RESULTING FROM ROTOR PITCHING MOMENT

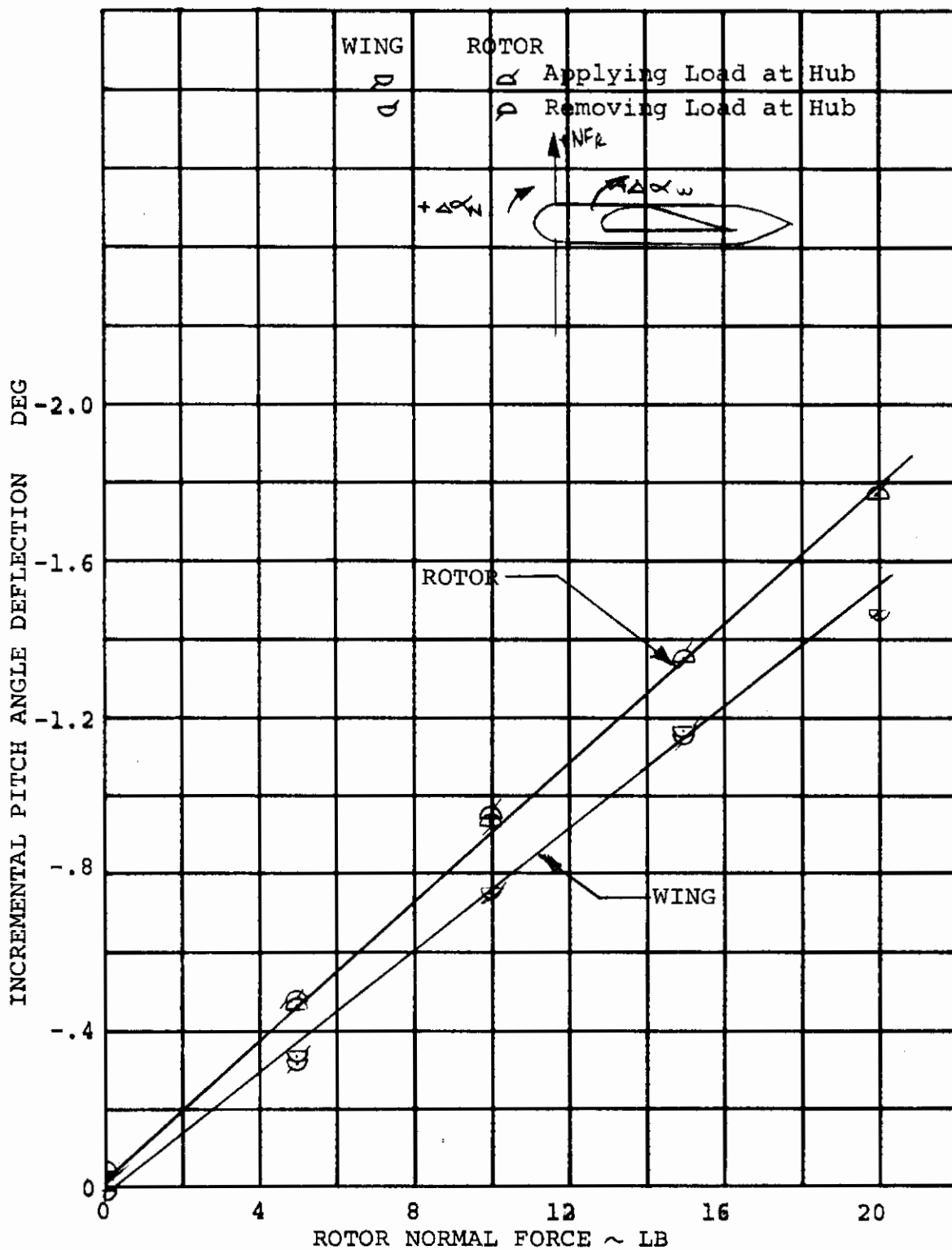
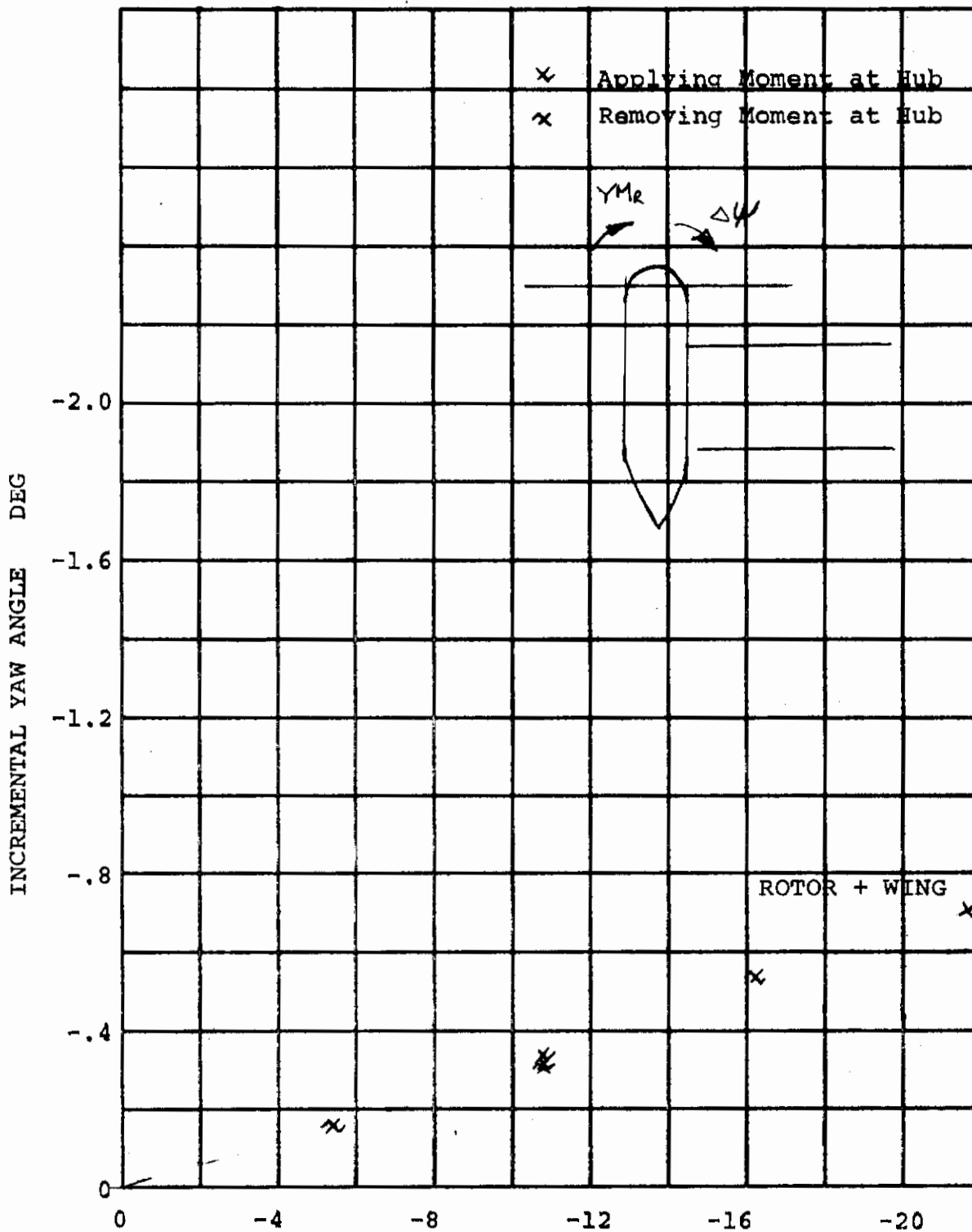


FIGURE A-2. PITCH ANGLE DEFLECTIVE OF THE ROTOR AND WING RESULTING FROM ROTOR NORMAL FORCE



ROTOR YAWING MOMENT FT LB  
 FIGURE A-3. YAW ANGLE DEFLECTION OF THE ROTOR DUE TO ROTOR YAWING MOMENT.

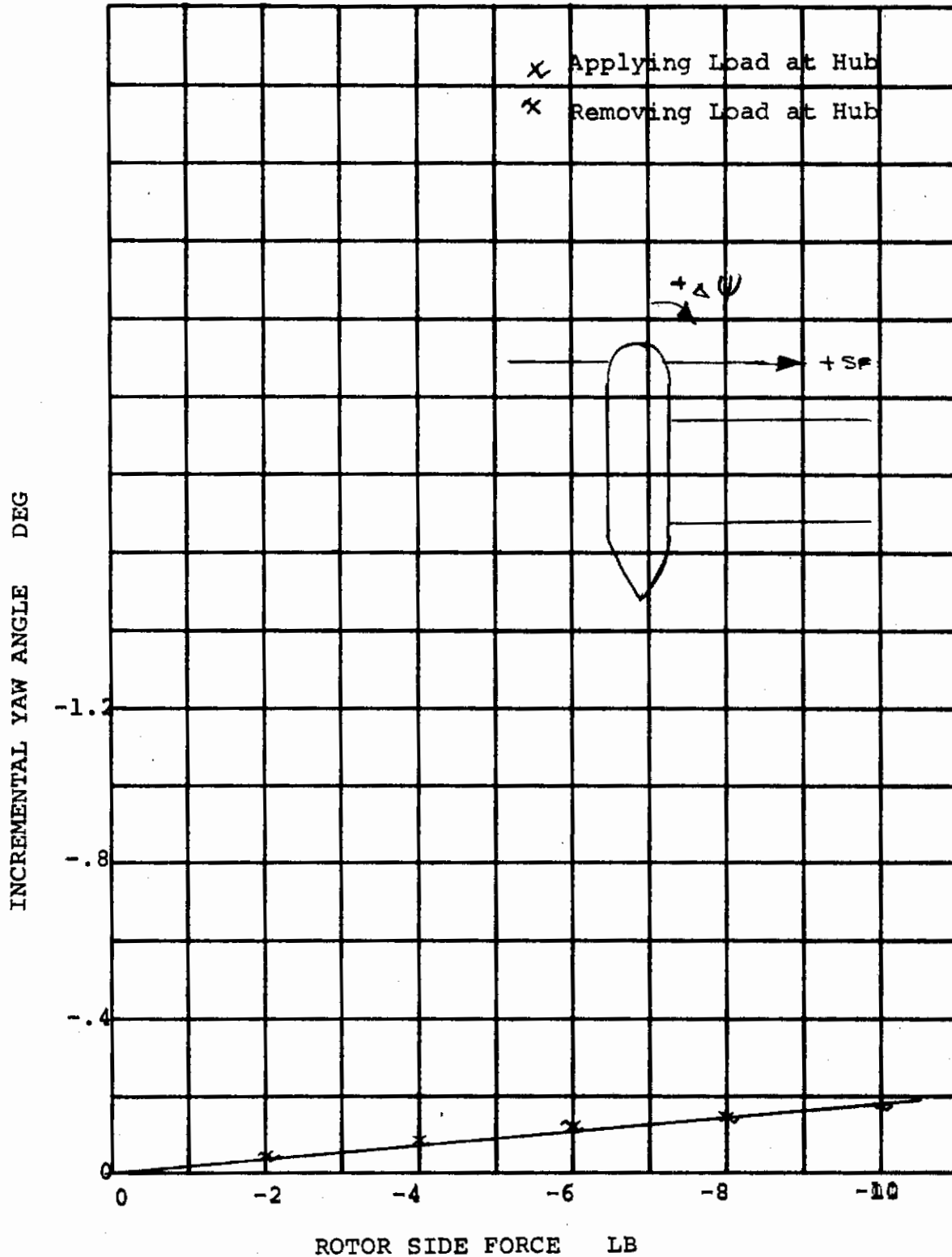


FIGURE A-4. YAW ANGLE DEFLECTION OR ROTOR DUE TO ROTOR SIDE FORCES.



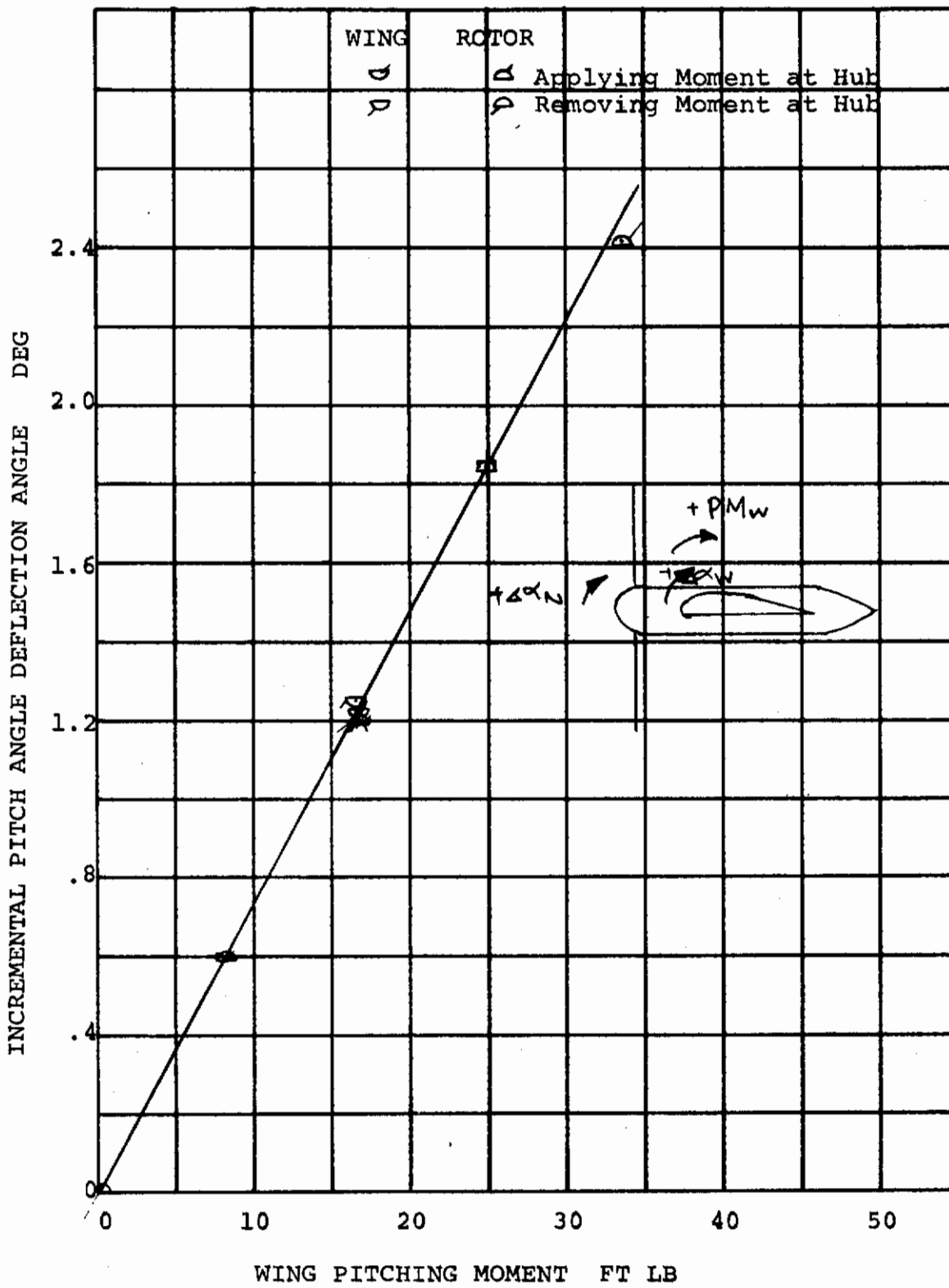


FIGURE A-5. WING PITCHING MOMENT FT LB  
 PITCH ANGLE DEFLECTION OF THE ROTOR AND  
 WING DUE TO WING PITCHING MOMENT.

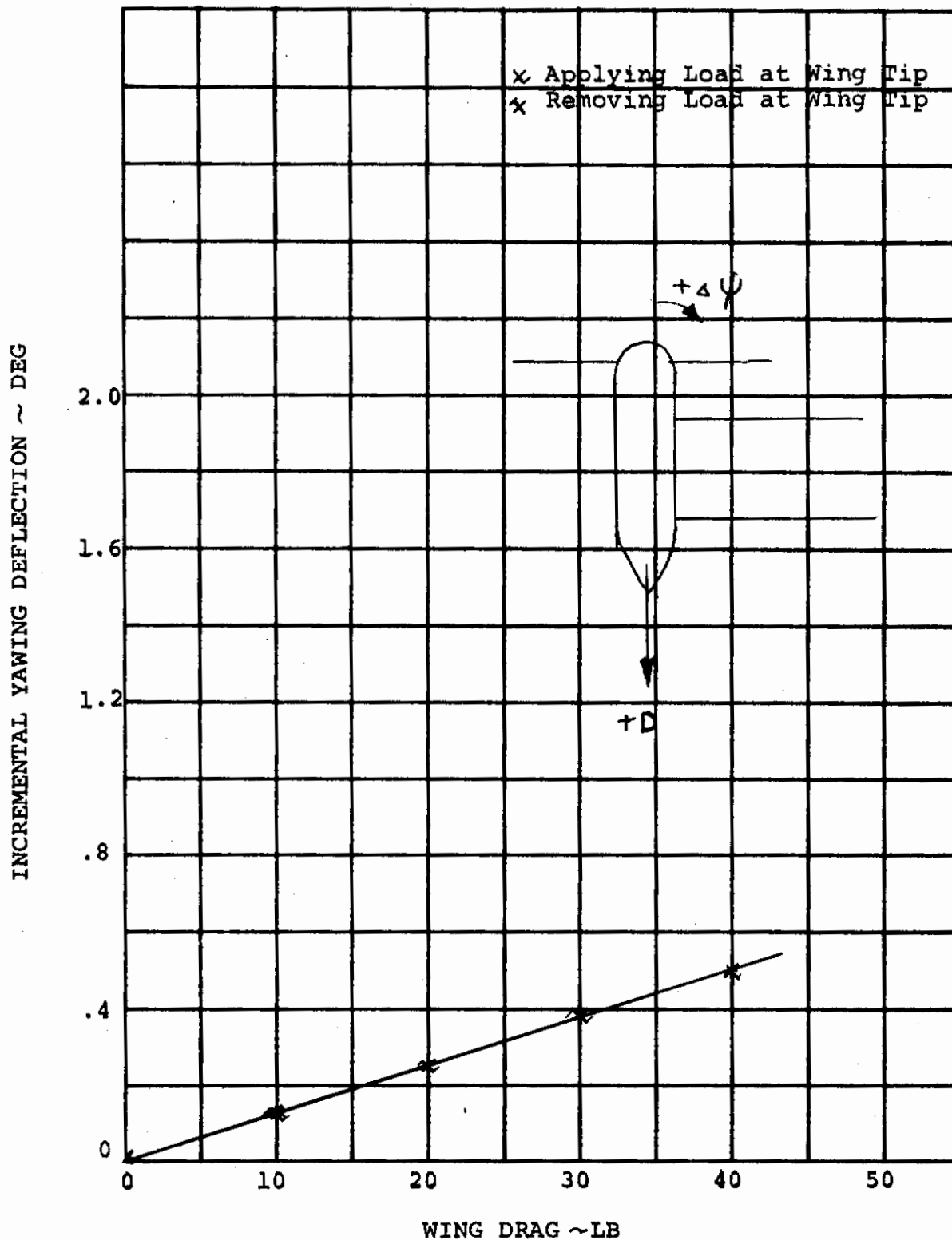


FIGURE A-6. YAW ANGLE DEFLECTION DUE TO WING AND ROTOR DRAG.

APPENDIX B

BASIC ROTOR DATA

The model was set at nominal angles of -2, 0, +2 and +4 degrees angle of attack. Basic rotor data recorded during steady windmilling was rotor pitching moment, normal force; yawing moment and side force are presented in Figures B-1 to B-24.

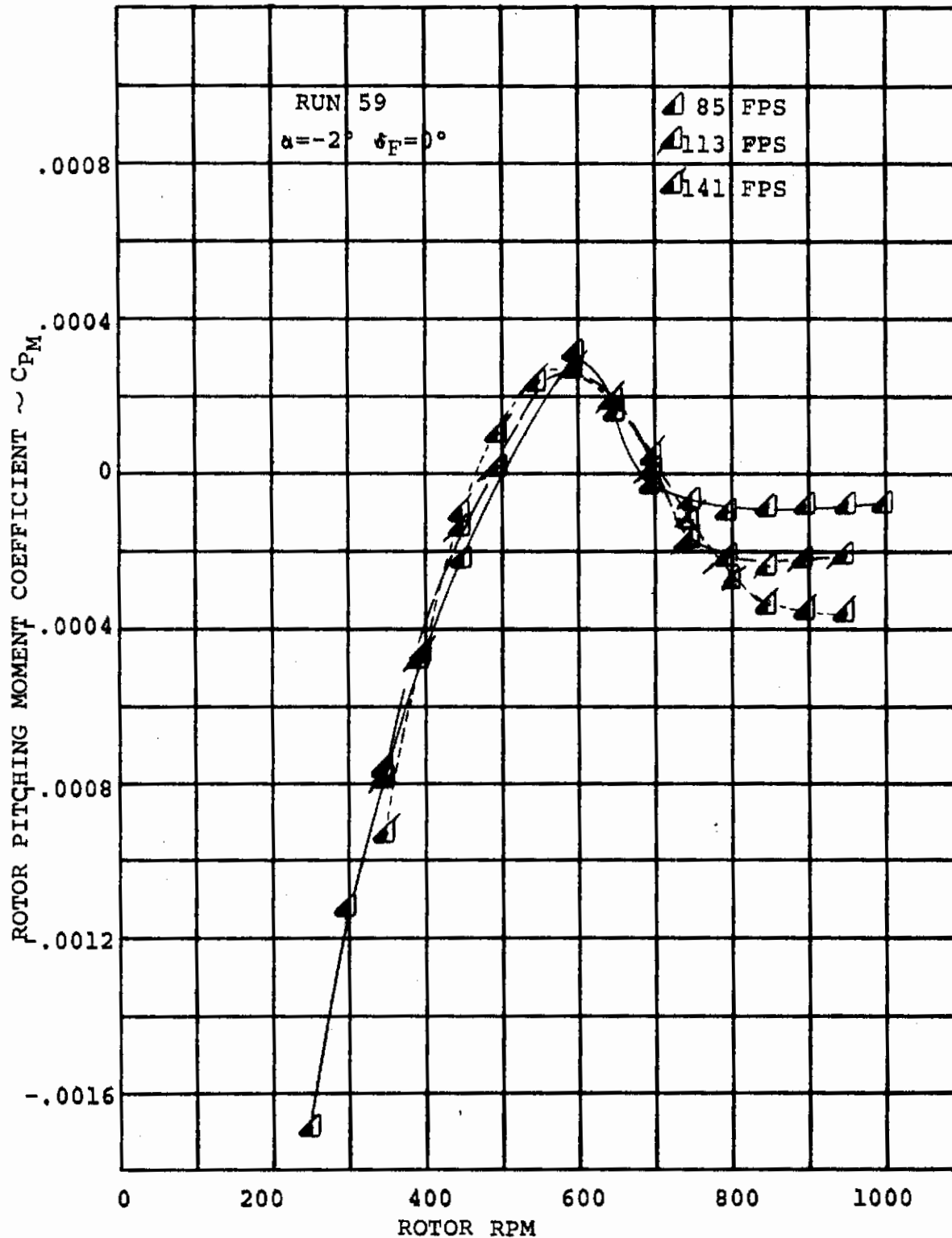


FIGURE B-1 ROTOR PITCHING MOMENT/RPM VARIATION  
FUSELAGE ATTITUDE =  $-2^\circ$   $\delta_F = 0^\circ$   
(STEADY WINDMILLING)

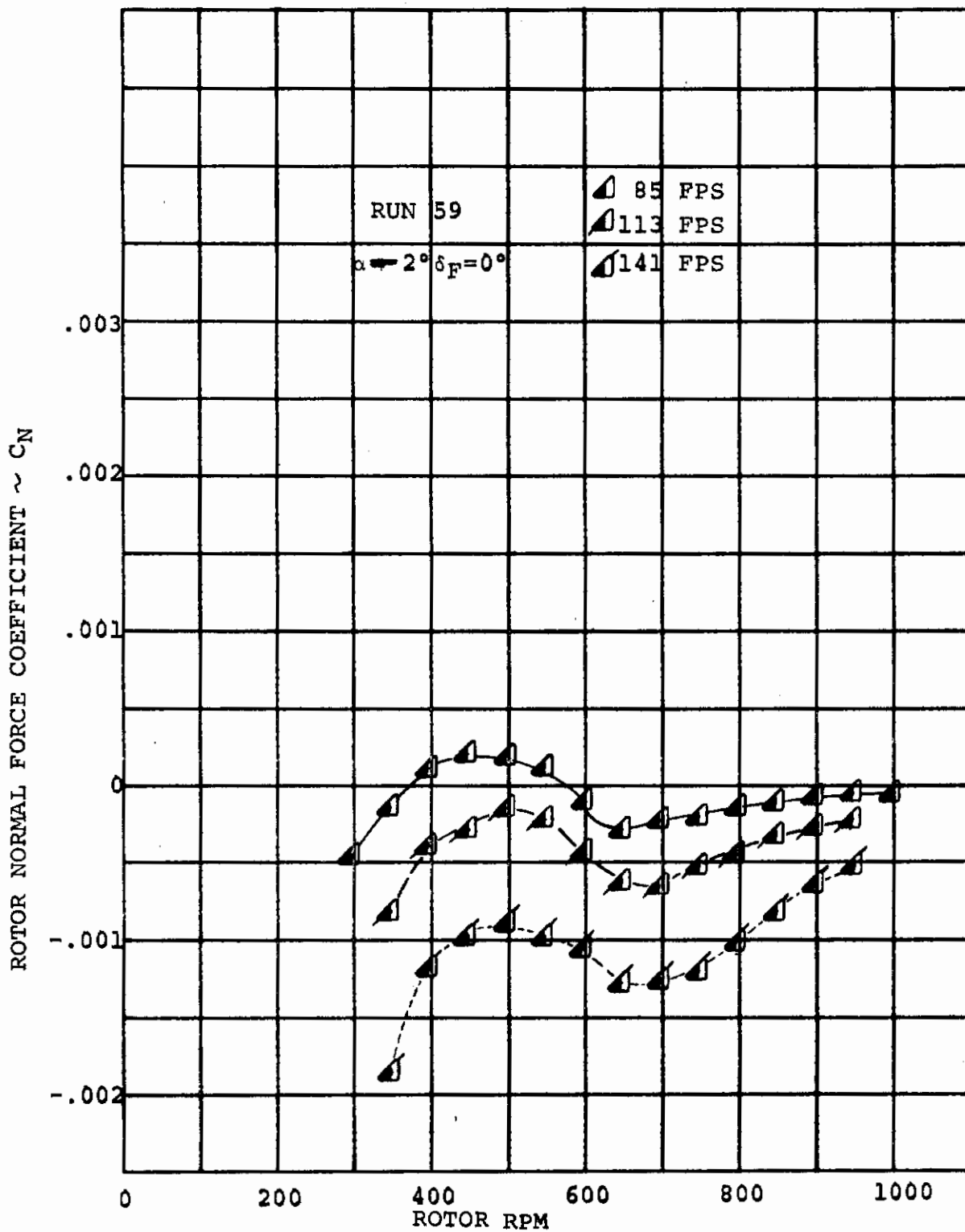


FIGURE B-2 ROTOR NORMAL FORCE/RPM VARIATION  
 FUSELAGE ATTITUDE  $= -2^\circ$   $\delta_F = 0^\circ$   
 (STEADY WINDMILLING)

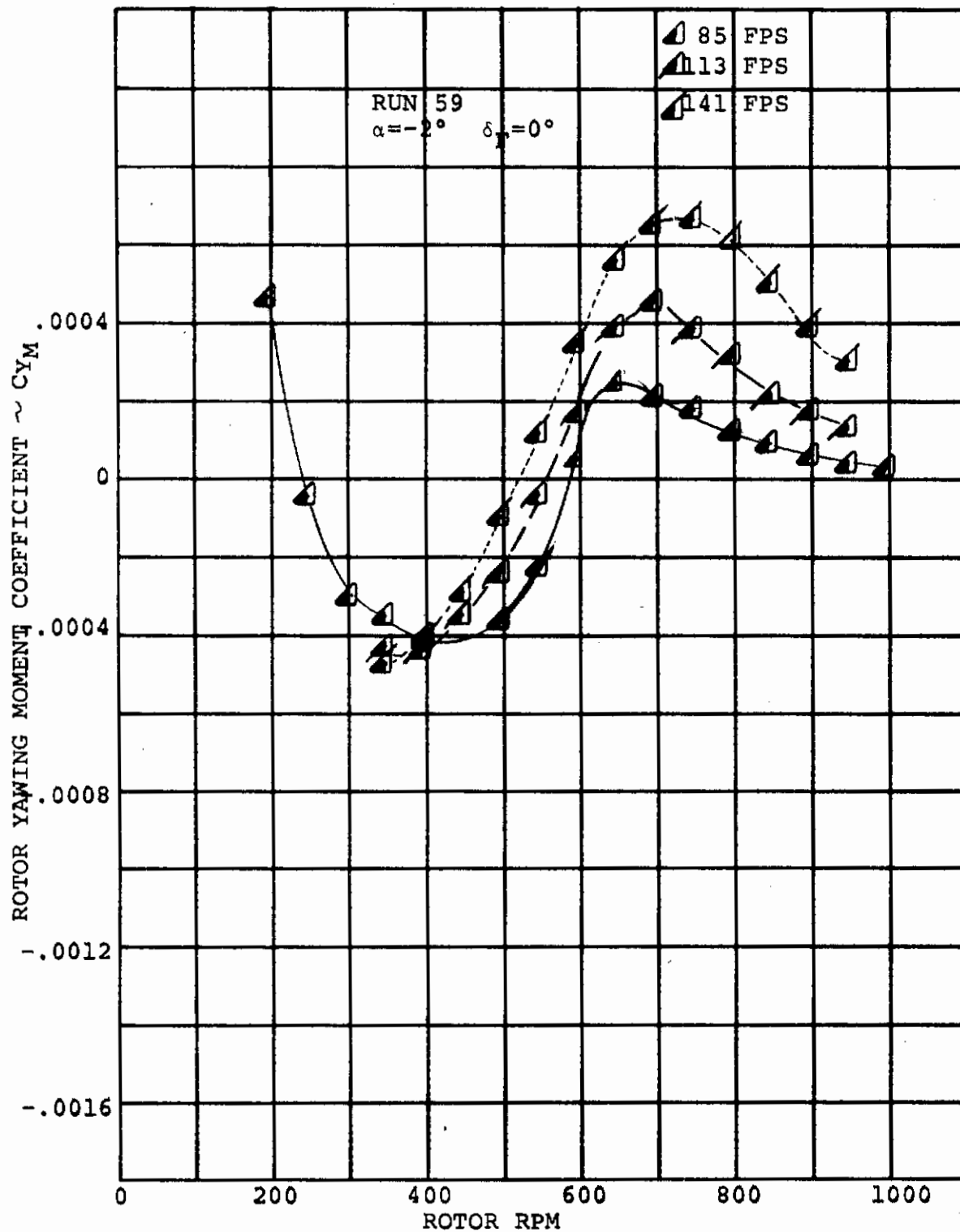


FIGURE B-3 ROTOR YAWING MOMENT/RPM VARIATION  
 FUSELAGE ATTITUDE =  $-2^\circ$   $\delta_F = 0^\circ$   
 (STEADY WINDMILLING)

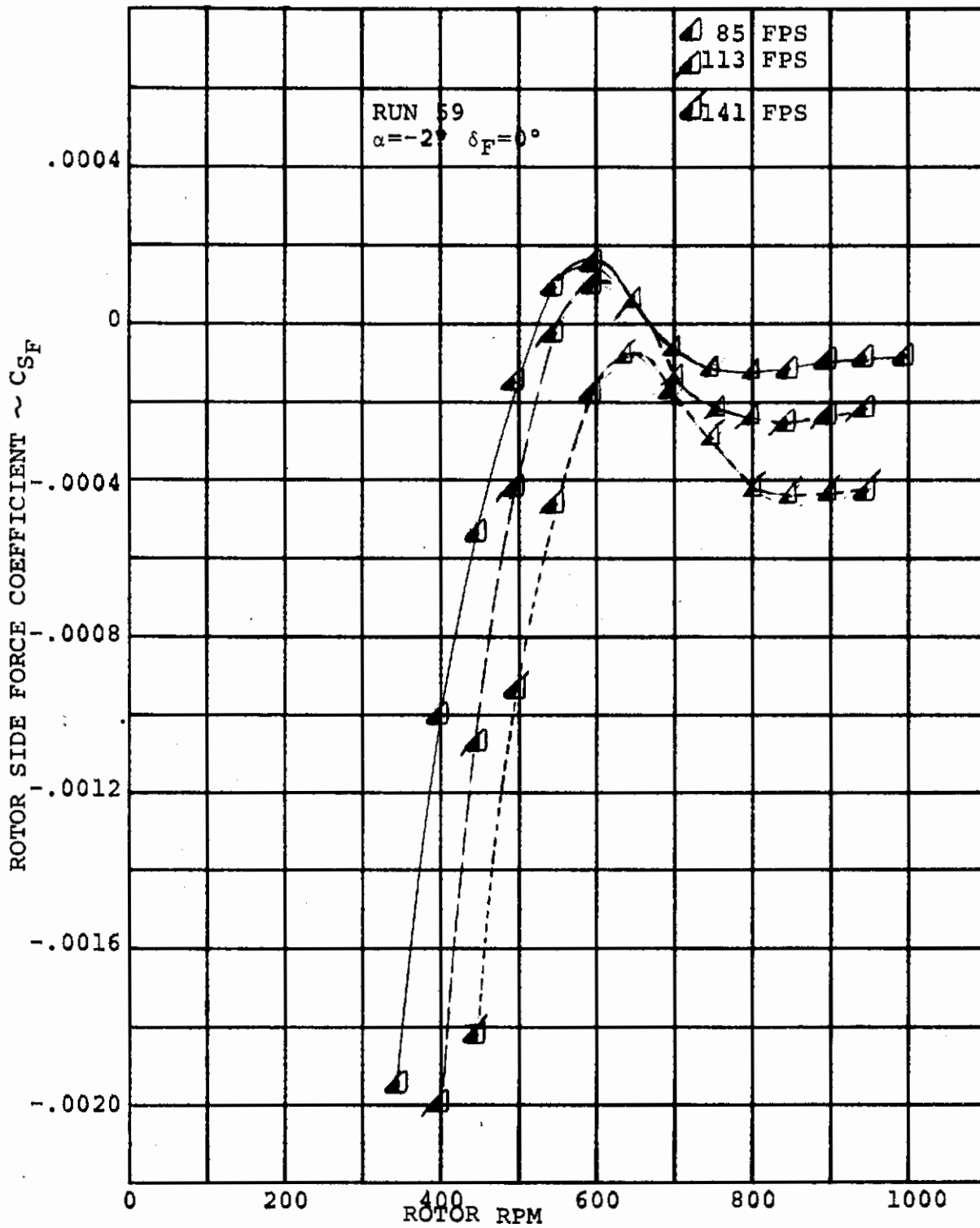


FIGURE B-4 ROTOR SIDE FORCE/RPM VARIATION  
 FUSELAGE ATTITUDE =  $-2^\circ$   $\delta_F = 0^\circ$   
 (STEADY WINDMILLING)

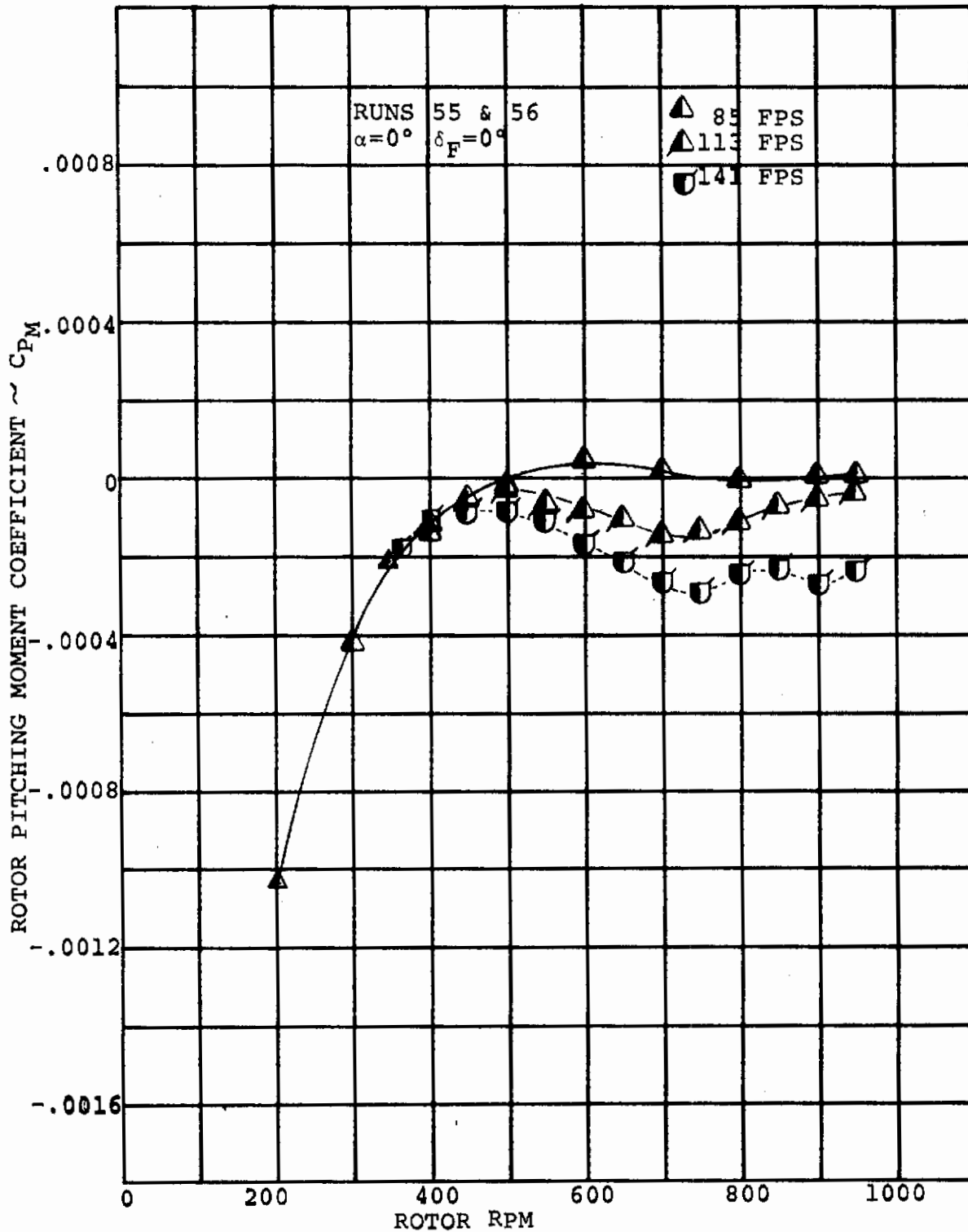


FIGURE B-5 ROTOR PITCHING MOMENT/RPM VARIATION  
FUSELAGE ATTITUDE =  $0^\circ$   $\delta_F = 0^\circ$   
(STEADY WINDMILLING)



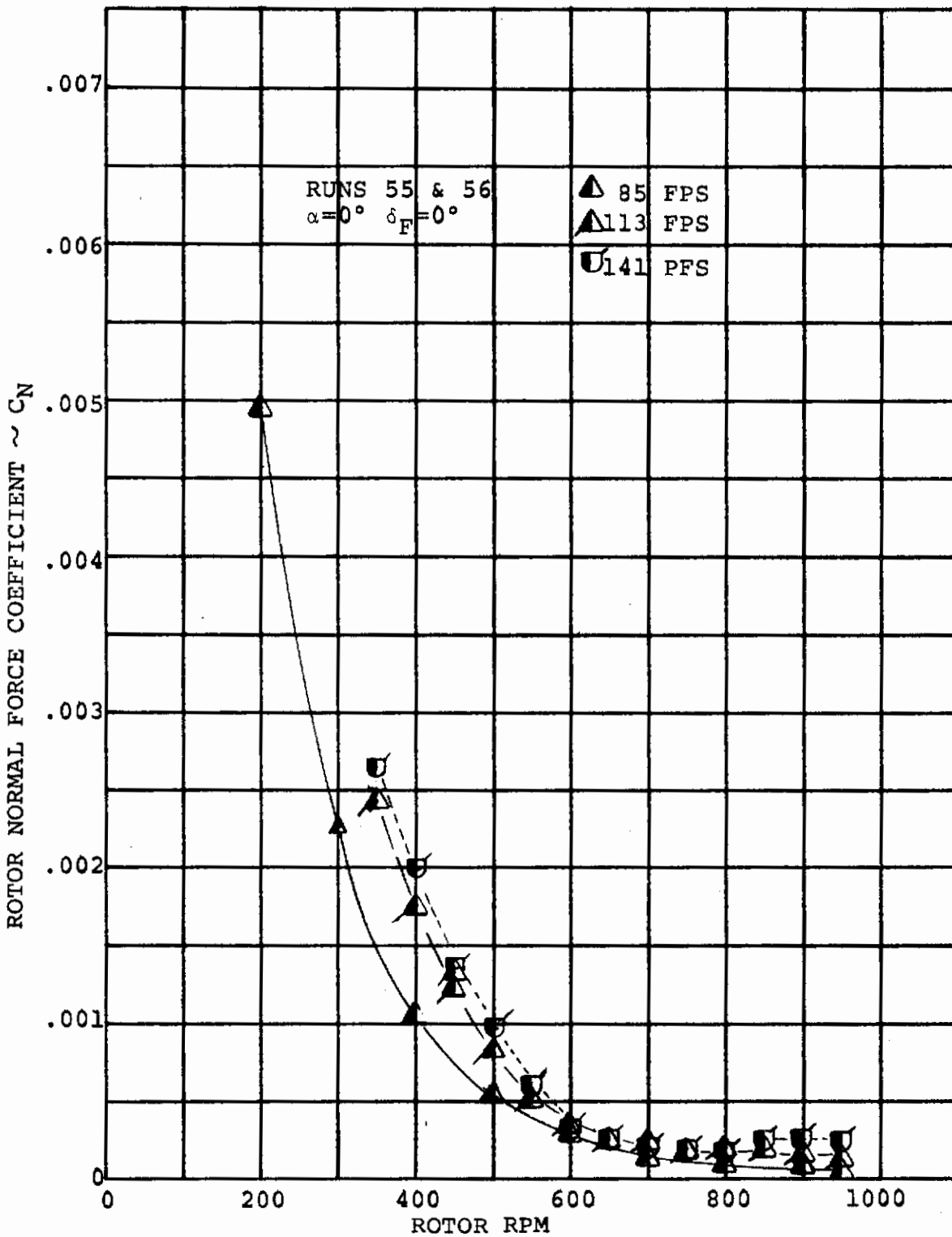


FIGURE B-6. ROTOR NORMAL FORCE/RPM VARIATION  
FUSELAGE ATTITUDE =  $0^\circ$   $\delta_F=0^\circ$   
(STEADY WINDMILLING)

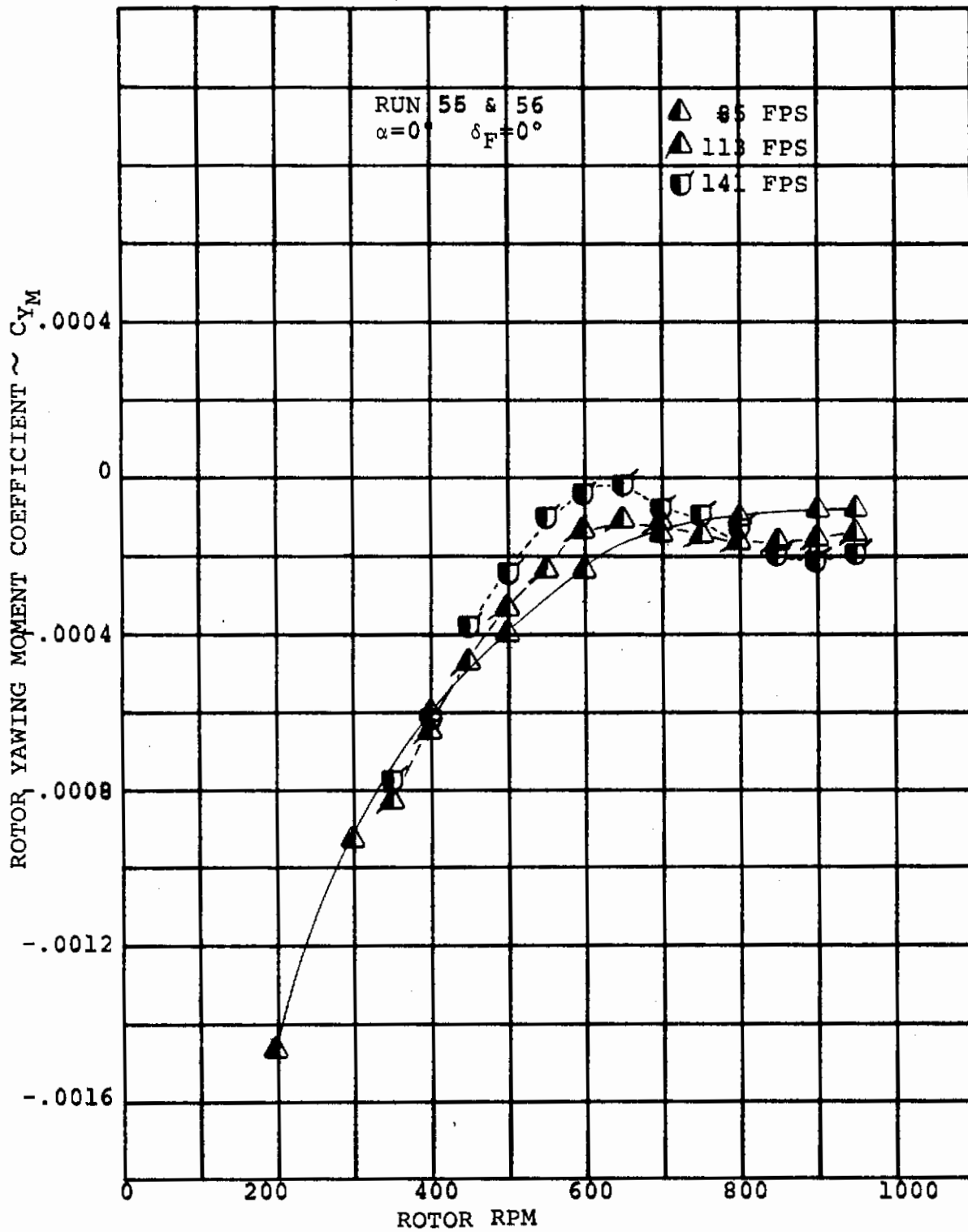


FIGURE B-7. ROTOR YAWING MOMENT/RPM VARIATION  
 FUSELAGE ATTITUDE =  $0^\circ$   $\delta_F = 0^\circ$   
 (STEADY WINDMILLING)

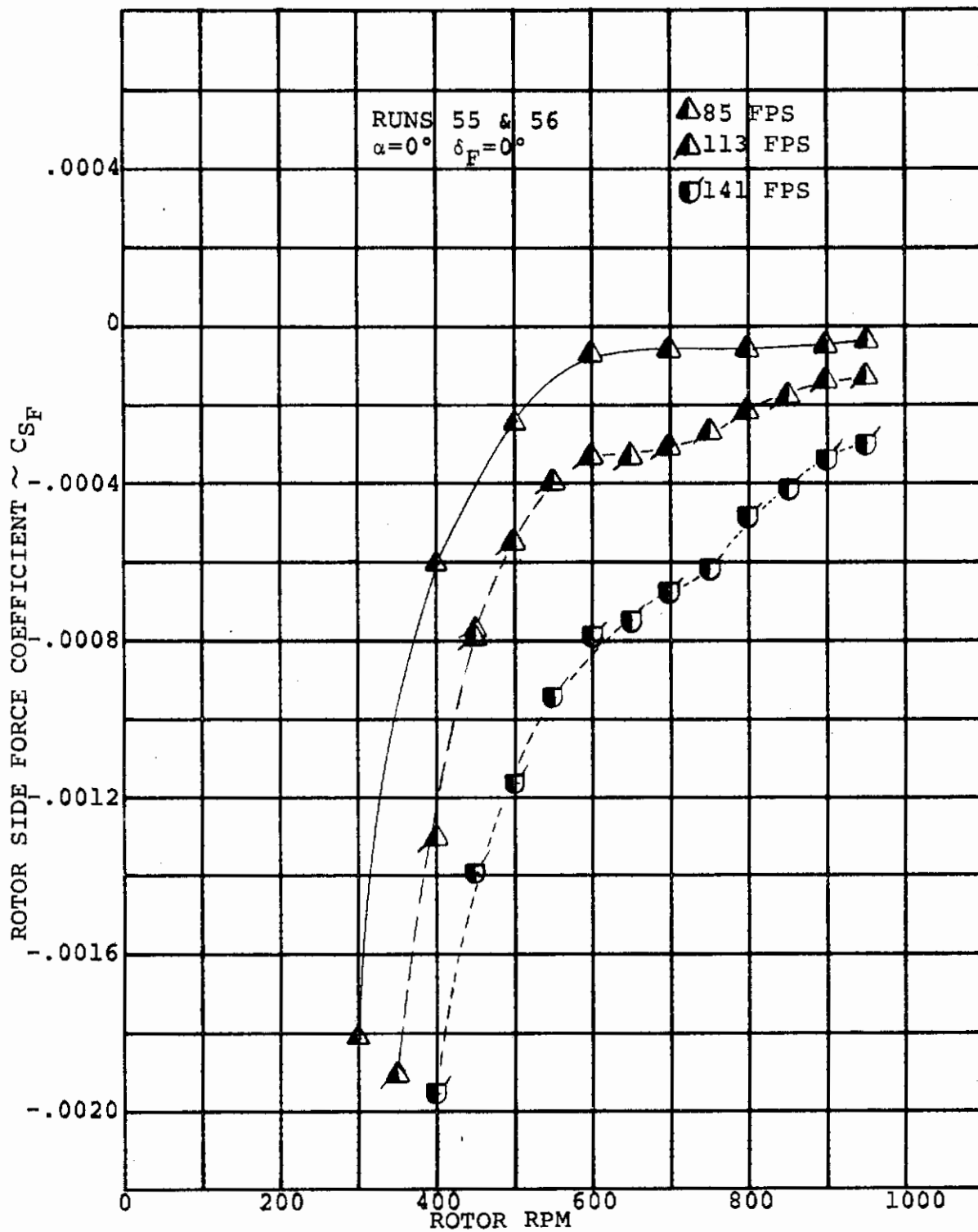


FIGURE B-8. ROTOR SIDE FORCE/RPM VARIATION  
FUSELAGE ATTITUDE =  $0^\circ$   $\delta_F=0^\circ$   
(STEADY WINDMILLING)

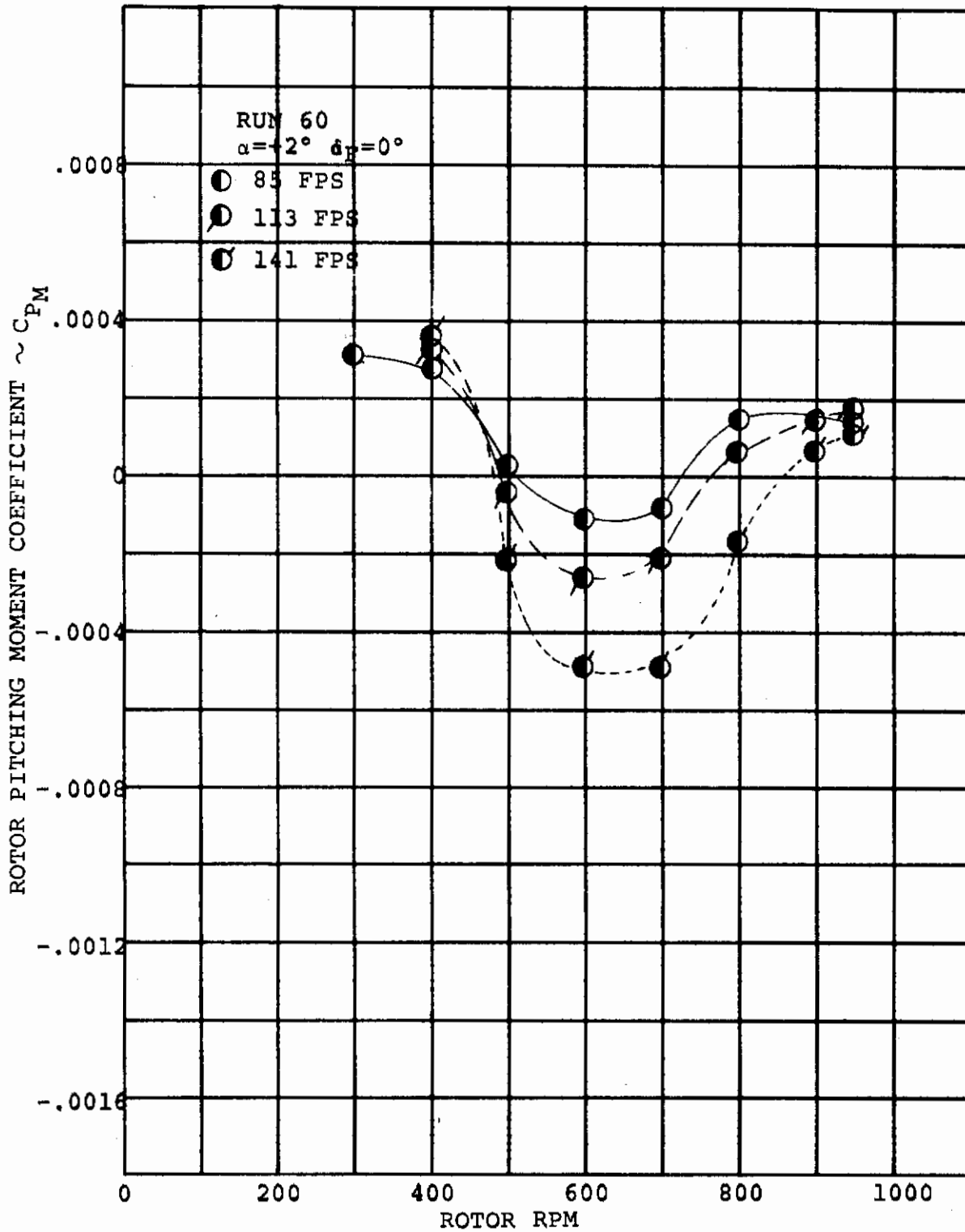


FIGURE B-9. ROTOR PITCHING MOMENT/RPM VARIATION  
FUSELAGE ATTITUDE =  $+2^\circ$   $\delta_F = 0^\circ$   
(STEADY WINDMILLING)

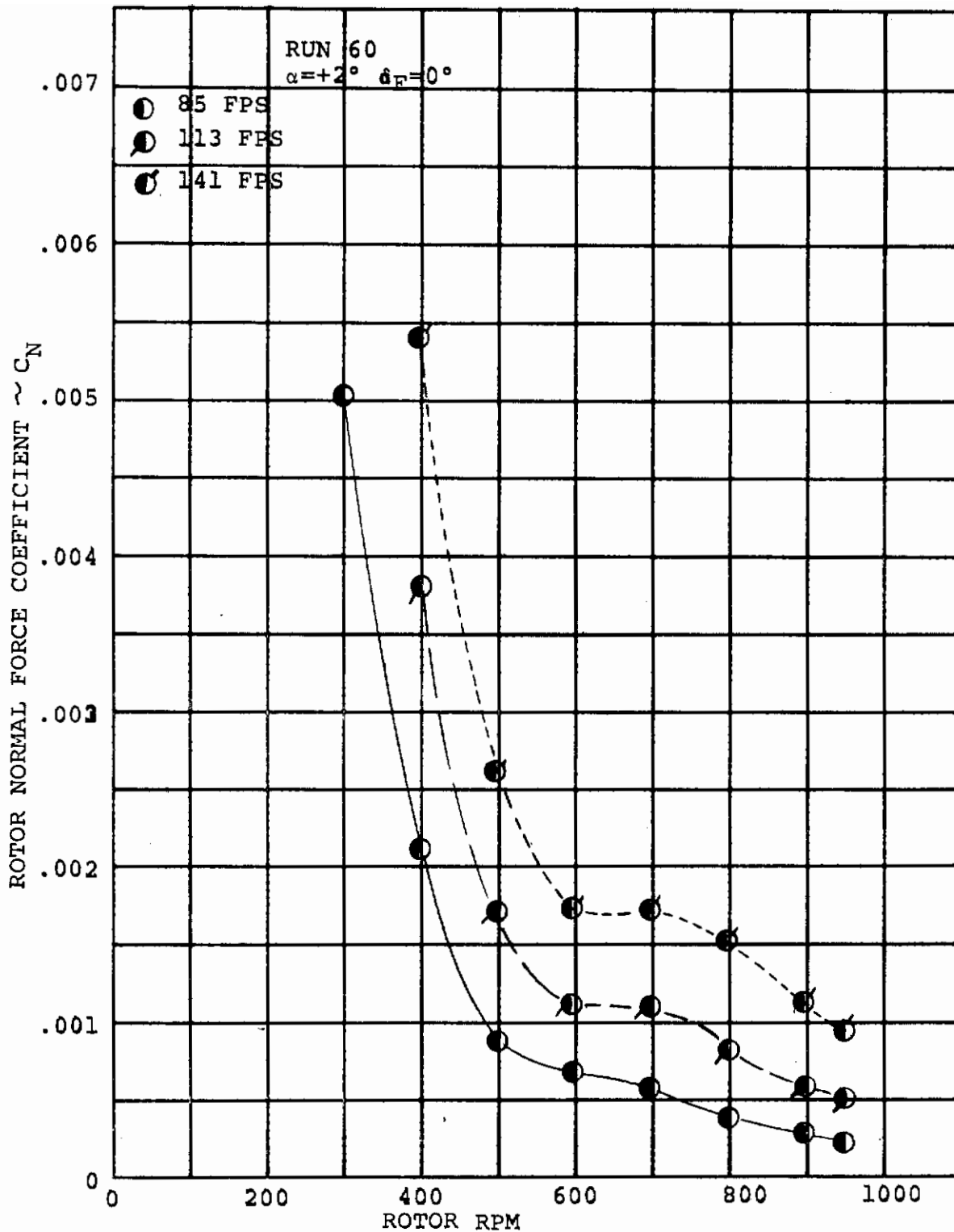


FIGURE B-10. ROTOR NORMAL FORCE/RPM VARIATION  
 FUSELAGE ATTITUDE =  $+2^\circ$   $\delta_F = 0^\circ$   
 (STEADY WINDMILLING)

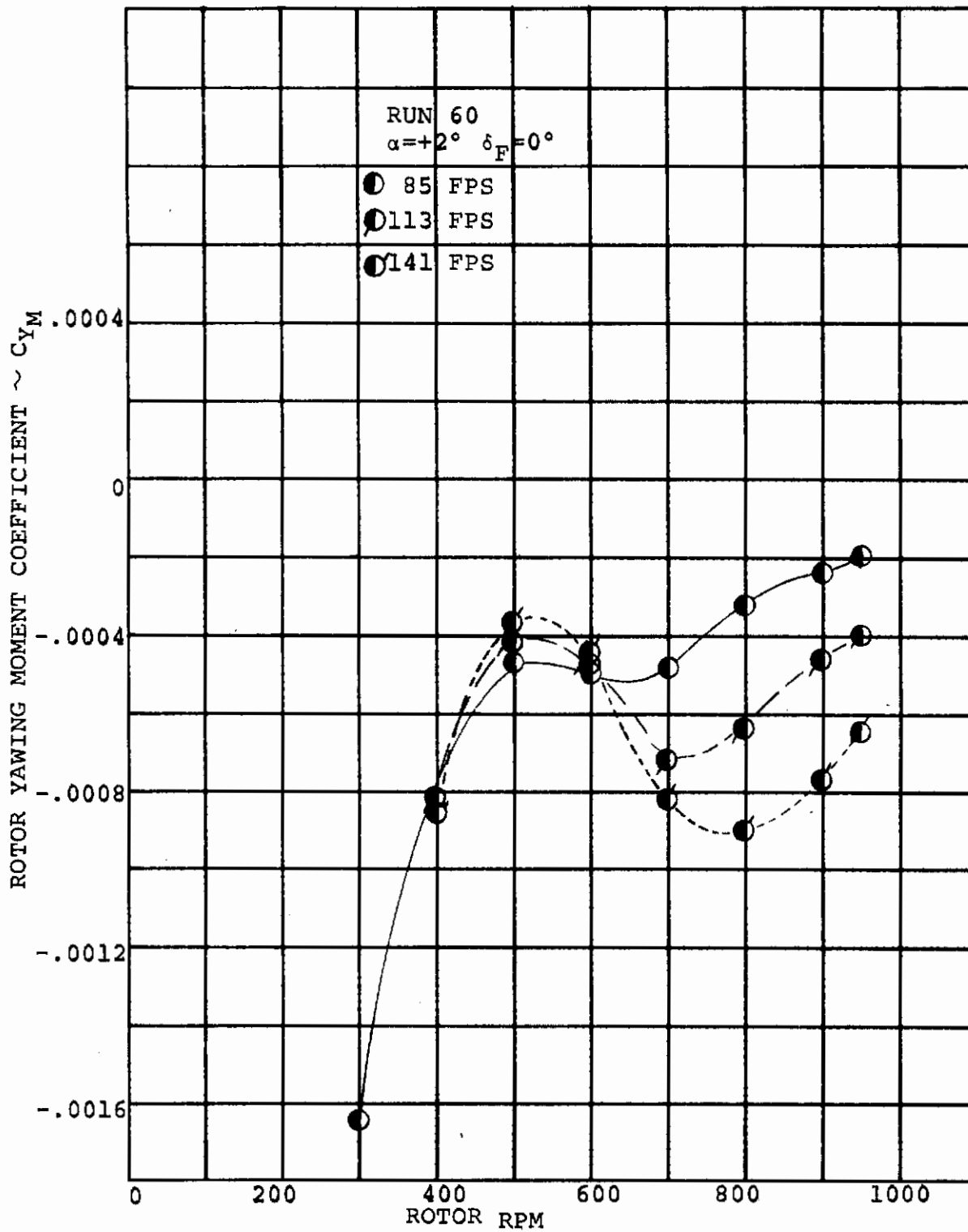


FIGURE B-11. ROTOR YAWING MOMENT/RPM VARIATION  
 FUSELAGE ATTITUDE  $= +2^\circ$   $\delta_F = 0^\circ$   
 (STEADY WINDMILLING)

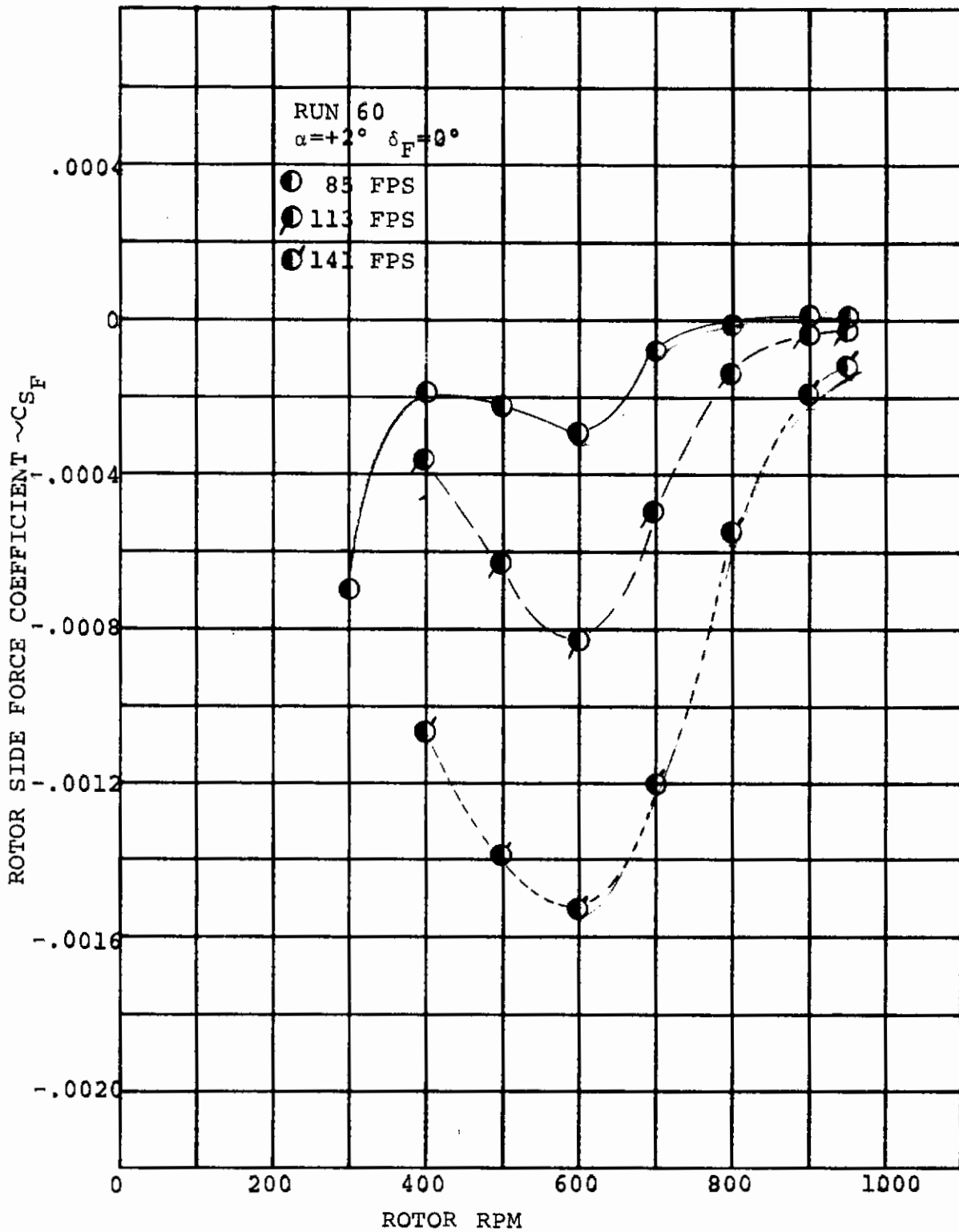


FIGURE B-12. ROTOR SIDE FORCE/RPM VARIATION  
 FUSELAGE ATTITUDE =  $+2^\circ$   $\delta_F = 0^\circ$   
 (STEADY WINDMILLING)

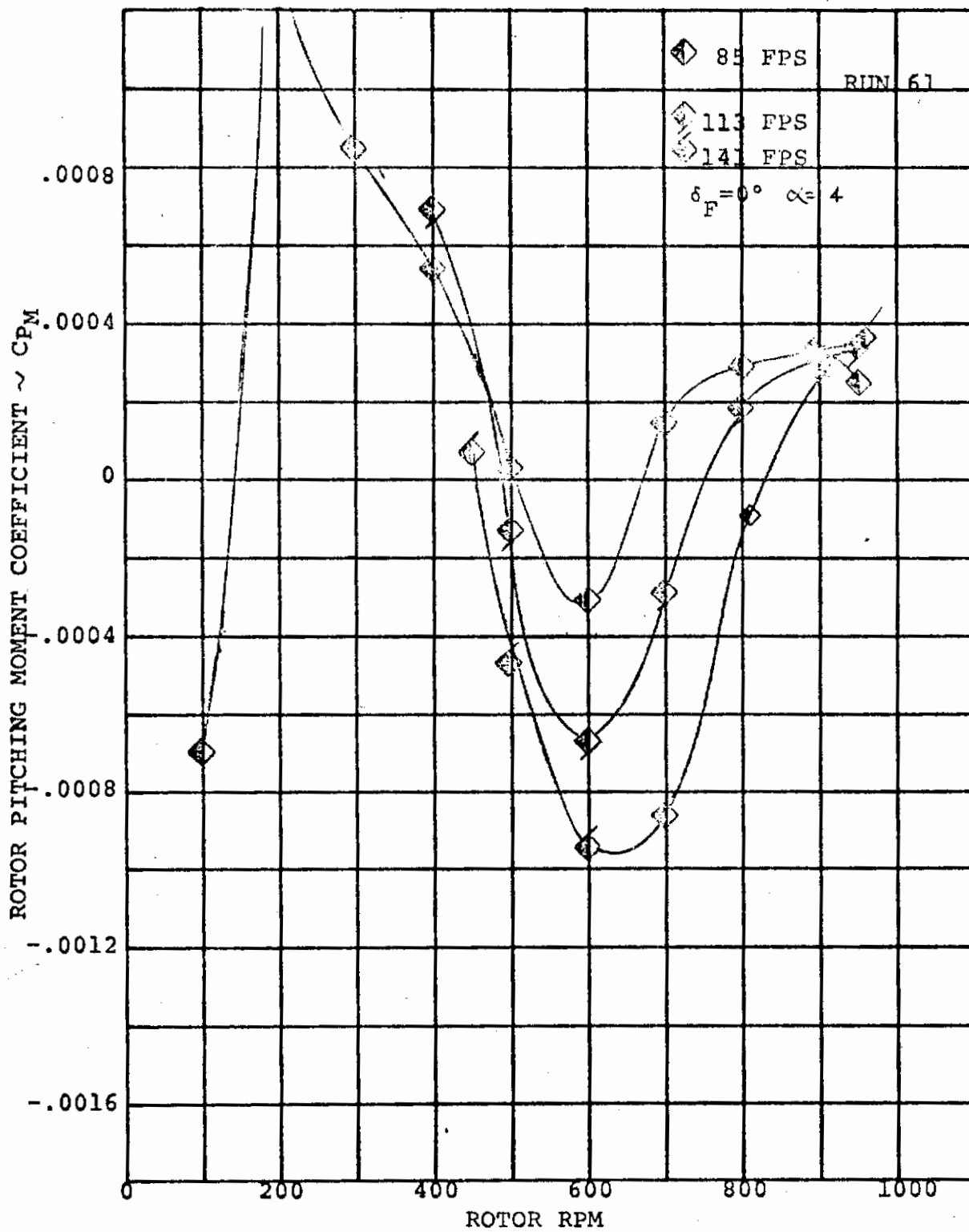


FIGURE B-13. ROTOR PITCHING MOMENT/RPM VARIATION  
 FUSELAGE ATTITUDE =  $4^\circ$   $\delta_F = 0^\circ$   
 (STEADY WINDMILLING)



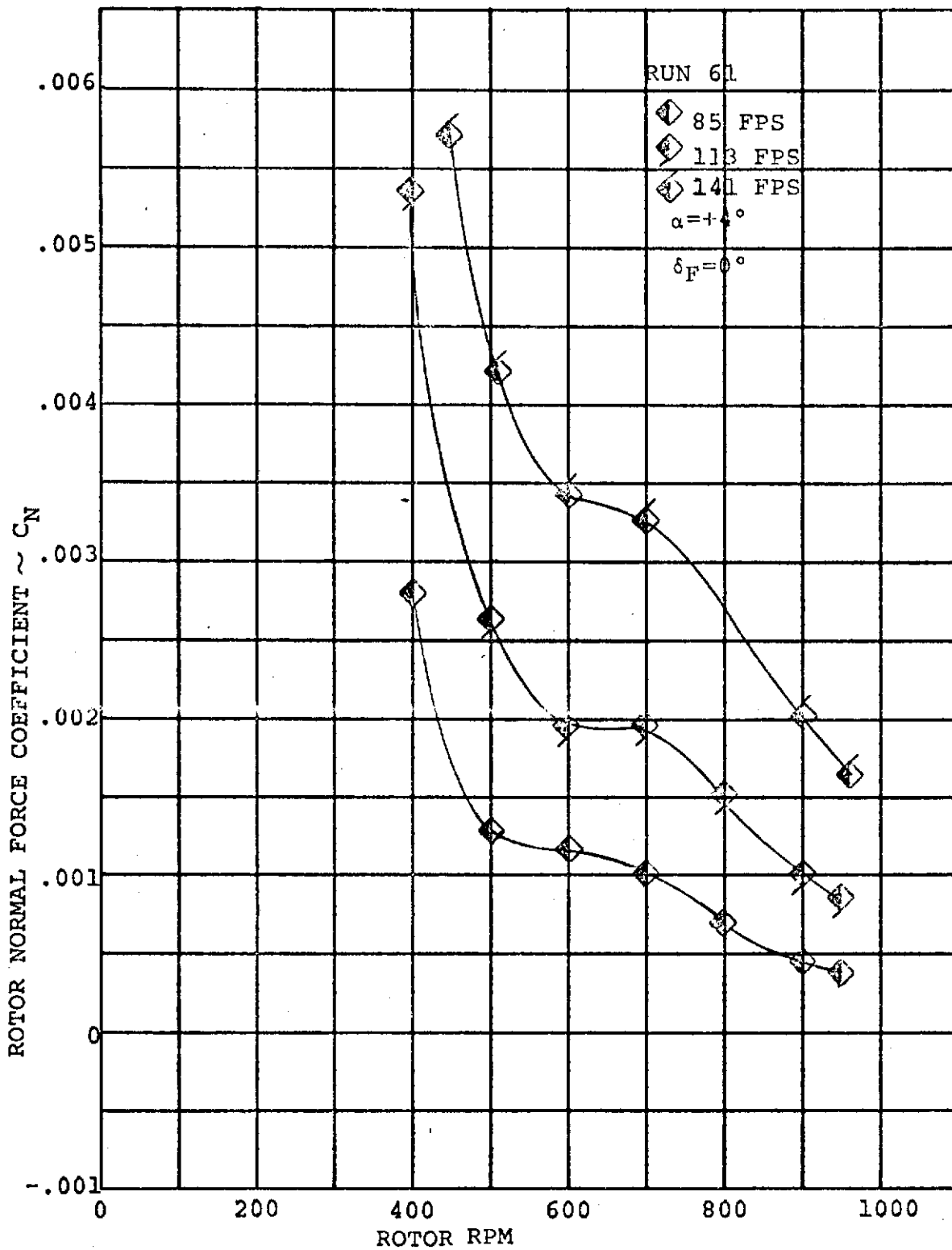


FIGURE B-14. ROTOR NORMAL FORCE/RPM VARIATION  
FUSELAGE ATTITUDE =  $+4^\circ$   $\delta_F = 0^\circ$   
(STEADY WINDMILLING)

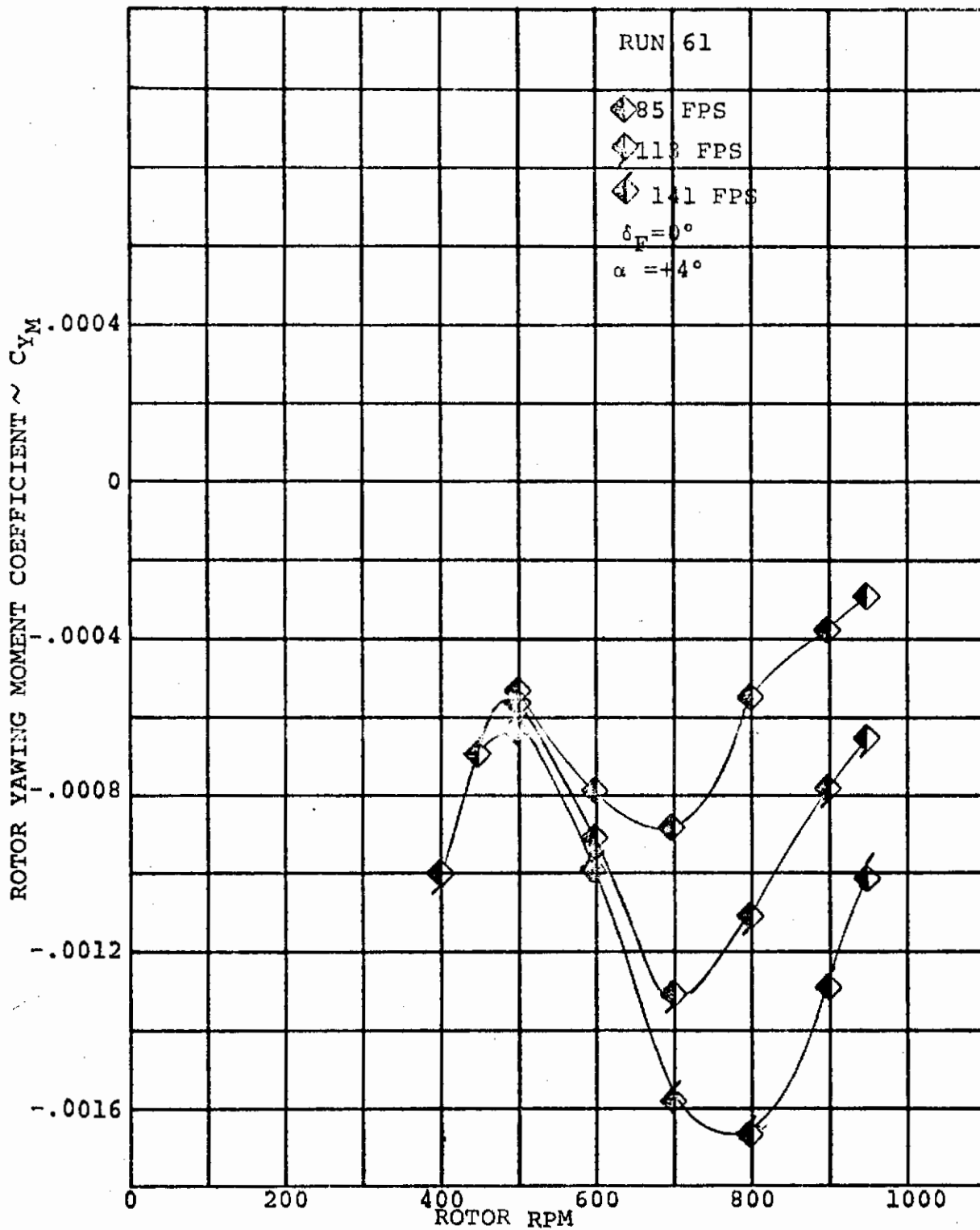


FIGURE B-15. ROTOR YAWING MOMENT/RPM VARIATION  
FUSELAGE ATTITUDE =  $+4^\circ$   $\delta_F = 0^\circ$   
(STEADY WINDMILLING)

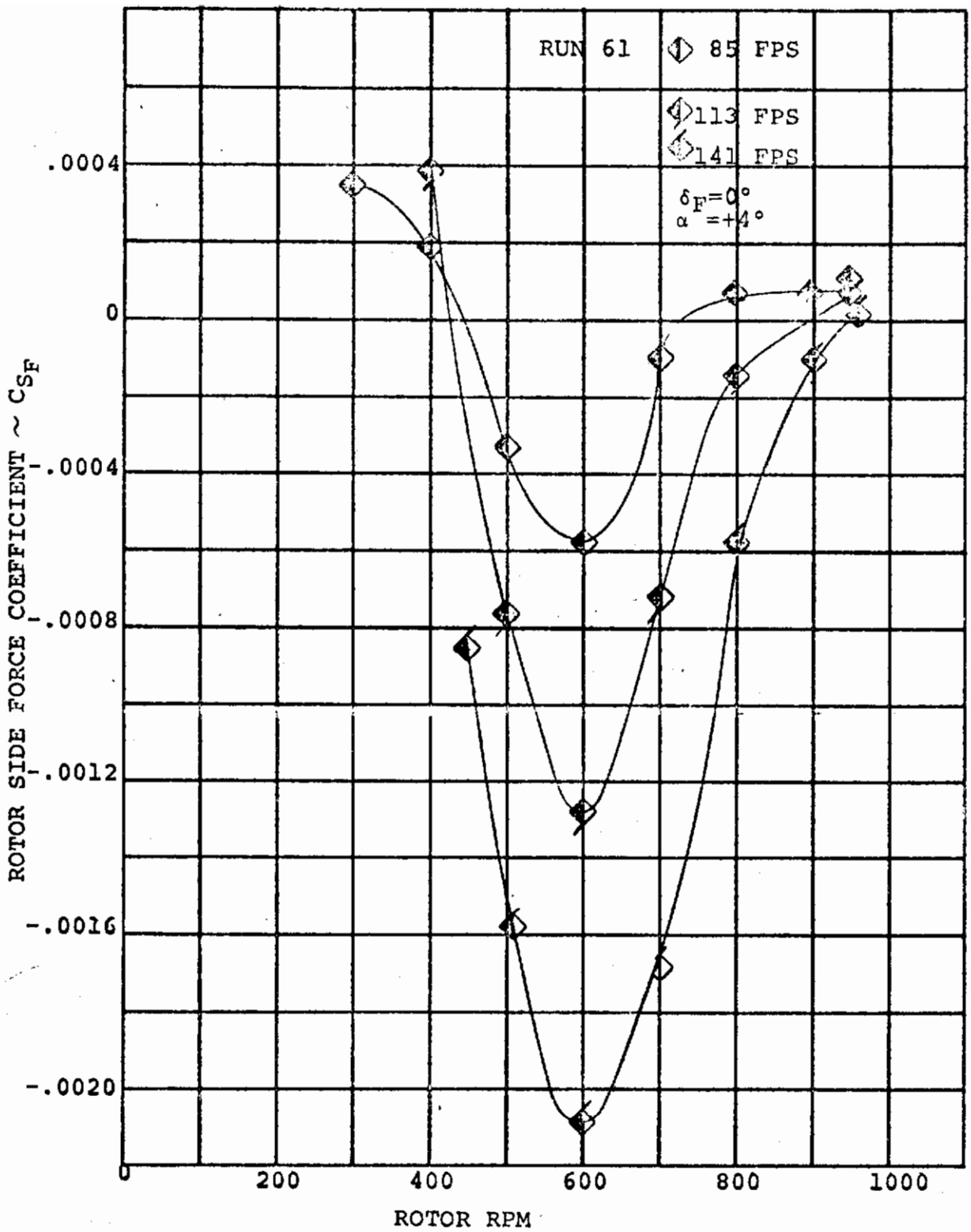


FIGURE B-16. ROTOR SIDE FORCE/RPM VARIATION  
FUSELAGE ATTITUDE  $= +4^\circ$   $\delta_F = 0^\circ$   
(STEADY WINDMILLING)

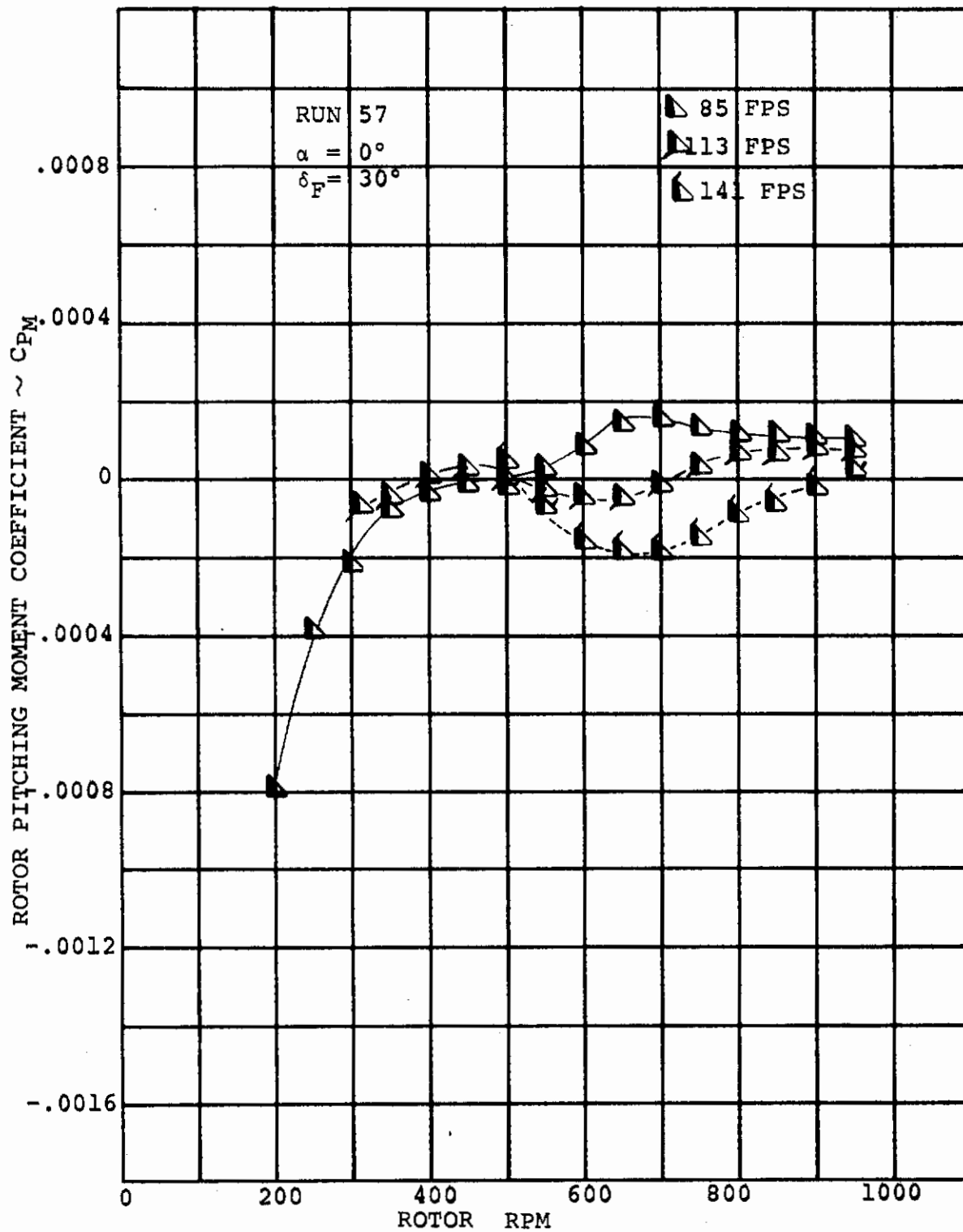


FIGURE B-17. ROTOR PITCHING MOMENT/RPM VARIATION  
 FUSELAGE ATTITUDE =  $0^\circ$   $\delta_F = 30^\circ$   
 (STEADY WINDMILLING)

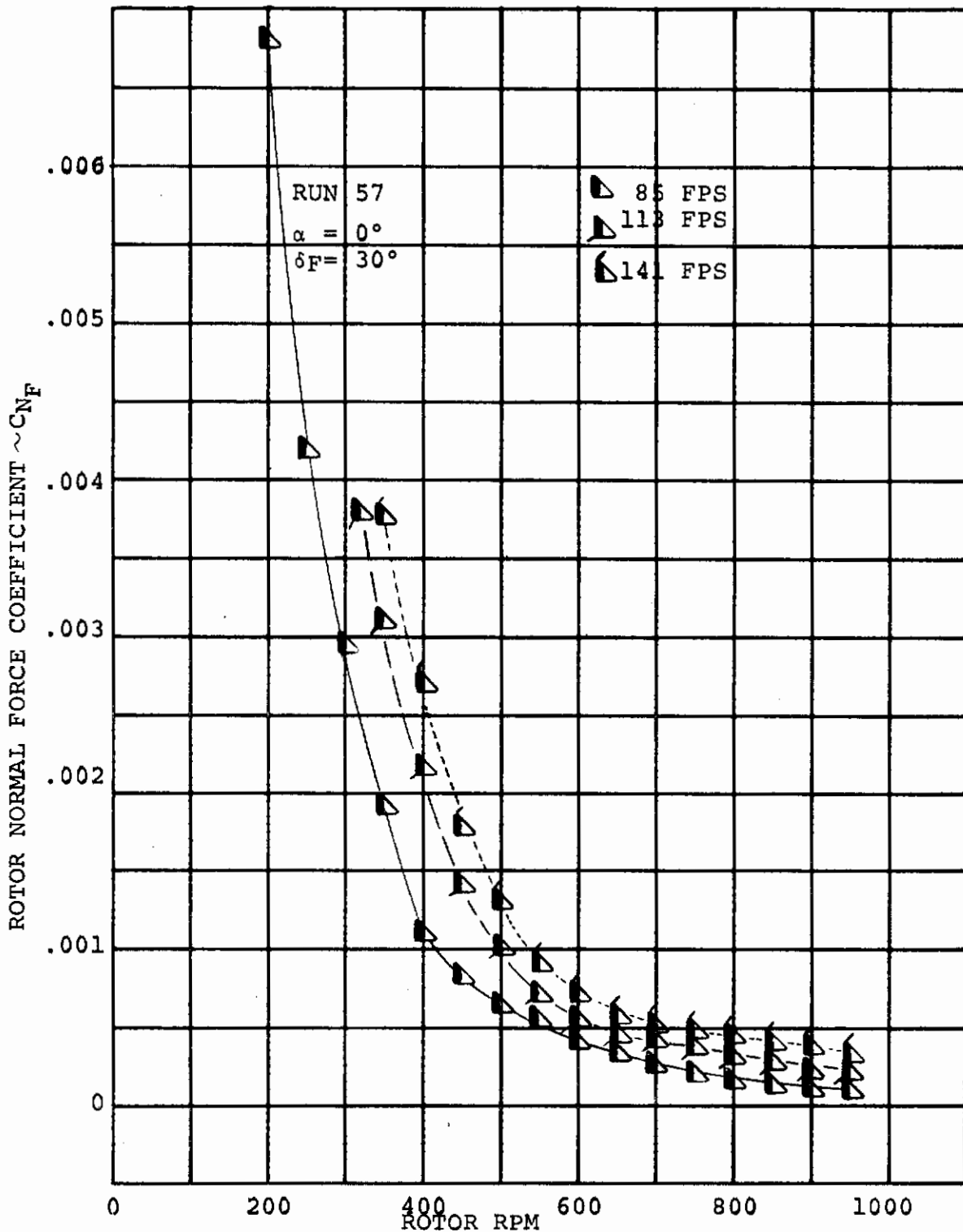


FIGURE B-18 ROTOR NORMAL FORCE/RPM VARIATION  
FUSELAGE ATTITUDE = 0°  $\delta F = 30^\circ$   
(STEADY WINDMILLING)

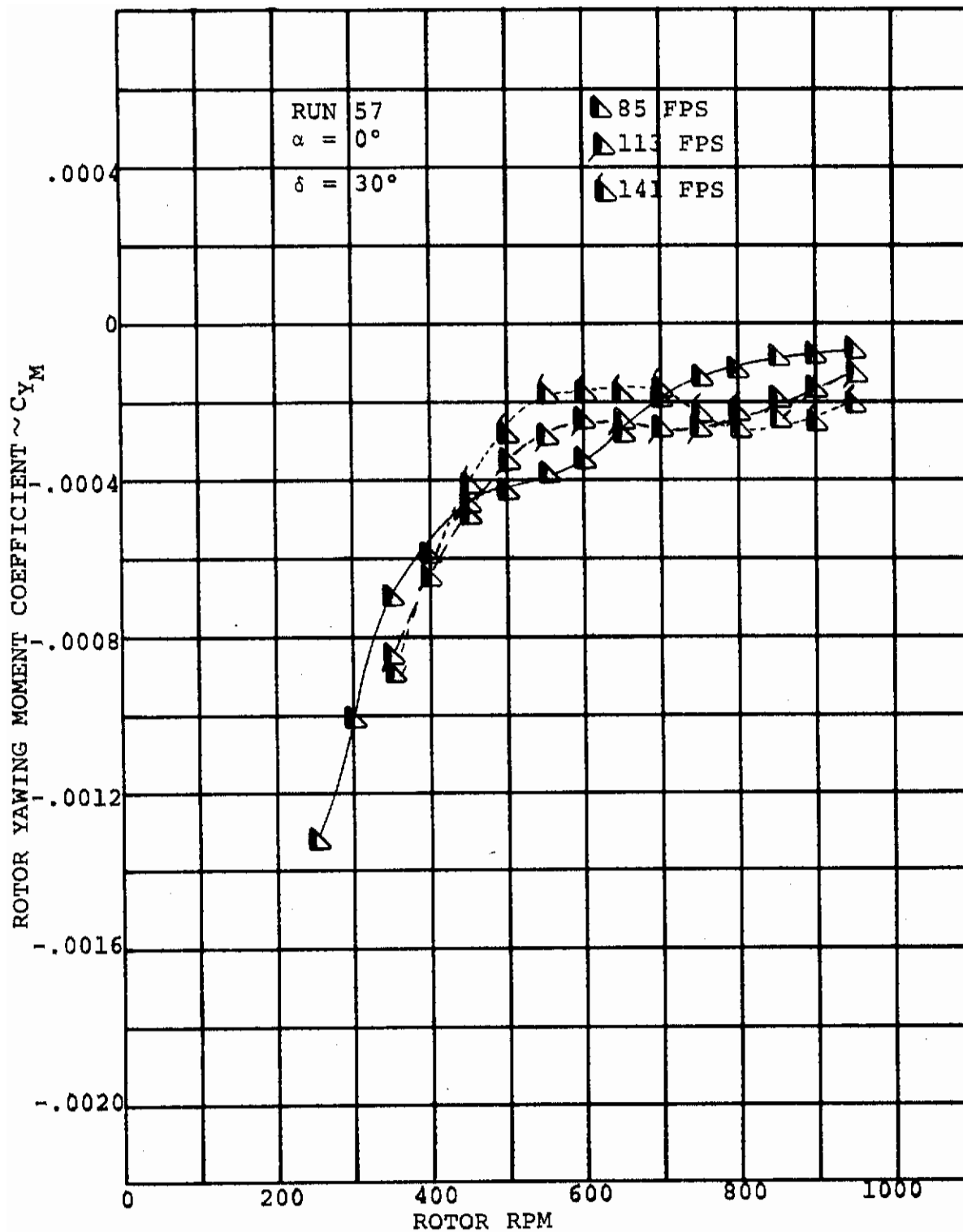


FIGURE B-19 ROTOR YAWING MOMENT/RPM VARIATION  
FUSELAGE ATTITUDE =  $0^\circ$   $\delta_F=30^\circ$   
(STEADY WINDMILLING)

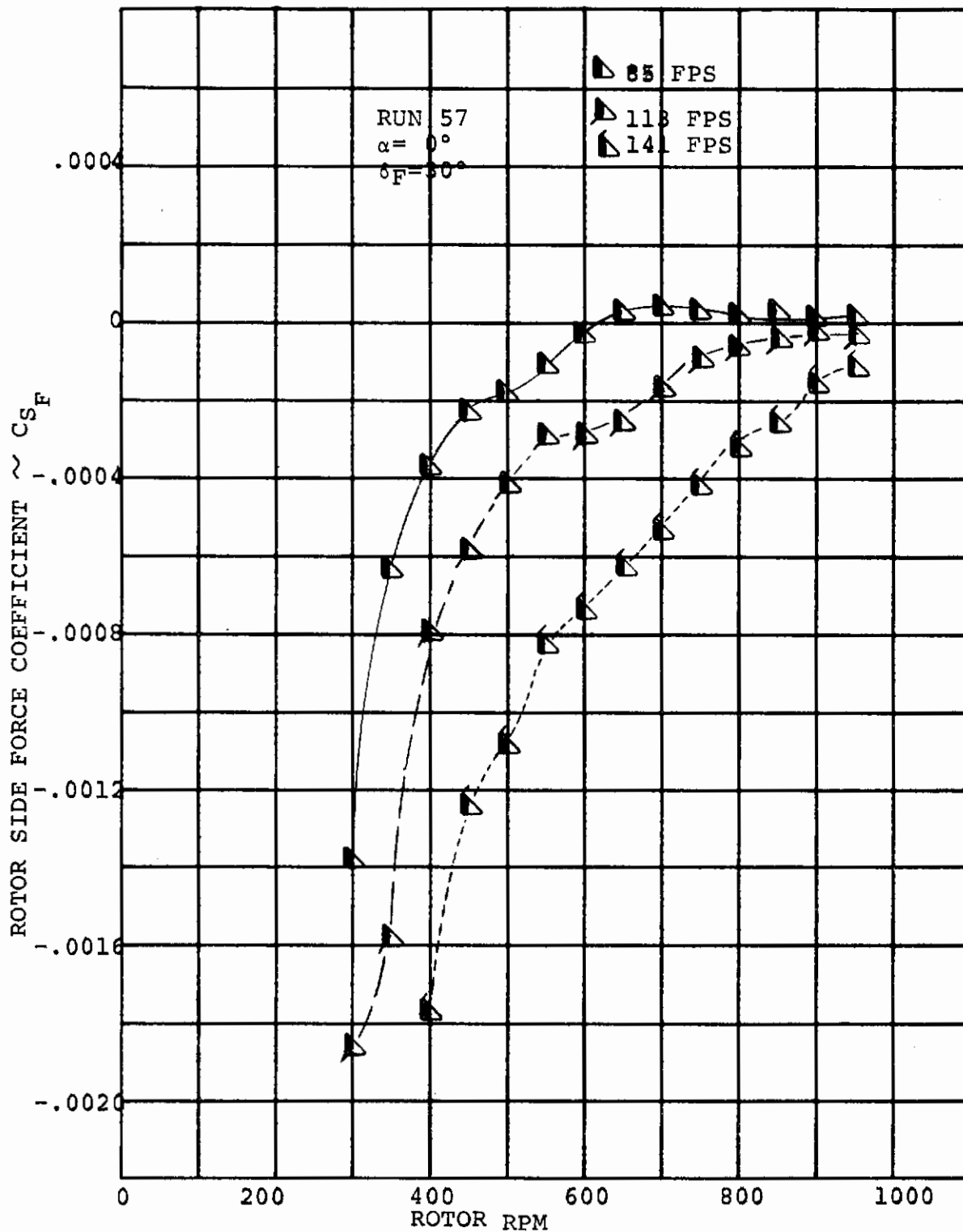


FIGURE B-20. ROTOR SIDE FORCE/RPM VARIATION  
 FUSELAGE ATTITUDE =  $0^\circ$   $\delta_F = 30^\circ$   
 (STEADY WINDMILLING)

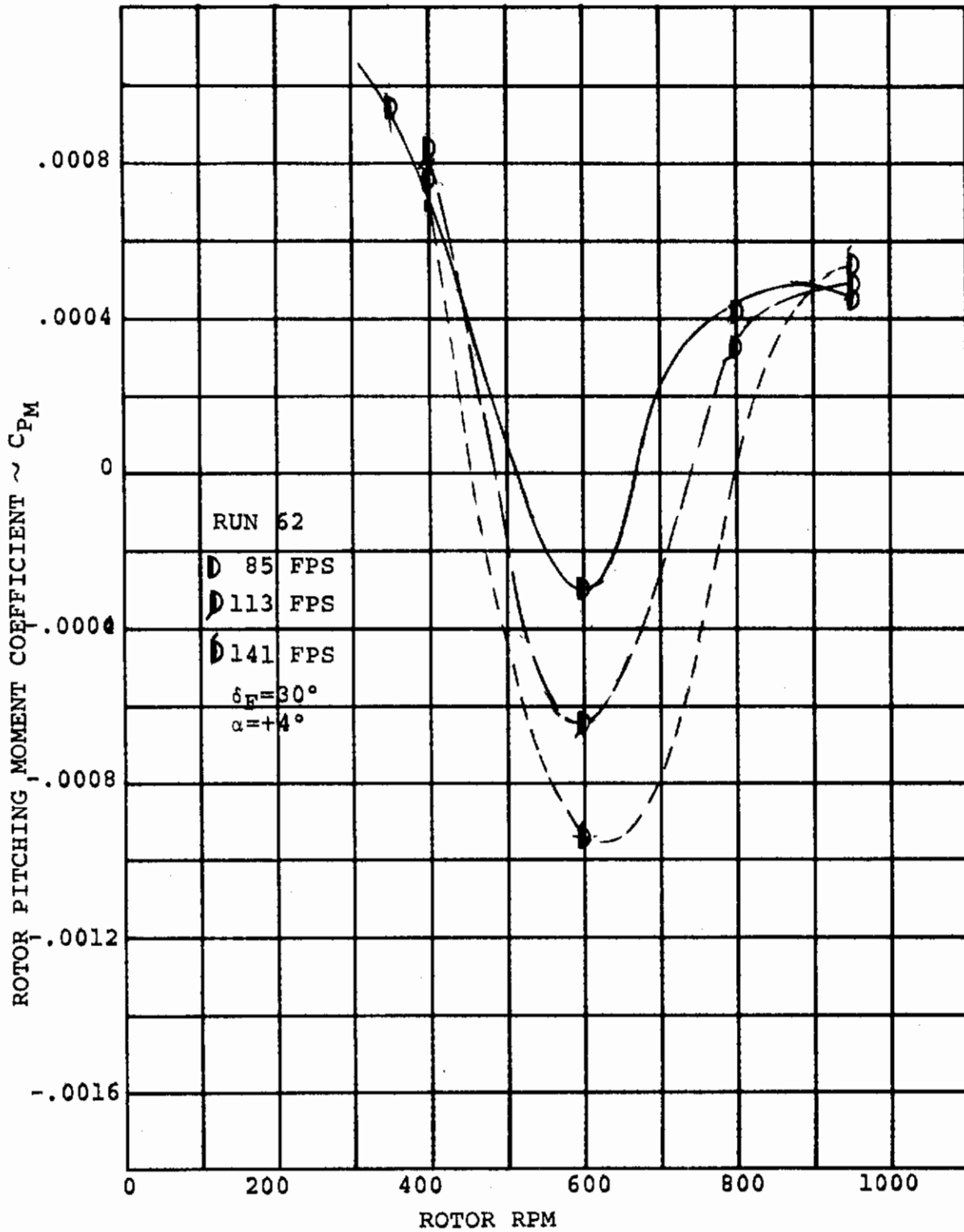


FIGURE B-2L. ROTOR PITCHING MOMENT/RPM VARIATION  
 FUSELAGE ATTITUDE =  $+4^\circ$   $\delta_F = 30^\circ$   
 (STEADY WINDMILLING)



# Contrails

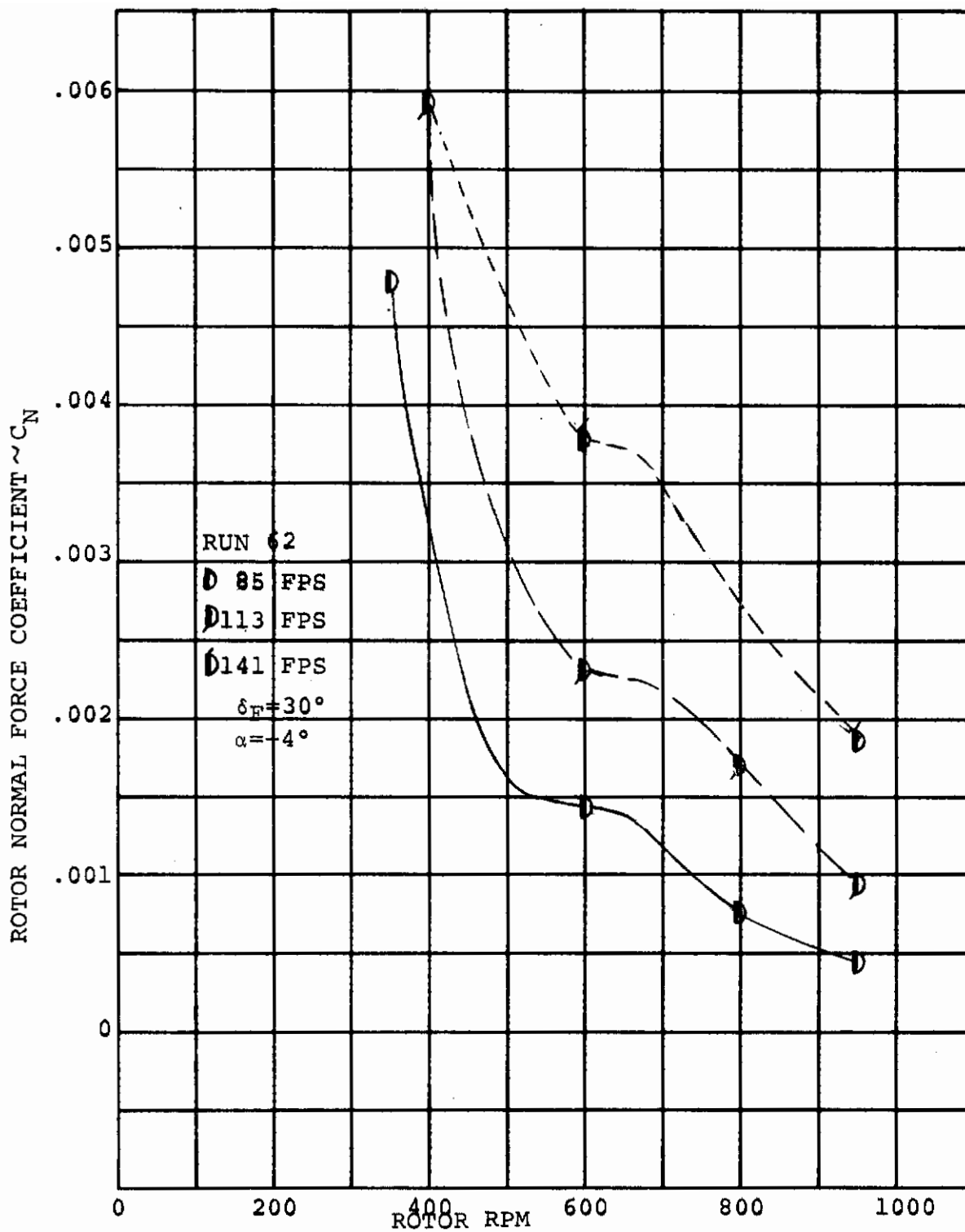


FIGURE B-22 ROTOR NORMAL FORCE/RPM VARIATION  
FUSELAGE ATTITUDE =  $+4^\circ$   $\delta_F = 30^\circ$   
(STEADY WINDMILLING)

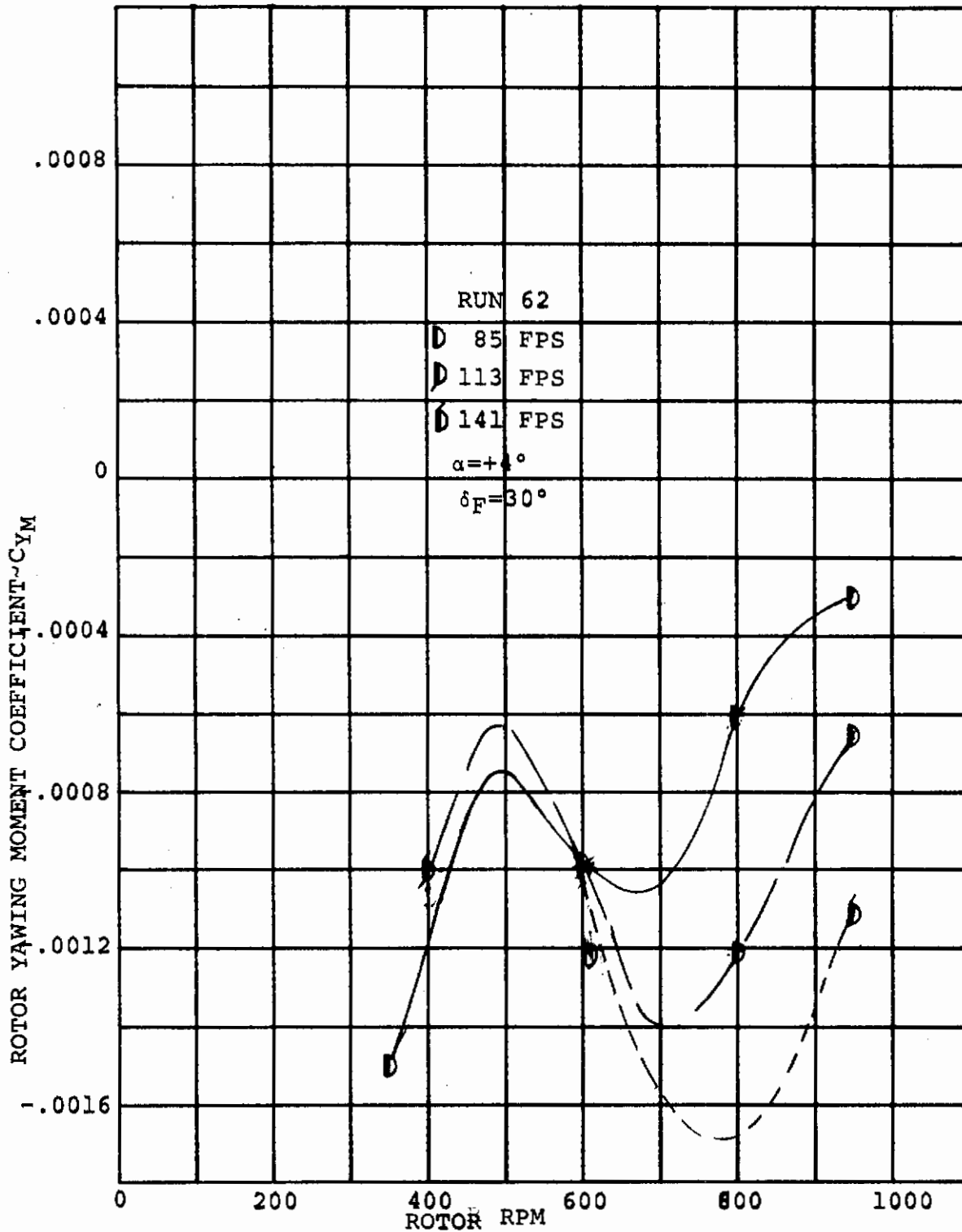


FIGURE B-23 ROTOR YAWING MOMENT/RPM VARIATION  
 FUSELAGE ATTITUDE  $= +4^\circ$   $\delta_F = 30^\circ$   
 (STEADY WINDMILLING)

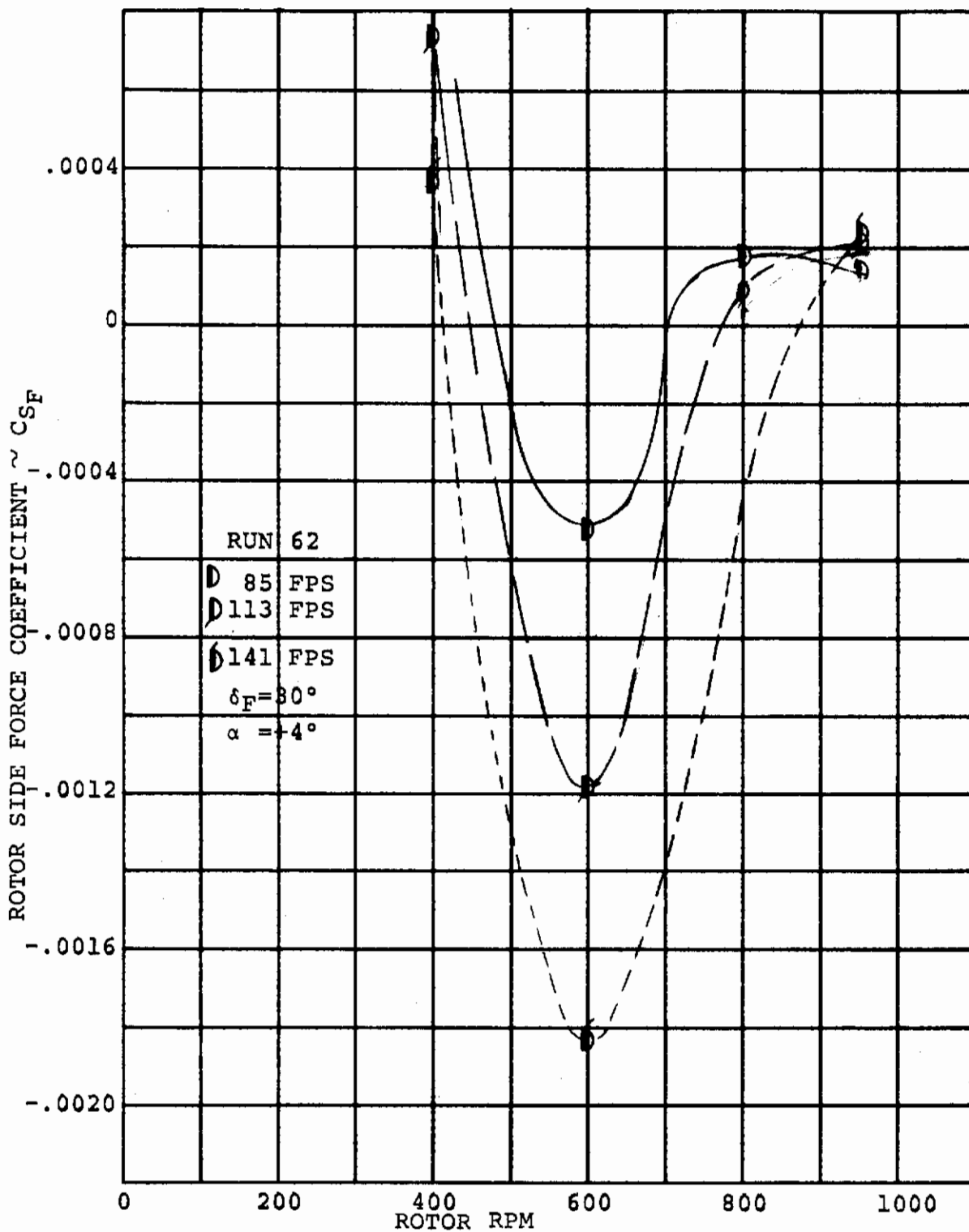


FIGURE B-24. ROTOR SIDE FORCE/RPM VARIATION  
FUSELAGE ATTITUDE  $+4^\circ$   $\delta_F = 30^\circ$   
(STEADY WINDMILLING)

## APPENDIX C

### CIRCULATION EFFECTS ON ROTOR CHARACTERISTICS

The rotor characteristics shown in Section 6 were plotted against airframe lift at constant nacelle angle of attack. This is done to provide a means of extrapolating back to zero lift and define data that is representative of an isolated rotor.

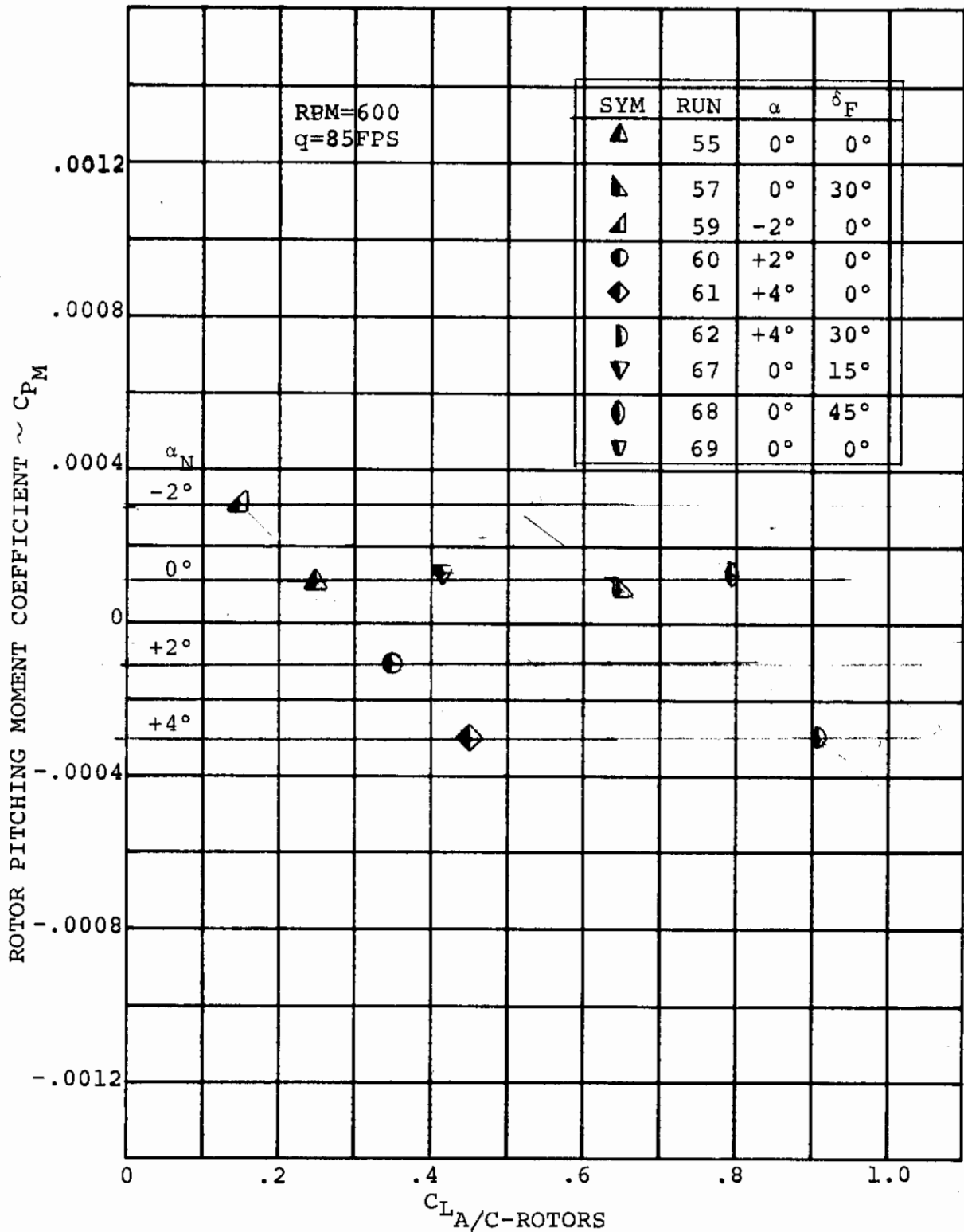


FIGURE C-1. EFFECT OF WING LIFT ON ROTOR PITCHING MOMENT  
(V = 85 FPS, RPM=600)

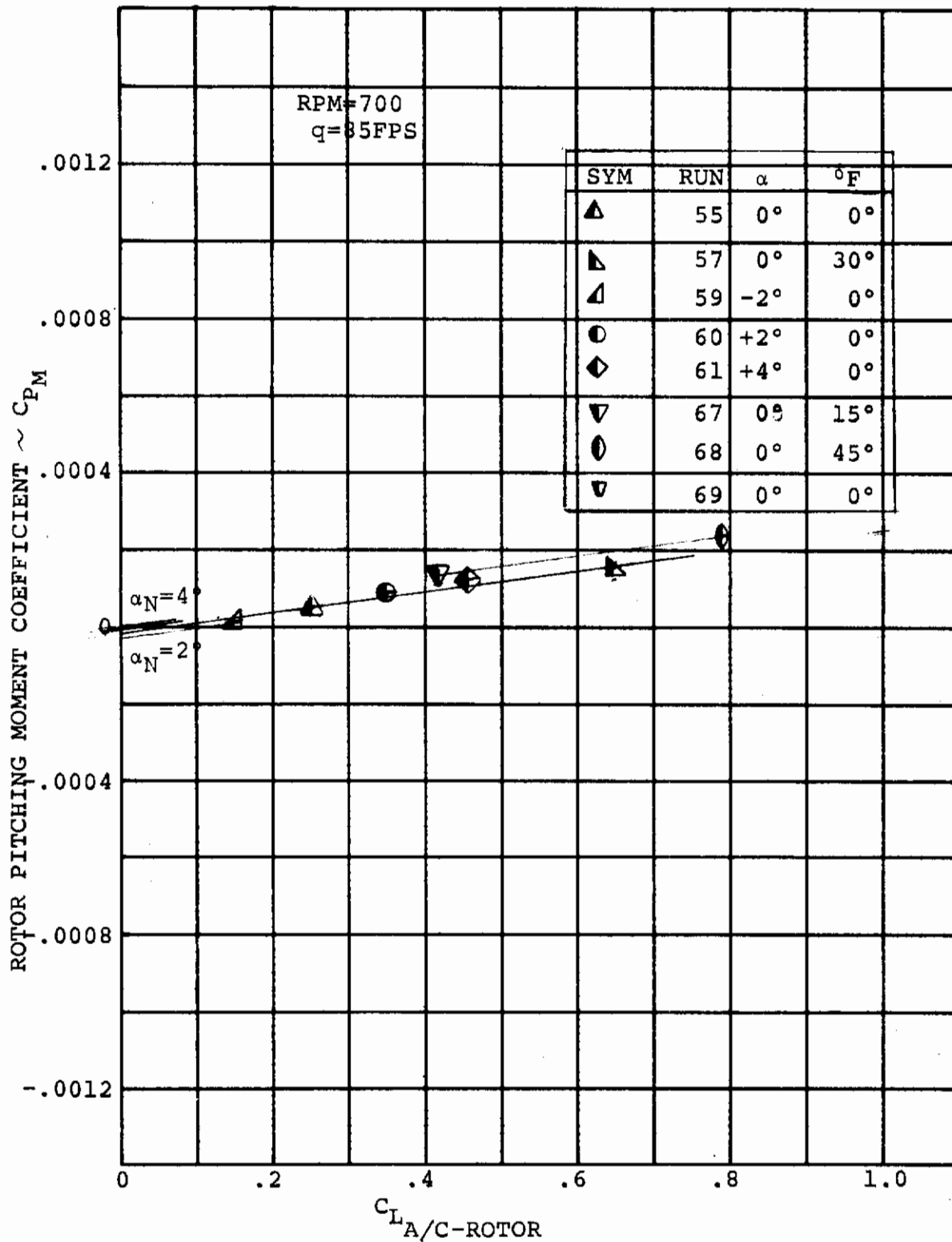


FIGURE C-2. EFFECT OF WING LIFT ON ROTOR PITCHING MOMENT  
(V = 85 FPS, RPM = 700)

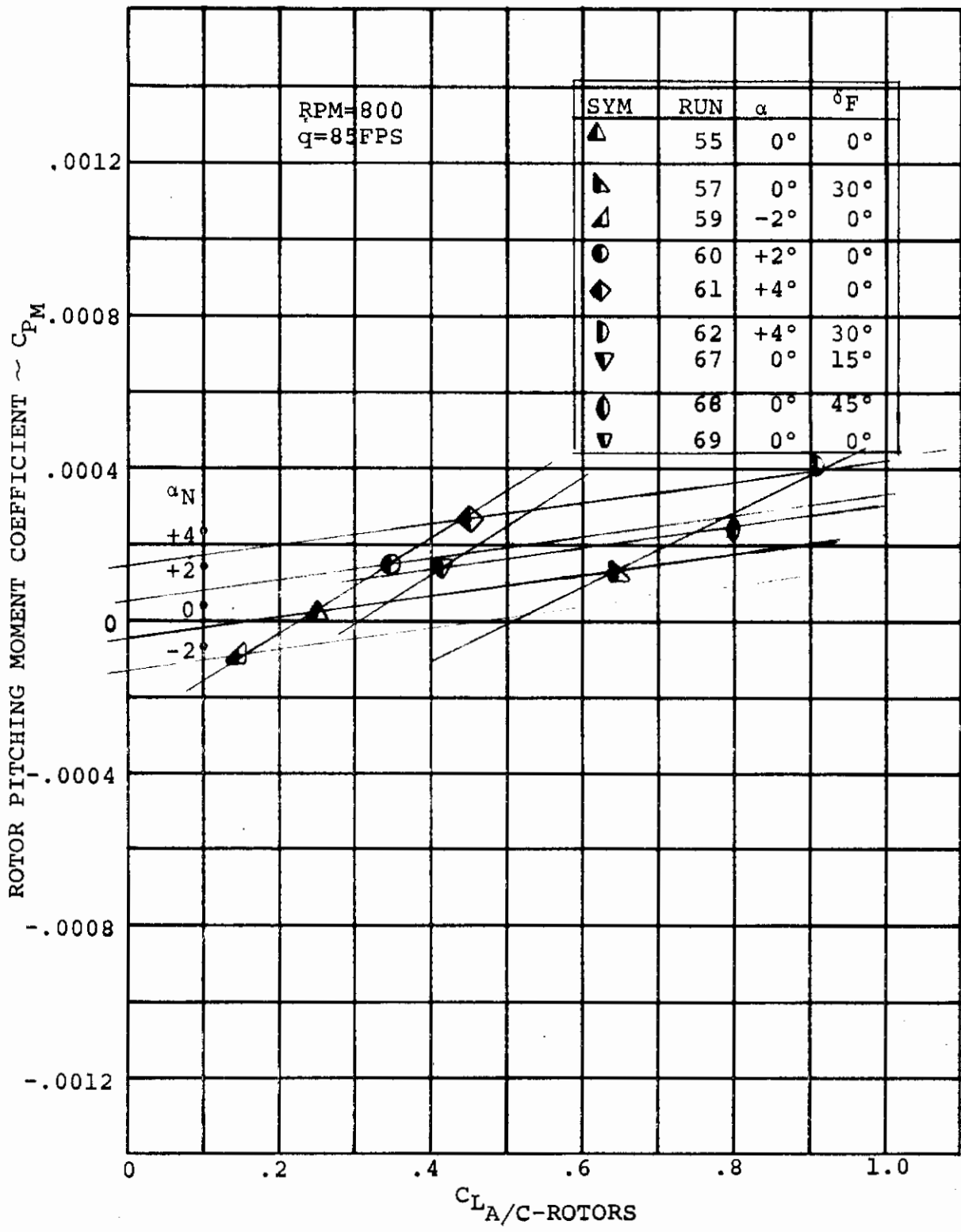


FIGURE C-3. EFFECT OF WING LIFT ON ROTOR PITCHING MOMENT (V = 85 FPS, RPM = 800)

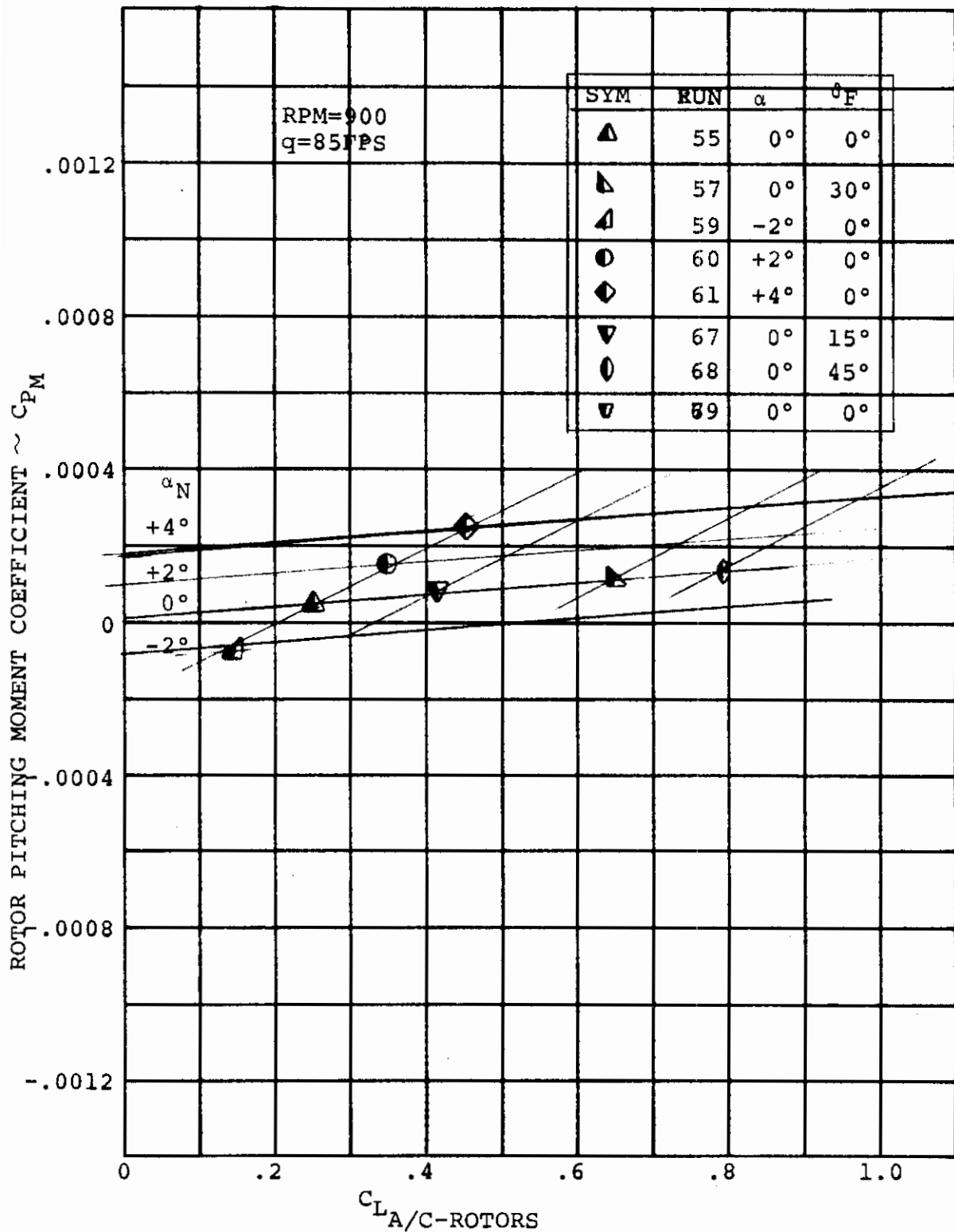


FIGURE C-4 EFFECT OF WING LIFT ON ROTOR PITCHING MOMENT  
(V = 85 FPS, RPM = 900)



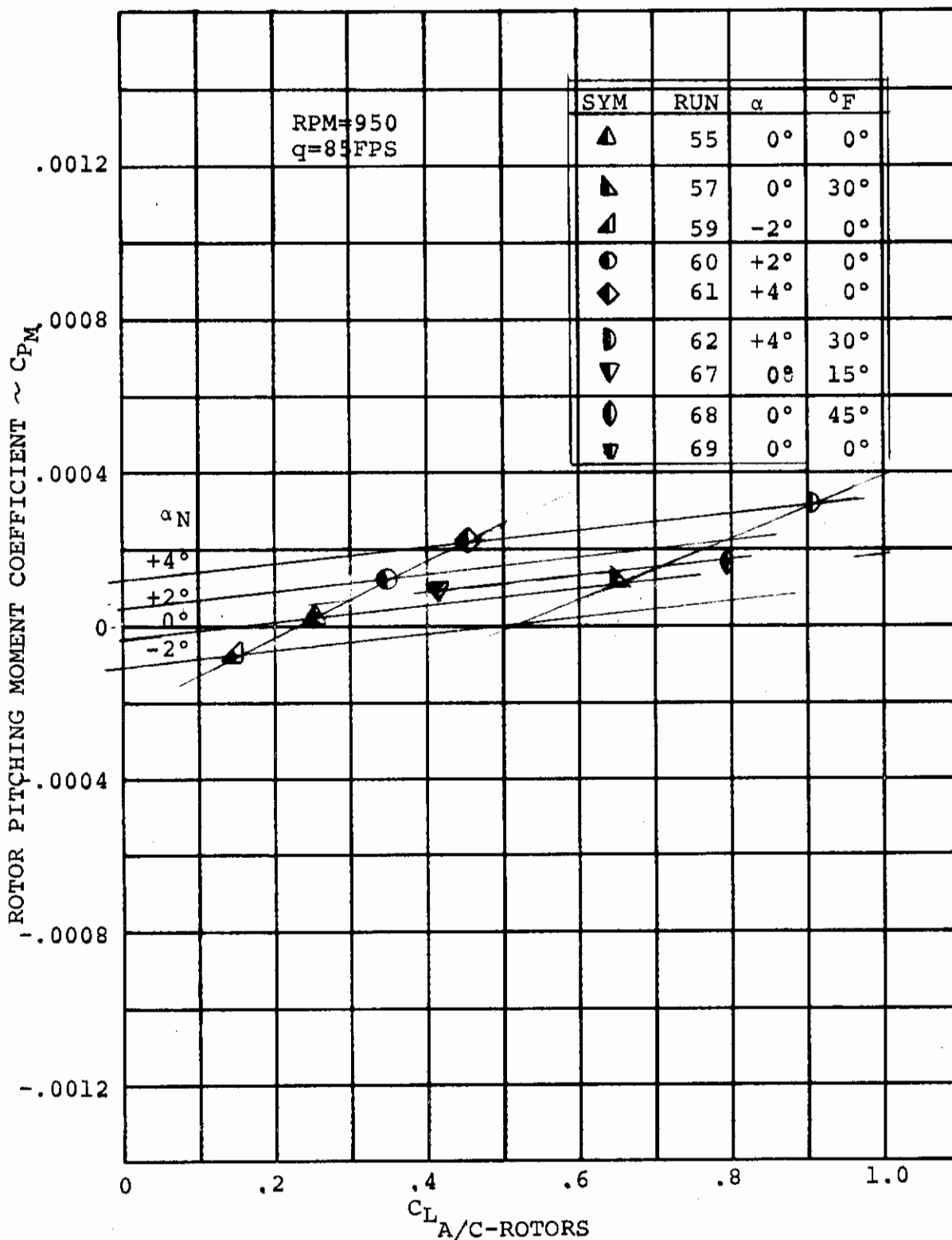


FIGURE C-5 EFFECT OF WING LIFT ON ROTOR PITCHING MOMENT  
(V = 85 FPS, RPM = 950)

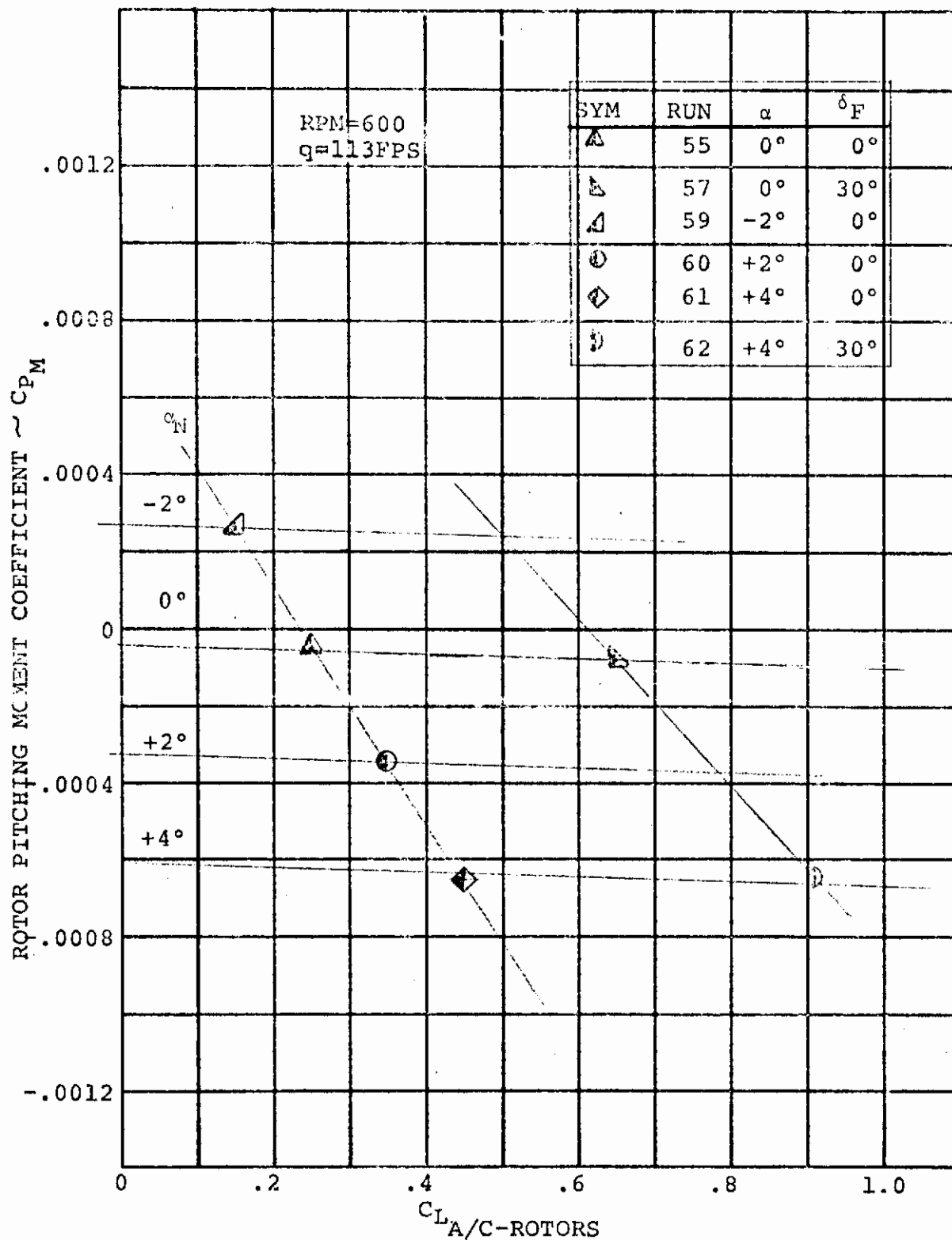


FIGURE C-6 EFFECT OF WING LIFT ON ROTOR PITCHING MOMENT  
(V = 113 FPS, RPM = 600)

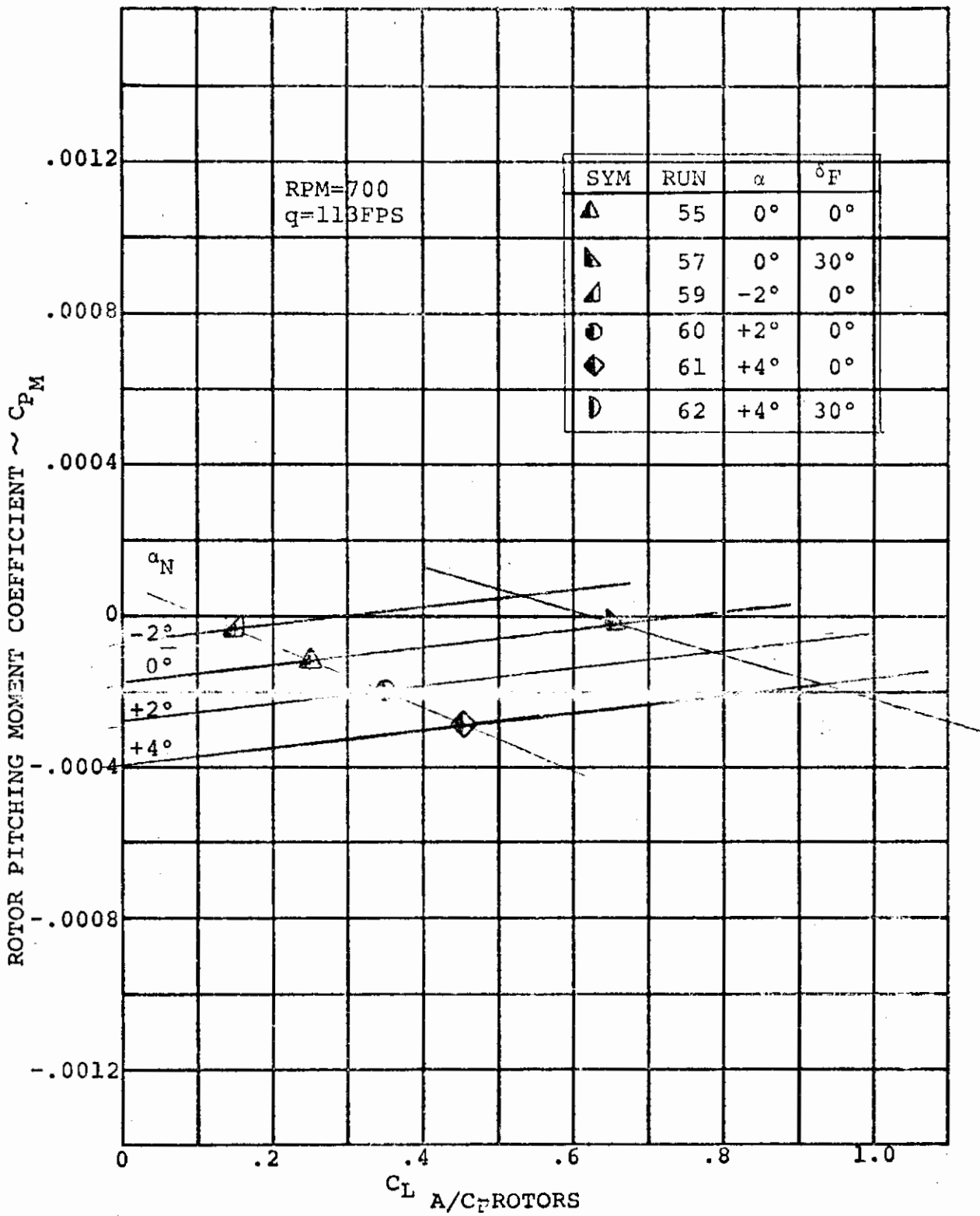


FIGURE C-7 EFFECT OF WING LIFT ON ROTOR PITCHING MOMENT  
(V = 113 FPS, RPM = 700)

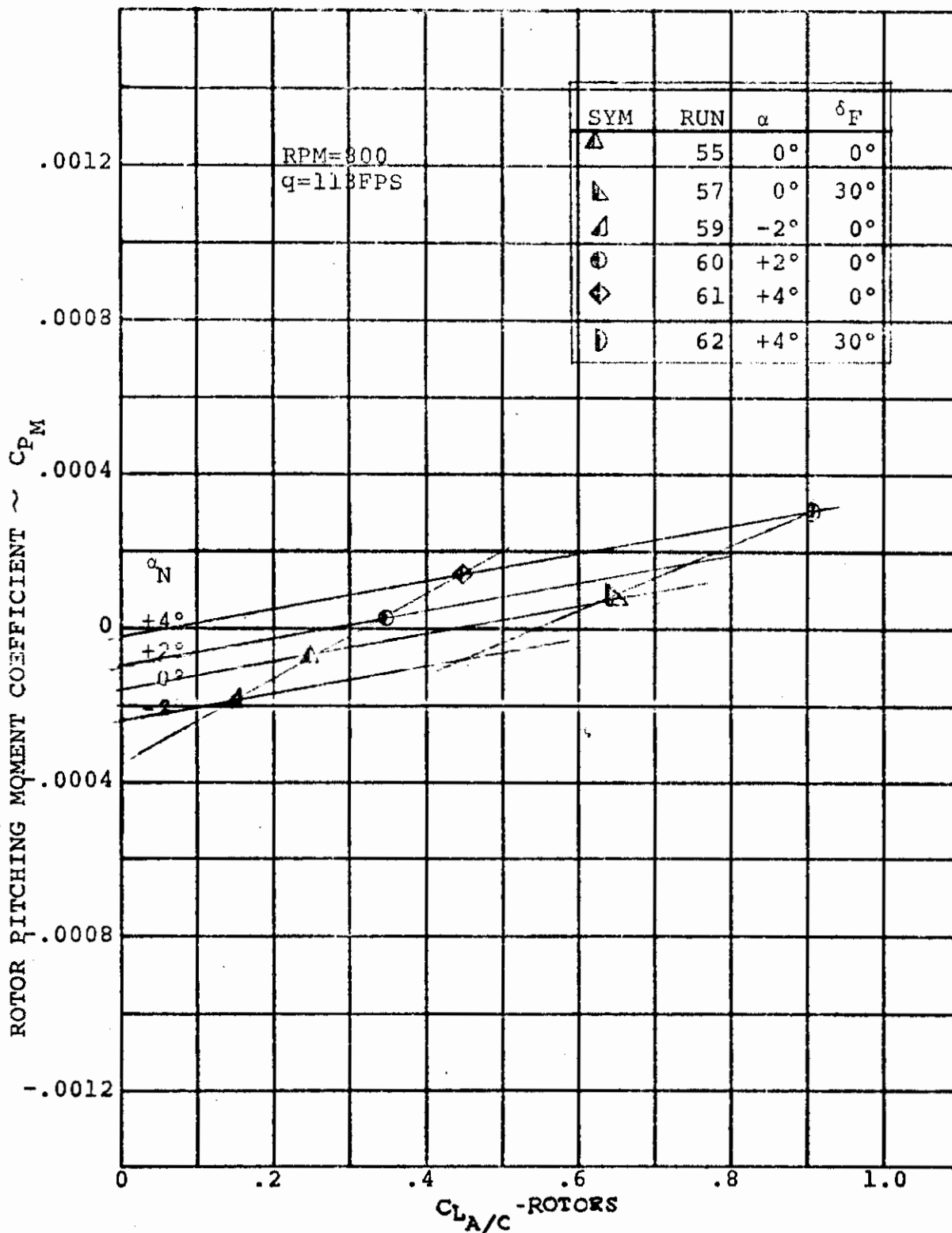


FIGURE C-8 EFFECT OF WING LIFT ON ROTOR PITCHING MOMENT  
(V = 113 FPS, RPM = 800)

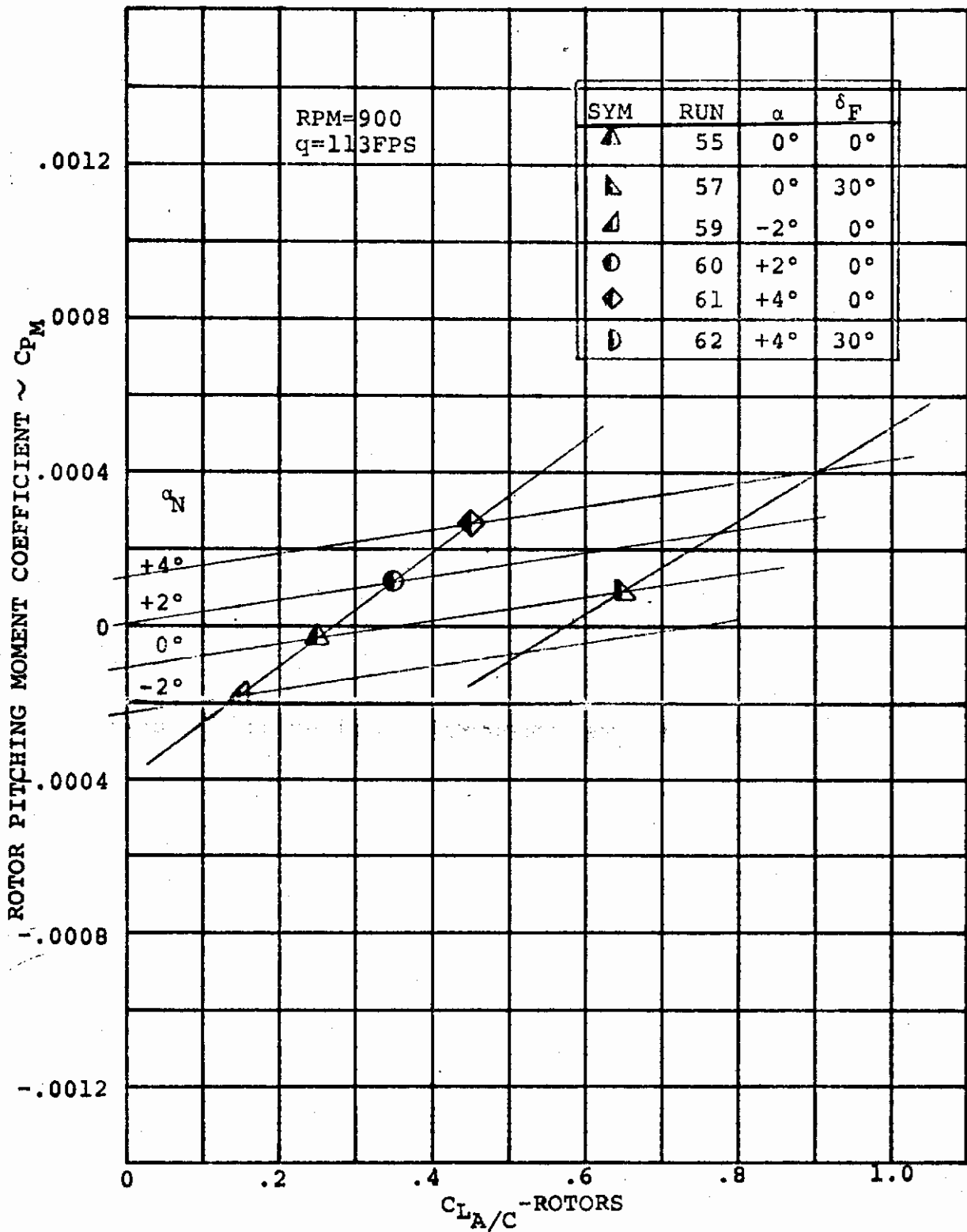


FIGURE C-9 EFFECT OF WING LIFT ON ROTOR PITCHING MOMENT  
(V = 113 FPS, RPM = 900)

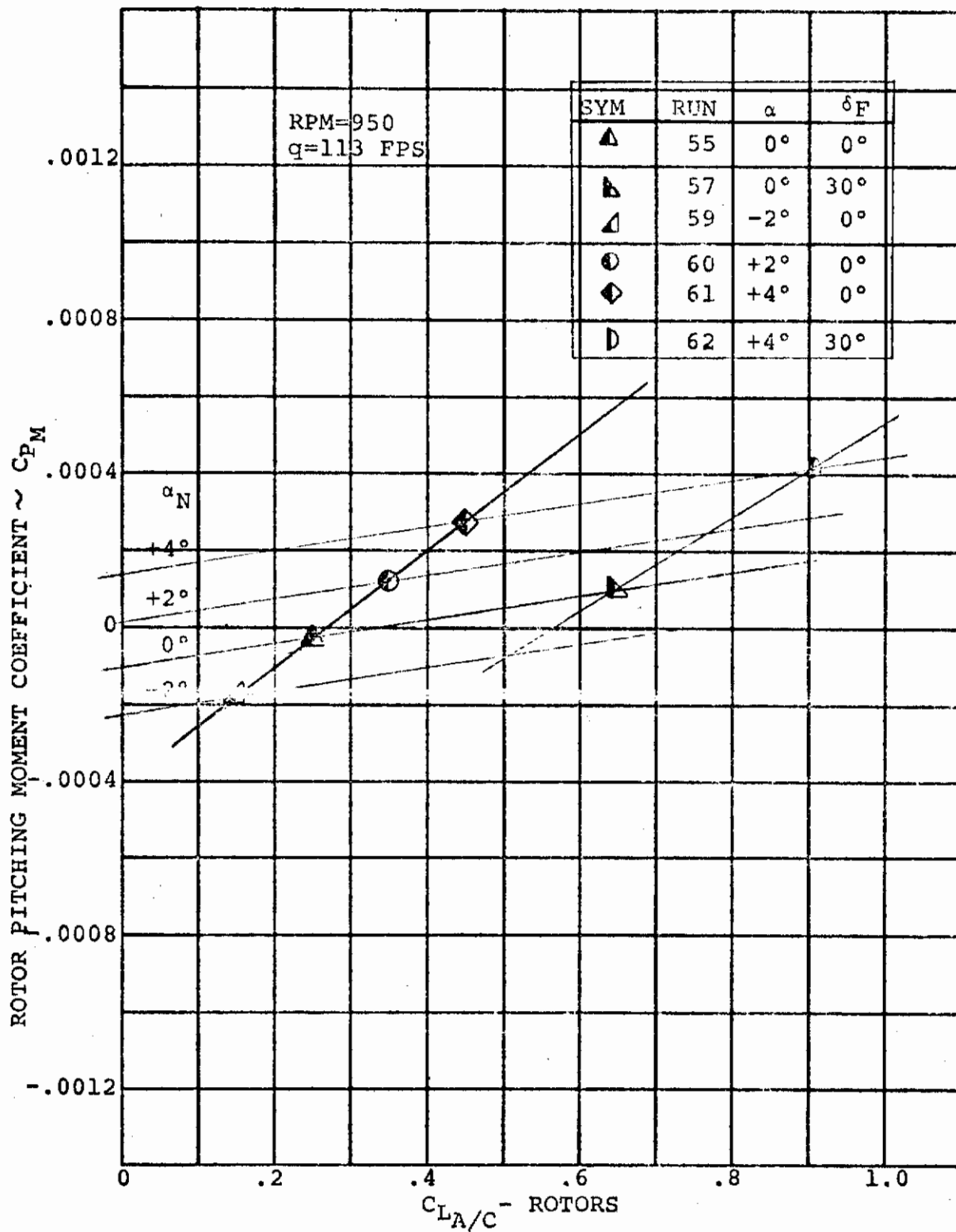


FIGURE C-10 EFFECT OF WING LIFT ON ROTOR PITCHING MOMENT  
(V = 113 FPS, RPM = 950)

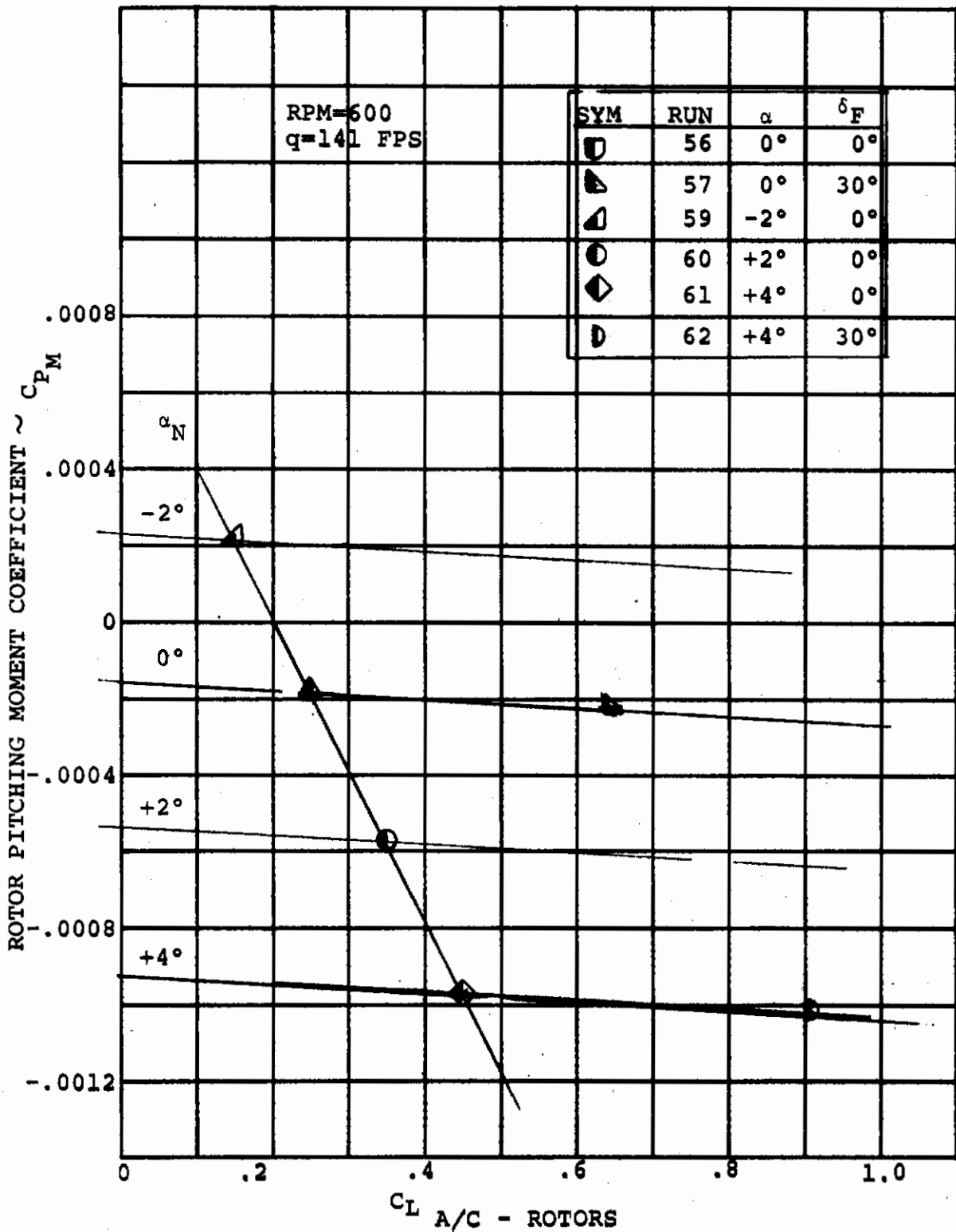


FIGURE C-11 EFFECT OF WING LIFT ON ROTOR PITCHING MOMENT  
(V = 141 FPS, RPM = 600)

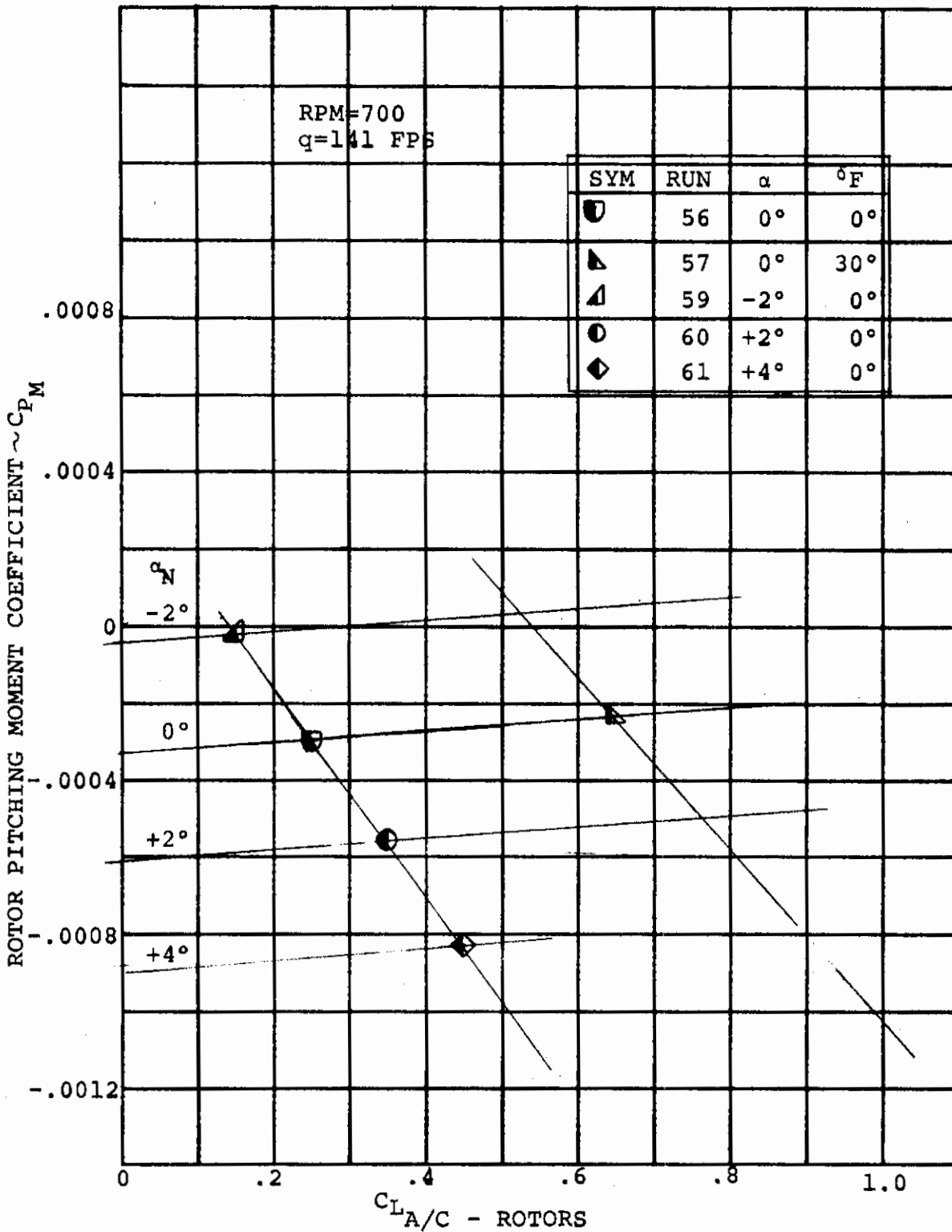


FIGURE C-12 EFFECT OF WING LIFT ON ROTOR PITCHING MOMENT  
(V = 141 FPS, RPM = 700)



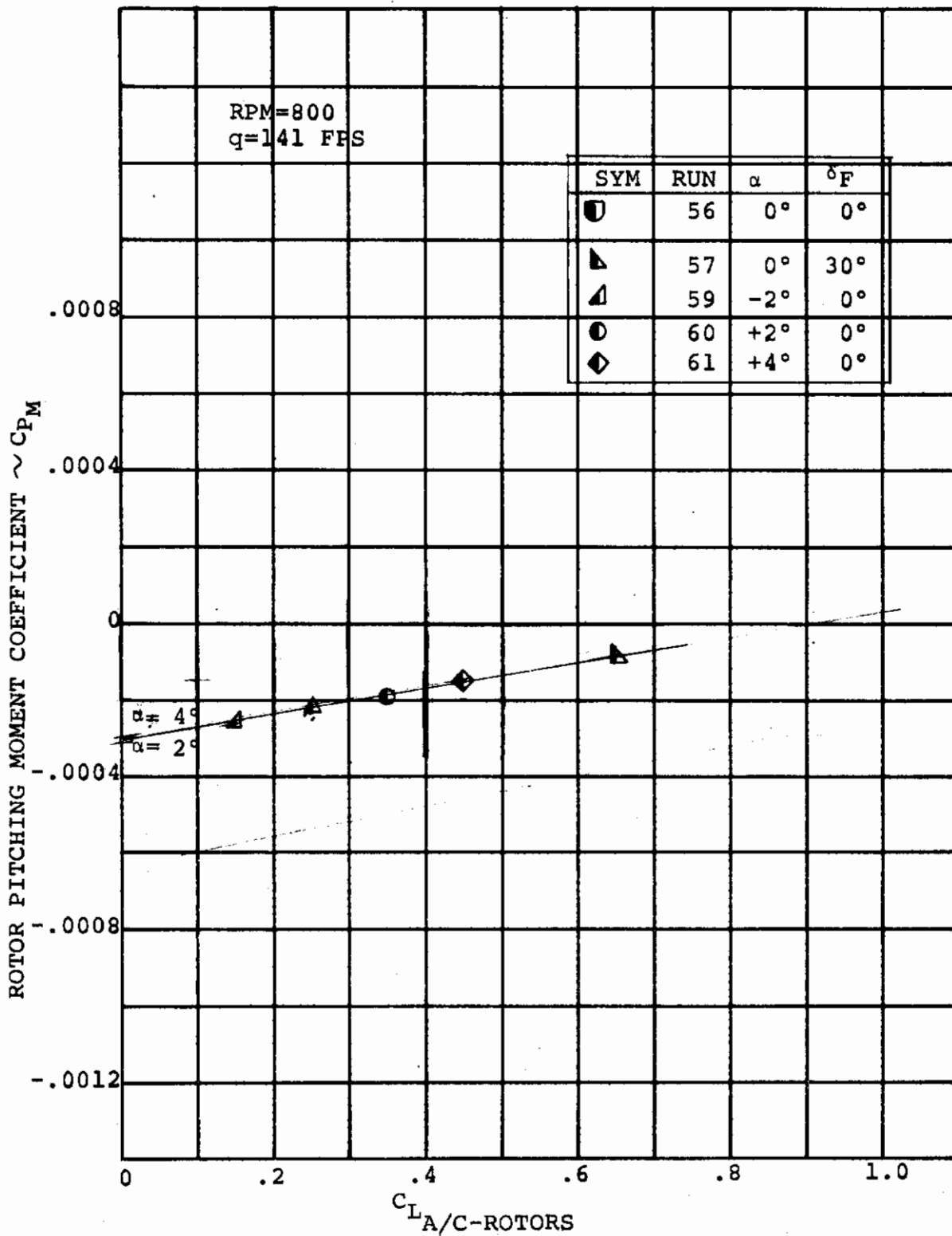


FIGURE C-13 EFFECT OF WING LIFT ON ROTOR PITCHING MOMENT  
(V = 141 FPS, RPM - 800)

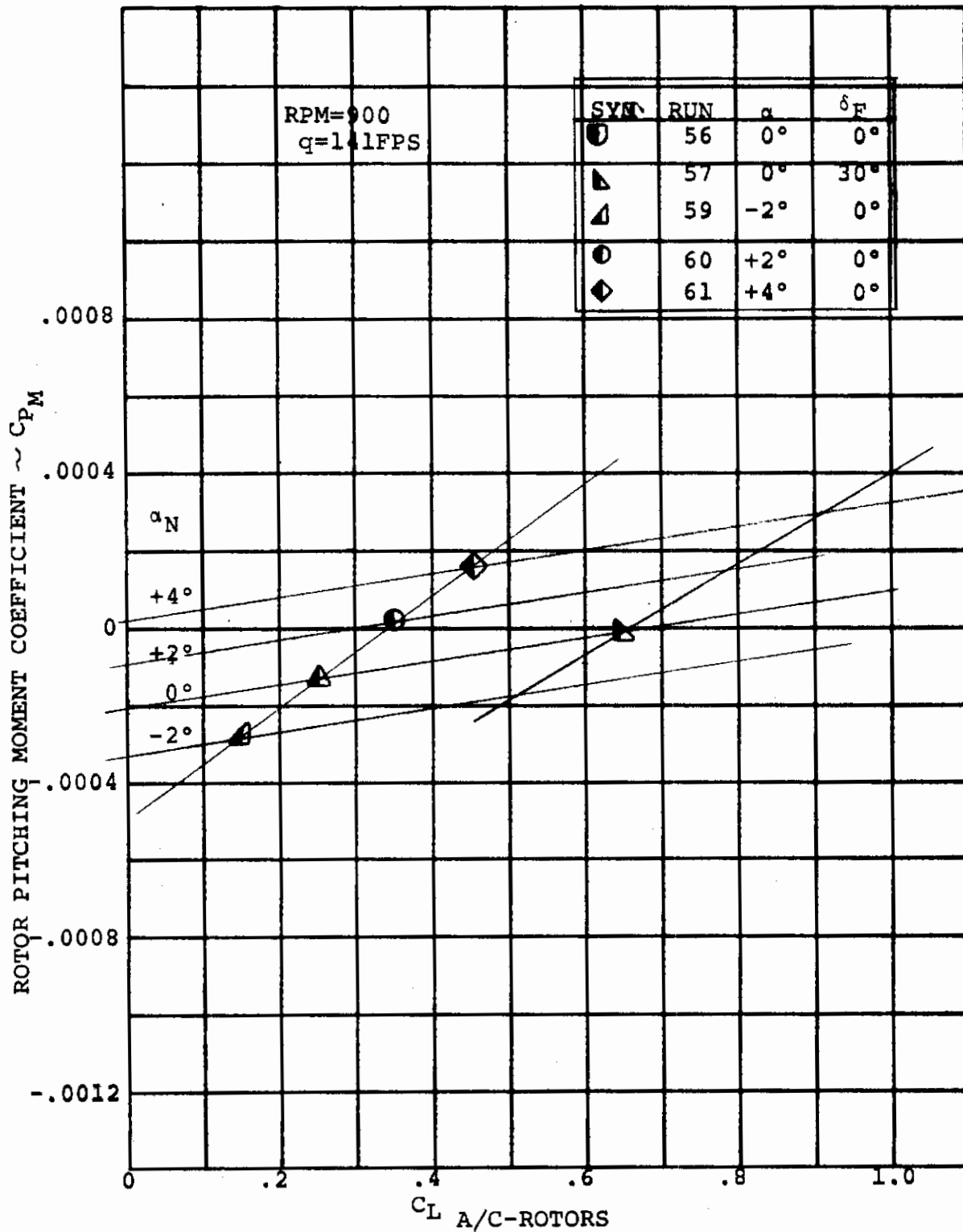


FIGURE C-14 EFFECT OF WING LIFT ON ROTOR PITCHING MOMENT  
(V = 141 FPS, RPM = 900)

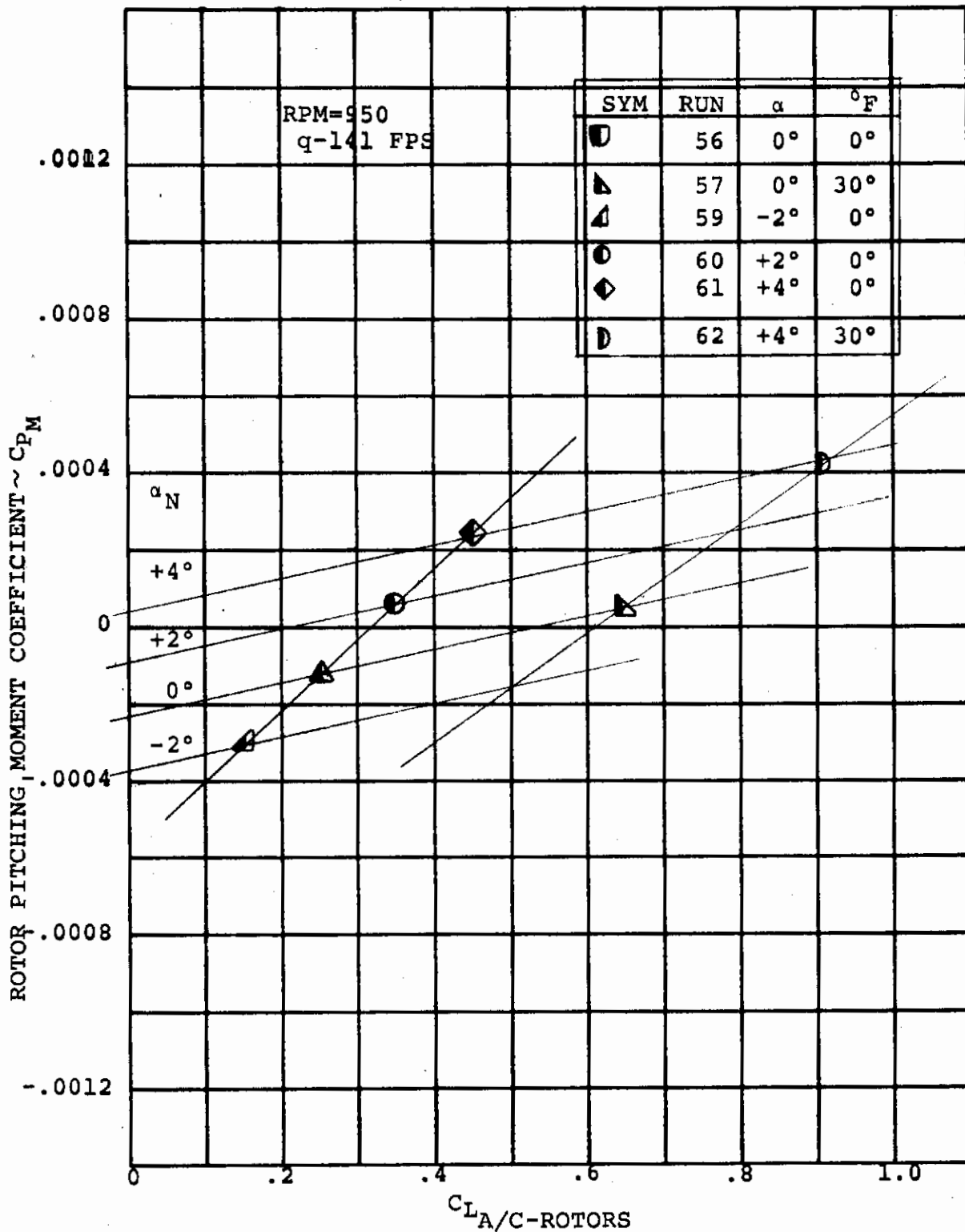


FIGURE C-15 EFFECT OF WING LIFT ON ROTOR PITCHING MOMENT  
(V = 113 FPS, RPM = 950)

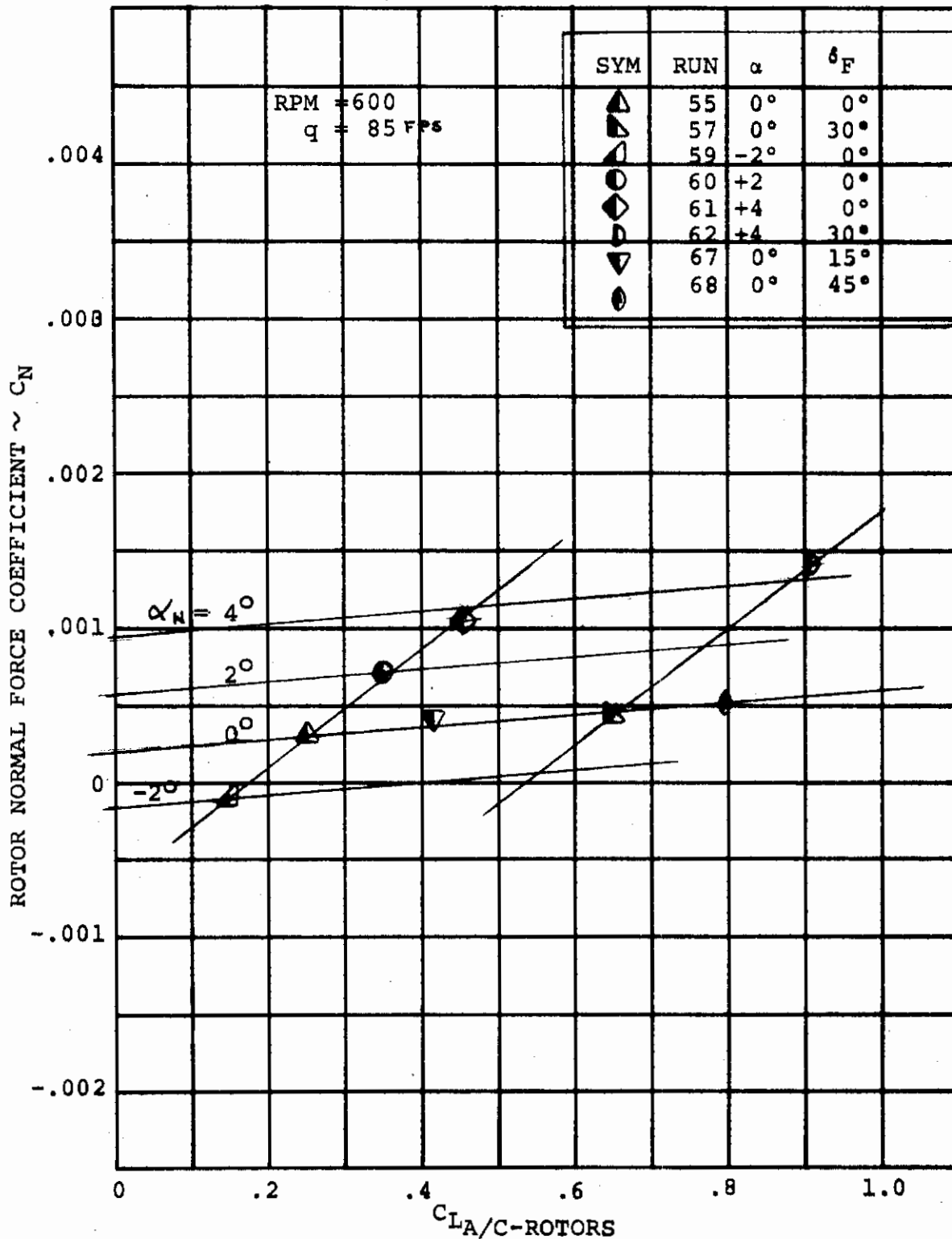


FIGURE C-16 EFFECT OF WING LIFT ON ROTOR NORMAL FORCE  
(V = 85 FPS RPM = 600)

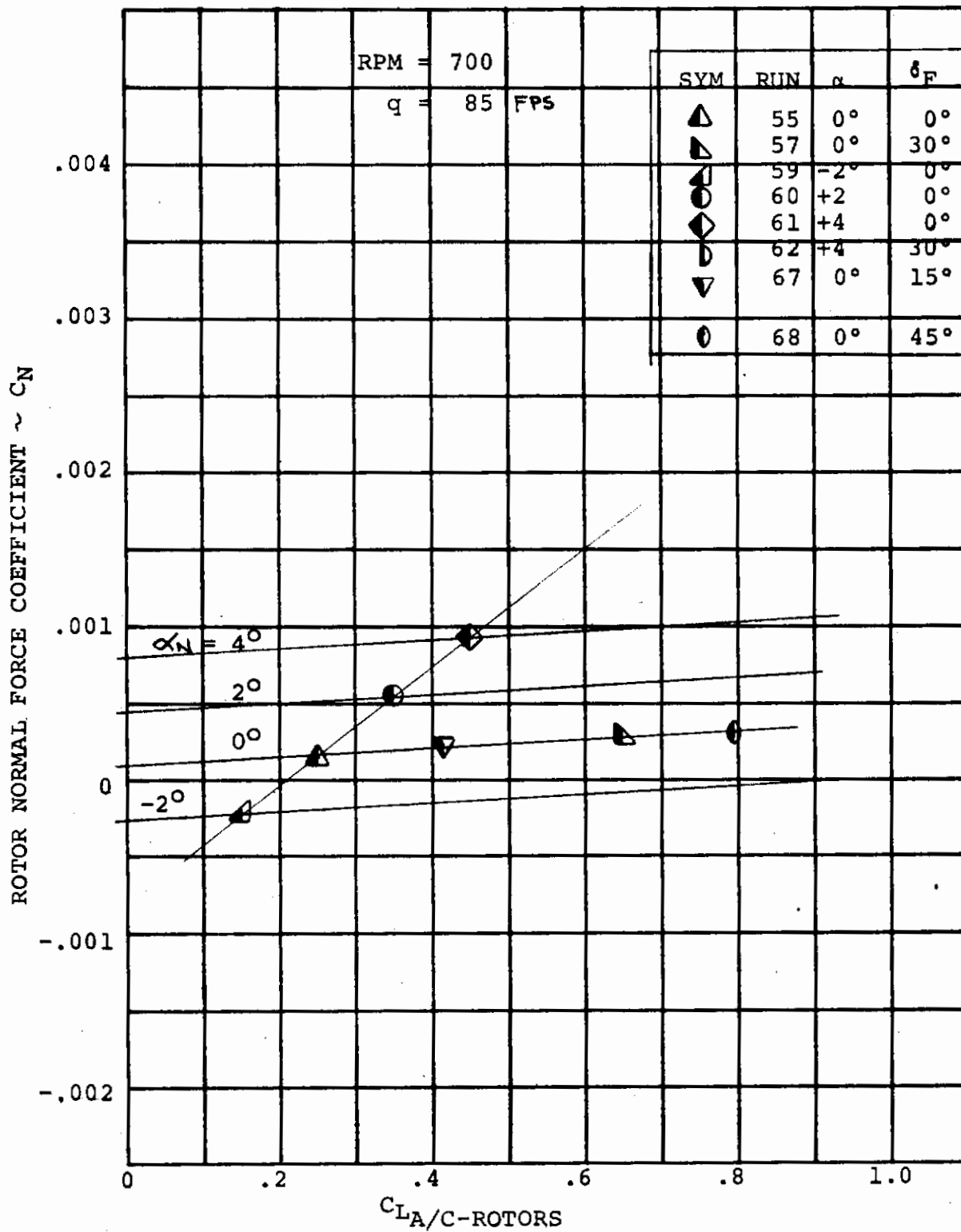


FIGURE C-17 EFFECT OF WING LIFT ON ROTOR NORMAL FORCE  
(V = 85 FPS RPM = 700)

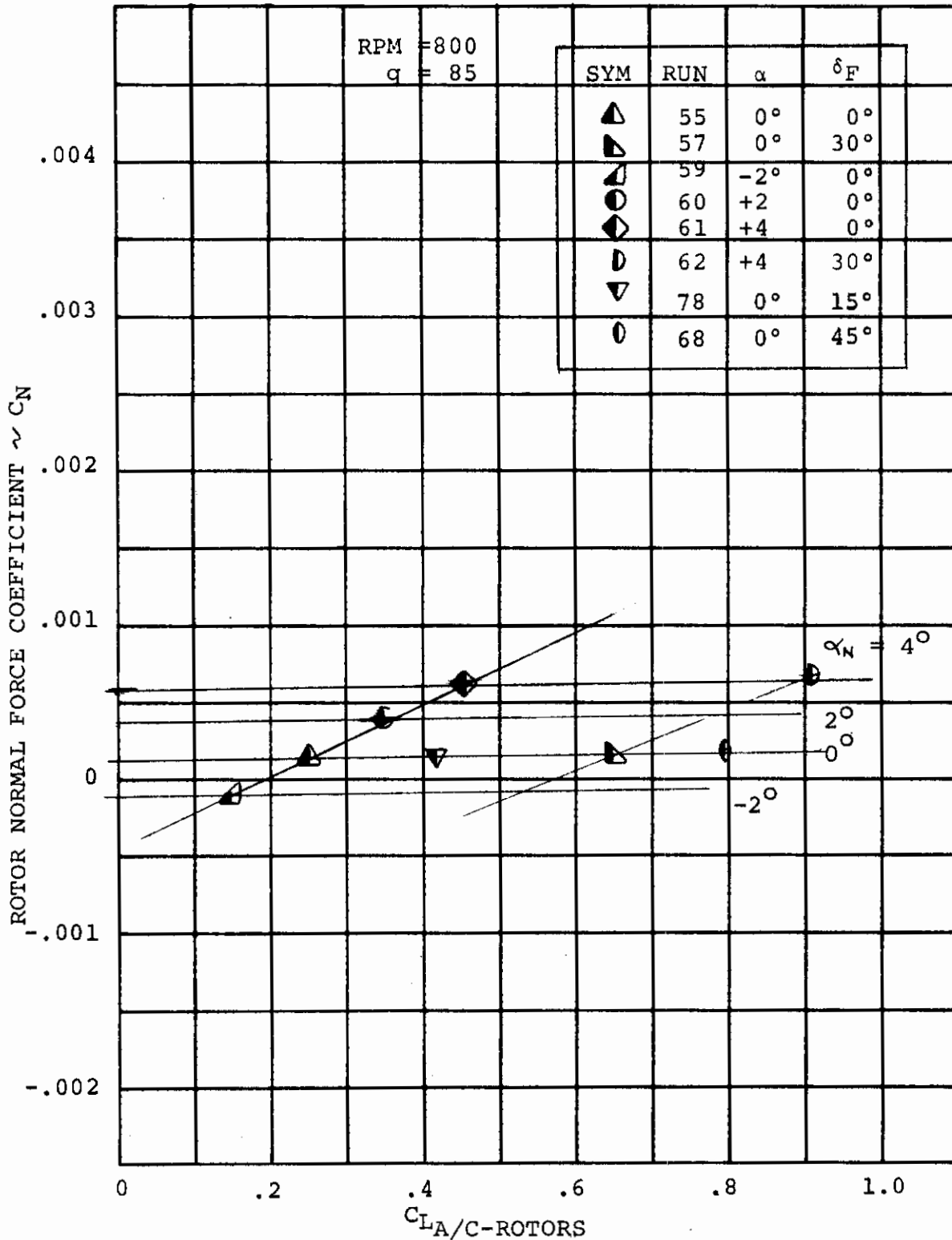


FIGURE C-18 EFFECT OF WING LIFT ON ROTOR NORMAL FORCE  
(V = 85 FPS RPM = 800)

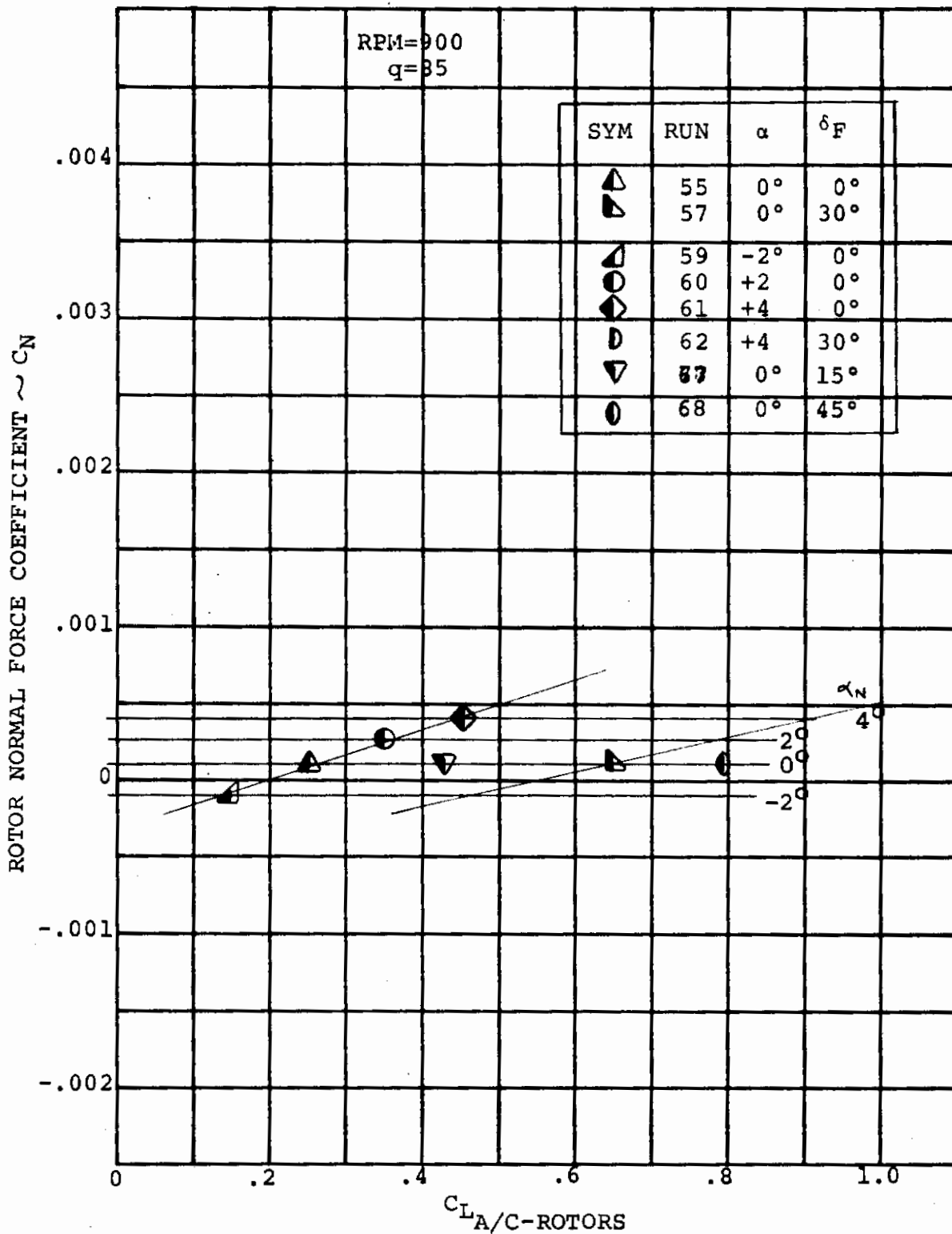


FIGURE C-19 EFFECT OF WING LIFT ON ROTOR NORMAL FORCE  
(V = 85 FPS RPM =900)

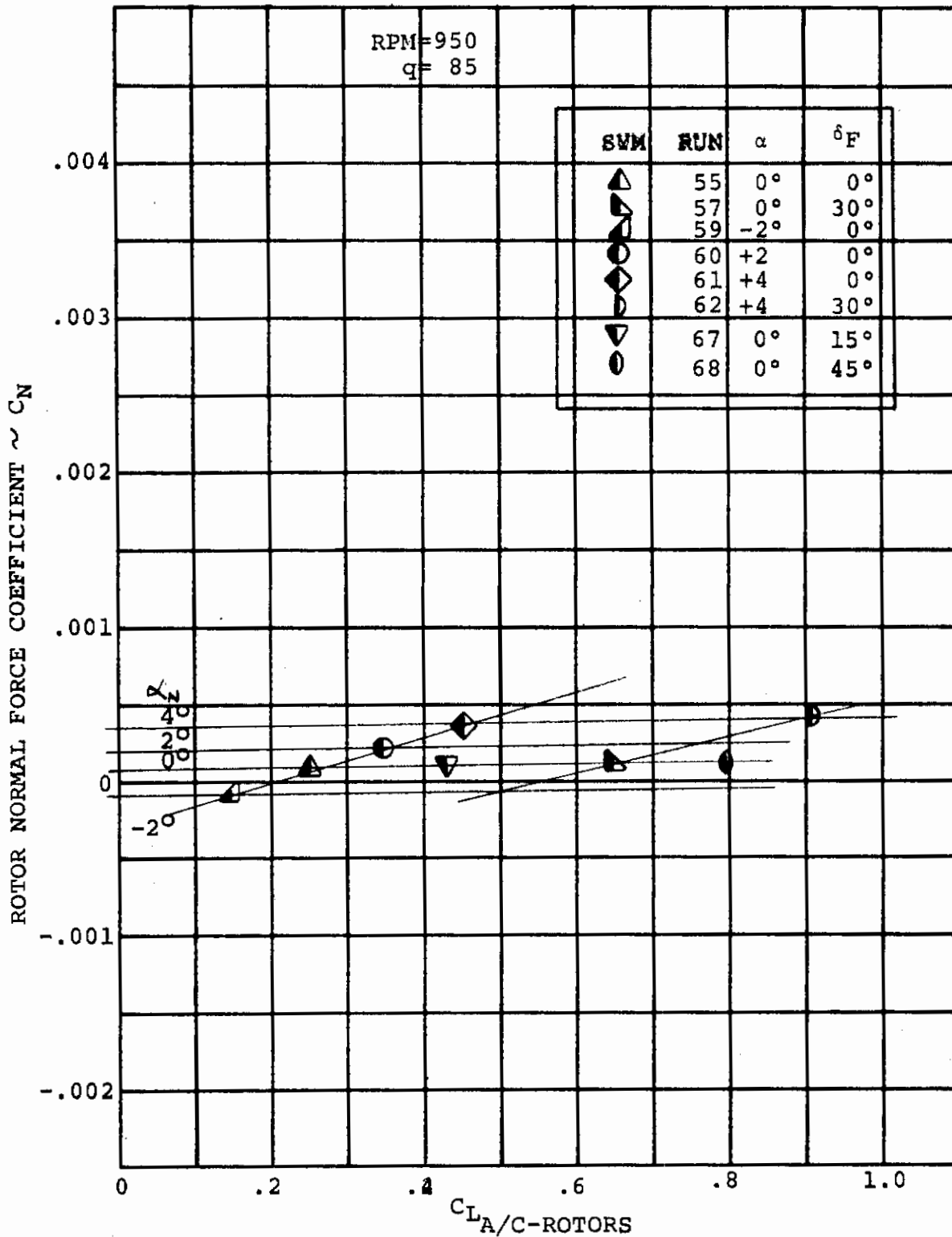


FIGURE C-20 EFFECT OF WING LIFT ON ROTOR NORMAL FORCE  
(V = 85 FPS RPM = 950)



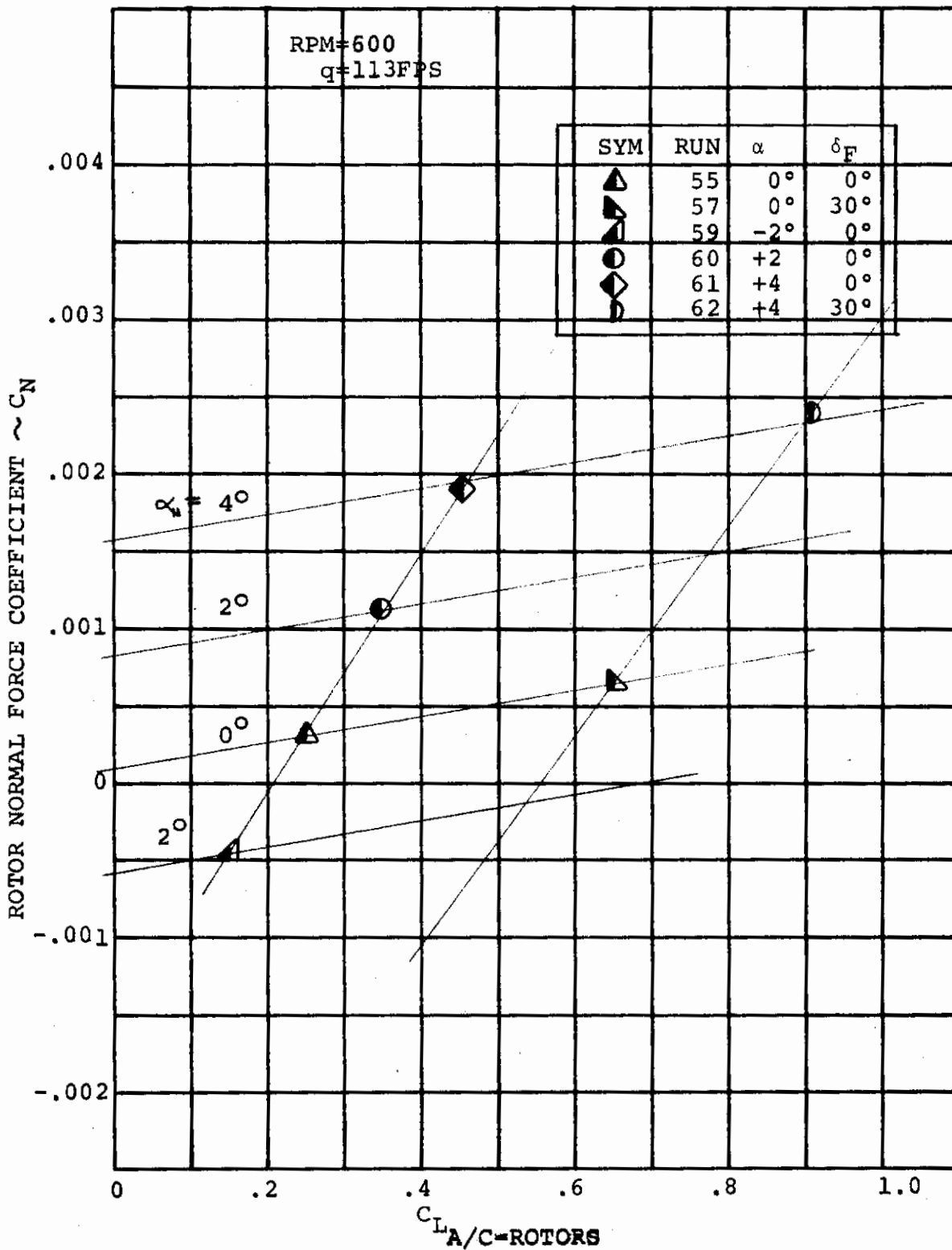


FIGURE C-21 EFFECT OF WING LIFT ON ROTOR NORMAL FORCE  
(V = 113 FPS RPM = 600)

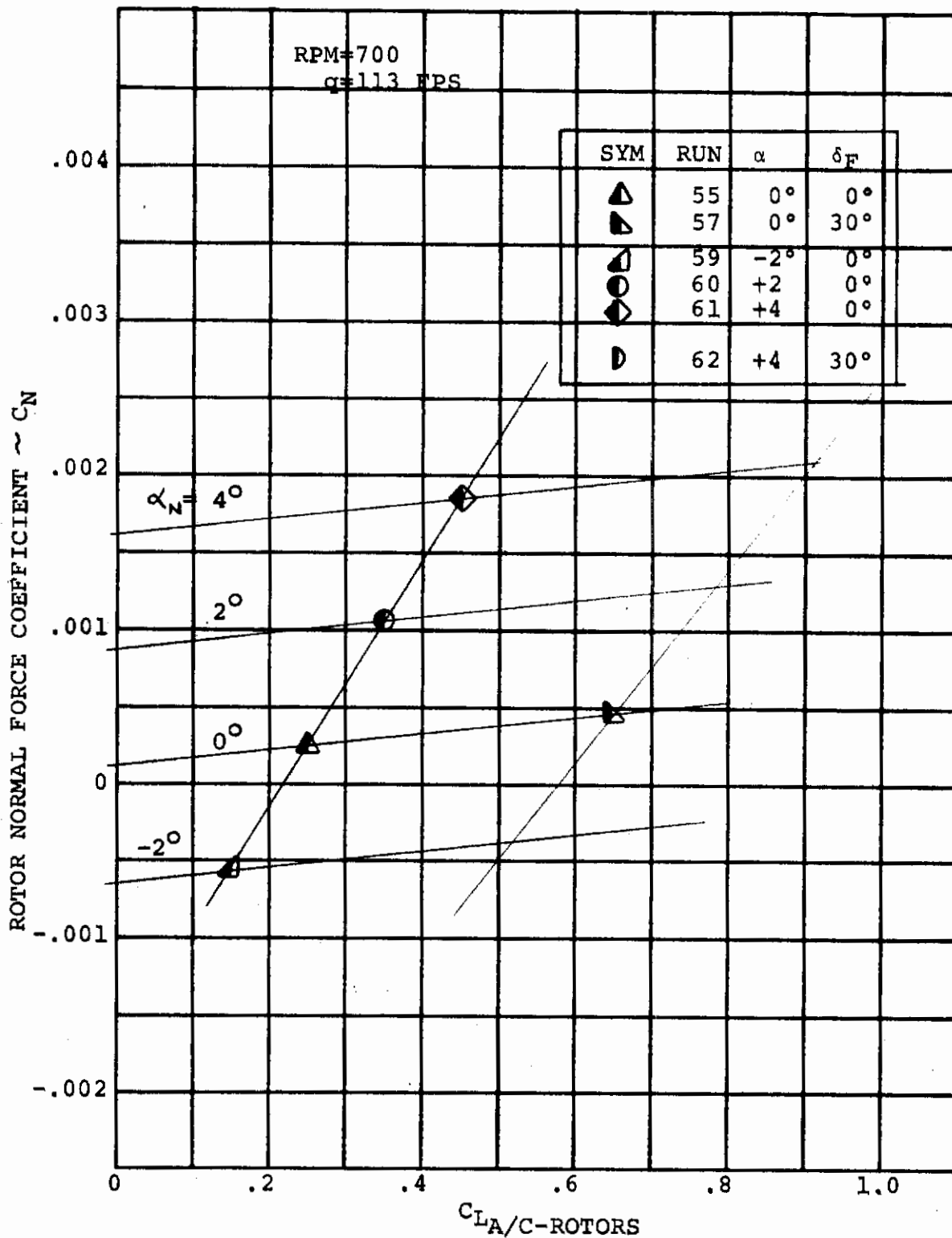


FIGURE C-22 EFFECT OF WING LIFT ON ROTOR NORMAL FORCE  
(V = 113 FPS RPM = 700)

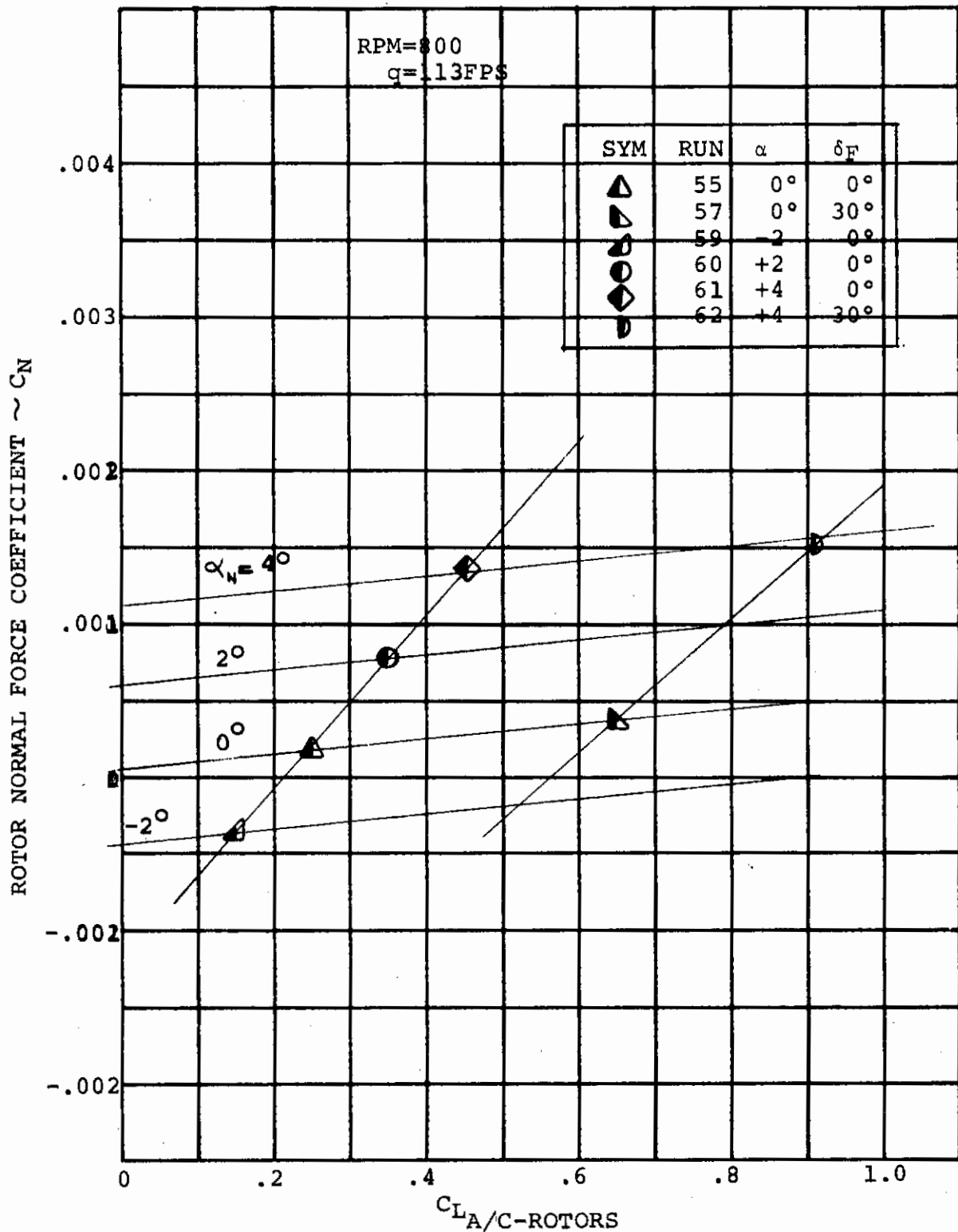


FIGURE C-23 EFFECT OF WING LIFT ON ROTOR NORMAL FORCE  
( $V = 113 \text{ FPS}$      $\text{RPM} = 800$ )

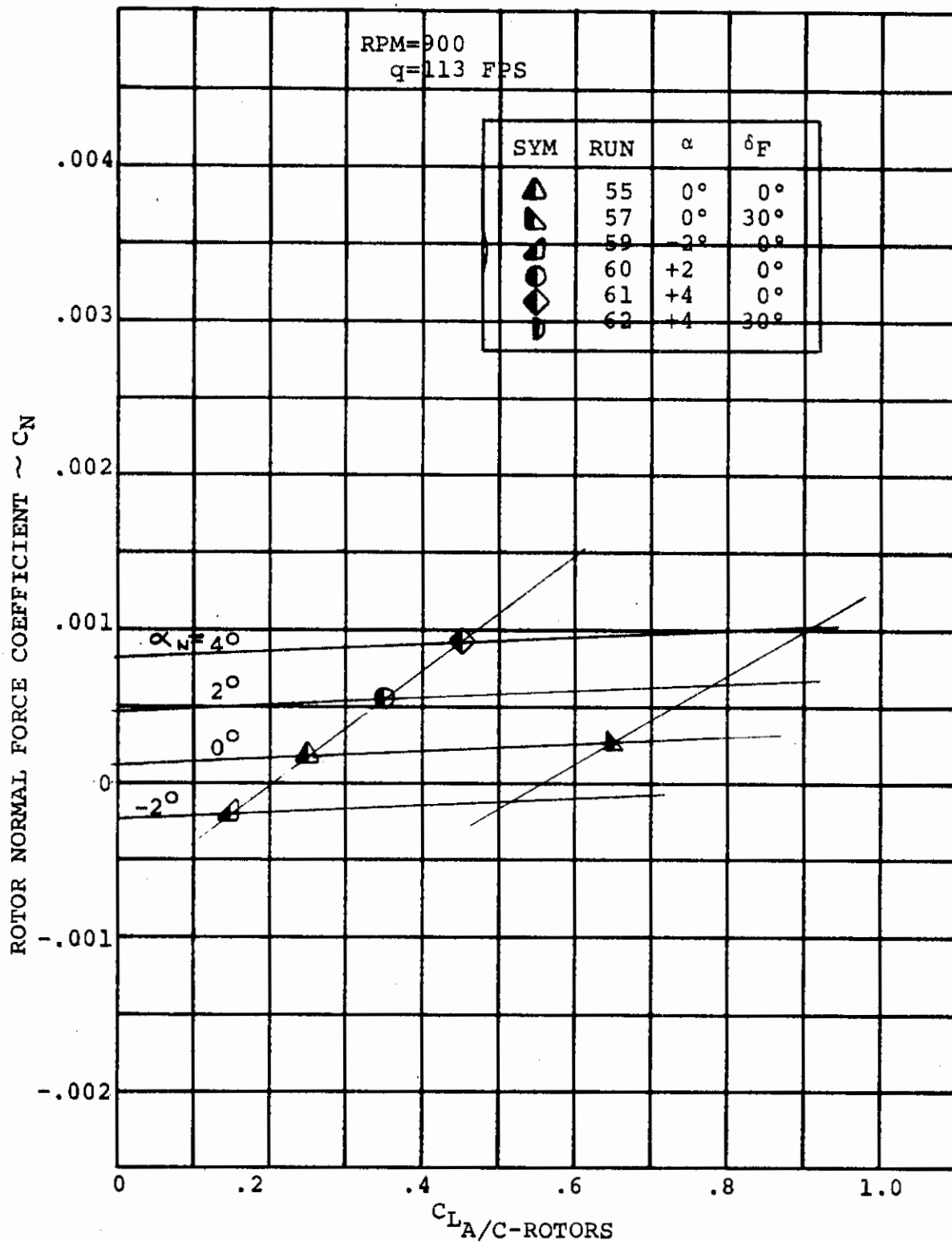


FIGURE C-24 EFFECT OF WING LIFT ON ROTOR NORMAL FORCE  
(V = 113 FPS RPM = 900)

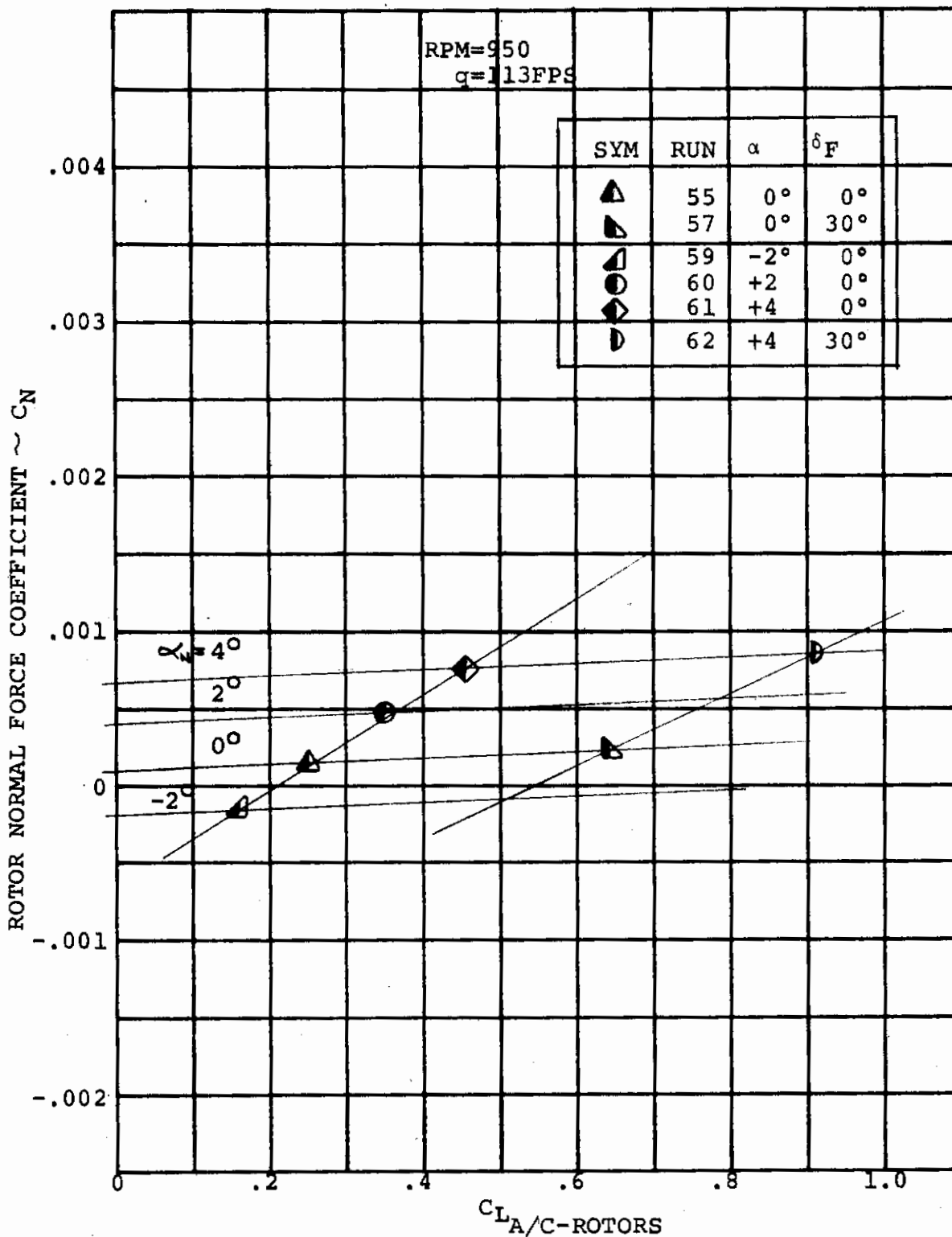


FIGURE C-25 EFFECT OF WING LIFT ON ROTOR NORMAL FORCE  
(V = 113 FPS RPM = 950)

# Contrails

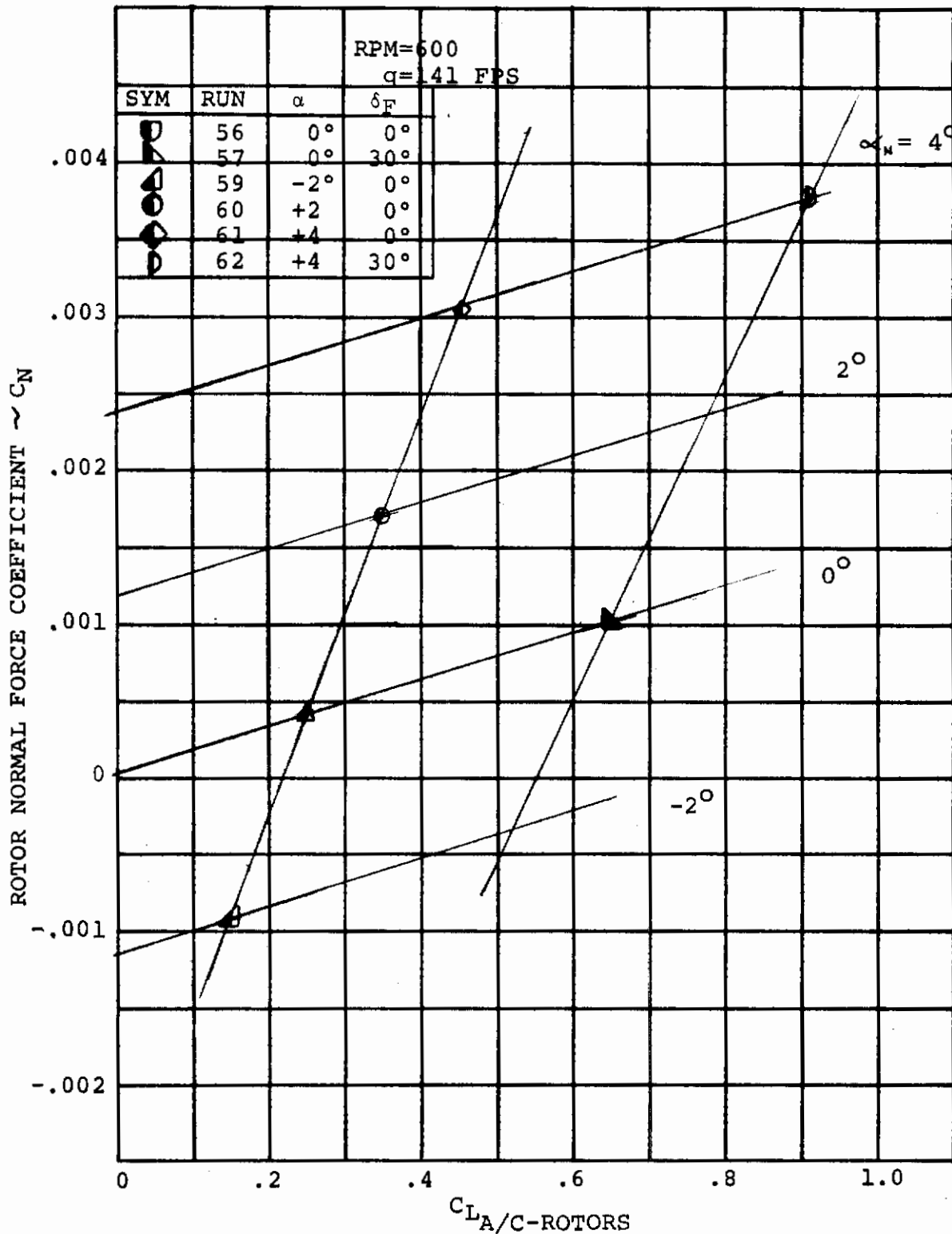


FIGURE C-26 EFFECT OF WING LIFT ON ROTOR NORMAL FORCE  
(V = 141 FPS RPM = 600)

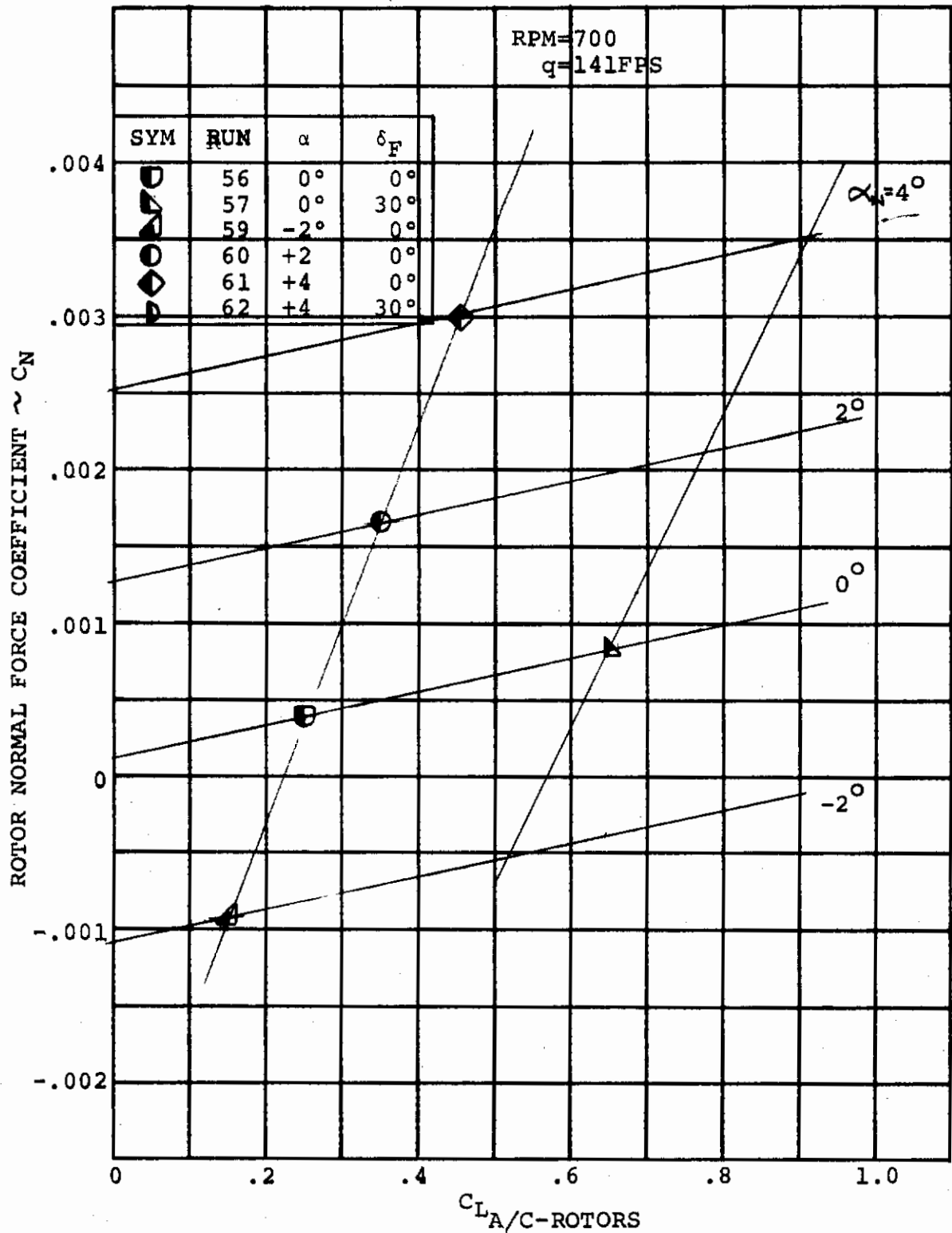


FIGURE C-27 EFFECT OF WING LIFT ON ROTOR NORMAL FORCE  
(V = 141 FPS RPM = 700)

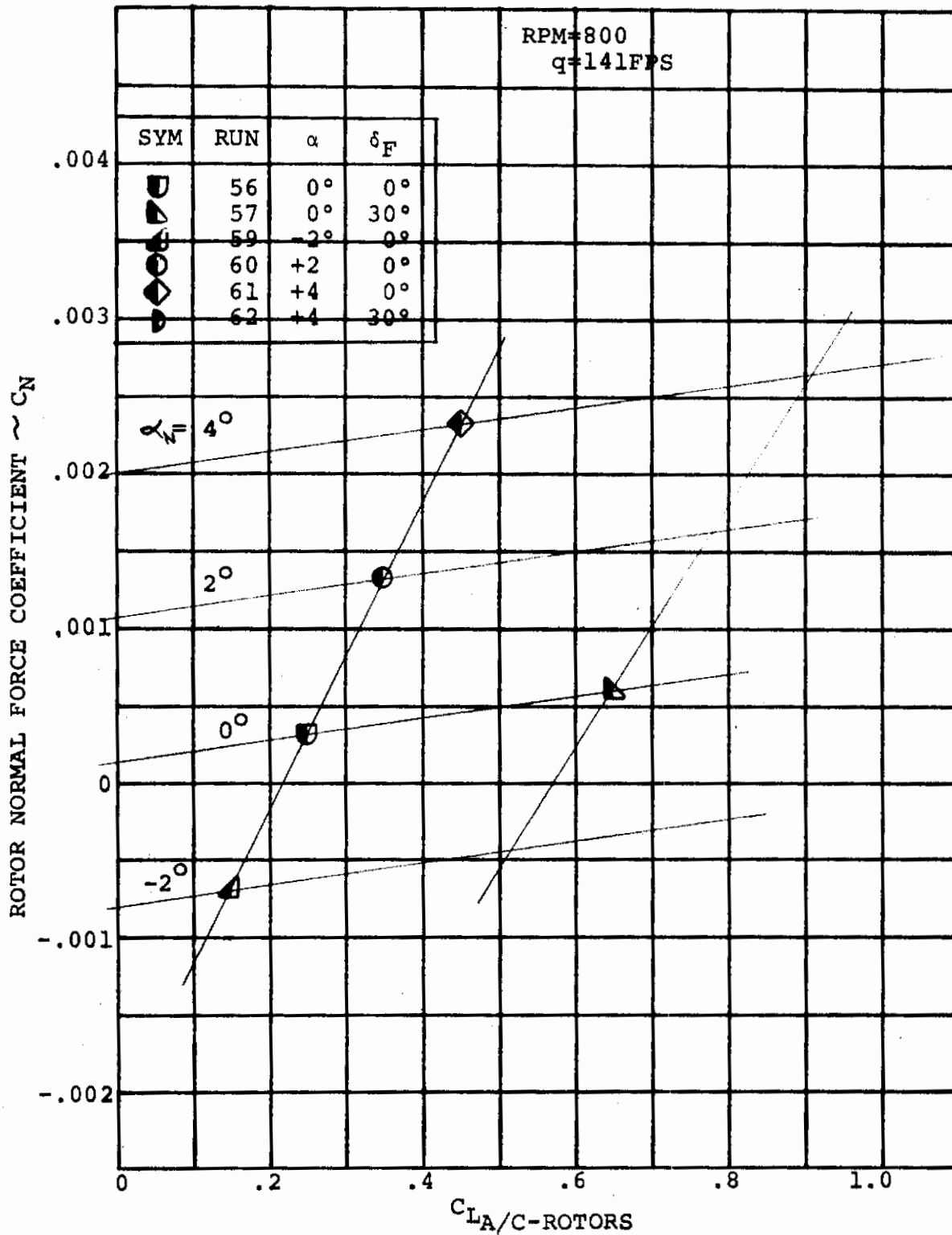


FIGURE C-28 EFFECT OF WING LIFT ON ROTOR NORMAL FORCE  
( V = 141 FPS RPM = 800)



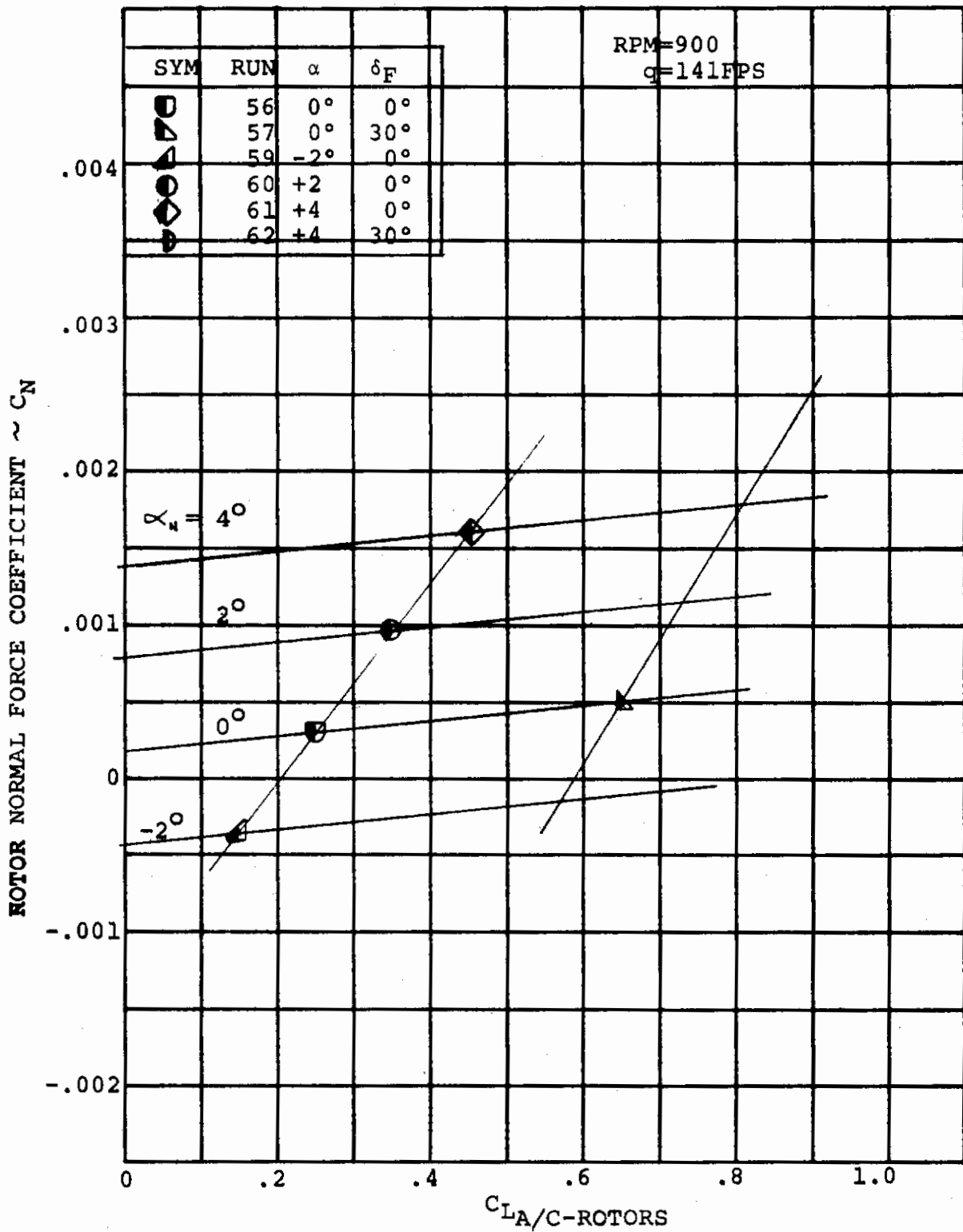


FIGURE C-29 EFFECT OF WING LIFT ON ROTOR NORMAL FORCE  
(V = 141 FPS RPM = 900)

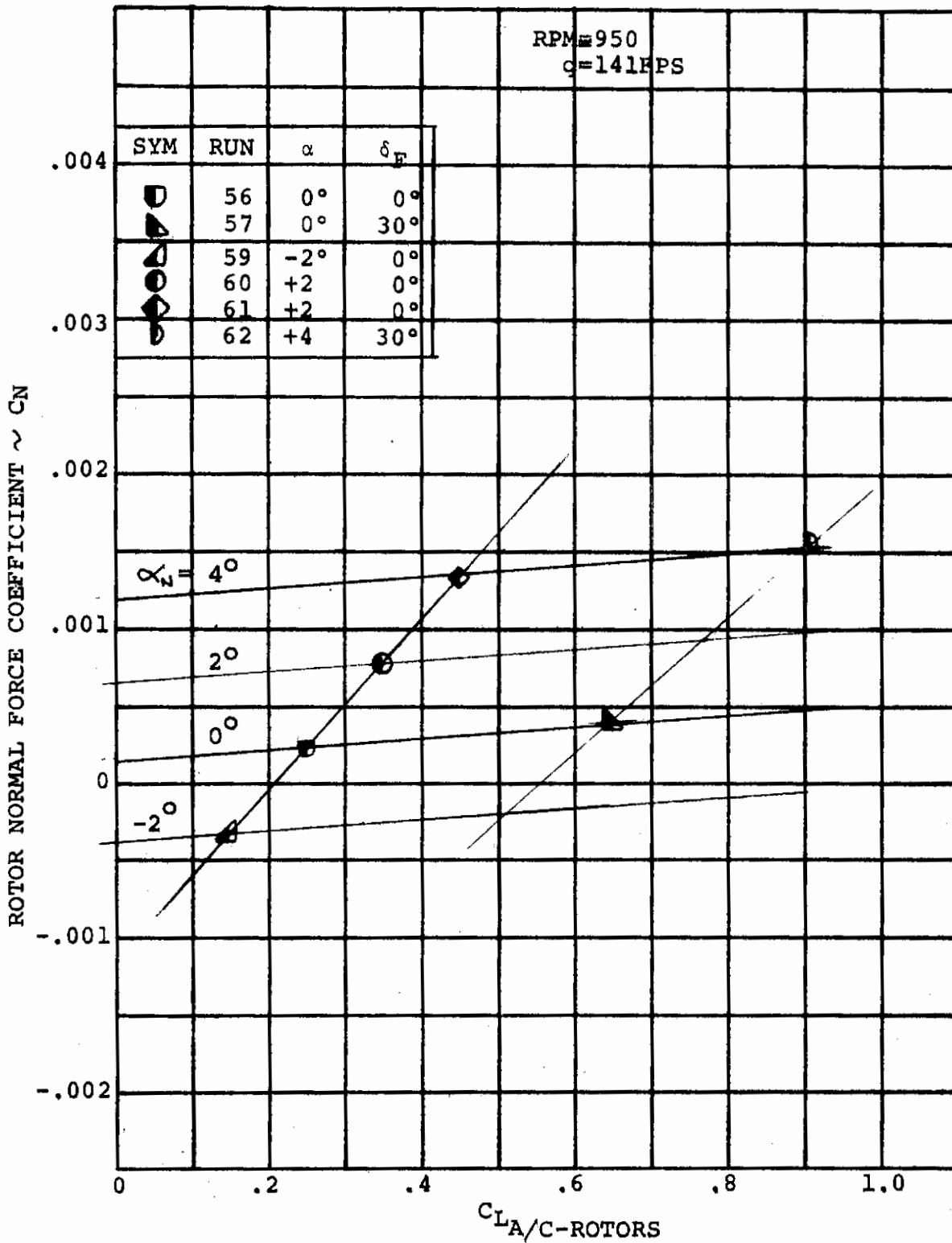


FIGURE C-30 EFFECT OF WING LIFT ON ROTOR NORMAL FORCE  
(V = 141 FPS RPM = 950)

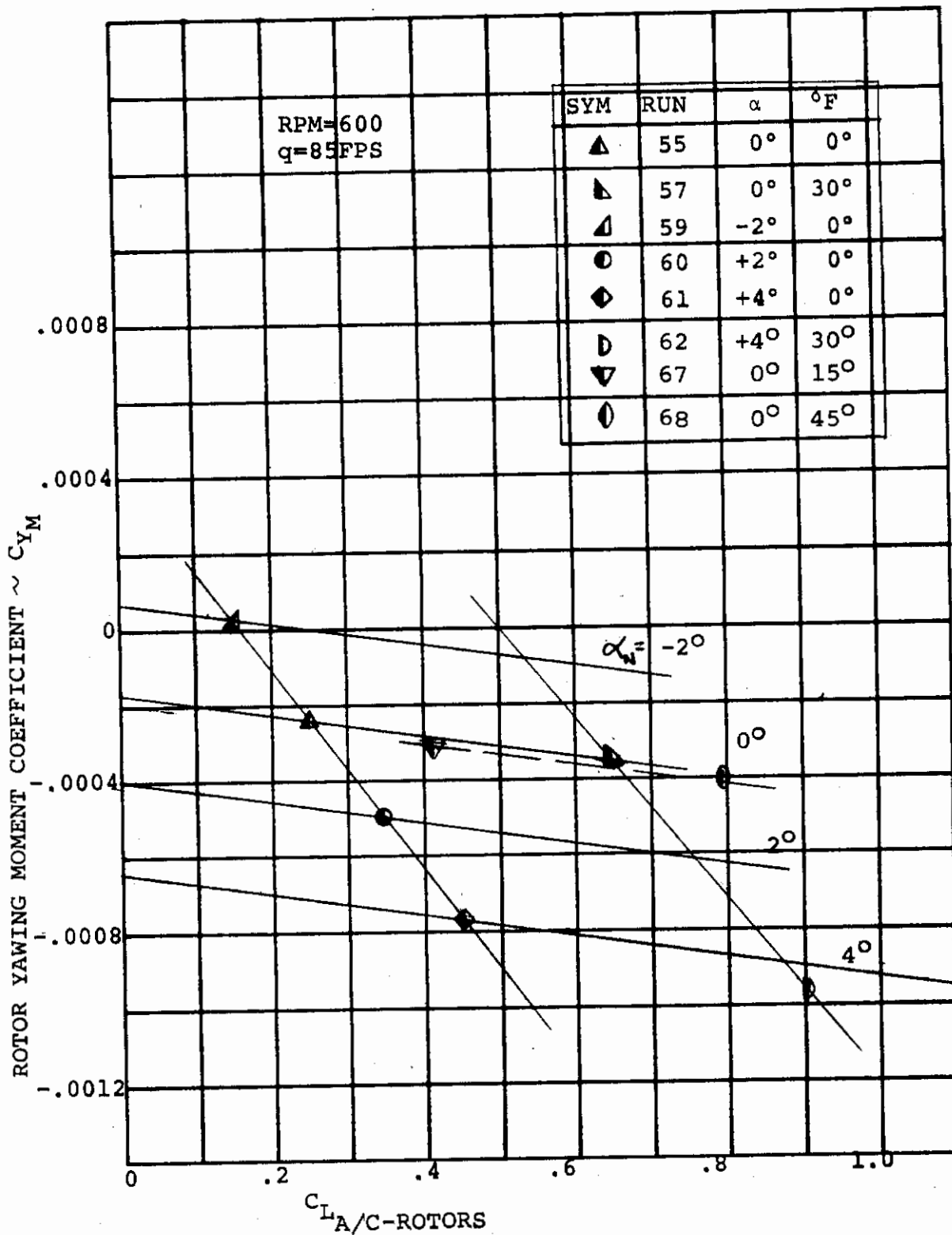


FIGURE C-31 EFFECT OF WING LIFT ON ROTOR YAWING MOMENT  
(V = 85 FPS RPM = 600)

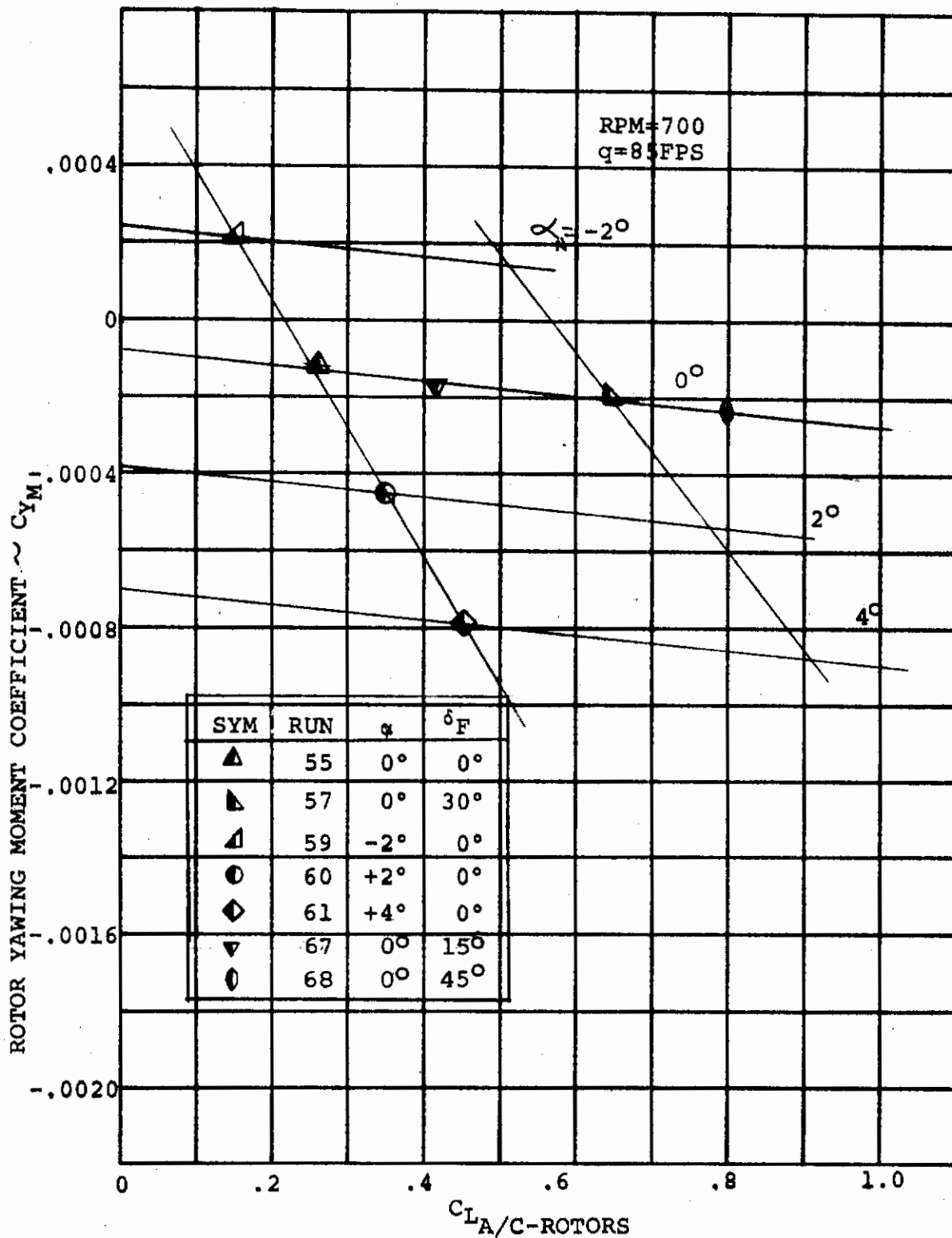


FIGURE C-32 EFFECT OF WING LIFT ON ROTOR YAWING MOMENT.  
(V = 85 FPS RPM = 700)

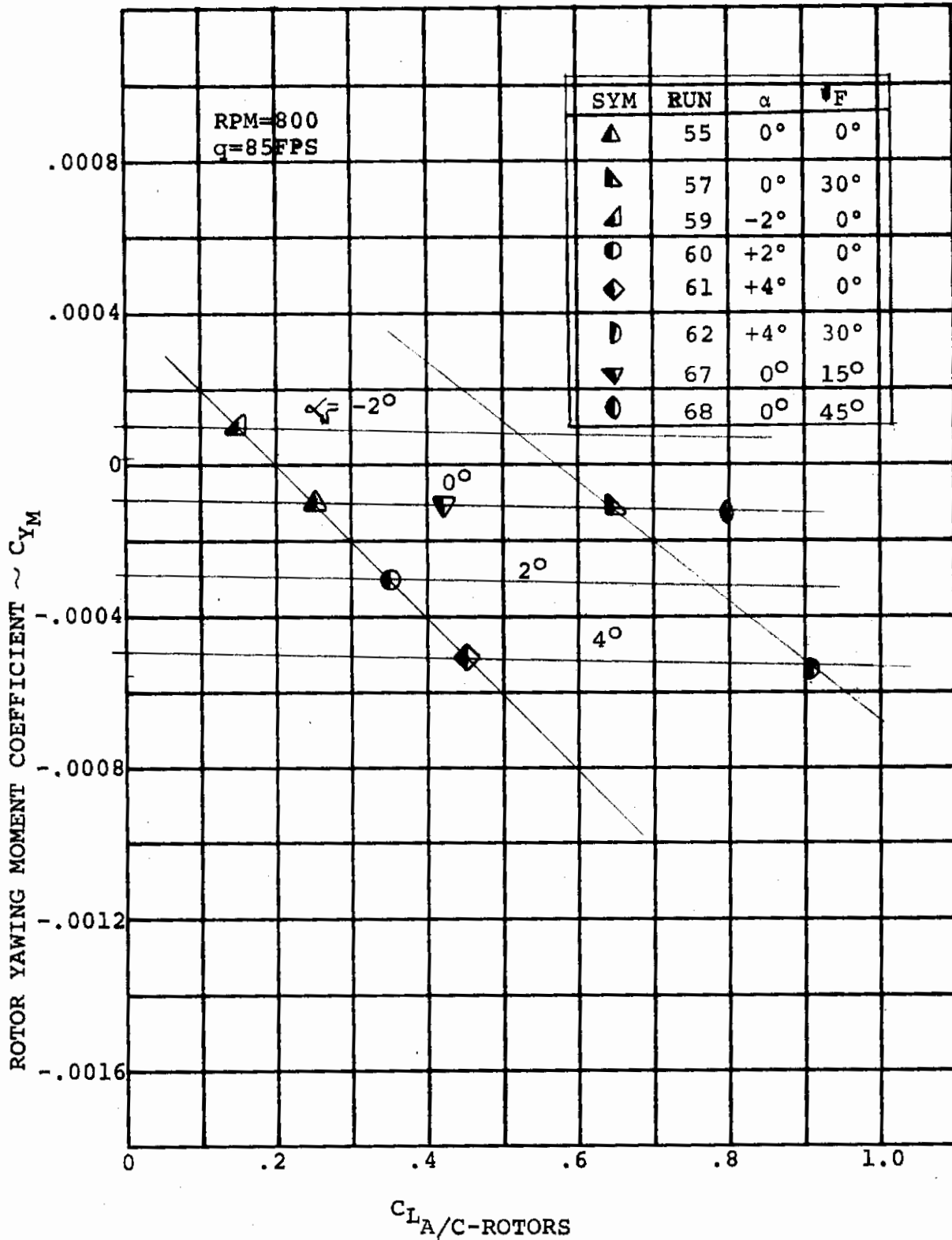


FIGURE C-33 EFFECT OF WING LIFT ON ROTOR YAWING MOMENT  
(V = 85 FPS RPM = 800)

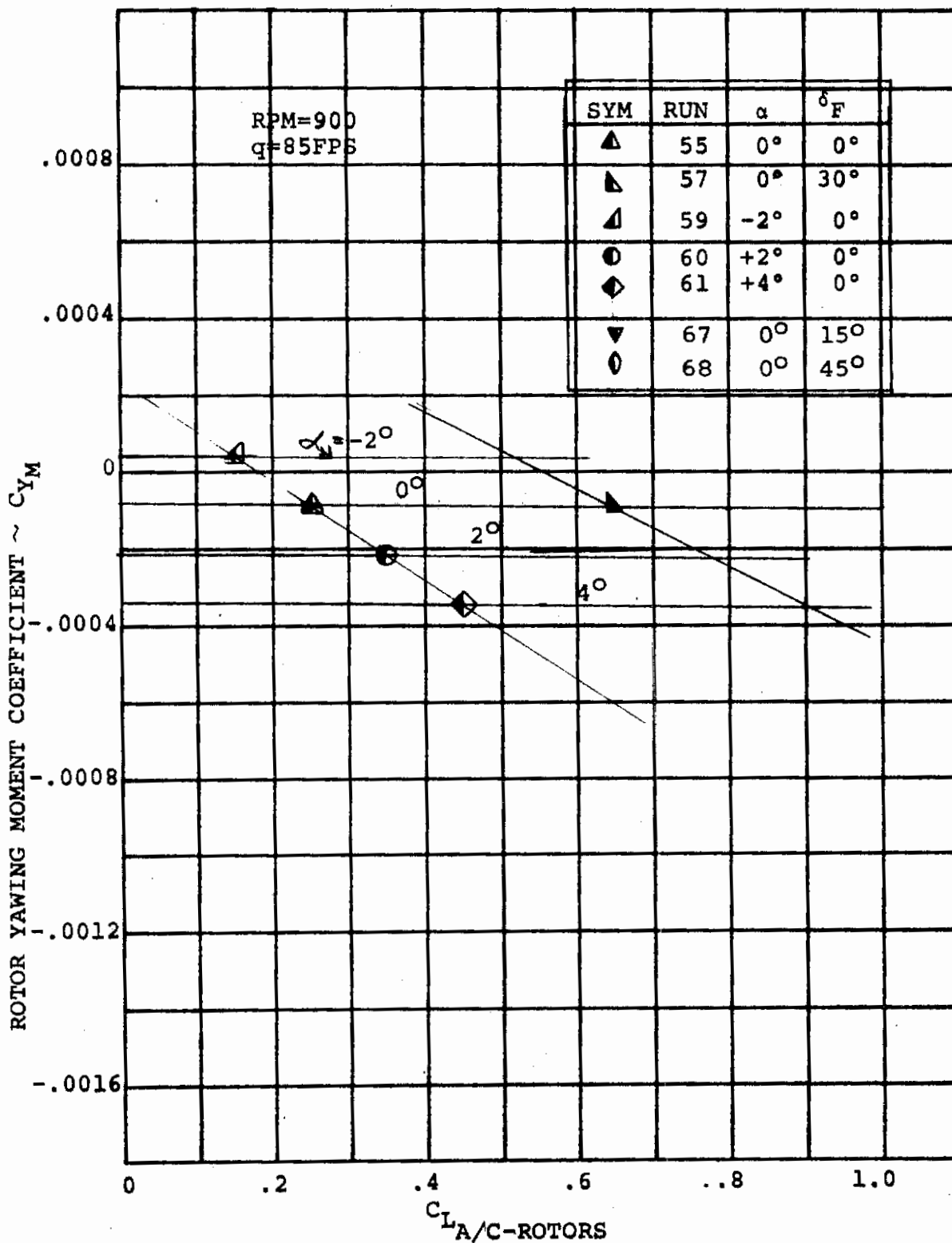


FIGURE C-34 EFFECT OF WING LIFT ON ROTOR YAWING MOMENT  
(V = 85 FPS RPM - 900)

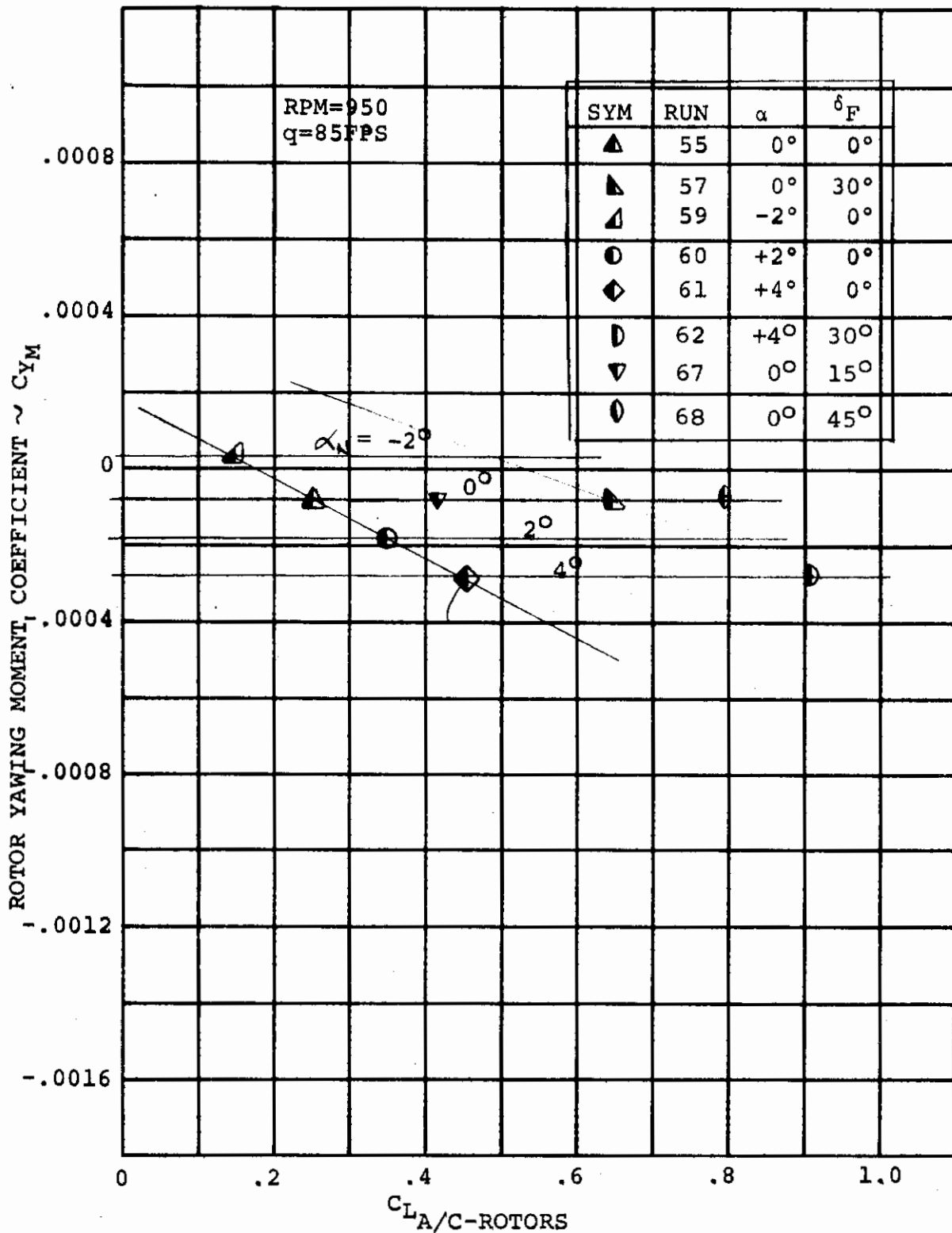


FIGURE C-35 EFFECT OF WING LIFT ON ROTOR YAWING MOMENT  
(V = 85 FPS RPM = 950)

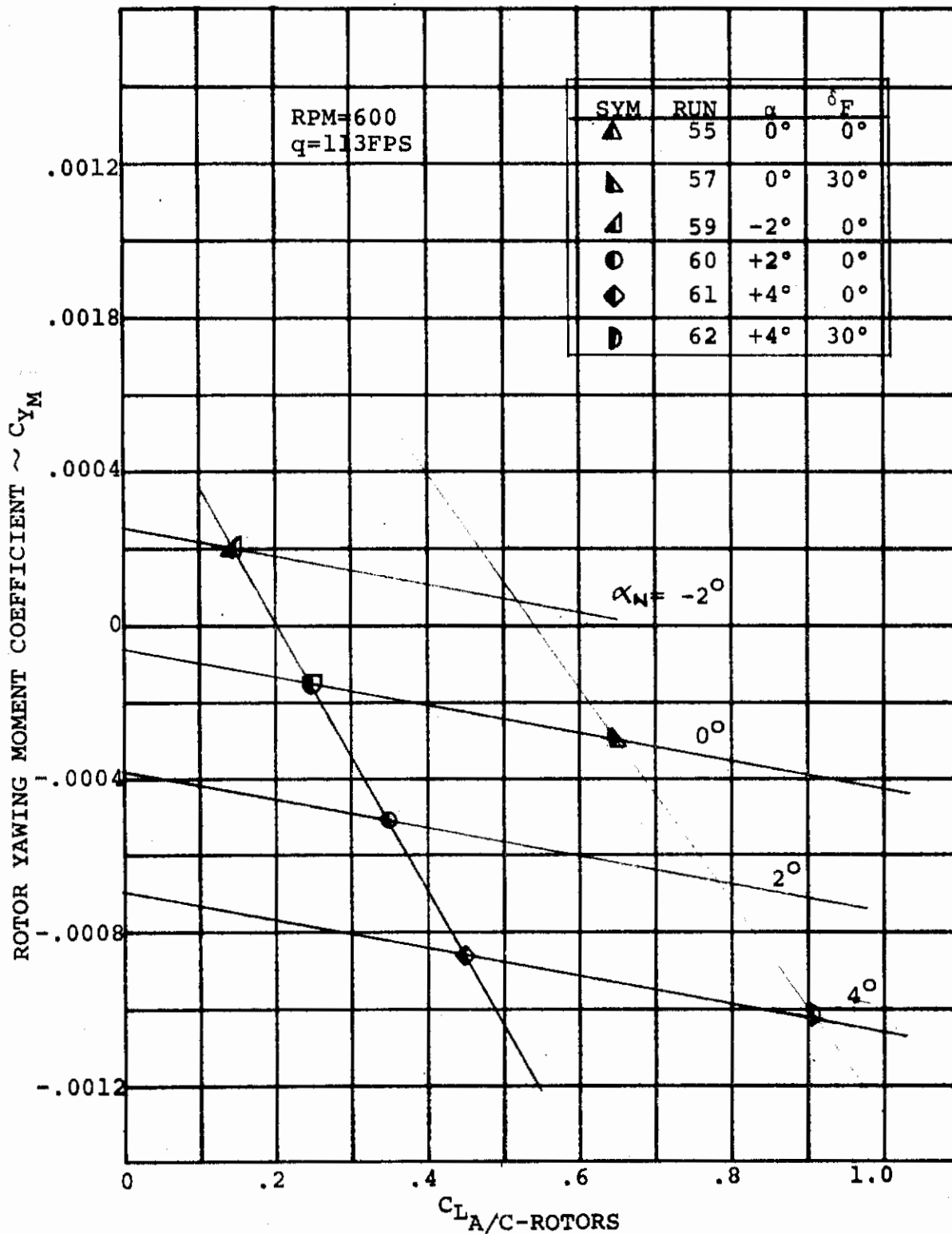


FIGURE C-36 EFFECT OF WING LIFT ON ROTOR YAWING MOMENT  
(V = 113 FPS RPM = 600)



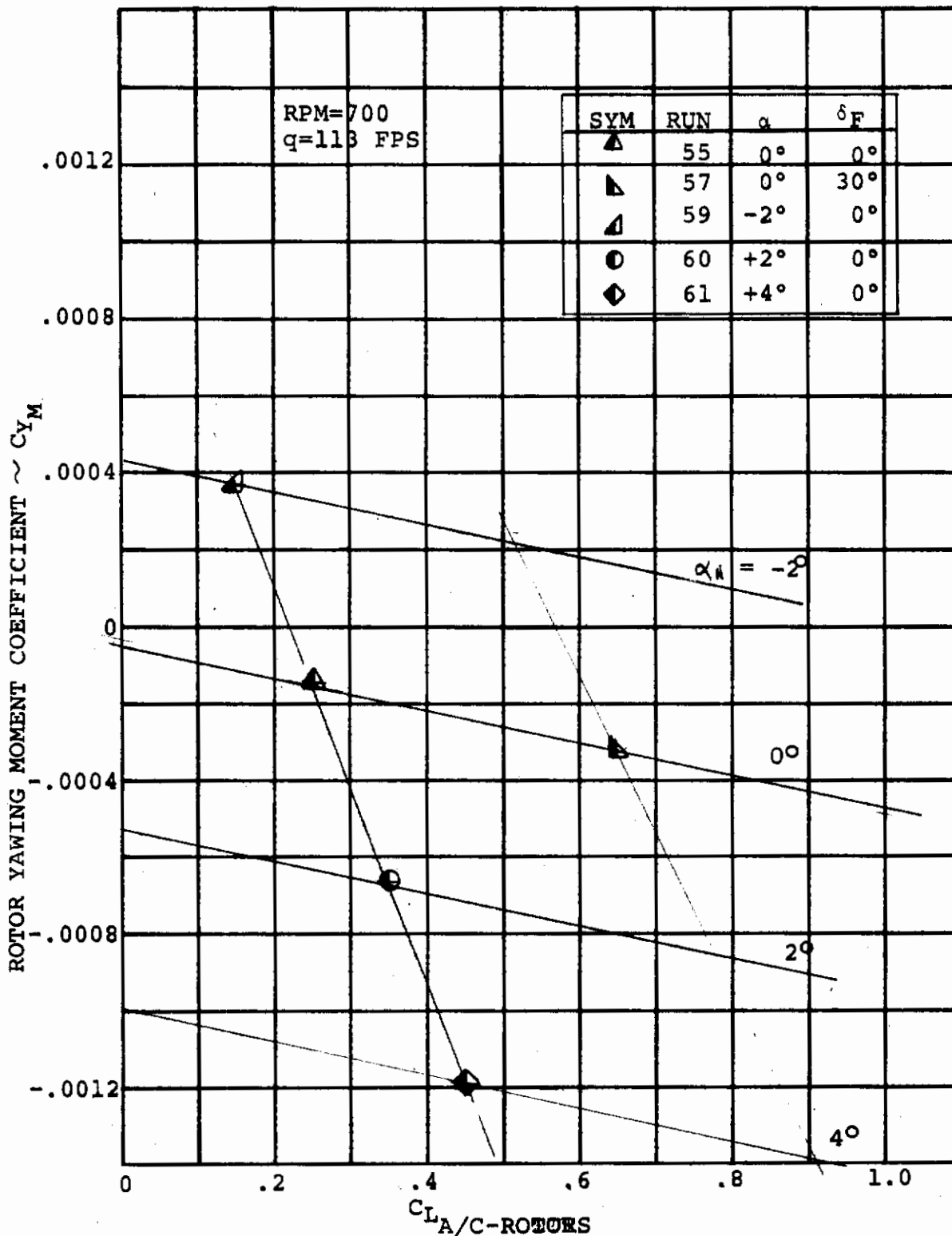


FIGURE C-37 EFFECT OF WING LIFT ON ROTOR YAWING MOMENT  
(V = 113 FPS RPM = 700)

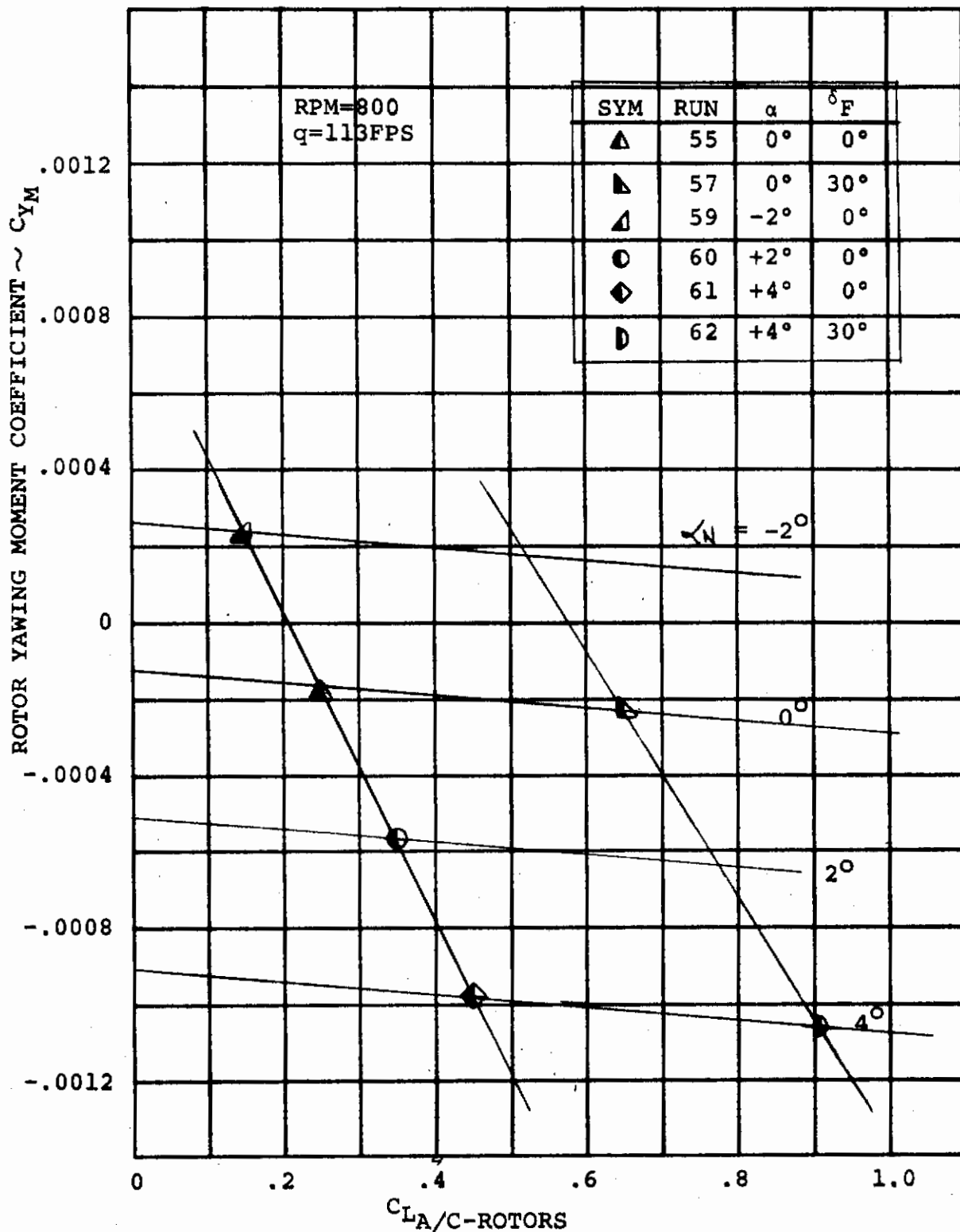


FIGURE C-38 EFFECT OF WING LIFT ON ROTOR YAWING MOMENT  
(V = 113 FPS RPM = 800)

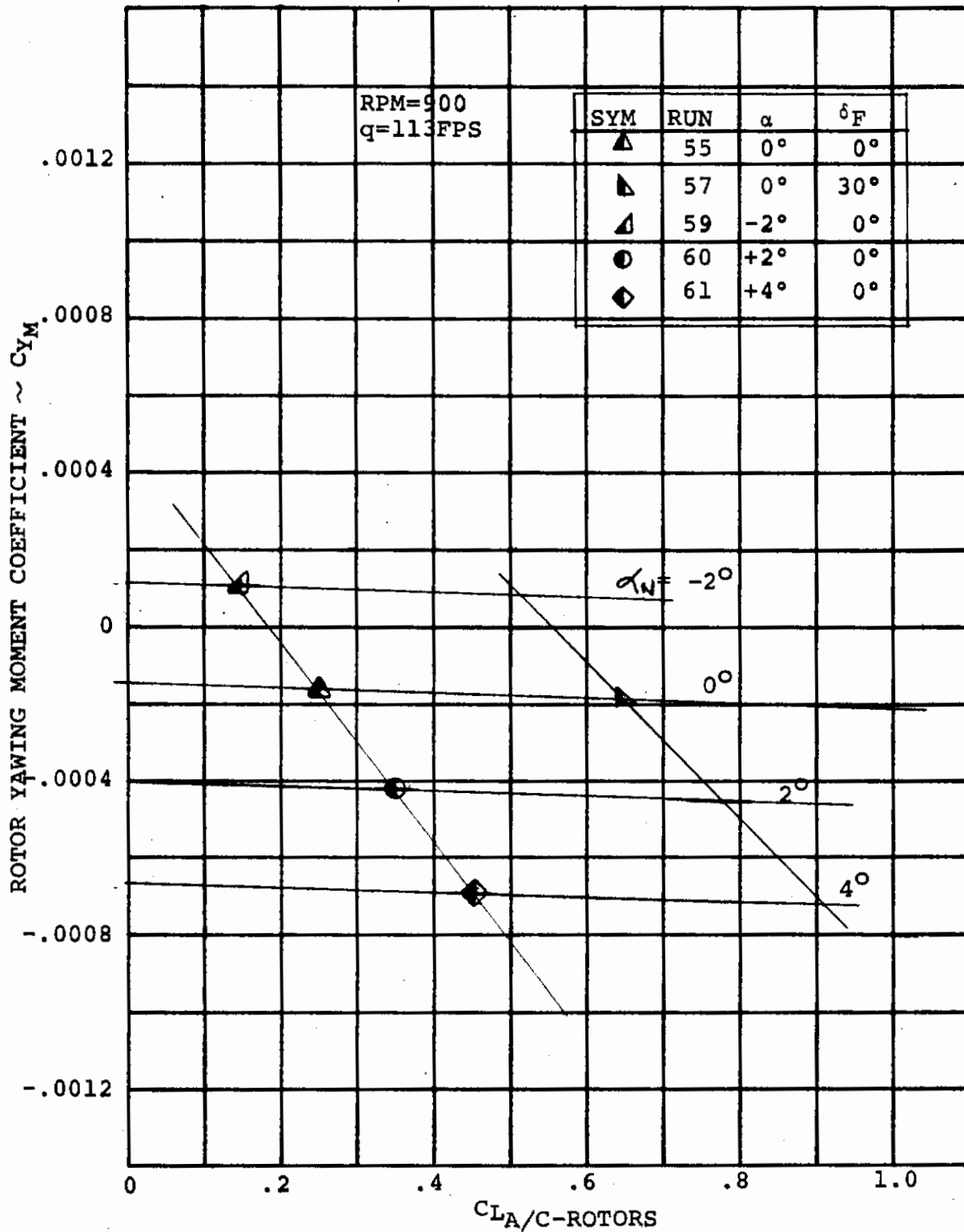


FIGURE C-39 EFFECT OF WING LIFT ON ROTOR YAWING MOMENT  
(V = 113 FPS RPM = 900)

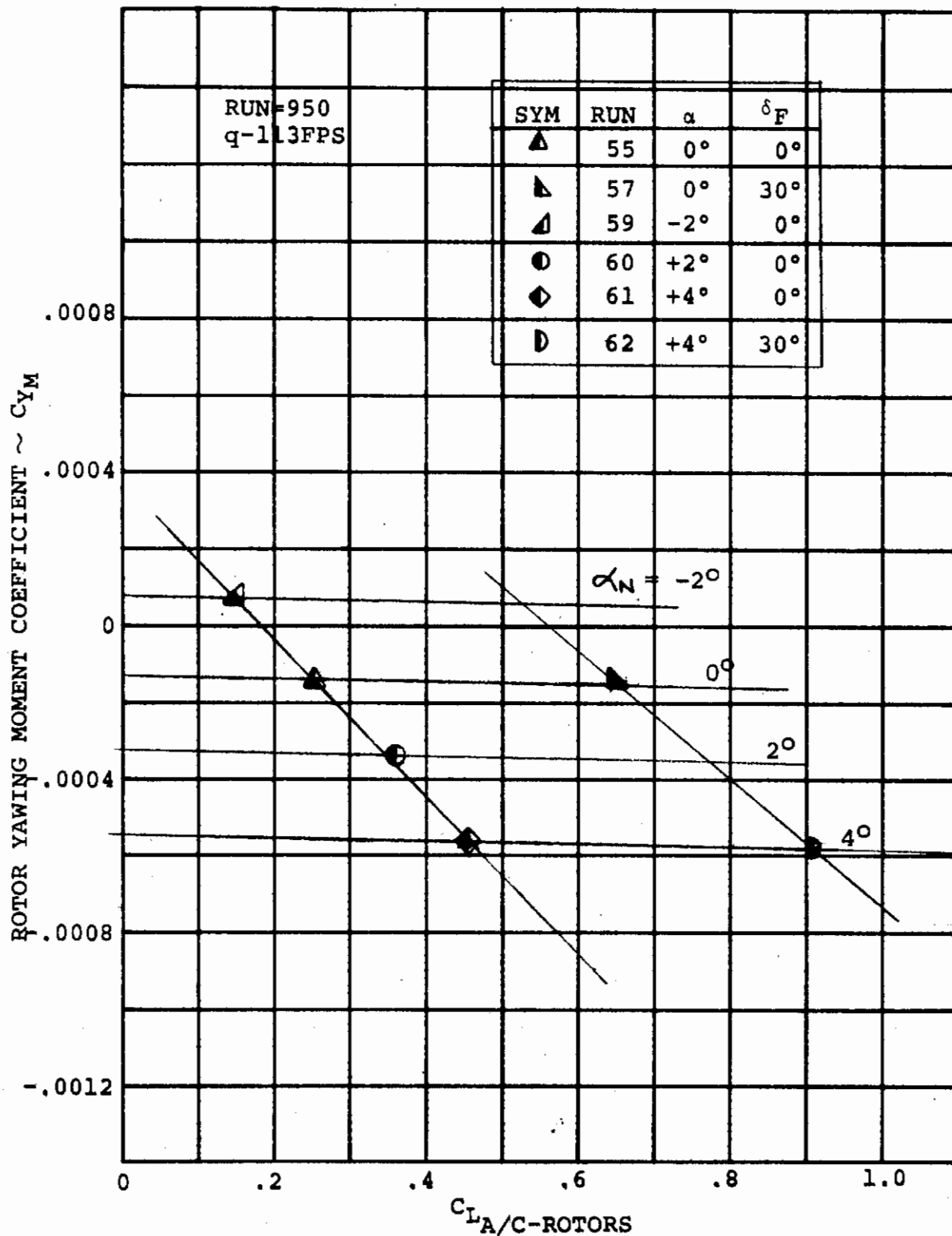


FIGURE C-40 EFFECT OF WING LIFT ON ROTOR YAWING MOMENT  
(V = 113FPS RPM = 950)

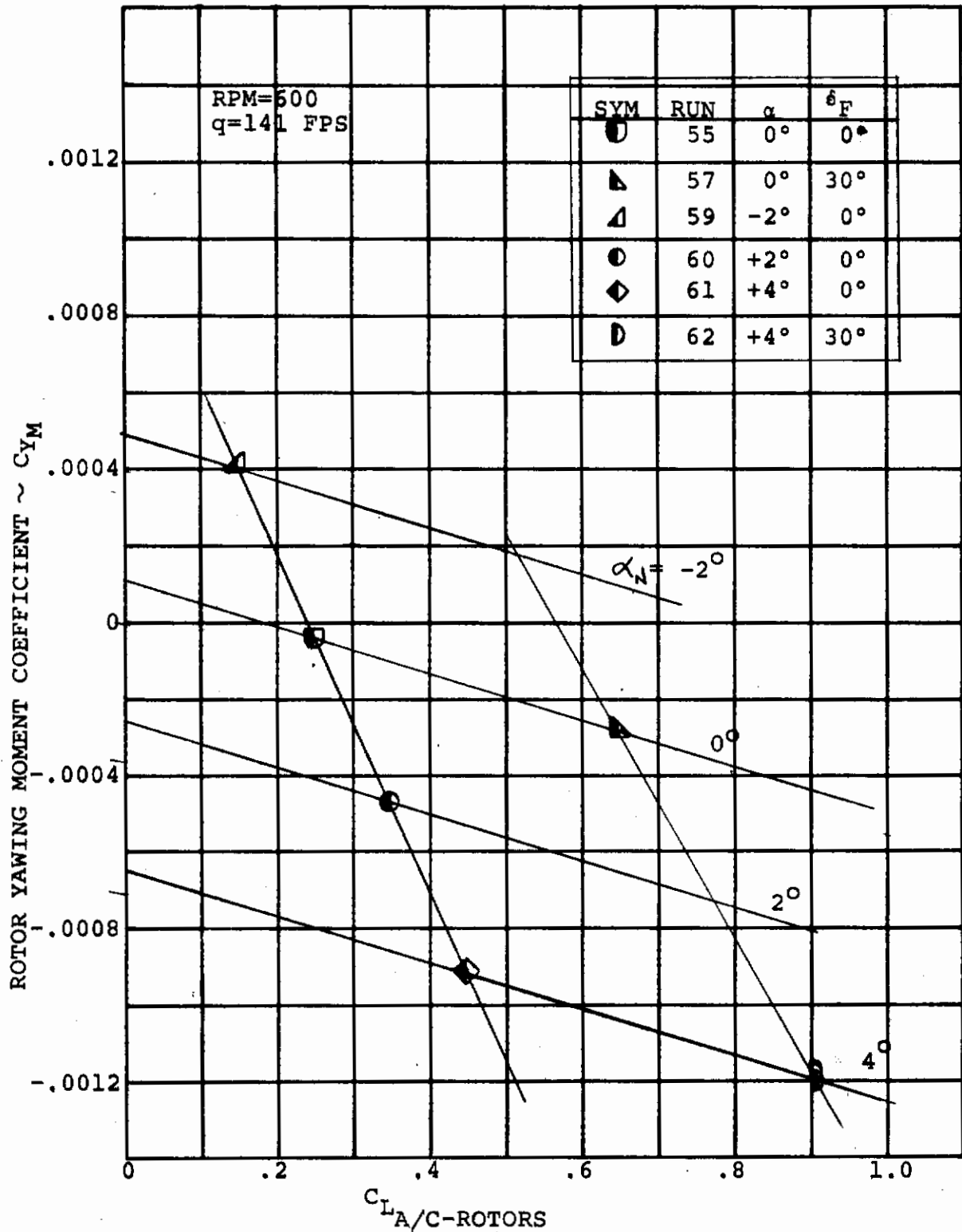


FIGURE C-41 EFFECT OF WING LIFT ON ROTOR YAWING MOMENT  
(V = 141 FPS RPM = 600)

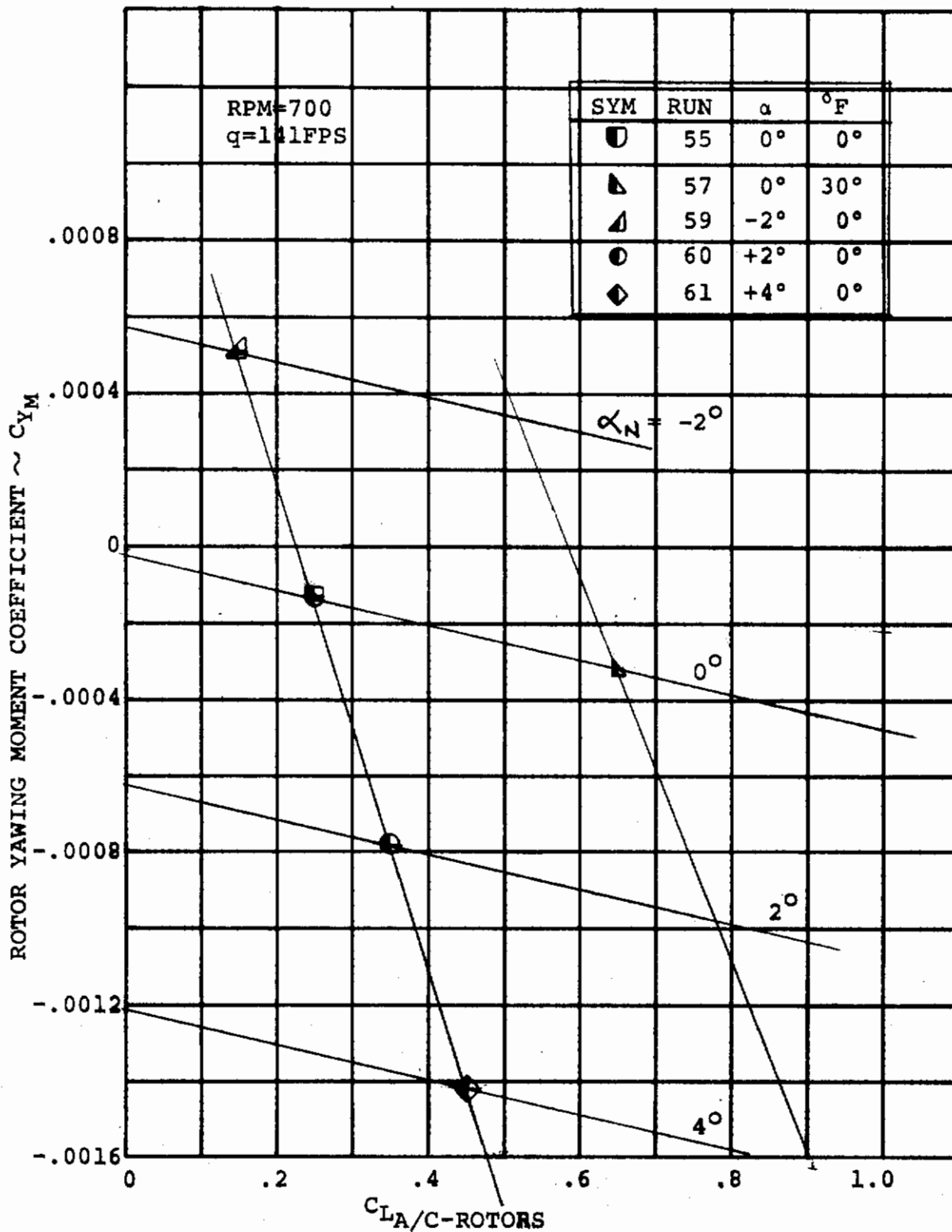


FIGURE C-42 EFFECT OF WING LIFT ON ROTOR YAWING MOMENT  
(V = 141 FPS RPM = 700)

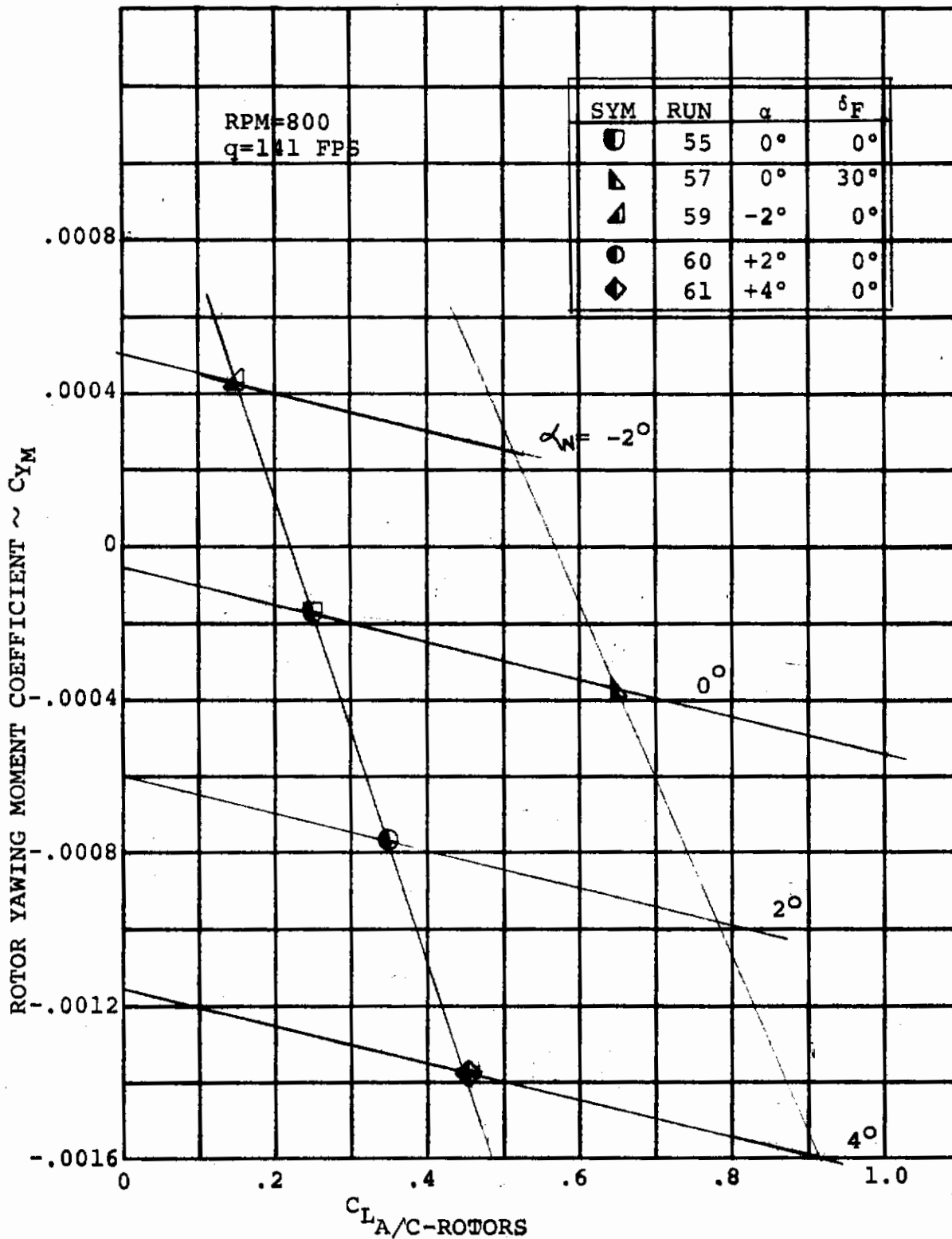


FIGURE C-43 EFFECT OF WING LIFT ON ROTOR YAWING MOMENT  
V = 141 FPS RPM = 800)

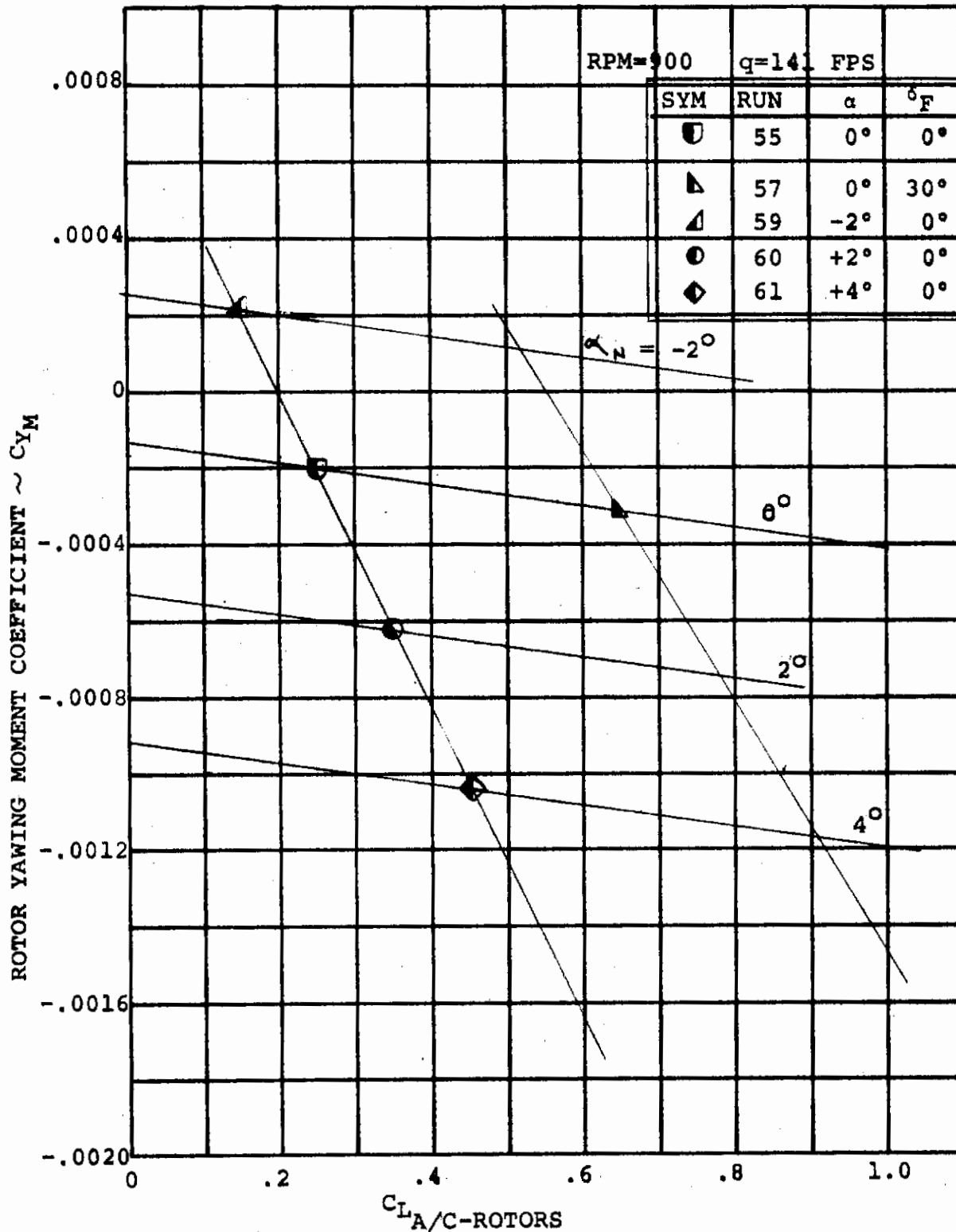


FIGURE C-44 EFFECT OF WING LIFT ON ROTOR YAWING MOMENT  
( V = 141 FPS RPM = 900 )



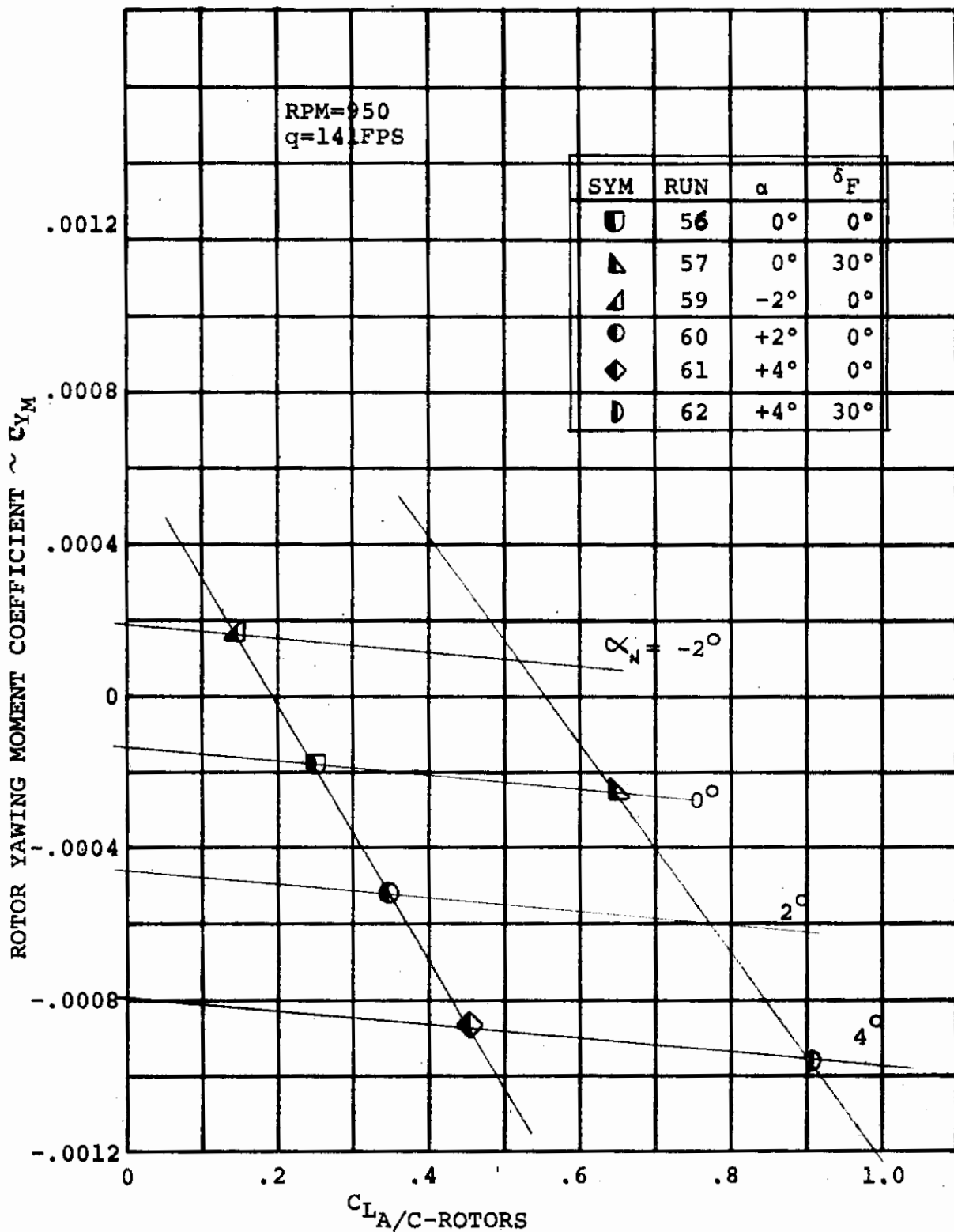


FIGURE C-45 EFFECT OF WING LIFT ON ROTOR YAWING MOMENT  
(V = 141 FPS RPM = 950)

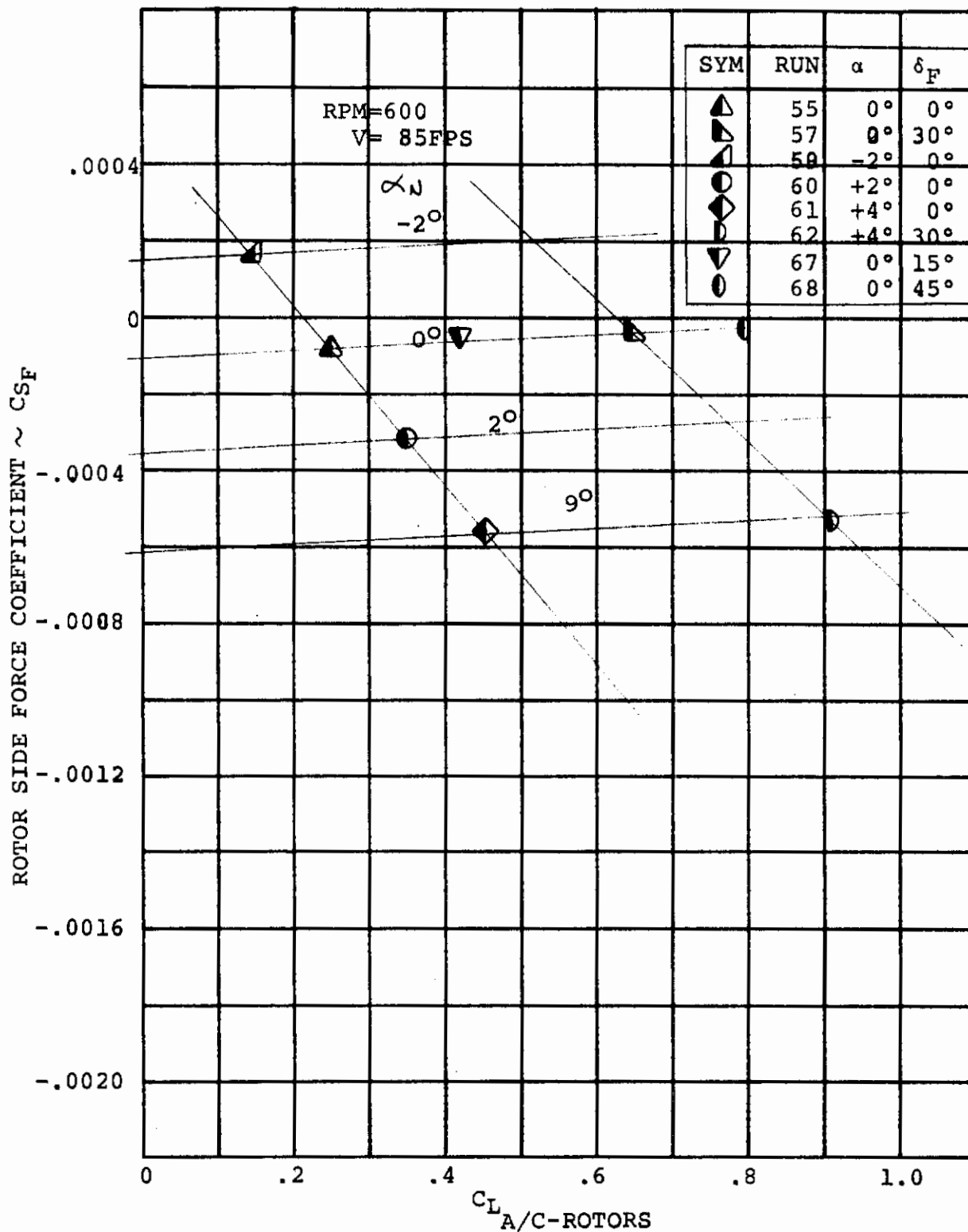
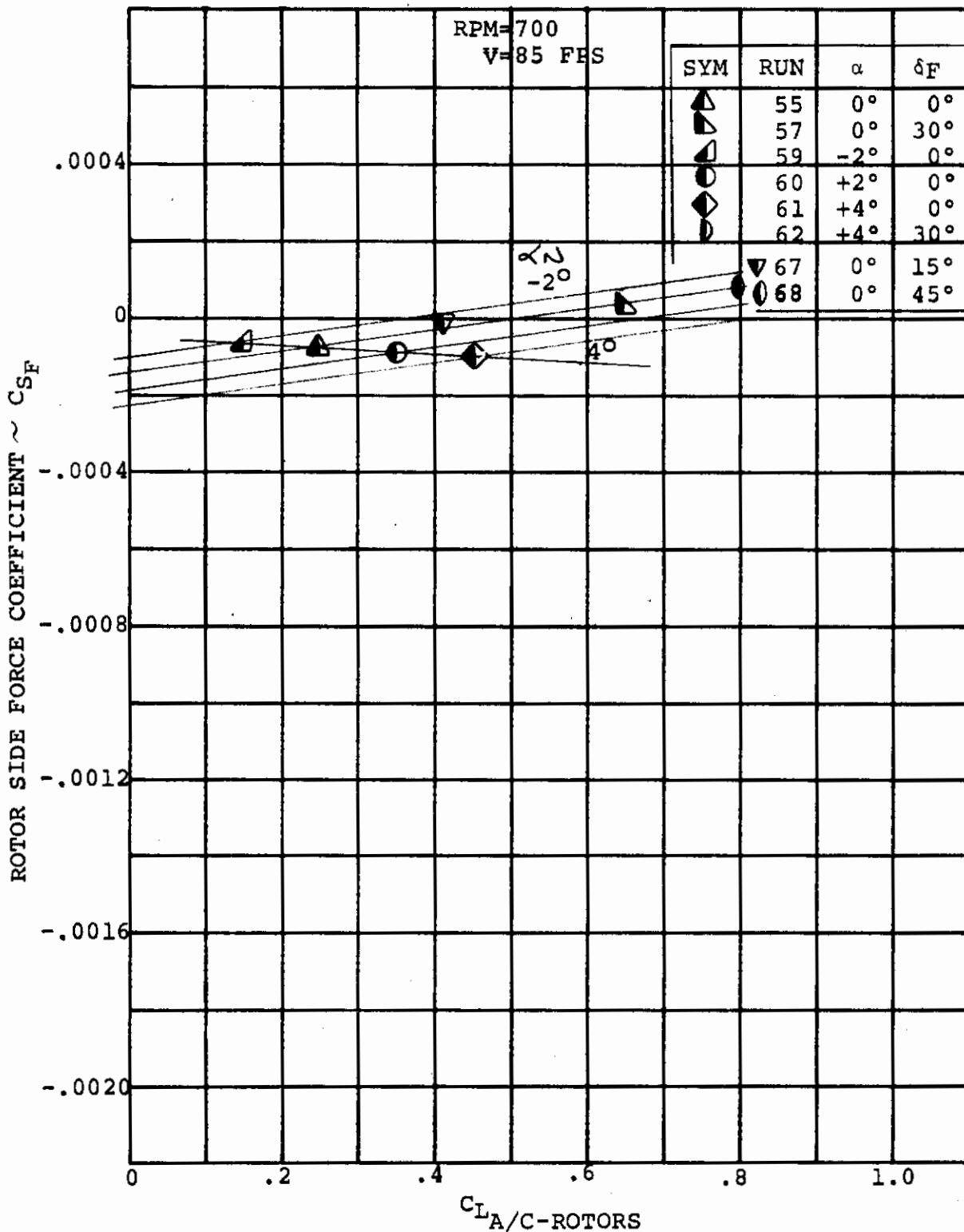


FIGURE C-46 EFFECT OF WING LIFT ON ROTOR SIDE FORCE  
(V = 85 FPS RPM = 600)



FIGURES C-47 EFFECT OF WING LIFT ON ROTOR SIDE FORCE  
(V = 85 FPS RPM = 700)

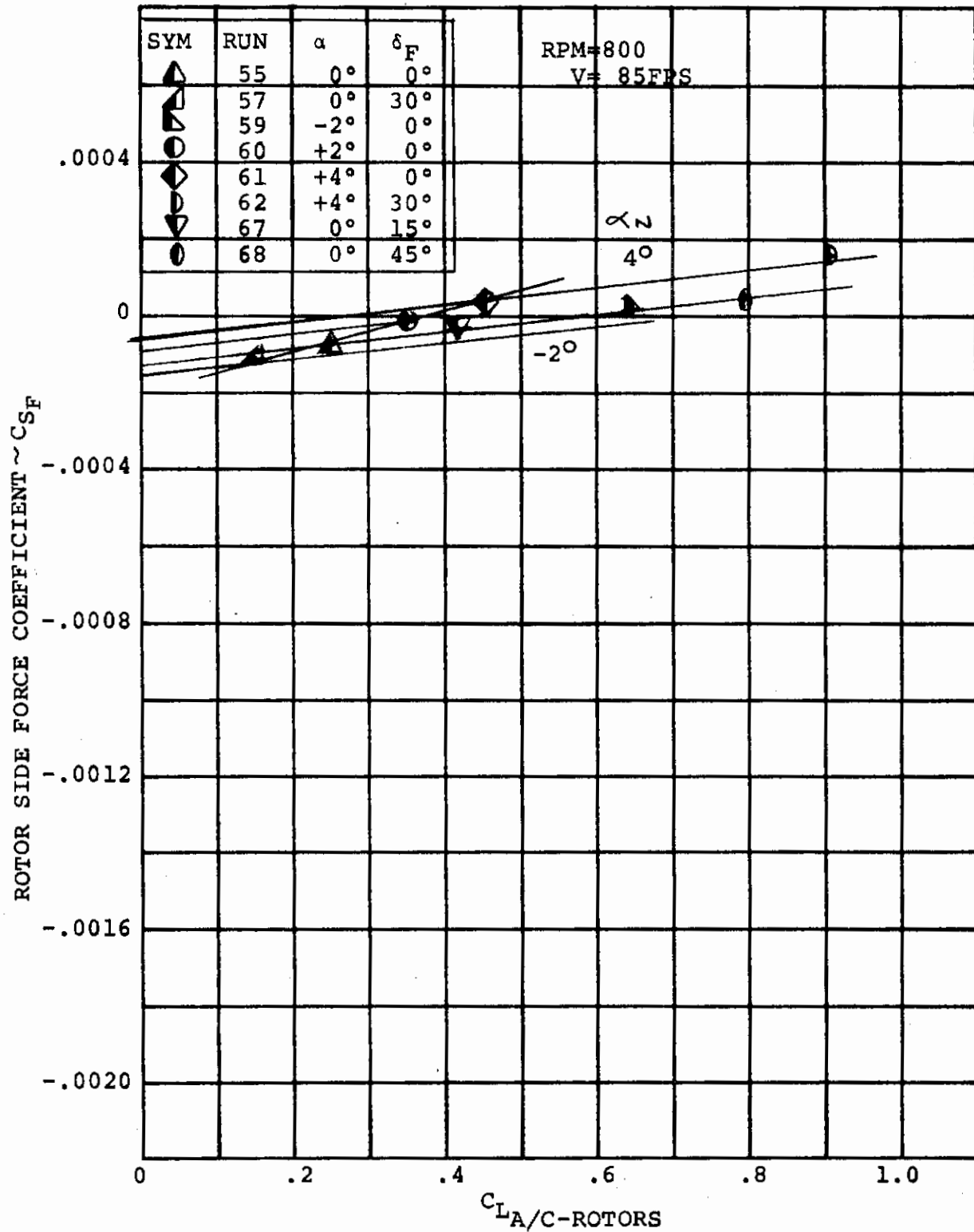


FIGURE C-48 EFFECT OF WING LIFT ON ROTOR SIDE FORCE  
(V = 85 FPS RPM = 800)

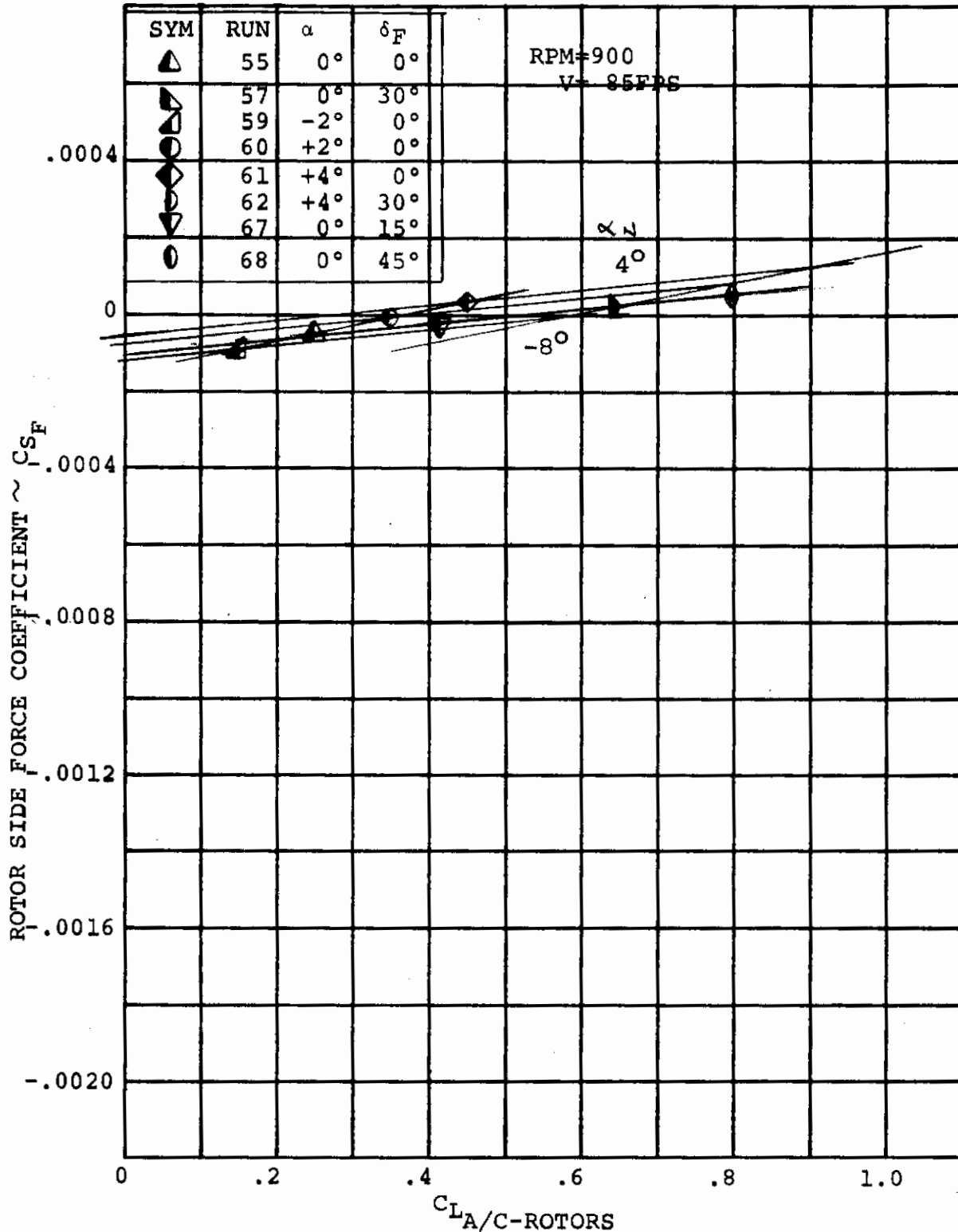


FIGURE C-49 EFFECT OF WING LIFT ON ROTOR SIDE FORCE  
(V = 85 FPS RPM = 900)

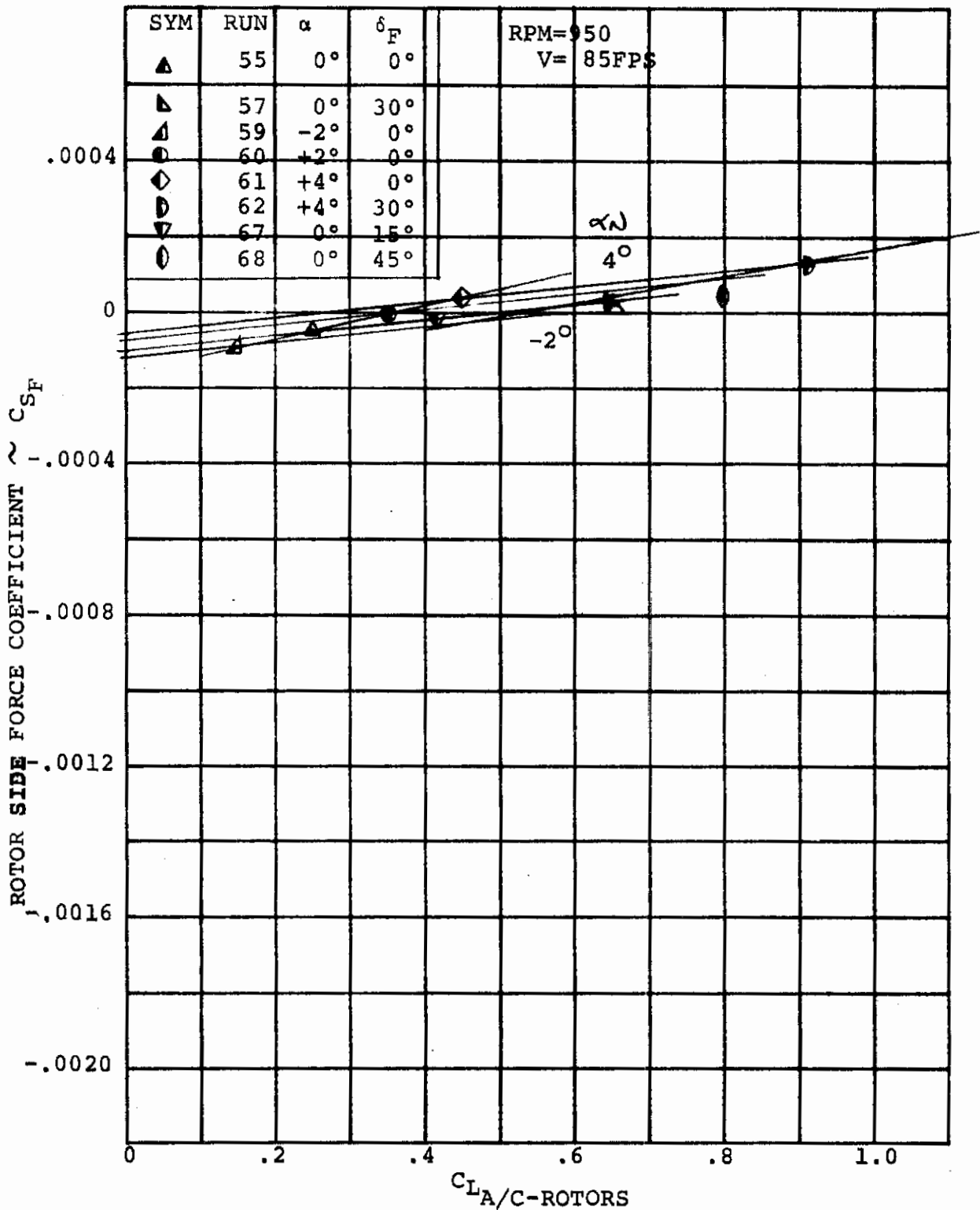


FIGURE C-50 EFFECT OF WING LIFT ON ROTOR SIDE FORCE  
(V = 85 FPS RPM = 950)

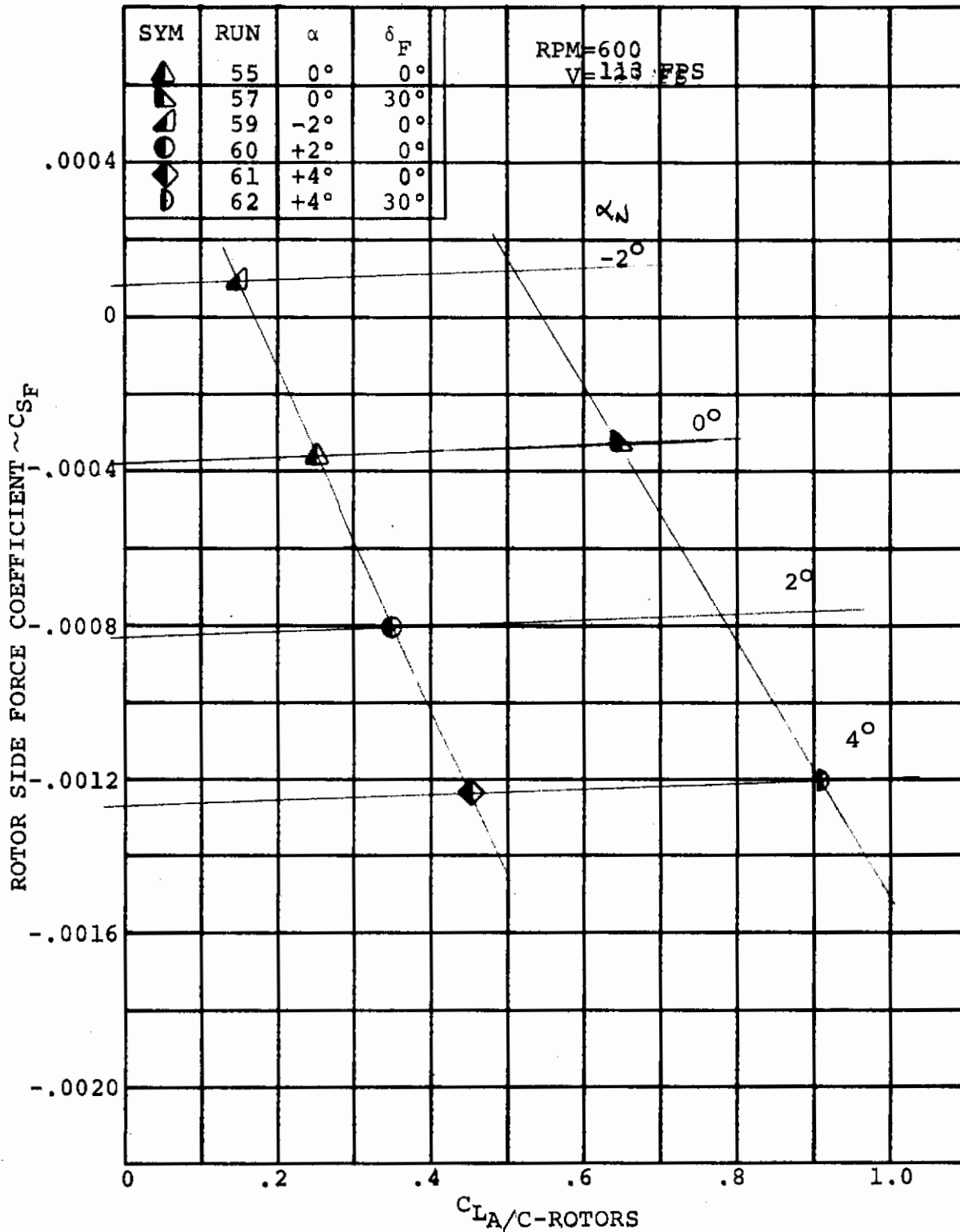


FIGURE C-51 EFFECT OF WING LIFT ON ROTOR SIDE FORCE  
(V = 113 FPS RPM = 600)

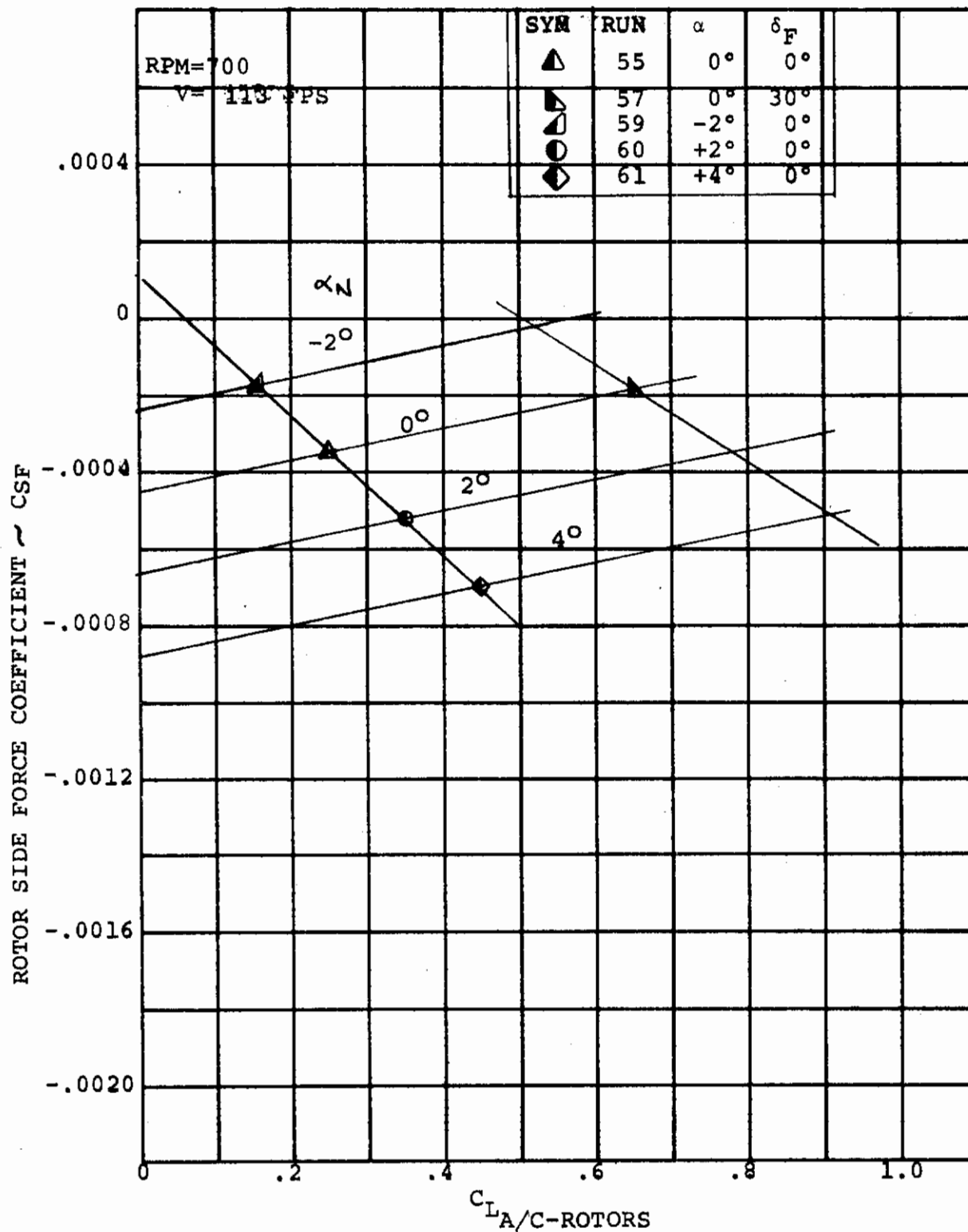


FIGURE C-52 EFFECT OF WING LIFT ON ROTOR SIDE FORCE  
( V = 113 FPS RPM=700)



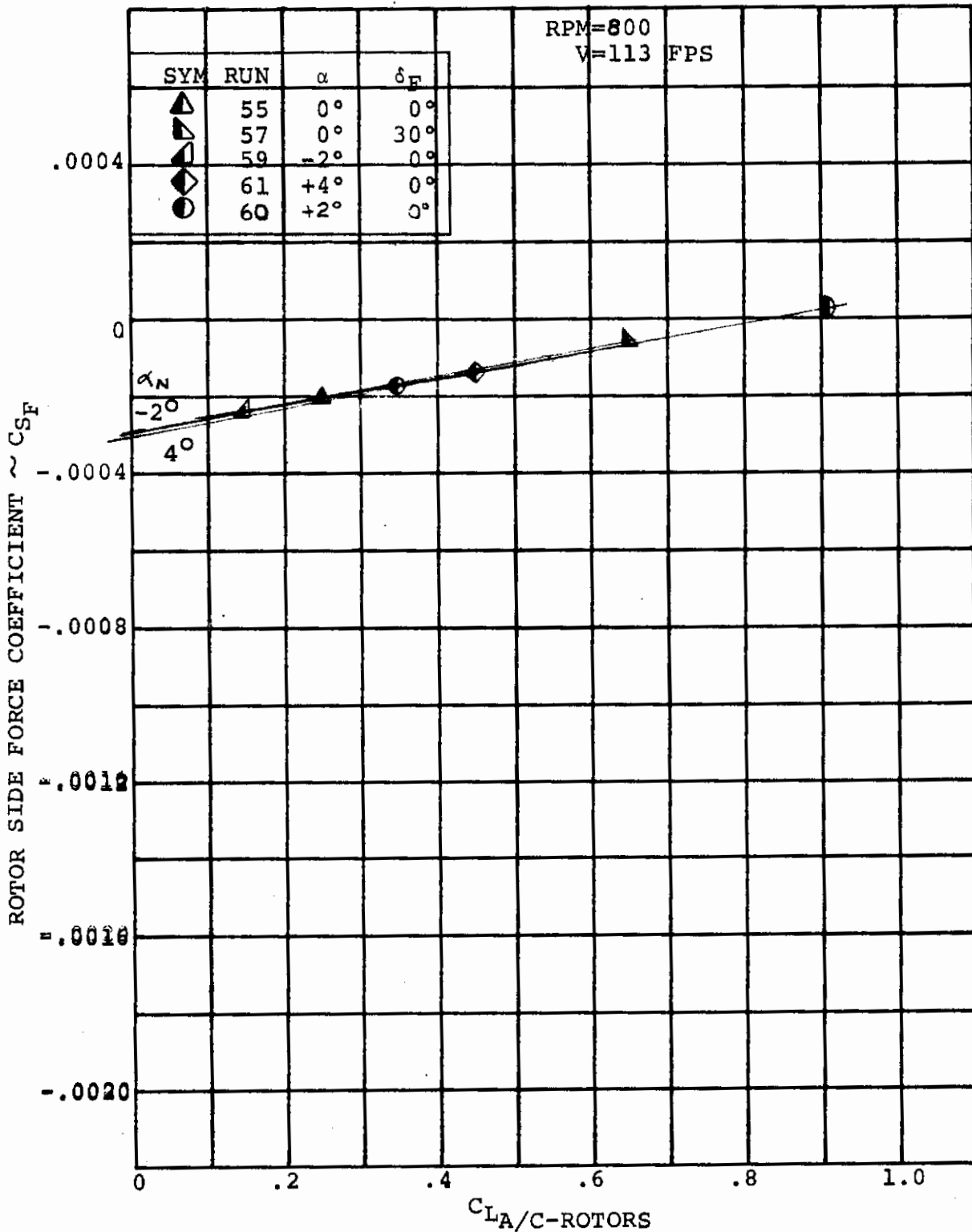


FIGURE C-53 EFFECT OF WING LIFT ON ROTOR SIDE FORCE  
( V = 113 FPS RPM = 800 )

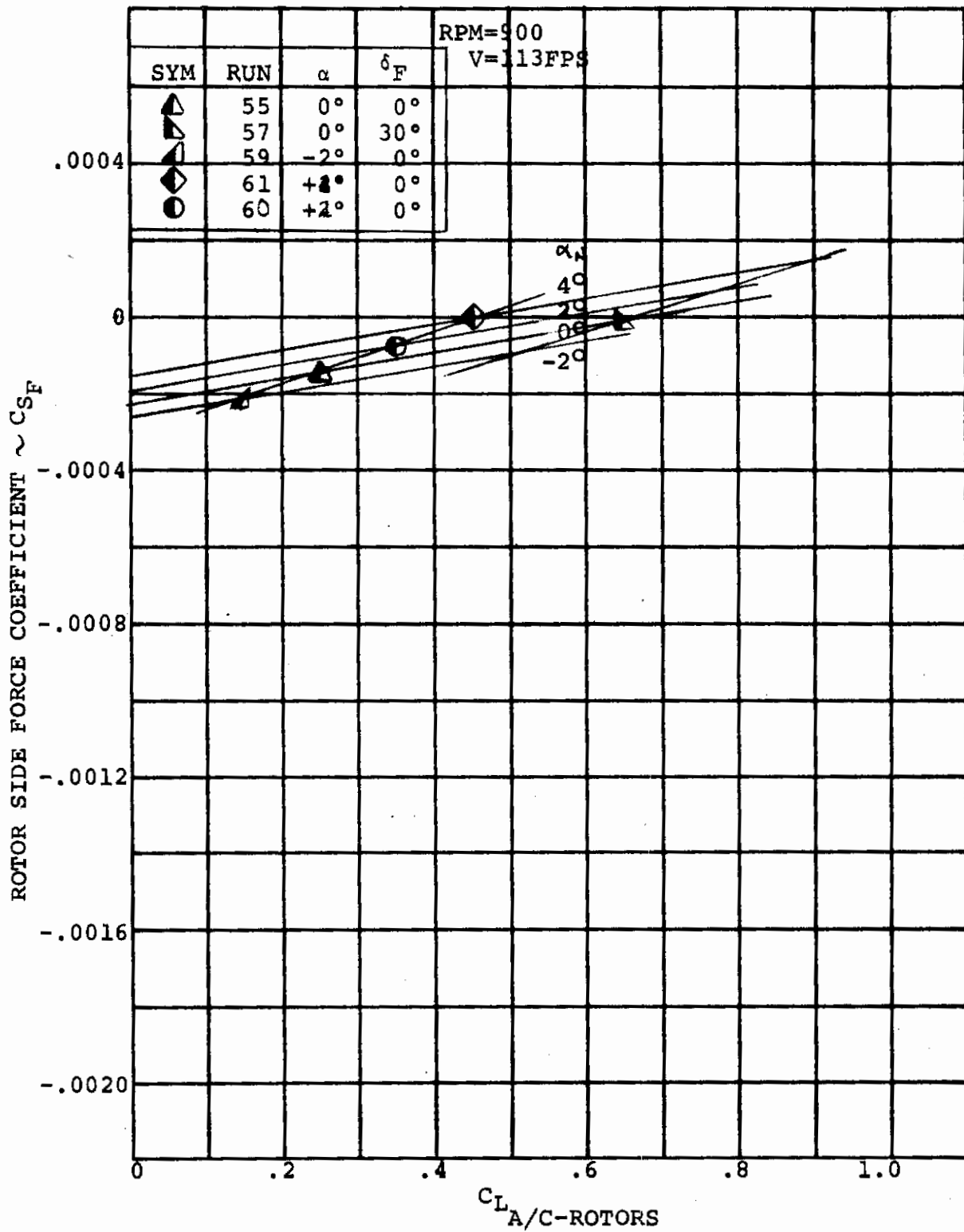


FIGURE C-54 EFFECT OF WING LIFT ON ROTOR SIDE FORCE.  
(V = 113 FPS RPM = 900)

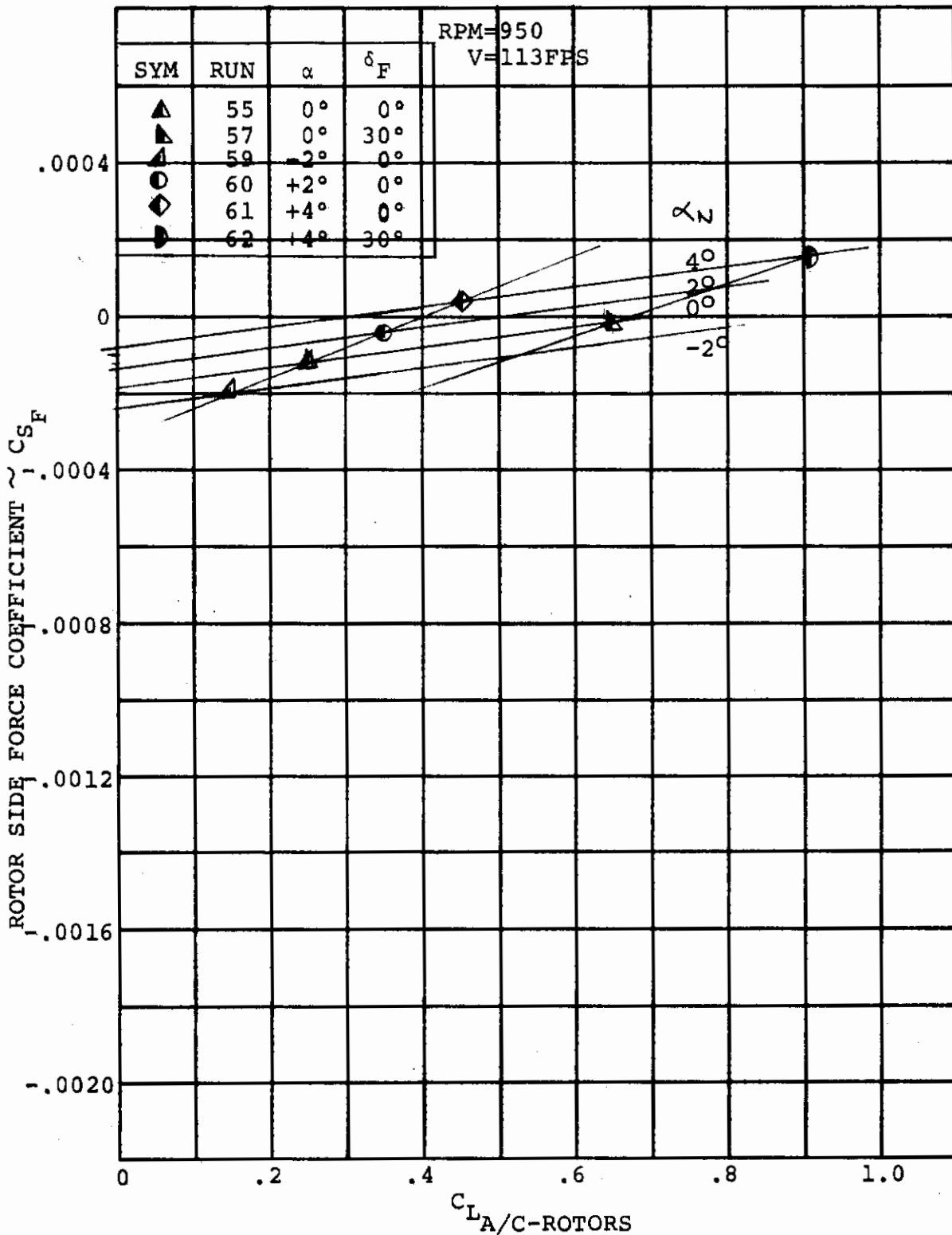


FIGURE C-55 EFFECT OF WING LIFT ON ROTOR SIDE FORCE  
( V = 113 FPS RPM = 950)

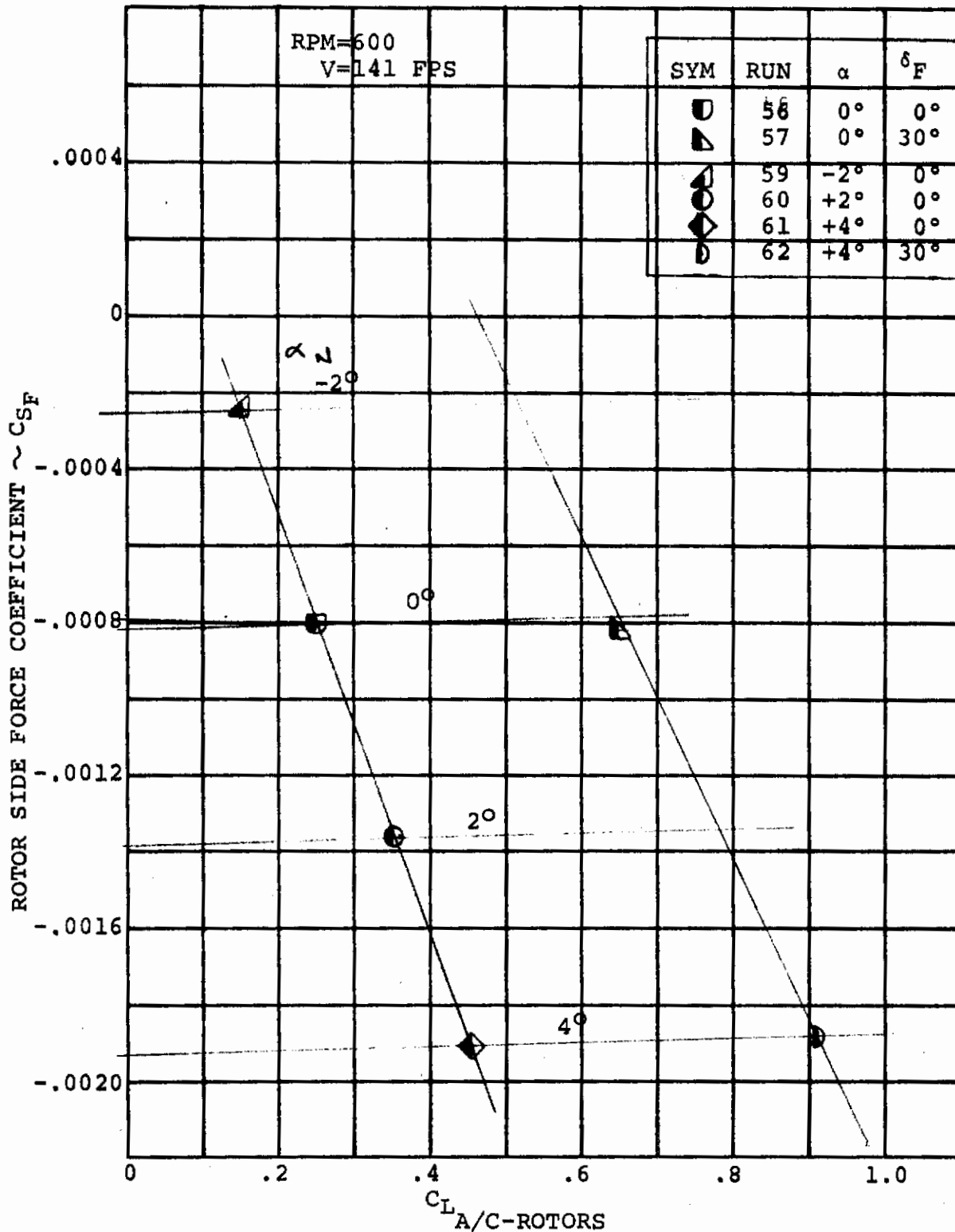


FIGURE C-56 EFFECT OF WING LIFT ON ROTOR SIDE FORCE  
( V = 141 FPS RPM = 600 )

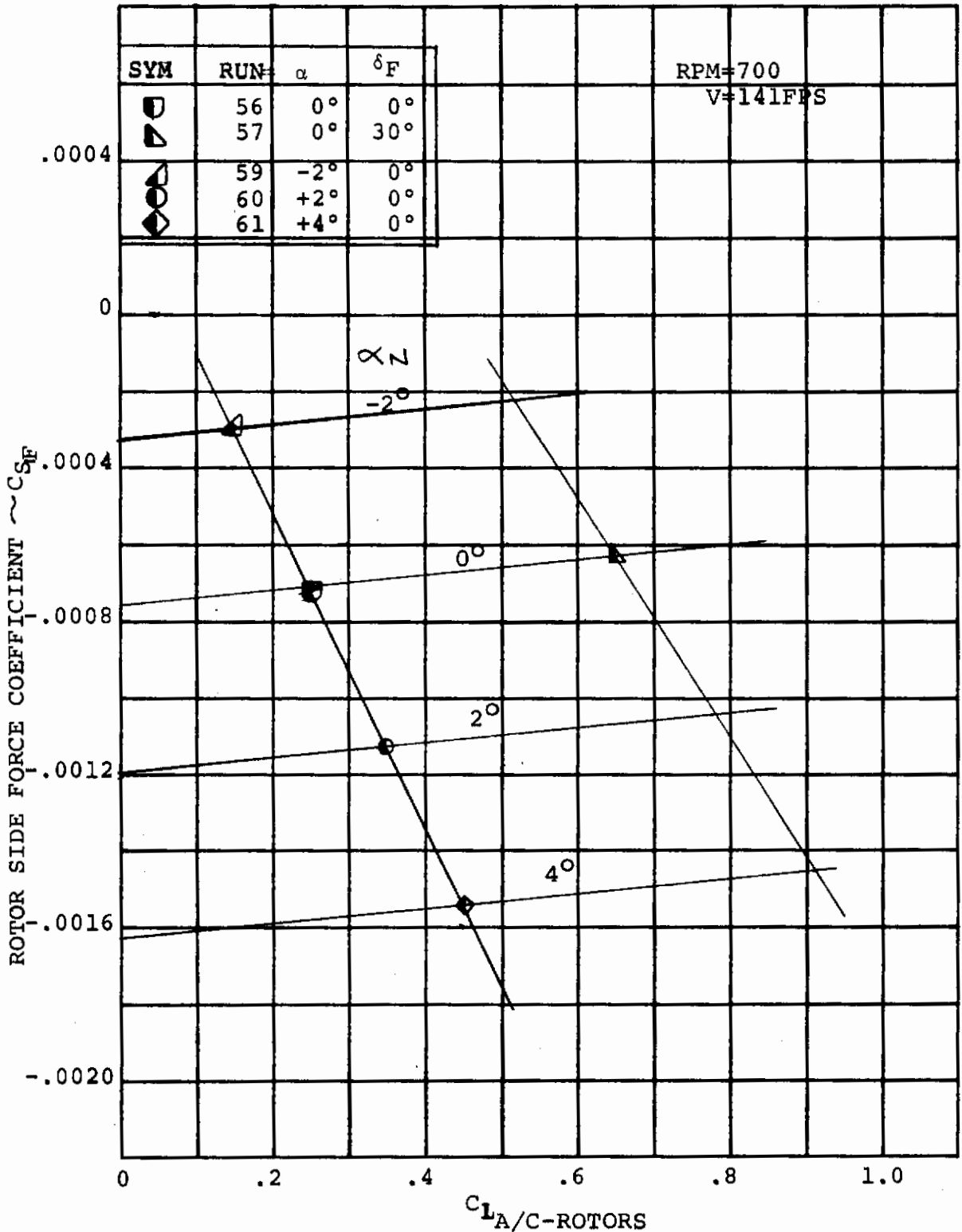


FIGURE C-57 EFFECT OF WING LIFT ON ROTOR SIDE FORCE  
( V = 141 FPS RPM = 700 )

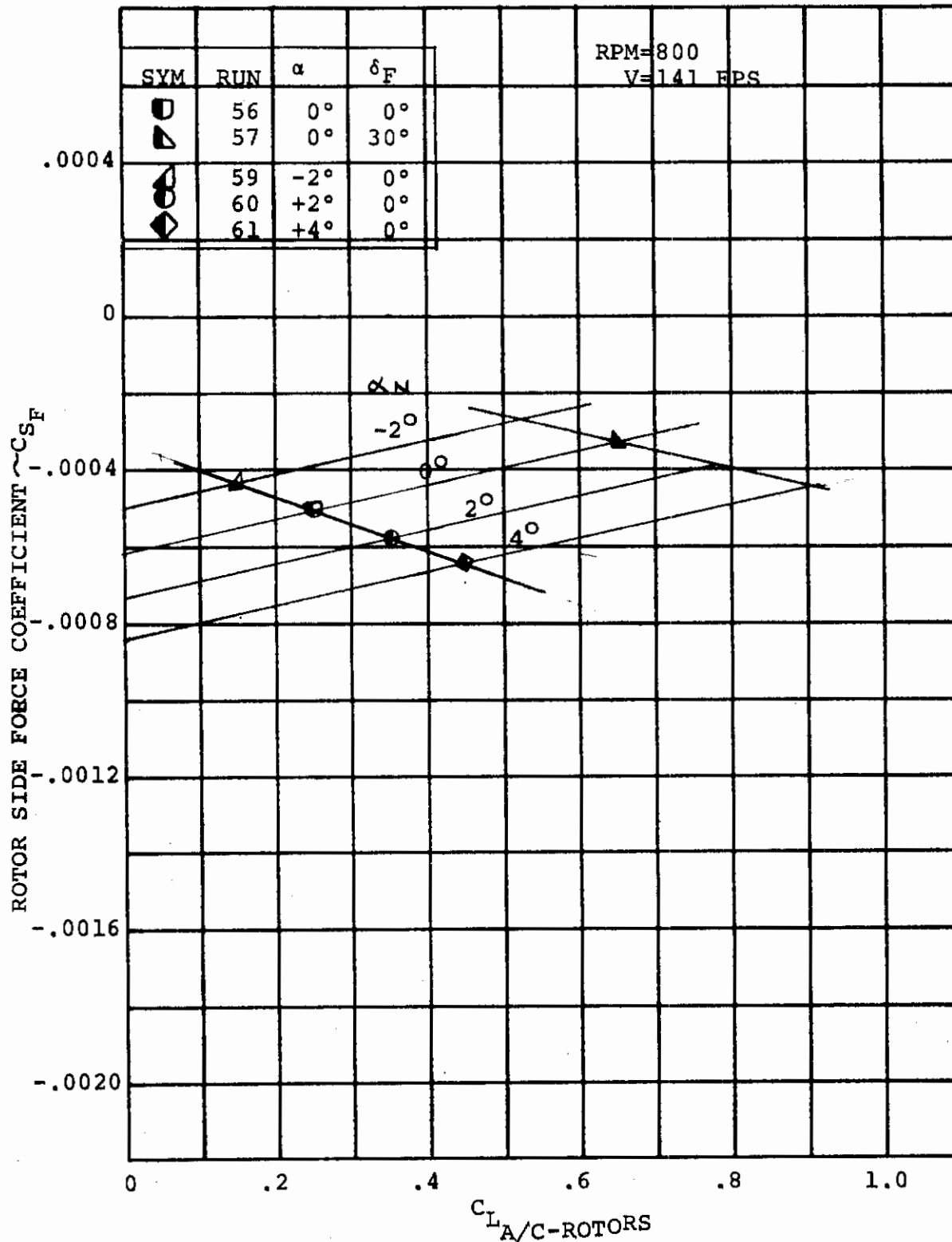


FIGURE C-58 EFFECT OF WING LIFT ON ROTOR SIDE FORCE  
(V = 141 FPS RPM = 800)

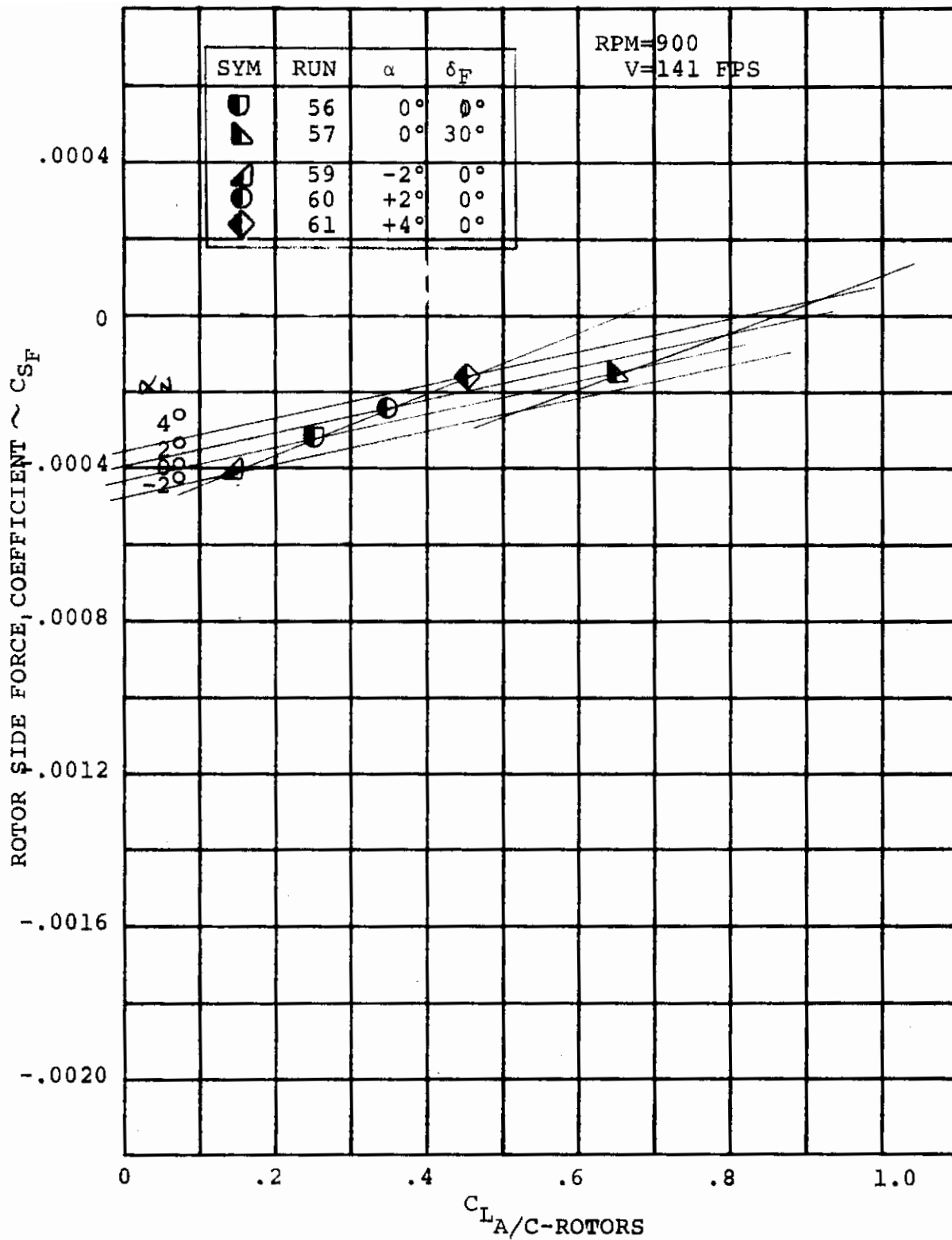


FIGURE C-59 EFFECT OF WING LIFT ON ROTOR SIDE FORCE  
(V = 141 FPS RPM = 900)

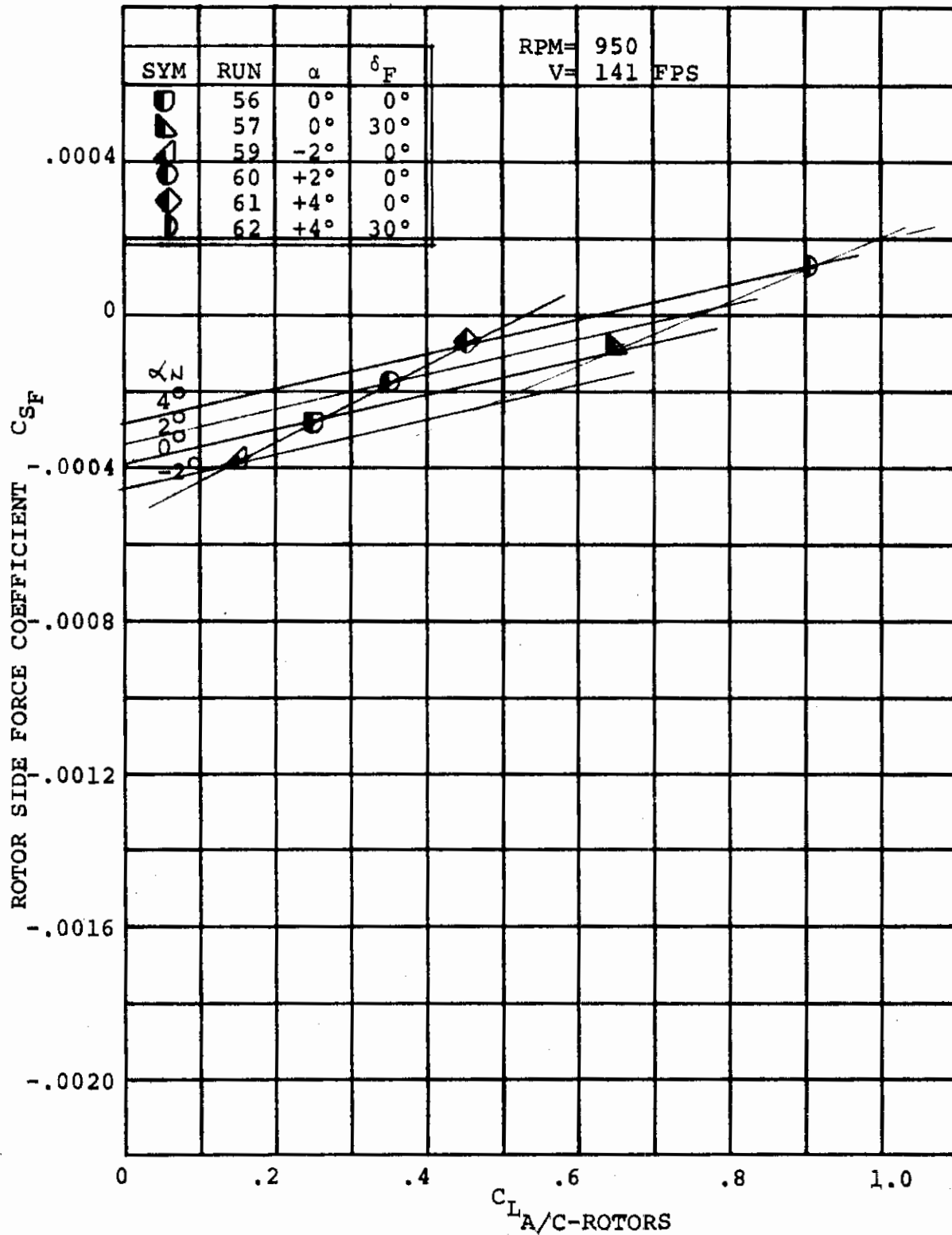


FIGURE C-60 EFFECT OF WING LIFT ON ROTOR SIDE FORCE  
(V = 141 FPS RPM = 950)



APPENDIX D

ROTOR CHARACTERISTICS WITHOUT CIRCULATION EFFECTS

The data presented here is a summary of the rotor characteristics presented in Appendix C at zero air-frame lift.

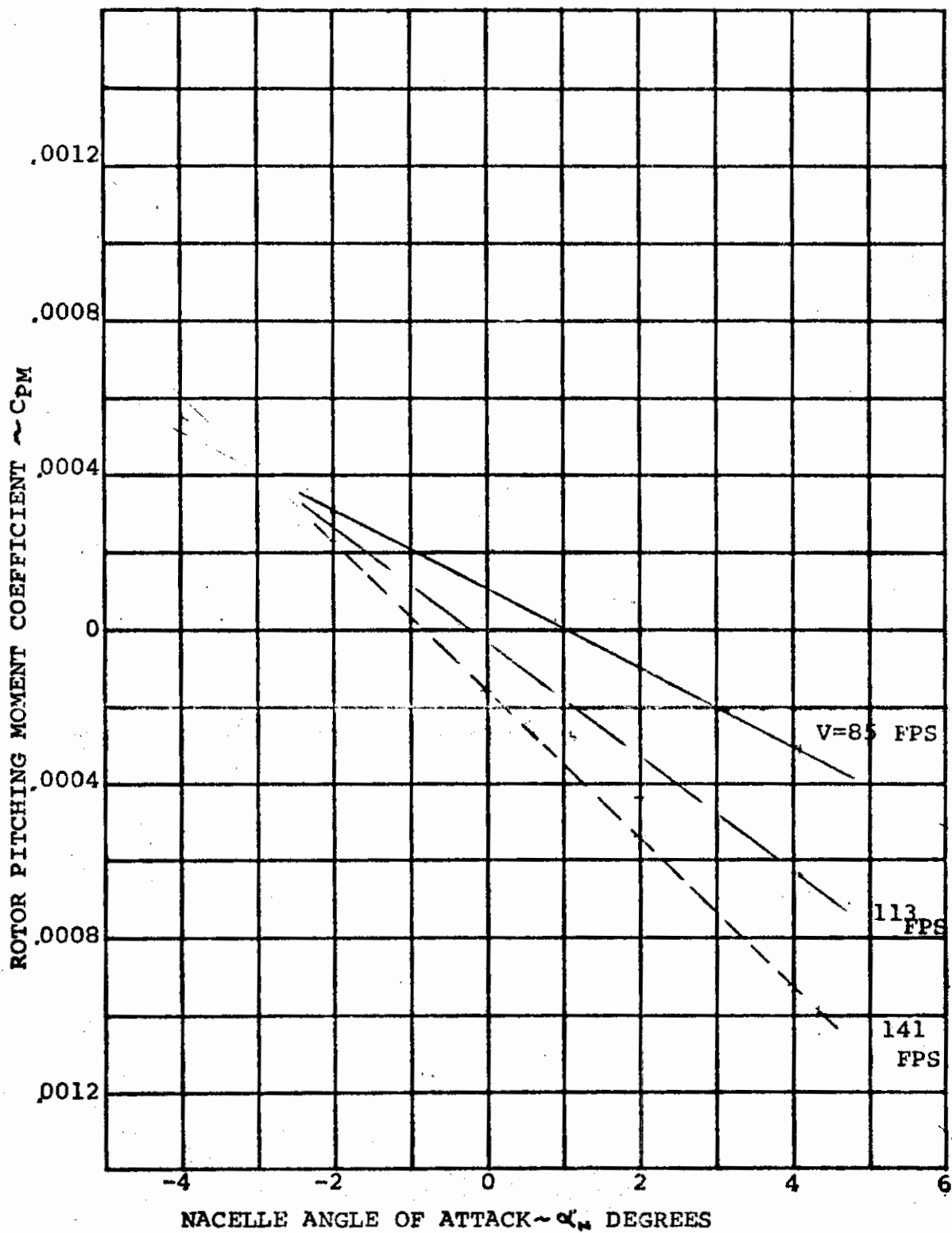


FIGURE D-1 ROTOR PITCHING MOMENT/NACELLE ANGLE OF ATTACK FOR ROTOR RPM = 600 δ<sub>r</sub> = 0°. (CIRCULATION EFFECTS REMOVED)

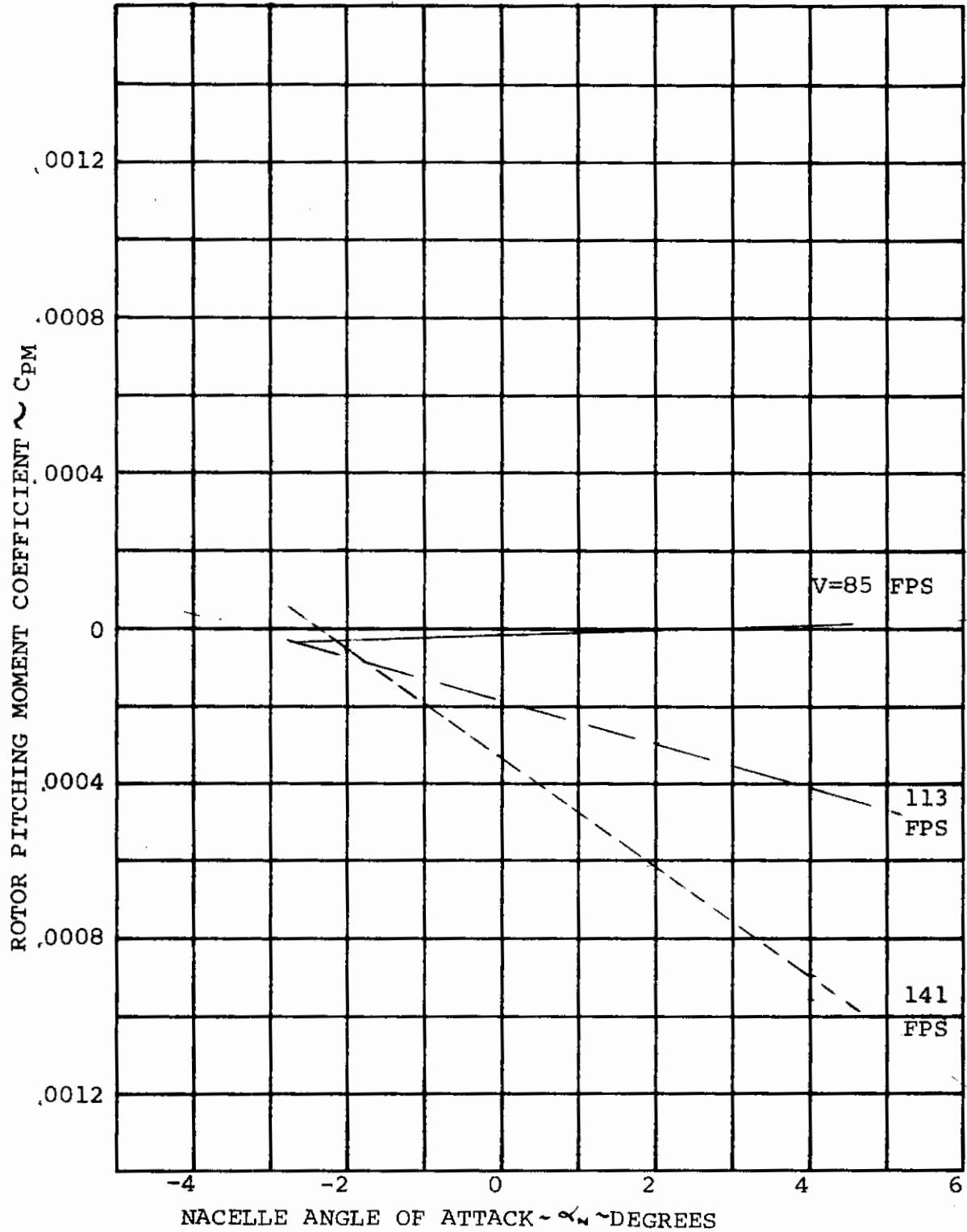


FIGURE D-2 ROTOR PITCHING MOMENT/NACELLE ANGLE OF ATTACK FOR ROTOR RPM = 700  $S_p = 0^\circ$  (CIRCULATION EFFECTS REMOVED)

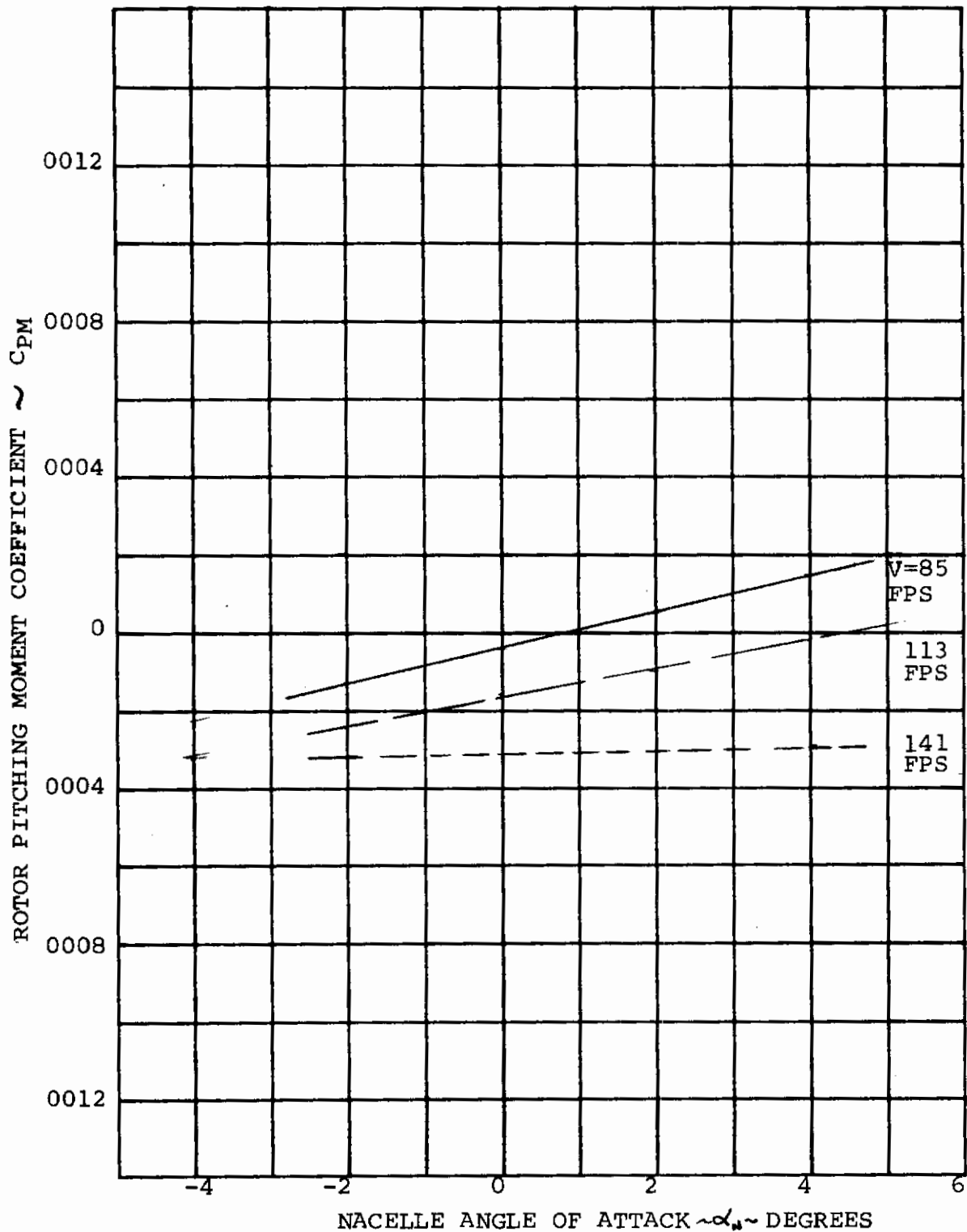


FIGURE D-3 ROTOR PITCHING MOMENT/NACELLE ANGLE OF ATTACK FOR ROTOR RPM = 800  $\delta_r = 0^\circ$  (CIRCULATION EFFECTS REMOVED)

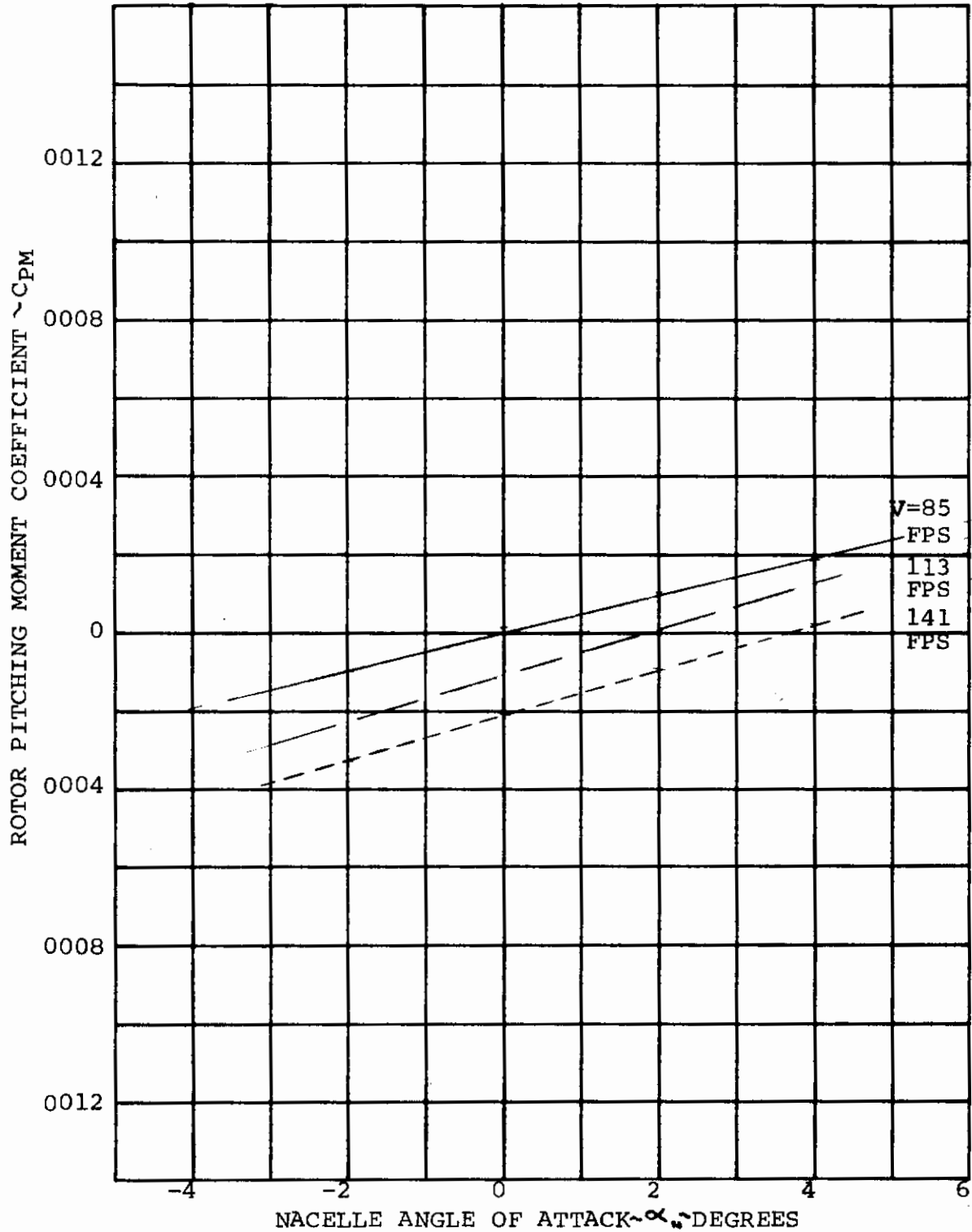


FIGURE D-4 ROTOR PITCHING MOMENT/NACELLE ANGLE OF ATTACK FOR ROTOR RPM = 900  $\delta_f = 0^\circ$  (CIRCULATION EFFECTS REMOVED)

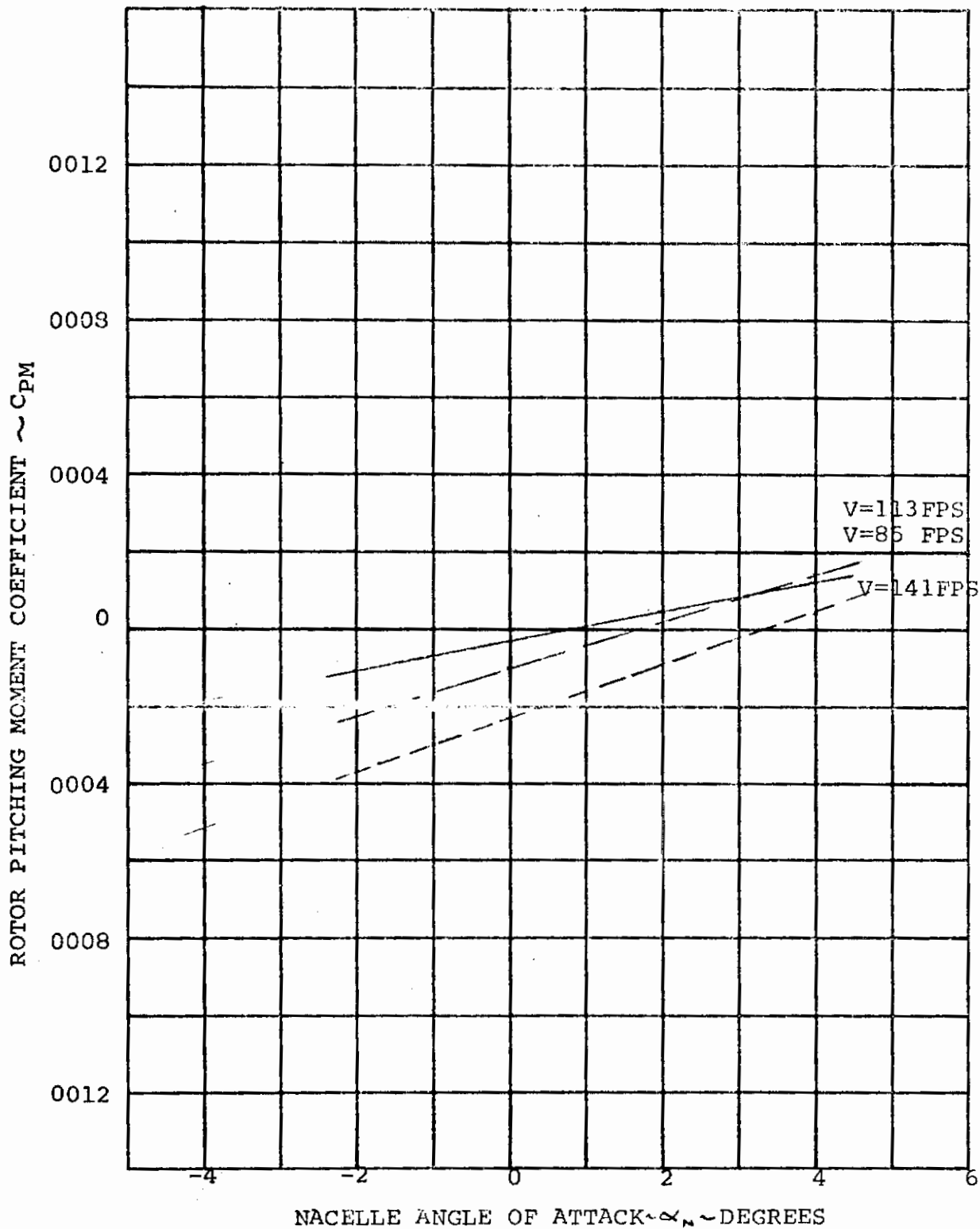


FIGURE D-5 ROTOR PITCHING MOMENT/NACELLE ANGLE OF ATTACK FOR ROTOR RPM = 950  $\beta_r = 0^\circ$  (CIRCULATION EFFECTS REMOVED)

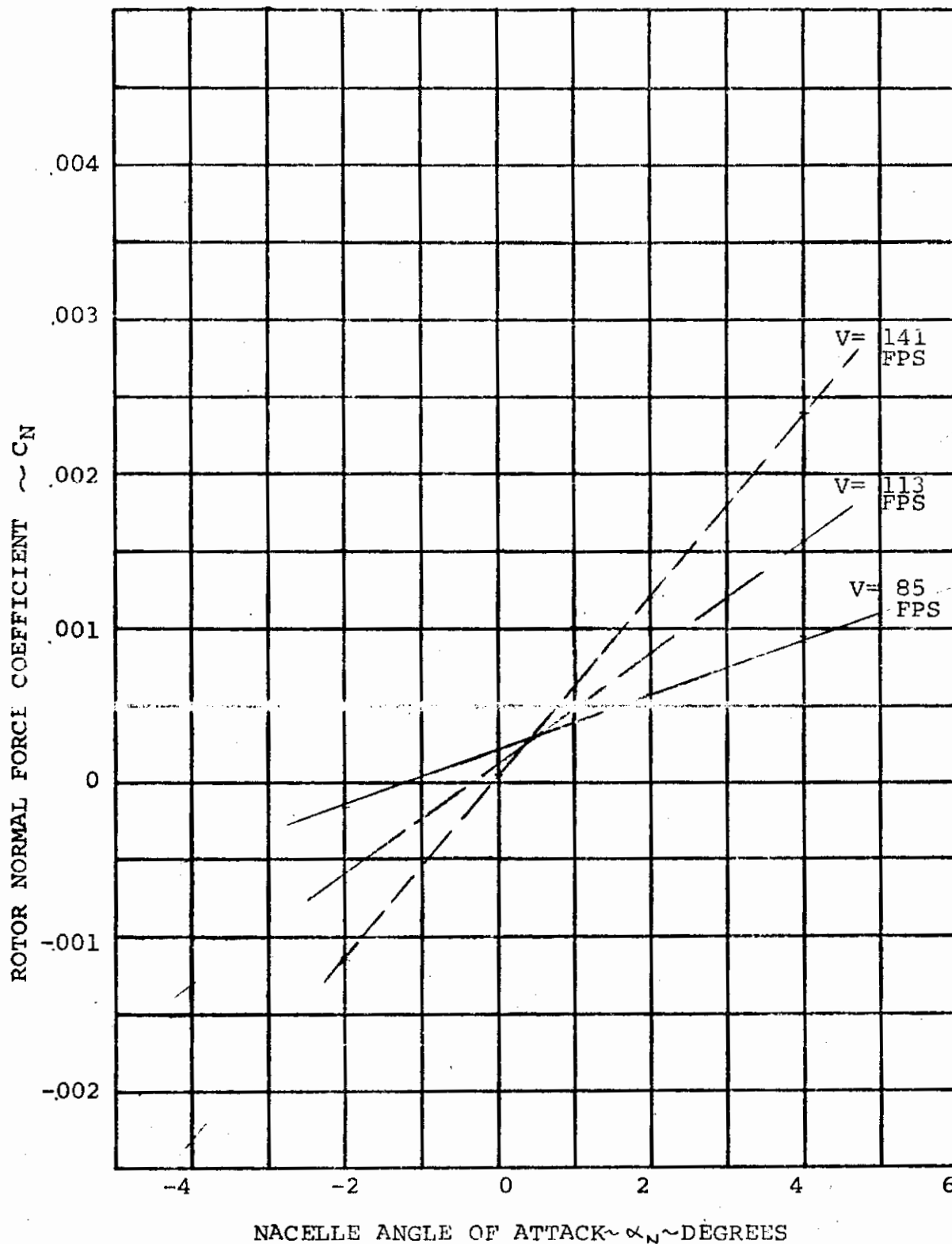


FIGURE D-6 ROTOR NORMAL FORCE/NACELLE ANGLE OF ATTACK VARIATION FOR ROTOR RPM = 600  $\delta_F = 0^\circ$   
(CIRCULATION EFFECTS REMOVED)

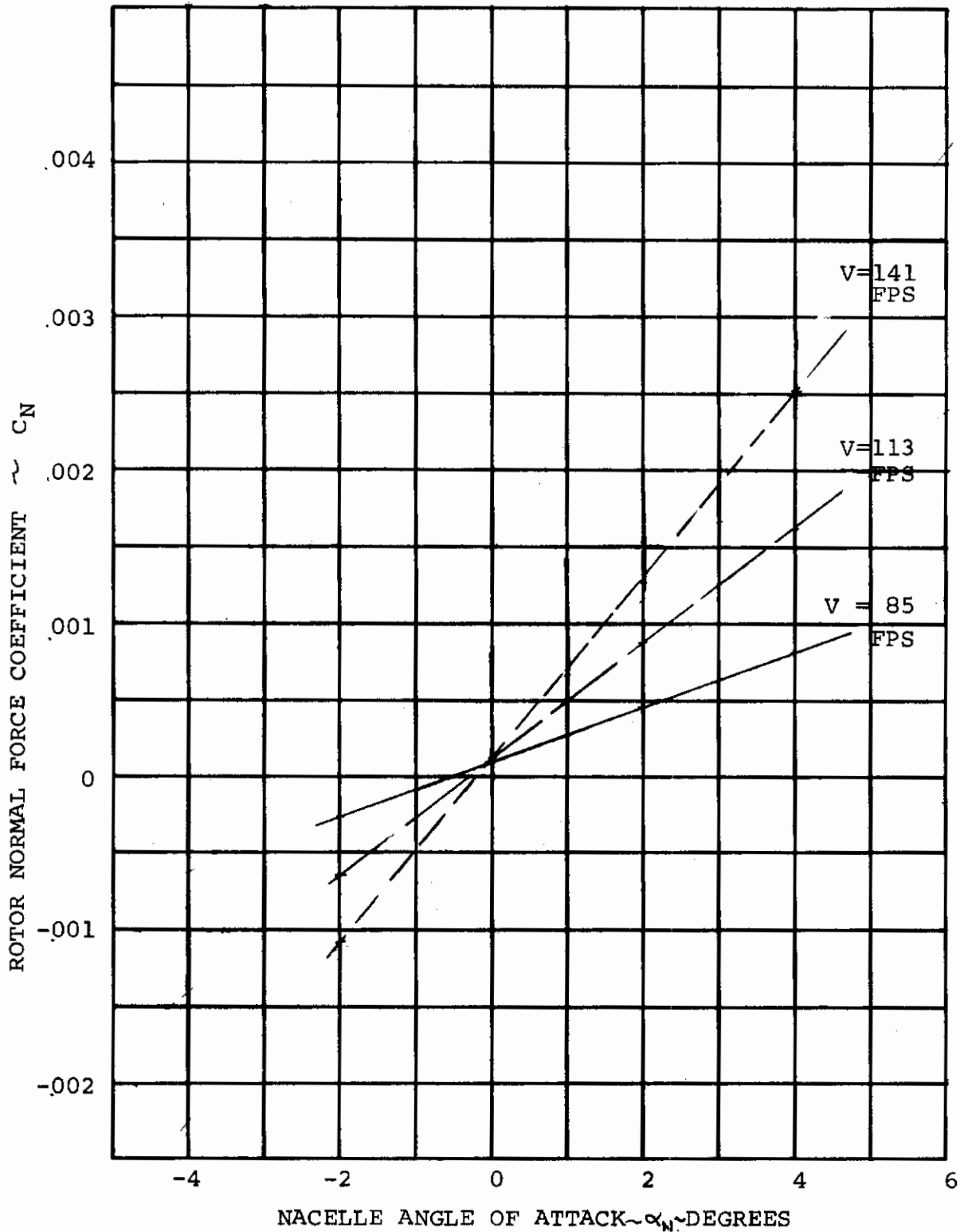


FIGURE D-7 ROTOR NORMAL FORCE/NACELLE ANGLE OF ATTACK VARIATION FOR ROTOR RPM = 700  $\delta_{\alpha} = 0^{\circ}$  (CIRCULATION EFFECTS REMOVED)



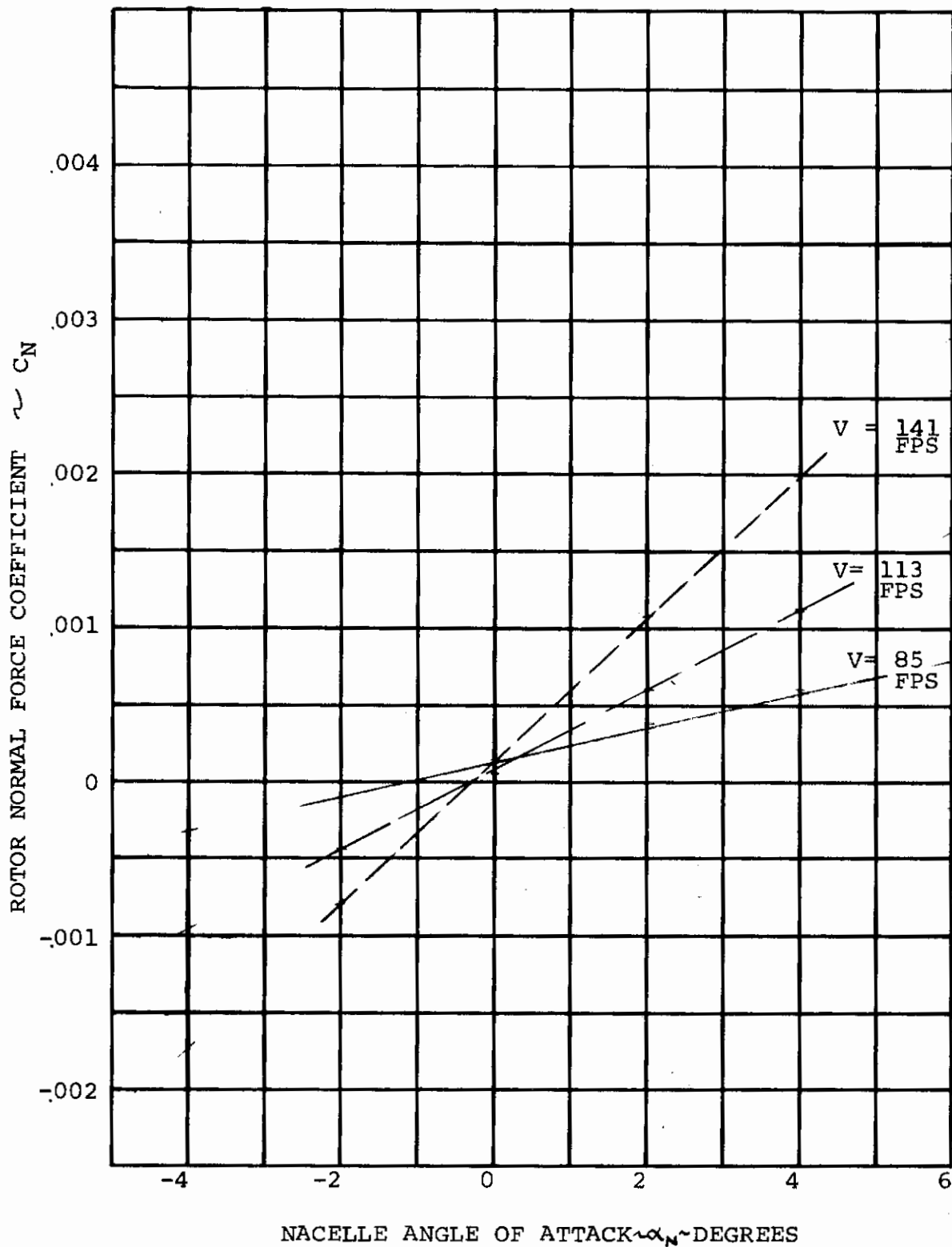


FIGURE D-8 ROTOR NORMAL FORCE/NACELLE ANGLE OF ATTACK VARIATION FOR ROTOR RPM = 800  $\delta_F = 0^\circ$  (CIRCULATION EFFECTS REMOVED)

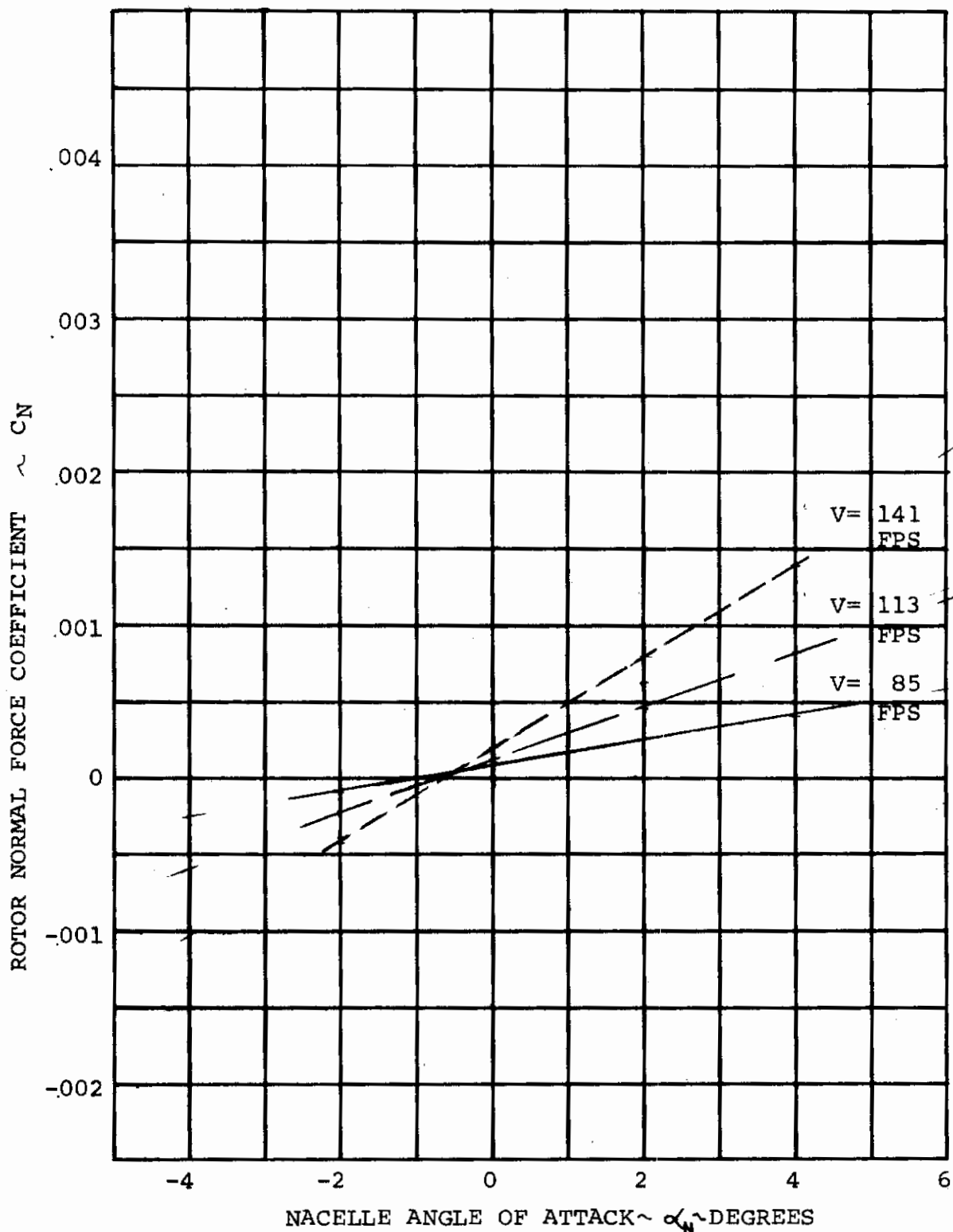


FIGURE D-9 ROTOR NORMAL FORCE/NACELLE ANGLE OF ATTACK VARIATION FOR ROTOR RPM = 900  $\delta_r = 0^\circ$  (CIRCULATION EFFECTS REMOVED)

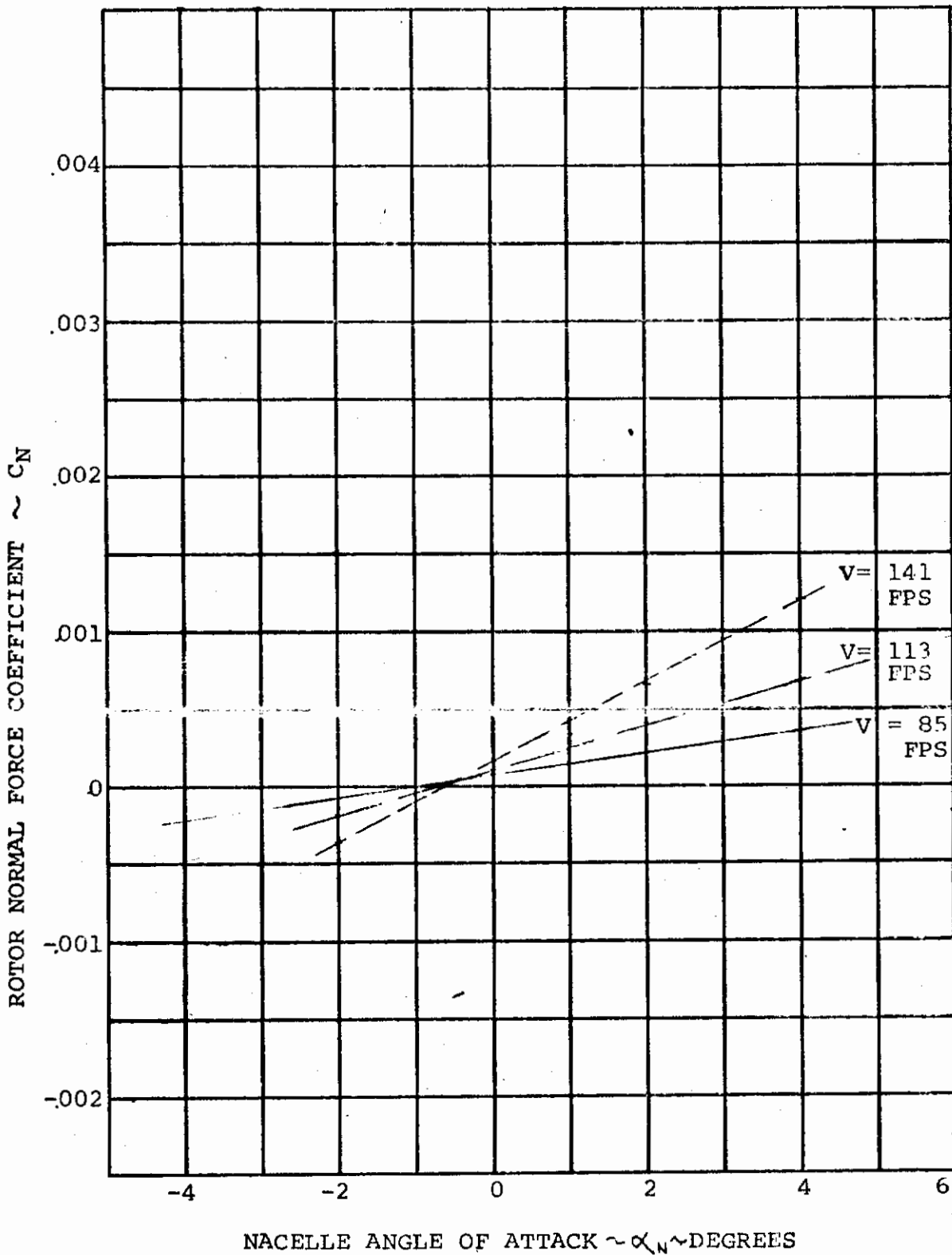


FIGURE D-10 ROTOR NORMAL FORCE/NACELLE ANGLE OF ATTACK VARIATION FOR ROTOR RPM = 950  $S_F = 0^\circ$  (CIRCULATION EFFECTS REMOVED)

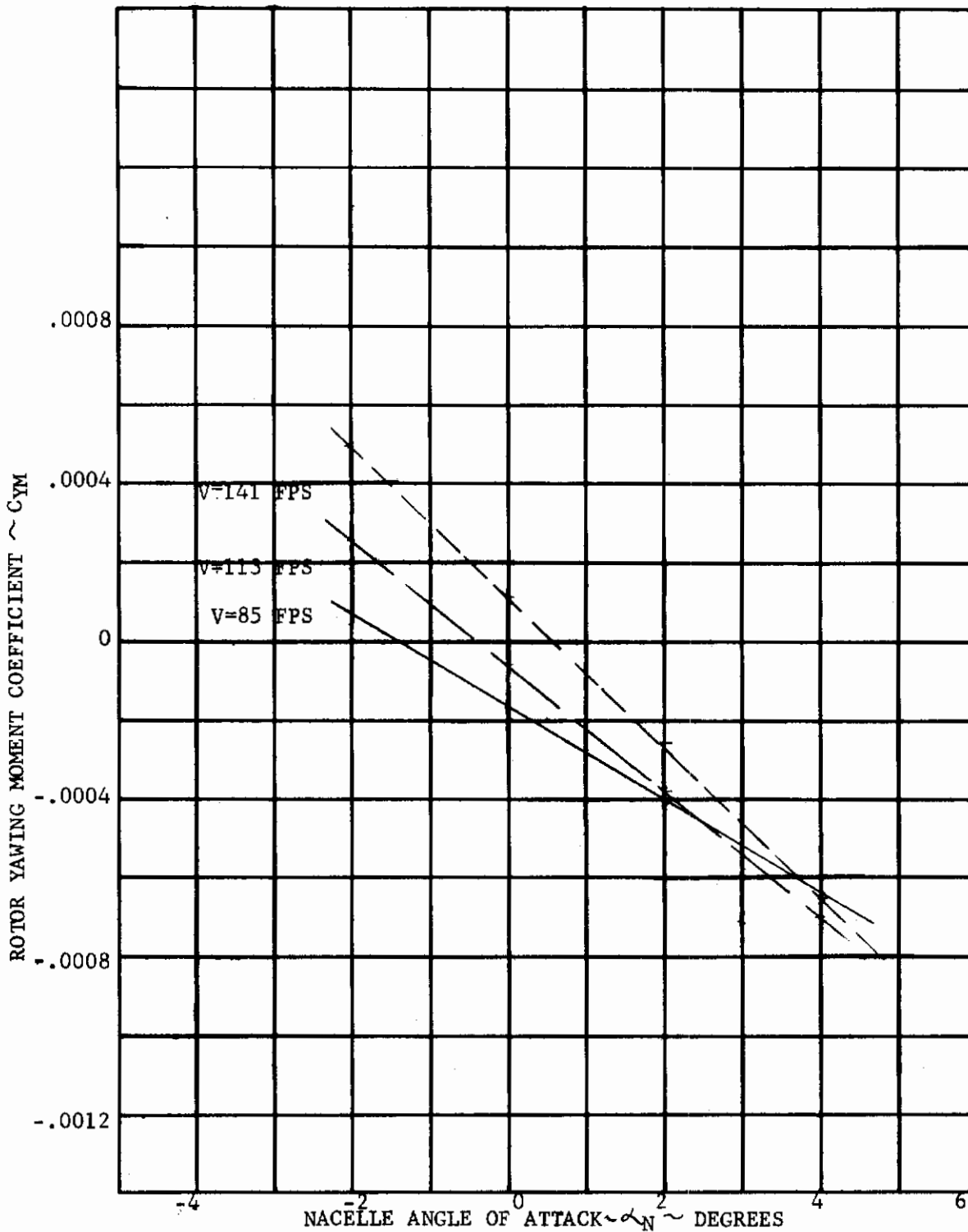


FIGURE D-11. ROTOR YAWING MOMENT/ANGLE OF ATTACK VARIATION  
FOR ROTOR RPM=600  $\zeta_F=0$   
(CIRCULATION EFFECTS REMOVED)

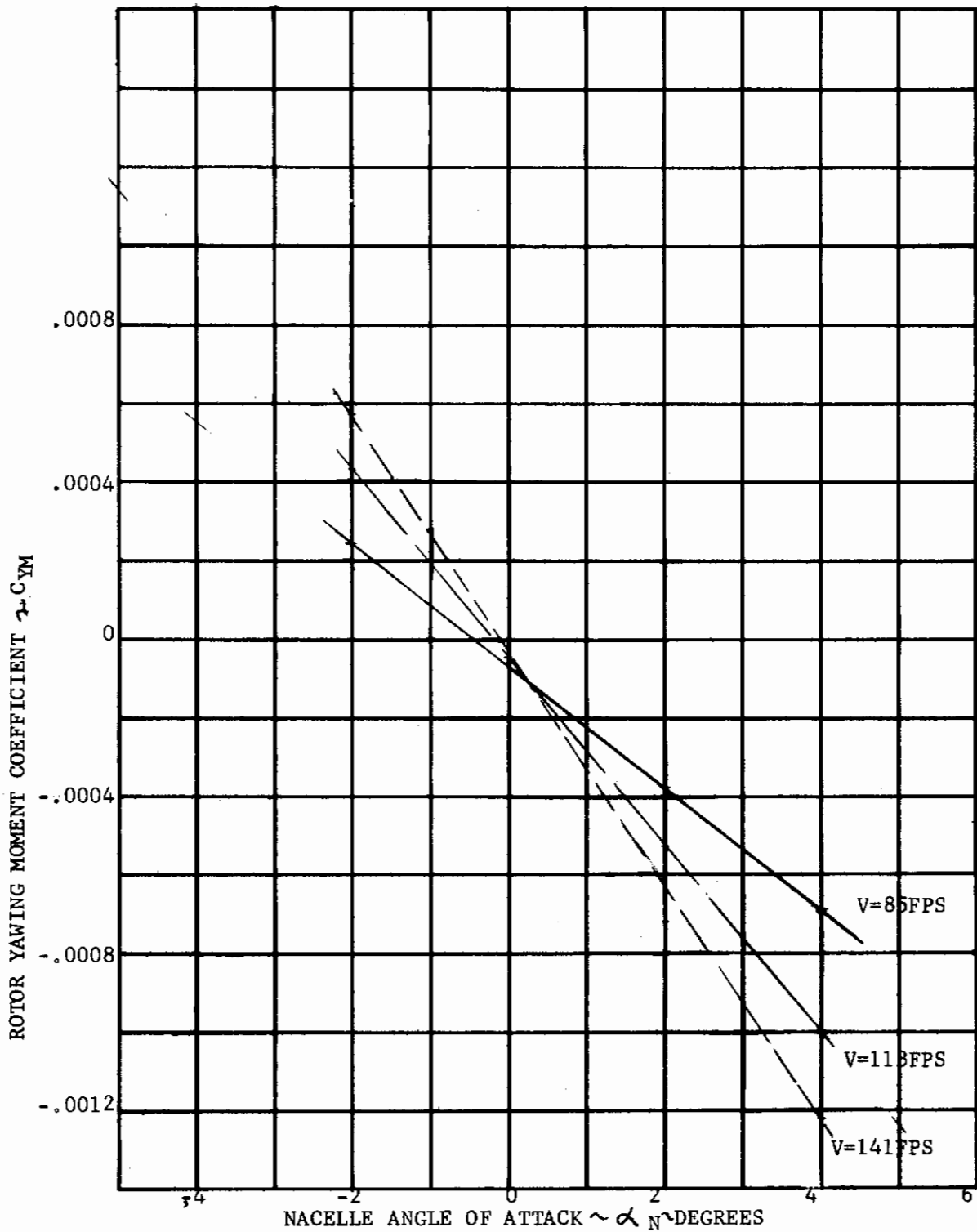


FIGURE D-12 ROTOR YAWING MOMENT/ANGLE OF ATTACK VARIATION FOR ROTOR RPM = 700  $\delta_F = 0$  (CIRCULATION EFFECTS REMOVED)

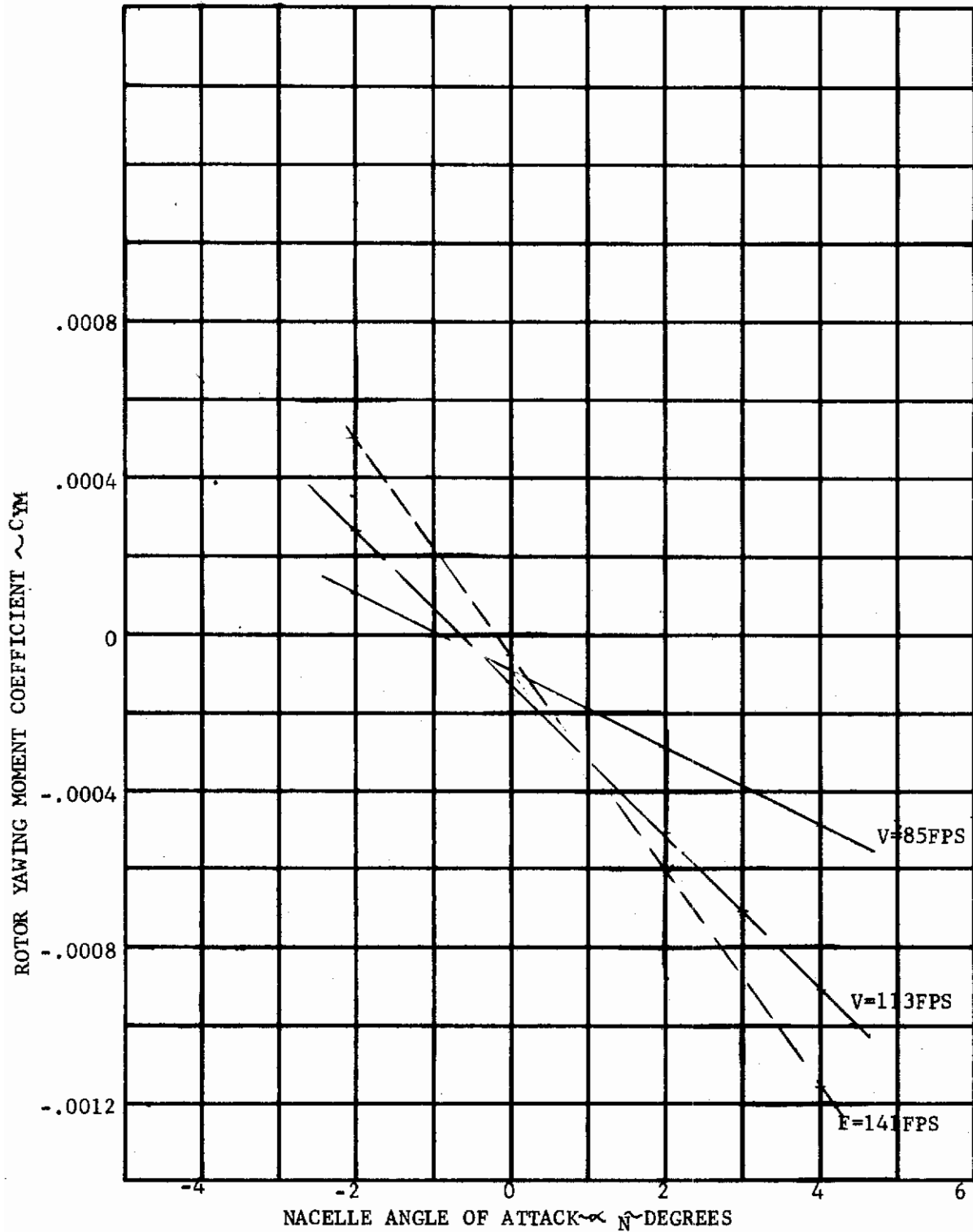


FIGURE D-13 ROTOR YAWING MOMENT/ANGLE OF ATTACK VARIATION FOR ROTOR RPM=800  $S_F=0$  (CIRCULATION EFFECTS REMOVED)

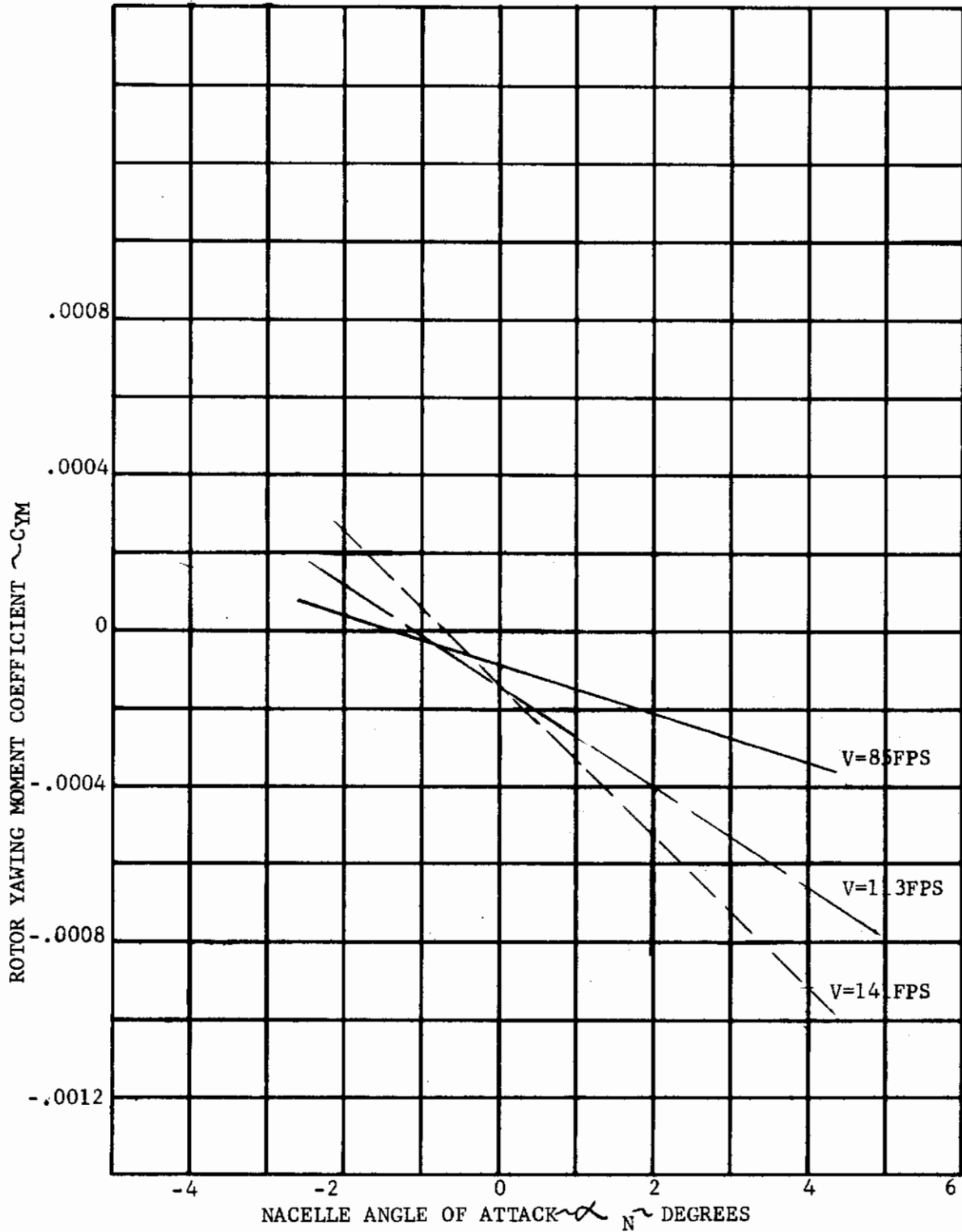


FIGURE D-14. ROTOR YAWING MOMENT/ANGLE OF ATTACK VARIATION FOR ROTOR RPM=900  $S_F=0$  (CIRCULATION EFFECTS REMOVED)

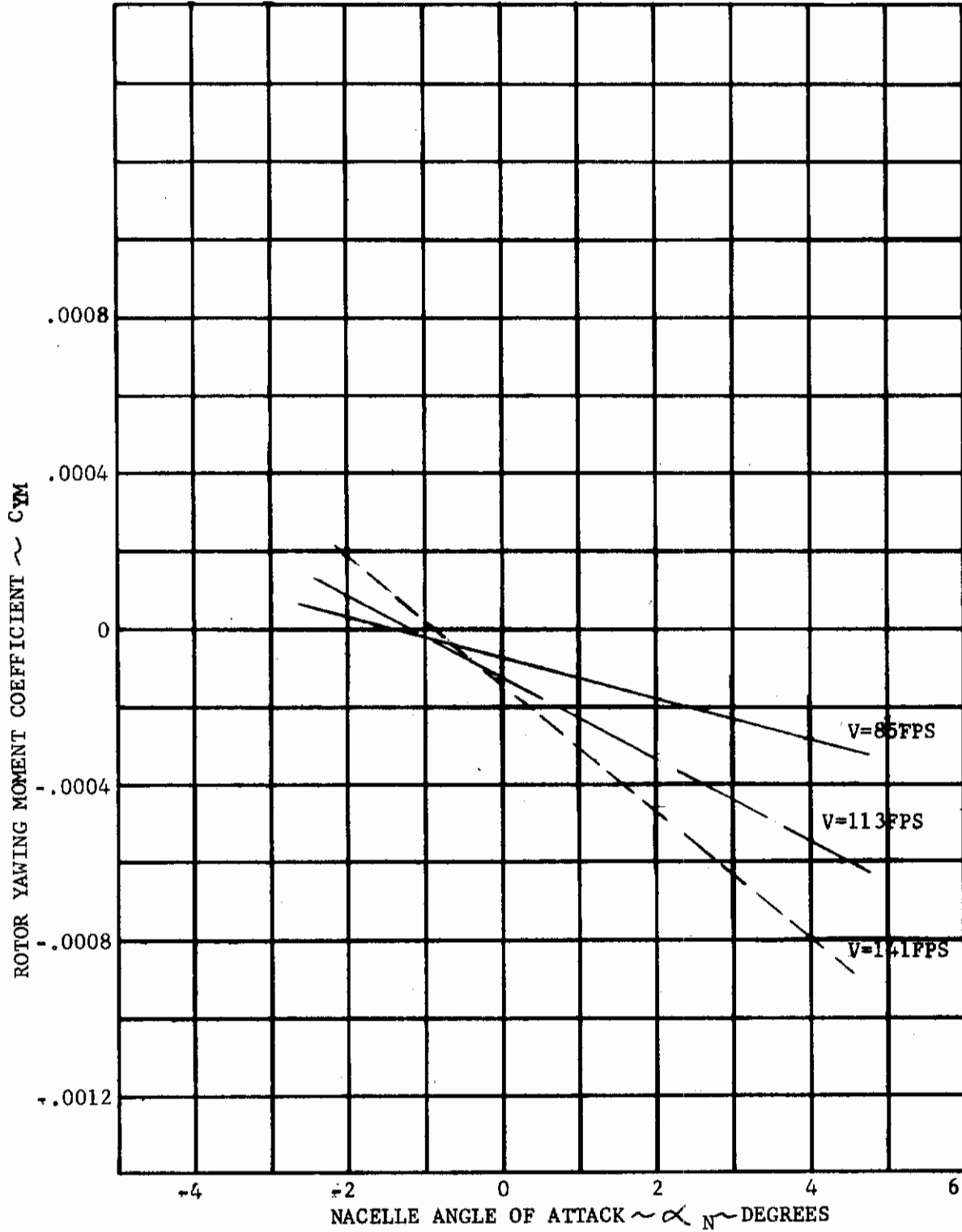


FIGURE D-15 ROTOR YAWING MOMENT/ANGLE OF ATTACK VARIATION FOR  
ROTOR RPM=950  $\delta_F = 0$   
(CIRCULATION EFFECTS REMOVED)



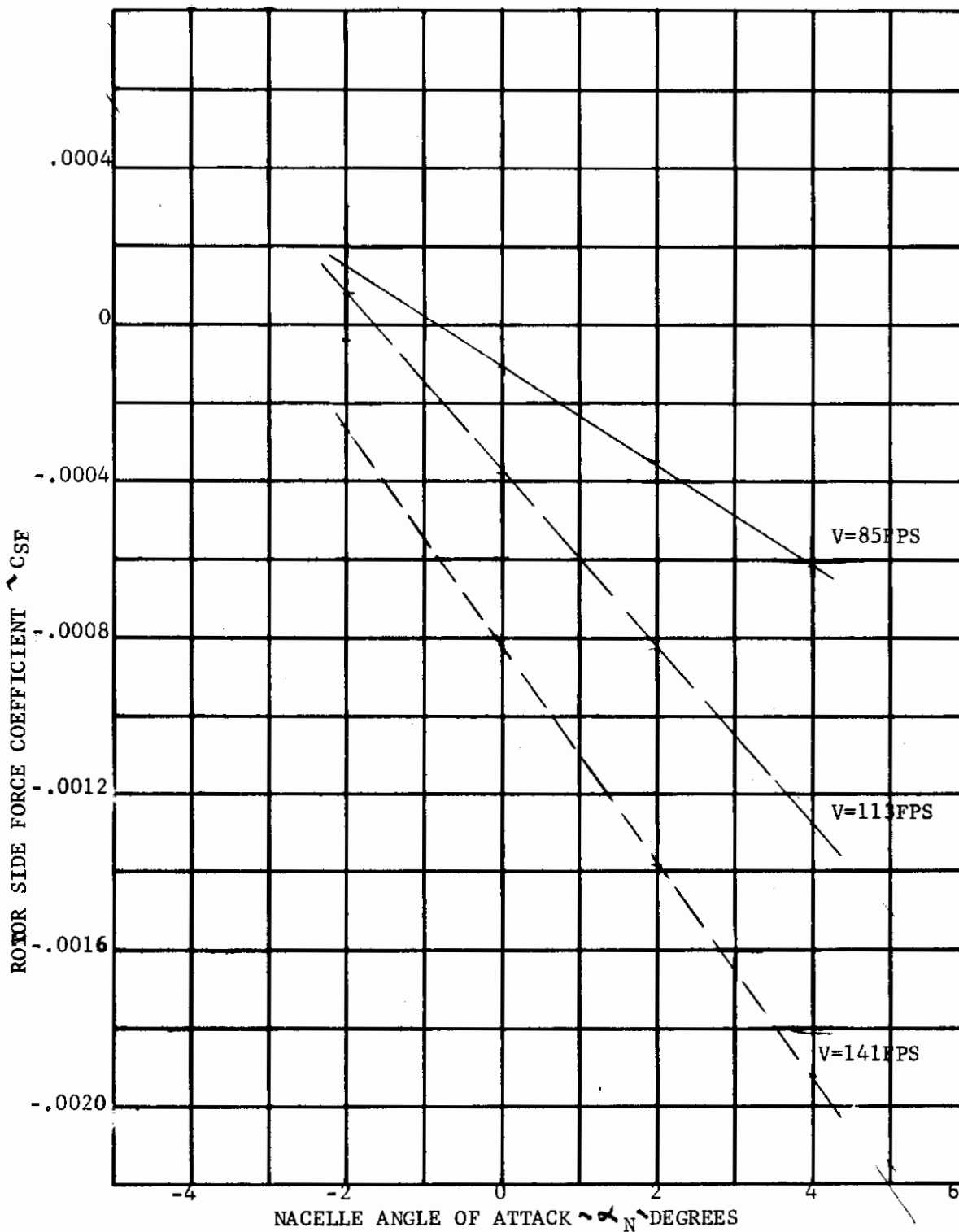


FIGURE D-16 ROTOR SIDE FORCE/NACELLE ANGLE OF ATTACK VARIATION  
FOR ROTOR RPM=600  $\delta_F=0^\circ$   
(CIRCULATION EFFECTS REMOVED)

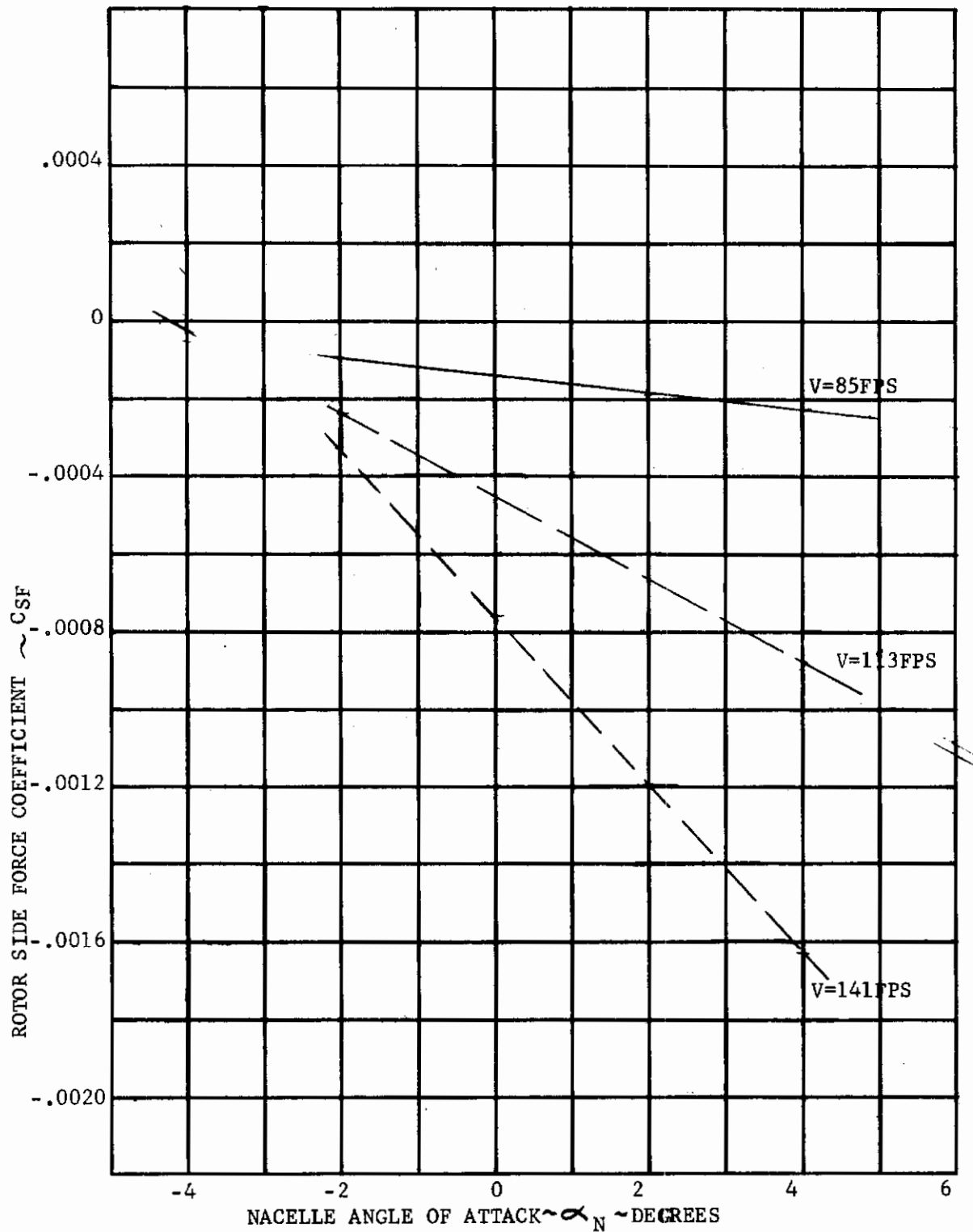


FIGURE D-17  
ROTOR SIDE FORCE/NACELLE ANGLE OF ATTACK VARIATION  
FOR ROTOR RPM=700  $\delta_F=0^\circ$   
(CIRCULATION EFFECTS REMOVED)

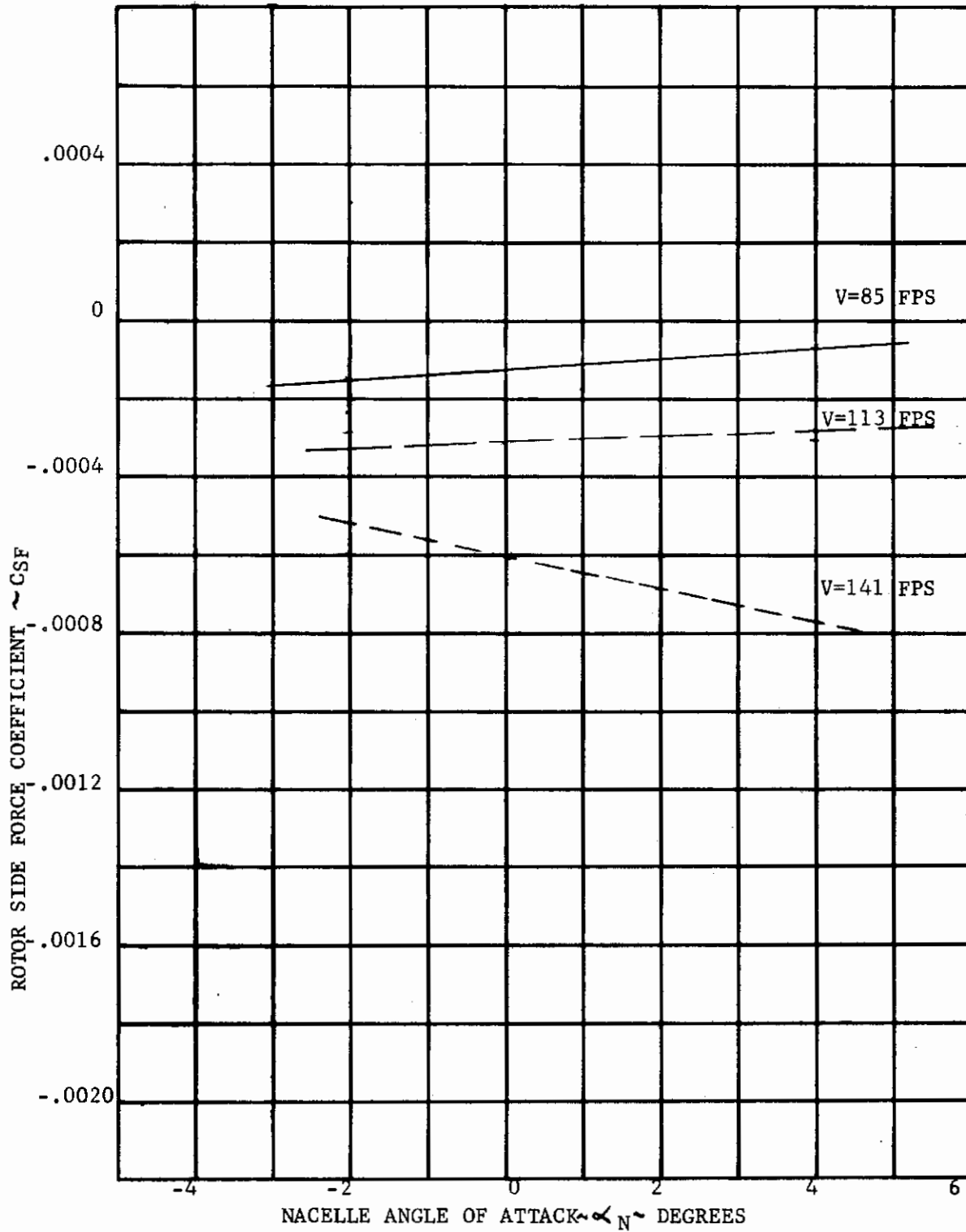


FIGURE D-18 ROTOR SIDE FORCE/NACELLE ANGLE OF ATTACK VARIATION  
FOR ROTOR RPM=800  $\delta_F=0^\circ$   
(CIRCULATION EFFECTS REMOVED)

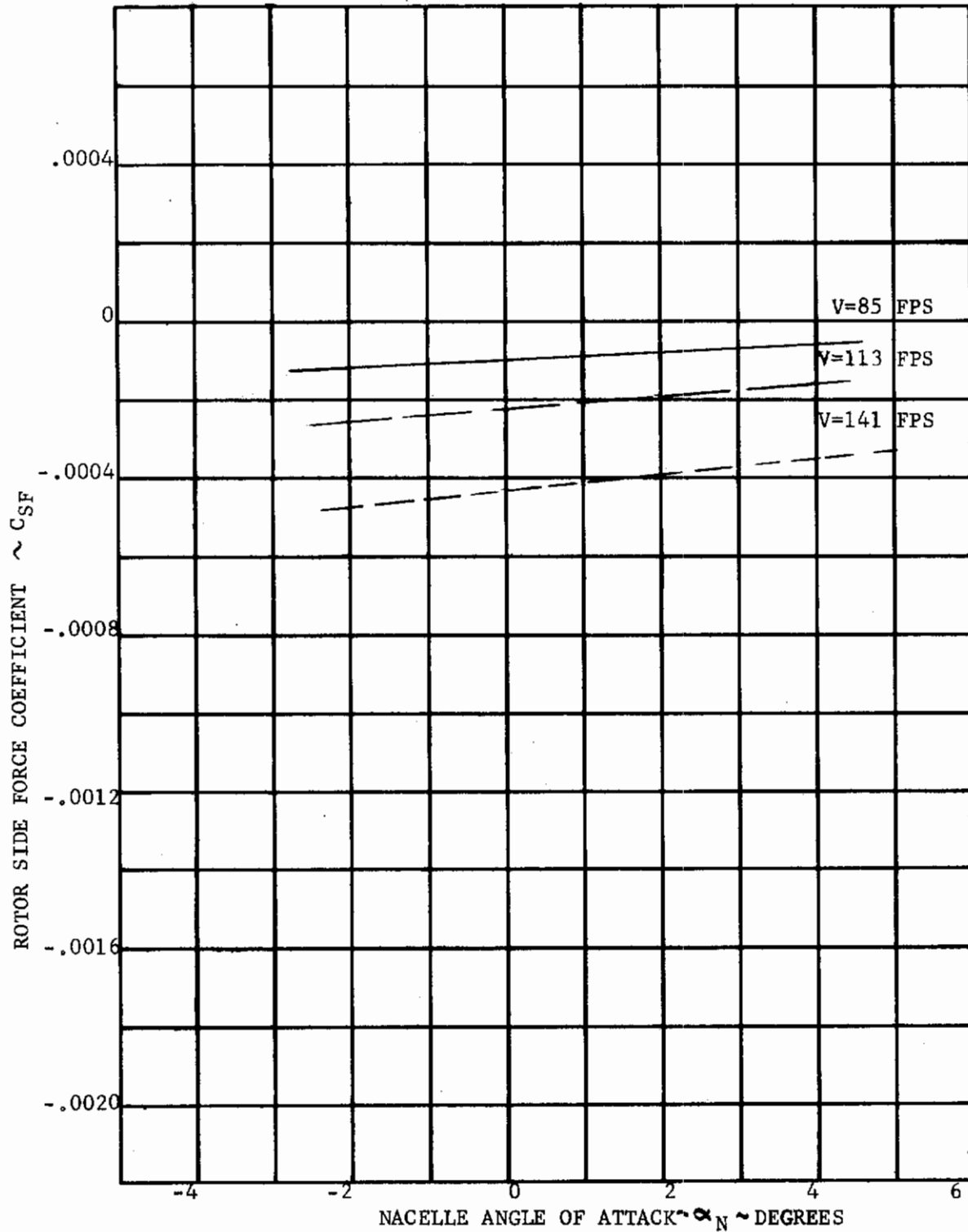


FIGURE D-19 ROTOR SIDE FORCE/NACELLE ANGLE OF ATTACK VARIATION  
FOR ROTOR RPM=900  $\delta_F=0^\circ$   
(CIRCULATION EFFECTS REMOVED)

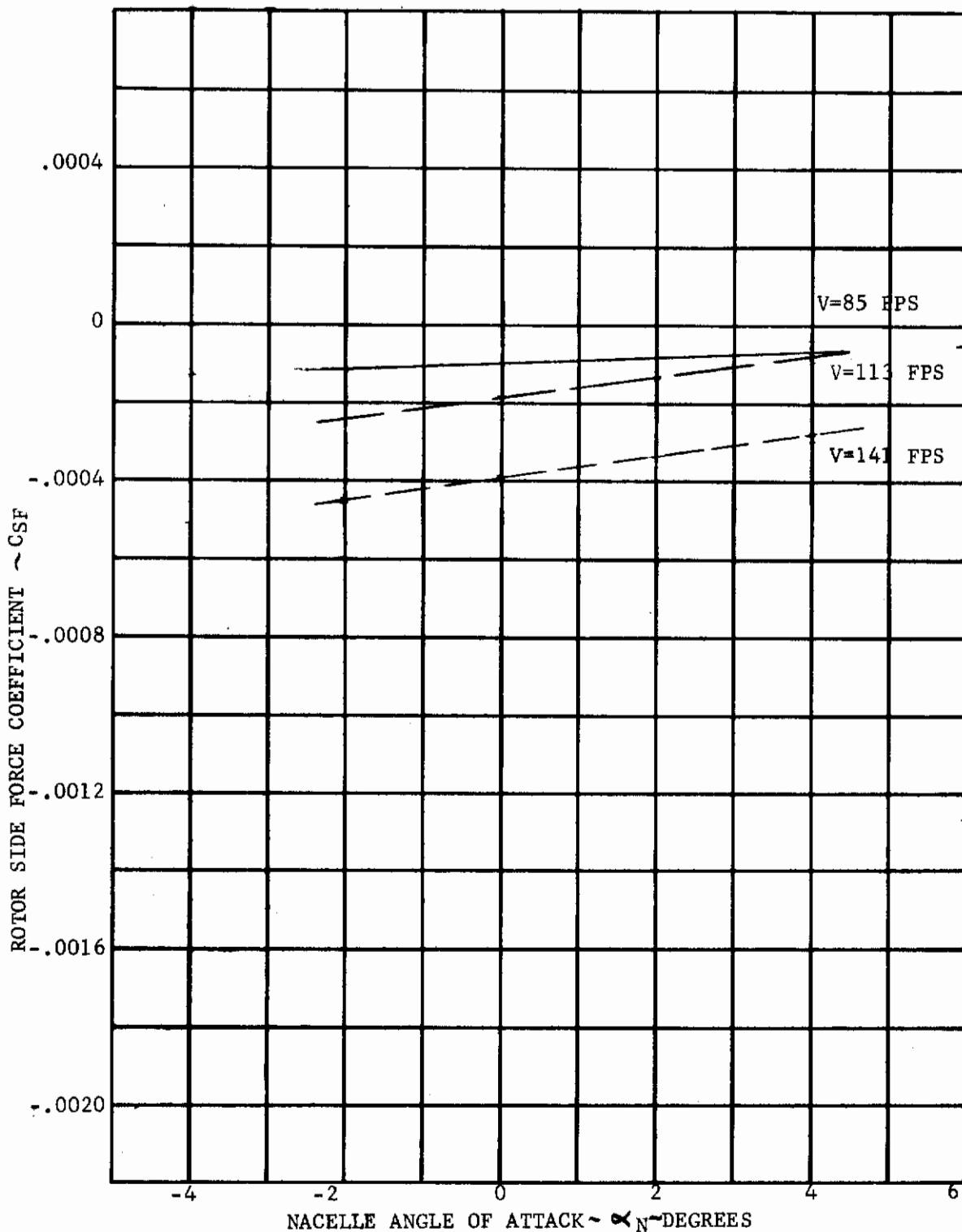


FIGURE D-20 ROTOR SIDE FORCE/NACELLE ANGLE OF ATTACK VARIATION  
FOR ROTOR RPM=950  $\delta_F=0^\circ$   
(CIRCULATION EFFECTS REMOVED)

APPENDIX E

PHYSICAL PROPERTIES OF WIND TUNNEL MODEL BLADES AND WING

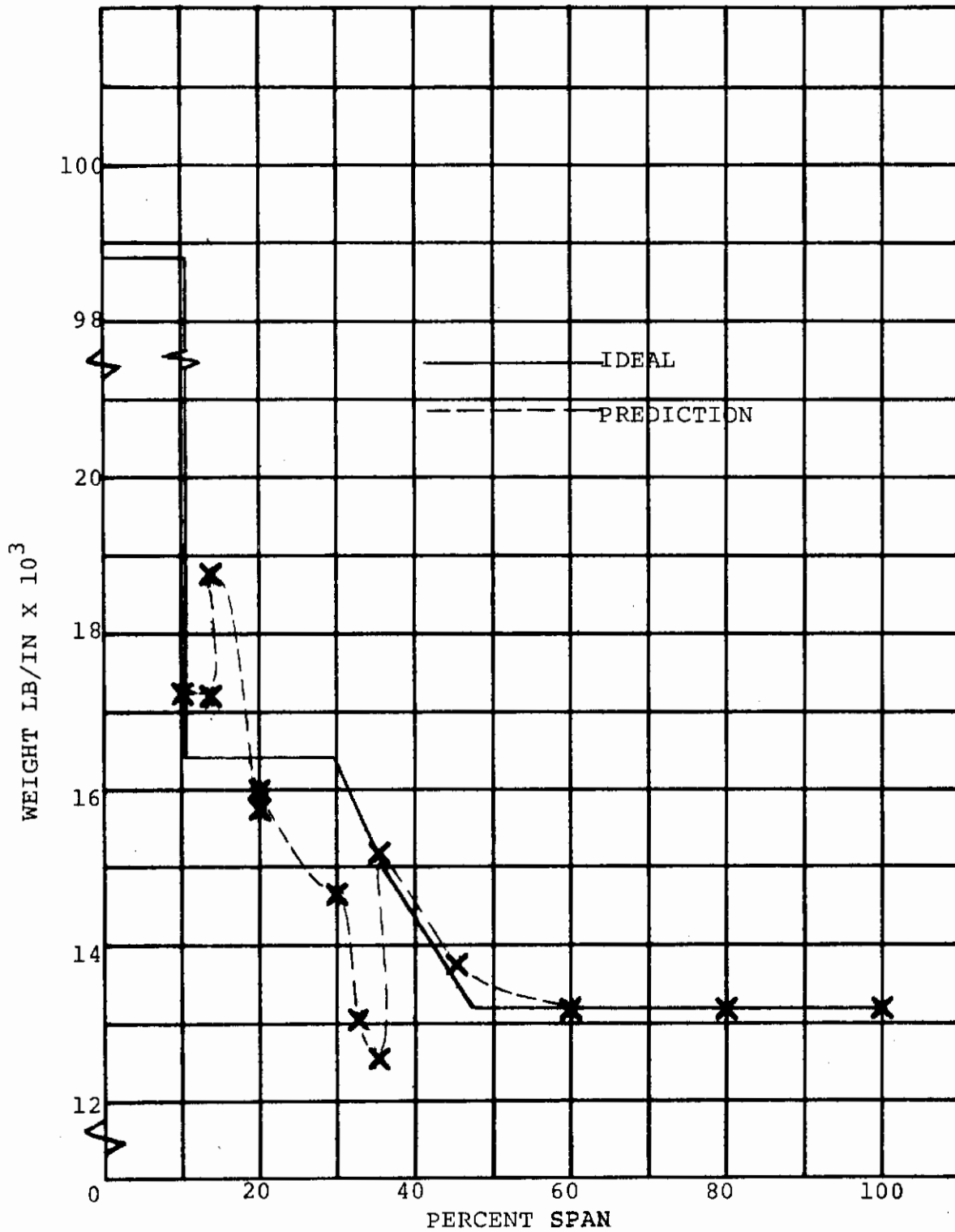


FIGURE E-1 BOEING 1/9 SCALE 213 SEMI-SPAN CONVERSION MODEL BLADE WEIGHT DISTRIBUTION

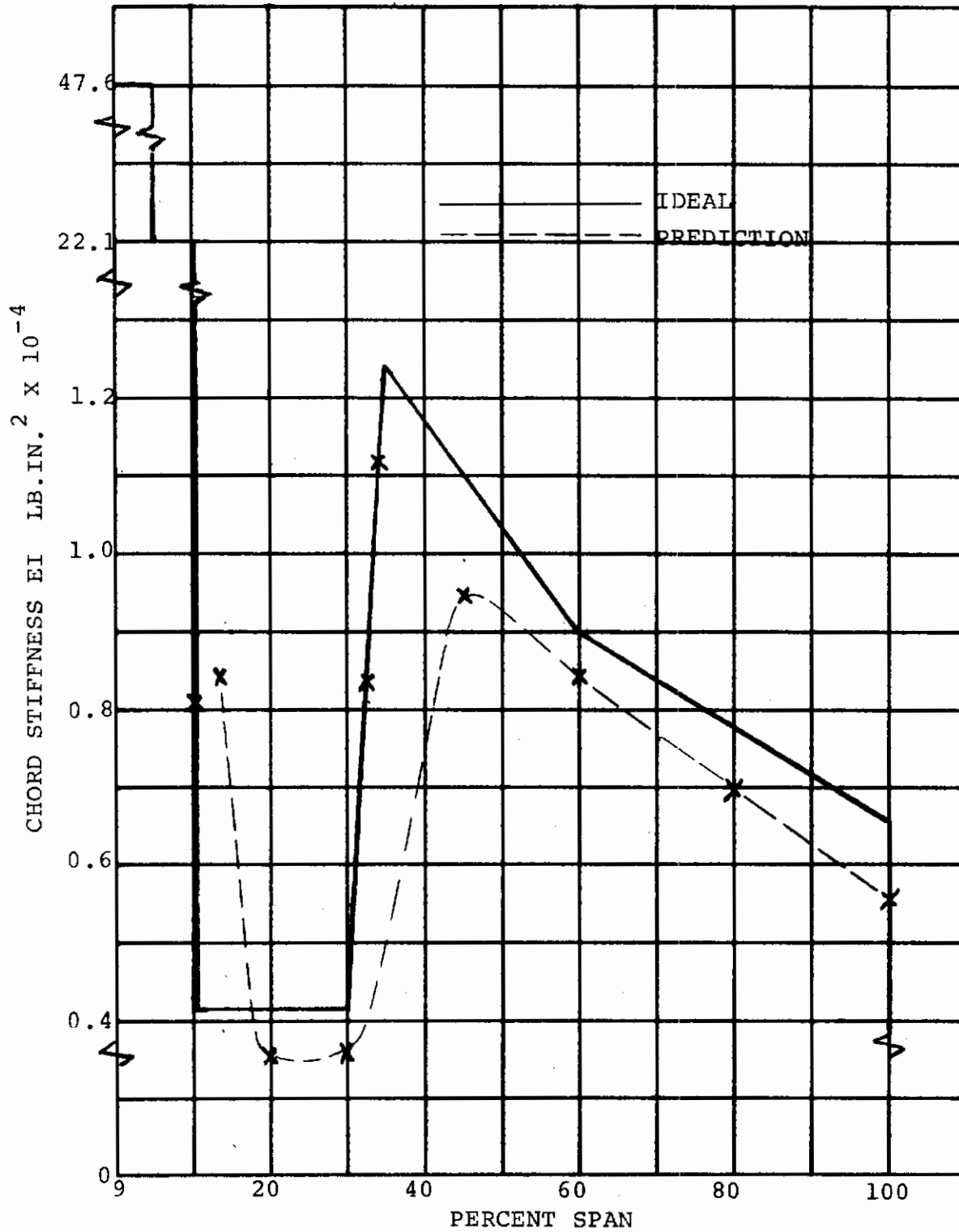


FIGURE E-2 BOEING 1/9 SCALE 213 SEMI-SPAN CONVERSION MODEL BLADE CHORD STIFFNESS



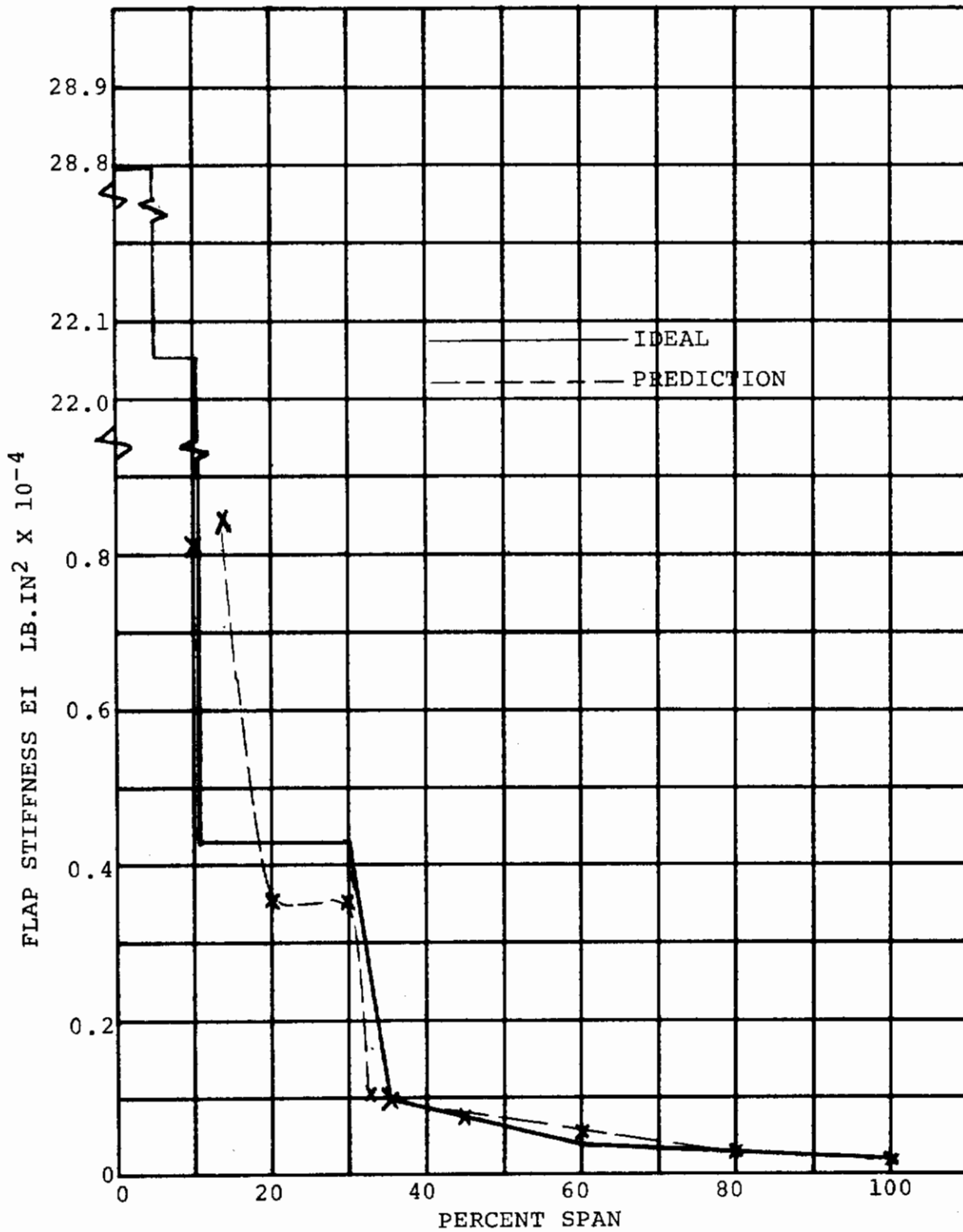


FIGURE E-3 BOEING 1/9 SCALE 213 SEMI-SPAN CONVERSION MODEL BLADE FLAP STIFFNESS

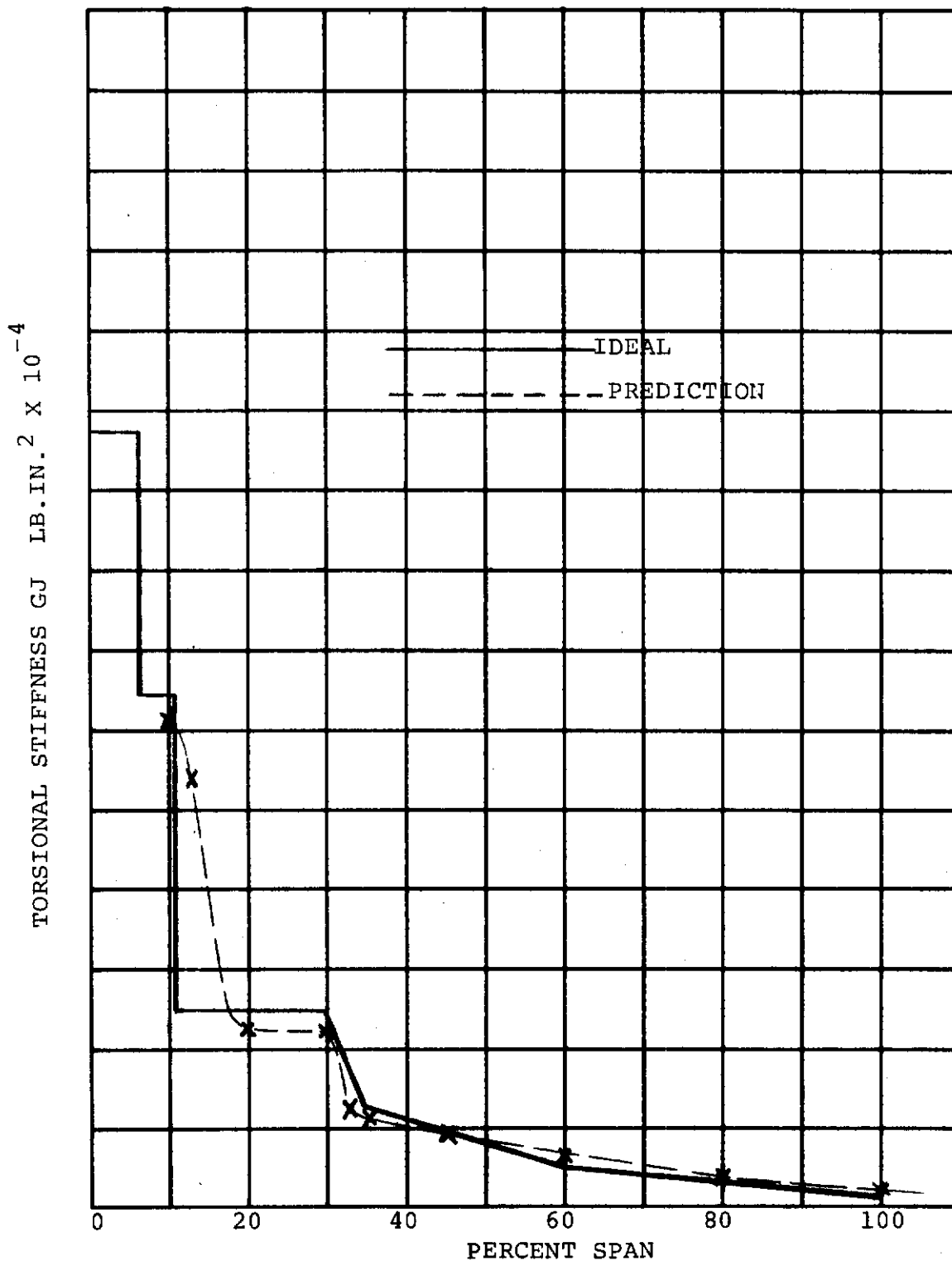


FIGURE E-4 BOEING 1/9 SCALE 213 SEMI-SPAN CONVERSION MODEL BLADE TORSIONAL STIFFNESS

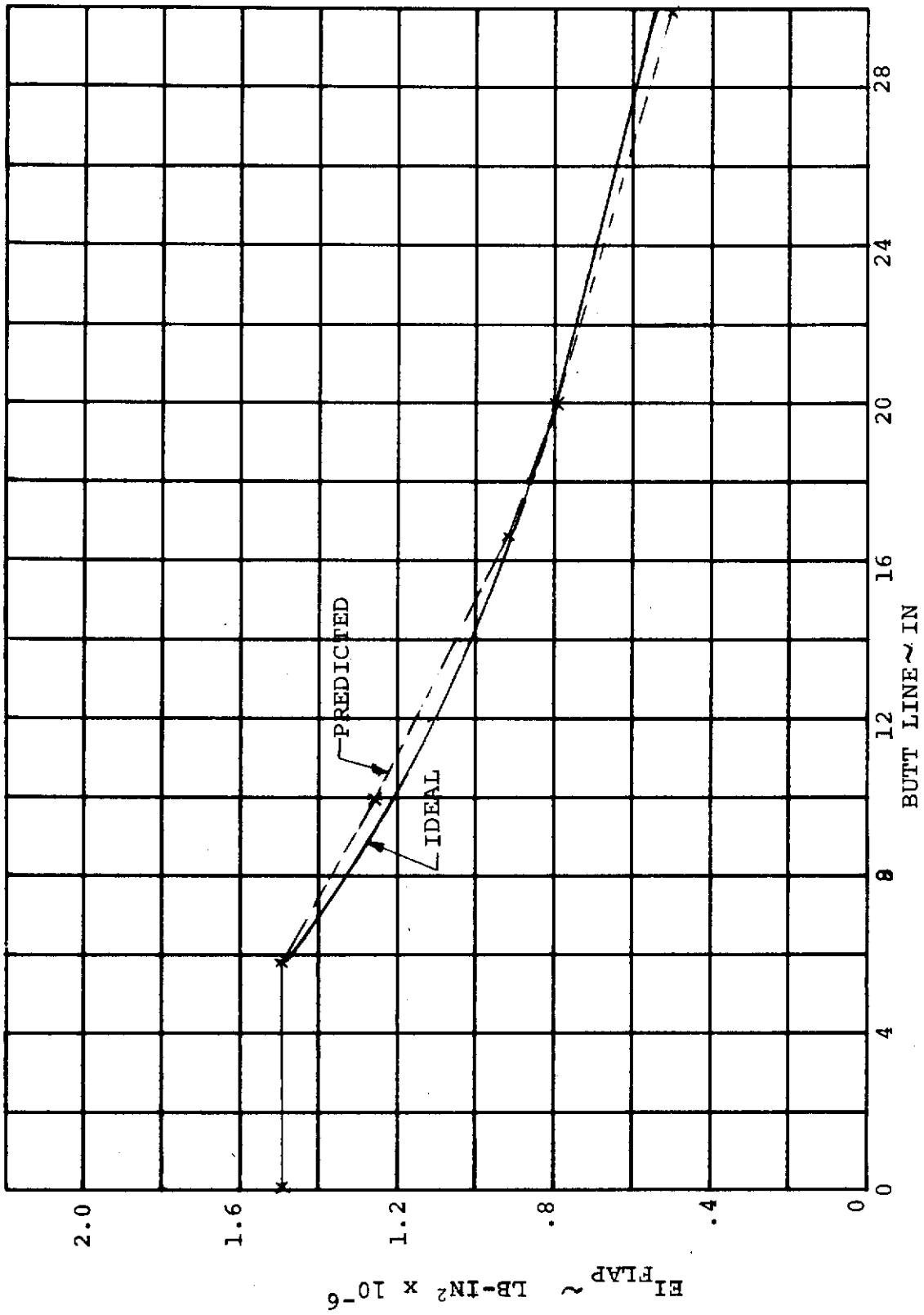


FIGURE E-5 WING FLAPWISE STIFFNESS DISTRIBUTION

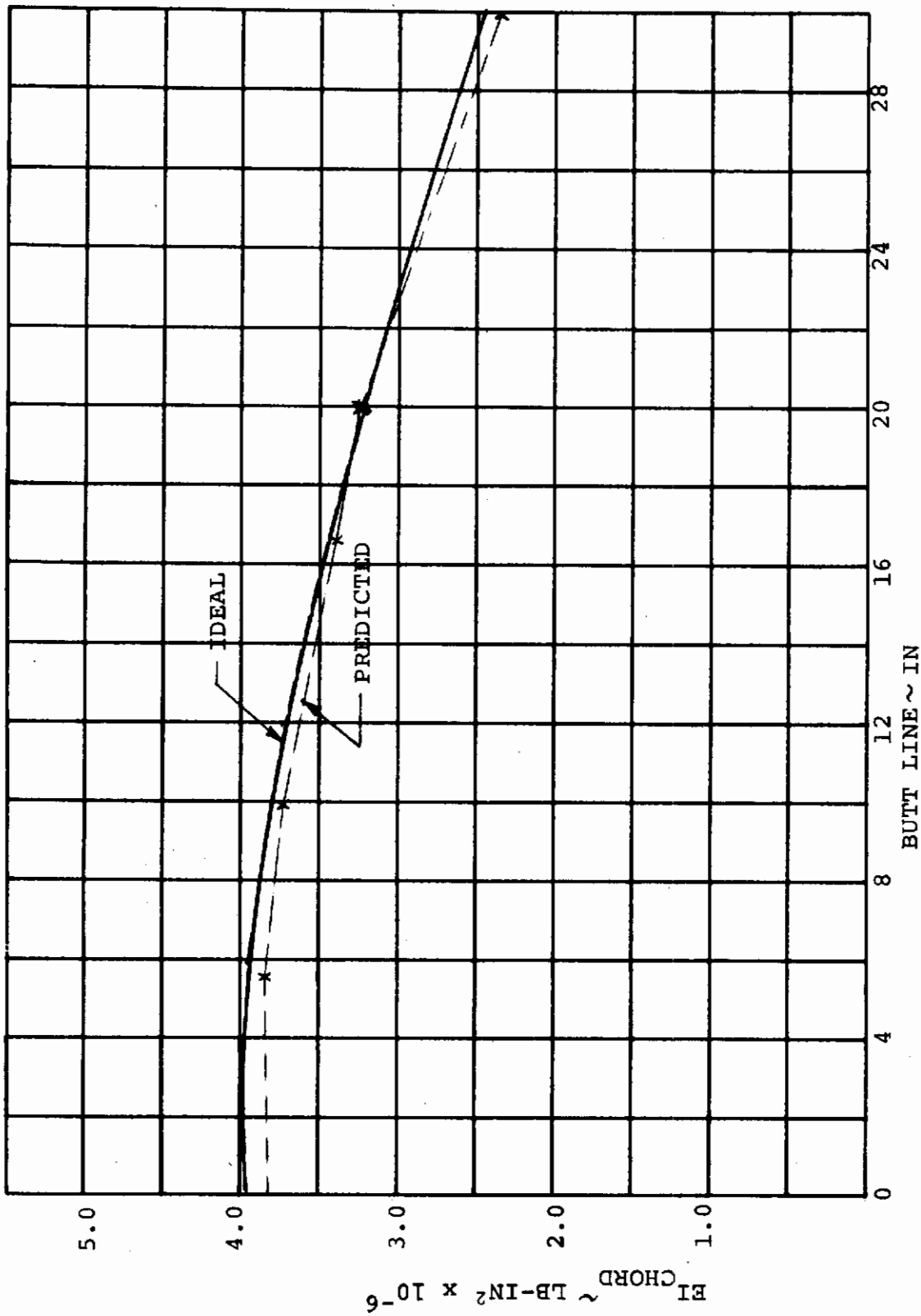


FIGURE E-6 WING CHORDWISE STIFFNESS DISTRIBUTION

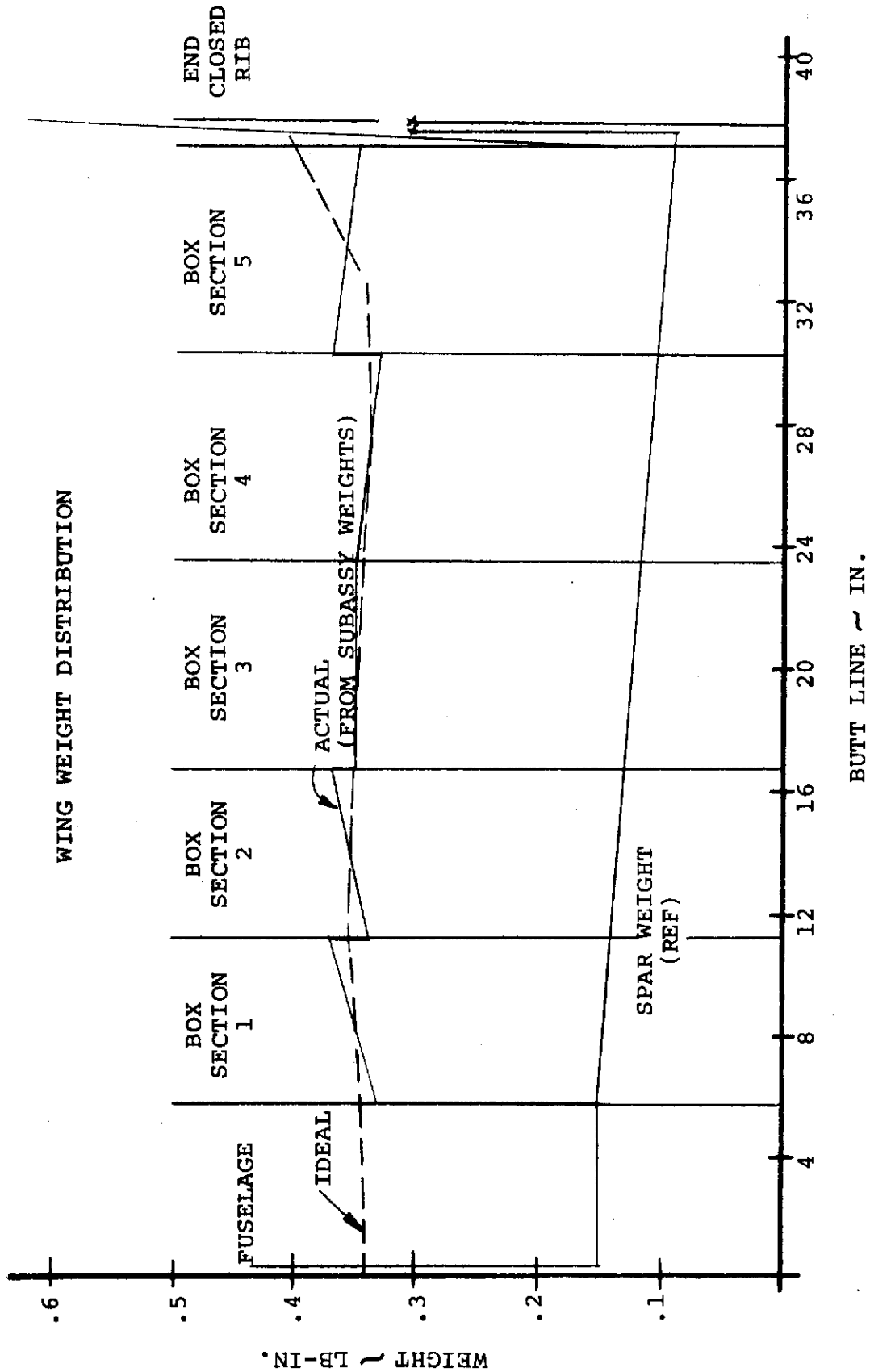


FIGURE E-7 WING WEIGHT DISTRIBUTION

APPENDIX F

TEST RUN LOG

Enclosed is a copy of the on line test run log that describes the model configuration for each test run and additional notes required to define test conditions.

PREP.	CHK.	APPR.	REVISED	DATE	CONFIGURATION	TYPE OF RUN	WT. TARE RUN	V	$\eta_T$	$\theta_{.75}$ RATE	RPM	$\alpha_F$	$\delta_F$	$\alpha_T$	TEST PROG. RUN#	NR OF DP'S	DATE / TIME
	XEZ				W <sub>1</sub> N <sub>3</sub> B.	T.B	-	85	89	SLOW	0-300	0	0	0	1	8	2/16/71 0052
					✓	T.B	-	✓	✓	✓	0-850	✓	✓	✓	1	11	2/17/71 1700
					✓	T.B	-	✓	✓	✓	0-850	✓	✓	✓	1	15	1930
					CHORDWISE	STATIC SHAKE	-	-	-	86	-	✓	✓	✓	✓	9	2013
					✓	✓	-	0	0	86	0	0	0	0	✓	12	2-18-71 0930
					✓	✓	-	0	0	86	0	0	0	0	✓	10	1400
					✓	✓	-	0	0	86	0	0	0	0	✓	6	
					✓	✓	-	0	0	86	0	0	0	0	✓	9	
					✓	✓	-	0	0	20	0	0	0	0	✓	9	

(89)

1. ENGINE NACELLE OFF, PRINCETON VRC BOX NOT OPERATIVE  
RPM = 0, 100, 200, 300. RPM LIMITATION DUE TO SF<sub>2</sub> ALT. ALLOW. BEING ATTAINED. BLADES CONSIDERABLY OUT OF TRACK. NO VREV UNTIL 300.
2. 0 - 800/100, 850. LIMITED BY INABILITY TO REDUCE COLLECTIVE PITCH INSUFFICIENT GAIN ON SYSTEM PROBABLE CAUSE. BASIC HUB. 0-ΔWT TRACK OK.
3. RPM = 0 → 850/50  
RPM AGAIN LIMITED BY INABILITY TO REDUCE COLLECTIVE BELOW 25" WITH 9" O/U.
4. TUNNEL D.C. BREAKER BECAME UNSTABLE. COIL BURNT OUT. SET UP FOR STATIC SHAKE TEST AS NO FURTHER TUNNING POSSIBLE.  
CHORDWISE SHAKING. 5 → 40 CPS / 5 CPS - CONSTANT SHAKER FORCE 1 1/4 LB (FROM PTP METER.) SEC DATA ONLY.
5. CHORDWISE SHAKE TEST ~ CONSTANT SHAKER FORCE = 1.0 1/2 LB TO 12 CPS
6. CHORDWISE SHAKE TEST ~ SHAKER FORCE = 1 LB 12 TO 21 CPS AND 2.5 LB FROM 21 TO 27 CPS.
7. CHORDWISE SHAKE TEST FORCE = 2.5 LB FROM 27-40 CPS

8. T = 2.56 LB FREQ = 0 TO 40 CPS  
9. T = 2.56 LB " " " " " "

VR 076-D	BVWT
1. CHECK-OUT, TRACK & BALANCE	071
2. STATIC SHAKE TEST	

RUN NO.	CONFIGURATION	TYPE OF RUN	WT. TARE RUN	V	$\eta_T$	$\theta_{79}$	COLL. RATE	RPM	$\alpha_F$	$\delta_F$	$i_T$	TEST PROG RUN#	NO OF DPS	DATE / TIME
10	W <sub>1</sub> N <sub>3</sub> B	CHECK OUT	-	99	11.65	SWEEP	SLOW	0-750	0	0	0	1	12	2/18/71 1750
11	✓	BAL	-	✓	✓	✓	✓	900	✓	✓	✓	1	8	2/18/71 1830
12	✓	A <sub>9</sub> SPEC	-	✓	✓	✓	✓	VAR	+4	✓	✓	-	7	2/13 2/14
13	✓	✓	-	85	8.6	✓	✓	VAR	+2	✓	✓	-	33	2/20 2/21
14	✓	✓	-	113	8.6	✓	✓	VAR	-2	✓	✓	-	32	2/22 0115
15	✓	C.O	-	-	8.6	✓	-	-	0	-	-	-	-	-
16	✓	BAL CNK	-	-	-	-	-	-	-	-	-	-	4	2-22-71 11:00
17	✓	✓	-	85	8.6	✓	✓	0-950	0	0	0	-	5	2/22/71 1750
18	✓	✓	-	✓	✓	✓	✓	✓	✓	✓	✓	-	6	1840 1905

10	RPM. 0 → 900 / 100, 750. RPM LIMIT - INABILITY TO REDUCE COLLECTIVE BELOW 270
11	CEC DATA ONLY. HUB BALANCING. 900 RPM.
12	RPM 0 → 1000. LIMITED BY COLLECTIVE SETTING. CWB @ 100% . SF @ 100%
13	RPM 0 → 950 / 50, $\eta = 8.59$ , $\eta = 9.0$ , $\eta = 15.0$
14	35 gm @ BLADE 91. 23 gm @ BLADE 95. 100% SF @ 550 RPM (RESIDUAL). AAND AT 150 RPM. POST RUN WOD. POINT - RM - 3. DIF - 15. RPM 0 → 250 / 50, $\eta = 8.59$ 0 → 850 / 50, $\eta = 15.0$ CWB = 100%
15	CHECK RUN TO INVESTIGATE COLLECTIVE PITCH SYSTEM
17	SPINNER, NACELLE FAIRING OFF. CEC DATA ONLY
18	SPINNER NACELLE FAIRING REPLACED. WEIGHTS IN SPINNER FOR BALANCING. BALANCE NOT ACHIEVED YET. CONTINUE WITH BASELINE RUNS. MODEL SET UP FOR BASELINE RUNS.

FORM 48610 (3/70)

VR 076-D  
CHECK-OUT & BALANCE RUNS

BWT  
071





PREP	CHK.	APPR	REVISED	DATE	WT. TARE RUN	V	q	DEG RATE	RPM	$\alpha_F$	$\delta_F$	$\mu_T$	TEST PROG RUN	NO OF D.P.'s	DATE / TIME
	K07				BASE LINE	85-140	8.59	-	-	+4	30	0	✓	6	0044 2/23/71 0033
					✓	✓	✓	-	-	+4	45	0	✓	6	0058 0104
					✓	✓	✓	-	-	+8	0	0	✓	6	0110 0115
					✓	✓	✓	-	-	+8	15	0	✓	6	0122 0129
					✓	✓	✓	-	-	+8	30	0	✓	6	0132 0140
					✓	✓	✓	-	-	+8	45	0	✓	6	0145 0154
					CHECK OUT	85	8.59	SNEEP SLOW	VAR	0	0	0		10	2/23/71 2000
✓					✓	140	23.3	SNEEP	✓	0	0	0		6	2040
36					DATA RPM SWEEP	85	8.59	✓	✓	✓	✓	✓		7	2220 2230

$\delta_F = 30^\circ$   
 $\delta_F = 45^\circ$   
 $\delta_F = 0^\circ$   
 $\delta_F = 15^\circ$   
 $\delta_F = 30^\circ$   
 $\delta_F = 45^\circ$

SNDBERS FITTED, NEW OPTICAL 1/26 SYSTEM TRY-OUT. NF SENSITIVITY CHANGE PRIOR TO THIS RUN AFTER CHECK LOADING. (AE, YM, RM, WITHIN LIMITS)  
 OK @  $q = 8.59$ , SF JUST W, YM 307%,  
 @  $q = 23.3$  SE ALT LIMITED RUN TO 500 (UP TO 150%) BUT SF WAS HIGH FROM 0-500 OPTICAL 1/REV NOT SUCCESSFUL. Q/P TOO LOW. NO D.D. (OK ON CEC.) BLADES, HUB V. ROCKY. DECISION TO DO ROTATING CHARACTERISTICS @ LOW  $q$ . SNDBERS OFF. REVERT TO MAG. 1/2R PICK-UP.

No 100 RPM UP TO 500 RPM USING MAG P.O. PHOTO-ELECTRIC 1.00 RE-HOUSING UP 1.00 OUTPUT BUT NO FLIP-FLIP. ALUMIN TAPE REFLECTOR RUN EVENTUALLY ABANDONED - SET UP FOR BASELINE CHARACTERISTICS

VR 076-D

BASELINE DATA - NO BLADES

BVWT 071

PREP.	CHK.	APPR.	REVISED	DATE	DATE / TIME
	K&Z			3/18	2/24/71 0055
					0105
					0110
					0119
					0135
					0140
					0145
					0150
					0155
					0200
					0204
					0209
					0213
					0219
					0224
					0229
					0234
					0237

(42)

37 ENGINE NAGELLE (N<sub>1</sub>) REMOVED FOR BASELINE DATA.  
 38 REFITTED FOR CHECK  
 39 REMOVED, FLAP CHANGE TO 30°  
 40  
 41  
 42  
 43  
 44  
 45  
 46

PREP.		REVISED	DATE
CHK.	K&Z		
APPR.			

VR 076 D BASELINE DATA - NO BLADES	BUWT 071
---------------------------------------	-------------

2078 a  
2046 c

PREP	CHK.	APPR	REVISED	DATE	NO. OF D.P.'S	TEST PROG RUN	DATE / TIME
	287				4	✓	2/24/71 0752
					12		2372
					7		2/25/71 0076
					20	✓	0252
					4		0328
					6		1710
					20	✓	2/25/71 1727
					3		1857
					20	✓	1930
					20		1755
					3		2006
					29	✓	2028
					16	✓	2047
					16	✓	2159
					16	✓	2242
					16	✓	2309
					16	✓	2340
(124)							
47	ENGINE NACELLE (N1) REMOVED						
48	BALANCE RUNS & AIR RESONANCE CHECKS AT 8.6 - 21.2 % UP TO 1050 RPM. DIVERGENT AIR RESONANCE IN WING FLAP MOISE AT 1050 RPM. EMERGO ON RUNNING AT MORE THAN 950 RPM WITHOUT SNAGGERS.						
49	REPEAT OF RUN 48 TYPE INVESTIGATION. CHECK OF MODEL BEHAVIOUR AT 23.5 q AND LOW RPM. RESONANCE AT 260 RPM. NO SPURIOUS MODEL BEHAVIOUR. HUB BALANCING ACHIEVED.						
50	BEGIN ROTATING - MODEL CHARACTERISTICS RUNNING. NO PRINTER DATA (OUT) q=8.6. RPM ~ 0, 100, 200, 300, 350, 400, 450, 500, 550, 600, 650, 700, 750, 800, 850, 900, 950. q=9.4. 9=10.3, 950.						
51	CHECKOUT						
52	HUB BALANCE RUNS 1, 2 & 3 BALANCE ACHIEVED. 20 gm on # 31.						
53	CEC DATA ONLY - SNAGGERS ON						
54	SNAGGERS OFF. NO VIB FOR INITIAL 100, 200, 300 RPM. RUN STOPPED TO ETX!						
55	REPEAT OF RUN 54. q=8.59. RPM: 0 - 900/100, 950. q=15.2. 350, 400 - 900/100, 950						
56	q=23.2. RPM: 0, 350, 400 - 100, 950. Hub to microswitch CRM PRIOR TO RUN.						

FORM 48810 (3/70)

VR 076-D

1. BASELINE DATA (NO BLADES)  
2. MODEL CHARACTERISTICS.

BWT  
071

PREP.	CHK.	APPR.	REVISED	DATE	NO. OF TEST RUNS	TEST SCHED. RUNS	NO. OF O.P.S.	DATE / TIME
	287				50	✓	50	2/25/71 0105
					2	—	2	2/25/71 1554
					65	✓	65	1804 1704
					29	✓	29	1842 2035
					29	✓	29	2116
					29	✓	29	2203
					16	✓	16	2308
					6	✓	6	2318
					6	✓	6	2350
					3	✓	3	0026
					2	✓	2	2/27/71
					6	✓	6	0100

57. FLAPS TO 30°.  $\eta = 8.6$  RPM 0, 100 → 950/50.  $\eta = 15.2$  RPM 320, 350 - 950/50

58. CHECKOUT & MOVE RUN: SPIN-UPS & FEATHER. BANG TEST PRIOR TO RUN 59

59. DATA RUN.  $\eta = 8.6$  RPM: 0, 100 → 1000/50. SHUT-DOWN TO CHECK @ CALIB AFTER  $\eta = 8.6$

REPEAT  $\eta = 8.6$  RPM: 0, 350, 600, 950. TOOK DEC RECORDING OF SLOW START-UP

UP TO 1 RPM AT 16"/SEC.  $\eta = 15.2$  RPM = 0, 350 → 950/50  $\eta = 23.3$  RPM 0, 350 - 950/50

60.  $\eta = 8.6$  RPM: 0, 100 - 900/100, 950  $\eta = 15.2$  RPM: 0, 400 → 900/100, 950

$\eta = 13.3$  RPM: 0, 400 → 900/100, 950

61.  $\eta = 8.6$  RPM: 0, 100 → 900/100, 950  $\eta = 15.2$  RPM: 0, 400 → 900/100, 950

$\eta = 23.3$  RPM: 0, 450, 500 → 900/100, 950. 100% COMBINED CWB, FBW 12% @ 700 RPM. SF 100%

62.  $\eta = 8.6$  RPM: 0, 350, 600, 950, 800.  $\eta = 15.2$ : 400, 600, 950, 800

$\eta = 23.3$  RPM: 0, 400, 600, 950. 120% ON COMB. CWB, FBW 12% @ 600 RPM

SF. ABOUT 200% @ 600 RPM (BAND EDGE)

63. SPIN-UP & FEATHER SCHEDULE (1) ~ TWO ATTEMPTS. T = 6 SECS

64. (2) T = 4 1/2 ✓

65. (3) T = 3 ✓

66. (4) T = 1.6 ✓

VR-076-D	BVWT
1. MODEL CHARACTERISTICS	071
2. SPIN-UP & FEATHER	

PREP.	CHK.	APPR.	REVISED	DATE	DATE / TIME	NO OF DP'S	TEST DEGS RUN	$\delta_F$	$\delta_P$	RPM	$\frac{\theta}{75}$ DEGR RATE	$\gamma$	WT. TARE RUN	TYPE OF RUN	CONFIGURATION	MODEL CHAR.	SWEEP	MAN	VAR	$\alpha_F$	$\delta_F$	$\delta_T$	NO OF DP'S	DATE / TIME
	KEZ			3/18/		13	✓	15	0	VAR	MAN	85	-	✓	W <sub>1</sub> N <sub>1</sub> N <sub>2</sub> B F <sub>1</sub>	✓	✓	✓	✓	0	0	0	13	3/1/71 1824
						15	✓	45	✓	✓	✓	✓	-	✓	✓	✓	✓	✓	✓	✓	✓	15	✓	1852 1915
						45	✓	0	✓	✓	✓	✓	-	✓	✓	✓	✓	✓	✓	✓	0	45	✓	1928 2012
						TRANSIT + (3)	✓	30	✓	0-900	AUTO ①	✓	-	✓	✓	✓	✓	✓	✓	✓	30	TRANSIT + (3)	✓	2009
						✓	✓	✓	✓	✓	✓	✓	-	✓	✓	✓	✓	✓	✓	✓	✓	✓	✓	✓
						✓	✓	✓	✓	✓	✓	✓	-	✓	✓	✓	✓	✓	✓	✓	✓	✓	✓	✓
						✓	✓	✓	✓	✓	✓	113	-	✓	✓	✓	✓	✓	✓	✓	✓	✓	✓	✓
						✓	✓	✓	✓	✓	✓	✓	-	✓	✓	✓	✓	✓	✓	✓	✓	✓	✓	✓
						✓	✓	✓	✓	✓	✓	✓	-	✓	✓	✓	✓	✓	✓	✓	✓	✓	✓	✓
						✓	✓	✓	✓	✓	✓	✓	-	✓	✓	✓	✓	✓	✓	✓	✓	✓	✓	✓
						✓	✓	✓	✓	✓	✓	✓	-	✓	✓	✓	✓	✓	✓	✓	✓	✓	✓	✓
						✓	✓	✓	✓	✓	✓	✓	-	✓	✓	✓	✓	✓	✓	✓	✓	✓	✓	✓

(90)

67.68 RPM SWEEP : 0, 100-900 / 100, 950

69 FINE RPM SWEEP : - 0, 25 → 950 / 25 (NO OFF-LINE DYNAMIC DATA)

70 ① - 6 SECS - LINEAR

71 ② - 2 1/2 SECS - LINEAR

72 ③ - 3 SECS - LINEAR

PREP.	CHK.	APPR.	REVISED	DATE
	KEZ			3/18/

<p><u>VR 076-D</u></p> <p>1. MODEL CHARACTERISTICS</p> <p>2. SPIN-UP AND FEATHER</p>	<p>BVWT</p> <p>071</p>
--	------------------------

PREP.	CHK.	APPR.	REVISED	DATE	DATE / TIME	NO OF D.P.'s	TEST PROG RUN	$i_T$	$\delta_F$	$\alpha_F$	RPM	$\omega_F$	DEG RATE	WT. TARE RUN	TYPE OF RUN	CONFIGURATION	END OF	SPIN-UP & FEATHER PROGRAM	
	KEZ				3/1/71	+2	✓	0	15	0	0-715	0	②	-	S & F	W <sub>1</sub> N <sub>1</sub> N <sub>2</sub> B F <sub>1</sub>	✓		
						+5	✓	✓	30	✓	✓	✓	②	-	✓	✓	8.6	✓	
						+5	✓	✓	✓	✓	0-950	✓	P②	-	✓	✓	✓	✓	
						+3	✓	✓	✓	✓	✓	✓	MAU. P②	-	✓	✓	✓	✓	
						+3	✓	✓	✓	✓	0-715	✓	P①	-	✓	✓	✓	✓	3/2/71
						+5	✓	✓	15	✓	0-950	✓	P①	-	✓	✓	152	✓	0005
						+2	✓	✓	✓	✓	0-715	✓	P①	-	✓	✓	✓	✓	0072
						+6	✓	✓	✓	✓	0-715	✓	VAR	-	✓	✓	✓	✓	0042
																	END OF		

79.	PARABOLIC COLLECTIVE INPUT SCHEDULE - 4.5 SECS (AUTOMATIC)																		
80	MANDAL PARABOLIC INPUT - CONDITIONS AS RUN #79, FEATHER PHASE REPEAT																		
81	✓	✓																	
82	✓	✓																	
83	✓	✓																	
84	✓	✓																	

FORM 49810 (8/70)

VR-076 D  
 SPIN-UP & FEATHER PHASE  
 BNWT  
 071

PREP	CHK.	APPR	REVISD	DATE	CONFIGURATION	TYPE OF RUN	WT. TARE RUN	V	FOLD ANGLE DEG. RATE	$\alpha_F^\circ$	$\delta_F^\circ$	$\delta_L^\circ$	TEST PROG. RUN	NO OF DP'S	DATE / TIME
	KEF				W, N, N <sub>2</sub> B F <sub>1</sub>	FOLD, CHECK	-	85	VAR STEP	0	0	0	-	11	3/3/71 0145
					FLAP.	STARTING FOLD	-	85	90-0 STEP	✓	✓	✓	✓	32	3/3/71 2127
						✓	-	✓	✓	-2	✓	✓	✓	21	2334
						✓	-	✓	✓	+2	✓	✓	✓	19	2336
						✓	-	✓	✓	+4	✓	✓	✓	20	2336
						✓	-	✓	✓	✓	✓	✓	✓	23	2341
						DYN FOLD	-	85	VAR.	✓	30	✓	✓	23	2359
							-	115		+2	30	✓	✓	17	0150
						COMPLETE			FLAPWISE FOLDING.						0227
85.					HOLD @ 90 → 23.3										
86					90 → 0/10° (APPROX)										
87.					90, 70, 50, 30, 0										
88.					FOLD @ 90, 70, 50, 30, 0										
89					FOLD ANGLES AS RUN 87										
90					✓										
91					✓										
91					DYNAMIC FOLD TESTS :-										
					1- INITIAL W.O. DATA PT										
					1- PRE SWEEPERS PT @ 90 = B.6										
					1- FINAL W.O. DATA PT.										
					T/P 3 NO GOOD										
					90° - DEPLOYED, 0° FOLDED										

VR-076 D  
FOLD TESTS - 1) FLAPWISE

BVWT  
071



PREP.	CHK.	REVISED	DATE	CONFIGURATION	TYPE OF RUN	WT. TARE RUN	V	γ	FOLD ANGLE DEG RATE	α <sub>F</sub>	δ <sub>F</sub>	L <sub>T</sub>	TEST PROG RUN	NO OF D.P.'S	DATE / TIME
	KEF		3/18	W <sub>1</sub> N <sub>1</sub> N <sub>3</sub> B <sub>F1</sub>	✓	85	8.6	90	-	0	0	0		7	3/5/71 00
				✓	✓	85	8.6	✓	-	✓	✓	✓		12	✓ 0120 0003
				✓	FOLD STEP	85	8.6	90-0	STEP	✓	✓	✓	✓	18	0200 0135
				✓	✓	86	8.6	✓	✓	+2	✓	✓	✓	15	0227 0723
				✓	FOLD & DENOT	115	15.2	✓	VAR.	+2	30	✓	✓	19	0314 0326
								END EDGE FOLDING.							
								END BWWT 071.							
														(71)	TOT: 1024.

92. CHECK OUT TO OBTAIN D-TORQUE : 1ST TRY -3.99 @ 1b, @ γ = 8.6 @ 75 ON γ<sub>N</sub> 92, 91 JACKRABBIT

93. Q<sub>2</sub> = -3.6

94. FURTHER ADJUSTMENTS γ = 8.6 FOLD @ 90, 70, 50, 25, 15, FOLDED (2.5)

95. γ = 15.2 ~ 90°, 70°, 50°, 30°, 12.5, FOLDED (2.3) γ = 23.3 ~ 90°, 70°, 40°, 15, FOLDED (2.4)

96. γ = 8.6 ~ 90°, 70°, 50°, 30, FOLDED, (2.47) γ = 15.2 ~ 90°, 70°, 50, 20, FOLD (2.69)

97. T/P IS NO GOOD

T/P	FOLD	DEPLOY	MOTOR VOLTS	APPROX TIME SECS	REMARKS
1	✓	✓	7.5	8.9	WOOD S.W. ON D
2	✓	✓	10.0	✓	D.D.
3	✓	✓	10.0	3-4	✓
4	✓	✓	15.0	✓	✓
5	✓	✓	15.0	3	✓
6	✓	✓	17.5	2 1/2	✓
7	✓	✓	15.2	6 1/2	S WOOD
8	✓	✓	7.5	✓	P.D.
9	✓	✓	10.0	✓	ONLY TO 77 - STOCK
10	✓	✓	10.0	7.0	D.P. RPT - 10
11	✓	✓	10.0	6.0	✓
12	✓	✓	10.0	5.0	✓
13	✓	✓	10.0	3.0	✓
14	✓	✓	10.0	3.0	✓
15	✓	✓	10.0	2.0	✓
16	✓	✓	10.0	✓	✓
17	✓	✓	10.0	✓	✓
18	✓	✓	10.0	✓	✓

PREP	CHK.	APPR	REVISD	DATE	CONFIGURATION	TYPE OF RUN	WT. TARE RUN	$\gamma$	$\alpha_w^\circ$	$i_w^\circ$	RPM	TEST PROG RUN	NO. OF D.P.S	DATE / TIME
					W <sub>1</sub> N <sub>1</sub> N <sub>2</sub> B F <sub>1</sub>	AUTO ROT. BEST	-	10	90	90	VARY	✓	1	3/8/71 2300
✓					✓		-	21	✓	✓	✓	✓	21	3/9/71 2340
101					-- N <sub>2</sub> B F <sub>1</sub>	✓	-	✓	✓	✓	✓	✓	8	0058 0115
102					✓	✓	-	VAR	✓	✓	✓	✓	9	1716 1813
103					✓	✓	-	VAR 3-5	✓	✓	✓	✓	8	1831 1913
104					W <sub>1</sub> N <sub>1</sub> N <sub>2</sub> B F <sub>1</sub>	AUTO ROTN	-	16	-1	121	✓	✓	9	2053
105					✓	✓	-	32	✓	✓	✓	✓	5	
106					✓	✓	-	47	✓	✓	✓	✓	5	2243
107					✓	✓	-	16	-1	111	✓	✓		2250
108					✓	✓	-	32	✓	✓	✓	✓		
100.					<p><math>\theta_{75}</math> SWEEP <math>\pm 90^\circ</math> TO <math>+10^\circ</math> RPM 5 <math>\alpha \rightarrow 270</math> SHUT DOWN @ <math>\theta_{75} = 10</math>  RESTART @ <math>\theta_{75} = +10^\circ</math> RPM @ 272 <math>\gamma = 12</math>. DECREASE <math>\theta_{75}</math> TO RESUME RPM. <math>\gamma</math> TO 52  <math>\sim</math> RPM 100 TO 47K - NF<sub>2</sub> LIMIT. (DOE TO WING TORSIONAL SHAKING)  BANK TEST HERE</p>									
101.					<p>WING BOXES OFF, ENGINE PODS OFF. <math>\gamma = 0.52</math> REPEAT RPM 300 <math>\rightarrow</math> 454  LIMITED BY NF<sub>2</sub> AGAIN</p>									
102					<p><math>\gamma</math> OF CEC DATA ONLY. START D.D. WITH <math>\gamma = 0.3</math>  RPM + 300, <math>\rightarrow</math> 434 (MAX @ <math>0^\circ \theta_{75}</math>) 434 <math>\rightarrow</math> 100(R) T.P #9 100 RPM BACKWARDS.  THEN, <math>\theta_{75} = 0</math>, RPM = 444 - INCREASE <math>\gamma</math> FROM 0.3 TO 0.41 RPM REACHED 500. CEC DATA ONLY.  START: <math>\gamma = 0.3 + \theta_{75}</math> FOR 400 RPM; INCREASE <math>\gamma</math> MAINTAINING 400 RPM BY <math>\theta_{75}</math> CHANGE; NO DATA  2ND TRY. <math>\gamma = 0.3 - \theta_{75}</math> FOR 200. (-30).  UP TO <math>\gamma = 1.2</math>. (RPM = 248, <math>\theta_{75} = -30</math>) THEN RPM 872  THEN FEATHER</p>									
103.					<p><math>\gamma = 1.3</math> RPM / <math>\theta_{75}</math> SWEEP 300 RPM TO <math>-175</math> (BACKWARDS) T.D #7 WTL # 120  <math>\gamma = 1.2</math> ✓  <math>\gamma = 2.7</math> RPM TO 940 (@ <math>\theta_{75} = -4^\circ</math>)  WTL = 110  RPM 0 <math>\rightarrow</math> 460</p>									
104.					<p>THRU RESONANCE @ 650-700 VERY FAST</p>									
105														
106														
107														
108														



RUN NO.	CONFIGURATION	TYPE OF RUN	WT. TARE RUN	V	γ	α <sub>N</sub> °	α <sub>TL</sub> °	θ <sub>SWEEP</sub> °	RPM	TEST PROG RUN	NO OF DIPs	DATE / TIME
119	W <sub>1</sub> N <sub>1</sub> N <sub>2</sub> B F <sub>1</sub> NO FUSE	AUTO ROT.	-	32	1.2	+5	120	SWEEP VARY		✓	6	3/10/71 2242
120	✓	✓	-	48	2.7	✓	✓	✓		✓	9	2330
121	✓	✓	-	0.3	90	180	✓	✓		✓	17	0042
122	✓	✓	-	1.2	90	180	✓	✓		✓	11	0126
	END AUTOROTATION PHASE											
<p>119 <del>B<sub>15</sub></del>: -30.4 -18.4 +4.7 -10 17  RPM: 94 156 208 310 422  120 <del>B<sub>15</sub></del>: -32 -23 -19.4 -16 -13.8 -11 -8.5 -6 -3.6 -2.3 -1.1 +0.9 1.6 2.9 3.9  RPM: 102 144 188 204 234 274 320 374 404 408 418 376 386 424 514  122 <del>B<sub>15</sub></del>: -24.5 -24.5 -17.2 -15.8 -13.5 -11.2 -8.5 -6.5 -4.7 -3.6 -1.6 -0.8  256 300 316 406 424 724 848 852 872 872  SEE 10076</p>												

FORM 49810 (3/70)

BVWT

072

PREP.	CHK.	APPR.	REVISED	DATE	NO. OF DIPS	$\alpha_F$	$\delta_F^\circ$	RPM	$\lambda_T^\circ$	$\theta_{75}^\circ$	$\alpha_{TL}^\circ$	$\alpha_W^\circ$	$q_T$	$V_T$	WT. TARE RUN	TYPE OF RUN	CONFIGURATION	DATE / TIME
					14	0	0	VAR	0	VAR	0	+3	8.6	85	-	DYN. INSTAB.	$W_2 N_1 N_2 B F_1$	3/11/71 1938 1935
					12	✓	✓	✓	✓	✓	✓	✓	15.7		✓		$W_2 - N_2 B F_1$	✓
					13	✓	✓	✓	✓	✓	✓	✓	20	130	✓		✓	2041
					29	+2	✓	✓	0	✓	+2	+5	20	130	✓		✓	2205 2310
					22	✓	✓	✓	✓	✓	✓	✓	20	131	✓		✓	0000 0050
																		3/12/71
																		3/14

123. BEGIN AERO-ELASTIC INSTABILITY TESTS.  $W_2 \neq$  SOFT SPAR WING ARRGT.  
 RPM = 320, 700, 1000, 1100, 950, 200, 1050, 1080, 1100. SNUBBERS FITTED

124 ENGINE POD OFF. HUB BALANCE WEIGHTS ADDED AS PER RUN # 52. 20gm (96) 8.6gm (91)  
 BALANCE CHECK @ 8.6g UP TO 1080. CHECK TWEAK & D.D @ 1080. ALL OK.  
 INCREASE  $q_T$  TO 15.7 RPM: 700, 800, 200, 1000, 1040, 1090.  $\rightarrow$  320

125  $q_T = 20$  RPM = 700,  $\rightarrow$  1090  $\rightarrow$  800. AT 800,  $q_T = 20, 25, 27, 29$ .

126 FLUSE  $\delta$  CHANGE TO +2°.  $q_T = 8.6$ . RPM: 0, 800  $q_T = 20$ . RPM: 700  $\rightarrow$  320.  $q_T = 23.0, 800 \rightarrow 325$  (WB)\*  
 $q_T = 25.0$  RPM = 800, 700, SPD, 450, 400, 350 (WB)

RPM = 1000,  $q_T = 20, 21, 22, 23, 24$ .

1070,  $q_T = 23, 24$ . LIMITED EIC COMBINED CWB + FBM ALLOWABLE.

BOUNDARY FOR STATIC DIVERGENCE NOT ESTABLISHED. LIMITED BY 1100 RPM LIMIT AND  $q_T$  (HIGH BLADE LOAD)

127 2 lb WT. ADDED TO NACELLE.  $q_T = 20$ . RPM. 800, 900, 960  $q_T = 23, 800, 890, 950, 1000, 1060$   
 $q_T = 24.0$  RPM = 900, 1000, 1050, 1080.  $q_T = 25, 1000, 1090$   
 $q_T = 26, 1040, 1080$ . APPARENT LOSS IN SPRING RATE. ONSET OF STATIC DIVERGENCE

\* (WB) ONSET OF W/FI BOUNDARY

RUN NO.	CONFIGURATION	TYPE OF RUN	WT. TARE RUN	V	$\eta$	$\theta_{15}$	RPM	$\alpha_F^\circ$	$i_T^\circ$	$\delta_F^\circ$	NO OF DIPS	DATE / TIME
128	W2 N1 N2 B F1	CHECK OUT	-	VAR	VAR	VAR	VAR	+4	0	30	-	3/12/71 1830
129	✓	ROTAT. CHARG.	-	8.5 11.3	8.0 15.7	✓	✓	+2	0	30	31	1941 2022
130	✓	✓	-	✓	✓	✓	✓	+2	✓	0	31	2026 2108
131	✓	✓	✓	✓	✓	✓	✓	-2	✓	0	31	2145 2224
132	✓	✓	✓	✓	✓	✓	✓	-2	✓	30	31	2251 2322
133	✓	✓	✓	✓	✓	✓	✓	-2	✓	45	31	2338 0012
134	✓	✓	✓	✓	✓	✓	✓	-2	✓	15	30	3/13/71 0054
135	✓	✓	✓	✓	✓	✓	✓	+2	✓	15	21	0054 0125
				END OF TEST								

128. CONTINUATION OF ROTATING MODEL CHARACTERISTICS - SNOBBERS FITTED FUSE ON. INVESTIGATION OF MODEL LOADS (BLADE SPECIFICALLY). NO COMPUTER DATA.

129. @ 23  $\eta$ , BLADE LOADS 7: HIGH. DECISION TO REDUCE  $\eta$  TO  $\pm 2^\circ$ . ADDED 58m WT TO SNOBBERS CABLES OFF, FOR 129 ET SEQ.  $\eta = 8.5$  RPM: 0, 400  $\rightarrow$  1015 STEADY OSCILLATION / AIR RESONANCE LIMIT @ 1015 RPM  $\eta = 15.7$  400  $\rightarrow$  1040  $\rightarrow$  1050 SOME TORSIONAL MODEL MOVEMENTS 400  $\rightarrow$  700 RPM

130.  $\eta = 8.6$  RPM: 0, 400  $\rightarrow$  1010 V. SMALL OSCILLATION @ 1010  $\eta = 15.7$  400  $\rightarrow$  1050

131.  $\eta = 8.6$  RPM: 0, 400  $\rightarrow$  1050 STEADY OSCILLATION @ 100. LOADS OK  $\eta = 15.7$  RPM: 400  $\rightarrow$  1050 BAL. TEST POST 131.

132.  $\eta = 8.6$  RPM: 0, 400  $\rightarrow$  1050 STEADY OSCILLATION AT LOAD - NO DATA, CEG RECORD  $\eta = 15.7$  RPM: 400  $\rightarrow$  1050

133.  $\eta = 8.6$  RPM: 0, 400  $\rightarrow$  1050  $\eta = 15.7$  RPM: 400  $\rightarrow$  1050

134.  $\eta = 8.6$  RPM: 0, 400  $\rightarrow$  1050  $\eta = 15.7$  RPM: 400  $\rightarrow$  1050

135.  $\eta = 8.5$  RPM: 0, 400  $\rightarrow$  1050  $\eta = 15.7$  400  $\rightarrow$  1050

BW/T  
072

UNCLASSIFIED

Security Classification

DOCUMENT CONTROL DATA - R&D		
<i>(Security classification of title, body of abstract and indexing annotation must be entered when the overall report is classified)</i>		
1. ORIGINATING ACTIVITY (Corporate author) The Boeing Company, Vertol Division Boeing Center, P.O. Box 16858 Philadelphia, Pa. 19142		2a. REPORT SECURITY CLASSIFICATION Unclassified
		2b. GROUP
3. REPORT TITLE VOLUME VII. WIND TUNNEL TESTS OF THE AERODYNAMICS AND DYNAMICS OF ROTOR SPINUP, STOPPING AND FOLDING ON A SEMISPAN FOLDING TILT-ROTOR MODEL		
4. DESCRIPTIVE NOTES (Type of report and inclusive dates) Final Report, January to July 1971		
5. AUTHOR(S) (Last name, first name, initial) Dirk Van Wagensfeld                      Walter L. Lapinski Frank J. McHugh                              John P. Magee Leon N. Delarm		
6. REPORT DATE October 1971	7a. TOTAL NO. OF PAGES 398	7b. NO. OF REFS 5
8a. CONTRACT OR GRANT NO. F33615-69-C-1577	9a. ORIGINATOR'S REPORT NUMBER(S) D213-10000-7	
b. PROJECT NO.		
c.	9b. OTHER REPORT NO(S) (Any other numbers that may be assigned this report) AFFDL-TR-71-62, Volume VII	
d.		
10. AVAILABILITY/LIMITATION NOTICES Approved for Public Release - Distribution Unlimited		
11. SUPPLEMENTARY NOTES	12. SPONSORING MILITARY ACTIVITY Air Force Flight Dynamics Laboratory Air Force Systems Command Wright-Patterson Air Force Base, Ohio	
13. ABSTRACT Wind tunnel test data obtained with a 1/9-scale, semispan, unpowered, dynamically-scaled Model 213 stowed/tilt rotor are reported. The objectives of the tests were to obtain aerodynamic, structural, and dynamics data during the spinup, feather and blade fold cycles of this vehicle.		

Security Classification

14. KEY WORDS	LINK A		LINK B		LINK C	
	ROLE	WT	ROLE	WT	ROLE	WT
Stowed Rotor Tilt Rotor Rotor Feathering Rotor Spinup Rotor Folding Rotor Deployment Soft In-plane Hingeless Rotor						

INSTRUCTIONS

1. **ORIGINATING ACTIVITY:** Enter the name and address of the contractor, subcontractor, grantee, Department of Defense activity or other organization (*corporate author*) issuing the report.
- 2a. **REPORT SECURITY CLASSIFICATION:** Enter the overall security classification of the report. Indicate whether "Restricted Data" is included. Marking is to be in accordance with appropriate security regulations.
- 2b. **GROUP:** Automatic downgrading is specified in DoD Directive 5200.10 and Armed Forces Industrial Manual. Enter the group number. Also, when applicable, show that optional markings have been used for Group 3 and Group 4 as authorized.
3. **REPORT TITLE:** Enter the complete report title in all capital letters. Titles in all cases should be unclassified. If a meaningful title cannot be selected without classification, show title classification in all capitals in parenthesis immediately following the title.
4. **DESCRIPTIVE NOTES:** If appropriate, enter the type of report, e.g., interim, progress, summary, annual, or final. Give the inclusive dates when a specific reporting period is covered.
5. **AUTHOR(S):** Enter the name(s) of author(s) as shown on or in the report. Enter last name, first name, middle initial. If military, show rank and branch of service. The name of the principal author is an absolute minimum requirement.
6. **REPORT DATE:** Enter the date of the report as day, month, year; or month, year. If more than one date appears on the report, use date of publication.
- 7a. **TOTAL NUMBER OF PAGES:** The total page count should follow normal pagination procedures, i.e., enter the number of pages containing information.
- 7b. **NUMBER OF REFERENCES:** Enter the total number of references cited in the report.
- 8a. **CONTRACT OR GRANT NUMBER:** If appropriate, enter the applicable number of the contract or grant under which the report was written.
- 8b, 8c, & 8d. **PROJECT NUMBER:** Enter the appropriate military department identification, such as project number, subproject number, system numbers, task number, etc.
- 9a. **ORIGINATOR'S REPORT NUMBER(S):** Enter the official report number by which the document will be identified and controlled by the originating activity. This number must be unique to this report.
- 9b. **OTHER REPORT NUMBER(S):** If the report has been assigned any other report numbers (*either by the originator or by the sponsor*), also enter this number(s).
10. **AVAILABILITY/LIMITATION NOTICES:** Enter any limitations on further dissemination of the report, other than those

imposed by security classification, using standard statements such as:

- (1) "Qualified requesters may obtain copies of this report from DDC."
- (2) "Foreign announcement and dissemination of this report by DDC is not authorized."
- (3) "U. S. Government agencies may obtain copies of this report directly from DDC. Other qualified DDC users shall request through \_\_\_\_\_."
- (4) "U. S. military agencies may obtain copies of this report directly from DDC. Other qualified users shall request through \_\_\_\_\_."
- (5) "All distribution of this report is controlled. Qualified DDC users shall request through \_\_\_\_\_."

If the report has been furnished to the Office of Technical Services, Department of Commerce, for sale to the public, indicate this fact and enter the price, if known.

11. **SUPPLEMENTARY NOTES:** Use for additional explanatory notes.

12. **SPONSORING MILITARY ACTIVITY:** Enter the name of the departmental project office or laboratory sponsoring (*paying for*) the research and development. Include address.

13. **ABSTRACT:** Enter an abstract giving a brief and factual summary of the document indicative of the report, even though it may also appear elsewhere in the body of the technical report. If additional space is required, a continuation sheet shall be attached.

It is highly desirable that the abstract of classified reports be unclassified. Each paragraph of the abstract shall end with an indication of the military security classification of the information in the paragraph, represented as (TS), (S), (C), or (U).

There is no limitation on the length of the abstract. However, the suggested length is from 150 to 225 words.

14. **KEY WORDS:** Key words are technically meaningful terms or short phrases that characterize a report and may be used as index entries for cataloging the report. Key words must be selected so that no security classification is required. Identifiers, such as equipment model designation, trade name, military project code name, geographic location, may be used as key words but will be followed by an indication of technical context. The assignment of links, rules, and weights is optional.